

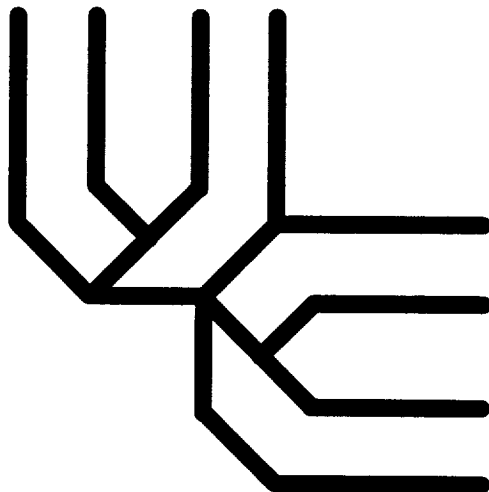
DESIGN OF AN UNMANNED MARTIAN POLAR EXPLORATION SYSTEM

(NASA-CR-197160) DESIGN OF AN
UNMANNED MARTIAN POLAR EXPLORATION
SYSTEM Final Report (Cincinnati
Univ.) 520 p

N95-12529

Unclassified

63/91 0026139 10



University of Cincinnati Space Engineering Research Center
NASA/USRA Advanced Design Program
Cincinnati, Ohio 45221-0343

July 30, 1994

DESIGN OF AN UNMANNED MARTIAN POLAR EXPLORATION SYSTEM

FINAL REPORT

NASA/USRA Advanced Design Program

Prepared By

Curt Baldwin	Tony Polakowski	Andy Stow
Denny Chitwood	Marc Richmond	Robert Stubbers
Brian DeMann	Todd Rothe	Maria Sychay
Jordan DuCheny	Marlon Santos	Tom Terrell
Richard Hampton	Neil Saunders	Lynn White
Jesse Kuhns	Shital Shah	Jeff Wiley
Amy Mercer	Jeff Skudlarek	Ralph Winiarski
Shawn Newman	Susan Slater	
Chris Patrick	Michael Sonby	

Lead Instructor

Dr. Larry Cooper

Teaching Assistant

Joe Lemanski

Assistant Instructors

James Anno
Ray Lin
Joseph Nevin
Trevor Williams
Richard Wysong

University of Cincinnati Space Engineering Research Center
NASA/USRA Advanced Design Program
Cincinnati, Ohio 45221-0343

July 30, 1994

ABSTRACT

The design of an unmanned Martian polar exploration system is presented. The system elements include subsystems for transportation of materiel from Earth to Mars, study of the Martian north pole, power generation, and communications.

Early next century, three Atlas 2AS launch vehicles will be used to insert three Earth-Mars transfer vehicles, or buses, into a low-energy transfer orbit. Capture at Mars will be accomplished by aerobraking into a circular orbit.

Each bus contains four landers and a communications satellite. Six of the twelve total landers will be deployed at 60° intervals along 80°N , and the remaining six landers at 5° intervals along 30°E from 65°N to 90°N by a combination of retrorockets and parachutes. The three communications satellites will be deployed at altitudes of 500 km in circular polar orbits that are 120° out of phase. These placements maximize the polar coverage of the science and communications subsystems.

Each lander contains scientific equipment, two microrovers, power supplies, communications equipment, and a science computer. The lander scientific equipment includes a micro weather station, seismometer, thermal probe, x-ray spectrometer, camera, and sounding rockets.

One rover, designed for short-range (<2 km) excursions from the lander, includes a mass spectrometer for mineral analysis, and auger/borescope system for depth profiling, a deployable thermal probe, and charge coupled device cameras for terrain visualization/navigation. The second rover, designed for longer-range (2-5 km) excursions

from the lander, includes radar sounding/mapping equipment, a seismometer, and laser ranging devices.

Power for all subsystems is supplied by a combination of solar cells, Ni-H batteries, and radioisotope thermoelectric generators. Communications are sequenced from rovers, sounding rockets, and remote sensors to the lander, then to the satellites, through the Deep Space Network to and from Earth.

PREFACE

This was the second year for the University of Cincinnati in the NASA/USRA Advanced Design Program. This association was initiated by the University of Cincinnati NASA Space Engineering Research Center to expose undergraduate students to space-related design opportunities.

More than thirty students and seven faculty from the Departments of Aerospace Engineering and Engineering Mechanics, Chemical Engineering, Electrical and Computer Engineering, Materials Science and Engineering, and Nuclear and Power Engineering collaborated under the leadership of the NASA Space Engineering Research Center in a unique design effort. This interdisciplinary approach to design is intended to provide the students with a "real-world" experience; it was the first opportunity for most of the students to work with people outside their respective disciplines on a common project.

During Fall Quarter, experts from NASA, industry, and academia gave seminars on space-related topics. The students were presented with an overall design goal, and divided into design teams to identify key technologies and parametrics associated with achieving this goal. Most of the actual design work was accomplished during Winter Quarter. Spring Quarter was devoted to report writing and preparing for the USRA/ADP Annual Conference. Weekly meetings attended by students and faculty were held to address problems and project direction. The students also submitted weekly progress reports.

Our presentation at the NASA/USRA ADP Tenth Annual Conference in Pasadena, CA on June 15, 1994 was well received by attendees from NASA, USRA, industry, and academia. The students viewed their participation in the program as an invaluable experience, and several students reported that talking about the experience during job interviews drew great interest from the interviewers.

Joe Lemanski, Teaching Assistant
July 21, 1994

ACKNOWLEDGMENTS

The students would like to thank all professors listed and unlisted whose help and guidance were invaluable to the completion of this design project. A special thanks goes to Larry Cooper from the University of Cincinnati NASA Space Engineering Research Center, whose efforts made this project possible and exciting to work on.

A final thanks to the USRA for making this experience available.

TABLE OF CONTENTS

1.0 EXECUTIVE SUMMARY	1.1
2.0 EARTH-MARS TRANSPORTATION SYSTEM.....	2.1
3.0 SHORT-RANGE MARTIAN ROVER.....	3.1
4.0 LONG-RANGE MARTIAN ROVER.....	4.1
5.0 REMOTE POWER SUPPLY	5.1
6.0 SOIL ANALYSIS	6.1
7.0 SOLAR TRACKING SYSTEM	7.1

1.0 EXECUTIVE SUMMARY

Curt Baldwin
Denny Chitwood
Richard Hampton
Joe Lemanski
Marc Richmond
Marlon Santos
Neil Saunders
Shital Shah
Jeff Skudlarek
Susan Slater
Michael Sonby
Robert Stubbers
Tom Terrell
Ralph Winiarski

TABLE OF CONTENTS

1.1 INTRODUCTION.....	1.1
1.2 MARS ORBITING BUS TRANSPORT	1.1
1.2.1 INTRODUCTION	1.1
1.2.2 LAUNCH SYSTEM	1.1
1.2.3 INTERPLANETARY CRUISE.....	1.2
1.2.4 ARRIVAL AT MARS	1.3
1.2.5 LANDER DEPLOYMENT	1.4
1.2.6 ORBITAL SYSTEMS	1.6
1.2.7 LANDER SYSTEMS	1.8
1.3 SHORT-RANGE ROVER.....	1.9
1.3.1 INTRODUCTION	1.9
1.3.2 DESIGN AND OPERATION.....	1.10
1.3.3 POWER SUPPLY AND ELECTRONICS.....	1.12
1.3.4 NAVIGATION, CONTROL, AND COMMUNICATIONS	1.13
1.3.5 SCIENCE EXPERIMENTS	1.14
1.4 LONG-RANGE ROVER	1.15
1.4.1 INTRODUCTION	1.15
1.4.2 ASSUMPTIONS.....	1.15
1.4.3 DESIGN AND OPERATION.....	1.17
1.4.4 FRAME DESIGN	1.17
1.4.5 DRIVE SYSTEM	1.18
1.4.6 SUSPENSION AND LATERAL STABILITY ASSEMBLY.....	1.21
1.4.7 POWER	1.22
1.4.8 TRACKING SYSTEM AND COMMUNICATIONS	1.23
1.4.9 HEATED COMPARTMENT.....	1.25
1.5 ROVER POWER SOURCE	1.25
1.6 SOIL ANALYSIS DEVICES.....	1.26
1.7 SOLAR TRACKING SYSTEM	1.26
1.8 ECONOMICS	1.26

1.1 INTRODUCTION

With the recent failure of the Mars Observer, NASA budget cuts, and the apparent abandonment of the Space Exploration Initiative by the present administration, missions to Mars in the foreseeable future will be unmanned. The polar regions have been the least studied and least understood on Mars. The composition and stratigraphy of the caps and the transport of volatiles to and from the polar regions are among the most important questions to be answered about Mars. This work summarizes the design of an unmanned mission to study the Martian north pole and related operations by students from the University of Cincinnati. The mission is designed using present to near-term technologies to be self-sufficient, i.e. it does not rely on the success or failure of other missions (e.g. Space Station).

1.2 MARS ORBITING BUS TRANSPORT

1.2.1 INTRODUCTION

The Mars Orbiting Bus Transport (MARS OR BUST) mission is designed as a follow up to the MESUR mission, but does not rely on its success. Specifically, it is a scientific exploration of the Martian Northern Polar Cap. The mission duration is one Martian year with the launch window set between the years 2010 and 2020. The mission consists of five stages: Launch, Interplanetary Cruise, Arrival at Mars, Lander Deployment, and Mission Duration.

1.2.2 LAUNCH SYSTEM

The Atlas 2AS-Centaur launch vehicle provides sufficient thrust to carry each transfer vehicle package which includes four landers, an orbiting communication satellite, structural

band and navigation sensors, (see Figure 1.2.1). A type-B adapter attaches each transfer vehicle to the inner fairing on the Centaur upper stage.

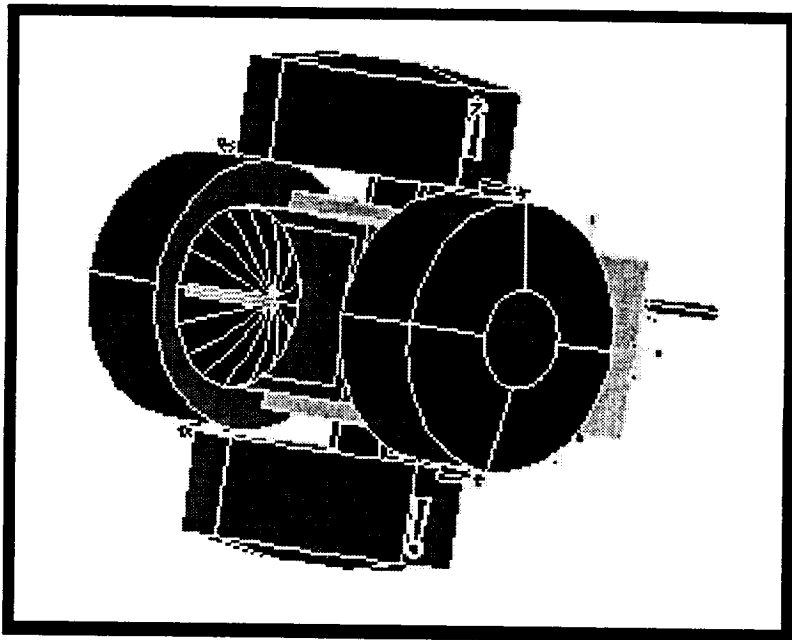


Figure 1.2.1 Earth-Mars Transfer Vehicle

1.2.3 INTERPLANETARY CRUISE

To minimize fuel requirements, a Hohmann transfer is flown to reach Mars. The total flight from Earth to Mars will last ~250 days. In-flight propulsive maneuvers, which account for a total ΔV of approximately 100 m/s, include a burn for upper-stage separation and mid-course corrections. A slow spin stabilizes the transfer vehicle, maintains accurate pointing of the communications equipment, and provides for uniform heating during cruise. Eight thrusters, aligned as shown in Figure 1.2.2, provide attitude control. One thruster aligned with the transversal axis provides three trajectory correcting propulsive ΔV s of 75, 15, and 10 m/s.

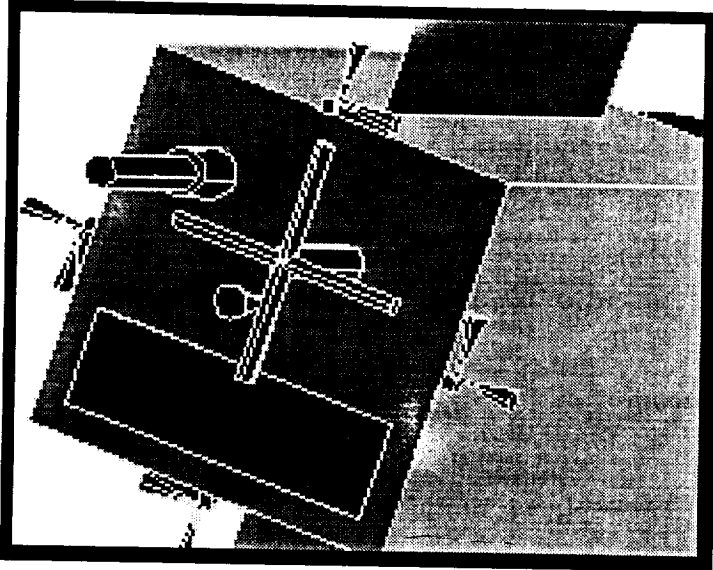


Figure 1.2.2 Transfer vehicle thrusters

The transmissions during cruise consist of Telemetry, Tracking, Command, and Communications (TTC&C). Downlinks, once every two to four days, occur at a low data rate (~400 bps). These communications are basic house- keeping tasks and only require a low 5 W EIRP which is provided for by the lander SNAP-19 RTGs.

The lander and transfer vehicle thermal systems include an Aluminized-Kapton coating which acts as a blackbody emitter and an insulating blanket to protect against the low temperatures during cruise. To maintain satisfactory operating temperatures at extreme flight conditions, the transfer vehicle also has an active temperature control system (louvers). The louvers are slats attached to temperature sensitive springs.

1.2.4 ARRIVAL AT MARS

An aerocapture maneuver is critical for orbit establishment with minimum fuel depletion. As the transfer vehicle passes through the Martian atmosphere, the following extreme conditions occur: a maximum velocity of 5.6 km/s, a minimum altitude of 52.8 km, a

maximum heating rate of 16.7 BTU/ft²-sec, and an atmospheric encounter time of ~16 minutes. The Thermal Protection System (heat shield) is an Alumina-Enhanced Thermal Barrier with a reaction cured glass coating to protect from space debris.

The final two passes are considered aerobrake maneuvers. They are necessary for orbit circularization from the initial capture orbit. Total fuel requirements account for a 100 m/s ΔV. By utilizing aerocapture/aerobraking in this way, fuel requirements are reduced by 1/3. The Thermal Protection System is jettisoned upon completion of the final pass, where a 500 km orbit is established.

1.2.5 LANDER DEPLOYMENT

Twelve landers are placed about the Martian northern polar cap as shown in Figure 1.2.3. Once the transfer vehicle has established a circular orbit, the Martian surface is mapped for lander placement. The process is an autonomous site selection with a quick-look downlink to the Earth for final verification. The medium resolution mapper creates 0.67 Mbps of information that is processed to select the specific locations of the polar sites.

Each lander is deployed from the transfer vehicle by the torsion disk system and two solid rocket motors (see Figure 1.2.4.) The vertical springs spin each lander at 30 RPM. Then the large horizontally located spring provides an initial ejective force from the transfer vehicle. The two solid rocket motors located on either side of the lander heat shield impart the deorbit burn of 104 m/s to send the lander from orbit to the Martian surface.

To decelerate the lander from it's orbital speed of 3,568 m/s, the following sequence is utilized: an aerobrake maneuver, parachute deployment and subsequent terminal velocity descent, heat shield release, tri-axial stabilization by three sets of hydrazine rockets,

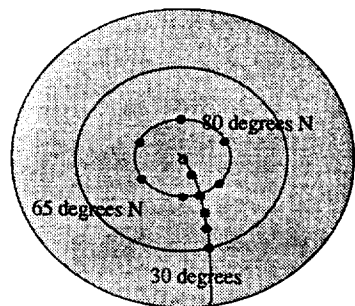


Figure 1.2.3 Lander deployment sites

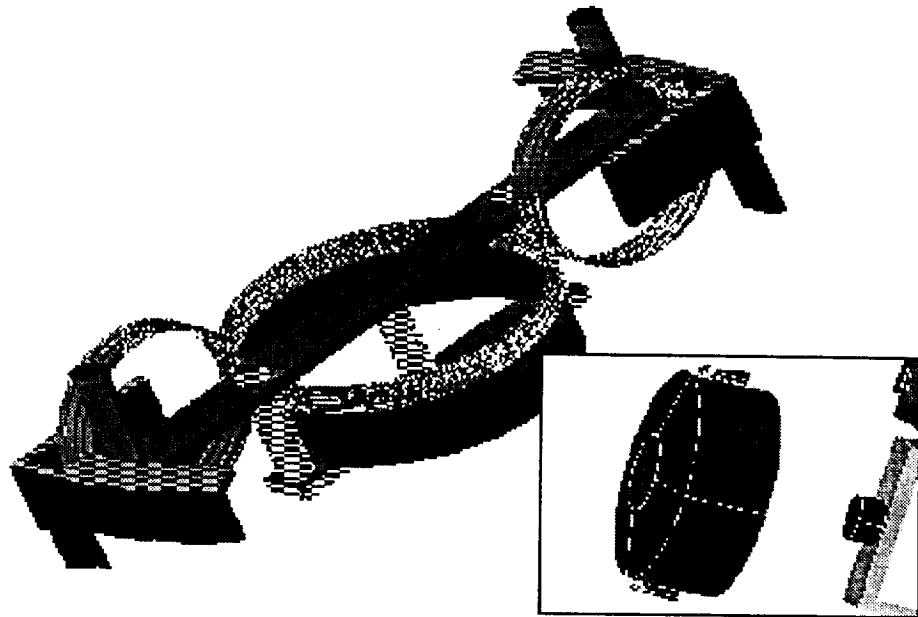


Figure 1.2.4 Torsion disk system

parachute/back shell release, final hydrazine rocket deceleration, and a soft landing (see Figure 1.2.5). The lander attitude and control system includes a frequency modulated carrier wave radar altimeter, three radar velocity sensors, and three single degree of freedom rate gyroscopes. The total deceleration process period is 8 minutes and 52 seconds. The lander decelerates 3,563 m/s to attain a soft landing of 5 m/s on the Martian surface. Crushable

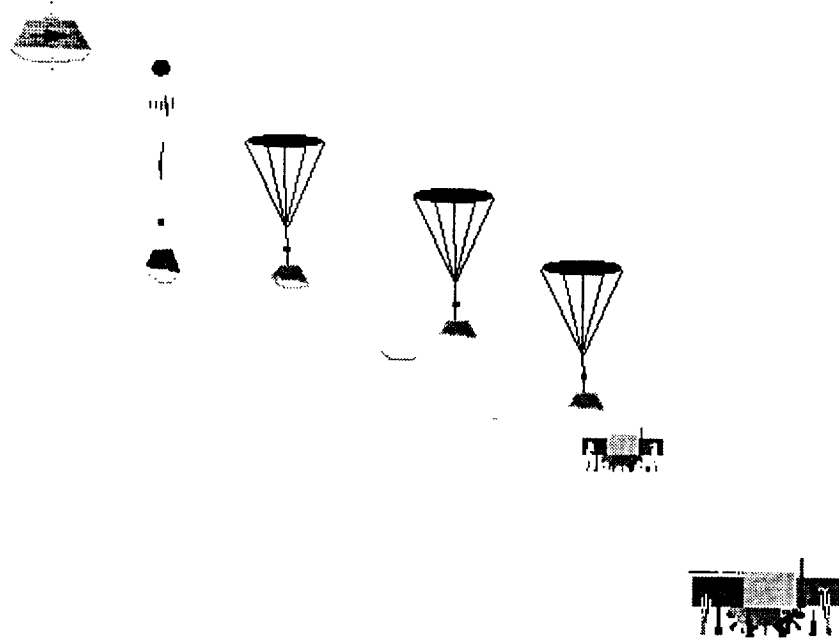


Figure 1.2.5 Lander deployment

honeycombed aluminum mechanical shocks and the lander exostructure absorb the impact energy of the 5 m/s landing.

1.2.6 ORBITAL SYSTEMS

During the operational, data-gathering phase of the mission, a total of three communications and science orbiters circle the planet in three 90° polar orbits. The three orbits (one per satellite) are 120° out of phase with one another, thereby providing the widest amount of polar surface coverage possible. Each 500 km orbit has a period of approximately 2 hours.

Power for the orbiter is provided by two gallium-arsenide solar cell arrays as shown in Figure 1.2.6. Each 7 m^2 cell is deployed via mechanical springs, thereby reducing the possibility of deployment failure. At the end of the mission, after two years of cell degradation and at the lowest solar efficiencies, the two cells together will provide 170 watt-

hours to the orbiter. To provide power while the orbiter is on the back side of the planet, three nickel-hydrogen batteries are manipulated. The 80 watt-hour batteries have the ability to be charged and drained simultaneously.

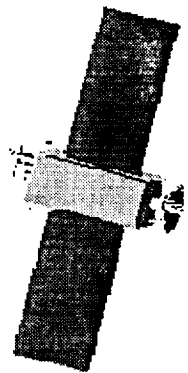


Figure 1.2.6 Orbital communications satellite

The largest power drain for the orbiter is the communications equipment. In order to communicate with Earth from the Mars vicinity the communications equipment can require as high as 53 watts. These transmissions are in the X-Band frequency range. The orbiters downlink data to the Deep Space Network for eight hours a day. In order to transmit the 2200 Mbits of data that are created at the lander sites each day, the orbiters will downlink at 8.5 kpbs. Diversity combining and 2:1 data compression techniques are utilized to maximize the data rates at the provided power. To compensate for the periods when data cannot be transmitted to Earth, a solid state memory device is employed. The 2 gigabyte recorder has the ability to read and write simultaneously. Additionally, further command and control signals are uplinked to the orbiter from operators on Earth and can be further transmitted from the orbiter to the landers. The data from the landers is communicated to the orbiter at

835 bps. By using an omnidirectional antenna and frequency spacing, multiple lander links can be transmitted/received simultaneously.

1.2.7 LANDER SYSTEMS

Each of the twelve landers is a platform for two microrovers and an assembly of science instruments. Power for the lander is provided by a radioisotope thermoelectric generator (RTG). A small SNAP-19 RTG can provide 35 watt-hours for up to two years on the Martian surface. The landers also house the communications equipment, an active thermal control system, and two sounding rockets. The sounding rockets are small devices used to autonomously probe the meteorological properties of the Martian atmosphere up to 13 km. The overall platform layout is depicted in Figure 1.2.7.

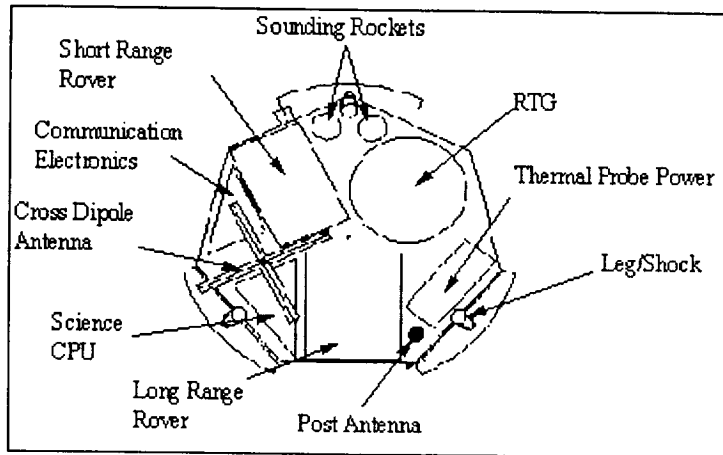


Figure 1.2.7

Communications with the rovers take place via a UHF transmitter such that the signals are transparent to the ice and rock that make up the polar cap. By using an

omnidirectional antenna, there are no rover tracking requirements and the rovers in turn, can transmit to the lander from any position. Additionally, the landers transmit to the orbiters in the S-Band frequency to downlink 180 Mbit/day.

1.3 SHORT-RANGE ROVER

1.3.1 INTRODUCTION

A short-range micro-rover (Figure 1.3.1), Red Rover, has been designed to conduct science experiments up to 2 km away from the lander site to obtain data on the environment of the polar cap. Each rover will commence at the lander and traverse in a circular pattern at intervals of 0.5 kilometers away from the lander as shown in Figure 1.3.2.

The basic operation of the rover includes traversing a distance of approximately 30 meters, collecting science data, then proceeding to the next test location. The entire cycle will last for a time period of about one third of a Martian day. The experiments that will take place include: compositional analysis of soil with a mass spectrometer, CCD imaging of the surrounding terrain, and meteorological data using a drill and borescope system. This experimentation will continue for one half of a Martian year. During this time period, the polar cap will be in complete sunlight. The second half year, when the polar cap is in complete darkness, the rover will remain stationary and will collect data as long as possible.

Because the data collection time period is to last at least one Martian year (which is equivalent to 1.8 Earth years), Red Rover is designed to endure the harsh environmental conditions of Mars for that time period. Navigational instruments on the rover will enable it

to detect terrain variations and avoid obstacles so that it will be able to traverse on the polar cap without being disabled.

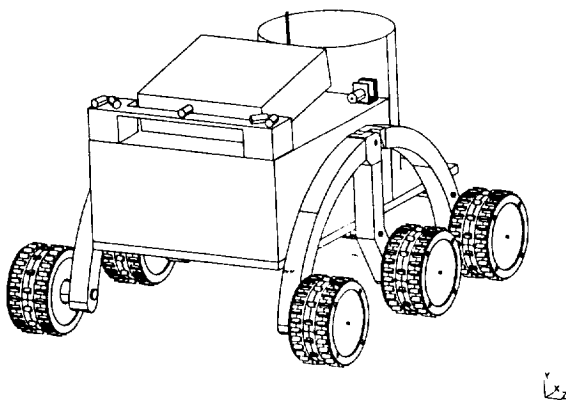


Figure 1.3.1 Short-range rover

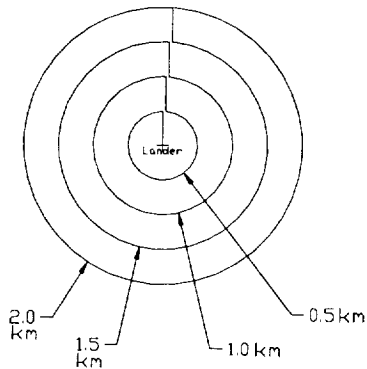


Figure 1.3.2 Rover pathway

1.3.2 DESIGN AND OPERATION

The proposed design of Red Rover consists of a six-wheel configuration. This allows for increased stability and also provides a good trade-off of power versus weight. The overall dimensions of the Rover envelope are 406.4 mm X 508.0 mm X 254.0 mm. The wheel base from the front to the center wheel is 236 mm. The wheel base from the front wheel to the

rear wheel is 406.4 mm. To obtain as much traction as possible, the width of each wheel is 50.8 mm. The diameter of each wheel is 101.6 mm in order to be able to traverse maximum protrusions. All six wheels are driven by independent motors and the steering is to be controlled by using tank steering methods. The Red Rover has two points of articulation for overcoming protrusions when traveling over the terrain. As a result of having just two articulation points, the Rover has two independent members per side. By attaching one of the articulation points to the platform, the left and right sides become independent of each other.

The platform supports all of the necessary scientific equipment, the power source, and the onboard electronics. The dimensions are 381.0 mm X 254.0 mm. It is pinned midway between the front and rear wheels to the sides. It is additionally supported by rear platform support cantilevers. There are two cantilevers, one on each rear member with a length of 101.6 mm. They protrude perpendicularly from the inner surface of the rear member beneath the platform. These cantilevers perform two major functions. The first is to utilize the weight of the platform to take advantage of the rear drive motors. If no weight were acting on the rear member, it would simply act as a trailer. The second function is to allow for an independent suspension while supporting the platform. The center of gravity of the platform payload (scientific equipment, experiments, etc.) should lie between the pinned attachment and the rear platform support cantilevers. One side of the basic configuration is shown in Figure 1.3.3.

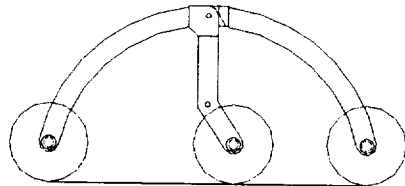


Figure 1.3.3 Basic Configuration

1.3.3 POWER SUPPLY AND ELECTRONICS

Depending on the tasks that are to be performed, Red Rover needs a variable amount of power. Preliminary estimates suggest that a minimal constant supply of approximately 2 Watts and a maximum supply of 8 Watts is needed; this power needed is DC. Power sequencing is to be employed so that minimum power is utilized at a given time.

The power supply for Red Rover is provided by a nuclear power source. The nuclear isotope being investigated is Strontium-90 and is in the form of Strontium Fluoride. The operating efficiency will be between 5 and 10 percent. The excess energy not turned into power will be given off thermally. This thermal energy will be used to maintain the temperature in a warm electronics box above a minimum of -40°C.

The warm electronics box sits on the platform. Most of the electronics and the central processing unit are encased within this box. Also, the electronics box is surrounded by a vacuum honeycomb wall of insulation to reduce heat loss. All other electronics which are outside of the box, will be designed to meet appropriate temperatures for successful operation.

1.3.4 NAVIGATION, CONTROL, AND COMMUNICATIONS

The Rover large-scale navigation is controlled from the Earth. It is based on lander-generated stereo images, rover imaging sensors, and rover contact sensors to obtain information concerning its location and surroundings. This information is transmitted to Earth so that Earth control can determine a path for the rover which is free of obstacles and/or hazards that could threaten the mobility of the rover.

The rover executes commands via on-board capabilities that involve traverse behaviors and dead reckoning. Traverse behaviors are based on range finders and contact sensors, while dead reckoning is based on gyro inclinometers and wheel revolution counters.. The rover also has three accelerometers and a gyro to determine the displacements and any angle changes of the platform during rover movement. The rangefinder portion of the control system has two forward-looking solid state imaging sensors (charge coupled device (CCD) cameras) and five strategically-placed light stiper projectors to aid rover navigation.

The rover has a antenna approximately 15 cm long. The antenna is linked to the RF modem, computer, and I/O electronics in the electronics box. The characteristics of the communication system will allow it to communicate with the lander effectively at all times. As a precautionary measure, “RF link checks” are made during rover movements so that the rover does not become lost in an area where it is unable to communicate effectively with the lander. Approximately every 30 seconds, the rover will send a signal to the lander and receive an echo. If RF contact is not made, the rover will traverse back to the last known point of effective RF contact.

1.3.5 SCIENCE EXPERIMENTS

There will be three experiments that the rover is responsible for: mass spectrometer, ice auger/borescope system, and a thermal probe. The mass spectrometer is a near-infrared spectrometer that will provide detailed mineral analysis which will aid in determining climatic and geological data on the polar cap of Mars. This instrument is mounted on the platform of the rover.

The ice auger/borescope system will be used to examine the layering of the polar ice cap. This layering is created as a result of the continually changing surface due to yearly weather variations. Much like the rings in the cross-section of a tree, each layer of ice contains information about the environmental conditions of a certain time period. The auger will drill a hole into the ice to a depth of approximately 15 cm and a diameter of 1 cm, then the borescope will be deployed into this hole to record a picture of the stratified layers of ice. The mechanical deployment mechanism for the auger and borescope system is mounted on the outside of one of the rear arms of the rover.

The Red Rover will drag a thermoprobe away from the lander and release it at a selected destination. The thermoprobe is initially on the lander and attached to the rover via a looped cord. This cord is connected to a solenoid unit placed on top of the electronics box, and will be actuated when the probe has traveled away from the lander, releasing the thermoprobe. The thermoprobe will then commence operation by melting its way through the layers of ice taking data as it goes.

Additionally, when computing power and memory are available, the rover will image the surface of Mars using the CCD imaging sensors. This will provide extra images for the researchers and scientists.

1.4 LONG-RANGE ROVER

1.4.1 INTRODUCTION

A rover that can travel 20 km from its lander has been designed to study the northern polar region of Mars (Figure 1.4.1). This polar region varies in size, depending on the season. This was a challenging design problem, because the rover and its subsystems will have to survive and perform at temperatures down to about -150°C. Also, specific information about the surface of the polar region was unknown. A lot of questions would have been answered by the Mars Observer spacecraft, but unfortunately, due to some system failure, it was lost in space just a short time ago. Therefore, a "best guess" approach has been used for certain aspects of the design.

The rover design is based upon considerations which involve frame design, drive systems, suspensions, materials, power requirements, computers, sensors and communications equipment.

1.4.2 ASSUMPTIONS

- ①** Most of the polar cap is very hard with patches of powdery dry ice.
- ②** The lowest temperature is -150°C and the highest is 40°C.
- ③** The solar panel will have a mechanism to keep array perpendicular to the sunlight to maximize power output

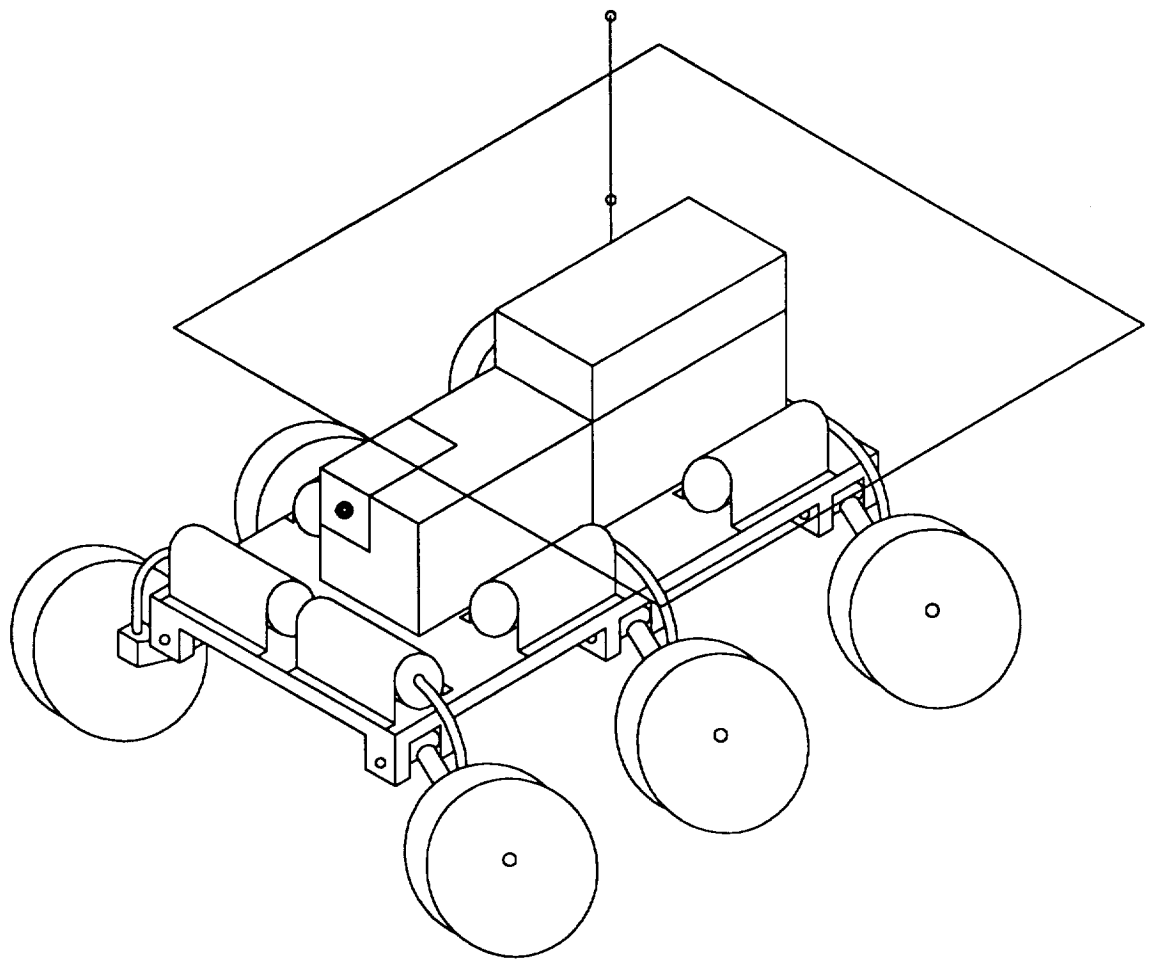


Figure 1.4.1 Long-range rover

- ⑥ Most of the polar cap is smooth with small rocks (<10cm in diameter).

1.4.3 DESIGN AND OPERATION

The goal is to design a vehicle capable of transporting payloads of experiments over a variable terrain in the Martian environment. Power is provided by a solar panel, batteries and RTGs. On-board science experiments, a computer, communications and other sensors will be standard equipment.

Four of the six wheels have the same tread for the harder surfaces. Two of the wheels have a different tread for any surface encountered. Using six frame mounted motors and six gear-reducers, the torque is transmitted to the wheels by flexible shafts. The solar panel will provide enough power to the motors for half a year based on the seasons. During the winter, the vehicle will be immobile with the batteries and the RTGs sustaining the science experiments, computer and communications. The RTGs main purpose is to keep the electronics package warm enough to operate and to provide power.

1.4.4 FRAME DESIGN

The basic frame is a single-piece design. A multi-piece unit was also considered, but the single-piece was preferred for the following reasons. A multi-piece unit would require the use of a joint or joints to connect the different sections. A failure in one of these joints would leave the rover at least partially disabled. Also, the controls for this design would be more complicated and would require more power. The multi-piece body would be preferable if extremely rugged terrain was to be traversed, but as far as is known, the polar region is not nearly as rugged as the rest of the planet. Material selection for the frame was a major factor. The temperature on Mars is estimated to be at a low of -150° C. Some metals in this range

become brittle and have other poor material properties. Some materials that were viable options were OFCH Copper, alpha brass, certain aluminum alloys, austenitic stainless steel, some titanium alloys, and some magnesium alloys. Non-metallic materials were also considered. Some examples were polyethylene, PVF, FEP (thermoplastics), glass fiber reinforced plastic (GFRP), and carbon fiber reinforced plastics (CFRP). The factors considered in material determination were yield strength, ultimate tensile strength, toughness, fatigue strength, thermal expansion coefficients (low number needed), and density.

The three materials that had the most desirable mechanical properties were aluminum alloys, titanium 6Al 4V, and CFRP. The material chosen from these three was CFRP. It had the best combination of factors. It has a high yield strength, a good fracture toughness, and the thermal expansion is very low. This is important because of the variation in temperature from launch on Earth, to the cold in the vacuum of space, and to the equally cold temperatures that will be experienced on the polar surface of Mars during the winter season. The material also has a low density value and retains its material properties at the low temperatures.

1.4.5 DRIVE SYSTEM

The drive system was one of the many challenging aspects of the design, because of the frozen CO₂ surface at the polar region. The variables used to choose the drive system were mobility, traction, reliability, ease of control, stability, power requirements, and weight. The following options were carefully reviewed to meet the needs of the mission: caterpillar-style treads similar to those on a tank; individually-controlled legs to give a "walking" effect; a snowmobile design that would entail a combination of skis mounted in the front and a

single drive tread mounted in the rear. A tread design would allow movement on a wide range of terrain and would provide inherent stability for the rover, but it would have a relatively high weight and would be prone to failure if one of the links should break. Legs are an interesting idea but just have too many potential problems. They would require a lot more control and computational power than other options and would, by nature, be unstable. Also, if one leg would fail, it would be extremely difficult to compensate for this loss. The snowmobile design was considered, because the polar surface most likely has some powdery CO₂ "snow." However, to be effective the ski part needs a very low coefficient of friction, while the tread portion needs a high friction coefficient. This could prove to be a seriously inefficient use of power.

The option that was decided upon was wheels. Wheels can be designed to handle a variety of surface conditions, are less vulnerable to failure than other options, and are easy to control. Also, they use power efficiently and are very stable if the vehicle has a low center of gravity. Wheels may have difficulty navigating rough, broken terrain, but it is assumed from what is known about the polar surface of Mars that the rover will be able to maneuver around any such conditions. It was decided that six wheels would be used; four wheels would not provide proper redundancy in the case of a single wheel failure, and more than six wheels would be too redundant and make the design needlessly complicated. The rover will have the ability to drive forwards and backwards in case it gets trapped somewhere and needs to back itself out of that area. Also, it will be able to turn around by having the wheels on one side spin one direction and the wheels on the other side spin the opposite direction.

The front and back wheels have a different tread design than the middle set of wheels in order to traverse different surface conditions. The front and back sets of wheels are designed to travel on solid CO₂ "ice," and the middle wheels are designed to drive on powdery "snow".

After six wheels were chosen, a method of power transmission to these wheels needed to be determined. Two main options were considered: slip rings and flexible shafts. Slip rings are conductive contacts which are used to transmit electrical power between rotating surfaces. A conductive strip is placed on one surface and a contact on the other. The contact is forced against the conductive strip by a spring to ensure a constant connection. Electricity would then be conducted by wires to the motors located in each wheel hub. A flexible shaft, on the other hand, is a set of wires twisted together in a uniform direction and held inside a flexible tube. Torque is supplied to the shaft at one end and is transmitted to the other end. The motors corresponding to the flexible shaft design would be mounted on the frame. There would still be one motor for each wheel to provide redundancy in case one or possibly two motors would fail.

The slip ring idea, with motors in the wheels, would increase the stability of the rover but would make the wheel design very complicated due to the need for a high gear reduction system to be placed in a small amount of space. Flexible shafts, with motors mounted on the frame, are considered to be the best choice for the following reasons. The flexible shaft allows for greater freedom on the part of the designers. Since the motors are to be mounted on the frame, they can be placed anywhere. This creates the flexibility to design for the most efficient use of space. The flexible shafts are also more efficient than a complex set of gears.

This system of shafts does not need the precise alignment or the high tolerances required by a gear or wheel mounted motor system. Being a less than smooth ride to Mars, this reduces the possibility of problems upon arriving at the destination. The flexible shafts are very efficient, low cost, and are low in weight. Overall, the flexible shaft design provides the best method of power transmission while eliminating some of the problems of other power transmission systems.

1.4.6 SUSPENSION AND LATERAL STABILITY ASSEMBLY

The suspension system is a fairly simple design. The struts connect the wheels to the frame and transfer the frame and equipment weight to the wheels. Material considerations were similar to those for the frame and wheels. The struts will be hollow shafts of circular cross section. They will be constructed out of titanium or CFRP due to its high strength/weight ratio. The bushings will be made out of CFRP impregnated with PTFE and with a reinforcing ring of 316 stainless steel. Torsional springs will allow damped vertical movement of the wheels and frame. The materials that were considered for the torsional springs are high carbon spring steel, Kromarc 55, and 310 stainless steel. Selection was based on high elastic limit, which was the most important factor, high surface hardness, toughness at low temperatures, and fatigue strength. The material that was best suited for this purpose was the 310 stainless steel because of its excellent low temperature strength and toughness. There will be two torsional springs per strut. This reduces the stresses in each individual spring and adds redundancy to the system.

1.4.7 POWER

Many different power systems were considered to run the rover and its subsystems. They included solar panels, radioisotope thermoelectric generators (RTG's), batteries, tethered power input, and an internal combustion engine. The internal combustion engine would provide high power output, but its need for refueling limits the range of the vehicle. This is obviously impractical for a long range rover such as the one being designed here. Tethered input would consist of a land line spooling from the lander to the rover to provide electric power to the rover and to transmit data to and from the lander. This option would also provide the rover with more power. However, since the rover will probably need to back up and maneuver itself along the surface, the tether would either get entangled with the rover or would break due to its fragility at the low Martian polar temperatures. Using a tether presents problems of length and additional mass. Therefore, tethered input is a very impractical choice for power.

Solar panels could be used to harness the energy of the sun. The solar intensity on Mars is not near what it is on Earth, however, solar panels are a proven technology and can be used at least as one power source.

RTG's, which convert thermal energy from a decaying radioisotope into electric power, are very dependable and last for a long time. Yet, they are terribly inefficient (around 6%) and have a high weight to power ratio. The excess heat that is given off by the radioisotope can be used to heat the electronics, which will be housed in an insulated box. Therefore, the RTG's are still a practical choice to be used on the rover.

The last power source considered was batteries. They would be charged by the other power sources on the rover, so they would not actually be supplying additional power. They would just allow the rover to store power to run different subsystems at the same time. It was decided that solar panels, RTG's, and batteries would all be used to power the rover.

1.4.8 TRACKING SYSTEM & COMMUNICATIONS

There are several factors that need to be considered when establishing a communication design: communication of the rover to the lander, communication of the lander to Earth, and positioning factors. Some designs considered were inertial tracking (gyroscopes and accelerometers), wheel movement tracking, radio tracking with receivers on the rover, on the lander, and in space, and visual tracking by way of cameras on the rover.

The design that will be used is a combination of a wheel movement tracking system and a radio tracking system. Gear speed sensors will keep track of essentially straight line motion, and this data will be transmitted to the lander. The transmission will be picked up by a small four-arm spiral antenna which will find the position of the rover in the horizontal and vertical planes relative to itself. These two angles, combined with the wheel movement data, will give the location of the rover. There will be as many receivers as there are rovers that report back to a particular lander. The advantages of such a system are explained next. The wheel movement tracking requires little or no power from the rover, and it would also take up minimal space on the wheel. The radio tracking provides accuracy regardless of terrain and can also relocate the rover if it falls out of communication for a period of time. The radio also requires little additional power which is an obvious advantage.

1.4.8.1 SENSORS

Laser ranging is the concept that will be used; it works similar to sonar. A laser beam pulse is emitted, and the return is monitored. The distance can be computed by knowing the time between emission and return. The system proposed for the rover would aim the laser at some angle downward. This angle would need to be calculated to determine an optimum, based on laser system location, vehicle dimensions, and travel speed. The laser would sweep out an arc in front of the rover, stopping at several positions and firing the laser. The return time given by the beam off a level surface would be known. Therefore, a longer return time would indicate a depression, and a shorter return time would indicate a raised area.

1.4.8.2 MICRO-CONTROLLER

The function of the micro-controller is to accept and process instructions sent to the rover via radio signals, as well as inputs from the wheel speed sensors and laser sensors. The processor will also output necessary responses over the radio, while producing drive signals for each of the six wheels. The micro-controller has the duty of activating experiment modules and transmitting experiment data back to the lander.

The micro-controller must meet several requirements:

- Sufficient computer power/speed to run the rover
- low power requirements
- large operating temperature range
- proven reliability

One chip meeting these requirements is the Intel 80C51BH. It is a single chip, 8-bit micro-controller capable of 12 MHz speed. Under normal operating conditions, it draws 16 mA from 5V; under a special sleep mode, it draws only 50 μ A. This sleep function shuts down everything but on-board and essential functions.

1.4.9 HEATED COMPARTMENT

To ensure proper operation of the micro-controller and other electronic equipment, a heated compartment will house these items as well as the rechargeable batteries. The insulation that was selected for the compartment is silica aerogel, or "santocel". This material has a very low thermal conductivity, which decreases with temperature drop. The heat for the compartment will be supplied by the RTG. It is a great source of heat due to a low (6%) efficiency. The placement of the RTG with respect to the compartment is centralized.

1.5 ROVER POWER SOURCE

To provide remote power generation for the Mars microrovers, several alternative methods were examined. These options included solar cells, batteries, fuel cells, thermionic direct energy converters (DEC), charged particle DEC, and radioisotope thermoelectric generators (RTG). In selecting among these alternative methods, several design criteria were used. These criteria included mission length, payload mass restrictions, and economic considerations. RTG's were selected because they best matched the design criteria. In order to provide the most efficient and economical power source, it was decided to design a RTG for the proposed mission, rather than use an existing one.

A computer code was written to perform all the necessary design calculations. A 10 watt RTG using strontium fluoride as the radioisotope was designed. It has an outer radius of 6.5 cm and a total mass of 600 g.

1.6 SOIL ANALYSIS DEVICES

Alternatives for a subsurface probe and an x-ray diffractometer are discussed. A subsurface probe has been designed that uses both heat and mechanical energy to penetrate the polar surface. The probe contains an imaging device to take pictures of the drilled layers, and temperature and pressure sensing devices. An x-ray diffractometer has been designed that is capable of obtaining mineralogical data on the polar deposits.

1.7 SOLAR TRACKING SYSTEM

An algorithm has been developed to move rover or lander based solar panels to maximize their exposure to solar radiation. This algorithm has been demonstrated using solar cells mounted on a robotic arm.

1.8 ECONOMICS

The cost of the delivery system including most relevant factors has been estimated at \$1 billion. The cost of all other systems, including only hardware and development, was estimated at \$500 million. This does not include legal fees for the RTD's and other administrative costs that we could not estimate. One observer from JPL estimated that our total mission cost would likely be in the \$10 billion range.

2.0 EARTH-MARS TRANSPORTATION SYSTEM

Curt Baldwin
Denny Chitwood
Chris Patrick
Jeff Skudlarek
Tom Terrell
Lynn White

ABSTRACT

The ability of mankind to explore the next frontier is essential for the advancement of society's technology and is critical as mankind dreams of habitation of future frontiers. The design of an unmanned polar Martian exploratory mission is presented. The mission elements include a set of three transfer vehicles each mounted with four landers containing a pair of rovers. Specific systems within the mission elements include deorbit and landing, power generation, communication, and thermal protection.

The multi-purpose vehicles provide interplanetary transportation to Mars. An aerocapture maneuver decelerates the transfer vehicle and a series of aerobraking passes establishes a circular orbit with minimal propellant. Once in position, surface mapping is used for site selection. At this time, the four landers are released sequentially from each vehicle and descend to specific Northern polar landing sites.

Upon landing on the surface, two rovers from each lander are activated for exploration within a five kilometer radius. Scientific data acquisition is conducted at each lander, rover, and orbiting satellite. Additionally, sounding rockets investigate the meteorological properties of the Martian atmosphere. All data is fed to the satellites via the lander, and then down linked to the Earth's Deep Space Network. To satisfy the power requirements of the satellites, solar arrays and Nickel-Hydrogen batteries are utilized. Radioisotope Thermoelectric Generators provide power for the interplanetary orbiter and the surface landers.

TABLE OF CONTENTS

<u>2.1. LAUNCH</u>	<u>1</u>
2.1.1 LAUNCH WINDOW ANALYSIS	1
2.1.2 LAUNCH VEHICLE CHOICE	1
2.1.3 TRANSFER VEHICLE DESIGN	3
<u>2.2. INTERPLANETARY CRUISE</u>	<u>5</u>
2.2.1 ORBITAL MECHANICS	5
2.2.2 PROPULSION AND ATTITUDE CONTROL	6
2.2.3 COMMUNICATIONS	8
2.2.4 POWER	9
2.2.5 THERMAL CONTROL DURING CRUISE	10
<u>2.3. ARRIVAL AT MARS</u>	<u>12</u>
2.3.1 AEROCAPTURE AND AEROBRAKE MANEUVERS	12
2.3.2 THERMAL PROTECTION SYSTEM	13
2.3.3 CIRCULARIZATION	14
2.3.4 POWER	14
2.3.5 COMMUNICATIONS	15
<u>2.4. LANDER DEPLOYMENT</u>	<u>17</u>
2.4.1 LANDER PLACEMENT	17
2.4.2 TRANSFER ORBIT	17
2.4.3 LANDER DROP SEQUENCING	19
2.4.4 COMMUNICATIONS	20
<u>2.5. LANDER DESCENT</u>	<u>22</u>
2.5.1 DESCENT SUMMARY	22
2.5.2 PARACHUTE SYSTEM	23
2.5.3 ROCKET SYSTEM	24
2.5.4 LANDER ATTITUDE AND CONTROL SYSTEM	27
2.5.5 LANDER IMPACT	28
<u>2.6. MISSION DURATION</u>	<u>30</u>
2.6.1 ORBITER	30
2.6.1.1 FINAL ORBIT	30

2.6.1.2 POWER	30
2.6.1.3 COMMUNICATION	32
2.6.1.4 ATTITUDE CONTROL	35
2.6.1.5 ATTITUDE CONTROL SYSTEM	37
2.6.2 LANDER	39
2.6.2.1 LANDER CONFIGURATION	39
2.6.2.2 COMMUNICATION AND SCIENCE	40
2.6.2.3 POWER	42
2.6.2.4 SOUNDING ROCKETS	43
2.7. CONCLUSION AND INITIAL ECONOMIC ASSESSMENT	45
2.8. APPENDIX A: LAUNCH WINDOW ANALYSIS CODE	47
2.8.1 ORBIT.CPP	48
2.8.2 VECTOR.H	54
2.9. APPENDIX B: ORBITAL MECHANICS EQUATIONS	57
2.9.1 CIRCULAR ORBITS	57
2.9.2 ELLIPTICAL ORBITS	57
2.9.3 HYPERBOLIC ORBITS:	57
2.10. APPENDIX C: ATMOSPHERIC FLIGHT SIMULATION	58
2.10.1 FLIGHT.CPP	60
2.10.2 TELEM.H	63
2.11. APPENDIX D: COMPUTATION OF HEATING RATE	75
2.12. APPENDIX E: DESCENT ANALYSIS	77
2.12.1 PARACHUTE ANALYSIS	77
2.12.2 ROCKET ANALYSIS	78
2.13. APPENDIX F: DESIGN OF LANDER STRUCTURE	80
2.13.1 FINITE ELEMENT MODEL	80
2.13.1.1 LOADING 1: EARTH BASED LAUNCH	83
2.13.1.2 LOADING 2: MARTIAN LANDING	83
2.13.1.3 FAILURE CRITERIA	85

<u>2.14. APPENDIX G: TANK DESIGN</u>	86
2.14.1 DETERMINATION OF HELIUM VOLUME (EXAMPLE FOR LANDER)	86
2.14.2 DETERMINATION OF TANK SIZES/MASSES	87
2.14.3 FINAL RESULTS	87
<u>2.15. APPENDIX H: ATTITUDE CONTROL SYSTEM</u>	90
2.15.1 PROGRAMS	90
2.15.2 PROGRAM START	90
2.15.3 PROGRAM ORBITER	90
2.15.4 FIGURES	91
<u>2.16. APPENDIX I: COMMUNICATIONS</u>	95
2.16.1 ORBITER TO EARTH LINK MARGIN	95
2.16.2 LANDER TO ORBITER LINK MARGIN	96
<u>2.17. APPENDIX J: TORSION DISK DESIGN</u>	97
<u>2.18. APPENDIX K: LAUNCH SUPPORT STRUCTURE</u>	103
2.18.1.1 FAILURE CRITERIA	105
<u>2.19. APPENDIX L: THERMAL ANALYSIS DURING CRUISE</u>	107
<u>2.20. APPENDIX M: SOLAR ARRAY AND BATTERY SIZING</u>	109
<u>2.21. APPENDIX N: THERMAL ANALYSIS ON SURFACE</u>	111

TABLES

TABLE 1: LAUNCH WINDOWS	1
TABLE 2: ATLAS 2AS LAUNCH VEHICLE	2
TABLE 3: TOTAL WET MASS BREAKDOWN.....	4
TABLE 4: ORBITER FUEL MASS BREAKDOWN FOR MISSION	8
TABLE 5: ORBITER PROPULSION/ATTITUDE CONTROL MASS BREAKDOWN.....	8
TABLE 6: CRUISE POWER BUDGET.....	9
TABLE 7: SOLAR ABSORBTIVITY AND EMISSIVITY FOR VARIOUS MATERIALS.....	10
TABLE 8: AEROBRAKE SUMMARY	13
TABLE 9: FLIGHT EXTREMES	13
TABLE 10: HEAT SHEILDS	14
TABLE 11: LANDER POSITIONS	17
TABLE 12: TRANSFER ORBIT CHARACTERISTICS	19
TABLE 13: LANDER DROP SEQUENCE.....	20
TABLE 14: DECELERATION PARAMETERS	22
TABLE 15: PARACHUTE SYSTEM MASS BREAKDOWN.....	23
TABLE 16: DESCENT SYSTEM MASS BREAKDOWN	27
TABLE 17: MASS BREAKDOWN OF LANDER STRUCTURE.....	28
TABLE 18: ORBITAL PARAMETERS	30
TABLE 19: SOLAR ARRAY CHARACTERISTICS.....	31
TABLE 20: ORBITER POWER/THERMAL MASS BREAKDOWN	32
TABLE 21: ORBITER COMMUNICATIONS/NAVIGATION MASS BREAKDOWN.....	34
TABLE 22: ORBITER POWER BUDGET	35
TABLE 23: MOMUNTUM WHEELS SPECIFICATIONS	36
TABLE 24: GAINS FOR DIFFERENT VEHICLE CONFIGURATIONS.....	38
TABLE 25: LANDER SCIENCE AND COMMUNICATION COMPONENT MASS BREAKDOWN.....	41
TABLE 26: SOUNDING ROCKET ENGINE DATA	43
TABLE 27: ECONOMIC ESTIMATE.....	45
TABLE 28: NODAL MASS DISTRIBUTIONS	82
TABLE 29: STRESS RESULTS	85
TABLE 30: SUMMARY OF TORSION DISK ELEMENTS.....	101
TABLE 31: SUMMARY OF SUPPORT STRUCTURE ELEMENTS	105
TABLE 32: MAXIMUM SUPPORT STRUCTURE STRESSES.....	105

FIGURES

FIGURE 1: LAUNCH SUPPORT STRUCTURE	2
FIGURE 2: ATLAS 2AS EARTH-ESCAPE PERFORMANCE	3
FIGURE 3: TRANSFER VEHICLE IMMEDIATELY AFTER LAUNCH	4
FIGURE 4: EARTH-MARS HOHMANN TRANSFER ORBIT.....	5
FIGURE 5: THRUSTER LOCATION ON ORBITER	7
FIGURE 6: TRANSFER VEHICLE DURING MAPPING STAGE.....	16
FIGURE 7: NORTHER POLAR CAP WITH LANDER POSITIONS	17
FIGURE 8: DESIGN OF TORSION DISK	18
FIGURE 9: DIRECTIONAL ROCKETS	25
FIGURE 10: ROLL AND PITCH ROCKETS	26
FIGURE 11: DESPIN ROCKETS	26
FIGURE 12: ROCKET DECELERATION	26
FIGURE 13: LEG ASSEMBLY	28
FIGURE 14: LANDER EXOSTRUCTURE	29
FIGURE 15: ORBITER WITH ALL LANDERS DEPLOYED AND SOLAR CELLS EXTENDED.....	32
FIGURE 16: MOMENTUM WHEEL CONFIGURATION	37
FIGURE 17: CONTROL SYSTEM BLOCK DIAGRAM	39
FIGURE 18: LANDER CONFIGURATION	40
FIGURE 19: PASS #1 AEROCAPTURE MANUEVER.....	72
FIGURE 20: PASS #2 AEROBRAKING MANUEVER	73
FIGURE 21: PASS #3 AEROBRAKE MANUEVER.....	74
FIGURE 22: LANDER STUCTURE FINITE ELEMENT MODEL	81
FIGURE 23: ONE RADIAN SLEW WITH NO LANDERS PRESENT.....	92
FIGURE 24: ONE RADIAN SLEW WITH ONE LANDER PRESENT	93
FIGURE 25: ONE RADIAN SLEW WITH TWO LANDERS PRESENT	94
FIGURE 26: SIDE, TOP, AND EXPLODED VIEWS OF TORSION DISK ASSEMBLY	101
FIGURE 27: SUPPORT STRUCTURE FINITE ELEMENT MODEL.....	103
FIGURE 28: SUPPORT STRUCTURE CROSS-SECTIONS	104

2.1. LAUNCH

2.1.1 Launch Window Analysis

(Denny Chitwood)

The lowest energy transfer between any two orbits is a Hohmann transfer. (See Orbital Mechanics for more details about a Hohmann transfer.) Using this transfer technique as the optimum, a computer simulation is utilized to evaluate the launch windows. Table 2.1 outlines the launch windows which allow for a C3 of less than 10.0 km²/sec². See Appendix A for more information.

Table 2.1: Launch Windows

Start Date	End Date
27 October 2011	1 December 2011
27 October 2013	30 November 2013
17 April 2016	27 May 2016
17 April 2018	28 May 2018
18 April 2020	28 May 2020

2.1.2 Launch Vehicle Choice

(Curt Baldwin)

In order to reach a compromise between payload size and cost, the Atlas 2AS is the vehicle of choice. The choice of launch vehicle defines several parameters for the transfer vehicle design. These parameters include mass, size, and structural integrity. Table 2.2 is a brief breakdown of the Atlas 2AS' important dimensions.

Table 2.2: Atlas 2AS Launch Vehicle

Maximum payload mass (large fairing)	2000 kg
Payload fairing height	9.4 m
Payload fairing usable diameter	3.7 m
Maximum longitudinal acceleration	5.5 g

During launch, the transfer vehicle sits atop a Type B launch adapter. This adapter is a 1.2 m diameter ring which attaches the support structure to the Centaur. In turn, this support structure cradles the transfer vehicle's landers through the 5.5g's encountered during launch. This support consists of a simple truss structure constructed from Aluminum 2024-T4. See Appendix K for details of the design. Figure 2.1 shows how this structure supports the landers. The entire assembly is covered by a shroud during launch. This shroud is connected only to the launch vehicle.

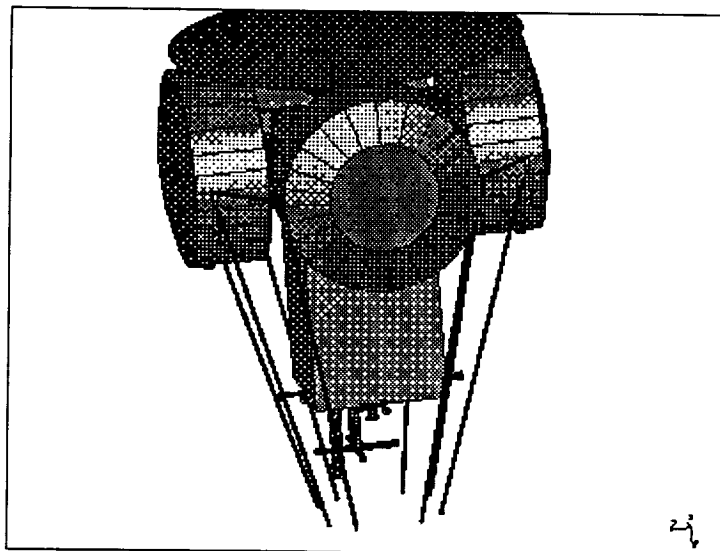


Figure 2.1: Launch Support Structure

Upon launch, the Atlas and the Centaur combine to put the vehicle in Earth orbit. A final firing of the Centaur sends the orbiter on interplanetary flight. Figure 2.2 shows several Earth-escape performance curves relating payload systems weight to the Atlas 2AS with

various payload fairings and an extra stage. Due to the value of C₃, approximately 10.0 km²/sec², an additional upper stage is not useful. At this line on the graph, the curves for the Atlas 2AS large payload fairing (LPF) and the Atlas 2AS with STAR 48B OIS have merged. This clearly states there is nothing to gain by adding another stage.

Figure 2.2: Atlas 2AS Earth-Escape Performance

2.1.3 Transfer Vehicle Design

(Curt Baldwin)

Collectively, the formation of the landers and the orbiter, have been termed the transfer vehicle. The orbiter consists of a communications satellite, mapping and navigational equipment, and various scientific instruments. Figure 2.3 shows the transfer vehicle just after launch.

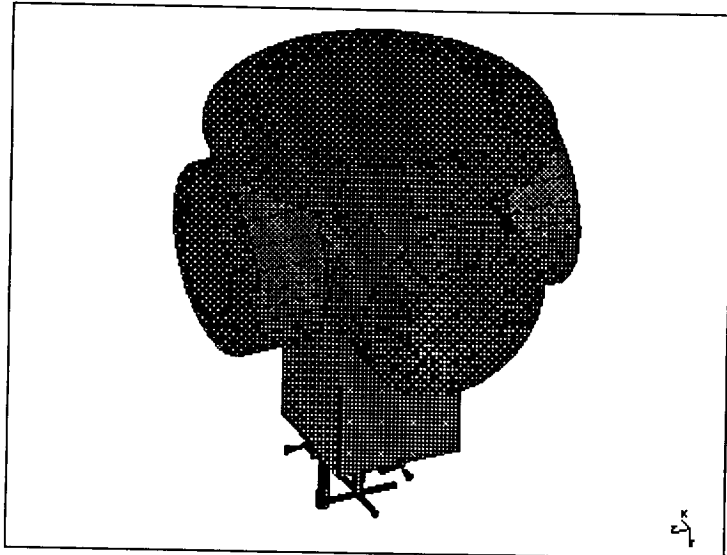


Figure 2.3: Transfer Vehicle Immediately After Launch

Each vehicle launched consists of four landers, each with an individual heat shield, a orbiter, and a main heat shield for the aerocapture at Mars. The total height of the transfer vehicle is 4.4 m while the principal diameter is 3.4 m. These dimensions allow the vehicle to make efficient use of the Atlas LPF. Table 2.3 gives a rough mass breakdown of the major systems at this stage. More detailed breakdowns will be given as each system is discussed. Total launch weight is 1629 kg, allowing for small mass gains at launch.

Table 2.3: Total Wet Mass Breakdown

Orbiter		Landers (4)	
propulsion/attitude	432.4 kg	deceleration/deorbit	116.7 kg
communications	78.7 kg	communications	6.4 kg
structure	50.0 kg	structure	26.6 kg
heat shield	22.2 kg	heat shield	6.2 kg
power/thermal	164.2 kg	power/science	69.4 kg
Total	747.5	Total	225.3 kg
Total			1648.7 kg

2.2. INTERPLANETARY CRUISE

2.2.1 Orbital Mechanics

(Denny Chitwood)

The minimum velocity change (ΔV) required for a transfer between two circular orbits is achieved by using a doubly-tangent transfer ellipse. This is called the Hohmann transfer orbit. It is considered the minimal energy transfer because it uses the least amount of propellant to achieve a new orbit. This type of transfer requires two ΔV s, one at the original orbit and one at the final orbit to circularize. The first ΔV at Earth is characterized by the parameter C3, which is V_∞^2 . V_∞ is the hyperbolic escape velocity from Earth. This is accomplished by the launch vehicle. The V_∞ at Mars is evaluated at the edge of its sphere of influence or the sphere in which Mars' gravity exceeds that of the Sun. The method employed is to use the Martian atmosphere to produce the second ΔV . This process is called aerocapturing. Figure 2.4 illustrates the heliocentric or Sun centered transfer orbit. See Appendix B for a listing of equations used.

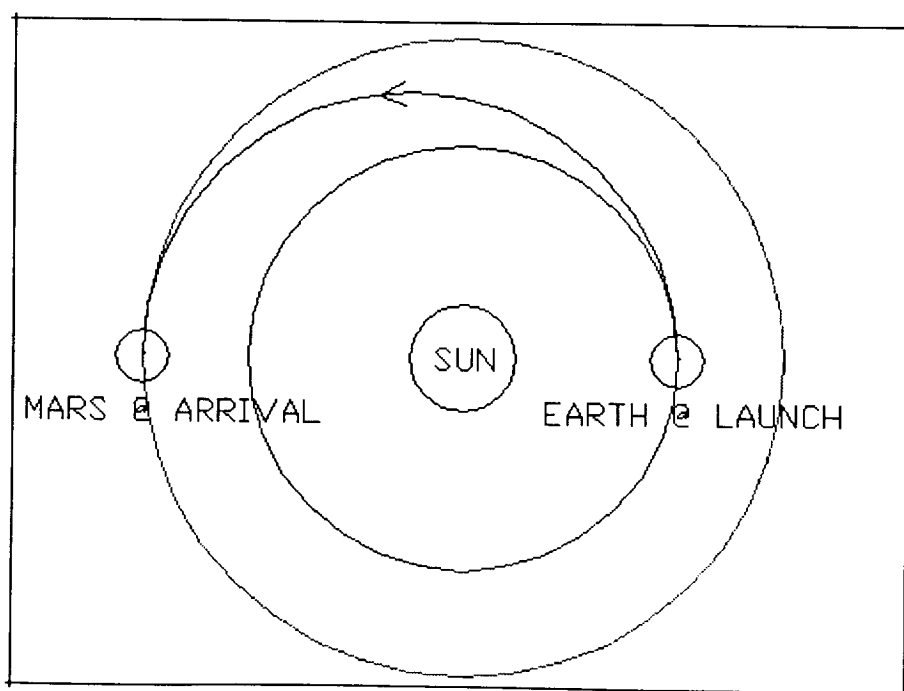


Figure 2.4: Earth-Mars Hohmann Transfer Orbit

2.2.2 Propulsion and Attitude Control

(Denny Chitwood and Lynn White)

To conserve mass and volume, the same propulsion system used on the orbiter is used by the transfer vehicle during the trip to Mars. The aft section of the orbiter, which houses the thrusters, is exposed to perform any mid-course corrections and maneuvers. Hydrazine, a monopropellant, was chosen over a bipropellant because of the simplicity of the monopropellant system. Although monopropellants have lower specific impulses than bipropellants, the savings in complexity and number of tanks needed to store the fuel is an advantage.

The control system employed by the satellite is a primary system of four momentum wheels and gas jet thrusters as a backup. This system was chosen over magnetic torquers, control moment gyroscopes and thrusters alone due to several factors. The first is that there is no appreciable magnetic field around Mars, therefore magnetic torquers could not operate. Control moment gyros were not chosen because of their cost and mass. The thrusters alone would not be suitable because the amount of fuel needed for station-keeping once in orbit would be tremendous. The momentum wheel/gas jet thruster combination provides the best control system with minimal mass and cost with the added benefit of being a very accurate system. With the momentum wheels spinning at high rates, small disturbances do not affect the attitude of the orbiter appreciably. During cruise, the momentum wheels slowly spin (5-10 RPM) to keep the wheel bearings from freezing. A complete discussion of the momentum wheels will be provided in a later section.

Several sensors are also used by the control system. Ring laser gyros, a horizon sensor and a star tracker are utilized to maintain the proper attitude. The ring laser gyro enables the satellite to interpret any changes in its orientation. The horizon sensor helps the satellite stay pointed in the proper direction once in orbit around Mars. The star tracker is used as a check on the cruise to ensure it is on the proper course. It will also be able to detect and correct any errors in the other sensors due to general wear.

The thruster locations are on the aft of the orbiter. Eight small thrusters (CHT-20's), clustered in pairs of two, are located around the edge of the orbiter and one main thruster located in the center (Figure 2.5). This configuration was chosen to provide thrust vectors along three axes. Each CHT-20 provides 7.2 N to 24 N of thrust. The small thrusters are clustered because this arrangement allows for the least amount of internal fuel piping from the tanks. The main thruster, a CHT-350, provides 110 N to 350 N of thrust. The small thrusters control rotation while the main thruster controls translation (eg. retro burns for circularization). The fuel requirements of the mission total 300 kg, as shown in Table 2.4.

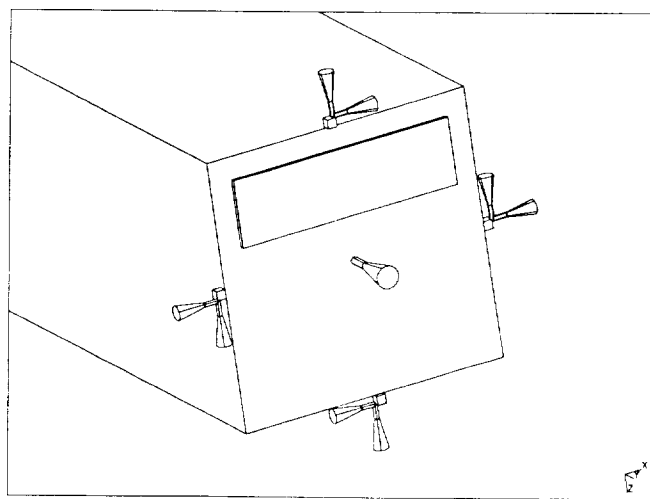


Figure 2.5: Thruster Location on Orbiter

This mission allows for three mid-course corrections. One major ΔV for a 75 m/s correction and two smaller ΔV s of 15 m/s and 10 m/s. The initial aiming point of the mission is slightly away from Mars so that the upper stage does not crash onto the Martian surface. The large ΔV is to change the vehicle course to intercept at the proper destination. A full summary of the sensors, thrusters, and other required attitude control mechanisms is included in Table 2.5.

Table 2.4: Orbiter Fuel Mass Breakdown for Mission

First Mid-Course Correction	75 kg
Second Mid-Course Correction	15 kg
Third Mid-Course Correction	10 kg
Circularization	100 kg
Desaturation	100 kg
Total	300 kg

Table 2.5: Orbiter Propulsion/Attitude Control Mass Breakdown

Star Tracker	6.8 kg
Ring Laser Gyro	6.8 kg
Static Horizon Sensors	.9 kg
Momentum wheels (4)	10 kg (each)
Momentum wheel motors (4)	2.5 kg (each)
Momentum wheel driver	2.25 kg
Hydrazine	300 kg
Helium	0 kg
Fuel Tank	18.4 kg
Pressure Tank	42.2 kg
CHT-20's (8)	.4 kg (each)
CHT-350	1.8 kg
Total	432.35 kg

2.2.3 Communications

(Jeff Skudlarek)

To communicate with the Earth during the trip to Mars, a small cross dipole antenna is used. During the cruise, the large, high gain dish antenna is obstructed by the heat shield. The medium gain, cross dipole antenna, which is on the aft face of the orbiter (adjacent to the suntracker and horizon sensors), provides an unobstructed medium for sending and receiving the S-Band 2200-2300 MHz signals. The uplink to the spacecraft serves two purposes. First, position and velocity tracking of the transfer vehicle is achieved via a semi-continuous

beacon that manipulates the Doppler shift of the return signal to calculate the spacecraft motion. The beacon only requires a few deciwatts of power, as it is without data. Second, command and control of the spacecraft must be accomplished for health monitoring and to maintain the trajectory to Mars. This uplink is sent every two to four days and a corresponding reply follows each transmission from Earth. The reply downlink is a short data stream of approximately 400 bits per second (bps) that lasts up to 10 min. In order to transmit to Earth, via the low gain antenna, 5 W transmissions are required. Using a 23% efficient amplifier, 22 W are drawn from the power source. A complete power budget for this portion of the mission is included in Table 2.6.

2.2.4 Power

(Chris Patrick)

During the interplanetary cruise phase of the mission, power is provided by the RTGs on the landers. On each orbiter, all four RTGs are wired into the communications satellite, which provide a total of 140 W. These power devices are wired into the orbiter through a central junction box. Each junction box contains four sockets into which the RTGs are plugged. Along with controlling the power flow, the junction box monitors the status of each RTG during the cruise phase. The power coupling between the lander and satellite disconnects prior to lander deployment.

The power from the RTGs is used to power the communications equipment and computer which provide attitude adjustment commands. The communications equipment requires 22 W for 10 min every three days and the computer requires a continuous 15 W. The RTGs additionally provide a preliminary charge on the batteries before entering orbit around Mars.

Table 2.6: Cruise Power Budget

Communications	22 W (10 min every 3 days)
Computer	15 W
Batteries Charging (3)	10 W/ hr for 6 hrs
Sensors and Mechanisms	5 W

2.2.5 Thermal Control During Cruise

(Chris Patrick)

In order to provide operating temperatures of 60°F during interplanetary cruise, two methods are employed: thermal coating and an active thermal control system (louvers).

Each lander is coated with Aluminized-Kapton which allows the body to have the characteristics of a blackbody. This assumption allows for a thermal analysis. The temperature of each lander was calculated at the two worst scenerios, at Earth and Mars.

Table 2.7: Solar Absorbitivity and Emissivity for Various Materials

Material	α	ϵ
Aluminum Paint	.35	.3
Polished Metal	.2	.05
White Paint	.3	.9
Silver-Teflon	.1	.9
Aluminized Kapton	.45	.8

Before heading to Mars the vehicle will orbit Earth. At this point, the vehicle is closest to the Sun and the most heating occurs. Using the Aluiminized-Kapton coating, the temperature of each lander was calculated to be 89°F. This temperature is 29°F over the recommended 60°F, but is within an acceptable range. On the way to Mars, the temperature drops linearly as the solar intensity decreases. Once in Martian orbit, the final temperature of each lander was calculated to be 15°F. This temperature was well below allowable limits, in order to control the the temperature drop and to keep within the 60°F limit, insulation is used.

Each orbiter is also coated with Aluiminized-Kapton. As for the lander, the orbiter temperature was calculated at the worst cases. While in orbit around Earth, the satellite temperature was calculated to be 110°F. This temperature is out of the acceptable range. In order to bring this temperature down to the proper temperature, the active thermal control system (ATCS) will be used. This system is then used until the solar intensity decreases and the temperature is in acceptable ranges (60°F-90°F). Once this temperature is reached,

insulation is used to maintain acceptable temperatures. See Appendix L for thermal calculations.

The ATCS used on the orbiter is composed of louvers. This device is similar to a Venetian blind. Each blade is controlled by a spring that is sensitive to temperature. When the blind reaches a certain temperature, the blind will open, allowing heat to escape. Once the proper temperature is reached, the blinds close. The inside of the louvers are coated with a white paint which acts as a blackbody emmiter. having a high emissivity ($\epsilon=1$) and low absorptivity. This allows for high levels of heat rejection and low levels of heat absorption. Louver are used because this system doesn't require any power, control systems or computers. Additionally, louvers have been proven in space; some example are the Voyager spacecraft, Viking and Pioneer missions.

2.3. ARRIVAL AT MARS

2.3.1 Aerocapture and Aerobrake Maneuvers

(Denny Chitwood)

Due to mass constraints when dealing with space flight, every possible mass savings needs to be considered. Aerocapture and aerobraking maneuvers greatly reduce propellant mass. By utilizing the drag forces encountered in the atmosphere, it is possible to reduce the speed of the spacecraft. The only additional mass associated with these maneuvers is that of the thermal protection system.

There are two possible options with these maneuvers. One involves a pure drag model with no lift generation. This requires a symmetrical shape with a balanced center of gravity. The other involves the generation of lift through body shape or propellant. This method adds complexity to the model.

An aerocapture is essentially an extreme aerobrake maneuver. Upon arrival at Mars, the transfer vehicle has an extremely high velocity relative to the planet. Therefore, the first pass captures the spacecraft by reducing the velocity considerably. Subsequent aerobrake maneuvers circularize the orbit about Mars.

Through the use of a computer simulation (Appendix C), a step-by-step force analysis was used to approximate the flight through the atmosphere. Appendix C also contains the data from each of the passes including: altitude, velocity and acceleration as functions of time. The following tables summarize information on the aerobraking maneuver:

Table 2.8: Aerobrake Summary

Pass	Target Periapsis (km)	ΔV to achieve (m/s)	Resultant Apoapsis (km)	Duration of pass	Eccentricity after pass
1	54.0	-	1325.4	14 min 16 s	.1574
2	78.0	8.61	597.0	28 min 37 s	.0702
3	93.125	4.97	500.1	35 min 23 s	.0556

Table 2.9: Flight Extremes

Minimum Altitude	52.78 km
Maximum Velocity	5.62 km/s
Maximum Acceleration	15.49 m/s
Maximum Heat Flow	16.71 BTU/ft ² ·s

2.3.2 Thermal Protection System

(Curt Baldwin)

A thermal protection system (TPS) is required for the aerobrake maneuver. During the passes through the Martian atmosphere, significant heat is produced due to drag. Without protection, this heat will damage the orbiter, landers, and onboard equipment. A combination of a thin Martian atmosphere and modern TPS technology make this possible. Appendix D gives a full description of how the heating rate analysis is accomplished. The results of this analysis yielded a heating rate that did not exceed 30 BTU/ft²·s.

Rates below 30 BTU/ft²·s allow for the possibility of flexible heat shields. However, flexible shields are not able to withstand these rates for extended periods of time. The aerocapture through the Martian atmosphere lasts beyond the limits of this type of TPS. Low heating rates, coupled with the need for reuse (several passes will be made through the atmosphere during the aerocapture), effectively rule out the use of ablative materials. These materials are reserved for extremely high heating rates and one time use. Typical heating rate

limits for rigid ceramic tiles are a minimum of 60 BTU/ft².s. Several materials, such as LI-900 and 2200, AETB-12/TUFI, ASMI, and AETB-8/RCG are suitable for this mission. Alumina-Enhanced Thermal Barrier (AETB) with Reaction Cured Glass (RCG) coating was picked for its low density of 128 kg/m³ (8 lb/ft³). The RCG coating also improves the toughness of the tile to prevent damage due to space debris.

The heat shields on the landers are used in conjunction with the main heat shield to protect the transfer vehicle during the aerocapture. Heating rates for the lander deployment have were calculated and found not to exceed 30 BTU/ft².s. Therefore the same material was chosen for the lander heat shields. Table 10 shows the volumes of the lander and main heat shields. An insulation thickness of .0254 m (1 in) was used.

Table 2.10: Heat Sheilds

	Lander	Transfer Vehicle
Volume (m ³)	.048	.173
Mass (kg)	6.2	22.2

2.3.3 Circularization

(Denny Chitwood)

Since the aerobraking maneuver positions the spacecraft such that its apoapsis is at the final desired orbit of 500 km, only one more propulsive ΔV is needed to complete the process. The ΔV required is 93.47 m/s. Prior to this burn, the TPS is released after having completed its mission. This allows it to re-enter the atmosphere and impact with the surface, keeping the final orbit free of unnecessary debris.

2.3.4 Power

(Chris Patrick)

Once in orbit around Mars, the RTGs continue to provide power to the communications equipment and computer, as well as power the surface mapping equipment and start the momentum wheels. The power required to start the motors of the momentum wheels is 79 W. After start-up only two RTGs are used to add additional momentum to the

momentum wheels. Along with powering these other systems, the RTGs provide a trickle charge to the batteries to keep them fully charged.

2.3.5 Communications

(Jeff Skudlarek)

Upon arrival at Mars, twenty-four hour communications are attempted with the spacecraft. During periods of high plasma attenuation, such as during the aerobrake, communications may be broken. However, once circularization is completed, the TPS is jettisoned and the high gain parabolic dish is utilized for higher data rates, such as those created by the mapping instrumentation. The dish antenna is steerable so that pointing of the entire spacecraft to a specific Earth position is not required. Once in orbit, the orbiter scans the surface using a mapping spectrometer. At 500 km, the satellite has a 6000 km footprint or surface coverage shadow. Based on the information generated by the spectrometer, the orbiter confirms the specific landing sites. Each image generates approximately .67 Mbps. This information is sent to Earth at a rate of 400 kbps for a quick-look image. The quick-look image is used for final verification of each of the four sites to be explored by the landers on that specific transfer vehicle. All four lander positions are verified prior to any lander deployment. Figure 2.6 depicts the transfer vehicle during the mapping phase.

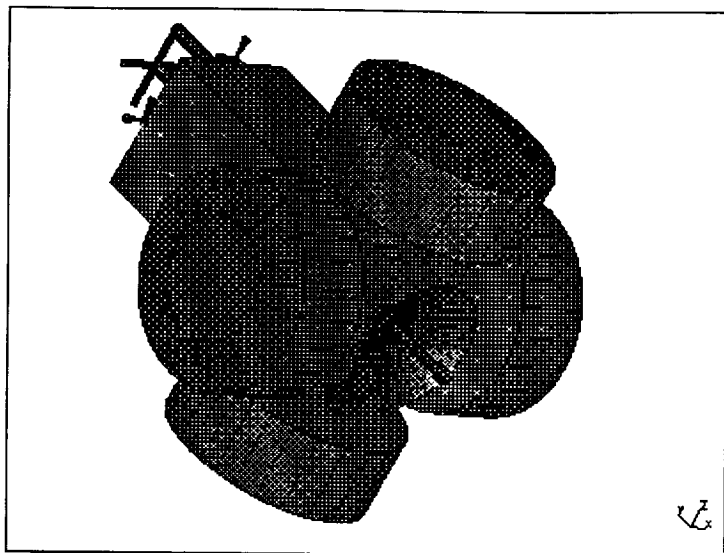


Figure 2.6: Transfer Vehicle During Mapping Stage

2.4. LANDER DEPLOYMENT

2.4.1 Lander Placement

(Lynn White)

Upon final verification of the site selection, the landers are released from the orbiter and descend to the surface. Six of the landers are positioned at 60° intervals along the 80° N latitude line and six are stationed at 5° intervals along the 30° longitudinal line from 90° N to 65° N. The positions along the 80° N are symmetric starting at the 0° longitudinal line. See Figure 2.7 for a schematic of the Northern Polar Region. The landers are identified according

Table 2.11: Lander Positions

Lander	Latitude	Longitude
1	90° N	30° E
2	85° N	30° E
3	80° N	30° E
4	75° N	30° E
5	70° N	30° E
6	65° N	30° E
7	80° N	0°
8	80° N	60° W
9	80° N	120° W
10	80° N	180°
11	80° N	120° E
12	80° N	60° E

to the site position number.

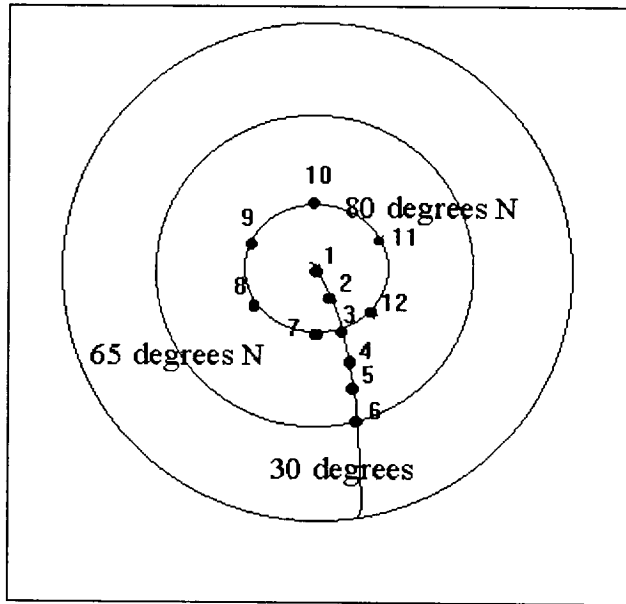


Figure 2.7: Northern Polar Cap with Lander Positions

2.4.2 Transfer Orbit

(Curt Baldwin and Lynn White)

To deploy a lander, a torsion disk is used to propel the lander away from the vehicle and at the same time giving it spin for stability. Figure 2.8 depicts the design of the disk.

Each disk consists of three springs. Two are arranged to produce a force couple about the lander and provide it with a spin of 30 RPM. The third spring simply propels the lander away

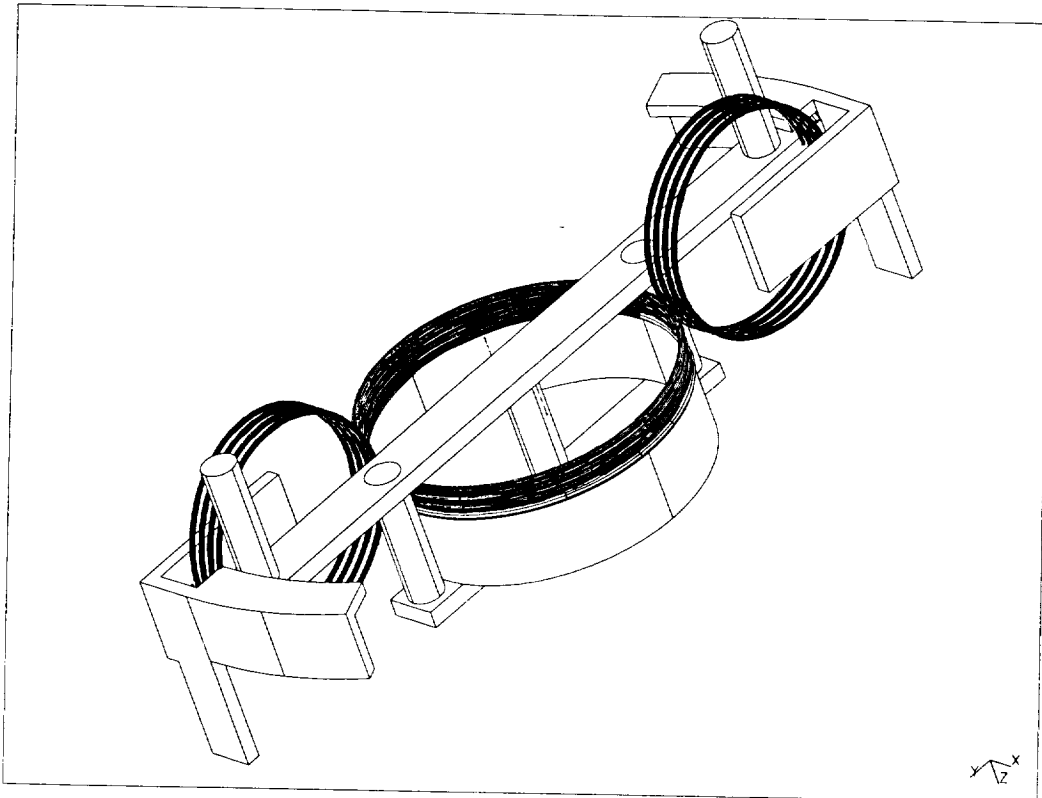


Figure 2.8: Design of Torsion Disk

at a rate of .25 m/s.

The decision to use springs, and their stored mechanical energy, was chosen over other alternatives such as powered spin tables for several reasons. First, this approach requires no additional power drain on the orbiter during the deployment stage. At this stage, power is limited because the solar cells have not yet been deployed. Their deployment has been delayed to prevent incidental damage from the landers. Also, this alternative is fairly simple; there are no motors to fail.

To avoid damage to the orbiter, the torsion disk pushes the lander away prior to the burn. The release occurs over the same latitude as the landing site, but one orbit before the

orbiter passes over the site. The lander remains in the same orbit as the orbiter for approximately half of an orbit. Two solid rockets, attached to the lander back shell, fire a small retrograde burn to send it on a transfer ellipse orbit with a 50 km periapse located over the target. The rockets of choice are the Star 6B (TE-M_790). Each delivers a 2.6 kN thrust in a vacuum over a 6.65 sec action time. Its total mass is 9.87 kg with a principal diameter of 116 mm and a length of 403 mm. The amount of fuel needed for this burn is 5.17% of the total lander mass. The ΔV produced to put it on the transfer ellipse is 104.2 m/s. The time of transfer from 500 km to 50 km is .93 hrs.

Table 2.12: Transfer Orbit Characteristics

Initial Height	500 km
Final Height	50 km
Initial Orbital Velocity	3.33 km/s
ΔV	104.16 m/s
Final Velocity	3.65 km/s
Time of Transfer	.93 hrs

2.4.3 Lander Drop Sequencing

(Lynn White)

The drop sequence minimizes the amount of time the orbiter is asymmetric, thereby minimizing the amount of wheel momentum required to stabilize the orbiter. By reducing the wheel momentum, the fuel required to desaturate the wheels is kept as low as possible. The lander drop positions around the pole are predominately symmetric and therefore it is conducive to launch two per pass. However, this cannot occur for all lander drops; therefore the drop sequence is “optimized”.

After the buses have arrived at Mars, the first week or so of orbiting encompasses radar mapping of the planet’s surface to insure that the predetermined drop sites are suitable. Once the landing sites are confirmed (see Figure 2.7), the buses begin releasing landers. Table 2.13 details which lander are dropped from which orbiter.

Table 2.13: Lander Drop Sequence

orbiter	first lander released	orbits until next release	second lander released	orbits until next release	third lander released	orbits until final release	final lander released
one	5	0	6	5	10	2	11
two	1	0	3	1	8	2	9
three	12	2	7	-1	2	0	4

On the first available pass the first orbiter launches the number five and six landers. Five orbits later, lander ten is dropped. Two more orbits are then needed before the orbiter is in the proper position for the number eleven lander to release. The second orbiter releases the number one and three landers on its first available pass. A one-orbit-delay occurs before the number eight lander is released. Again, two more orbits occur before the number nine lander is launched. The third orbiter, on its first pass, releases the number twelve lander. Two orbits pass before the number seven lander is released. On the next orbit, the final two landers, numbers two and four, are released. During all of these releases, the orbiter is rotating between positioning the landers for launch and the Sun so that the folded solar panels can provide power to the orbiter. This rotation causes the momentum in the wheels to increase, thus the amount that the lander release needs is minimized. Further discussion into the folded solar panels follows in the Power section.

2.4.4 Communications

(Jeff Skudlarek)

As a result of the presence of the large obstructive Martian planet, all lander deployments are not made while in Earth coverage of the launches. Continuous coverage would be advantageous for release verification and attitude monitoring. Turn-around times for data prevent Earth from having any realtime effect on the lander drop sequence. The actual descent of the landers is autonomous. However, the orbiting transfer vehicle tracks the each lander descent to the Martian surface. Once all four landers have descended and arrival

and checkout is complete, all communications from the satellite to the Earth are restricted to eight hours per day. As a result, the manpower requirements on Earth are kept to a minimum.

2.5. LANDER DESCENT

2.5.1 Descent Summary

(Tom Terrell)

The mission requires for 12 soft landings on the Martian surface. This is accomplished with a parachute, rocket and control system which will be detailed in the following section. Table 2.14 contains stage to stage parameters. The criteria for this process are as follows:

- (1) Reduce velocity to attain a soft landing. A soft landing is defined as 5 m/s.
- (2) Remain under launch mass ceiling. The total deceleration system mass must not contribute to an inability to lift-off.
- (3) The lander must be stabilized while decelerating.
- (4) The lander deceleration process must be autonomous.

Table 2.14: Deceleration Parameters

Stage	Initial Altitude	Final Altitude	Initial Velocity	Final Velocity	Stage time Period
Aerobrake Maneuver	60 km	5,000 m	3,568 m/s	778 m/s	394 s (6.57 min)
Parachute Deployment	5,000 m	4,915 m	778 m/s	778 m/s	.1 s
Terminal Velocity Achieved	4,915 m	2,915 m	778 m/s	32 m/s	42 s
Heat Shield Release	2,915 m	2,900 m	32 m/s	32 m/s	.5 s
Stabilization	2,900 m	265 m	32 m/s	32 m/s	82 s
Parachute / Back Shell Release	265 m	250 m	32 m/s	32 m/s	.5 s
Major Rocket Burn	250 m	0 m	32 m/s	5 m/s	13 s
Touchdown	0 m	0 m	5 m/s	5 m/s	instantly

2.5.2 Parachute System

(Tom Terrell)

The packed parachute is stored in a .2 m long cylindrical case with a .25 m radius centered on the top surface of the back shell. Current parachute packaging technology utilizes vacuum packing, thus maximizing space. The packing density is 640 kg/m³. This value was developed from tests performed by Richard A. Lau for the Viking mission to Mars.

Small drogue chutes are widely utilized in the Earth's atmosphere to deploy parachutes. However, the Martian atmosphere is thin compared to the Earth's. Therefore, the required parachute deployment devices are spreader guns. A spreader gun is a gas propelled gun. Spreader guns are currently used by the United States Air Force when large vehicles are air dropped at low altitudes. Five spreader guns are attached to the parachute suspension cables, one gun every nine cables. Each gun is designed to travel a designated distance and deploy the parachute.

The parachute diameter is 15 m. There are 45 suspension cables, each 15 m in length. The additional length from the spindle to the back shell is 1 m. These parameters were obtained from tests done for the Viking mission.

The parachute canopy consists of 15 triangular sections (gores). Each gore contains a flexible panel covering about two-thirds of the width, with an air slot extending one edge of the panel to intersect the outer edge of the canopy. A spindle, secured to the suspension lines and to the lander, enables free and continuous parachute rotation after deployment. After inflation, each panel balloons into an airfoil shape as the air hits the underside. The panel edge next to the air flow bulges so that the panel assumes an angle of attack relative to the oncoming airstream, causing the panels to rotate the parachute. As the parachute rotates,

Table 2.15: Parachute System Mass Breakdown

Cloth (Dacron)	5.3 kg
Thread	.9 kg
Radials	4.3 kg
Suspension Lines (45)	.18 kg (each)
Reinforcements	.8 kg
Riser / Bridle	4.5 kg
Spindle	1.5 kg
Bag	1.1 kg
Miscellaneous	.6 kg
Spreader Guns (5)	.9 kg (each)
Total	31.5 kg

centrifugal force flattens the canopy, increasing drag and deceleration of the lander. High rotational speed also provides a high degree of gyroscopic stability with oscillations of less than three degrees. Parachute tests have been performed by Sandia National Laboratories in low and supersonic speed wind tunnels and in rocket boosted free flights.

2.5.3 Rocket System

(Tom Terrell)

The rocket system consists of two solid deorbit rockets, six liquid attitude rockets, two liquid trajectory rockets and four liquid deceleration rockets. The twelve hydrazine liquid rockets are attached to the lander main fuel and pressure system located in the center of the lander bottom surface. To guard against a single rocket consuming all of the mission fuel, pre-set shut-off valves are attached to each rocket. Since all fuel calculations have been done for worst case scenarios, no rocket requires more fuel than allocated. Additionally, all liquid rockets are attached to the lander attitude and control system. Rockets were chosen instead of other torque input devices, such as momentum wheels, because of the short stage period and large torque requirements.

Two CHT-350 rockets are mounted to the lander bottom surface perpendicular to the lander vertical axis and provide translational correction. Shown in Figure 2.9, these rockets are utilized during descent prior to parachute deployment. The trajectory initiated by the deorbit rockets should be sufficient to place the lander near the landing site. Therefore, these rockets are used as auxiliary, not primary thrusters. Ten kilograms of fuel have been allocated for trajectory correction.

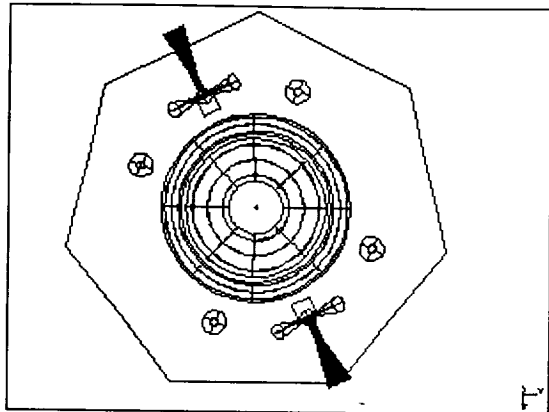


Figure 2.9: Directional Rockets

During descent, the lander is tri-axially stabilized by six CHT-20 liquid rockets located on the lander bottom surface. As depicted in Figure 2.10, two rockets are vertically aligned. The lander is initially spin stabilized with an angular rate about its vertical axis of 30 RPM. As the two rockets fire and the lander spins about the vertical axis, the upward force will be uniform about the entire lander platform. However, both rockets do not necessarily fire at the same time. The worst case of a pure spin about the local pitch axis (y-axis) was utilized to determine that .06 kg of hydrazine and a burn time of 5.81 s stabilizes the platform from an angular velocity of 30 RPM. See Appendix E for fuel calculations.

The other four CHT-20 rockets are aligned at a 45° declination from the lander platform, as depicted in Figure 2.11. Therefore, the rocket plumes do not contact the platform. The rockets are utilized such that a coupling reaction force is applied about the lander center of gravity; rockets located diagonal to one another will fire simultaneously. These rockets despin the lander from the initial deorbit spin and provide stability from unpredictable wind gusts during parachute descent. A burn time of 5.9 s and .24 kg of fuel stabilize the lander from the initial spin of 30 RPM.

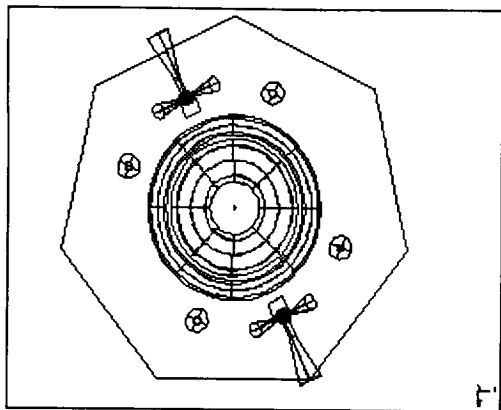


Figure 2.10: Roll and Pitch Rockets

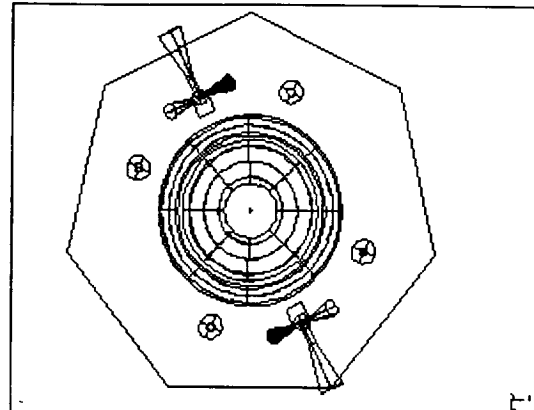


Figure 2.11: Despin Rockets

In order to achieve a soft landing (5 m/s), a final rocket stage is required. As depicted in Figure 2.12, four CHT-350 rockets are aligned symmetrically on the platform bottom surface .5 m from the center. Fuel is allocated to decelerate the lander to the required 5 m/s. The burn time is 13 s.

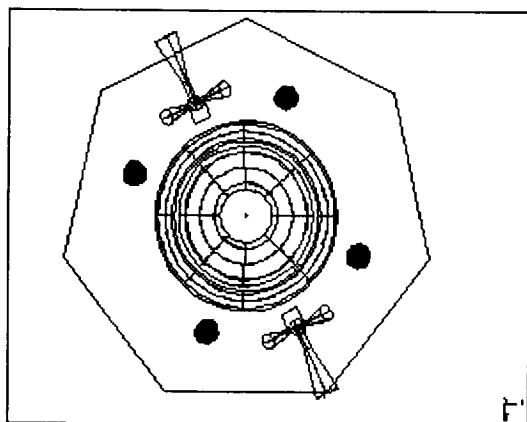


Figure 2.12: Rocket Deceleration

The following is a detailed mass breakdown of the lander descent system.

Table 2.16: Descent System Mass Breakdown

Torsion Disk	21.7 kg
Parachute System	31.5 kg
Rocket System	
Deorbit Rockets	9.9 kg
Deorbit Fuel	15.0 kg
Translational Rockets (2)	1.8 kg (each)
Translational Fuel	10.0 kg
Stabilization Rockets (2)	.4 kg (each)
Stabilization Fuel	.12 kg
Despin Rockets (4)	.4 kg (each)
Despin Fuel	.24 kg
Deceleration Rockets (4)	1.8 kg (each)
Deceleration Fuel	7.9 kg
Fuel Tank	3.9 kg
Pressure Tank	3.2 kg
Helium	0 kg
Total Lander Deceleration System	116.7 kg

2.5.4 Lander Attitude and Control System

(Tom Terrell)

While the lander performs the aerobrake maneuver, communications with the orbiter are broken. However, the orbiter continuously tracks the lander trajectory with respect to the designated landing site. Upon reaching 60 km, the lander receives coordinates from the orbiter. From this information, the lander control system determines the amount of thrust required from the translational rockets to adjust the trajectory to reach the designated landing site. At this altitude, a radar altimeter begins tracking the lander altitude and three radar velocity sensors track changes in velocity, with respect to the Martian surface. A FM/CW radar altimeter is chosen over a pulse altimeter because a pulse altimeter cannot operate at low altitude due to difficulty in separating the return and transmitted pulses.

The radar altimeter data initializes the following descent stages: release of the heat shield, ignition of the parachute spreader guns, release of the back shell and the final rocket deceleration ignition.

Three single degree of freedom rate gyroscopes measure the lander angular rates. The angular rates are sent to a central computer which sends a thrust command to the respective rocket(s).

2.5.5 Lander Impact

(Curt Baldwin)

After the deceleration process, the lander impacts the surface with a final velocity of 5 m/s. Some of this kinetic energy must be dissipated or the structure and its onboard equipment will be critically damaged. In consideration of minimum mass and complexity, a honeycomb energy absorption structure was chosen.

Figure 2.13 depicts a close up of the leg.

Each leg consists of a foot-pad, strut, and shock. The shock is composed of a honeycomb aluminum cylinder. Each leg dissipates energy, leaving a final kinetic energy to be absorbed by the structure. The structure consists of various size Aluminum 2024-T4 I-beams. This cross-section provides a large moment of inertia to account for the high bending stresses encountered upon impact. Table 2.17 gives a mass break down of the lander structure. Also, Figure 2.14 shows the solid model of the lander's exostructure. See Appendix F for a full explanation of the techniques used to model the impact.

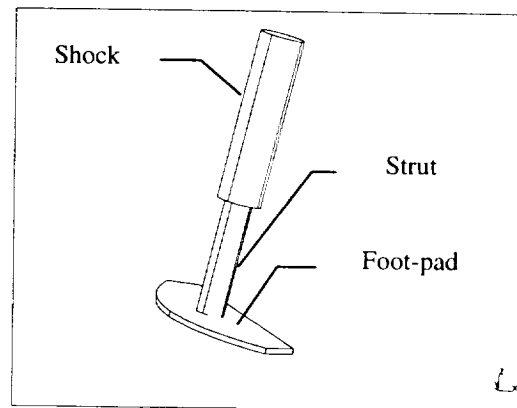


Figure 2.13: Leg Assembly

Table 2.17: Mass Breakdown of Lander Structure

Beam structure	10.5 kg
Foot pad (3)	2.3 kg (each)
Strut (3)	2.7 kg (each)
Shock (3)	.36 kg (each)
Total	26.6 kg

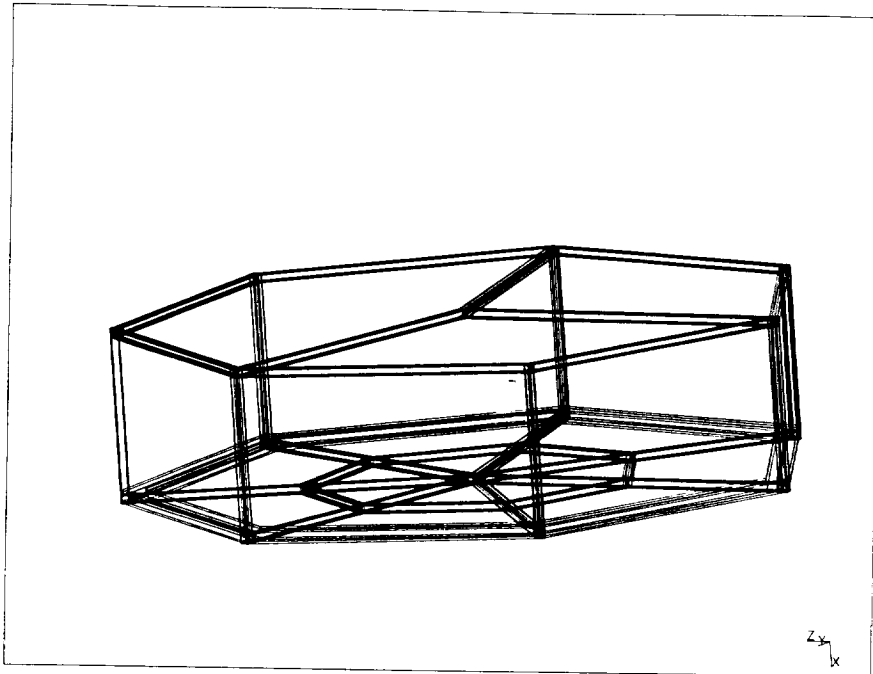


Figure 14: Lander Exostructure

Although the landing sites have been mapped prior to touchdown, the possibility of landing on an uneven surface is very likely. However, the lander is extremely stable due to the fact that the center of gravity is concentric with the geometric center. Stability, both during and after touchdown, is the reason three legs were chosen for the lander. Fewer legs would be unstable while more legs would most likely leave the lander precarious. Analytically, this statement is confirmed with the fact that three points define a plane.

2.6. MISSION DURATION

2.6.1 ORBITER

2.6.1.1 Final Orbit

(Lynn White)

An altitude of 500 km was chosen so as to obtain complete coverage of the Northern Polar region where the landers will reside. The field of view of the orbiter as it tracks the surface encompasses the entire polar region from 65° N latitude on the eastern side to 65° N latitude on the western side of Mars. This insures that the orbiter can see the lander at the 65° N latitude no matter which longitudinal line the orbiter tracks to the pole. The orbit is circular so as to eliminate any possibility that the apoapsis will “slip” to the Southern Polar region and oscillate between the two. This effect is a result of the oblateness of Mars. The three orbiters are in a 90° inclination orbit (completely polar). The reason behind this was to hold the orbiters in a particular orbital plane. The planes would rotate with respect to the ground with any other inclination angle. The 500 km altitude gives the orbiters a period of 2.03 hrs. This time is approximately 1/12 of the Martian day (24.62 hrs) which allows for twelve passes of the polar region per day by one orbiter. For communication purposes, the orbiters are arranged in orbital planes that are 120° out of phase. Essentially, the spacing of the orbiters is as if equally spaced in one orbital plane and then each orbiter is rotated out by 120° to form the constellation. This allows for 20 min of communication then 20 min of silence.

Table 2.18: Orbital Parameters

Altitude	500 km
Velocity	3.33 km/s
Period	2.03 hrs
Inclination	90°

2.6.1.2 Power

(Chris Patrick)

After the landers are launched, power is provided to the orbiter by a solar array and battery combination. This combination provides power to the communications equipment,

momentum wheel motors, computer and other scientific equipment. The solar array also charges the batteries. See Appendix M for power calculations.

The solar array provides 170 W of power to the orbiter. The array is composed of Gallium Arsinide cells. These cells have a circular shape with a diameter of .057 m and provide a solar to electric conversion efficiency of 18%. The total array contains 2112 cells which are fitted into modules that are .365 x .468 x .015 m. Each of the modules can hold 34 cells, which works out to a total of 64 modules being used. The arrays have 32 modules on each side of the satellite, 16 modules long and 2 modules wide. The total mass of the array including all the components (i.e. structure, wiring) is 149 kg and has a total area of 7.04 m². The solar arrays are summarized in Table 2.19.

Table 2.19: Solar Array Characteristics

Module Dimensions	.365 x .468 x .015 m
Number of Modules	64
Total Mass	149 kg
Total Area	7.04 m ²

The substrate of the array is composed of aluminum and each module is connected and stabilized by hinged beams at the edges. By being hinged at the ends this allows the array to be folded-up while in transit. Once in orbit the array opens using a series of torsional springs.

To provide additional power to the satellite when launching the landers, the unfolded surface of the solar array is employed. The folded area of the array has a total area of 2.05 m², producing a total of 50 W.

During the periods the orbiter is not in view of the Sun, Nickel-Hydrogen batteries are employed. Each orbiter has three batteries, which produce 60 W an hour and have a mass of 2.42 kg. Nickel-Hydrogen batteries were chosen over Ni-cad because of several factors. One reason is that Nickel-Hydrogen batteries can be charged many of times and still have close to a maximum charge level, compared to Ni-cad which need to be fully discharged after a period to obtain maximum charge. Compared to Ni-cad, Nickel-Hydrogen batteries are lighter and much more efficient.

Table 2.20: Orbiter Power/Thermal Mass Breakdown

Solar Cell Array	149 kg
Array Structure / Deployment Device	15 kg
Batteries (3)	.08 kg (each)
Total	164.2

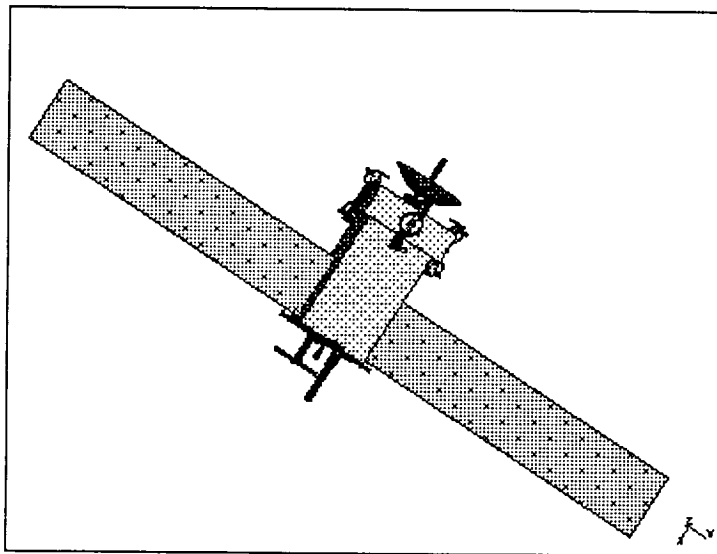


Figure 15: Orbiter with all Landers Deployed and Solar Cells Extended

2.6.1.3 Communication

(Jeff Skudlarek)

The total amount of data that can be received at the Earth DSN stations will be 2448 Megabits per day. This total is based on DSN data rate restrictions at the worst case elevation angle (approx. 20°), and the eight hours per day downlink restriction. At 2448 Mbits per day, the 12 Martian ground sites can transmit to Earth approximately 180 Mbits per day. This is based on the assumption that each ground site and each orbiter have command and control data rate requirements of about 1/10th the data rate of the scientific information that is sent home. In addition, the orbiter continues topographical surface mapping via an infrared spectrometer to observe the motion of the polar cap over the course of the entire year. The overall communications architecture is summarized as follows:

- I. The rovers communicate to the landers at 300-500 Mhz.
- II. The landers communicate to the orbiters at 2300 Mhz.
- III. The orbiters communicate to the DSN at 8400 Mhz.
- IV. The DSN communicates to the orbiters at 3200 Mhz.
- V. The orbiters communicate to the landers at 3200 Mhz
- VI. The orbiters communicate to the rovers at 300-500 Mhz.

Due to the nature of the orbiter flight paths, the availability to each ground site is limited to approximately 20 min per day. Each ground site must be able to transmit at 835 bps to achieve a daily data rate of 180 Mbits. Using Reed Solomon data compression techniques, the data rate can be effortlessly improved 2:1 to almost 1650 bps of data. The landers, however, do not have the ability to communicate directly to Earth. In case of catastrophic failure of one of the orbiters, the redundant network compensates for the loss and the total downlink data rate is diminished. Alternatively, the time the DSN allocates to reception of the signal could be increased.

During the primary mission, the orbiter downlink data rate is 8.5 kbps. Due to the high data rates, as well as the extraordinary distances between Earth and Mars, the downlink is the most precarious of all signals in the communications architecture. At orbital conjunction, that is, when Earth and Mars are furthest from each other, the distance between the planets can be as high as 375 million km. The resulting space loss is 282.5 dB. By comparison, the gain on the large 34 m High Efficiency DSN dish is 66 dB. To accommodate the large space loss, the downlink signal is sent via a 1.5 m diameter parabolic dish antenna and received at one of the three Deep Space Network sites on Earth. To send the 8.5 kbps signal from the Mars vicinity to Earth, 12 W effective isentropic radiated power (EIRP) are required. EIRP is the power of the signal being broadcast. The power draw is a function of the efficiency of the power amplifiers. Using 23% efficient solid state amplifiers, 53 W are required from the batteries or solar cells. A complete link budget for this transmission is provided in Appendix I.

To provide for data storage requirements, an additional memory device is utilized. This provides the ability to store all information generated from the landers and orbiter, but while the orbiter is either behind the planet (out of the Earth line of sight), or while not within the allotted eight hour DSN manpower window. Additionally, the ability to store all data generated during the 16 day solar eclipse of Mars is required. This eclipse occurs once every 2.3 years. The memory device used to handle the large storage requirements is an off the shelf solid state component. This piece of hardware has data storage capabilities up to 2 gigabits and can be accessed at a rate of 25 Mbits / s. The ability to read and write simultaneously is also imperative. This piece of equipment is no longer state of the art and is practically available off the shelf. The total breakdown of the orbiter communication hardware and respective contributions to the overall mass is included in Table 2.21.

Table 2.21: Orbiter Communications/Navigation Mass Breakdown

computer (2)	.7 kg (each)
memory	3.6 kg
dish	6 kg
mast	2.2 kg
dipole	4 kg
amplifier (2)	.15 kg (each)
transponder (2)	20 kg (each)
mapping spectrometer	18.2 kg
antenna pointing mechanism	3 kg
Total	78.7 kg

The communications to Earth from the orbiter are via the X-Band (7900-8500 MHz). While a Ka-Band transmission could have provided greater data rates and a better bit error rate, a large amount of research is yet to be done on the Ka-Band transmissions and most X-Band equipment can at this time, be purchased “off the shelf.” As a result, X-Band was selected for the downlink for economic reasons, as well as to limit the dependency on future innovations. A complete power budget for the multiple communications opportunities while orbiting Mars is included in Table 2.22.

2.6.1.4 Attitude Control

Table 2.22: Orbiter Power Budget

Mode	Spacecraft Activity	Typical (hrs.)	Average Power Utilization (W-hr)	
1	Comm to Earth, comm to lander, acquire science data, use solar power	1/3	RF	62
			Computer	15
			Batteries	45
			Science	05
			Momentum Whls.	15
			Misc.	05
			Total	147
2	Comm to lander, acquire science data, use batteries	1/3	RF	09
			Computer	15
			Batteries	00
			Science	05
			Momentum Whls.	15
			Misc.	05
			Total	49
3	No communications, use batteries	2/3	RF	00
			Computer	15
			Batteries	00
			Science	00
			Momentum Whls.	15
			Misc.	05
			Total	35
4	Comm to Earth, charge batteries, use solar power	2/3	RF	53
			Computer	15
			Batteries	45
			Science	00
			Momentum Wheels	15
			Misc.	05
			Total	133

(Lynn White)

The communication satellites require a complex control system since they have several different tasks to complete in this single mission. The primary system of choice, as stated previously, is momentum wheels and gas jet thrusters utilized for the desaturation of the wheels. Reaction wheels are continually being spun up from zero and desaturated back to zero RPM. As a result, the bearings tend to stick when restarted and lubricant can leak from lack of use. Momentum wheels are never stationary, thus the rotation should cancel out any problems that commonly occur with reaction wheels.

The momentum wheels are operating at a nominal rate of 7000 RPM. This nominal operating speed can be varied by 2000 RPM to provide any torques that are needed to change the attitude of the orbiter. Desaturation of the wheels occurs at 9000 RPM (the maximum speed for these wheels) or 5000 RPM (the minimum speed for these wheels) and the thrusters only have to compensate for the extra 2000 RPM. Table 2.23 contains the momentum wheel specifications.

Table 2.23: Momentum Wheels Specifications

Wheel Nominal Speed	7000 RPM
Adjustable Wheel Speed	5000-9000 RPM
Wheel Mass (4)	10 kg (each)
DC Motor (4)	2.5 kg (each)
Wheel Inertia	0.05 kg-m ²
Wheel Radius	0.1 m
Wheel Height	0.1 m

Four wheels are employed. Three primary wheels lie parallel with the three body axes and the fourth wheel lies at a 45° angle to the other three (see Figure 16). The fourth wheel is used as a precautionary measure in the event that one of the three primary wheels fail. The rotation of the wheel is driven by a small, brushless DC motor. The DC motor was chosen over an AC motor because the DC is more efficient than the AC since no gears are necessary to step-up or down the torque. Additionally, no friction or backlash problems are associated with DC motors (Wertz, 1978 p 209).

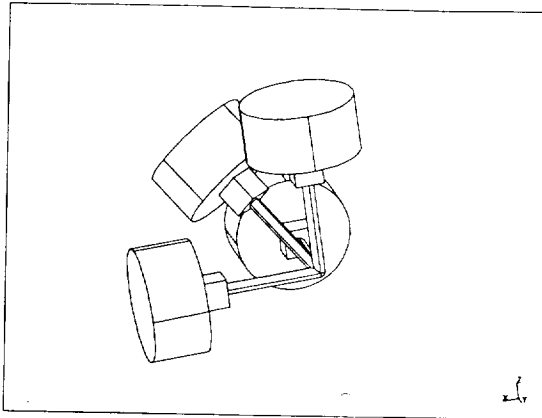


Figure 2.16: Momentum Wheel Configuration

2.6.1.5 Attitude Control System

(Lynn White)

The attitude control system employs rate and position feedback of the vehicle to determine the necessary wheel angular momentum to stabilize the system. This control system is complicated by the fact that all three axes must be controlled, additionally they are coupled through the products of inertia. The equations of motion of the vehicle plus the momentum wheels are as follows:

$$\frac{d}{dt}(I\omega) = -\omega \times h - N_w$$

$$\frac{d}{dt}(h) = N_w$$

The I and ω term represent the inertias and angular rates of the vehicle while N_w and h represent the torque and angular momentum associated with the momentum wheels. There are also disturbance torques acting on the system, but for the purpose of designing the control system, are being ignored. The basis of the control system is the control law; the implemented equation is as follows:

$$N_w = G_p * \theta_p + G_r * \omega_r$$

The G_p and G_r represent gain matrices for position and rate respectively and N_w is the control torque applied to the wheels. The gain matrices are dependent on the current vehicle

configuration. The gains are significantly different between the four lander case and the zero lander case; these differences are due to the changing moments of inertia of the transfer vehicle as landers are released. Since different gains must be used, gain scheduling is utilized. Gain scheduling is the act of changing the gains according to a predetermined “schedule” for different operating conditions. The gains are changed just prior to the release of the lander so as to anticipate any attitude disturbances caused by the release. The gain matrices are essentially a constant multiplied by the identity matrix. The gains for this mission are listed in Table 2.19.

Table 2.24: Gains for Different Vehicle Configurations

Vehicle Configuration	G_p	G_r
Four Landers	700	80000
Three Landers	700	80000
Two Landers	50	5000
One Lander	50	500
Zero Landers	2.5	2.5

The gains are chosen so as to obtain decent steady state responses as well as trying to keep the settling time within 40-60 s for the zero and one lander cases and between 100-200 s for the other configurations. This “long” settling time is necessary so that the attitude control system does not excite any structural modes in the vehicle. It is desired to keep the bandwidth of the control system low so as not to excite any vibrational modes (for example the solar panels).

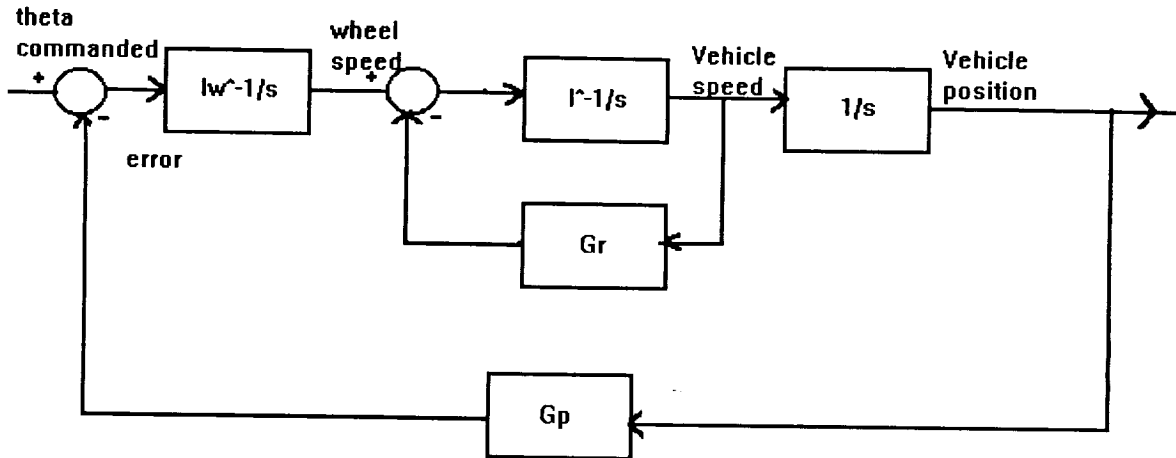


Figure 2.17: Control System Block Diagram

The block diagram of the vehicle control system shows the breakdown of the system dynamics (see Figure 2.17). The commanded change in position adds to the actual position (position feedback) to produce an error signal to the wheel controller. This controller then changes the error signal into a torque command that is produced by the wheels on the spacecraft. Internally, the rate at which the spacecraft is moving is fed back to the desired rate. The controllers, as stated previously, are simple gain matrices.

The vehicle dynamics were modeled using state equations (see Appendix H). The initial conditions of the vehicle were set to zero, meaning no initial rates or positions of the spacecraft. The initial angular momentum of the wheel was set to the nominal wheel speed multiplied by the wheel inertia. For this particular configuration the angular momentum is 36.7 kg-m²/s. The maximum change in angular momentum is 10.5 kg-m²/s positive or negative. A step input was given to the system to simulate a position change command. See Figures 2.23-2.25 located in Appendix H for the attitude, angular velocity of the vehicle and the angular momentum of the wheels with the one, two and no lander configurations.

2.6.2 LANDER

2.6.2.1 Lander Configuration

(Curt Baldwin)

The purpose of this mission is purely scientific; upon lander arrival, most of the scientific data will be collected. Figure 2.18 and Table 2.25 combine to show the layout of the lander components and mass break down.

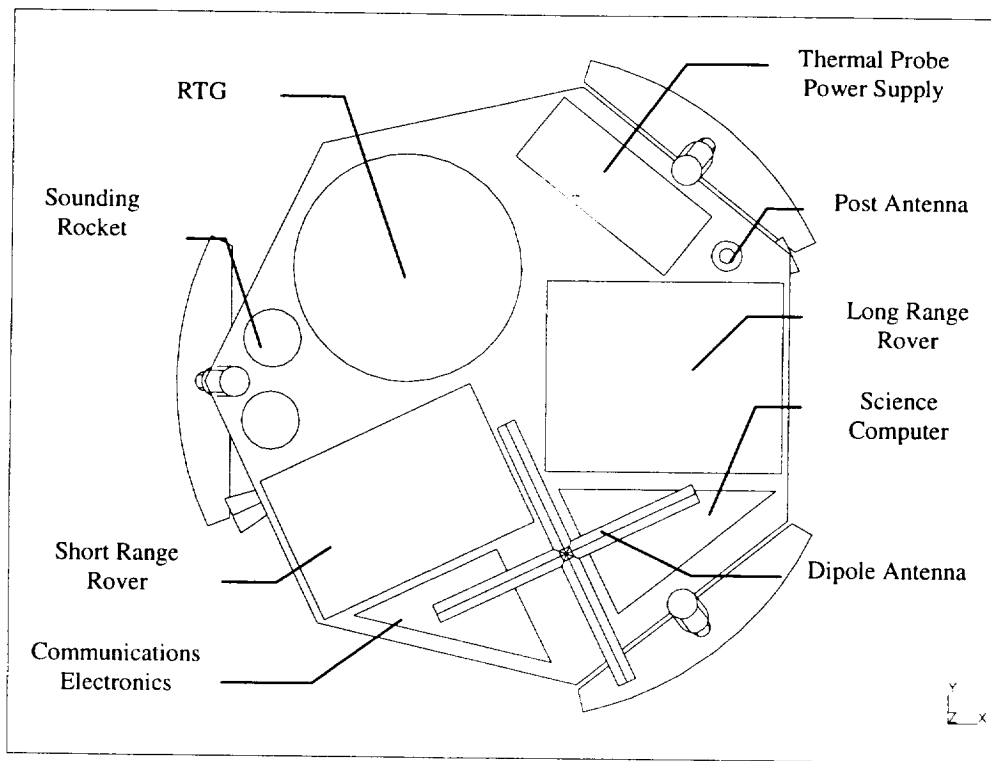


Figure 2.18: Lander Configuration

Note on the configuration layout the science experiments and communications electronics are grouped into two boxes of sufficient volumes to hold all the individual parts.

2.6.2.2 Communication and Science

(Curt Baldwin and Jeff Skudlarek))

At each lander there is an entire suite of science measurement and instrumentation equipment, in addition to the scientific data that is generated at each of two rovers per lander. A full list of equipment that is at the surface sites is as follows:

Lander: Temperature, pressure, wind speed, humidity, seismometer, thermal probe(which is dragged off the lander)

Short range rover: B/W video, mass spectrometer, ice auger, boroscope

Long range rover: Color video, subsurface radar mapper, seismometer

Each science experiment is fixed to the lander except for the rovers, the thermal probe, and the sounding rockets. Both rovers exit the lander via ramps deployed along rollers and expelled by springs. This method was chosen for its simplicity. Once off the lander, the short range rover moves around the lander to drag the thermal probe off the platform. The probe is dragged a distance away from the lander while still tethered to its power source, which lies on the lander. Although not shown separately in the lander configuration (because of its small size), the probe is essentially part of the power supply with its tether coiled in the supply box. The tether is extended as the rover drags the probe. This was done to eliminate the chance of tangling or snagging the tether on any parts of the lander or rover.

Table 2.25: Lander Science and Communication Component Mass Breakdown

micro-weather	.5 kg
seismometer	.16 kg
camera	.25 kg
thermal probe	1 kg
sounding rockets (2)	1.8 kg (each)
x-ray spectrometer	.06 kg
science cpu	12 kg
Rover - long range	9.8 kg
Rover - short range	18 kg
communications cpu	.7 kg
dipole antenna	2.5 kg
mast antenna	1 kg
amplifier	.15 kg
transponder	2 kg
RTG	14 kg
thermal probe power	10 kg
Total	75.7 kg

A small cross dipole antenna is used on the landers to transmit a S-Band signal to the orbiting satellites at a very low power of 4 W EIRP. Using solid state amplifiers, power efficiencies as high as 23% can be seen, yielding transponder power requirements of 17 W from the batteries or solar cells. The link budget calculations for this link is in Appendix I.

To communicate with the rovers, a UHF modem is employed. The modem transmits and receives a 300-500 MHz signal via an omnidirectional mast antenna on the lander. At UHF frequencies, the transmissions have no problem penetrating the ice and any rock particles that make up the polar ice cap. As a result, the rovers are never obstructed from view of the lander. By using an omnidirectional antenna, the lander is not required to track either rover. Different frequencies are used to distinguish the signals of each rover, with a minimum of a 25 kHz bandwidth separation. The UHF transmissions require a maximum of 2 W EIRP to traverse the short ranges of the two rovers. This corresponds to a 10 W draw from the lander power source.

2.6.2.3 Power

(Chris Patrick)

The landers use the SNAP-19 RTG. This power source generates 35 W of power for all the equipment on the lander for over two years. RTGs are space proven as they have been used in many other space mission such as Viking, Pioneer and Apollo missions. Along with providing power, the RTG also provides heat to keep the electronics on the lander at an optimum temperature (60°F). To dissipate the heat generated by the decay of Plutonium-238 the landers use louvers and conductive heat transfer methods. See Appendix N for an expanded view of the SNAP-19 RTG.

Thermal Control of Landers On Surface

(Chris Patrick)

Once on the planet the main thermal source of each lander is the RTG. Each lander is to be kept at a temperature that allows proper operation of the on-board electronics, between 60°F and 80°F. The analysis was done at the worst case scenario, that is at night. The type of analysis was taken as a conduction problem. From the early Viking mission the average

nightime temperature on Mars is -197°F. With the RTG emitting 682 W and using the basic conduction equations, in order to obtain 70°F, a thermal conductivity (k) of the lander material is calculated to be .907.

During the day the average temperature on the surface is -20°F. Using the calculated thermal conductivity, the temperature inside the lander reaches a temperature of 350°F. This temperature is beyond the accepted operating temperature. In order to get the temperature to acceptable levels, louvers are used to vent the excess heat. See Appendix O for calculations.

2.6.2.4 Sounding Rockets

(Chris Patrick)

In order to meteorologically probe the Martian atmosphere, sounding rockets were chosen. The sounding rocket design uses the I132W rocket motor designed by Aerotech Consumer Aerospace. The specifications are as follows:

Table 2.26: Sounding Rocket Engine Data

Thrust	226 N
Specific Impulse	473 s
Burn Time	4.8 s
Propellant Weight	.36 kg
Casing Dimensions	.038 x .30 m

This engine carries the 1.81 kg mass of the rocket to a height of 16.84 km. Due to the thin Martian atmosphere, drag forces are neglected. The horizontal range of the rocket is variable because of atmospheric conditions and because the rocket is "floating" down to the surface (See Table 2.24 for performance data). The height of the rocket is now .5 m due to limited height available inside of the lander. The diameter is .152 m. See Appendix P for calculations.

Once the rocket is finished taking upper atmospheric readings and is floating back to the surface, the landing sequence begins. While floating back to the surface, the lower section of the rocket containing the motor is jettisoned. The remaining instrument package lands softly on the surface using a cushioning system and begins recording data. Power to the

probes is provided by combination solar array and battery. These probes take meteorological measurements and pictorial images. The distance at which the sounding rocket lands from the lander is variable, therefore, communication is back to the orbiters, not the landers.

2.7. CONCLUSION AND INITIAL ECONOMIC ASSESSMENT

(Jeff Skudlarek)

The Mars Orbiting Bus Transport is designed to follow up the Mars Polar Pathfinder by providing a thorough exploration of the Martian polar cap. With the advent of the "lighter, faster, better" concept at NASA, every effort has been made to provide a design which develops a spacecraft in two to three years at minimal cost. All cost estimates are in 1995 dollars and are expected to inflate at a yearly rate of 5-12%. The lion's share of the expense will be the launch vehicle which costs approximately 100 million dollars from womb to tomb, including launch operations and payload integration expenses.

Table 2.27: Economic Estimate

FY 95 Dollars	
Spacecraft Systems	
-A&T, Launch Ops	4,200,000
-Lander Bus	4,000,000
-Lander Comm	3,600,000
-Lander Power	3,000,000
-Management	3,000,000
-Orbiter Bus	15,000,000
-Orbiter Comm	6,500,000
-Orbiter Power	900,000
-Product Assurance	2,500,000
-Propulsion	1,500,000
-Total Thermal	1,300,000
Project Management	3,000,000
Integration	550,000
Mission Eng & Ops	10,000,000
Project Subtotal	59,050,000
Contingency (33%)	19,700,000
Project Total	78,750,000

While actual manufacturing and hardware costs are at this time unknown, early estimates put the single vehicle costs at \$550,000 for vehicle integration and assembly costs alone. This is based on vehicle total mass and power requirements. When considering a subsystem breakdown, the orbiter bus, that is, the orbiter structure, computer, sensors, momentum wheels, batteries, power distribution and circuitry, could cost 15 million dollars. This is based on the complexity of the orbiter structure, the redundant attitude control system, and spacecraft pointing accuracy requirements. Likewise, the structure of the landers are in the neighborhood of 2-4 million each. The complete cost breakdown is estimated in Table 2.27. With a 33% contingency, total costs are

expected to be in the neighborhood of \$80 million dollars per transfer vehicle, plus rover and Atlas 2AS launch vehicle. This compares favorably with the MESUR Pathfinder budget of \$150 million, plus launch vehicle. However, the total system, which relies on the launch of three such transfer vehicles, puts the total system cost at \$240 million. Nonetheless, the total Mars Or Bust space network is the best option for exploration of the next frontier.

2.8. APPENDIX A: LAUNCH WINDOW ANALYSIS CODE

(Denny Chitwood)

The following C++ source code was used in analyzing the launch windows. Starting from a known set of orbital positions, the first step was to store daily position & velocity vectors for each of the planets. By doing this, it was possible to allow for the gravity due to all the planets and the sun. This data was stored in a binary file on the system disk. The second step was to advance from the beginning of the launch window time frame. For each day, the launch position and velocity were taken along with a projected arrival position and velocity. With this information, the transfer orbit was calculated. If the resultant C3 was less than 10.0 km²/sec², the transfer data was output to another text file for later import into a spreadsheet.

2.8.1 orbit.cpp

```
/** Includes **/  
  
#include <stdio.h>  
#include <stdlib.h>  
#include <conio.h>  
#include <time.h>  
#include "vector.h"  
  
/** Defines **/  
  
#define START 2449920.5  
#define D2010 2455197.5 // 1 Jan 2010  
#define D2020 2459214.5 // 31 Dec 2020  
  
#define AU 1.4959965e8 // km - mean earth orbit radius  
#define GravParm 6.672e-20 // km3/sec2*kg  
  
#define RESETSCR gotoxy(1,20)  
#define GOTOMSG gotoxy(1,15)  
#define LineLength 80  
  
/** Global Variables **/  
  
time_t StartTime = time( NULL ),  
       CurrentTime;  
double SecondsInADay = 60.0 * 60.0 * 24.0,  
      RadToDeg = 180.0 / PI;  
  
/** Function Declarations **/  
  
double Square( const double &D ) { return D * D; }  
  
void InitializeScreen(),  
     InitializeScreen2(),  
     ScreenOutput( const double &, Vector *, Vector * ),  
     ScreenOutput2( const double &, const int & ),  
     LogPlanetData( FILE *, const double &, Vector *, Vector * ),  
     GetPlanetData( FILE *, const double &, const int &, Vector &, Vector & ),  
     CalculateTransfer( const double &, const double &,  
                        Vector &, Vector &, Vector &, Vector &,  
                        const double &, FILE * );  
  
int LoadPlanetInfo( double *, Vector *, Vector * );  
  
char *TimeString( void ),  
     *SecondConvert( const double & );  
  
Vector EvaluateAcceleration( const int &, double *, Vector * );  
  
/** Main Program **/  
  
int main()  
{  
    /* Variables */  
  
    int Planet;  
    double TimeStep = SecondsInADay, // sec  
          Mass[10], // kg  
FILE *planetStep;  
Vector P[10], PrevP[10], StartP[10], // km  
      V[10], PrevV[10], // km/sec  
      A[10], TotalA; // km/sec2  
  
    /* Start of Code */  
  
    #if 1 // don't re-create "runtime.dat" every time!  
    if ( ( PlanetStep = fopen( "runtime.out", "rb+" ) ) == NULL ) abort();
```

```

#else
    if ( ( PlanetStep = fopen( "runtime.out", "wb+" ) ) == NULL ) abort();
    InitializeScreen();

    if ( LoadPlanetInfo( Mass, P, V ) != 0 ) return 1;

    for ( Planet = 1; Planet <= 9; Planet++ )
        *( StartP + Planet ) = *( P + Planet );

    for( double Date = START;
        Date <= D2020 + 600.0;
        Date += TimeStep / SecondsInADay )
    {

        // Store previous steps position & velocity
        for ( Planet = 1; Planet <= 9; Planet++ )
        {
            *( PrevP + Planet ) = *( P + Planet );
            *( PrevV + Planet ) = *( V + Planet );
        }

        // Evaluate step on each planet from Mercury out to Pluto
        for ( Planet = 1; Planet <= 9; Planet++ )
        {
            TotalA = EvaluateAcceleration( Planet, Mass, PrevP );
            *( V + Planet ) = *( V + Planet ) + TimeStep * TotalA;
            *( P + Planet ) = *( P + Planet ) + TimeStep * *( V + Planet );
        }

        ScreenOutput( Date, P, V );

        if ( Date >= D2010 )
            LogPlanetData( PlanetStep, Date, P, V );
    }
#endif

    // Evaluate launch windows throughout the 10 year period
    Vector LaunchP, LaunchV, ArrivalP, ArrivalV;
    FILE *OutFile;

    InitializeScreen2();

    for ( double LaunchDate = D2010;
          LaunchDate <= D2020;
          LaunchDate += TimeStep / SecondsInADay )
    {
        double StartDate = LaunchDate + 200.0,
              EndDate   = LaunchDate + 300.0;

        OutFile = fopen( "C3.OUT", "at+" );
        GetPlanetData( PlanetStep, LaunchDate, 3, LaunchP, LaunchV );

        for ( double ArrivalDate = StartDate;
              ArrivalDate <= EndDate;
              ArrivalDate += TimeStep / SecondsInADay )
        {
            GetPlanetData( PlanetStep, ArrivalDate, 4, ArrivalP, ArrivalV );
            CalculateTransfer( LaunchDate, ArrivalDate,
                               LaunchP, LaunchV,
                               ArrivalP, ArrivalV,
                               1.327e11, OutFile );
        }
        fclose( OutFile );
        ScreenOutput2( LaunchDate, int( D2020-LaunchDate ) );
    }

    fclose( PlanetStep );
    return 0;
}

/** Support Function Definitions ***/

```

```

void InitializeScreen()
{
    int line = 1;
    CurrentTime = time( NULL );
    clrscr();
    gotoxy(1,line++); printf( "Start Time : %s", TimeString() );
    gotoxy(1,line++);
    printf( "Current Time : %s", SecondConvert(difftime(CurrentTime,StartTime)) );
    gotoxy(1,line++); printf( "Duration : " );
    line++;
    gotoxy(1,line++); printf( "Date: " );
    line++;
    gotoxy(1,line++); printf( "Planet P V" );
    gotoxy(1,line++); printf( "Mercury : " );
    gotoxy(1,line++); printf( "Venus : " );
    gotoxy(1,line++); printf( "Earth : " );
    gotoxy(1,line++); printf( "Mars : " );
    gotoxy(1,line++); printf( "Jupiter : " );
    gotoxy(1,line++); printf( "Saturn : " );
    gotoxy(1,line++); printf( "Uranus : " );
    gotoxy(1,line++); printf( "Neptune : " );
    gotoxy(1,line++); printf( "Pluto : " );
    RESETSCR;
}

void ScreenOutput( const double &Date,
                  Vector *P,
                  Vector *V )
{
    int line = 2;
    CurrentTime = time( NULL );
    gotoxy(16,line++); printf( "%s", TimeString() );
    gotoxy(15,line++);
    printf( "%s", SecondConvert(difftime(CurrentTime,StartTime)) );
    line++;
    gotoxy(7,line++); printf( "%9.1f %9.1f", Date, Date - START );
    line+=2;
    for ( int Planet = 1; Planet <= 9; Planet++ )
    {
        gotoxy(11,line++);
        printf( "%10.3e %10.3f %10.3f",
               ( P + Planet )->Mag(),
               ( V + Planet )->Mag(),
               ( P + Planet )->Longitude() * RadToDeg );
    }
    RESETSCR;
}

void InitializeScreen2()
{
    int line = 1;
    CurrentTime = time( NULL );
    clrscr();
    gotoxy(1,line++); printf( "Start Time : %s", TimeString() );
    gotoxy(1,line++);
    printf( "Current Time : %s", SecondConvert(difftime(CurrentTime,StartTime)) );
    gotoxy(1,line++); printf( "Duration : " );
    line++;
    gotoxy(1,line++); printf( "Date: " );
    line++;
    gotoxy(1,line++); printf( "Days Remaining: " );
    RESETSCR;
}

void ScreenOutput2( const double &Date,
                   const int &Remaining )
{
    int line = 2;
    CurrentTime = time( NULL );
    gotoxy(16,line++); printf( "%s", TimeString() );
    gotoxy(15,line++);
    printf( "%s", SecondConvert(difftime(CurrentTime,StartTime)) );
    line++;
    gotoxy(7,line++); printf( "%9.1f", Date );
    line++;
    gotoxy(17,line++); printf( "%-10d", Remaining );
}

```

```

RESETSCR;
}

int LoadPlanetInfo( double *Mass,
                    Vector *P,
                    Vector *V )
{
double dP[3], dV[3];
/* char Line[LineLength], *endptr; */
FILE *PlanetData;

if (! ( PlanetData = fopen( "planets.dat", "rt" ) ) )
{
GOTOMSG;
printf( "ERROR: Unable to open PLANETS.DAT!" );
RESETSCR;
return 1;
}

for ( int Planet = 0; Planet <= 9; Planet++ )
fscanf( PlanetData, "%le", Mass+Planet );

for ( Planet = 1; Planet <= 9; Planet++ )
{
fscanf( PlanetData, "%13lf%13lf%13lf%13lf%13lf", dP+0, dP+1, dP+2,
        dV+0, dV+1, dV+2 );
for ( int Loop = 0; Loop < 3; Loop++ )
{
*( dP + Loop ) *= AU;
*( dV + Loop ) *= AU / SecondsInADay;
}

( P + Planet )->Set( dP );
( V + Planet )->Set( dV );
}

fclose( PlanetData );
return 0;
}

Vector EvaluateAcceleration( const int &Planet,
                            double *Mass,
                            Vector *PrevP )
{
Vector A, R, Runit;
double Amag;
for ( int Loop = 0; Loop <= 9; Loop++ )
if ( Loop != Planet )
{
R = *( PrevP + Loop ) - *( PrevP + Planet );
Runit = R / R.Mag();
Amag = ( GravParm * *( Mass + Loop ) / Square( R.Mag() ) );
A = A + Runit * Amag;
}
return A;
}

void LogPlanetData( FILE *PlanetStep,
                    const double &Date,
                    Vector *P,
                    Vector *V )
{
fprintf( PlanetStep, "%9.1f", Date );
for ( int Planet = 1; Planet <= 9; Planet++ )
fprintf( PlanetStep, "%16.9e%16.9e%16.9e%16.9e%16.9e",
        ( P + Planet )->X(), ( P + Planet )->Y(), ( P + Planet )->Z(),
        ( V + Planet )->X(), ( V + Planet )->Y(), ( V + Planet )->Z() );
}

void GetPlanetData( FILE *PlanetStep,
                    const double &Date,
                    const int &Planet,
                    Vector &Pos,
                    Vector &Vel )
{
double InpDate, Px, Py, Pz, Vx, Vy, Vz;

```

```

long RecLen = 9 + 16 * 6 * 9,
Offset = RecLen * long( Date - D2010 );

fseek( PlanetStep, Offset, SEEK_SET );
fscanf( PlanetStep, "%9lf", &InpDate );

if ( InpDate != Date )
{
    printf( "ERROR: unable to find correct data!\n" );
    abort();
}

fseek( PlanetStep, long( 16 * 6 * ( Planet - 1 ) ), SEEK_CUR );
fscanf( PlanetStep, "%16le%16le%16le%16le%16le%16le",
        &Px, &Py, &Pz, &Vx, &Vy, &Vz );

Pos.Set( Px, Py, Pz );
Vel.Set( Vx, Vy, Vz );
}

void CalculateTransfer( const double &LaunchDate,
                      const double &ArrivalDate,
                      Vector &LaunchP,
                      Vector &LaunchV,
                      Vector &ArrivalP,
                      Vector &ArrivalV,
                      const double &Mu,
                      FILE *OutFile )
{
double Theta = ArrivalP ^ LaunchP;

if ( ( Theta < ( 0.95 * PI ) )
     || ( Theta > ( 1.05 * PI ) ) )
    return;

double Rp = LaunchP.Mag(),
      R = ArrivalP.Mag(),
      e = ( R - Rp ) / ( Rp - R * cos( Theta ) ),
      a = Rp / ( 1.0 - e ),
      Vp = sqrt( 2.0 * Mu / Rp - Mu / a );

Vector TransferPlaneNorm = ( LaunchP | ArrivalP ),
      Tmp = ( TransferPlaneNorm | LaunchP ),
      TransferVelocity = Tmp / Tmp.Mag();

double Ang = TransferVelocity ^ LaunchV;

if ( ( Ang < ( 1.8 * PI ) ) && ( Ang > ( 0.2 * PI ) ) )
    TransferVelocity = TransferVelocity * -1.0;

Vector dV = LaunchV - ( Vp * TransferVelocity );
double C3 = Square( dV.Mag() );

if ( C3 < 10.0 )
{
    fprintf( OutFile,
             "%9.1f;%9.1f;%G;%G;%G\n",
             LaunchDate, ArrivalDate, ArrivalDate - LaunchDate,
             C3, Theta * RadToDeg );
}
}

/** Time Function Definitions ***/

char *TimeString( void )
{
struct tm *time_now;
time_t secs_now;
char String[80];

tzset();
time( &secs_now );
time_now = localtime( &secs_now );
strftime( String, 80, "%A, %d %B %Y, %I:%M:%S %p", time_now );

return( String );
}

```

```
}

char *SecondConvert( const double &Time )
{
    char String[80], Temp_String[80];
    int iTime = (int) Time,
        Hours = ( iTime / 3600 ),
        Minutes = ( ( iTime - Hours*3600 ) / 60 ),
        Seconds = iTime % 60;

    sprintf( String, "%3d hrs %2d mins %2d secs", Hours, Minutes, Seconds );
    return( String );
}
```

2.8.2 vector.h

```
#include <math.h>

double PI = acos( -1 );

/** Class Definitions **/

class Vector
{
private:

    /** Members Instances **/

    double x, y, z;

public:

    /** Constructors & Destructors **/

    Vector( const double &a = 0.0,
            const double &b = 0.0,
            const double &c = 0.0 )
    {
        x = a;
        y = b;
        z = c;
    }
    Vector( const Vector &Source );
    ~Vector() { ; }

    /** Member Functions **/

    char *StringOutput(); // ( #####.##, #####.##, #####.## )

    void Set( const double &a, const double &b, const double &c )
    { x = a; y = b; z = c; }
    void Set( double *V )
    { x = *( V + 0 ); y = *( V + 1 ); z = *( V + 2 ); }
    double X() { return x; }
    double Y() { return y; }
    double Z() { return z; }
    double Mag() { return sqrt( x * x + y * y + z * z ); }
    double Longitude();

    double operator *( const Vector & ); // Dot Product

    Vector operator *( const double & ); // Vector * double
    friend Vector operator *( const double &, const Vector & ); // double * Vector
    Vector operator *=( const double &D ) { return *this * D; }

    Vector operator /( const double & ); // Vector / double
    Vector operator /=( const double &D ) { return( *this / D ); }

    Vector operator |( Vector & ); // Cross Product

    Vector operator +( const Vector & ); // Addition
    Vector operator +=( const Vector &V ) { return( *this + V ); }

    Vector operator -( const Vector & ); // Subtraction
    Vector operator -=( const Vector &V ) { return( *this - V ); }

    Vector operator =( const Vector & );

    double operator ^( Vector & ); // Angle between Vectors
};

Vector::Vector( const Vector &Source )
{
    x = Source.x;
    y = Source.y;
    z = Source.z;
}
```

```

char *Vector::StringOutput()
{
    char String[80];
    sprintf( String, "( %9.2e, %9.2e, %9.2e )", x, y, z );
    return String;
}

double Vector::operator *( const Vector &A ) // Dot Product
{
    return( ( x * A.x ) + ( y * A.y ) + ( z * A.z ) );
}

Vector Vector::operator *( const double &D ) // Vector * double
{
    Vector Temp;
    Temp.x = x * D;
    Temp.y = y * D;
    Temp.z = z * D;
    return Temp;
}

Vector operator *( const double &D, const Vector &V ) // double * Vector
{
    Vector Temp;
    Temp.x = V.x * D;
    Temp.y = V.y * D;
    Temp.z = V.z * D;
    return Temp;
}

Vector Vector::operator /( const double &D ) // Vector * double
{
    Vector Temp;
    Temp.x = x / D;
    Temp.y = y / D;
    Temp.z = z / D;
    return Temp;
}

Vector Vector::operator ()( Vector &A ) // Cross Product
{
    Vector Temp;
    double Ang = acos( ( *this * A ) / ( sqrt(x*x+y*y+z*z) * A.Mag() ) );
    if ( Ang == PI )
    {
        printf( "WARNING: Cross Product of co-linear vectors!" );
        return Temp;
    }
    Temp.x = y * A.z - z * A.y;
    Temp.y = z * A.x - x * A.z;
    Temp.z = x * A.y - y * A.x;
    return Temp;
}

Vector Vector::operator +( const Vector &A ) // Addition
{
    Vector Temp;
    Temp.x = x + A.x;
    Temp.y = y + A.y;
    Temp.z = z + A.z;
    return Temp;
}

Vector Vector::operator -( const Vector &A ) // Subtraction
{
    Vector Temp;
    Temp.x = x - A.x;
    Temp.y = y - A.y;
    Temp.z = z - A.z;
    return Temp;
}

Vector Vector::operator =( const Vector &Source )
{
    x = Source.x;
}

```

```
Y = Source.y;
z = Source.z;
return *this;
}

double Vector::operator ^( Vector &V ) // Lead angle of V1 to V2
{
    double Angle = this->Longitude() - V.Longitude();
    while( Angle < 0.0 ) Angle += 2.0 * PI;
    while( Angle > ( 2.0 * PI ) ) Angle -= 2.0 * PI;
    return Angle;
}

double Vector::Longitude()
{
    double Angle = atan2( y, x );
    while( Angle < 0.0 ) Angle += 2.0 * PI;
    while( Angle > ( 2.0 * PI ) ) Angle -= 2.0 * PI;
    return Angle;
}
```

2.9. APPENDIX B: ORBITAL MECHANICS EQUATIONS

(Denny Chitwood)

2.9.1 Circular orbits

$$\text{Velocity, } V = \sqrt{\frac{\mu}{r}}$$

$$\text{Period, } P = \sqrt{r^3/\mu}$$

2.9.2 Elliptical orbits

$$\text{Semi - major axis, } a = \frac{(r_a + r_p)}{2}$$

$$\text{Eccentricity, } e = \frac{(r_a - r_p)}{(r_a + r_p)}$$

$$\text{Velocity, } V = \sqrt{\frac{2\mu}{r} - \frac{\mu}{a}}$$

$$\text{Period, } P = 2\pi \sqrt{\frac{a^3}{\mu}}$$

2.9.3 Hyperbolic orbits:

Semi - major axis, a

$$\text{Hyperbolic escape velocity, } V_\infty = \sqrt{\frac{\mu}{a}}$$

$$C3 = V_\infty^2$$

2.10. APPENDIX C: ATMOSPHERIC FLIGHT SIMULATION

(Denny Chitwood)

Given:

C_D = coefficient of drag

C_L = coefficient of lift

mass = total mass of orbiter

S = frontal surface area

V_∞ = velocity at which orbiter enters Mars' sphere of influence (SOI)

R_p = initial projected radius of periapse

Outline:

- Calculate approach to atmosphere.
- Force analysis step-by-step through atmosphere including: gravity, drag forces, temperature.
- Evaluate orbit upon departure from atmosphere: is it captured?
- Evaluate best method for circularization at final orbit: burn or use atmosphere?
- Execute of final circularization

Output:

- Step-by-step file output of flight duration, altitude, velocity and acceleration.
- Pass summary including pass duration, flight maximums, pass parameters and results.

Program philosophy

In terms of the atmospheric flight, to model the orbital flight appropriately it was necessary to use Cartesian coordinates. A simple x-y system is the easiest to model in a computer program. By using this, it was not necessary to model any kind of centrifugal force. The only complexity introduced was the evaluations of the various angles involved. The program was checked prior to adding any kind of drag forces due to the atmosphere by verifying the periapsis point. By using a time increment of 1 second, the proximity was within 0.5 km.

2.10.1 flight.cpp

```
#include "telem.h"

ErrorCondition main( void )
{
    /*** Variables ***/
    int line,
        Pass = 0; // Pass Counter
    char Filename[LineLength];
    double FlightTime = 0.0,
           StepInc = 2.0,
           dV = 0.0,
           Vi = 2.65,
           Projected_Periapsis = 50.0;
    Boolean FinalIteration = False;
    HighLow Side = Low;
    Telemetry T, Current, Next;

    /*** Begin ***/
    PassOut = fopen( "flight.out", "wt" );
    T.ScreenOutputInit();
    T.PassFileOutputInit( Vi, S, Cd, Cl );
    InputMarsData();

    do /*** do-while: Passes Iteration ***/
    {
        gotoxy(1,5); printf( "Pass #%-d", ++Pass );

        Retry:
        sprintf( Filename, "pass%d.out", Pass );
        StepOut = fopen( Filename, "wt" );

        gotoxy(10,5); printf( "Ap = %-10G", Projected_Periapsis ); ResetScreen;
        if ( Pass == 1 )
            T.Hyperbola_Entry( Vi, Projected_Periapsis );
        else if ( Pass > 1 )
            T.Elliptic_Entry( Projected_Periapsis );

        gotoxy(30,5);
        printf( "dV = %G m/s          ", (dV=fabs(LastVa-T.Va)*1000.0) );
        ResetScreen;

        Current = T; // temporary to allow for iterations
        Next = T; // allows transference of time & extremes

        // Next.Set_Time( Current.ReadTime() );

        do /*** do-while: Atmospheric Pass walk-thru ***/
        {
            Next.Increment_Time();
            Next.Step( Current );
            CurrentTime = time( NULL );
            Next.ScreenOutput();
            Next.StepFileOutput();
            Next.StepCheck();
            Current = Next;
        }
        while ( ( Current.QueryAltitude() < Mars_Atmosphere )
                && ( Current.FlightStatus == Good ) );
    }

    fclose( StepOut );

    if ( Current.FlightStatus == Impact )
    {
        // Since the Projected Periapsis caused an impact, then increase
        // it & try again.
        Projected_Periapsis += StepInc;
        goto Retry;
    }
}
```

```

    }

FlightTime = Current.ReadTime() - T.ReadTime();

Current.PassCheck();
gotoxy(1,18); printf( "Apo of previous iteration = %G", Current.Ra - Mars_Radius );
if ( Current.FlightStatus == TooLow )
    FinalIteration = True;

if ( FinalIteration == True )
{
    if ( Current.Ra < ( FinalOrbit - ErrorMargin + Mars_Radius ) )
    {
        if ( Side == High ) { StepInc /= 2.0; Side = Low; }
        Projected_Periaxis += StepInc;
        goto Retry;
    }
    else if ( Current.Ra > ( FinalOrbit + ErrorMargin + Mars_Radius ) )
    {
        if ( Side == Low ) { StepInc /= 2.0; Side = High; }
        Projected_Periaxis -= StepInc;
        goto Retry;
    }
}

LastVa = Current.Va;
T = Current;
dV_total += dV;

T.PassFileOutput( Pass, Projected_Periaxis, dV, FlightTime );
T.FlightExtremes.UpdateScreen();

switch( T.FlightStatus )
{
case Good:
case TooLow:
    break;
case Impact:
    gotoxy(20,5);
    printf( "WARNING: Spacecraft has impacted with surface!" );
    break;
case NoMass:
    gotoxy(20,5);
    printf( "WARNING: Spacecraft has no mass!" );
    break;
case Escaped:
    gotoxy(20,5);
    printf( "WARNING: Spacecraft has escaped Mars!" );
    break;
default:
    gotoxy(20,5);
    printf( "WARNING: Unknown Flight Status!" );
}
ResetScreen;
}
while( ( T.QueryRa() > FinalOrbit + Mars_Radius + ErrorMargin )
    && ( T.FlightStatus == Good ) );

// Circularization calculations for final orbit

double Va = EllVelAtRad( T.Ra, FinalOrbit + Mars_Radius, T.Ra ),
Vp = EllVelAtRad( T.Ra,
                    FinalOrbit + Mars_Radius,
                    FinalOrbit + Mars_Radius );

dV_total += fabs( T.Va - Va )*1000.0;
dV_total += fabs( Vp - CirVel( FinalOrbit + Mars_Radius ) )*1000.0;

gotoxy(1,19);
printf( "Total dV = %G m/s", dV_total );
fprintf( PassOut, "Total dV = %G m/s\n\n", dV_total );

T.FlightExtremes.FileOutput();

ResetScreen;

```

```
fclose( PassOut );
return( NoError );
}
```

2.10.2 telem.h

```

***** Includes *****/
#include <conio.h>
#include <stdio.h>
#include <stdlib.h>
#include <string.h>
#include <math.h>
#include <time.h>

***** Defines *****/
#define LineLength 80
#define Square( X ) ( ( X ) * ( X ) )
#define Cube( X ) ( ( X ) * ( X ) * ( X ) )
#define Magnitude( X, Y ) sqrt( Square( X ) + Square( Y ) )
#define ResetScreen gotoxy(1,20)

#define Mars_Mu 42828.3 // km3/sec2
#define Mars_Radius 3397.4 // km
#define Mars_Atmosphere 200.0 // km
#define Mars_Gravity( R ) ( Mars_Mu / Square( R ) )

***** Type Definitions *****/
typedef struct { double x, y, Mag; } Vector;

typedef struct { double Temperature, // K
                 Density, // kg/km3
                 SpeedOfSound; // km/sec
             } Atmosphere;

typedef enum { False = 0,
              True = 1
            } Boolean;

typedef enum { Good = 10,
              Impact = 11,
              TooLow = 12,
              NoMass = 13,
              Escaped = 14
            } FlightCondition;

typedef enum { NoError = 10,
              FileError = 11
            } ErrorCondition;

typedef enum { High = 10,
              Low = 11
            } HighLow;

***** Global Variable Definitions *****/
const double PI = acos( -1 ),
            RadToDeg = 180.0 / PI,
            TimeIncrement = 1.0, // sec
            InitialMass = 1500.0, // kg
            FinalOrbit = 500.0, // km
            ErrorMargin = 0.5, // km
            Cd = 1.5, // should be between 1.0 & 2.0
            C1 = 0.0, // initial analysis is for no lift
            S = 13.73 / 1.0e6; // km2 - heat shield surface area

double dV_total = 0.0, // m/sec - delta V
      LastVa = 0.0;
FILE *PassOut, *StepOut;
time_t StartTime = time( NULL ),
      CurrentTime;
Atmosphere Mars_Data[201];

```

```

***** Inline Functions *****

inline double Angle( const Vector &V )
{ return atan2( V.y, V.x ); }

inline double HypVelAtRad( const double &Vi,
                           const double &R )
{ return sqrt( 2.0 * Mars_Mu / R + Square( Vi ) ); }

inline double EllVelAtRad( const double &Ra,
                           const double &Rp,
                           const double &R )
{ return sqrt( Mars_Mu * ( 2.0 / R - 2.0 / ( Ra + Rp ) ) ); }

inline double CirVel( const double &R )
{ return sqrt( Mars_Mu / R ); }

***** Prototype Definitions *****

double HeatingRate( const double &,
                     const double & ),
TotalTemperature( const double &,
                  const double & ),
Temperature( const double & ),
SpeedOfSound( const double & ),
Mars_Density( const double & );
ErrorCondition InputMarsData( void );
char *TimeString( void ),
*SecondConvert( const double & );

***** Class Definition *****

class Extremes
{
private:
    double MinAlt, // km
           MaxVel, // km/sec
           MaxAcc, // km/sec2
           MaxQdot; // BTU/ft2*sec
public:
    Extremes( void )
    {
        MinAlt = 1.0e99;
        MaxVel = 0.0;
        MaxAcc = 0.0;
        MaxQdot = 0.0;
    }
    void EvalAlt( const double &Alt ) { if ( Alt < MinAlt ) MinAlt = Alt; }
    void EvalVel( const double &Vel ) { if ( Vel > MaxVel ) MaxVel = Vel; }
    void EvalAcc( const double &Acc ) { if ( Acc > MaxAcc ) MaxAcc = Acc; }
    void EvalQdot( const double &Qdot )
    { if ( Qdot > MaxQdot ) MaxQdot = Qdot; }
    void UpdateScreen( void )
    {
        gotoxy(45,6+1); printf( "(%12G km)", MinAlt );
        gotoxy(45,6+4); printf( "(%12G km/sec)", MaxVel );
        gotoxy(45,6+5); printf( "(%12G m/sec2)", MaxAcc*1.0e3 );
        gotoxy(45,6+7); printf( "(%12G BTU/ft2*sec)", MaxQdot );
    }
    void FileOutput( void )
    {
        fprintf( PassOut, "Flight Extremes:\n" );
        fprintf( PassOut, " Minimum Altitude = %G km\n", MinAlt );
        fprintf( PassOut, " Maximum Velocity = %G km/sec\n", MaxVel );
        fprintf( PassOut, " Maximum Acceleration = %G km/sec2\n", MaxAcc );
        fprintf( PassOut, " Maximum Qdot = %G BTU/ft2*sec\n", MaxQdot );
        fprintf( PassOut, "\n" );
    }
};

class Telemetry

```

```

{
private:

    /*** Private Variables ***/

    Vector Position,      // km
    Velocity,        // km/sec
    double Acceleration, // km/sec2
    Altitude,        // km
    gamma,           // rad - angle below local horizontal
    Lastgamma,       // rad
    theta,           // rad - angle of passage from entry
    eccentricity,
    mass,            // kg - instantaneous mass
    Qdot,            // BTU/ft^2*sec - heating rate
    T_total,         // K - stagnation temperature
    time;           // sec - time since entry
    Boolean BottomedOut;
    void SetPosition( const double & ),
        SetPosition( const double &, const double & ),
        SetVelocity( const double &, const double & );

public:

    /*** Constructors & Destructor ***/

    Telemetry( void );
    Telemetry( const Telemetry & );
    ~Telemetry( void ) { ; }

    /*** Public Variables ***/

    double Ra, Va,
          Rp, Vp;
    Extremes FlightExtremes;
    FlightCondition FlightStatus;

    /*** Member Functions ***/

    inline double QueryAltitude( void ) { return Altitude; }
    inline double QueryRa( void ) { return Ra; }
    inline double ReadTime( void ) { return time; }
    inline void Set_Time( const double &Time ) { time = Time; }
    inline void Increment_Time( void ) { time += TimeIncrement; }
    void ScreenOutputInit( void ),
        ScreenOutput( void ),
        PassFileOutputInit( const double &,
                            const double &,
                            const double &,
                            const double & ),
        PassFileOutput( const int &,
                      const double &,
                      const double &,
                      const double & ),
        StepFileOutput( void ),
        StepCheck( void ),
        PassCheck( void ),
        Hyperbola_Entry( const double &, const double & ),
        Elliptic_Entry( const double & );
    Telemetry Step( const Telemetry & );
};

    /*** Member Function Definitions ***/

Telemetry::Telemetry( void )
{
    /*** Default Constructor - zero initialization ***/
    Position.x = Position.y = Position.Mag = Altitude = 0.0;
    Velocity.x = Velocity.y = Velocity.Mag = 0.0;
    Acceleration = 0.0;
    theta = gamma = 0.0;
    Lastgamma = 1e10;
    eccentricity = 0.0;
    mass = 0.0;
    Qdot = 0.0;
    T_total = 0.0;
}

```

```

time = 0.0;
Ra = Va = 1.0e10;
FlightStatus = Good;
BottomedOut = False;
}

Telemetry::Telemetry( const Telemetry &Source )
{
/** Copy Constructor **/
Position.x = Source.Position.x;
Position.y = Source.Position.y;
Position.Mag = Source.Position.Mag;
Altitude = Source.Altitude;

Velocity.x = Source.Velocity.x;
Velocity.y = Source.Velocity.y;
Velocity.Mag = Source.Velocity.Mag;

gamma = Source.gamma;
Lastgamma = 1e10;
theta = Source.theta;
eccentricity = Source.eccentricity;
mass = Source.mass;
Qdot = Source.Qdot;
T_total = Source.T_total;
time = Source.time;

Ra = Source.Ra;
Va = Source.Va;

FlightStatus = Source.FlightStatus;
FlightExtremes = Source.FlightExtremes;

/* Reset Flag */
BottomedOut = False;
}

void Telemetry::SetPosition( const double &Alt )
{
Position.x = Mars_Radius + Alt;
Position.y = 0.0;
Position.Mag = ( Altitude = Alt ) + Mars_Radius;
}

void Telemetry::SetPosition( const double &Px,
                           const double &Py )
{
Position.x = Px;
Position.y = Py;
Altitude = ( Position.Mag = Magnitude( Px, Py ) ) - Mars_Radius;
}

void Telemetry::SetVelocity( const double &Vx,
                           const double &Vy )
{
Velocity.x = Vx;
Velocity.y = Vy;
Velocity.Mag = Magnitude( Vx, Vy );
}

void Telemetry::Hyperbola_Entry( const double &Vi,
                                 const double &Ap )
{
Rp = Ap + Mars_Radius;
Vp = HypVelAtRad( Vi, Rp );

this->SetPosition( Mars_Atmosphere );

Velocity.Mag = HypVelAtRad( Vi, Position.Mag );
gamma = acos( ( Rp * Vp ) / ( Position.Mag * Velocity.Mag ) );
Velocity.x = -Velocity.Mag * sin( gamma );
Velocity.y = Velocity.Mag * cos( gamma );

theta = 0.0;
}

```

```

mass = InitialMass;
Qdot = HeatingRate( Velocity.Mag, Altitude );
time = 0.0;

Ra = 1.0e99; // hyperbola
Va = 0.0;

/** flight status must be good since this is the first pass **/
FlightStatus = Good;

/* Reset Flag */
BottomedOut = False;
}

void Telemetry::Elliptic_Entry( const double &Ap )
{
double Rp = Ap + Mars_Radius;

gotoxy(1,16);
printf( "Altitude at Apo of last Pass = %8.1f", Ra-Mars_Radius );
ResetScreen;

this->SetPosition( Mars_Atmosphere );

Velocity.Mag = EllVelAtRad( Ra, Rp, Position.Mag );
Va = EllVelAtRad( Ra, Rp, Ra );
gamma = acos( ( Ra * Va ) / ( Position.Mag * Velocity.Mag ) );
Velocity.x = -Velocity.Mag * sin( gamma );
Velocity.y = Velocity.Mag * cos( gamma );

theta = 0.0;
mass = InitialMass;
Qdot = HeatingRate( Velocity.Mag, Altitude );

/** flight status must be good if it's re-entering **/
FlightStatus = Good;

/* Reset Flag */
BottomedOut = False;
}

Telemetry Telemetry::Step( const Telemetry &Initial )
{
// Force Analysis for Individual Point in Flight from Previous Point

double Gravity = Mars_Gravity( Initial.Position.Mag ),
Density = Mars_Density( Initial.Altitude );

Vector Acc, Drag, Lift;

Drag.Mag = 0.5*Density*Square(Initial.Velocity.Mag)*Cd*S/Initial.mass;
Drag.x = Drag.Mag * sin( Initial.gamma + Initial.theta );
Drag.y = -Drag.Mag * cos( Initial.gamma + Initial.theta );

Lift.Mag = 0.5*Density*Square(Initial.Velocity.Mag)*Cl*S/Initial.mass;
Lift.x = Lift.Mag * cos( Initial.gamma + Initial.theta );
Lift.y = Lift.Mag * sin( Initial.gamma + Initial.theta );

Acc.x = Drag.x + Lift.x - Gravity * cos( Initial.theta );
Acc.y = Drag.y + Lift.y - Gravity * sin( Initial.theta );
Acceleration = Magnitude( Acc.x, Acc.y );

this->SetVelocity( Initial.Velocity.x + Acc.x * TimeIncrement,
Initial.Velocity.y + Acc.y * TimeIncrement );

this->SetPosition( Initial.Position.x + Velocity.x * TimeIncrement,
Initial.Position.y + Velocity.y * TimeIncrement );

theta = Angle( Position );
gamma = Angle( Velocity ) - PI / 2.0 - theta;
if ( gamma < -PI ) gamma += 2.0*PI;

Qdot = HeatingRate( Velocity.Mag, Altitude );
mass = Initial.mass;
T_total = TotalTemperature( Velocity.Mag, Altitude );
}

```

```

        return *this;
    }

void Telemetry::ScreenOutputInit( void )
{
    int line = 7;

    clrscr(); // Clear Screen

    gotoxy(1,1); printf( "Start Time : %s", TimeString() );
    gotoxy(1,2); printf( "Current Time : %s", TimeString() );
    gotoxy(1,3); printf( "Duration : " );

    gotoxy(1,line++); printf( " Altitude : " );
    gotoxy(1,line++); printf( " Gamma : " );
    gotoxy(1,line++); printf( " Theta : " );
    gotoxy(1,line++); printf( " Velocity : " );
    gotoxy(1,line++); printf( " Acc : " );
    gotoxy(1,line++); printf( " Mass : " );
    gotoxy(1,line++); printf( " Qdot : " );
    // gotoxy(1,line++); printf( " T_total : " );
    gotoxy(1,line++); printf( " Time : " );

    ResetScreen;
}

void Telemetry::ScreenOutput( void )
{
    int line = 7;

    gotoxy(16,2); printf( "%s", TimeString() );
    gotoxy(15,3); printf( "%s", SecondConvert(difftime(CurrentTime,StartTime)) );

    gotoxy(15,line++); printf( "%15.1f km", Altitude );
    gotoxy(15,line++); printf( "%15.1f deg", gamma * RadToDeg );
    gotoxy(15,line++); printf( "%15.1f deg", theta * RadToDeg );
    gotoxy(15,line++); printf( "%15.1f km/s", Velocity.Mag );
    gotoxy(15,line++); printf( "%15.1f m/s^2", Acceleration*1000.0 );
    gotoxy(15,line++); printf( "%15.1f kg", mass );
    gotoxy(15,line++); printf( "%15.1f BTU/ft^2*sec", Qdot );
    // gotoxy(15,line++); printf( "%15.1f K", T_total );
    gotoxy(15,line++); printf( "%s", SecondConvert( time ) );

    ResetScreen;
}

void Telemetry::PassFileOutputInit( const double &Vi,
                                    const double &S,
                                    const double &Cd,
                                    const double &C1 )
{
    fprintf( PassOut, "Start Time : %s\n", TimeString() );
    fprintf( PassOut, "\n" );
    fprintf( PassOut, " Vi = %G km/s\n", Vi );
    fprintf( PassOut, " Initial Mass = %G kg\n", InitialMass );
    fprintf( PassOut, " S = %G m2\n", S*Square(1000.0) );
    fprintf( PassOut, " Cd = %G\n", Cd );
    fprintf( PassOut, " C1 = %G\n", C1 );
    fprintf( PassOut, "\n" );
}

void Telemetry::PassFileOutput( const int &Pass,
                               const double &Ap,
                               const double &dv,
                               const double &FlightTime )
{
    fprintf( PassOut, "Pass #&d @ %s\n", Pass, TimeString() );
    fprintf( PassOut, " Propulsive dv to achieve Proj_Apo = %G m/s\n", dv );
    fprintf( PassOut, " Apoapsis = %G (%G) km\n", Ra-Mars_Radius, Ap );
    fprintf( PassOut, " Eccentricity after pass = %G\n", eccentricity );
    fprintf( PassOut, " Time of pass = %s\n", SecondConvert(FlightTime) );
    fprintf( PassOut, "\n" );
}

void Telemetry::StepFileOutput( void )
{
}

```

```

/*
fprintf( StepOut, " Altitude : %12G km\n", Altitude );
fprintf( StepOut, " Gamma     : %12G\n", gamma );
fprintf( StepOut, " Theta      : %12G\n", theta );
fprintf( StepOut, " Velocity   : %12G\n", Velocity.Mag );
fprintf( StepOut, " Acc        : %12G\n", Acceleration );
fprintf( StepOut, " Mass       : %12G\n", mass );
fprintf( StepOut, " Qdot       : %12G\n", Qdot );
fprintf( StepOut, " T_total    : %12G\n", T_total );
fprintf( StepOut, " Time       : %s\n", SecondConvert( time ) );
fprintf( StepOut, "\n" );
*/
fprintf( StepOut, "%18G %18G %18G %18G\n",
          time, Altitude, Velocity.Mag, Acceleration );
}

void Telemetry::PassCheck( void )
{
// Orbit Analysis
double H = Velocity.Mag * Position.Mag * cos( gamma ),
P = Square( H ) / Mars_Mu,
E = 0.5 * Square( Velocity.Mag ) - Mars_Mu / Position.Mag;

eccentricity = sqrt( 1.0 + 2.0 * E * Square( H / Mars_Mu ) );
Rp = P / ( 1.0 + eccentricity ); Vp = H / Rp;
Ra = P / ( 1.0 - eccentricity ); Va = H / Ra;

Lastgamma = 1e10;

// Flight Condition Evaluation
if ( Vp >= sqrt( 2.0 * Mars_Mu / Rp ) )
    FlightStatus = Escaped;
else if ( Ra < FinalOrbit + Mars_Radius )
    FlightStatus = TooLow;
}

void Telemetry::StepCheck( void )
{
// Evaluate Flight Conditions

if ( Lastgamma < gamma )
    FlightStatus = Impact;
else if ( Altitude < 25.0 )
    FlightStatus = Impact;
else if ( ( BottomedOut == False ) && ( gamma < 0.0 ) )
    BottomedOut = True;
else if ( ( BottomedOut == True ) && ( gamma > 0.0 ) )
    FlightStatus = Impact;

if ( mass <= 0.0 )
    FlightStatus = NoMass;

Lastgamma = gamma;

// Evaluate Flight Extremes
FlightExtremes.EvalAlt( Altitude );
FlightExtremes.EvalVel( Velocity.Mag );
FlightExtremes.EvalAcc( Acceleration );
FlightExtremes.EvalQdot( Qdot );
FlightExtremes.UpdateScreen();

ResetScreen;
}

***** Support Functions *****

ErrorCondition InputMarsData( void )
{
FILE *infile;
char line[LineLength], *endptr;

if ( ( infile = fopen( "mars.dat", "rt" ) ) == NULL )
{
fprintf( PassOut, "ERROR: Cannot open input file.\n" );
return( FileError );
}

```

```

}

for ( int i = 0;
      i <= Mars_Atmosphere;
      i++, fgets( line, LineLength, infile ) )
{
  (Mars_Data+i)->Temperature = strtod( line, &endptr ); // K
  (Mars_Data+i)->Density = strtod( line+12, &endptr )* 1.0e12; // kg/km^3
  (Mars_Data+i)->SpeedOfSound = strtod( line+25, &endptr ) / 1.0e3; // km/s
}

fclose( infile );

return( NoError );
}

double HeatingRate( const double &Velocity,
                    const double &Altitude )
{
// Calculate heating rate for given Velocity & Altitude

// Radius of the Body - BodyRadius      = ft
// Molecular Weight - MolecularWeight   = dimensionless
// ??? - C                           = BTU*sec^2/ft^3*lb^1/2
// Heating Rate - Qdot                = BTU/ft^2*sec
// Density - Density                 = lbm/ft^3

double BodyRadius = 6.068,
      MolecularWeight = 44.4,
      C = ( 9.18 + 0.663 * MolecularWeight ) * 1.0e-10,
      Density = Mars_Density( Altitude ) / ( 1.0e9 * 16.018 ),
      Qdot = C * sqrt( Density / BodyRadius ) * Cube( Velocity * 3280.0 );
return( Qdot );
}

double TotalTemperature( const double &Velocity,
                        const double &Altitude )
{
// Calculate total/stagnation temperature for given Velocity & Altitude

double SpeedOfSoundV = SpeedOfSound( Altitude ), // km/s
      TemperatureV = Temperature( Altitude ); // K

return( TemperatureV * ( 1.0 + 0.15 * Square( Velocity / SpeedOfSoundV ) ) );
}

double Temperature( const double &Altitude )
{
// Temperature Interpolation from an Atmosphere Model

int iAltitude = (int) Altitude; // conversion from double to int
return( ( Altitude - (double) iAltitude )
       * ( (Mars_Data+iAltitude+1)->Temperature
           - (Mars_Data+iAltitude)->Temperature )
       + (Mars_Data+iAltitude)->Temperature );
}

double SpeedOfSound( const double &Altitude )
{
// Speed of Sound Interpolation from an Atmosphere Model

int iAltitude = (int) Altitude; // conversion from double to int
return( ( Altitude - (double) iAltitude )
       * ( (Mars_Data+iAltitude+1)->SpeedOfSound
           - (Mars_Data+iAltitude)->SpeedOfSound )
       + (Mars_Data+iAltitude)->SpeedOfSound );
}

double Mars_Density( const double &Altitude )
{
// Density Interpolation from an Atmosphere Model

int iAltitude = (int) Altitude; // conversion from double to int
}

```

```

    return( ( Altitude - (double) iAltitude )
        * ( (Mars_Data+iAltitude+1)->Density
        - (Mars_Data+iAltitude)->Density )
        + (Mars_Data+iAltitude)->Density );
}

char *TimeString( void )
{
    struct tm *time_now;
    time_t secs_now;
    char String[80];

    tzset();
    time( &secs_now );
    time_now = localtime( &secs_now );
    strftime( String, 80, "%A, %d %B %Y, %I:%M:%S %p", time_now );

    return( String );
}

char *SecondConvert( const double &Time )
{
    char String[80], Temp_String[80];
    int iTime = (int) Time,
        Hours = ( iTime / 3600 ),
        Minutes = ( ( iTime - Hours*3600 ) / 60 ),
        Seconds = iTime % 60;

    sprintf( String, "%3d hrs %2d mins %2d secs", Hours, Minutes, Seconds );

    return( String );
}

```

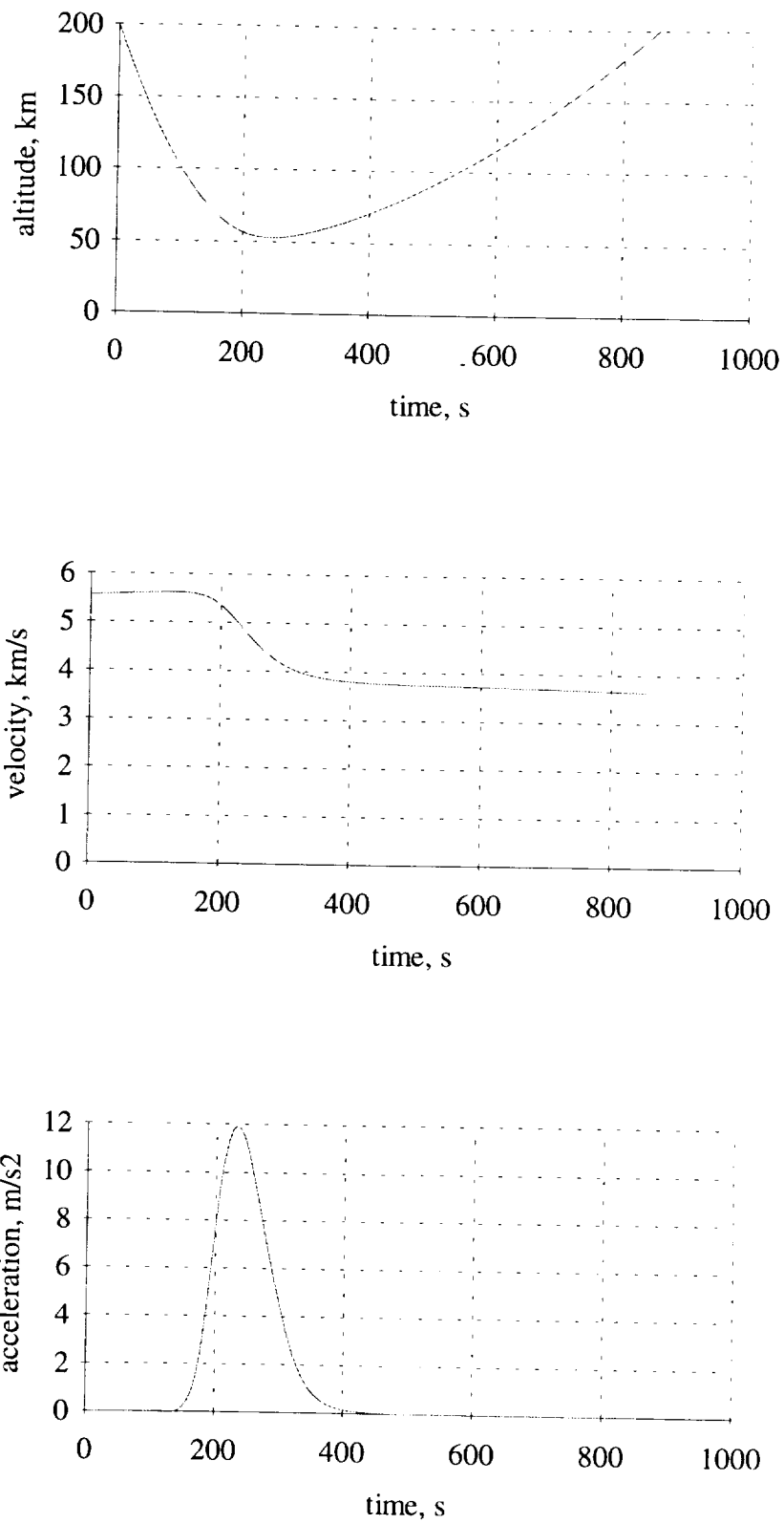


Figure 2.19: Pass #1 Aerocapture Manuever

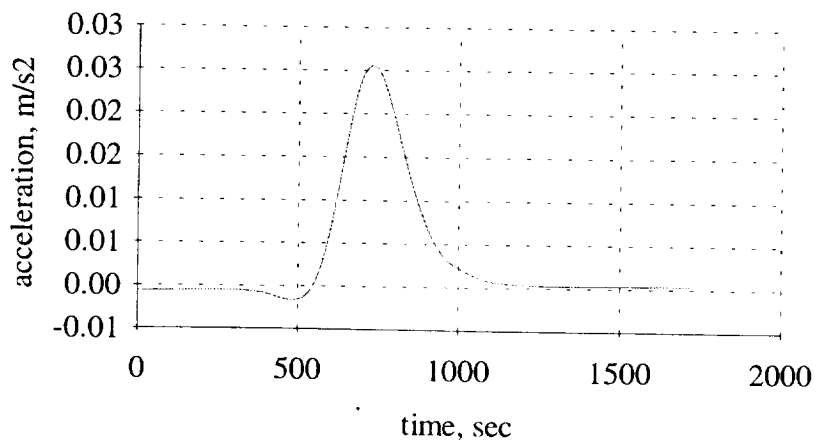
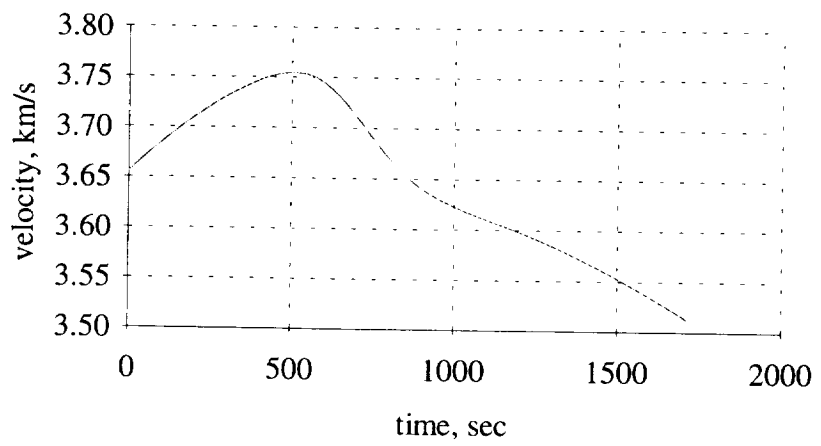
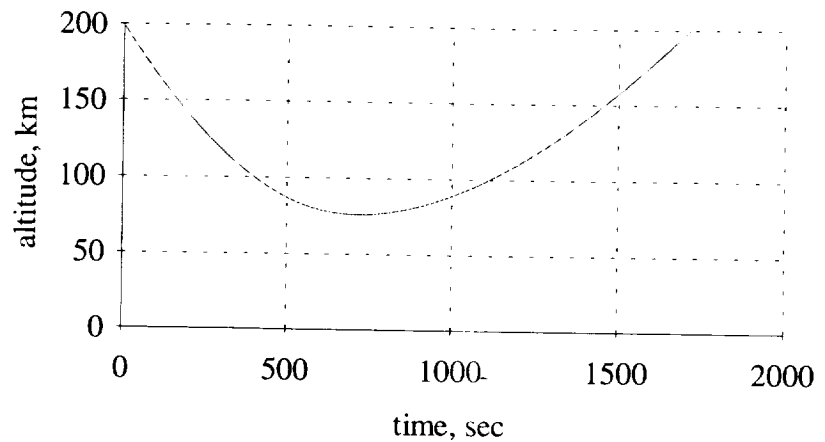


Figure 2.20: Pass #2 Aerobraking Manuever

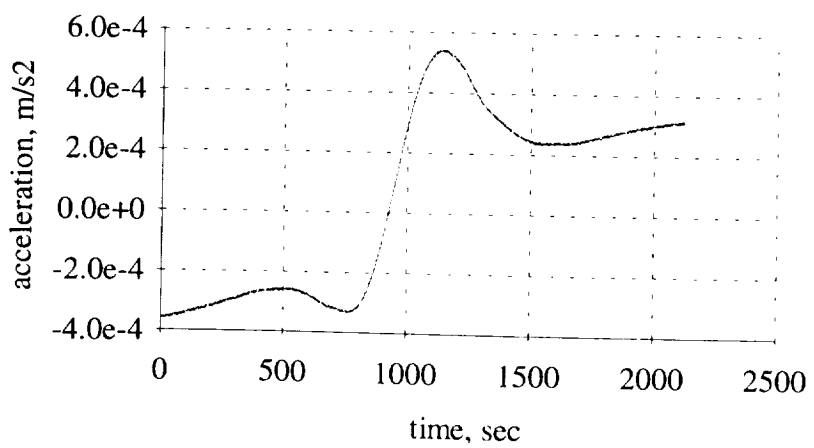
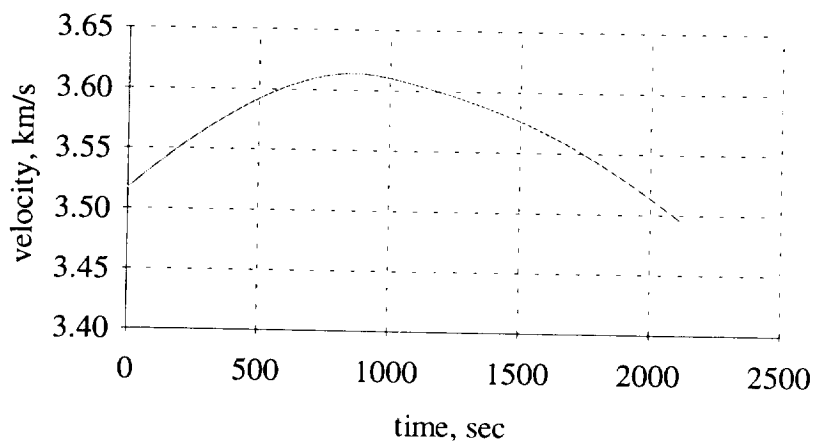
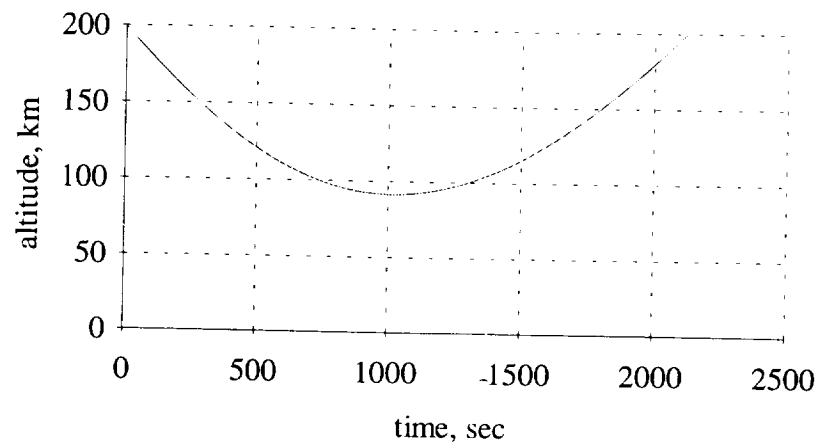


Figure 2.21: Pass #3 Aerobrake Manuever

2.11. APPENDIX D: COMPUTATION OF HEATING RATE

(Curt Baldwin)

The following is a brief description of the formula used in determining the heating rate needed to chose an appropriate thermal protection system. This formula was used in the program which calculated the passes through the atmosphere during the aerocapture maneuver. It should be noted that the formula was obtained from a source (source 2 below) which used empirical methods to derive it. The gases used in the experiments were meant to approximate the atmosphere of Mars. No direct data relating the experimental results in the lab to experimental results on a Martian aerocapture were available. However, the formula agrees well with the lab results it was derived from:

$$Q_w = \frac{c}{\sqrt{RB}} \sqrt{\rho_\infty V_\infty^3}$$

where the physical quantities have dimensions given by:

ρ_∞ - ambient density, lb/ft³

R_B - nose radius, ft

V_∞ - flight speed, ft/s

then the coefficient C has the value:

$$C = (9.18 + 0.663 \overline{M}_\infty) \times 10^{-10} \frac{BTU}{ft^3} \frac{sec^2}{lb^5}$$

As mentioned above the formula was placed in a program where the heating rate was computed at every time step. This same procedure will be used to verify the heating rates are within acceptable limits for the lander deployment.

Sources

Hankey, Wilbur L. Re-Entry Aerodynamics

Loh, W. H. T. Re-Entry and Planetary Entry

Dr. Paul Orkwis of University of Cincinnati

Regan, Frank J. Re-Entry Vehicle Dynamics

2.12. APPENDIX E: DESCENT ANALYSIS

(Tom Terrell)

2.12.1 Parachute Analysis

By knowing the density at discrete fifty meter steps, an iteration process was utilized to determine the velocity, time elapsed, and acceleration of the lander system during the parachute stage. Terminal velocity is achieved when the drag force is equal to the weight force and thus, acceleration becomes negligible. The following is a process equation listing.

$$(1) \quad \text{Drag acceleration} = C_D \rho A V^2 / 2m$$

where, the velocity, V , is the final velocity of the previous step

the coefficient of drag, C_D , = 0.7

ρ is a function of altitude

A is the canopy area

m is the total lander mass

$$(2) \quad \text{Total Acceleration} = g_{MARS} - \text{Drag Accel.}$$

where, g_{MARS} = 3.75 m/s²

$$(3) \quad V = (V_0^2 + 2a(\Delta x))^{0.5}$$

where, V_0 is the final velocity of the previous step

a is the total acceleration from #2

Δx is the step of 50 m

Assumptions : density and acceleration are constant during each step

acceleration due to gravity is constant

The time for each step is calculated by dividing the step distance by the change in velocity. The iteration is discontinued when the change in total acceleration decreases to .004 m/s².

2.12.2 Rocket Analysis

The following is an explanation of the analysis utilized to determine the required rocket fuel mass.

ROLL AND PITCH ROCKETS

The worst case for the roll and pitch rockets is a pure spin about the y-axis. The case of a single rocket providing the thrust force to stop a 30 RPM spin is analyzed.

The units for the angular velocity are converted to radians per second:

$$(30 \text{ RPM}) * (2\pi \text{ rad/rev}) * (\text{min}/60 \text{ s}) = 3.14 \text{ rad/s}$$

By knowing the applied force, moment arm, and the moment of inertia, the angular acceleration can be calculated.

$$M = F * d = I * \text{angular acceleration}$$

$$\text{angular acceleration} = (F * d) / I$$

The burn time is then calculated:

$$\text{burn time} = \text{angular velocity} / \text{angular acceleration}$$

The propellant mass is calculated with the following known quantities:

thrust force, burn time, specific Impulse, and gravity on earth (earth calibrated rockets).

$$m_p = (F * \text{burn time}) / (\text{specific Impulse} * \text{gravity})$$

To obtain the fuel requirements for both rockets, the final propellant value is doubled.

DESPIN ROCKETS

The despin rockets are required to stop the spin stabilization of the lander. The angular acceleration was determined first. Due to the rocket alignment only the horizontal component of the force is utilized when calculating the required angular acceleration.

$$\alpha = (F \cos\theta) * d / I_{zz}$$

where, F = the total force applied

d = the applied moment arm

I_{zz} = mass moment of inertia about the vertical axis

Two rockets provide a coupling moment therefore, the total force equals two times the individual rocket force. The angular velocity was calculated previously.

burn time = angular velocity / angular acceleration

$$m_p = (F*t) / (I_s * g)$$

This propellant value is doubled to account for the opposite set of despin rockets utilized for unpredictable spin in the opposite direction.

MAIN ROCKET DECELERATION

Four CHT-350 rockets provide 1400 N of thrust. The acceleration due to the rockets is simply Thrust / lander mass. To determine the total acceleration, acceleration due to gravity on Mars is subtracted from the acceleration due to the rockets. The burn time is determined by dividing the required change in velocity by the total acceleration.

The propellant mass is calculated with the following equation:

$$m_p = (\text{Force} * \text{burn time}) / (I_s * g)$$

2.13. APPENDIX F: DESIGN OF LANDER STRUCTURE

(Curt Baldwin)

2.13.1 Finite Element Model

To design the lander structure, a finite element model was constructed and analyzed using the software package IDEAS. Two key periods in the mission of the lander were studied, the initial Earth based launch and the controlled landing on Mars. The same model was used in both cases with different loadings approximating each situation. Aluminum 2024-T4 I-beams were used throughout the structure. A thin skin encases the entire structure and is used as an environmental barrier only. It plays no part in the structure and was therefore ignored in the model. The array of cargo and deceleration rockets were overlapped on the model and each mass was divided among the nodes in proximity. A lumped mass element was then placed on each mass-carrying node. Table 2.28 gives the breakdown of the nodal masses while Figure 2.22 shows the finite element model.

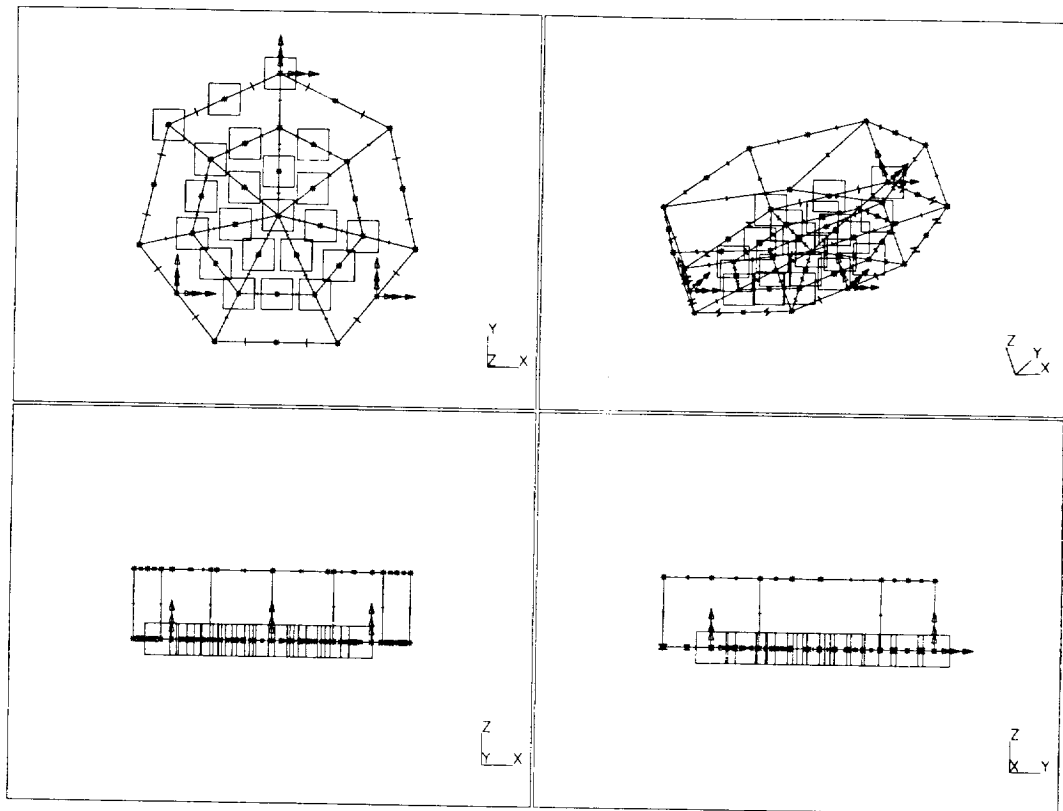


Figure 2.22: Lander Structure Finite Element Model

Table 2.28: Nodal Mass Distributions

Node	Deceleration		Rovers		Communications			Science/Power			Sum kg
	rckts	tanks	long	short	dpole	post	box	s rckts	rtg	cpu	
1		4.9									5
38		4.9									5
39		4.9		3.6							8.5
40		4.9			1.25		.72				7
41		4.9	3.27				.72				8.5
42		4.9	3.27								11
43		4.9									2.5
44		4.9							14		7
16											19
17				3.6							3.6
18					1.25						1.25
19	.36										.36
20	1.44					1					2.5
21	.36									2.5	3
22											
45	.36										.36
46											
47										2.5	2.5
48			3.27								3.6
49							.72				.72
50	.36									.7	1.25
51	1.44			3.6							5
8				3.6							3.6
12				3.6							3.6
2								3.6			3.6

2.13.1.1 Loading 1: Earth based launch

The launch vehicle currently being used produces a nominal load of 5.5g's vertically and .4g's horizontally. Since the landers are mounted sideways relative to their final orientation on Mars, this case was an important criterion. This case was approximated by using an acceleration loading. The orientation of the lander relative to the orbiter was chosen such that the points of contact between the legs and the structure carry most of the load in an efficient manner.

2.13.1.2 Loading 2: Martian landing

The impact of the landing is difficult to model using a static analysis. An important consideration is the energy absorbed by the legs upon impact. This dissipation of energy is key in that it is the primary reason the impact can be survived by a structure so limited in mass and therefore material strength. Here is an outline of the procedure:

- (1) Run the static analysis using Martian gravity with clamps on the structure where the legs would be in contact

- (2) Sum the strain energies in all elements

$$E_{\text{strain}} = .266 \text{ J}$$

- (3) Determine the energy absorbed by each leg and subtract it from the kinetic energy of the lander

$$\begin{aligned} E_{\text{final}} &= .5mv^2 - E_{\text{legs}} \\ &= 3250 \text{ J} - 2080 \text{ J} \\ &= 1170 \text{ J} \end{aligned}$$

- m is the mass of the lander and v the impact velocity a more detailed explanation of E_{legs} will be given later

- (4) Rerun the static analysis with an adjusted Martian gravity which accounts for the impact

$$\begin{aligned} g_{\text{adjusted}} &= g_{\text{Mars}} * \sqrt{E_{\text{final}} / E_{\text{strain}}} \\ &= 3.75 * \sqrt{1170 / .266} \\ &= 248.7 \text{ m/s}^2 \end{aligned}$$

- this acceleration is equivalent to roughly 25g's on Earth which is an acceptable impact

The legs on the lander consist of a foot pad, strut, and shock. Each shock is a cylinder of honeycomb aluminum which absorbs energy upon its crushing. This energy absorbed may be evaluated by approximating the shocks as springs. The analysis manipulated three graphs of experimental data obtained from a source at Martin Marietta Aerospace. As a whole, the graphs provided the necessary sizing and mass of the shocks and the energy each absorbed. This analysis is performed as if the three shocks were combined as one. Here is a brief summary:

- (1) Graph 1: obtain minimum thickness (t) of honeycomb using impact velocity and G limit.

$$\begin{aligned} G \text{ limit} &= 20g && (\text{anything less than } 50g \text{ accepted}) \\ t &= .102 \text{ m} && (\text{actual cylinder height is } .3 \text{ m}) \end{aligned}$$

- (2) Graph 2: obtain crush strength (F) using G limit, impact weight, and impact area.

$$\begin{aligned} G \text{ limit} &= 20g \\ \text{impact weight} &= 975 \text{ N} && (219 \text{ lbf}) \\ \text{impact area} &= .015 \text{ m}^2 && (\text{total area of all three shocks}) \\ \text{crush strength} &= 13867 \text{ N} \end{aligned}$$

- (3) Graph 3: obtain density of honeycomb using crush strength

$$\begin{aligned} \text{crush strength} &= 13867 \text{ N} \\ \text{density} &= 80 \text{ kg/m}^3 \end{aligned}$$

- (4) determine spring constant

$$\begin{aligned} k &= F/x \\ &= 13867 \text{ N} / .3 \text{ m} \\ &= 46222 \text{ N/m} \end{aligned}$$

- (5) evaluate total energy absorbed by all three legs

$$\begin{aligned} E_{\text{legs}} &= .5kx^2 \\ &= .5(46222 \text{ N/m})(.3\text{m})^2 \\ &= 2080 \text{ J} \end{aligned}$$

2.13.1.3 Failure Criteria

With each of the above analyses came stresses and displacements. To determine acceptable levels for each, various criteria were used. For stresses, the von Mises yield condition was used. In general, this method is less conservative than other methods such as the Tresca yield condition. Simply stated, the yield stress of any member was not to exceed $1/\sqrt{3} \times (\text{yield stress of aluminum 2024-T4})$. This less conservative estimate was chosen since mass is of great concern in the design of this unmanned structure. Displacements were not as critical, although there was one important restraint. To avoid an additional load upward upon impact, the rockets and tanks, which were mounted on the underbody, must have clearance above the ground at the time of maximum displacement. After a first run of the model it was apparent the very small displacements occurring were incapable of interfering with ground clearance. Table 2.29 gives the results of the analyses.

Table 2.29: Stress Results

	Maximum Allowable Stress (MPa)	Actual Stress (MPa)
Loading 1	127	15.5
Loading 2	127	101.1

Sources

Dr. Byron Newberry of University of Cincinnati

Popov, Egor P. Engineering Mechanics of Solids

Dr. Bill Willcockson of Martin Marietta Astronautics Flight Systems

2.14. APPENDIX G: TANK DESIGN

(Curt Baldwin)

For both the orbiter and each lander, Hydrazine was used as the chosen fuel with helium providing the pressure in the gas feed system. In all cases, an amount of fuel was given and the amount of helium needed along with the tank sizes for both the fuel and the gas were to be determined. The following is the process used along with any chosen variables fully explained.

2.14.1 Determination of helium volume (example for lander)

Input

mass of Hydrazine (used to determine volume of propellant V_p)

Chosen variables

ullage 5%

propellant tank pressure (P_p) 6 MPa (typically in the range 1.3 - 9)

initial gas tank pressure (P_o) 36 MPa (typically 4 - 8 times P_p)

tank temperature (T_o) 239 K (atmospheric temperature of Mars)

instantaneous gas pressure (P_g) = P_p (assumption)

Constants

K (helium) 1.67

R (helium) 207.7 J/kg-K

Output

$$\text{mass of helium} = (P_p V_p / RT_o)(K/(1 - P_g/P_o)(1 + \text{ullage})$$

2.14.2 Determination of tank sizes/masses

Input

volume of propellant or gas

Chosen variables

<i>tank material</i>	<i>aluminum 2024-T4 (density = 2770 kg/m³)</i>
<i>wall thickness</i>	<i>determined by stress levels</i>
<i>tank geometry</i>	<i>varies for each tank</i>

Output

compute stresses

compute tank volume

*mass of tank = density*volume*

2.14.3 Final Results

As mentioned previously the material is Aluminum 2024-T4. The stresses which are listed below must all fall below the material's ultimate tensile strength of 414 MPa.

satellite fuel tank

geometry cylindrical

height 1.75 m

radius (r) .2 m

thickness (t) .003 m

stresses $\sigma_1 = pr/2t$ 200 MPa

$\sigma_2 = pr/t$ 400 MPa

mass 18.4 kg

satellite pressure tank

geometry cylindrical

height 2.6 m

radius (r) .1 m

thickness (t) .009 m

stresses $\sigma_1 = pr/2t$ 200 MPa

$\sigma_2 = pr/t$ 400 MPa

mass 42.2 kg

lander fuel tank

geometry toroid

o radius (r) .2 m

c radius (r) .09 m

thickness (t) .002 m

stresses $\sigma_1 = pr/2t$ 133 MPa

$\sigma_2 = \sigma_1$ (symmetry)

mass 3.9 kg

lander pressure tank

geometry toroid

o radius (r) .35 m

c radius (r) .04 m

thickness (t) .002 m

stresses $\sigma_1 = pr/2t$ 367 MPa

$\sigma_2 = \sigma_1$ (symmetry)

mass 3.2 kg

Sources

Popov, Egor P. Engineering Mechanics of Solids

Sutton, George P. Rocket Propulsion Elements

2.15. APPENDIX H: ATTITUDE CONTROL SYSTEM

(Lynn White)

2.15.1 Programs

The following programs simulate the spacecraft's motion using a Runge-Kutta integration function in Matlab. The Start program "starts" the simulation. Orbiter is the function that ode23 calls to numerically solve the equations of motion.

2.15.2 Program Start

```
x0=[0 0 0 0 0 36.7 36.7 36.7].';  
  
[t,y] = ode23('orbiter',0,100,x0);  
  
figure(1)  
  
subplot(311),plot(t,y(:,1),t,y(:,2),'--',t,y(:,3),':')  
  
title('Spacecraft Angular Velocity vs. Time'); xlabel('Time, sec'); ylabel('Angular Velocity, rad/sec');  
  
subplot(312),plot(t,y(:,4),t,y(:,5),'--',t,y(:,6),':')  
  
title('Spacecraft Attitude vs. Time'); xlabel('Time, sec'); ylabel('Angular Perturbations, rad');  
  
subplot(313),plot(t,y(:,7),t,y(:,8),'--',t,y(:,9),':')  
  
title('Angular Momentum of Mom. Wheels vs. Time'); xlabel('Time, sec'); ylabel('Angular Momentum, kg-m^2/sec');
```

2.15.3 Program Orbiter

```
function xdot = f(t,x)  
  
I4 =[1328 -.04 -.3;-.04 1331 -.02;-.3 -.02 2471];  
  
I3 =[516 1.3 3; 1.3 1300 -7; 3 -7 1658];
```

```

I2 =[98 -.04 4.4;-.04 1266 -.02;4.4 -.02 1238];
I1 =[65 19 -.6;19 73 1.3;-.6 1.3 44.6];
I0 =[10 -.25 -.3;-.25 13.5 -.05;-.3 -.05 5.8];
Iw = .05*eye(3);
N = 50*eye(3)*(x(4:6)-[0 0 1].')+500*eye(3)*x(1:3);
xdot(1:3)=inv(I1)*(-cross(x(1:3),I1*x(1:3))-cross(x(1:3),Iw*x(7:9))-N);
xdot(4:6) = x(1:3);
xdot(7:9) = N;

```

2.15.4 Figures

These figures represent the spacecraft's attitude and angular momentum. Two cases are shown to compare the responses for two different configurations.

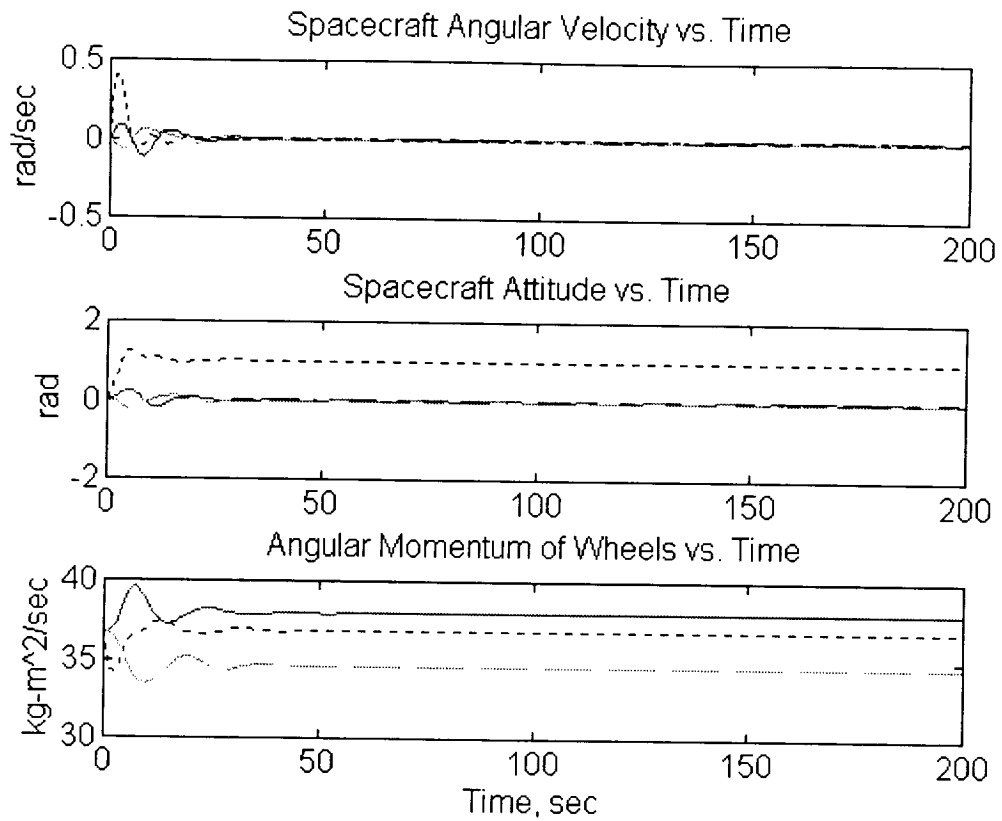


Figure 2.23: One Radian Slew with No Landers Present

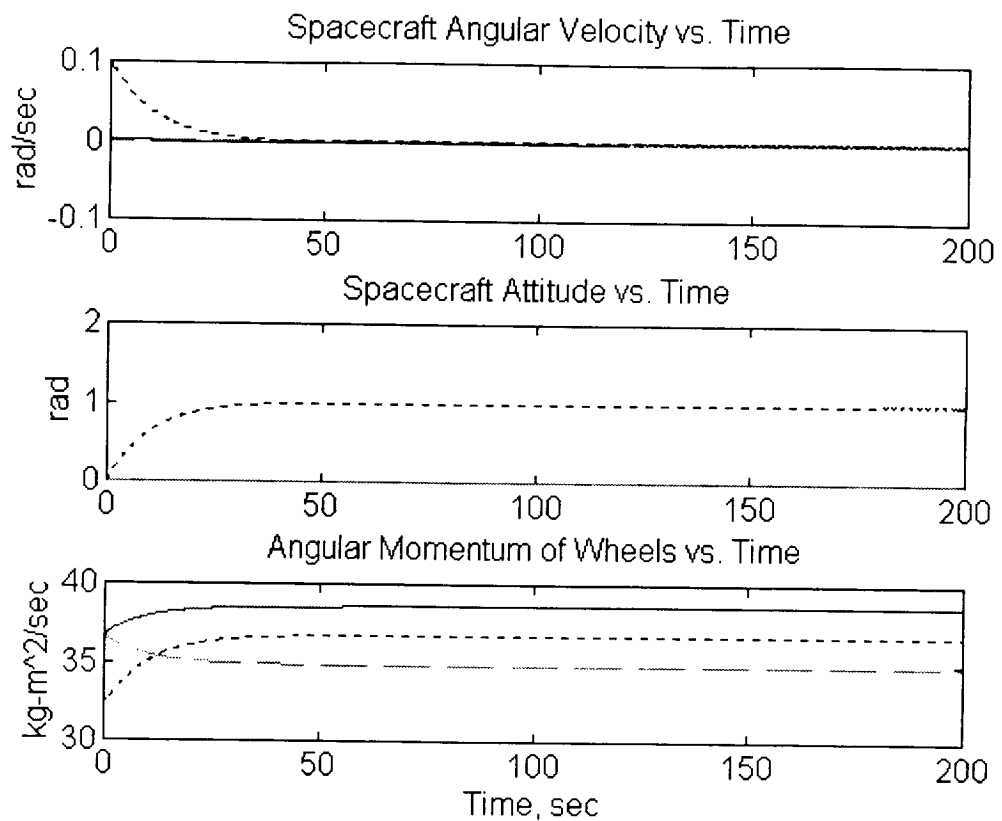


Figure 2.24: One Radian Slew with One Lander Present

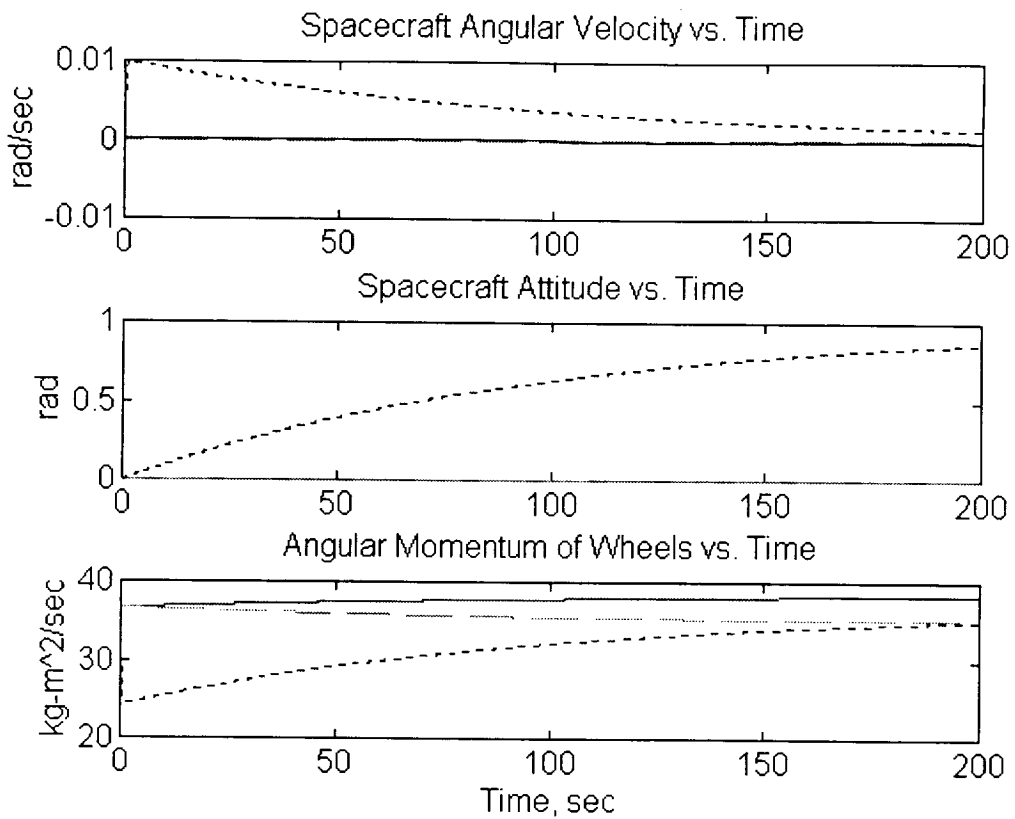


Figure 2.25: One Radian Slew with Two Landers Present

2.16. APPENDIX I: COMMUNICATIONS

(Jeff Skudlarek)

2.16.1 Orbiter to Earth Link Margin

Link Margin Analysis				
Orbiter to Earth Link				
Element	Symbol	value	Units	Formula/Remarks
Orbiter information				
Transmitter Power	Pvt	12.00	W	
Losses to Antenna	Lvt	3.00	dB	
Orbiter Antenna Gain	Gv	39.00	dBi	
Vehicle EIRP=	EIRP	76.79	dBm	$10 * \log(Pvt * 1000) - Lvt + Gv$
Transmission Loss				
Link Frequency	f	8417.00	MHz	
Range	Range	213150684.9	nmi	
Space Loss	Ls	282.88	dB	$37.8 + 20 * \log(f) + 20 * \log(\text{Range})$
Polarization Loss	Lpol	0.00	dB	
Atmospheric Loss	Lat	0.12	dB	
Multipath Margin	Lm	0.00	dB	
Re-entry Plasma Attenuation	Lplas	0.00	dB	
Transmission loss=	Lt	283.00	dB	$Ls + Lat + Lpol + Lm + Lplas$
Receiver Signal Strength				
Receiver Antenna Gain	Ga	66.00	dBic	
Antenna Pointing loss	La	0.10	dB	
Receiver S/S=	S_S	-140.21	dBm	$EIRP - Lt + Ga - La$
Receiver Noise Power (kTB)				
Receiver IF BW	B	0.75	KHz	Subcarrier bandwidth
System Noise Temperature	Tsys	34.60	kelvins	
Receiver Noise Power=	Pnifr	-154.4578785	dBm	$10 * \log((1.380622E-23) * Tsys * (B * 1000) * 1000)$
Receiver IF C/N Ratio	C_N	14.25	dB	$S_S - Pnifr$
Link Margin				
Diversity Combiner Improvement	Gc	2.50	dB	
Required IF C/N ratio	C_Nr	10.00	dB	
Implementation Margin	Mi	3.00	dB	
Link Margin=	LMargin	3.75	dB	$C_N + Gc - C_Nr - Mi$

2.16.2 Lander to Orbiter Link Margin

Link Margin Analysis				
Lander to Orbiter Link				
Element	Symbol	value	Units	Formula/Remarks
Lander information				
Transmitter Power	Pvt	4.00	W	
Losses to Antenna	Lvt	3.00	dB	
Lander Antenna Gain	Gv	8.00	dBi	
Lander EIRP=	EIRP	41.02	dBm	$10^{\log(Pvt*1000)-Lvt+Gv}$
Transmission Loss				
Link Frequency	f	3120.00	MHz	
Range	Range	213150684.9	nmi	
Space Loss	Ls	274.26	dB	$37.8+20\log(f)+20\log(\text{Range})$
Polarization Loss	Lpol	0.00	dB	
Atmospheric Loss	Lat	0.00	dB	
Multipath Margin	Lm	0.00	dB	
Re-entry Plasma Attenuation	Lplas	0.00	dB	
Transmission loss=	Lt	274.26	dB	$Ls+Lat+Lpol+Lm+Lplas$
Receiver Signal Strength				
Orbiter Antenna Gain	Ga	6.00	dBi	
Receiver S/S=	S_S	-227.24	dBm	$EIRP-Lt+Ga$
Receiver Noise Power (kTB)				
Carrier Deviation	Dev_C	0.01	KHz	
Bit Rate	BR	0.84	kbps	
Effective Frequency	f_eff	0.42	KHz	for NRZ-L modulation $f_{eff}=0.5 BR$
Receiver IF BW	B	0.86	KHz	$2(Dev_C+f_eff)$
System Noise Temperature	Tsys	578.63	kelvins	
Receiver Noise Power=	Pnifr	-141.6555815	dBm	$10^{\log((1.380622E-23)*Tsys*(B*1000)*1000)}$
Receiver IF C/N Ratio	C_N	-85.58	dB	$S_S-Pnifr$
Link Margin				
Diversity Combiner Improvement	Gc	0.00	dB	
C/N Threshold	C_Nt	-89.50	dB	
Implementation Margin	Mi	2.00	dB	
Link Margin=	LMargin	1.92	dB	C_N+Gc-C_Nt-Mi

2.17. APPENDIX J: TORSION DISK DESIGN

(Curt Baldwin)

In order to deploy each lander a safe distance from the orbiter, a new mechanism was developed. This mechanism has been termed a "Torsion Disk." A torsion disk consists of three springs. One spring propels the lander away from the lander. The two remaining springs act as a force couple to spin stabilize the lander. Design of this mechanism seeks to minimize two features: torque applied to the orbiter and mass. To achieve the optimum balance several iterations of various parameters were made in no distinct order. For clarity, the approach taken to this design will be explained as if only one iteration were needed. Steel was used for the spring design and its material properties are given first. The remaining sections explain the design of the propelling spring, torque springs, and the general mechanism.

Material Properties of Steel

shear modulus	G	80 GPa
maximum shear stress	τ_{\max}	200 to 700 MPa

Propelling Spring

Responsible for propelling the lander away from the orbiter at .25 m/s

Given

lander mass	m	260 kg
velocity	v	.25 m/s

- equate kinetic energy of lander to potential energy of propelling spring

$$\frac{1}{2}mv^2 = \frac{1}{2}kx^2$$

- define the spring constant k through the geometry of the helical spring

$$k = \frac{Gd^4}{64\bar{r}^3 N}$$

where these parameters are chosen:

cross section diameter	d	.0113 m
mean spring radius	\bar{r}	.175 m
number of live coils	N	4

$$= 950 \text{ N/m}$$

- define the maximum deflection x of the helical spring

$$\text{compressed length} \quad x_c = N \cdot d \quad .0452 \text{ m}$$

$$\text{extended length} \quad x_e = 4 \cdot x_c \quad .18 \text{ m}$$

$$\text{maximum deflection} \quad x = x_e - x_c \quad .1356 \text{ m}$$

Evaluation of design

needed energy 8.1 Nm

$$t_{\max} = \frac{16kx\bar{r}}{\pi d^3} \left(\frac{d}{4\bar{r}} + 1 \right)$$

actual energy 8.7 Nm

$$= 81 \text{ Mpa (well below max)}$$

Force applied to Orbiter is 130 N. This is a reasonable torque for the Orbiter control system to handle.

Mass of spring is 3.45 kg which will prove to be reasonable as the total mechanism is assembled.

Torque Springs

Responsible for spin stabilizing the lander to a rotation of 30 RPM.

Given

<i>lander rotation</i>	ω	<i>30 RPM</i>
<i>principle moment of inertia</i>	I_z	40 kgm^2

- determine minimum spring constant k needed for each spring

$$\frac{1}{2} I_z \omega^2 = \int_{\theta_{\min}}^{\theta_{\max}} M d\theta \quad \text{where} \quad M = 2Fd \quad (2 \text{ springs acting as a couple})$$

$$\begin{array}{ll} \text{force} & F = k d \tan \theta \\ \text{moment arm} & d \quad .45 \text{ m} \end{array}$$

- this equation may be rewritten with the integral evaluated to solve for k

$$k = \frac{I_z \omega^2}{4d^2 [\ln(\cos \theta_{\min}) - \ln(\cos \theta_{\max})]}$$

$$\theta = \tan^{-1} \left(\frac{x}{d} \right) \quad x \text{ is the spring length compressed or elongated}$$

- define the spring constant k through the geometry of the helical spring

$$k = \frac{Gd^4}{64\bar{r}^3 N} \quad \text{where these parameters are chosen:}$$

<i>cross section diameter</i>	<i>d</i>	.0134 m
<i>mean spring radius</i>	<i>r̄</i>	.125 m
<i>number of live coils</i>	<i>N</i>	4

$$= 5158 \text{ N/m}$$

- define the maximum deflection x of the helical spring

<i>compressed length</i>	$x_c = N * d$.0536 m
<i>extended length</i>	$x_e = 4 * x_c$.2144 m
<i>maximum deflection</i>	$x = x_e - x_c$.1608 m

$$\text{spring constant needed} \quad 5117 \text{ N/m}$$

Evaluation of design

As shown above, k can be defined by either the angular velocity needed or by the physical geometry of the spring. The two methods are coupled through the compressed and extended lengths of the spring. It was determined that the minimum spring constant needed is 5117 N/m. Through the geometry of the spring, the constant turns out to be 5158 N/m. This is sufficient to spin the lander to 30 RPM in a rotation of roughly 19 degrees. The geometric limitation to this rotation would be roughly 160 degrees. Within the remaining 141 degrees of rotation, before the torsion disk spins into itself, the propulsive spring will separate the lander from the orbiter. By the same method above, the maximum shear stress was calculated to be 225 MPa. This is still well below the ultimate maximum of 700 MPa. A force of 830 N is applied by each 3.5 kg spring. This should be a reasonable torque for the Orbiter control system to handle.

Mechanism design

The previous sections have dealt with the design of the springs on the torsion disk. This portion of the design pulls the springs together into a working mechanism which, upon a single command, governs the spinning of the lander and then propels it away from the lander. This procedure is mechanically automated rather than relying on electronics. Figure 2.27 gives side, top, and exploded views of the torsion disk.

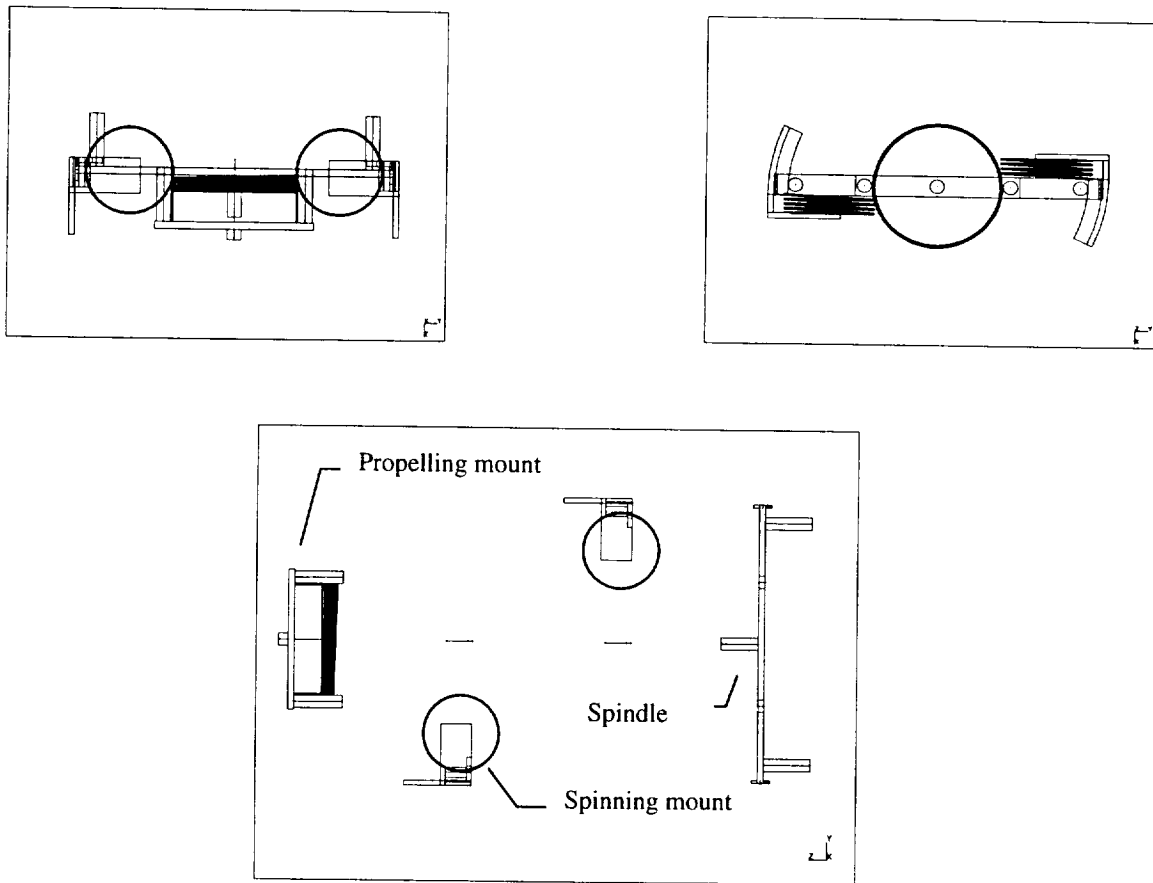


Figure 2.26: Side, Top, and Exploded Views of Torsion Disk Assembly

As seen above, the assembly consists of a propelling mount, two spinning mounts, and a spindle. The propelling mount is attached to the structural band about the satellite. It houses the propelling spring. Each spinning mount is also fixed to the structural band. These mounts consist of rails which guide the spindle during its rotation. Each mount also houses a torque spring which causes the rotation of the spindle. Below is a table giving the final masses of each element of the torsion disk assembly. The structural elements of the disk are constructed from Aluminum 2024-T4.

Table 2.30: Summary of Torsion Disk Elements

	Mass (kg)	Comments
Propulsive Spring	3.45	$k = 950 \text{ N/m}$; $x = .14 \text{ m}$; $F = 130 \text{ N}$
Torque Springs (2)	3.5 (each)	$k = 5158 \text{ N/m}$; $x = .16 \text{ m}$; $M = 743 \text{ Nm}$
Structure	11.22	
Total	21.67	

Sources

Dr. Byron Newberry of University of Cincinnati

Popov, Egor P. Engineering Mechanics of Solids

2.18. APPENDIX K: LAUNCH SUPPORT STRUCTURE

(Curt Baldwin)

During launch, the transfer vehicle must withstand up to 5.5gs. The landers are most vulnerable to this load since they are quite massive and attached to the rest of the vehicle in a manner such that they may be deployed easily. For these reasons, a support structure was developed to cradle the landers during the launch. The structure consists of four curved I-beams, one for each lander, and pipes to withstand the compressive forces. Figure 2.28 shows the finite element model and its loads while Figure 2.29 gives the cross-sections of the beams used.

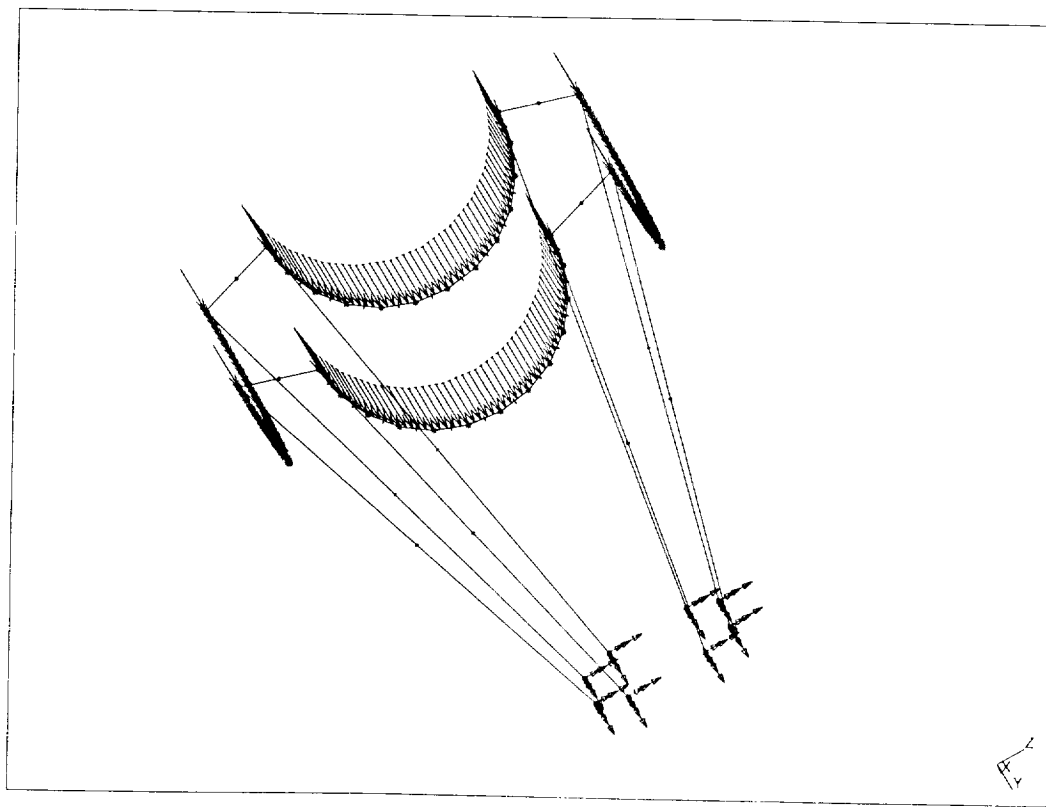


Figure 2.27: Support Structure Finite Element Model

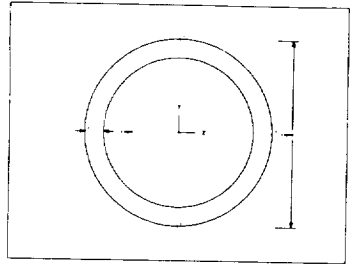
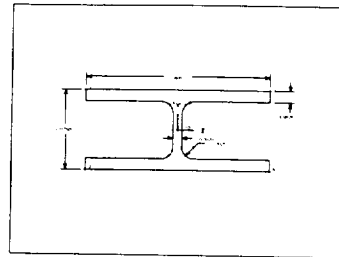


Figure 2.28: Support Structure Cross-Sections



All elements of the truss were constructed from Aluminum 2024-T4. This material was chosen for its combination of strength and lightweight. Although the structure is only physically attached to the fairing adaptor, and therefore will not travel with the transfer vehicle to Mars, it is critical that it is of low mass. Table 2.31 gives a summary of the components.

Table 2.31: Summary of Support Structure Elements

Element	Total Length (m)	Total Mass (kg)	Cross section dimensions (m)
pipe	32	16	OD = .025 thk = .0025
I-beam	11.3	7.2	Height = .0175 Width = .04 Flange = .002

To analyze the structure a finite element model was created. The model consisted of linear beam elements with the cross-sections listed in the above table. Distributed beam loads were applied to simulate the landers under a 5.5g launch condition.

2.18.1.1 Failure Criteria

With the above analyses came stresses. To determine acceptable levels, the von Mises yield condition was used. In general, this method is less conservative than other methods such as the Tresca yield condition. Simply stated, the yield stress of any member was not to exceed $1/\sqrt{3} \times (\text{yield stress of aluminum 2024-T4})$. This less conservative estimate was chosen since mass is of great concern in the design of this unmanned structure. Table 2.32, shown below, gives the maximum stresses achieved in the analysis in comparison with the maximum allowable stresses. All stresses are given in Mega-Pascals.

Table 2.32: Maximum Support Structure Stresses

Axial	Y-Bend	Z-Bend	Torque	Y-Shear	Z-Shear
11.6	119.0	84.0	23.9	22.5	3.86
Maximum Allowable			Maximum Allowable		
239.0			127.0		

As can be seen, a factor of safety of two was allowed for in the stress levels. This structure is essential to the success of the launch, and therefore the entire mission. For this reason, a conservative approach was taken towards its design.

Sources

Popov, Egor P. Engineering Mechanics of Solids

2.19. APPENDIX L: THERMAL ANALYSIS DURING CRUISE

(Chris Patrick)

In order to do the thermal analysis on the lander and satellite the assumptions were made, that with the Aluminized Kapton coating the vehicle would act as a blackbody radiator. With this assumption the equations for radiative heat transfer can be used. This analysis was done for each piece of equipment individually.

First the total contributions of heat input into the system had to calculated. The first input into the system is the heat output from the RTG, this value is known and assumed constant. The heat reflected from the Earth was assumed to be negligible. The input from the sun is a function of the solar intensity, which changes as the distance from the sun increases, the projected area the sun is hitting on the vehicle, and the absorptivity. The equation is as follows:

$$Q_{\text{sun}} = (S.I.) * \alpha * A_{\text{projected}}$$

S.I.= Solar intensity

α = Absorptivity of coating

$A_{\text{projected}}$ = Area sun effects

Then to solve for the temperature of the vehicle, the thermal equilibrium equation is used. Solving for the spacecraft temperature (T_s), the equation becomes:

$$T_s = ([Q_{\text{sun}} + Q_i] / \epsilon_s * \sigma * A_s)^{(1/4)}$$

Q_{sun} = Heat input from sun

Q_i = Internal heat source from vehicle

ϵ_s = Emissivity of coating

σ = Stefan-Boltzmann Constant

A_s = Total area of vehicle

This same process is repeated for the satellite. The following is a table of temperatures of the lander and satellite at various solar intensities:

Intensity (W/m ²)	$Q_{\text{sun}}(\text{lander})$ W	Q_{sun} (satellite) W	T(lander) °F	T(satellite) °F
1350 (Earth)	984	1040	89	125
1300	948	1001	86	120
1250	911	963	83	114
1200	875	324	79	109
1150	838	886	76	103
1100	802	847	73	97
1050	765	809	70	91
1000	729	770	66	85
950	693	732	63	78
900	656	693	59	71
850	620	655	56	64
800	583	616	52	57
750	574	578	49	50
700	510	539	45	42
650	474	501	41	33
600 (Mars)	437	462	37	24

2.20. APPENDIX M: SOLAR ARRAY AND BATTERY SIZING

(Chris Patrick)

To size the solar arrays the following equations were used:

$$\text{Array Voltage} = \text{battery volt.} * 20\%$$

This is calculated because the array voltage must exceed the battery voltage in order to charge the battery. A good rule of thumb is to assume 20% above battery voltage. Then array capacity was calculated:

$$\text{Array Cap.} = \text{Total power/degradation} * \cos \text{sun angle} * \text{temp effect}$$

Next the total cell area is calculated:

$$\text{Tot. Cell Area} = \text{Array Cap.} / \text{solar intensity} * \text{efficiency}$$

The number of cells needed:

$$\# \text{ of cells} = \text{Tot. Cell Area} / \text{Cell Size}$$

Finally the array size:

$$\text{Array Size} = \text{Tot. Cell Area} / \text{Packing Factor}$$

2.21. APPENDIX N: THERMAL ANALYSIS ON SURFACE

(Chris Patrick)

The analysis of the thermal analysis of the lander on the planet was assumed to be a conductive heat transfer problem. This analysis was done at worst condition, which is at night. First, the thermal conductivity (k) required of the lander material is calculated. Since the required temperature of the lander is known, k can be solved for by using the conduction equation:

$$k = -(q / A * (T_1 - T_2))$$

q = Heat from lander

A = Area of lander

T_1 = Temperature of lander

T_2 = Temperature of Mars Atmosphere

Once k is known the temperature of the lander can be calculated at any time. Final note, for this analysis the heat from the sun and the heat emitted from the planet was assumed to be small.

Appendix O: Sounding Rocket Calculations

(Chris Patrick)

The calculations for the sounding rocket was a simple analysis. The engine performance was obtained from the Aerotech Consumer Aerospace Company (ACAC). Once an engine was chosen, and the specific impulse known (given by ACAC), the range and height of the rocket were found using the equations of motion.

2.22. APPENDIX O: REFERENCES

- 1) Joel S. Greenberg and Henry R. Hertzfeld, ed., Progress in Astronautics and Aeronautics, Vol. 144, Space Economics. Washington, D.C.: American Inst. of Aero. and Astro., 1992.
- 2) P.R.K. Chetty, Satellite Technology , Its applications, Second Edition, Blvd Ridge Summit: TAB Professional and Reference Books, 1991.
- 3) Wilbur Pritchard, Satellite Communication Systems Engineering, Englewood Cliffs: Prentice Hall, 1986.
- 4) James R. Wertz, Spacecraft Attitude Determination and Control, Kluwer Academic Pub., 1978.
- 5) Royce D. Harbor and Charles L. Phillips, Basic Feedback Control Systems, Englewood Cliffs: Prentice Hall, 1991.
- 6) Jerry G. White, Fundamentals of Astrodynamics, Dover Publications, 1921.
- 7) Richard A. Burke, Fundamentals of Solar Cells: Photovoltaic, New York: Academic Press, 1983.
- 8) H. S. Rauschenbach, Solar Cell Array Design Handbook, New York: Litton Educational Publishing, 1980.

- 9) S. Griffith, Radiation Heat Transfer and Thermal Control of Spacecraft, Board of Regents for the Oklahoma State University: Still Water, 1960.
- 10) George P. Sutton, Rocket Propulsion Elements, New York: Wiley and Sons, 1992.
- 11) Charles D. Brown, Spacecraft Mission Design, Washington, D.C.: American Institute of Aeronautics and Astronautics, 1992.
- 12) Michael D. Griffin and James R. French, Space Vehicle Design, Washington, D.C.: American Institute of Aeronautics and Astronautics, 1991.

3.0 SHORT-RANGE MARTIAN ROVER

Jesse Kuhns
Amy Mercer
Shawn Newman
Marc Richmond
Susan Slater
Maria Sychay
Jeff Wiley

TABLE OF CONTENTS

3.1	INTRODUCTION	1
3.2	PROPOSED CONCEPTUAL DESIGN	3
3.2.1	Body Structure	3
3.2.2	Drivetrain	8
3.2.3	Steering	9
3.2.4	Power Supply	10
3.2.5	Navigation and Control	11
3.2.6	Electronics and Instrumentation	13
3.2.6.1	Central Processing Unit	15
3.2.7	Communications Network	16
3.2.8	Science Experiments	16
3.2.8.1	Mass Spectrometer	16
3.2.8.2	Ice Auger/Borescope	17
3.2.8.3	Thermal Probe	20
3.3	ANALYSIS	22
3.3.1	Structural	22
3.3.2	Thermal and Power	28
3.3.3	Traction and Mobility	32
3.3.4	Motor Selection	35
3.3.5	Rover Mass and Power Budget	37
3.4	NOMENCLATURE	38
3.5	LIST OF FIGURES	39
3.6	REFERENCES	40
3.7	SCALE DRAWINGS	43

3.1 Introduction (Susan Slater)

An unmanned mission to the planet Mars, designed as a follow-up to the Mars Polar Pathfinder Mission (tentatively planned by the Jet Propulsion Laboratory to launch in 1998), is presented. The follow-up mission's objective is to obtain science data on the northern polar cap of Mars for one Martian year. This research and data collection will be performed in approximately 10-12 locations so that maximum area can be covered. At each location, a lander assembly will house a variety of science instruments to study the atmosphere and the polar ice cap. One such instrument is a short-range micro-rover. This rover, Red Rover, will then conduct science experiments up to 2 km away from the lander site to obtain data on the environment of the polar cap.

A rover will commence at the lander and traverse in a circular pattern at intervals of 0.5 kilometers away from the lander as depicted in Figure 3.1.1. The basic operation of the rover includes traversing a distance of approximately 30 meters, collecting science data, then proceeding to the next test location. The entire cycle will last for a time period of about one third of a Martian day. The experiments that will take place include: compositional analysis of soil with a mass spectrometer, CCD imaging of the surrounding terrain, and meteorological data using a drill and borescope system. This experimentation will continue for one half of a Martian year. During this time period, the polar cap will be in complete sunlight. The second half year, when the polar cap is in complete darkness, the rover will remain stationary and will collect data as long as possible.

Because the data collection time period is to last at least one Martian year (which is equivalent to 1.8 Earth years), Red Rover is designed to endure the harsh environmental conditions of Mars for that time period. Navigational Instruments on the rover will enable it to detect terrain variations and avoid obstacles so that it will be able to traverse on the polar cap without being disabled.

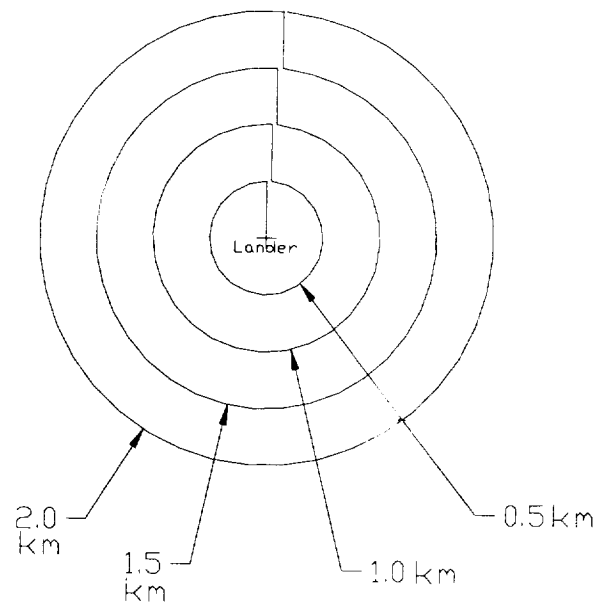


Figure 3.1.1 Rover Pathway

3.2 Proposed Conceptual Design

3.2.1 Body Structure

(Amy Mercer and Marc Richmond)

The design of the structure of Red Rover must meet certain requirements. Because the Red Rover will be placed on the polar cap of the Mars planet, it will need to be able to travel over icy terrain. Due to the fact that the surface of the polar caps is unknown, it is best assumed that the terrain will be similar to that of the polar caps on Earth which are relatively smooth. Red Rover is designed to traverse protrusions with a maximum height of 101.6 mm; this is the ground clearance of the rover. If larger protrusions exist, the Red Rover will avoid them. Also, due to the unknown terrain, the rover will also need to have an independent suspension system. The rover will also need to support a platform that will hold various experiments and scientific equipment. Due to the severe climate, the rover will need to be able to withstand extreme cold temperatures. The rover will need to be able to function independent of the Lander. The rover has also been minimized in size and weight for the utilities it provides.

The proposed design consists of a six-wheel configuration. This allows for increased stability and also provides a good trade-off of power versus weight. The overall dimensions of the Rover envelope are 406.4 mm X 508 mm. The wheel base from the front to the center wheel is 236 mm. The wheel base from the front wheel to the rear wheel is 406.4 mm. To obtain as much traction as possible, the width of each wheel is 50.8 mm. The diameter of each wheel is 101.6 mm in order to be able to traverse maximum protrusions. All six wheels are driven by independent motors and the steering is to be controlled by using tank steering methods. The Red Rover has two points of articulation for overcoming protrusions when traveling over the terrain. As a result of having just two articulation points, the Rover has two independent members per side. By attaching one of the articulation points to the platform, the left and right sides become independent of each other.

The platform supports all of the necessary scientific equipment, the power source, and the onboard electronics. The dimensions are 381 mm X 254 mm. It is pinned midway between the front and rear wheels to the sides. It is additionally supported by the

rear platform support cantilevers. There are two cantilevers, one on each rear member with a length of 101.6 mm. They protrude perpendicularly from the inner surface of the rear member beneath the platform. These cantilevers perform two major functions. The first is to utilize the weight of the platform to take advantage of the rear drive motors. If no weight were acting on the rear member, it would simply act as a trailer. The second function is to allow for an independent suspension while supporting the platform. The center of gravity of the platform payload (scientific equipment, experiments, etc.) should lie between the pinned attachment and the rear platform support cantilevers.

One side of the basic configuration is shown in Figure 3.2.1.1.

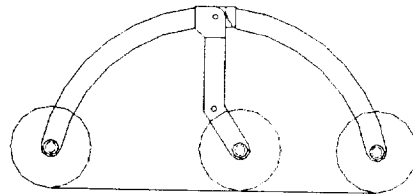


Figure 3.2.1.1 Basic Configuration

There are two independent members per side. The front member attaches the front and center wheels. The curved section is in the shape of an arc. This is to minimize stress concentrations and to carry loads more effectively. The lower portion of the curved section is vertical, a distance of 50.8 mm. This is to avoid interference when steering the front wheels. The large vertical section of the front member serves as a connection between the top of the curved section and the attachment point to the platform. The center wheel attachment is rotated rearward. This feature is necessary to allow the front member to rotate back to its original position after traversing protrusions. When the front wheel is raised in order to climb the protrusions, the entire front member rotates about the bottom of the vertical section. The back member has a similar curved section. There is a 50.8 mm vertical section at the bottom that attaches the rear wheel to the back member. This is also to avoid interference with steering.

The center wheel attachment is rotated rearward (cant) for two reasons. The first, as mentioned previously, is to allow the front wheel to return to the ground after being

raised. This is accomplished by a simple moment analysis. By summing the moments applied to this member, the necessary rotation angle of the attachment bar can be determined. A plot of the sum of the moments versus the bar rotation angle (β) for various angles of inclination (Θ) of the front wheel are given in Figure 3.2.1.2b. Figure 3.2.1.2a describes the variables related in Figure 3.2.1.2b.

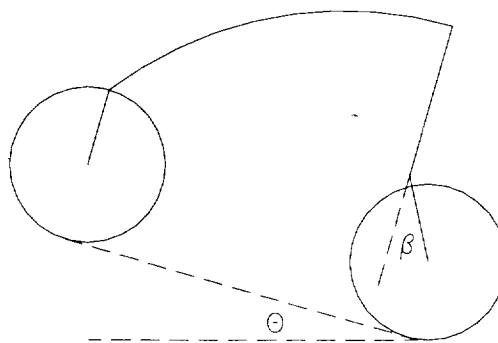


Figure 3.2.1.2a Incline Angle and Cant Angle

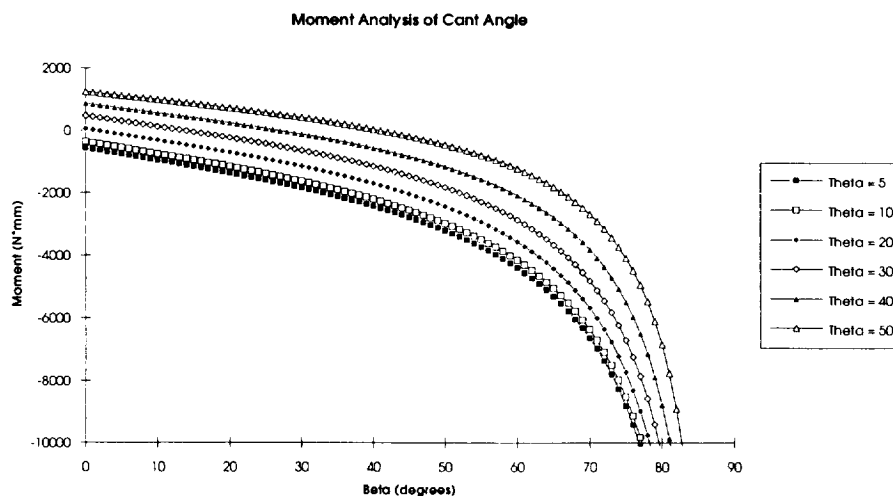


Figure 3.2.1.2b Moment Analysis of Cant Angle

Negative values of the moment are desirable because they indicate a moment in the counterclockwise direction, which returns the front wheel to the ground. The second reason is because of the geometry of the maximum protrusion position. The angle of rotation of 32.8° is chosen for the Red Rover. In this position, the desirable condition of

the rotated bar being vertical is achieved. The moment analysis of Figure 3.2.1.2b supports the fact that this is an acceptable angle.

Different scenarios for the Red Rover have been examined when one side is traversing a protrusion of the maximum height of 101.6 mm. The first scenario is shown in Figure 3.2.1.3a.

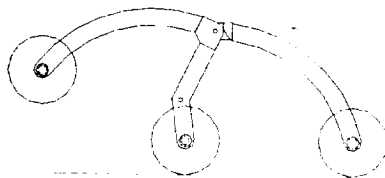


Figure 3.2.1.3a Front Wheel Scenario

In this position, the front wheel has encountered the obstacle. The rear platform support cantilever slides rearward. The front member rotates clockwise about the rotation point. This rotation point also lifts. The rear member rotates counterclockwise about the rotation point. In the second scenario (Fig. 3.2.1.3b), the center wheel has encountered the obstacle.

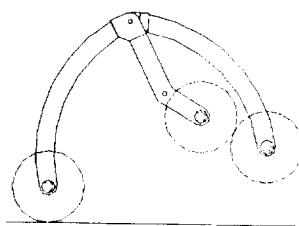


Figure 3.2.1.3b Center Wheel Scenario

A restriction must be imposed to inhibit the rear member from rotating too far in the clockwise direction. This is to prevent the rear wheel and center wheel from coming in contact with each other. Mechanical stops are located at the pivot for the front

curved member and the rear curved member. Due to this rotation restriction, the platform will be raised in the rear. The Rover will also tilt between 14° and 18° in this situation due to the fact that the two center wheels are rigidly attached to the platform. The front member will rotate in the counterclockwise direction and the rear member will rotate in the clockwise direction. In the third scenario (Fig. 3.2.1.3c), the rear wheel has encountered the obstacle.

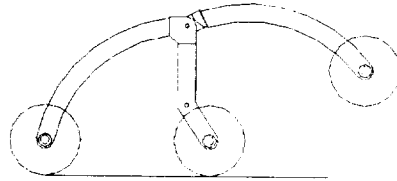


Figure 3.2.1.3c Rear Wheel Scenario

The rear of the platform is raised by the rear cantilever. This makes the platform rotate counterclockwise. The rear member rotates counterclockwise. By analyzing these separate scenarios, each wheel on one side is shown to be independent. With respect to each side, the front and rear wheels are shown to be independent but the center wheels are not.

There are many cost-saving guidelines that are implemented in the structural design of the Red Rover. First, aluminum alloy is the material to be used because it maintains sufficient material properties at low temperatures. In addition, it is lightweight, cheap, and available. Second, the tubing used for the members is hollow and square. It is hollow to save weight and to have the ability to run wiring through the members. It is square to increase the available area inside. The square tubing is easier to obtain and is therefore more cost effective because of its simple geometry. Finally, the complex corners of the Red Rover are machined pieces to make assembly and manufacturing easier, therefore reducing cost. These joints are not hollow, but this additional mass is negligible.

3.2.2 Drivetrain

(Jeff Wiley)

The Red Rover configuration consists of six-wheels with independent drive motors and solid wheels. Preliminary designs consisted of tires made from bent sheet metal into a desired form, acting as the wheel. Although these redesigned wheels account for a greater percentage of Red Rover's total weight, the solid wheels provide greater strength over the unpredictable strength of sheet metal variations. The new tread is constructed from a long strip of spring steel/sheet metal which fits into the outer groove of the tire. Screws hold the tread secure and can be removed if necessary. This configuration allows for variable tread patterns to be used and easily changed during testing. Slots are cut into the tread and bent at 45° to provide traction. (The exact tread dimensions and pattern can be seen in the 'Drawings' section.) Overall dimensions of the tires are 102mm in diameter by 51mm wide. The wheels are made of 20-24 T4 Aluminum. The entire wheel assembly can be seen in the following figure.

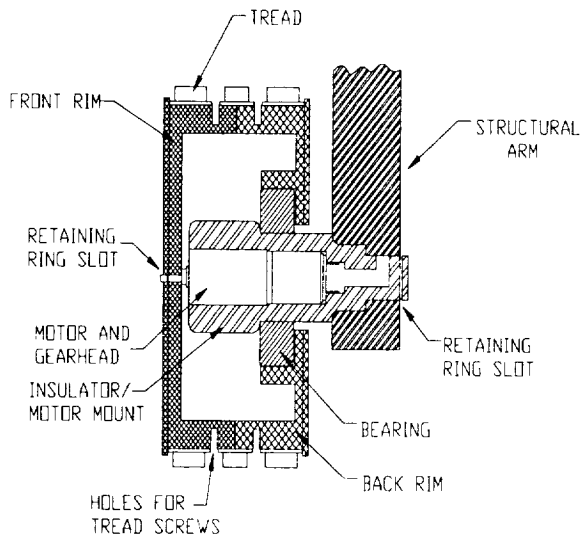


Figure 3.2.2.1 Cross-Sectional View of Wheel Assembly.

The insulator provides two important features; it mounts the motor and gearhead to the structural arm, and shields the motor from harsh environmental conditions. Lateral support of the wheel is attained by the use of retaining rings on the inside of the structural arm and outside the wheel at the output gearshaft. Radial motion of the insulator/structural arm junction is prevented by an interior Woodruff Key located inside the arm. The insulator is also made of 20-24 T4 Aluminum. While this material does not provide a high degree of insulation, its strength is important and further research is being done on an alternative. Bearings that are suited for use at low temperature are being utilized to support the entire wheel structure.

3.2.3 Steering

(Shawn Newman)

To eliminate the problems of using steering motors on the wheels of Red Rover, which were weight concerns and placement problems, a steering system similar to the type used for track laying vehicles such as tractors and tanks has been designed. Red Rover is designed to make two different types of turns. Turns while it is moving forward or backward, and turns when its translational motion has been stopped.

In order for Red Rover to turn while it is moving backwards or forwards, the wheels on the opposite side of the direction of the turn will provide more torque than the wheels on the same side of the direction of the turn. In other words, for a right turn the wheels on the left will provide more torque than the wheels on the right, and for a left turn the wheels on the right will provide more torque than the wheels on the left. The effect of having one side of wheels provide more torque than the other side is a moment about the center of mass of Red Rover which will cause it to move in a circular path. The path that Red Rover is desired to traverse will be fed into a controller that will control the radius of curvature and speed of the turn.

Red Rover's turning ability will be significantly reduced if the wheels are slipping rather than rolling over the surface. Wholesale slippage between wheel and road will occur if more torque is supplied to the wheels than can be maintained by the friction between the wheel and the Martian surface. The control system will be able to detect if a wheel is slipping rather than rolling on the ice by using the sensors that monitor torque input, wheel angular velocity and acceleration. Slipping of the wheels can be detected if the wheels' angular velocity and acceleration do not correspond with the velocity or

acceleration of Red Rover motion. It can also be detected if the wheels' angular velocity and acceleration are much greater than what would be expected for pure rolling with a given torque. When a wheel is slipping, the control system will try to compensate by increasing torque to the wheels that are not slipping and decreasing torque to the wheels which are slipping while still guiding Red Rover along the desired path.

Red Rover has the additional advantage of being able to make turns when its forward or backward motion has been stopped. This is accomplished by rotating one side of the wheels forward while rotating the other side of wheels backward, creating a moment about the center of gravity of Red Rover. This type of turn can be used to take a 360° panoramic view of the surroundings around Red Rover. This type of turning also enhances Red Rover maneuverability and ability to avoid obstacles.

3.2.4 Power Supply

(Susan Slater)

Depending on the tasks that are being performed, Red Rover needs a variable amount of power. By performing a power analysis, there needs to be a minimal and constant supply of approximately 2 Watts and a maximum supply of approximately 8 Watts is needed.

The power supply for Red Rover is provided by a nuclear source. This source is being designed by the Nuclear Space Design team. Two systems are being designed: a 2.5 Watt and a 10 Watt system. Consideration must be taken into how much power is needed at any one time and how the this power is allocated before either system can be incorporated. One option is that a 2.5 Watt system is utilized with batteries that are trickle-charged; the batteries would be able to provide the maximum power when needed. Because of weight considerations and power requirements, this method of power supply isn't used.

The nuclear isotope being used is Strontium 90, and will be in the form of Strontium Fluoride. The operating efficiency will be between 5 and 10 percent. The excess energy not turned into power will be given off thermally. This thermal energy will be utilized in maintaining the temperature in the warm electronics box above a minimum of -40°C. This can be done by radiation, convection, or conduction methods, and the method chosen will be integrated within the resulting power supply that is designed.

To conserve energy and weight, Red Rover will incorporate power management sequencing. This technique utilizes a control system to sequence the power consumers so that power surges are minimized. One example of this method is the start up of each motor sequentially while all other non-essential utilities are turned off. This maximizes the total power margin at any one time. From preliminary analysis, the maximum power needed at any one time is approximately 8 Watts. To provide this, multiple 2.5 Watt supplies could be implemented in parallel or a 10 Watt supply could be used. When both systems are designed, a comparison will be made, and the most advantageous system will be used. The primary characteristics to consider are mass, size, and amount of heat given off.

3.2.5 Navigation and Control

(Jesse Kuhns)

Rover large-scale navigation is controlled from Earth. It is based on lander-generated stereo images supported by on-board tilt and heading sensors. Rover terminal guidance can use lander and rover stereo images, rover ranging sensors, and rover contact sensors to obtain information concerning its location and surroundings. This information is transmitted to Earth so that Earth control can determine a path the rover which is free of obstacles and/or hazards that could threaten the mobility of the rover. This navigation and control diagram is shown in Figure 3.2.5.1. The rover executes commands via on-board capabilities that involve transverse behaviors and dead reckoning. Traverse behaviors are based on range finders and contact sensors, while dead reckoning is based on gyro inclinometers and wheel revolution counters. To determine the total wheel revolution, an average count will be calculated on all wheels. This accounts for any rise of the wheels off of the ground. The rover also has three accelerometers and a gyro to determine the displacements and any angle changes of the platform that occur during rover movement. Specifically, the accelerometers will be used to measure the orientation of the platform with respect to vertical to indicate how close the vehicle is to tipping over, to measure instantaneous accelerations during traversal in support of the technology experiments and to compensate for the rate gyro readings. A Shaevitz Linear SM Series Servo Accelerometer will be used. This model was chosen based on its general use in the measurement of acceleration, guidance control systems, and vehicle ride analysis. Also, the accelerometer mass (60 grams), operating temperature (-55 to +95°C), input voltage (+/-15VDC), and overall volume (40mm³) were important characteristics. Incorporated

with the accelerometer will be a Systron Donner Quartz Rate Sensor (a gyroscope). The small size (50 x 50 x 25mm), excellent performance, low power requirements (<0.8Watts), operating temperature range (-40 to +80°C) and mass (60 grams) make this sensor adequate for the rover. These components, accelerometers and gyro, are located within the warm electronics box and will be maintained at the appropriate operating temperature with other power supplies.

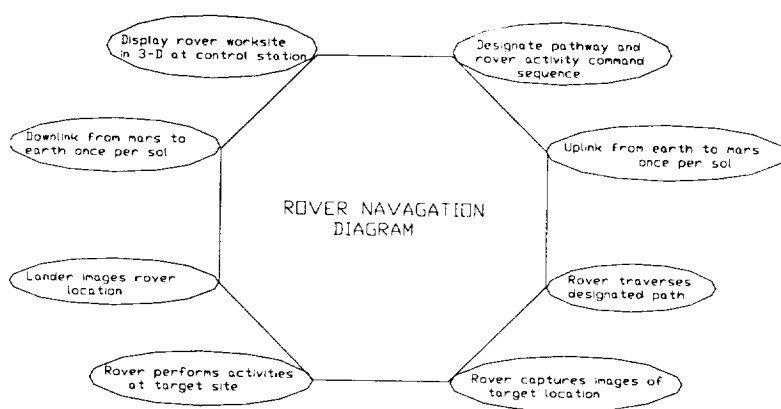


Figure 3.2.5.1 Navigation and Control Diagram

The rangefinder portion of the control system has two forward looking solid state imaging sensors (charged coupled device (CCD) cameras) and five strategically placed light stripe projectors to aid rover navigation by allowing technicians to plot a course to the next test site. The cameras are used for the detection of navigational hazards, including excessive terrain rise, excessive terrain drop-off, and obstacles. The sensors can also capture complete images to be transmitted to earth for engineering and science purposes, including showing status of the lander and viewing the terrain for path designation. The CCD cameras are manufactured by the Eastman Kodak Company. These solid state imaging sensors were chosen for their capabilities, characteristics, and success in previous applications. The Kodak KAI-0370 series image sensor has several beneficial characteristics including: high data rate (14.3MHz), photosensitive pixel range (768H x 484V), low dark current, high output sensitivity, no image lag or smear, operating temperature (-25 to +40°C), and small size (30 x 20 x 10mm). This imaging sensor has been used previously for surveillance cameras and robotic vision. Also, a Kodak KASP-305M ASIC will be included to provide a high-performance solution to the

analog signal processing requirements. A multiplexer combines the processed signals into a single output channel. It has a sampling rate of 1-5 MHz, power dissipation of 0.25 Watts per channel (3), and small signal noise. The CCD camera and ASIC will be placed in an insulated box (50 x 40 x 40mm) with a total mass of less than 150 grams.

The light stripe projectors (10mm dia. x 20mm) will have a range of 0.5 meters and weigh less than 4 grams each including mounting hardware. The stripe projectors generate vertical planes of visible stripes on the surface of obstacles and the terrain in front of the vehicle. The five projectors generate one stripe out over the right front wheel, one out over the left front wheel, one out the center of the vehicle, and two stripes which are projected diagonally out across the front of the vehicle. The CCD cameras and light stripe projectors will be placed on top of the warm electronics box. Less memory can be used by repeatedly taking, reading out, and sending complementary sections of the CCD's view. The rover uses the CCD's sequentially, powering and reading only one at time. Each CCD draws 0.4 W during exposure, and 0.8 W during readout. Each light-striper draws 0.7 W during CCD exposure. The stripers are used in pairs but can be used individually in low power situations.³⁶

3.2.6 Electronics and Instrumentation

(Jesse Kuhns)

All electronics are single point grounded and are floated above the frame with a high level of impedance ($1\text{ k}\Omega$). Most of the electronics will be encased in an electronics box. This electronics box contains all the items listed in Figure 3.2.6.1 in addition to other small components. The electronics box is also surrounded by a vacuum honeycomb wall of insulation to reduce heat loss. All other electronics, which are outside the box, will be designed to meet appropriate temperatures for successful operation. Also, all cables between the electronics box and external equipment will be pigtailed at their source. A connector panel will be provided outside the insulated opening to the electronics box; the electronics box equipment connectors will mate to the external connectors at this panel.

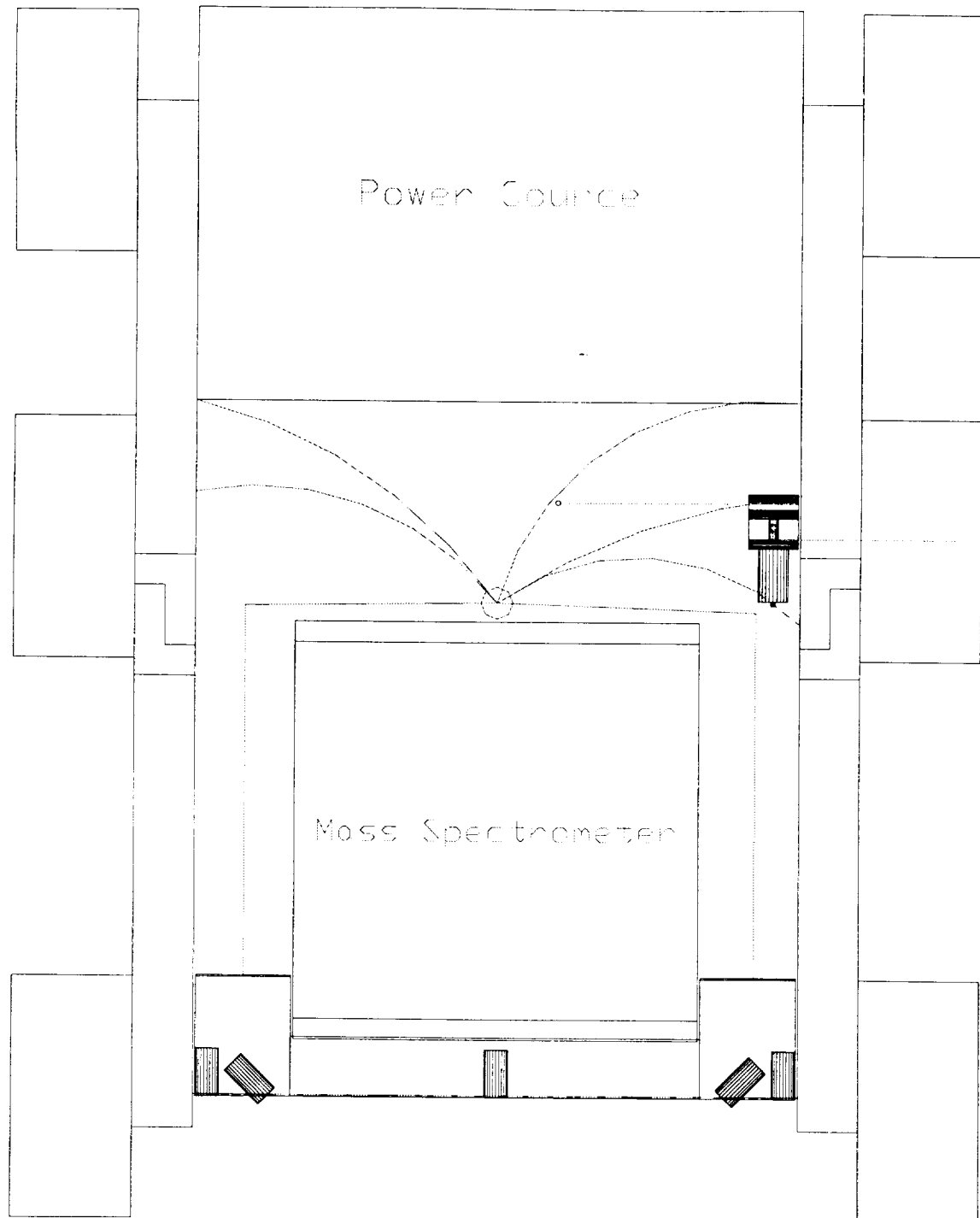


Figure 3.2.6.1: External Wiring Diagram

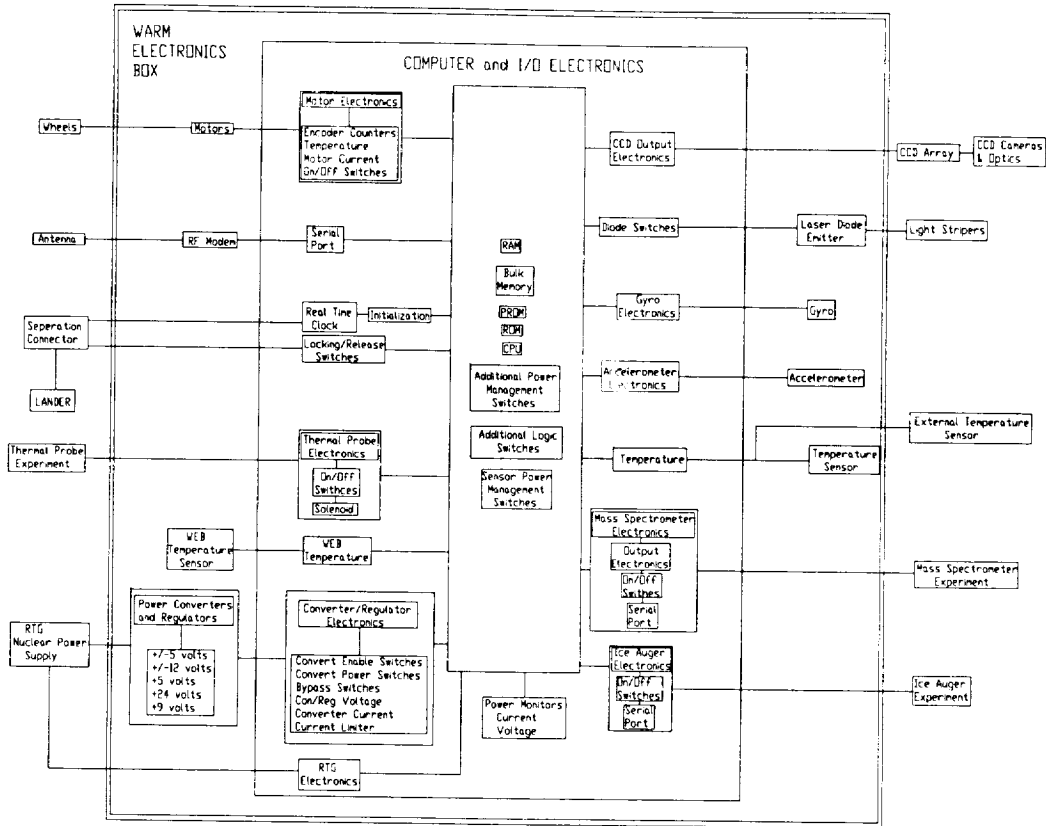


Figure 3.2.6.2 Rover Electric Functional Diagram

3.2.6.1 Central Processing Unit

The microprocessor, located in the warm electronics box, is based upon the Motorola 80C85 CPU which has been used extensively on other planetary spacecraft. It is fully flight qualified, and immune to Single Event Latchups (SELs). The 80C85 is a 100Kips, 8 bit machine with a 16 bit address space (i.e., 64Kbyte address space). Bank Switching will be used to extend the on board memory to 672 Kbytes (16Kbytes of core ROM, 16Kbytes of core RAM, 128Kbytes of Flash EEprom, and 512Kbytes of bulk RAM). The bulk RAM is for storing images and engineering data prior to transmission to Earth. The on board control code is expected to occupy approximately 60-80Kbytes of the core ROM and EEprom.³⁶

3.2.7 Communication Network

(Jesse Kuhns)

The rover has a whip antenna approximately 15cm long. The antenna is linked to the RF modem, computer, and I/O electronics in the electronics box. It is released by a latch mechanism or solenoid after being deployed from the lander. The rover/lander UHF radio communicator utilizes a Motorola R-Net Radio 9600 Modem (SLM 2 Watt Package) that is placed within the warm electronics box. This modem will require a space of 105 x 60 x 30mm, an operating temperature of -30 to +60°C, and a supply DC voltage of 10-17V. Some other benefits of this modem are: frequency range (403-416MHz), channel spacing (25kHz), data rate (9600 BPS), and a low mass (200 grams). These characteristics will allow the rover to effectively communicate with the lander at all times. As a precautionary measure, "RF link checks" are made during rover movements so that the rover does not become lost in an area where it is unable to communicate effectively with the Lander. Approximately every 30 seconds, the rover will send a signal to the lander and receive an echo. If RF contact is not made, the rover will traverse back to the last known point of effective RF contact. Also, when the antennas on both the rover and lander are deployed, successful communication can occur over 0.5 meter high obstacles. Communication from the lander to a control station on Earth may be direct or through the use of a satellite.

3.2.8 Science Experiments

3.2.8.1 Mass Spectrometer

(Susan Slater)

Red Rover will be instrumented with a near-infrared spectrometer. The near-infrared spectra will provide detailed mineral analyses which will aid in determining climatic and geological data on the polar caps of Mars. The spectrometer is currently being developed and tested at the Jet Propulsion Laboratory. It has a minimal weight of 500 grams and requires approximately 2 Watts of power. The instrument's box sits above the warm electronics box at an optimum angle, so that surrounding environment can be easily investigated. This can be seen in more detailed drawings in Appendix A.

3.2.8.2 Ice Auger/Borescope System

(Marc Richmond)

The polar ice cap is a continually changing surface due to yearly weather variations. These yearly changes are recorded in the ice cap by the stratified layers of ice. Much like the rings in the cross section of a tree, each layer of ice contains information about the environmental conditions of a certain time period. By examining these layers of ice, an environmental or climatic history can be established²³. A method used to examine this layering of the polar ice cap is an ice auger and borescope system. The auger will drill a hole into the ice to a depth of approximately 150 mm and a diameter of 10 mm, then a borescope will be deployed into this hole to record a picture of the stratified layers of ice.

The deployment mechanism for the auger and borescope system is mounted on the outside of one of the rear arms of the rover. The mechanical deployment system consists of a servo motor, an attachment to the rear arm of the rover, a two-bar linkage, and a mechanical stop. The servo motor is attached to the outside of one of the rear arms of the chassis of the rover, and the servo output must be pointing outwards toward the wheel. The opposite side of the servo motor must be flush with the inside of the rear arm. This is to eliminate any interference with the platform while the rover traverses a protrusion. The servo motor is approximately 25.4 mm in diameter and can be up to 50 mm in length. The servo is attached to the rover by a strap of metal formed around the servo housing, shaped like the capital Greek letter Omega (Ω). The permanence of this attachment is subjective. If the auger or borescope get jammed in the hole for some reason, the servo is simply detached from the rover rear arm and the auger and borescope system are left behind so the rover can continue its data collection. The two-bar linkage consists of an input bar and an output bar. The input bar of the linkage is 260 mm long. In the stored position, the servo is attached to the rearward end of the input bar. The forward end of the input bar is attached to the output bar of the linkage. This attachment is free to rotate for any angle. This joint is supported by a mechanical stop on the outside of the middle arm which supports the input bar to the linkage. This mechanical stop prevents the linkage from rotating into the middle wheel. The length of the input bar is sufficient to maintain contact with the mechanical stop for the various configurations of the rover

chassis as it traverses protrusions. In the stored position, the output bar of the linkage is connected to the input bar at the forward end and to the auger and borescope system at the rearward end. The auger and borescope system is supported, in the stored position, at the rearward end by the servo motor housing and at the forward end by the linkage input bar.

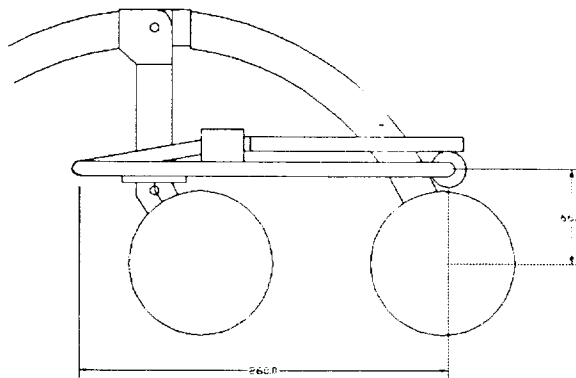


Figure 3.2.8.2.1 Auger in stored position.

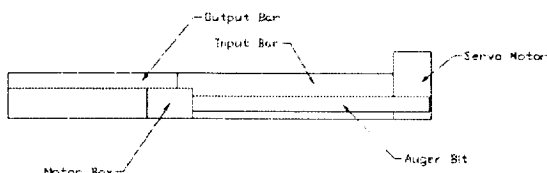


Figure 3.2.8.2.2 Auger Top View

The servo motor will rotate the linkage to deploy the auger to drill at a site behind the rover. The auger and borescope system remain supported by the servo housing and the input bar until the servo rotates the input bar a small increment past vertical. When

the auger and borescope system become unsupported by the servo motor housing, the auger and borescope system will hang freely like a two jointed pendulum. The motion of the servo motor will be very slow to minimize oscillations. The desired deployment is to simply lower the auger and borescope system vertically. This type of deployment will aid in creating a vertical hole (to achieve maximum depth and thus maximum climatic history). The sizes of the linkage components prevent the auger and borescope system from contacting the rear wheel upon deployment.

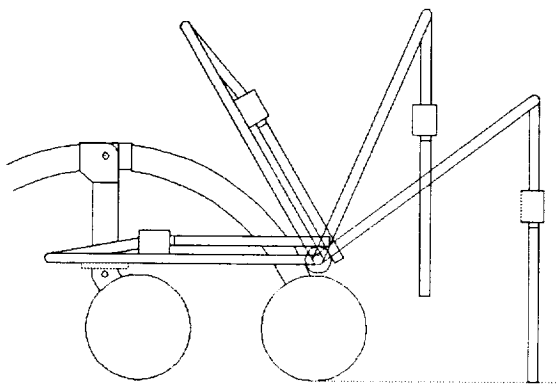


Figure 3.2.8.2.3 Auger deployment.

Once the auger and borescope system are in contact with the ground, the auger will begin to drill the hole. The auger drill bit is rotated by an electric motor. This is the same type of motor used to power the wheels. These motors provide very high RPM and not much torque. Consequently, a very slow drilling operation results. The weight of the auger and borescope system should be sufficient to create enough downward force to drill into the ice cap²³. The auger bit should have a flat bottom like a reamer to aid in creating a vertical hole. In addition, the linkage will act as a support to keep the auger and borescope system vertical. When the auger and borescope system is deployed, the servo will have feed back to determine if the auger is vertical. A simple feedback input is a mercury level switch on the auger and borescope system to determine verticality. If the servo were to continue deploying the auger and borescope system after contact with the ground, the auger and borescope system could rotate about the contact point and tilt away from the rover. Therefore, the servo must stop deploying and wait for the auger to drill a hole. This is also important because it is unknown what the surface will be like on the ice cap. This creates an ambiguity in the configuration of the rover arms and the surface

proximity for the drilling operation. Once the hole has been drilled, the electric motor rotating the auger will reverse. The servo motor must aid in lifting the auger from the hole. This upward force, transmitted through the two bar linkage and supplied by the servo motor, combined with the auger bit spinning, should create an easy, slow extraction.

Once a hole has been drilled, the borescope can take pictures of the inside of the hole. The borescope is internal to the auger bit. A 1 mm fiber optic cable is implanted down the center of the auger bit. A hole in the side of the bit will allow the borescope camera to take pictures. This hole will be covered with a transparent surface to protect the camera lens during drilling. The camera lens will be angled at 2° from the vertical. This will allow maximum visibility of the sides of the hole. The field of view of the camera lens is 70°. Allowing a bit of overlap, two pictures can be taken to fully characterize the hole. After the hole has been drilled and the auger bit removed, the auger and borescope system will be lowered back into the hole to take the two pictures. After the pictures are taken, the auger and borescope system can be removed from the hole and put back into the stored position.

3.2.8.3 Thermal Probe

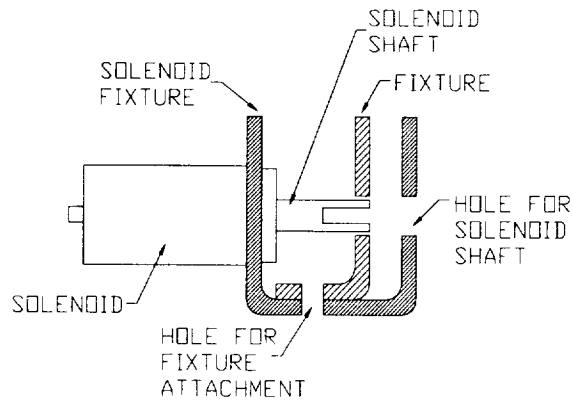
(Jeff Wiley)

Red Rover's mission consists of a special task to drag a thermoprobe away from the lander and release it at a selected destination. The thermoprobe will have a 'looped' cord attached to it, which, in turn will be connected to a solenoid unit on the rover. This tubular solenoid will be located on top of the rover's electronic box.

The communications antenna on top of the electronics box also needs to be released upon leaving the lander. The 15mm long antenna will be restrained by this same solenoid in a bent position. When the solenoid is actuated, the antenna will spring to a vertical position, ready for transmission.

The solenoid works like a piston. In its starting position, the solenoid shaft will extend beyond both fixtures (see Figure 3.2.8.4.1). The thermoprobe loop attachment will wrap around the solenoid shaft between the two fixtures, thus restraining the loop. The antenna will be in a horizontal position and will pass under the shaft, between the

fixtures. Upon an excitation voltage, the solenoid will move backward, releasing the antenna and thermoprobe loop. The antenna will then be vertical and the thermoprobe will be released.



Newark® Tubular Solenoid #24F2972

Solenoid Data

Nominal Voltage	24 V
Coil Resistance	131 Ω
Maximum Stroke	0.25 in. at 1 oz.

Figure 3.2.8.3.1 Antenna and Thermoprobe Release Solenoid.

3.3 Analysis

3.3.1 Structural

(Amy Mercer and Maria Sychay)

To ensure that the rover will withstand the applied forces, a stress analysis was performed. The rover is made out of an aluminum alloy (Al 2024 - T4). It has the following material properties:

Al (2024 - T4)

$E = 73 \text{ GPa}$	Ultimate Strength (Tensile)	- 414 MPa
$G = 27.6 \text{ GPa}$	(Shear)	- 220 MPa
$\rho = 2.77 \times 10^3 \text{ kg/m}^3$	Yield Strength (Tensile)	- 300 MPa
$\alpha = 23.2 \times 10^{-6} /^\circ\text{C}$	(Shear)	- 170 MPa

The above properties do not vary significantly within the temperature range in which the Rover will be functioning¹¹. These are the properties that are used in the stress analysis. The loading of the analysis consists of the different weights (using Earth's gravity) of the science experiments that the Rover will carrying. Table 3.3.1.1 lists the total weight of each science experiment.

Table 3.3.1.1 Total Weights

EXPERIMENT	TOTAL WEIGHT (N)
CCD (2)	1.4715
Electronic Box	39.24
Ice Auger	1.962
Power Supply	49.05
Mass Spectrometer	4.905

For the analysis the restraints are set at the point at which the wheels are attached to the body. There are four different cases of restraints. These restraints are summarized in Table 3.3.1.2a-b. In the first case the analysis simulates the Rover resting on level ground on Earth. The second case simulates the Rover with one back leg raised to its maximum height of 0.1016m. The third case simulates the Rover resting on level ground

in a Martian atmosphere. The fourth case simulates the Rover with one back leg raised to its maximum height in a Martian atmosphere. The Martian atmosphere is assumed to have a temperature of -60° C. Although the gravity of Mars is one third the gravity of Earth, the loading of the structure is kept at Earth's gravity to incorporate a factor of reliability.

Table 3.3.1.2 Boundary Conditions

Case 1 and 3

Attachment Points	x-trans	y-trans	z-trans	x-rot	y-rot	z-rot
front pair	0	0	0	0	0	free
middle pair	free	0	0	0	0	free
rear pair	free	0	0	0	0	free

(a)

Case 2 and 4

Attachment Points	x-trans	y-trans	z-trans	x-rot	y-rot	z-rot
front pair	0	0	0	0	0	free
middle pair	free	0	0	0	0	free
right rear	free	0	0	0	0	free
left rear	free	0.1016m	0	0	0	free

(b)

Three different cross-sections are used in the design of the Rover. The curved members have a square cross-section with a width of 0.0254 m and wall thickness of 0.003816 m. The straight members have a square cross-section with a width of 0.0254 m and a circular hole of 0.0051 m diameter. The cantilever beams are solid circular beams with a diameter of 0.0127 m.

A finite element analysis was performed to calculate the stresses within the structure. Table 3.3.1.3a-d shows the resulting stresses for the four different cases. The stresses given are for the beam members and the platform.

Table 3.3.1.3a Case 1

Beams	Maximum Stresses (MPa)
Von Mises	0.797
Axial	-0.058
Shear (y-dir.)	0.0187
Platform	
Von Mises	0.610
Maximum Principle	-0.456
Shear	0.346

The maximum Von Mises stress occurs at the point of attachment of the platform for both the beams and the platform.

Table 3.3.1.3b Case 2

Beams	Maximum Stresses (MPa)
Von Mises	1.26
Axial	-0.00736
Shear (y-dir.)	0.00358
Bending (y-dir)	0.333
Bending (z-dir)	1.26
Platform	
Von Mises	0.779
Maximum Principle	-0.433
Shear	0.45

The maximum Von Mises stress occurs at the attachment point of the cantilever to the curved beam member. This is also the point of maximum bending in the z-direction. The maximum stresses in the platform occur at the hinge point on the right side of the Rover.

Table 3.3.1.3c Case 3

Beams	Maximum Stresses (MPa)
Von Mises	58.4
Axial	-30.2
Shear (y-dir.)	6.44
Bending (y-dir)	28.2
Bending (z-dir)	12.4
Platform	
Von Mises	6.84
Maximum Principle	6.64
Shear	3.51

The maximum Von Mises stress occurs at the bottom of the cant beam. This is the point of maximum bending in the y-direction. The maximum stresses in the platform occur at the hinge points.

Table 3.3.1.3d Case 4

Beams	Maximum Stresses (MPa)
Von Mises	58.5
Axial	-30.2
Shear (y-dir.)	6.44
Bending (y-dir)	28.2
Bending (z-dir)	12.6
Platform	
Von Mises	6.97
Maximum Principle	6.65
Shear	3.62

The maximum Von Mises stress occurs at the bottom of the cant beams. This is also the point of maximum bending in the y-direction. The maximum stresses in the platform occur at the hinge points.

The shear stresses are relatively small in the beams for all cases. The decrease in temperature for Cases 3 and 4 results in significant increases in stresses. This is apparent when comparing Cases 1 and 3. The Von Mises stress in the beams increase from 0.797 MPa to 58.4 MPa. Likewise the Von Mises stress in the platform increases from 0.610 MPa to 6.84 MPa.

The maximum displacements in the x and y directions for Cases 1 and 3 are given in Table 3.1.4. For both cases, the maximum displacement in the y-direction occurred at the front end of the platform. For Case 1 the maximum displacement in the x-direction occurred in the rearward direction at the bottom of the cant beam. For Case 3 the maximum displacement in the x-direction occurred in the forward direction at the rear end of the platform. The x-direction displacements for Case 3 for the bottom back curved beam and the bottom of the cant beam are 1.57×10^{-4} m and 0.7×10^{-4} m in the forward direction, respectively. The change in direction of the x-direction displacement is due the decrease in temperature. Since the front attachment points are pinned to avoid singularities in the analysis, the structure contracts, pulling the structure forward.

Table 3.3.1.4

Case	x-dir (m)	y-dir (m)
1	2.03×10^{-5}	-4.09×10^{-5}
3	-1.74×10^{-4}	-1.34×10^{-4}

One final analysis was performed on the structure. This is to simulate a 5G loading during take-off. The structure will be mounted vertically in the Lander during take-off. Therefore the loading due to gravity will be in the positive x-direction. The restraints are modified so that all six wheel attachments are fixed. Table 3.3.1.5a-b summarizes stress and displacement results. The maximum Von Mises stress in the beam occurs at the bottom of the cant beams. The maximum Von Mises stress for the platform occurs directly fore and aft of the hinge points. The maximum displacement in the y-direction occurs at the front of the platform. The maximum displacement in the x-direction occurs at the hinge point.

Table 3.3.1.5a Maximum Stresses

Beams	Maximum Stress (MPa)
Von Mises	2.57
Axial	-0.195
Shear (y-dir)	0.107
Bending (y-dir)	0.442
Bending (z-dir)	-2.38
Platform	
Von Mises	0.188
Maximum Principle	0.192
Shear	0.0959

Table 3.3.1.5b Maximum Displacements

Maximum x-dir displacement (m)	3.47×10^{-6}
Maximum y-dir displacement (m)	3.12×10^{-6}

The yield stress of the aluminum alloy is 300MPa in tension and 170 MPa in shear. For all cases, both the maximum Von Mises and shear stresses are well beneath these values. This analysis shows that the structural integrity of the model will not be compromised during this mission.

3.3.2 Thermal

(Susan Slater)

Temperature fluctuations in the Martian environment can be very drastic with minimum temperatures at -120°C in the dark to +40°C in the sunlight²⁵. This temperature differential can have many adverse effects on materials. One of the major considerations for choosing a material is its behavior in a low temperature environment and its reaction to large temperature fluctuations. Aluminum and its alloys have been chosen for this among many other reasons (such as strength and weight). Aluminum has a low coefficient of thermal expansion when compared to other structural materials ($\alpha = 23.2 \times 10^{-6}/^{\circ}\text{C}$) of the same or less strength. To determine the maximum thermal strain that occurs as a result of the temperature fluctuations in the Martian environment, a preliminary calculation was made under the assumption that the rover was manufactured within the temperature range -120°C to +40°C. Using this, the maximum thermal potential is 160°C given $\epsilon_{\text{th}} = \alpha\Delta T = 0.0037$. Therefore, the length increase or decrease of an aluminum rod is approximately 0.37%. For a rover of the proposed dimensions, this expansion or contraction is negligible.

Another area of thermal concern is the amount of excess heat resulting from the on-board power source. If great enough, the heat given off can soften or melt the polar cap surface causing concern for the traction, mobility, and operation of the rover. A worst case calculation was performed under the following assumptions:

- 1) The efficiency of the power source was 5%, resulting in the excess, 95%, given off as heat.
- 2) It is assumed that approximately 20% of this excess heat is applied directly to the Martian surface.
- 3) The initial temperature of the ice surface is -40°C and the solar flux, which is assumed to be 0.03 W/m², is negligible.
- 4) Martian surface is composed of water ice which will melt at 0°C²³. Because the atmospheric pressure of Mars is approximately one percent that of Earth (0.01 atm), the melting point is higher than that on Earth, but it is still relatively close to 0°C. (The actual melting point is less than 0.01°C).

The amount of energy that it takes to melt ice when it is at -40°C is composed of two portions. The amount to raise the temperature of the ice to its melting point and the energy needed for the phase change. Per unit mass:

$$\left(\frac{Q}{m}\right) = c_p \Delta T + H_{\text{fusion}} = 8.19 \times 10^5 \text{ J/kg} \quad (3.3.2.1)$$

The area or region that will be affected by the power source is assumed to be the surrounding area of 1 m² with a depth of 0.03 m. The heat needed to melt this amount of ice is 2.26 x 10⁷ J.

The rover is planned to be stationary for a maximum of one Martian day (8.86x10⁴ seconds) during the summer. Then it is to traverse to another location. In one day, the power supply can generate energy at a rate of P Watts. Typically, 95% of this energy is given off as heat and the other 5% is for the required power dedicated to the operation of the rover.

For energy at a generation rate of T, the amount of heat that reaches the ice is 20% of 95% of P within the given time frame. This heat must be less than that required to melt the ice, i.e. 2.26 x 10⁷ J.

$$2.26 \times 10^7 \text{ J} \geq (.20)(.95)(T)(8.86 \times 10^4 \text{ seconds})$$

$$T \leq 1.34 \text{ kW}$$

The total output energy dedicated to the operation of the rover with only a 5% efficiency is:

$$P = 0.05 * T = 67.1 \text{ Watts}$$

This energy is well within the required energy limits of the rover, therefore, melting ice should not be a problem and is independent of the power source that is used. Using this information, a nuclear source was chosen so that at least 8 Watts could be supplied at any one time. This is the maximum amount of power needed during the course of action of the rover. To determine this maximum power and to minimize power usage at all times, a power sequencing scenario was developed. This is displayed in Tables 3.3.2.1 and 3.3.2.2.

Table 3.3.2.1 Power Sequencing

PROCEDURE	POWER
Engine Start -up #1	3.4
Engine Start-up #2	3.4
Engine start-up #3	3.4
Engine start-up #4	3.4
Engine start-up #5	3.4
Engine start-up #6	3.4
Traversing	
Drive Motors	3.99
Lasers	1.4
Accelerometer	0.15
Gyros	0.8
TOTAL	6.34
Condensing Traverse Data	
CCD imaging of next traverse path(s)	0.4
(time == 1 min/picture)	
Condensing CCD image data	0.8
(time == 2 min/picture)	
Transmit data to lander	
Lander needs to transmit CCD	4.4
image pictures	
Perform Mass Spectrometer Exp.	2
Perform Ice Auger Exp.	1.5
Transmit Data to Lander	4.4

Table 3.3.2.2 Power Sequencing/Timeline

CPU ongoing power ==1.5 Watts	Power	Time	Computer Memory Required
Engine Start -up #1	3.4	NA	minimal
Engine Start-up #2	3.4	NA	minimal
Engine start-up #3	3.4	NA	minimal
Engine start-up #4	3.4	NA	minimal
Engine start-up #5	3.4	NA	minimal
Engine start-up #6	3.4	NA	minimal
Traversing			
Drive Motors	3.99		
Lasers	1.4		
Accelerometer	0.15		
Gyros	0.8		
TOTAL	6.34	20 min	150 Kbytes
Engine Shut-off	-	NA	minimal
CCD imaging of next traverse path(s) (time == 1 min/picture)	0.4	4 min	400 Kbytes
Condensing CCD image data (time == 2 min/picture)	0.8	10 min	approx. 100 Kbytes/pic
Transmit data to lander			
Lander needs to transmit CCD image pictures	4.4	25 min	
Perform Mass Spectrometer Exp.	2		400 Kbytes
Transmit Data to Lander	4.4	10 min	
Perform Ice Auger Exp.	1.5	60 min	350 Kbytes
Transmit Data to Lander	4.4	10 min	
This timeline will be performed 3 times per Martian Day.			

3.3.3 Traction and Mobility

(Shawn Newman)

The configuration of the Red Rover must ensure a desirable weight distribution over the wheels and a low position for the center of gravity. It is also beneficial to have the platform relatively high off of the ground. All of these characteristics enable greater mobility over various types of terrain.

The design of Red Rover's wheel layout was based to address the following items: first, it must give Red Rover the ability to cross depressions; second, it must give Red Rover dynamic stability; finally, the wheel layout must provide Red Rover maneuverability over various types of terrain since there is so little known about the Mars Polar Region terrain at the present time.

Red Rover's wheel layout is a variation of the 1-1-1 wheel alignment. The 1-1-1 wheel alignment consists of three wheels, one wheel under the middle of the vehicle and the two remaining wheels equally spaced from the middle wheel. This classic 1-1-1 wheel design, however, could not be used with the pivoting system designed for Red Rover. It was noted during preliminary analysis that if the wheel rotated up after going over an obstacle, there would not be a moment large enough to rotate it back to the ground. In order to give Red Rover dynamic stability the middle wheel, instead of being supported by a vertical beam coming straight down from the rotation pin, would be moved 32.8 mm aft of the rotation pin. Using this design, sufficient moment would always exist to rotate the front wheels back to the ground throughout Red Rover's designed operating conditions.

There are two types of clearance failure modes which must be addressed during preliminary design: (1) hang-up failure (HUF), when the bottom of the vehicle interferes with the obstacle, and (2) Nose-in Failure (NIF), when the front end of the vehicle interferes with the obstacle. Red Rover's high geometric profile, with a ground clearance and tire diameter of 101.6 mm, and the 1-1-1 wheel layout, greatly reduces the possibility of HUF. Obstacle types that could cause HUF for Red Rover are short steep objects with slopes greater than 47.5° relative to the horizontal (See Figure 3.3.1). In order to prevent Red Rover from experiencing NIF, the front wheels are designed to be in front of the platform. Similarly the rear wheels are extended behind the platform to keep the aft end of the platform from interfering with the ground.

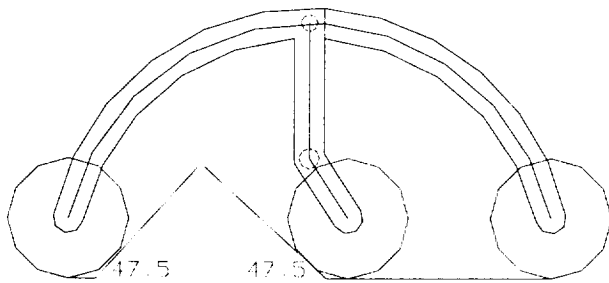


Figure 3.3.3.1 Maximum HUF Angle

The parameters that Red Rover will use to tell whether or not it will be able to climb an obstacle are the obstacle height(h_s), Red Rover velocity (V), wheel-rolling surface contact length ($\sum l_k$), coefficient accounting for inertia of wheels (δ), and the angle at which the wheel meets the obstacle (β). The velocity Red Rover needs in order to cross an obstacle is found by equating the kinetic energy of Red Rover and the energy spent on overcoming the resistance to motion. This velocity is found from the equation;

$$V = (2g[h_s + (\sum l_k)\tan\beta]/[\delta + \sin^2\beta])^{1/2} \quad 21 \quad (3.3.3.1)$$

The maximum transverse angle (Θ_t), depicted in Figure 3.3.3.2, that Red Rover can be tilted with respect to horizontal without tipping over is 71.6° due to body geometry. The maximum transverse slope that Red Rover can negotiate on Martian ice (Coefficient of Friction = 0.15) without sliding down the slope is 8.53° .

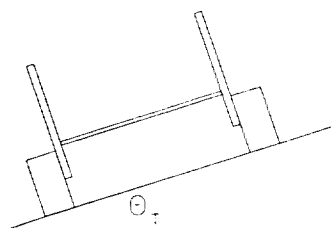


Figure 3.3.3.2 Maximum Transverse Angle, Θ_t

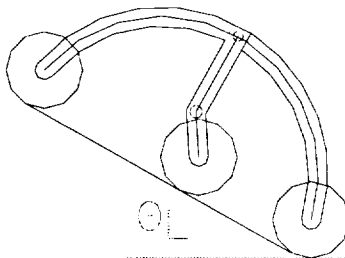


Figure 3.3.3.3 Maximum Longitudinal Angle, Θ_l

The maximum longitudinal angle (Θ_l), depicted in Figure 3.3.3.3, which Red Rover can negotiate without tipping over is 51.3° also due to body geometry. The maximum incline that Red Rover can ascend with all six motors generating maximum torque of $0.3 \text{ N} \cdot \text{m}$ is dependent on the coefficient of traction between the tire and the rolling plane. The coefficient of traction determines the amount of reaction force the rolling surface can generate on the wheels due to the torque of the motors. There is always less force generated from the rolling surface to the wheels than the force the torque of the motor generates at the outer radius of the wheel. The amount of force lost depends on the type of surface being negotiated. Since the characteristics of the polar surface on Mars are unknown, the maximum incline Red Rover can negotiate was found for varying percentages of surface reactions, depicted in Table 3.3.3.1

Table 3.3.3.1 Maximum Incline

Coefficient of Traction	Θ_l max. (deg)*
0.85	63.5°
0.80	55.0°
0.75	46.5°
0.65	38.5°
0.60	33.5°
0.50	25.0°
0.25	8.0°

*note: Since Red Rover is moving at a low speed and the wind velocity on the polar ice caps are unknown, aerodynamic drag was neglected for calculation of maximum slope.

$$\text{Aerodynamic Drag} = (1/2 * \rho * A * (V + V_w)^2). 21 \quad (3.3.3.2)$$

ρ = Air Density

V = Red Rover Velocity

A = Frontal Area

V_w = Wind Velocity

3.3.4 Motor Selection

(Jeff Wiley)

Selection of the drive motors came after a simple analysis of forces, masses, and the torque required on the designated surface. This analysis is shown below.

Total mass of rover = 20 kg

Mass concentrated/wheel = 20 kg/6 wheels = 3.33 kg/wheel

Radius of wheel = 51mm = 0.051 meters

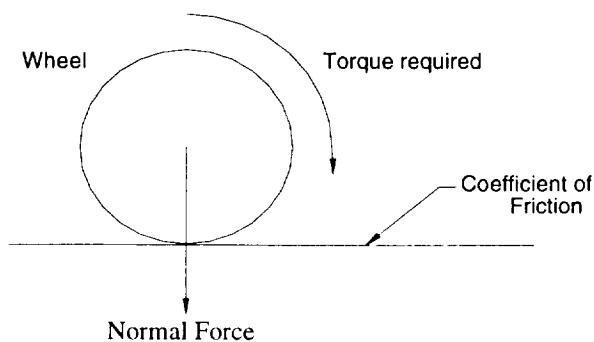
Coefficient of friction on ice = 0.15

Gravity on Mars = 1/3 of earth's gravity = 3.27 kg*m/s^2

Normal force on ground/wheel = 10.89 N

Force required to turn wheel = $\mu N = 0.15 * 10.89 \text{ N} = 1.63 \text{ N}$

Torque required to turn wheel = $F * \text{radius} = 1.63 \text{ N} * 0.051 \text{ meters} = 0.083 \text{ N*m}$



To attain a high torque with such small DC motors, the use of planetary gears was incorporated into the design of the rover drive system. The following motor and gearhead were selected:

Table 3.3.3.2 Motor Specifications

<u>Maxon® Motor and Gearhead Specifications for Red Rover Drivetrain</u>	
Motor Data	
Assigned power rating	1.6 W
Nominal voltage	3.00 V
Terminal resistance	2.66 Ohm
Max. permissible speed	11000 rpm
Max. continuous current	500 mA
Planetary Gearhead Data	
No. of stages	5
Reduction Ratio	1620.5 : 1
Max. continuous torque	0.3 N*m
Assembled Data	
Overall length	51.7 mm
Weight	55 grams

The torque required to turn Red Rover's wheels is 0.083 N*m. It can clearly be seen that the selected motor provides 0.3 N*m of torque, which is more than adequate and will compensate if more torque is needed.

3.3.5 Rover Mass and Power Budget

(Susan Slater)

Table 3.3.5.1 Rover and Mass Budget

	Qty.	Mass (g) (each)	Total Mass (g)	Power (W) (Max/Min)
Control/Navigation				
CCD Assembly	2	100	200	0.8/0.4
CPU-I/O-Card	1	600	600	1.5
Lasers	5	6	30	1.4
Accelerometer	3	60	60	0.2
Gyro	1	60	60	0.8
Telecommunications				
RF Modem	1	200	200	1.1/0.3
Antenna	1	50	50	
Power Equipment				
5V, 10W	1	95	95	
24V, 10W	1	95	95	
+/-12V, 2.5W	1	26	26	
9V, 2.5W	1	26	26	
+/-5V, 2.5W	1	26	26	
Board & Misc Comp	1	50	50	
Power Source (approx.)	1	2500	2500	
Mechanical				
Motor Drives	6	55	330	5.0/2.0
Platform	1	650	650	
Frame	1	700	700	
Cabling	1	250	250	
Antenna Launch	1	70	70	
Solenoid				
Antenna Deploy Device	1	50	50	
Antenna Structure	1	100	100	
Wheels	6	700	4200	
Thermal				
Electronics Box	1	4000	4000	
RHU's	2	55	110	
Science Packages				
Mass Spectrometer	1	500	500	2
Ice Auger/Borescope	1	200	200	1.5
Total Rover Mass (g)			15,178	

3.4 NOMENCLATURE

CCD	Charged Coupled Device
c_p	Coefficient of Pressure
F	Force
H_{fusion}	Heat of Fusion
h_s	Height of Obstacle
HUF	Hang-up Failure
m	Mass
N	Normal Force
NIF	Nose-in Failure
P	Power
Q	Heat
T	Temperature
V	Velocity
α	Coefficient of Thermal Expansion
β	Angle which a wheel meets an obstacle
δ	Inertial Coefficient
ΔT	Change in Temperature
Σl_k	Wheel-rolling surface contact length
μ	Coefficient of Friction
θ_t	Maximum Transverse Angle
θ_l	Maximum Longitudinal Angle

3.5 LIST OF FIGURES

3.1.1	Rover Pathway	2
3.2.1.1	Basic Configuration	4
3.2.1.2a	Incline Angle and Cant Angle	5
3.2.1.2b	Moment Analysis of Cant Angle	5
3.2.1.3a	Front Wheel Scenario	6
3.2.1.3b	Center Wheel Scenario	6
3.2.1.3c	Rear Wheel Scenario	7
3.2.2.1	Cross-Sectional View of Wheel Assembly	8
3.2.5.1	Navigation and Control Diagram	12
3.2.6.1	External Wiring Diagram	14
3.2.6.2	Rover Electric Functional Diagram	15
3.2.8.2.1	Auger In Stored Position	18
3.2.8.2.2	Auger Top View	18
3.2.8.2.3	Auger Deployment	19
3.2.8.3.1	Antenna and Thermoprobe Release Solenoid	21
3.3.3.1	Maximum HUF Angle	33
3.3.3.2	Maximum Transverse Angle	33
3.3.3.3	Maximum Longitudinal Angle	34
3.7.1-11	Scale Part Diagrams	44
3.7.12	Red Rover 3-D View	56

3.6 REFERENCES

- 1 Ageikin, Ia.S., Off-the-Road Wheeled and Combined Traction Devices, Amerind Publishing Co. Ovt. Ltd., New Delhi 1987.
- 2 Ageikin, Ia.S., Off-the-Road Mobility of Automobiles, Amerind Publishing Co. Ovt. Ltd., New Delhi 1987.
- 3 ASTM Special Publication 470, Manual on the Use of Thermocouples in Temperature Measurement, ASTM, 1970.
- 4 ASTM Special Publication 556, Fatigue and Fracture Toughness-Cryogenic Behavior, ASTM, 1973
- 5 Baker, Victor R., The Channels of Mars, University of Texas Press, Austin, Texas, 1982.
- 6 Beer, Ferdinand P., Vector Mechanics for Engineers, McGraw Hill Inc, USA, 1988.
- 7 Bekker M.G., Introduction to Terrain-Vehicle Systems, The University of Michigan Press, Ann Arbor 1969.
- 8 Boer, Karl W., Advances in Solar Energy, American Solar Energy Society, Inc., Boulder, Colorado, Vol. 7, 1992.
- 9 Brock, John E., Stresses in Curved Beams, Machine Design, 88-91, March 4, 1971.
- 10 Chang, Raymond, Chemistry Second Edition, Random House, 1981.
- 11 Clark, Alan E. et. al., Material at Low Temperatures, American Society for Metals, New York, 1983.
- 12 Cook, William, The Invasion of Mars, US News and World Report, 50-57, 1993
- 13 Eastman Kodak Company
- 14 Garg, H.P., Advances in Solar Energy Technology, D. Reidel Publishing Co., Dordrecht, Holland, Vol. 3, 1987.
- 15 Grabe, Ron, Traction Control, Motor Trend 1990, Jul p. 81-84.
- 16 Holman, J.P., Heat Transfer Seventh Edition, McGraw-Hill, 1990.
- 17 Johnson, Ralph Winthrop, Approximating Shear-center Location to Get Bending Without Twisting, Machine Design, Nov. 11, 1965
- 18 Kaplan, David, Environment of Mars, NASA Technical Memorandum 100470, 1988.

- 19 Kreider, Ian, Stine, William, and Wanatanabe, Koichi, Solar Engineering 1992, The American Society of Mechanical Engineers, New York, 1992.
- 20 Layman, W.E. and Matijevic, J.R., Micro-Rover Technical Baseline: Highlights and Design Philosophy, JPL Interoffice Memorandum 352:92:64:WEL Rev N.
- 21 Lucas, G.G., Road Vehicle Performance, Gordan and Breach Science Publications, 1986.
- 22 Michaux, C.M., Handbook of the Physical Properties of Mars, NASA 1967.
- 23 Motorola Inc.
- 24 Mutch, Thomas A., et.al., The Geology of Mars, Princeton University Press, Princeton, New Jersey, 1976.
- 25 Paige, David A., The Mars Polar Pathfinder, Discovery Program Workshop, 1992.
- 26 Pathfinder: Design, Implementation, Cost Review, Industry Copy, Vol 1&2, Jet Propulsion Laboratory.
- 27 Pivirotto, Donna Shirley, Finding a Better Path to Mars, Aerospace America, 12-15, Sept. 1993.
- 28 Popov, Egor P., Engineering Mechanics of Solids, Prentice Hall, Englewood Cliffs, New Jersey, 1990.
- 29 Reynolds, Kim, Rocky IV, Road and Track, 44, 1993.
- 30 Sack, Ronald L., Matrix Structural Analysis, PWS-KENT Publishing Co., Boston, 1989.
- 31 Schaevitz Inc.
- 32 Sherwood, Brent, Mars Vehicle Design: The Fourth Generation, Aerospace America, 16-19, Sept. 1993.
- 33 Smith, A. E., Mars, The Next Step, IOP Publishing Ltd., New York, 1989.
- 34 Smith, G., Storage Batteries Third Edition, Pitman Publishing Limited, Boston, 1980.
- 35 Space Resource News, 2, 1-4, 1993.
- 36 Stone, Henry W., Mechanical System Components, Allyn and Bacon Publishing, Boston, 1989.
- 37 Systrondonner.
- 38 Thorpe, James F., Mechanical System Components, Allyn and Bacon Publishing, Boston, 1989.
- 39 Wang, Ting-San, Shear Stresses in Curved Beams, Machine Design, 175-178, Dec. 7, 1967.

- 40 Wells, R.A., Geophysics of Mars, Elsevier Scientific Publishing Company, Amsterdam, 1979.
- 41 Zubrin, Robert, et.al., A New Map for Mars, Aerospace America, 20-24, Sept. 1993.

SCALE DRAWINGS

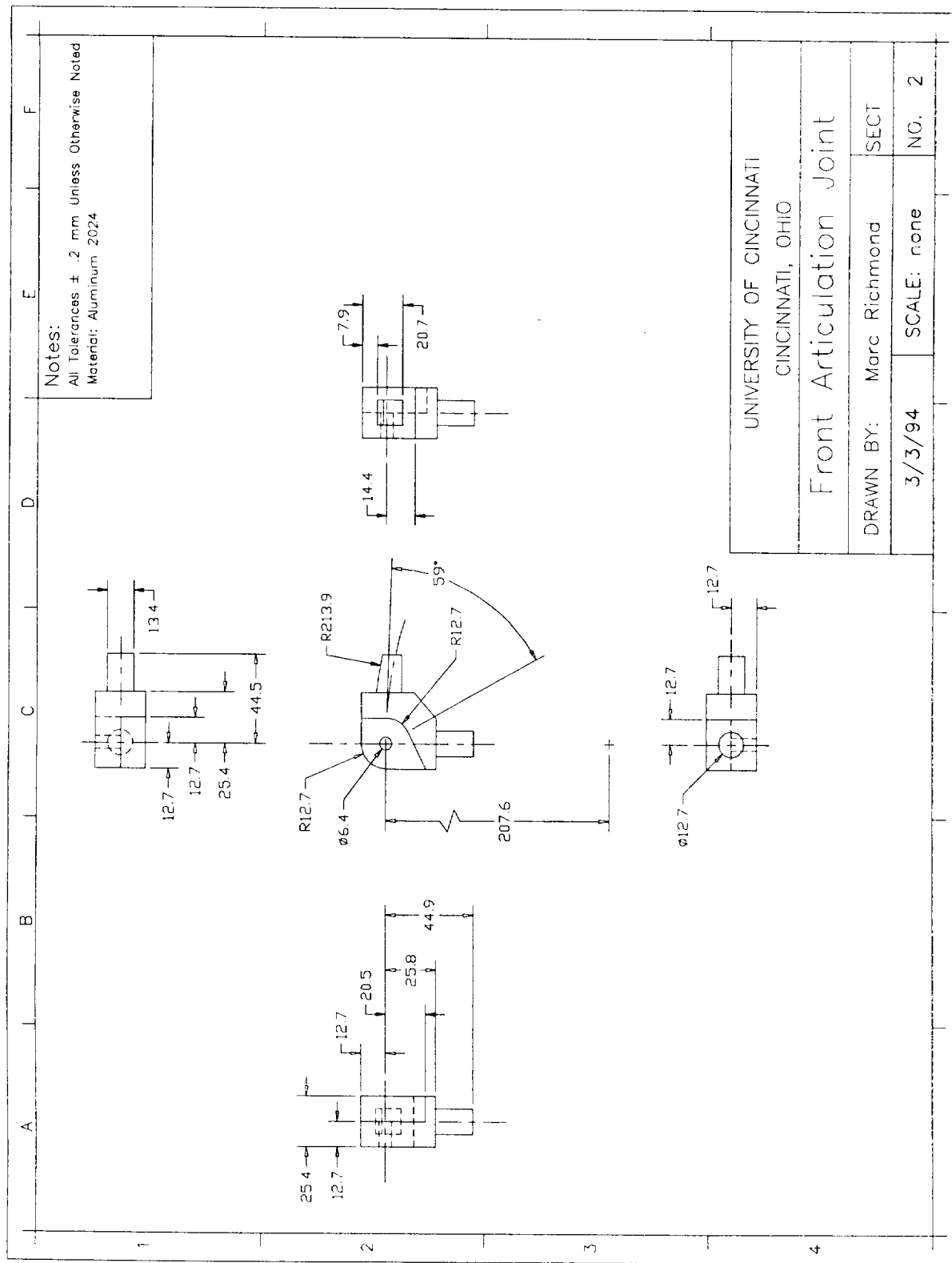


Figure 3.7.1

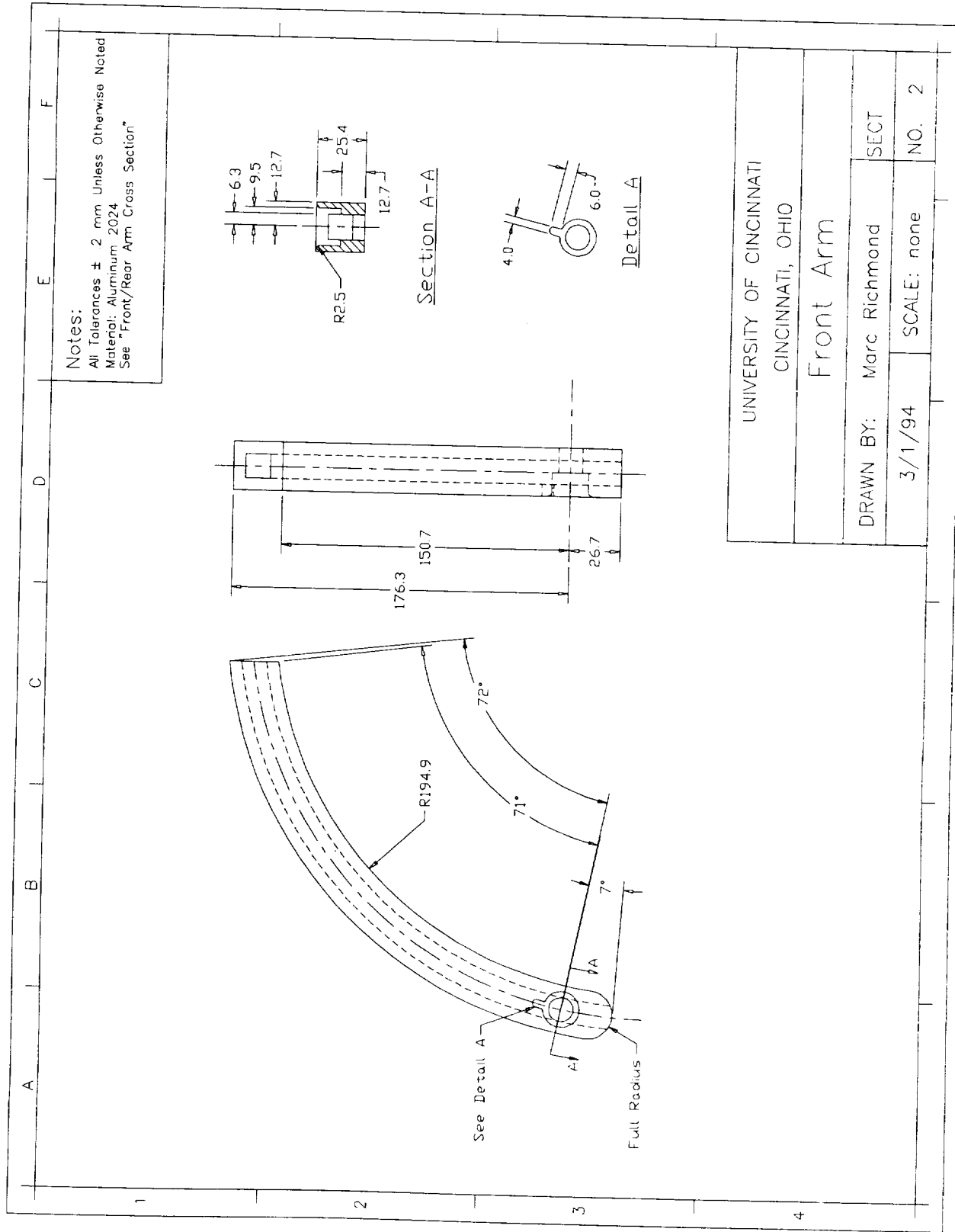


Figure 3.7.2

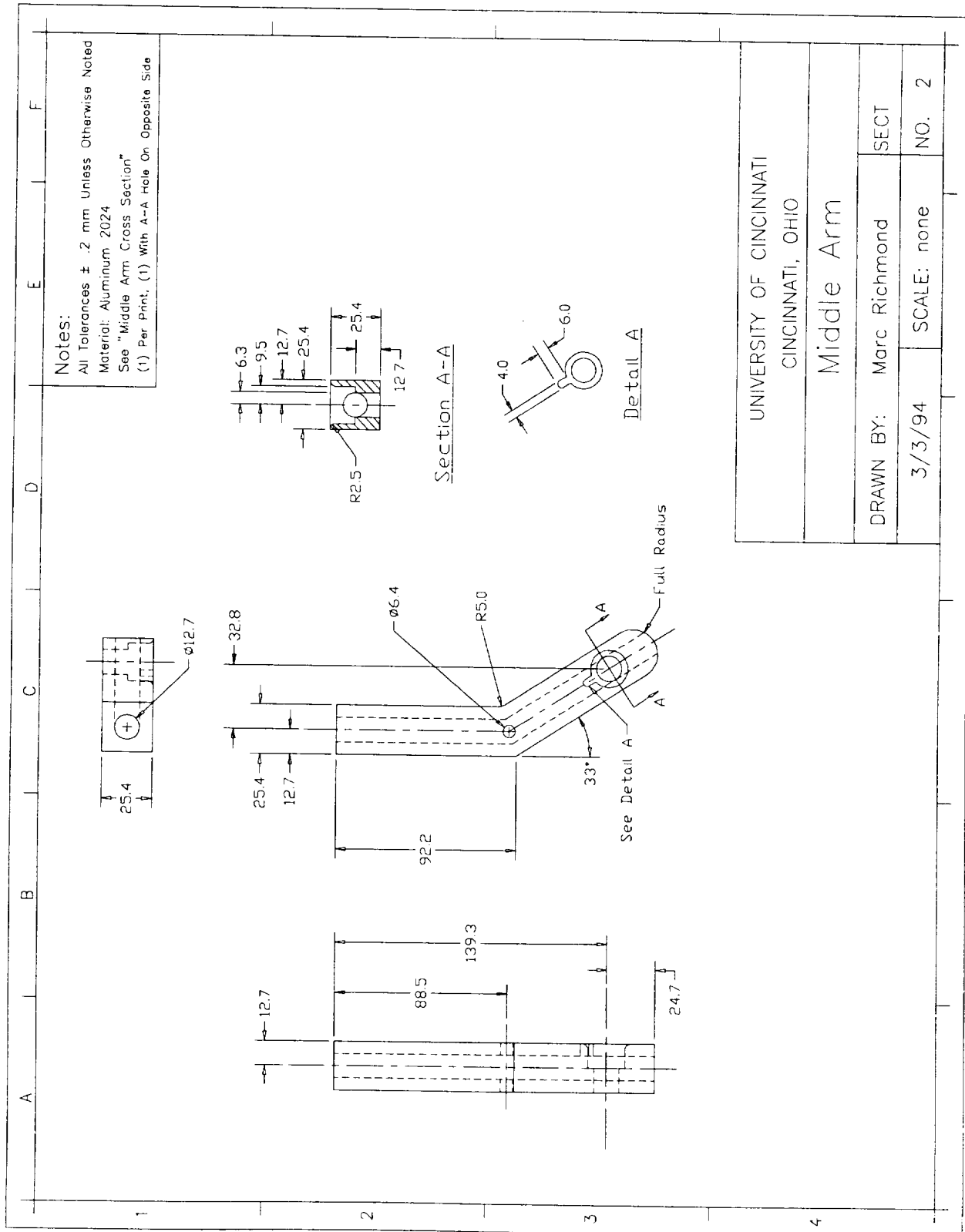


Figure 3.7.3

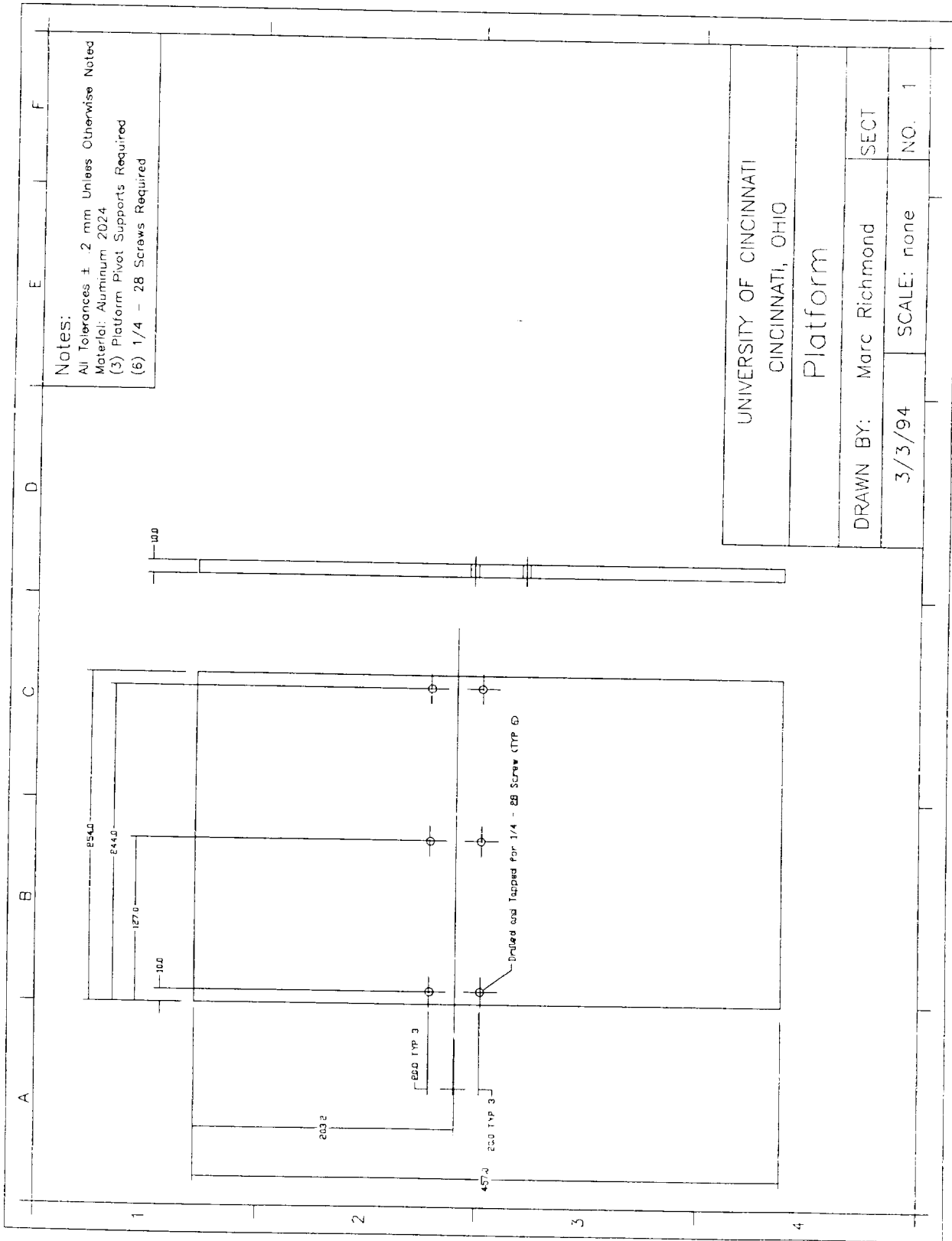


Figure 3.7.4

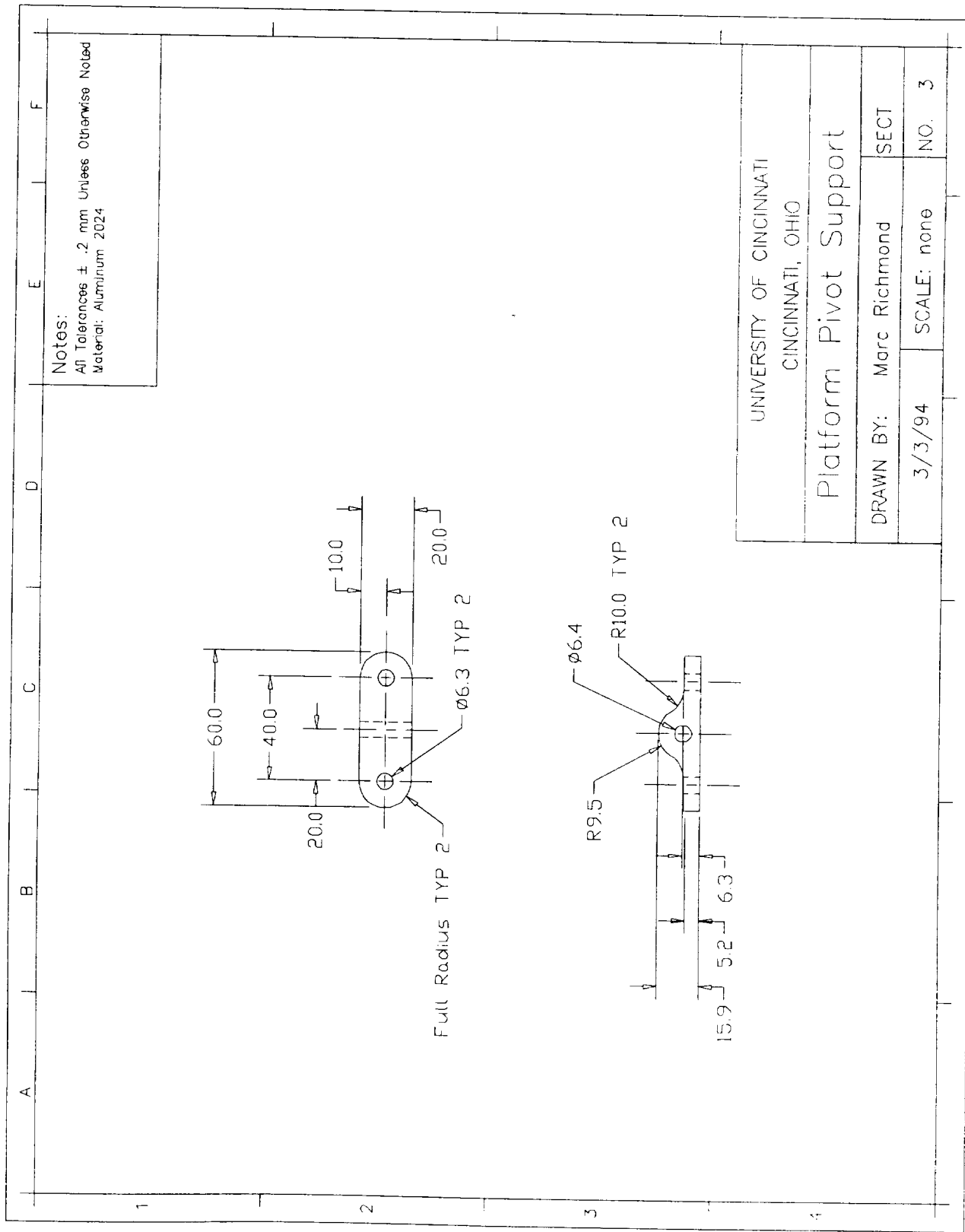


Figure 3.7.5

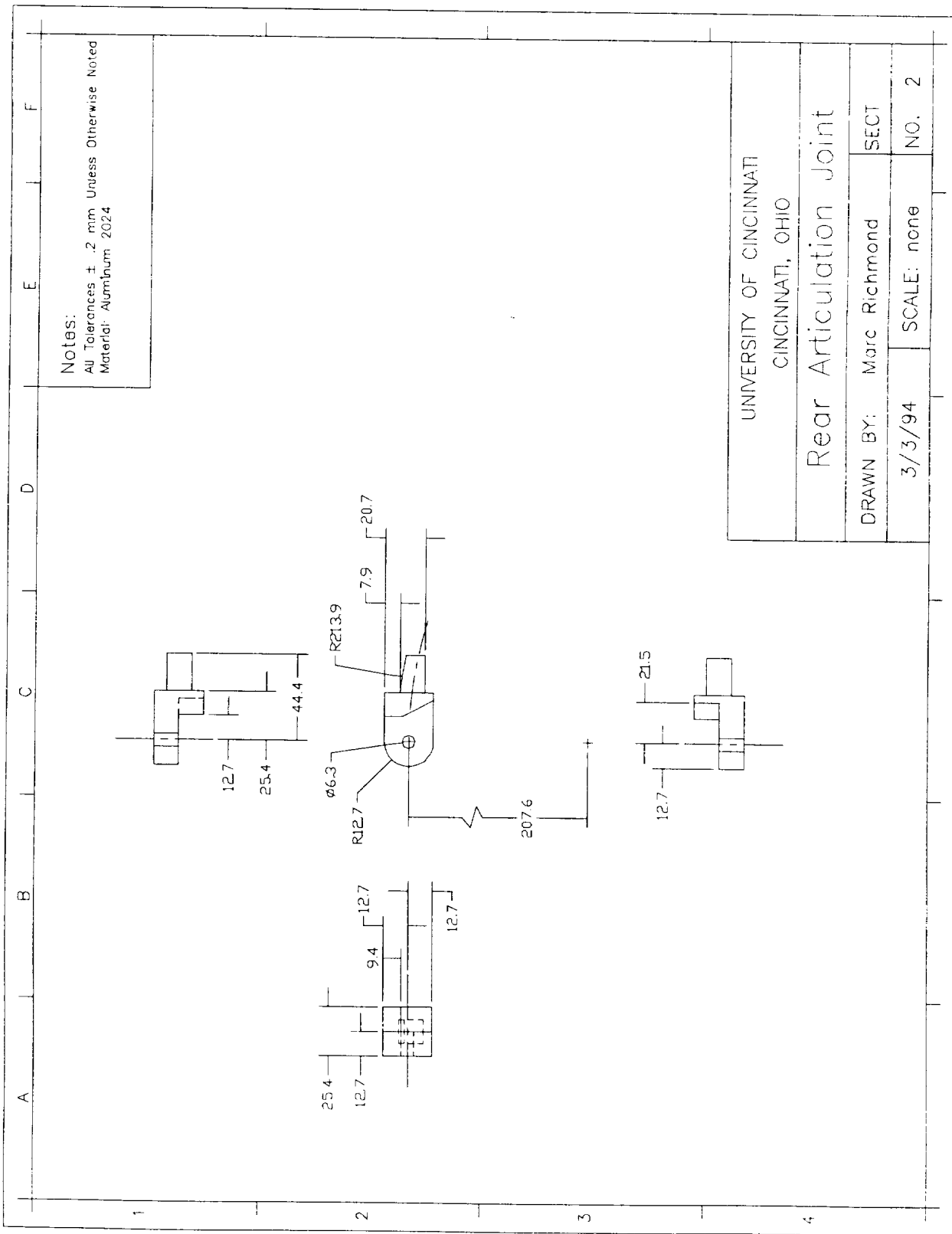


Figure 3.7.6

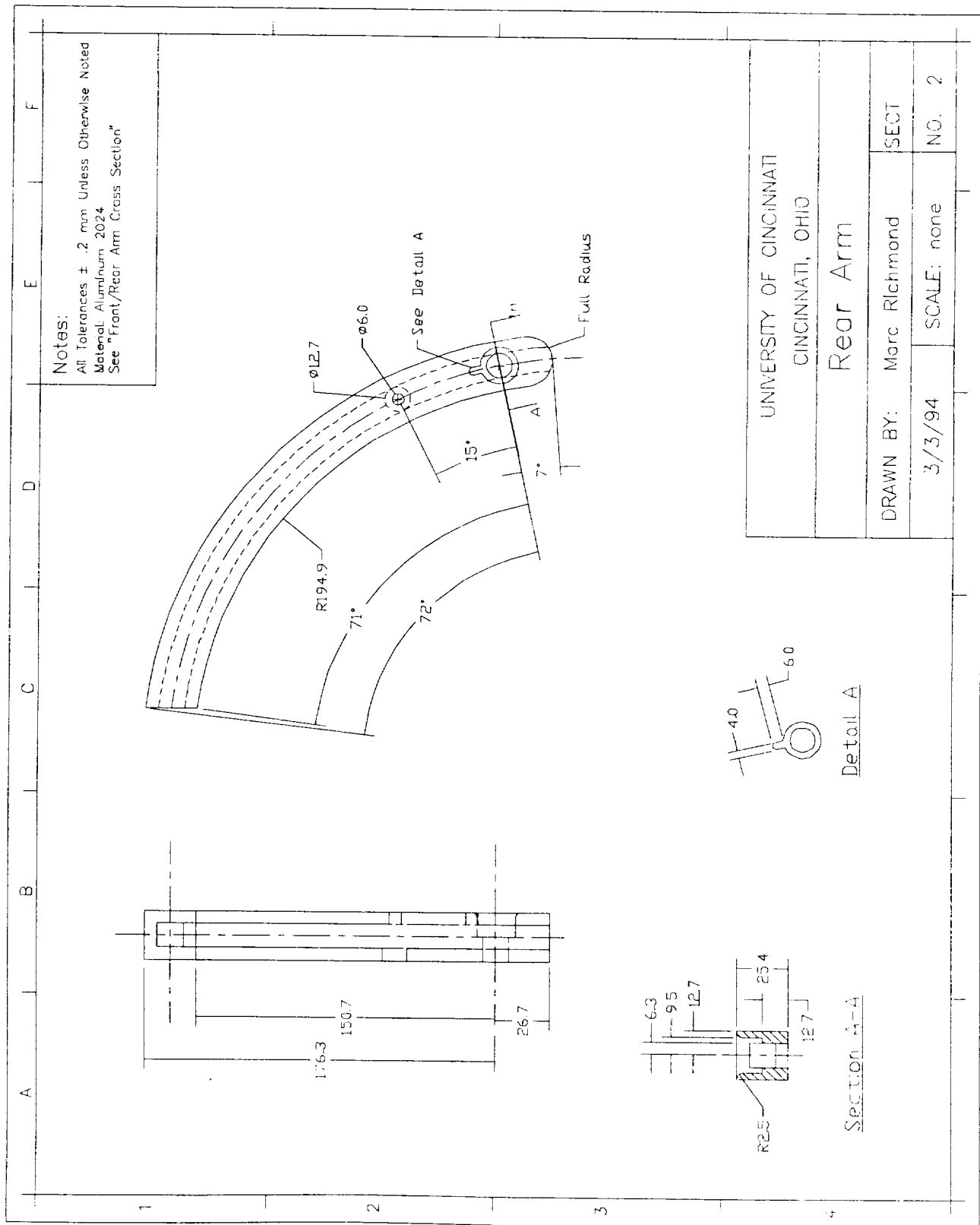


Figure 3.7.7

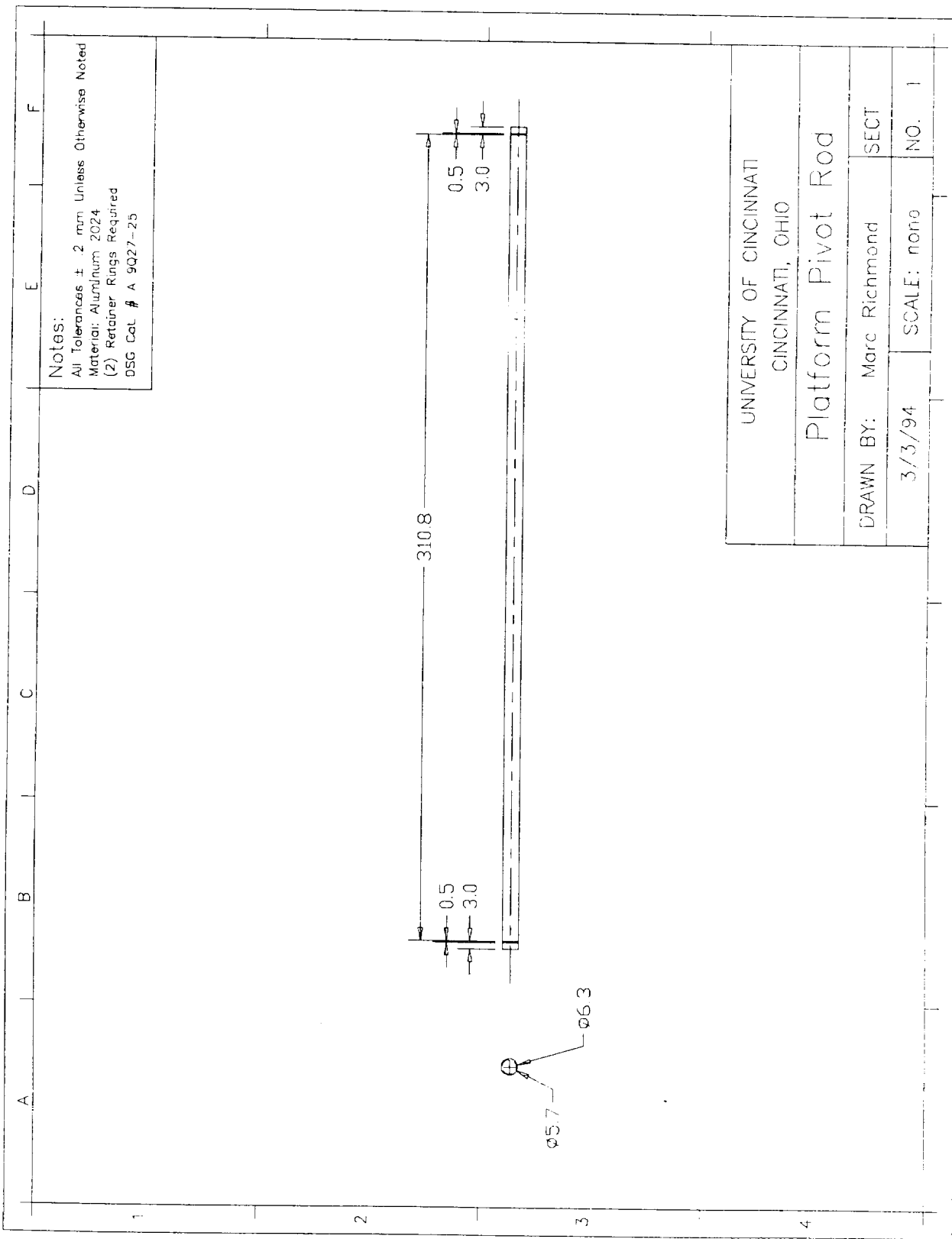


Figure 3.7.8

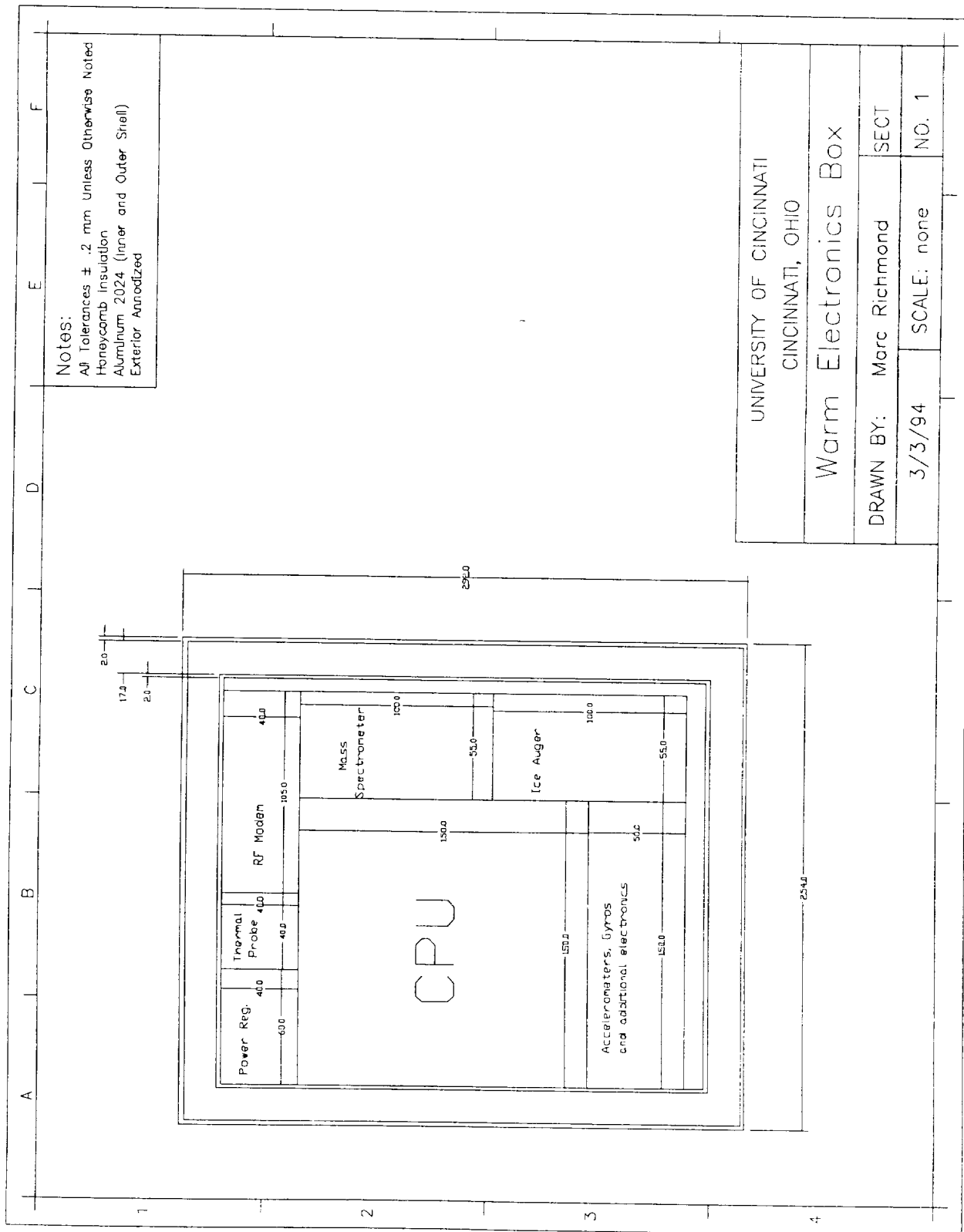


Figure 3.7.9

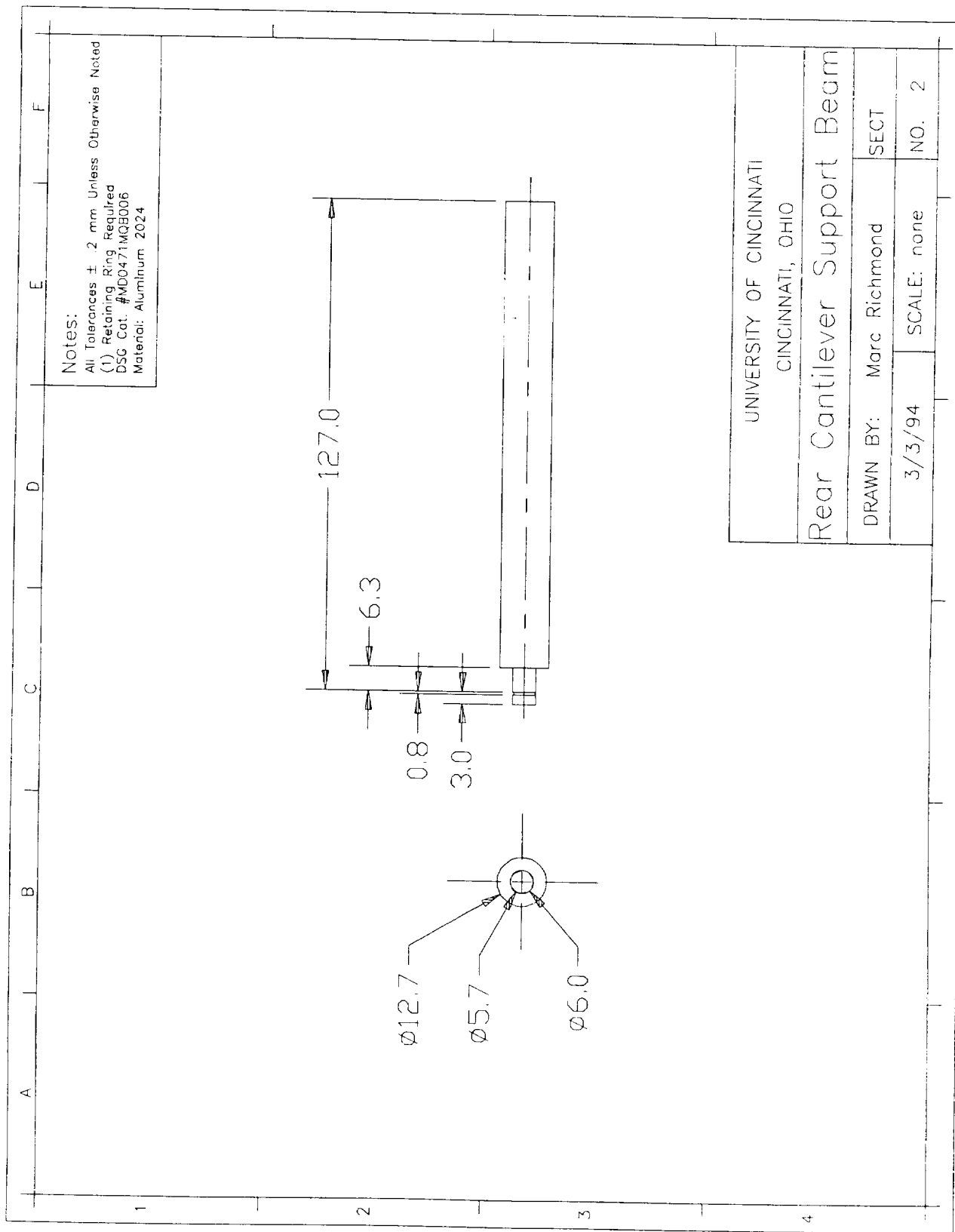


Figure 3.7.10

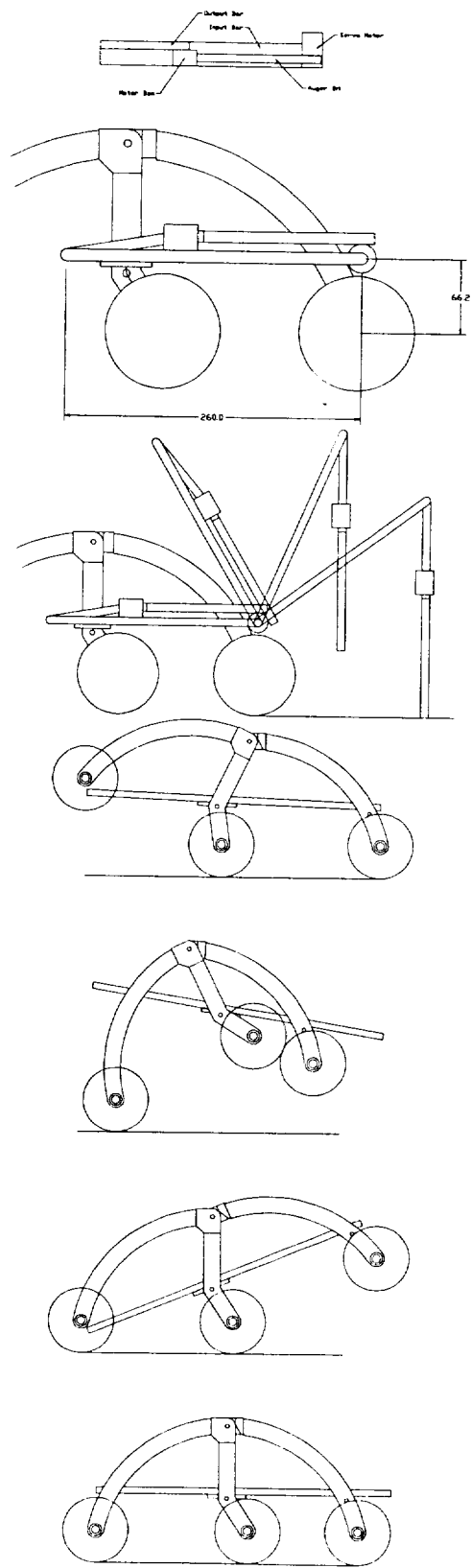


Figure 3.7.11

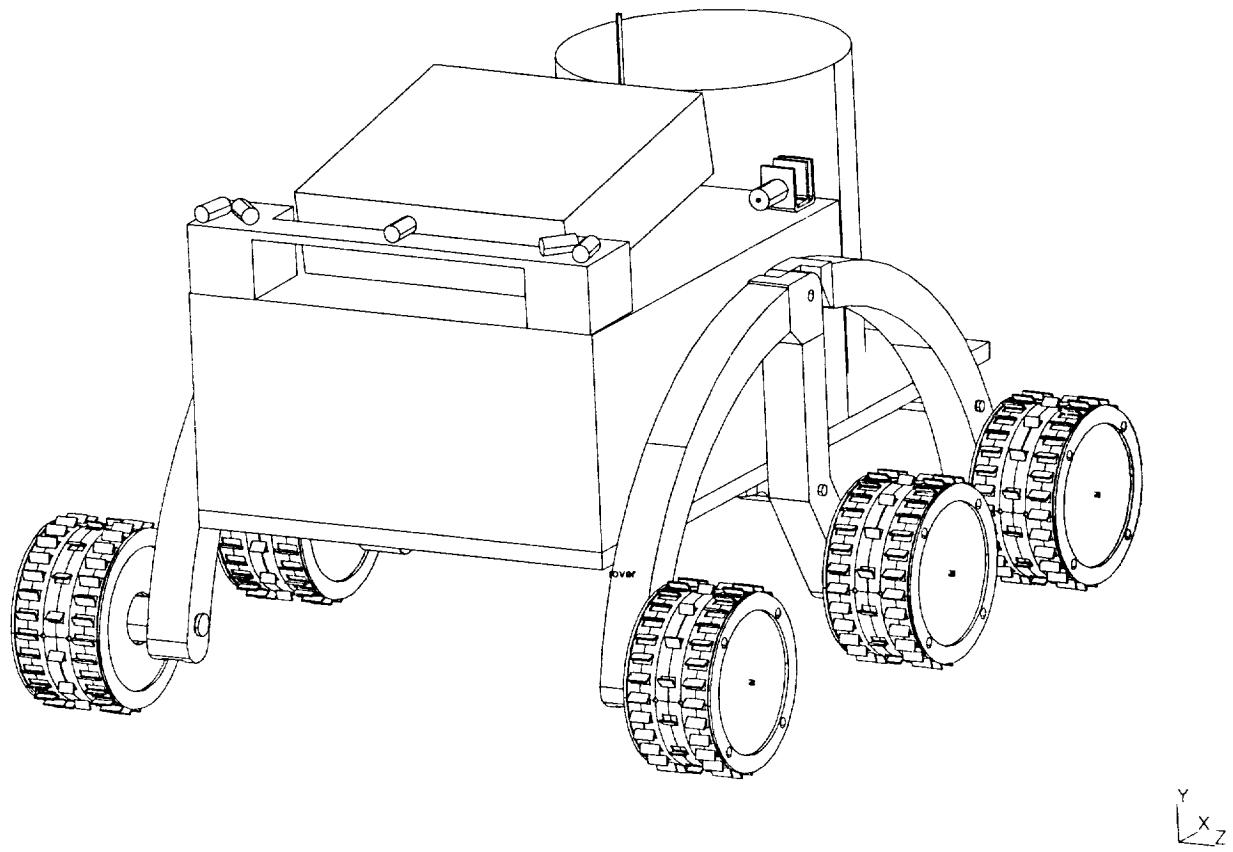


Figure 3.7.12 Red Rover

4.0 LONG-RANGE MARTIAN ROVER

Brian DeMann
Jordan DuCheny
Tony Polakowski
Todd Rothe
Neil Saunders
Shital Shah
Andy Stow

Table of Contents

ABSTRACT	2
NOMENCLATURE	5
INTRODUCTION	8
PROPOSED DESIGN	
Frame Design	10
Drive System	11
Suspension	15
Power	15
Tracking System and Communications	17
Sensors	18
Micro-controller	19
Heated Compartment	20
FIGURES	21
ANALYSIS	48
Suspension	49
Power	53
Navigation and Communications	65
Laser Systems	72
Heated Compartment	79
Takeoff and Landing Impact	83
Stress Analysis	85
Failure Analysis	91
Cost Analysis	93
APPENDIX A - Gear Selection Code.....	94
APPENDIX B - Material Properties	98
APPENDIX C - Mechanical Power Requirements Code	100
APPENDIX D - Rover Specifications Table	102
REFERENCES	104

Abstract

In the near future, rovers will be sent to Mars to explore the surface. The reason for doing this is to gain a greater understanding of the Martian weather, geology, and history. Also, it could be determined if it is possible to use indigenous material on Mars to sustain a colony.

The rovers will experience harsh environments and this makes the design very challenging. The surface conditions are not known so the design approach used for this project was to consider the worst case scenario. The design goal is to create a rover that can survive in a harsh environment for one Martian year or more, and send scientific data back to Earth via the lander.

The major assumptions used for this project are:

- ❶ Most of the polar cap is very hard with patches of powdery dry ice.
- ❷ The lowest temperature is -150°C and the highest is 40°C.
- ❸ The solar panel will have a mechanism to keep array perpendicular to the sunlight to maximize power output
- ❹ Most of the polar cap is smooth with small rocks (<10cm in diameter).

The following is a summary of the design goals and results:

Design goal: Design a vehicle capable of transporting payloads of experiments over a variable terrain in the Martian environment. Power is provided by a solar panel, batteries and Radioisotope Thermoelectric Generators (RTGs). On-boards science experiments, a computer, communications and other sensors will be standard equipment.

Design results: The basic design of the rover is a single piece frame upon which the on board scientific equipment will be secured. The six wheels are connected to the frame by articulating struts which feature damped movement by torsional springs. The wheels are a rim and spoke design. The front and back wheels have the same tread, which is designed for harder surfaces such as ice. The middle wheels have a different tread for

any softer, powdery surfaces encountered. Using six frame mounted motors and six gear-reducers, the torque is transmitted to the wheels by flexible shafts. A directional solar panel will provide enough power to the motors for half a year based on the seasons. During the winter, the vehicle will be immobile with batteries and RTGs sustaining the science experiments, computer and communications. The RTGs will also produce heat necessary to maintain the electronic equipment at operating temperatures.

Acknowledgments

The long range rover team would like to thank the following individuals for their assistance on this project.

Michael Brown

Dr. Larry Cooper

John Haney

Tyler Langley

Joseph Lemanski

Dr. David Page

Cindy Ross

Dr. Dick Wysong

NOMENCLATURE

d	density of a material	g/cm ³
F_s	static friction between wheels and surface	kg m/s ²
F_b	friction of the bearings	kg m/s ²
G	force of rover on bearing	kg m/s ²
g	acceleration of gravity on Mars	m/s ²
l	lever arm of rolling resistance	m
n	normal force	kg m/s ²
p	force required to move rover up a 15° incline	kg m/s ²
s	speed of rover	m/s
r_b	radius of balls in bearing	m
v	volume	cm ³
w	weight on Mars	g
μ_b	coefficient of friction of the bearings	----
μ_s	coefficient of static friction of the surface	----
A	total surface area of the compartment walls	m ²
k	thermal conductivity	W/m K
h	heat transfer coefficient	W/m ² K
Q	heat energy rate	W
q	heat flow per unit area	W/m ²

T_{fl}	temperature inside the compartment	K
T_{f3}	temperature on Mars surface	K
ϵ	emissivity	
σ	Stefan-Boltzmann constant	kW/m ² K ⁴

Nomenclature for motors and gearboxes

F ----- Force (Newtons)

I ----- Current (Amps)

P_M --- Mechanical Power (Watts)

R ----- Resistance of rotor at final temperature (Ohms)

R_{th} --- Thermal resistance of rotor-body and body-ambient (Deg Celsius/Watt)

R_{22} -- Rotor resistance at 22 deg C (Ohms)

T ----- Torque

T_{amb} - Ambient temperature (Deg Celsius)

T_r ---- Temperature of the rotor (Deg Celsius)

V ----- Voltage required by the motors (Volts)

i ----- Gear reduction

k ----- Torque constant of the motor (mNm/Amp)

n_L ---- Speed of the wheel (revolutions per minute)

n_m ---- Speed of the motor (rpm)

n_{max} - Maximum input speed for the gearbox (rpm)

r ----- Wheel radius (meters)

v ----- velocity (meters/sec)

α ----- Copper temperature coefficient (1/deg C)

η ----- Efficiency of the gearbox (%)

ω ----- Angular velocity of motor (rad/sec)

Nomenclature for solar array

A_A ----- Array area (m^2)

F ----- Degradation factor of the solar cells

P_A ----- Array power output (W)

s ----- Solar intensity (mW/cm^2)

Γ ----- Incident angle (degrees)

η ----- Solar cell efficiency (%)

INTRODUCTION

The Mars rover will be an essential component of the new Mars exploration plan. The rover will give researchers on Earth a tremendous amount of new data on the characteristics of Mars. This information will help researchers determine whether Mars is capable of sustaining life and of being used for a space station.

The rovers will be placed on the surface of the red planet by a series of landers. The landers will open in a petal-like formation with rovers attached to the "petals". These petals will be the solar panels to supply power for the landers. Each lander will carry two of these rovers; one will be designed to perform a variety of scientific tasks and will travel a relatively short distance, whereas the other will be designed to make geographical and climatic observations over a much greater area with few experiments. The long distance rover is the subject of this report.

The rover will be landing on the northern polar region of Mars. This polar region varies in size, depending on the season. This is a challenging design problem, because the rover and its subsystems will have to survive and perform at temperatures down to about -150 °C. Also, specific information about the surface of the polar region is unknown. A lot of questions would have been answered by the Mars Observer spacecraft, but unfortunately, due to some system failure, it was lost in space just a short time ago. Therefore, a "best guess" approach has been used for certain aspects of the design.

The plan for the long range exploration of the northern polar cap is outlined as follows. The lander will reach the surface in September of 1999, immediately deploying the long and short range rovers. Each of the long range rovers will have a specific navigation course pre-programmed into memory. The rovers will orient themselves with respect to the lander, and begin to proceed on their preset routes. When the rovers detect obstacles which could be a hazard, they will employ their built in logic for avoiding an obstacle. No communication with Earth will be necessary for most obstructions such as rocks, cliffs, or craters. The rovers will stop every few meters in order to conduct radar mapping of the

immediate surroundings. A change in angle of the solar array will also be necessary every so often. While these processes are taking place, the rovers will also relay data back to the lander which will enable the lander's computer to determine the coordinates of the rover. If any change of course is necessary due to motor or tracking errors, the lander will communicate to the rover that it needs to adjust its course, and will provide the coordinates to get the rover back on track. This entire process will be entirely automated, without communication with Earth.

The lander will send back its rover data to mission control on Earth about once every 12 hours. Based on the data received, the operators will determine whether or not they want a particular rover to alter its course, in order to explore an area not covered. If so, the change of course information can reach the rover in less than an hour. If not, the rover continues on course until it hears otherwise.

Through the summer months, when good lighting provides adequate solar power for the motors, that will be the general cycle of the rovers. When the rotation of Mars reaches a point when sunlight is no longer always powerful enough to provide adequate power to the motors, the rover will shift into a more relaxed schedule, only moving when the solar power is the greatest. During other times of the day, the solar cells will trickle charge the batteries, to get them ready for the winter. Science experiments will continue during this time.

Eventually the polar region will be completely shrouded in darkness for the winter. During this period, no motion will take place in the rovers. The communications and science equipment will continue to be powered by the batteries and the RTG. In the following spring, the rovers will attempt to thaw out and continue their mission.

The following proposed design section goes into detail about the design process from which this rover was conceived. The design is based upon considerations which involve frame design, drive systems, suspensions, materials, power requirements, computers, sensors and communications equipment.

PROPOSED DESIGN

Section 1.1: Frame Design

The basic frame was determined to be a single-piece design (See Figure 2.1a). A multi-piece unit was also considered, but the single-piece was preferred for the following reasons. A multi-piece unit would require the use of a joint or joints to connect the different sections. A failure in one of these joints would leave the rover at least partially disabled. Also, the controls for this design would be more complicated and would require more power. The multi-piece body would be preferable if extremely rugged terrain was to be traversed, but as far as is known, the polar region is not nearly as rugged as the rest of the planet. The assumption has been made that the largest "rock" size will be less than 10cm in diameter. If the rover encountered a larger obstacle, it would have the option of going over it or around it depending on the size and orientation of the obstacle. This determination would be made by the sensors recording the obstacle size and by the central computer which would determine the alternative that is most plausible. The sensors would record this information, send it to the lander, which in turn sends the signal back to Earth. On Earth, scientists would be plotting the surface and make the determination on what course the rover should follow. Also, when coupled with the suspension design to be discussed later, the single-piece body would provide more than adequate clearance and maneuverability for the rover. Other views of the rover are offered in Figures 2.1b and c. An isometric view is shown in Figure 2.1d.

Material selection for the frame was a major factor. The temperature on Mars is estimated to be at a low of -150° .¹⁵ Some metals in this range become brittle and have other poor material properties. Some materials that were viable options were OFCH Copper, alpha brass, certain aluminum alloys, austenitic stainless steel, some titanium alloys, and some magnesium alloys. Non-metallic materials were also considered. Some examples were polyethylene, PVF, FEP (thermoplastics), glass fiber reinforced plastic

(GFRP), and carbon fiber reinforced plastics (CFRP). The factors considered in material determination were yield strength, ultimate tensile strength, toughness, fatigue strength, thermal expansion coefficients (low number needed), and density.

The three materials that had the most desirable mechanical properties were aluminum alloys, titanium 6Al 4V, and CFRP. The material chosen from these three was CFRP. It had the best combination of factors. It has a high yield strength and a good fracture toughness. The thermal expansion is very low, such that it can be considered negligible.¹⁷ This is important because of the variation in temperature from launch on Earth, to the cold in the vacuum of space, and to the equally cold temperatures that will be experienced on the polar surface of Mars during the winter season. The material also has a low density value and retains its material properties at the low temperatures. The material can be tailored specifically for the needs of the mission by varying the fiber type, the plastic type, and the geometric arrangement of the fibers within the composite.¹⁷

Section 1.2: Drive System

The drive system was one of the many challenging aspects of the design, because of the frozen CO₂¹⁵ surface at the polar region. The variables used to choose the drive system were mobility, traction, reliability, ease of control, stability, power requirements, and weight. The following options were carefully reviewed to meet the needs of the mission: caterpillar-style treads similar to those on a tank; individually-controlled legs to give a "walking" effect; a snowmobile design that would entail a combination of skis mounted in the front and a single drive tread mounted in the rear; "Christie" drive, which consists of a tread on either side placed over a series of wheels; and four to eight wheels mounted independently on actuated arms. A tread design would allow movement on a wide range of terrain and would provide inherent stability for the rover, but it would have a relatively high weight and would be prone to failure if one of the links should break. Legs are an interesting idea but just have too many potential problems. They would

require a lot more control and computational power than other options and would, by nature, be unstable. Also, if one leg would fail, it would be extremely difficult to compensate for this loss. The snowmobile design was considered, because the polar surface most likely has some powdery CO₂ "snow."¹⁵ However, to be effective the ski part needs a very low coefficient of friction, while the tread portion needs a high friction coefficient. This could prove to be a seriously inefficient use of power. The "Christie" drive could be a viable option by providing stability and reasonable clearance, and if the treads fail, the wheels could still be used to drive. Nevertheless, a major problem arises of how to control the vehicle with treads on one side and wheels on the other should that situation occur. Therefore, this option is useless for our design.

The option that was decided upon was wheels. Wheels can be designed to handle a variety of surface conditions, are less vulnerable to failure than other options, and are easy to control. Also, they use power efficiently and are very stable if the vehicle has a low center of gravity. Wheels may have difficulty navigating rough, broken terrain, but it is assumed from what is known about the polar surface of Mars that the rover will be able to maneuver around any such conditions. It was decided that six wheels would be used; four wheels would not provide proper redundancy in the case of a single wheel failure, and more than six wheels would be too redundant and make the design needlessly complicated. The rover will have the ability to drive forwards and backwards in case it gets trapped somewhere and needs to back itself out of that area. Also, it will be able to turn around by having the wheels on one side spin one direction and the wheels on the other side spin the opposite direction.

The wheel and tread design are seen in Figure 2.2. The front and back wheels have a different tread design than the middle set of wheels in order to traverse different surface conditions. The front and back sets of wheels are designed to travel on solid CO₂ "ice," and the middle wheels are designed to drive on powdery "snow".

The wheels will be constructed from titanium 6Al 4V. This was determined after considering aluminum alloys, stainless steels, thermoplastics, and reinforced composites. Materials considerations similar to those for the frame design were made for the wheels. The properties of primary concern were fracture toughness, strength, and thermal expansion. The fracture toughness is approximately $60 \text{ MPa} \sqrt{\text{m}}$. This was very high compared to other materials. Titanium 6Al 4V had the highest strength/density ratio of all materials considered.

After six wheels were chosen, a method of power transmission to these wheels needed to be determined. Two main options were considered: slip rings and flexible shafts. Slip rings are conductive contacts which are used to transmit electrical power between rotating surfaces. A conductive strip is placed on one surface and a contact on the other. The contact is forced against the conductive strip by a spring to ensure a constant connection. Electricity would then be conducted by wires to the motors located in each wheel hub. A flexible shaft, on the other hand, is a set of wires twisted together in a uniform direction and held inside a flexible tube. Torque is supplied to the shaft at one end and is transmitted to the other end. The motors corresponding to the flexible shaft design would be mounted on the frame. There would still be one motor for each wheel to provide redundancy in case one or possibly two motors would fail.

The slip ring idea, with motors in the wheels, would increase the stability of the rover but would make the wheel design very complicated due to the need for a high gear reduction system to be placed in a small amount of space. Flexible shafts, with motors mounted on the frame, are considered to be the best choice for the following reasons. The flexible shaft allows for greater freedom on the part of the designers. Since the motors are to be mounted on the frame, they can be placed anywhere. This creates the flexibility to design for the most efficient use of space. The flexible shafts are also more efficient than a complex set of gears. This system of shafts does not need the precise alignment or the high tolerances required by a gear or wheel mounted motor system.

Being a less than smooth ride to Mars, this reduces the possibility of problems upon arriving at the destination. The manufacturer's data sheets show a 90-95% ⁹ efficiency. This is important in terms of minimizing wasted power. As will be shown later, power is a valuable commodity that cannot be afforded any waste. Also, a major plus for the flexible shafts is that they remain flexible in extreme temperatures (-189 to 537°F).

Being on the long range rover is also not a problem for the flexible shafts. The shafts are designed to sustain high speeds of rotation for exceptionally long periods of time. The flexible casing of the shaft helps to retain lubrication for the shaft and adds a protective layer. The outer shaft also prevents helixing within the shaft and provides a continuous guide for the shaft enabling smoother operation. Other benefits are the low cost and low weight constraints. Overall, the flexible shaft design provides the best method of power transmission while eliminating some of the problems of other power transmission systems. The motor to be used with the flexible shafts is the EscapTM 28L28-416E shown in Figure 2.3a. Appendix A shows the code for a program used to analyze power requirements and selection based on EscapTM guidelines.

There are two possible ways to reduce the RPM of a motor. These are shown in Figure 2.3b and c. The first is a basic gearbox, and the second is a gear motor which combines a motor and a gear reduction system in one unit.

A 90° gearbox will be used to take the flexible shafts into the wheels, since this will increase the radius of curvature of the flexible shafts and will make them more efficient. A drawing of the x-contact bearing that will be used in the gearbox is provided in Figure 2.4. The materials that were candidates for the bearing were CFRP, GFRP, and 316 stainless steel. They were evaluated on the basis of good toughness properties at low temperatures and low coefficient of friction. The 316 stainless steel was chosen for its excellent hardness and strength at low temperatures.¹² It will also be impregnated with PTFE to reduce friction.

Section 1.3: Suspension and Lateral Stability Assembly (SALSA)

The suspension system is a fairly simple design. The struts connect the wheels to the frame and transfer the frame and equipment weight to the wheels.. Material considerations were similar to those for the frame and wheels. The struts will be hollow shafts of circular cross section. They will be constructed out of titanium or CFRP due to its high strength/weight ratio. A drawing of the suspension system can be found in Figure 2.5. The bushings will be made out of CFRP impregnated with PTFE and with a reinforcing ring of 316 stainless steel. The CFRP and PTFE will provide dry lubrication, since the coefficient of friction of a carbon composite on steel is approximately 40% that of lubricated steel on steel.¹² Torsional springs will allow damped vertical movement of the wheels and frame. The materials that were considered for the torsional springs are high carbon spring steel, Kromarc 55, and 310 stainless steel. Selection was based on high elastic limit, which was the most important factor, high surface hardness, toughness at low temperatures, and fatigue strength. The material that was best suited for this purpose was the 310 stainless steel because of its excellent low temperature strength and toughness. It is completely stable at low temperatures, meaning it will not undergo martensitic transformation and hence have reduced fatigue strength.²⁴ Also, it has a high carbon content (25%) which insures high surface hardness. There will be two torsional springs per strut. This reduces the stresses in each individual spring and adds redundancy to the system.

Section 1.4: Power

As was mentioned earlier, power has turned out to be a valuable commodity for this project. Many different power systems were considered to run the rover and its subsystems. They included solar panels, radioisotope thermoelectric generators (RTG's), batteries, tethered power input, and an internal combustion engine. The internal combustion engine would provide high power output, but its need for refueling limits the

range of the vehicle. This is obviously impractical for a long range rover such as the one being designed here. Tethered input would consist of a land line spooling from the lander to the rover to provide electric power to the rover and to transmit data to and from the lander. This option would also provide the rover with more power. However, since the rover will probably need to back up and maneuver itself along the surface, the tether would either get entangled with the rover or would break due to its fragility at the low Martian polar temperatures. Using a tether presents problems of length and additional mass. Therefore, tethered input is a very impractical choice for power.

Solar panels can be used to harness the energy of the sun. The solar intensity on Mars is not near what it is on Earth, however, solar panels are a proven technology and can be used at least as one power source.

RTG's, which convert thermal energy from a decaying radioisotope into electric power, are very dependable and last for a long time. Yet, they are terribly inefficient (around 6%) and have a high weight to power ratio. The excess heat that is given off by the radioisotope can be used to heat the electronics, which will be housed in an insulated box. Therefore, RTGs are still a practical choice to be used on the rover.

The last power source considered was batteries. They would be charged by the other power sources on the rover, so they would not actually be supplying additional power. They would just allow the rover to store power to run different subsystems at the same time. It was decided that solar panels, an RTG, and batteries would all be used to power the rover. (Figure 1.1). The rover will be landing on Mars sometime at the beginning of the summer, and sunlight will be constant until the onset of winter. Therefore, the solar panels and the batteries will be used to run the drive system, the sensors, and some science experiments. The RTG will provide power for the computer and probably the communications equipment, recharge the batteries and will also be used as a heat source for the heated compartment on the rover. During winter, the polar region experiences continual darkness which makes the solar panels useless. Also, due to the

Figure 1.1: Power Usage As a Function of Time

	Sept.-Mar. 2000 (Max. solar power range)	July-Sept. 2000, Apr.-July 2001 (Limited movement, slower speed)	June-July 2001 (No movement - total darkness)
Motors	Solar	Solar, RTG, Battery	N/A
Computers	RTG, Battery, Solar	RTG, Battery	RTG, some Battery
Communications	RTG, Battery, Solar (No movement)	RTG, Battery (No movement)	RTG, Battery
Radar Sounding/ Mapping	Solar, RTG, Battery (No movement)	Solar, RTG, Battery (Very limited use)	RTG, Battery (Limited use or not at all)
Seismometer	RTG, Solar	RTG, Solar	RTG
Video Camera	RTG, Solar	RTG, Solar	N/A
Sensors	RTG, Solar	RTG, Solar, Battery	N/A
Trickle-charge Batteries	RTG, Solar	RTG, Solar	RTG

layer of CO₂ frost that settles on the polar cap during the winter, the rover will probably be covered and unable to move. The RTG and batteries will be a source of power in the winter. The combination of both will be adequate to keep the computers and communications equipment and possibly some small experiments heated and running during this time. If the rover manages to survive the harsh Martian winter, it could potentially continue its mission into the next year.

Section 1.5: Tracking System and Communications

There are several factors that need to be considered when establishing a communication design: communication of the rover to the lander, communication of the lander to Earth, and positioning factors. Some designs considered were inertial tracking (gyroscopes and accelerometers), wheel movement tracking, radio tracking with receivers on the rover, on the lander, and in space, and visual tracking by way of cameras on the rover.

The problem with inertial systems is that the size would be too bulky for the rover to handle. The numerous moving parts such as bearings could be impractical at -150°F. This system would also require power from the rover. The visual tracking would require considerable computing power from the rover and the lander. This system would also be hard to design and implement. The most important disadvantage is that, since this is to be a long distance rover, a visual system doesn't allow for much exploration.

The design that will be used is a combination of a wheel movement tracking system and a radio tracking system. Gear speed sensors will keep track of essentially straight line motion, and this data will be transmitted to the lander. The transmission will be picked up by a small four-arm spiral antenna which will find the position of the rover in the horizontal and vertical planes relative to itself. These two angles, combined with the wheel movement data, will give the location of the rover. There will be as many receivers as there are rovers that report back to a particular lander. The advantages of

such a system are explained next. The wheel movement tracking requires little or no power from the rover, and it would also take up minimal space on the wheel. The radio tracking provides accuracy regardless of terrain and can also relocate the rover if it falls out of communication for a period of time. The radio also requires little additional power which is an obvious advantage. This system does, however, have some small problems.

One problem is wheel slip during rotation. This could cause a discrepancy between each separate wheel on a particular rover. There is potential loss of accuracy over hilly or rough terrain. This has a simple solution, though, of keeping track of elevation angles and using this in the distance/location computation. The antenna which receives the signal is bulky ($\approx 3"$ radius) but is only going to be on the lander. Radio interference is a minor concern, because only the ice will provide an obstacle. The ice will appear largely transparent at the expected frequency to be used (100MHz), which will eliminate the interference problem.

Section 1.6: Sensors

Laser ranging is the concept that will be used; it works similar to sonar. A laser beam pulse is emitted, and the return is monitored. The distance can be computed by knowing the time between emission and return. The system proposed for the rover would aim the laser at some angle down. This angle would need to be calculated to determine an optimum, based on laser system location, vehicle dimensions, and travel speed. The laser would sweep out an arc in front of the rover, stopping at several positions and firing the laser. The return time given by the beam off a level surface would be known. Therefore, a longer return time would indicate a depression, and a shorter return time would indicate a raised area. This system is described in detail in the analysis section 3.4.

Section 1.7: Micro-controller

Figure 2.6 shows a schematic diagram for the rover electronics. The function of the micro-controller is to accept and process instructions sent to the rover via radio signals, as well as inputs from the wheel speed sensors and laser sensors. The processor will also output necessary responses over the radio, while producing drive signals for each of the six wheels. The micro-controller has the duty of activating experiment modules and transmitting experiment data back to the lander.

It is not anticipated that the micro-controller needs to be as powerful as the large, power-hungry chips used in modern PC's. Instead, micro-controllers from five years ago should be sufficient. The micro-controller must meet several requirements:

- Sufficient computer power/speed to run the rover
- low power requirements
- large operating temperature range
- proven reliability

One chip meeting these requirements is the Intel 80C51BH. It is a single chip, 8-bit micro-controller capable of 12 MHz speed. Under normal operating conditions, it draws 16 mA from 5V; under a special sleep mode, it draws only 50 μ A. This sleep function shuts down everything but on-board and essential functions. The ambient temperature operating range is -40° to 85°C.⁷

Another candidate is from the Motorola MC68000 family. It has essentially the same specifications. This chip has the advantage of being more widely used in industrial applications, and also features a sleep mode.⁸

Most likely, one of these chips with sufficient peripheral I/O, and RAM and ROM chips, would be sufficient for the task of running the rover. Final research showed that the Motorola MC68000 chips would be ideal for the purposes outlined here.

Section 1.8: Heated Compartment

To ensure proper operation of the micro-controller and other electronic equipment, a heated compartment will house these items as well as the rechargeable batteries. The insulation that was selected for the compartment is silica aerogel, or "santocel". This material has a very low thermal conductivity, which decreases with temperature drop. The heat for the compartment will be supplied by the RTG. It is a great source of heat due to a low (7.6%) efficiency. The placement of the RTG with respect to the compartment is centralized. A small duct which connects the compartment to the RTG will funnel the heat to the compartment.

Section 2: Figures

Figure 2.1 a) Rover Assembly - Top View

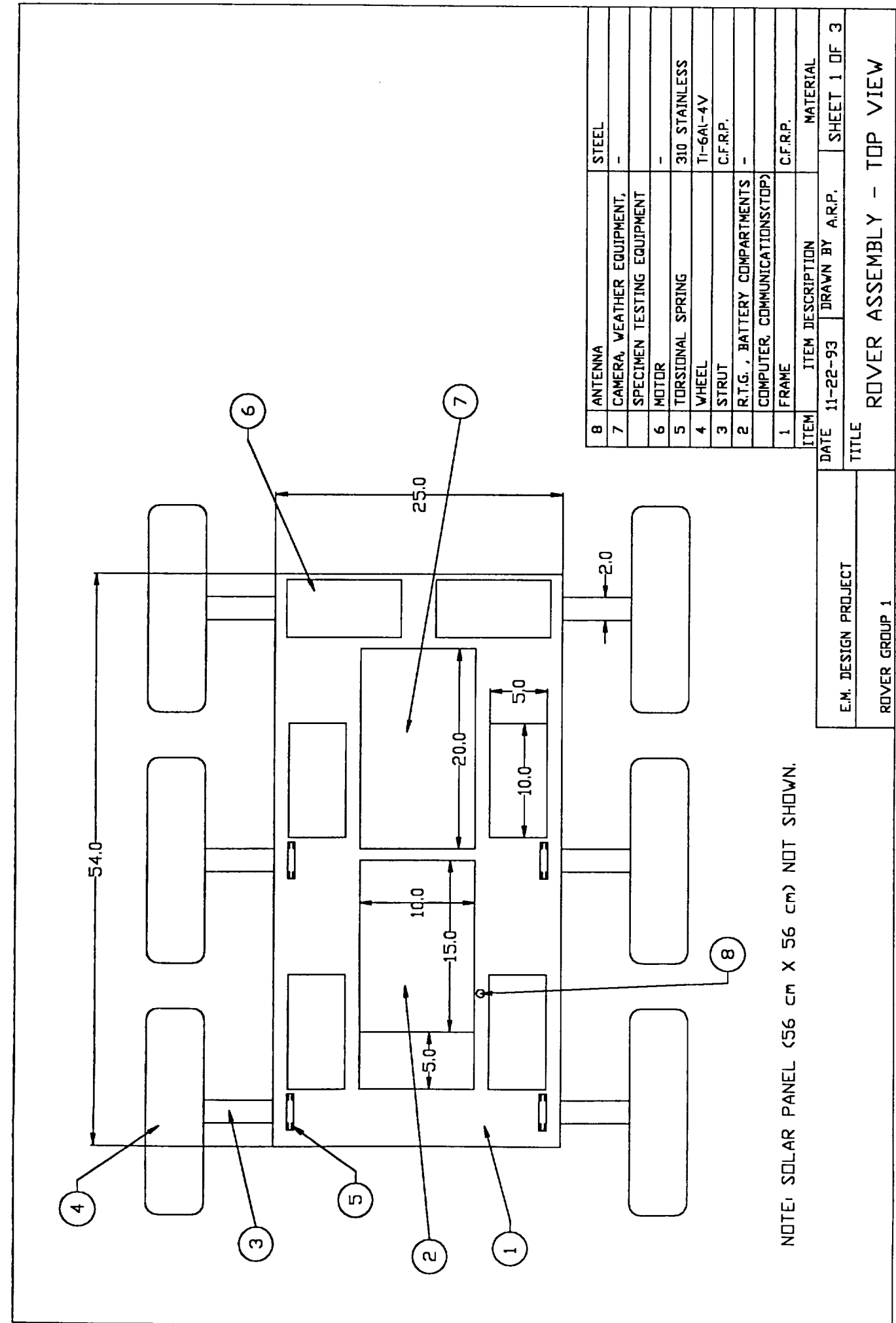


Figure 2.1 b: Rover Assembly - Side View

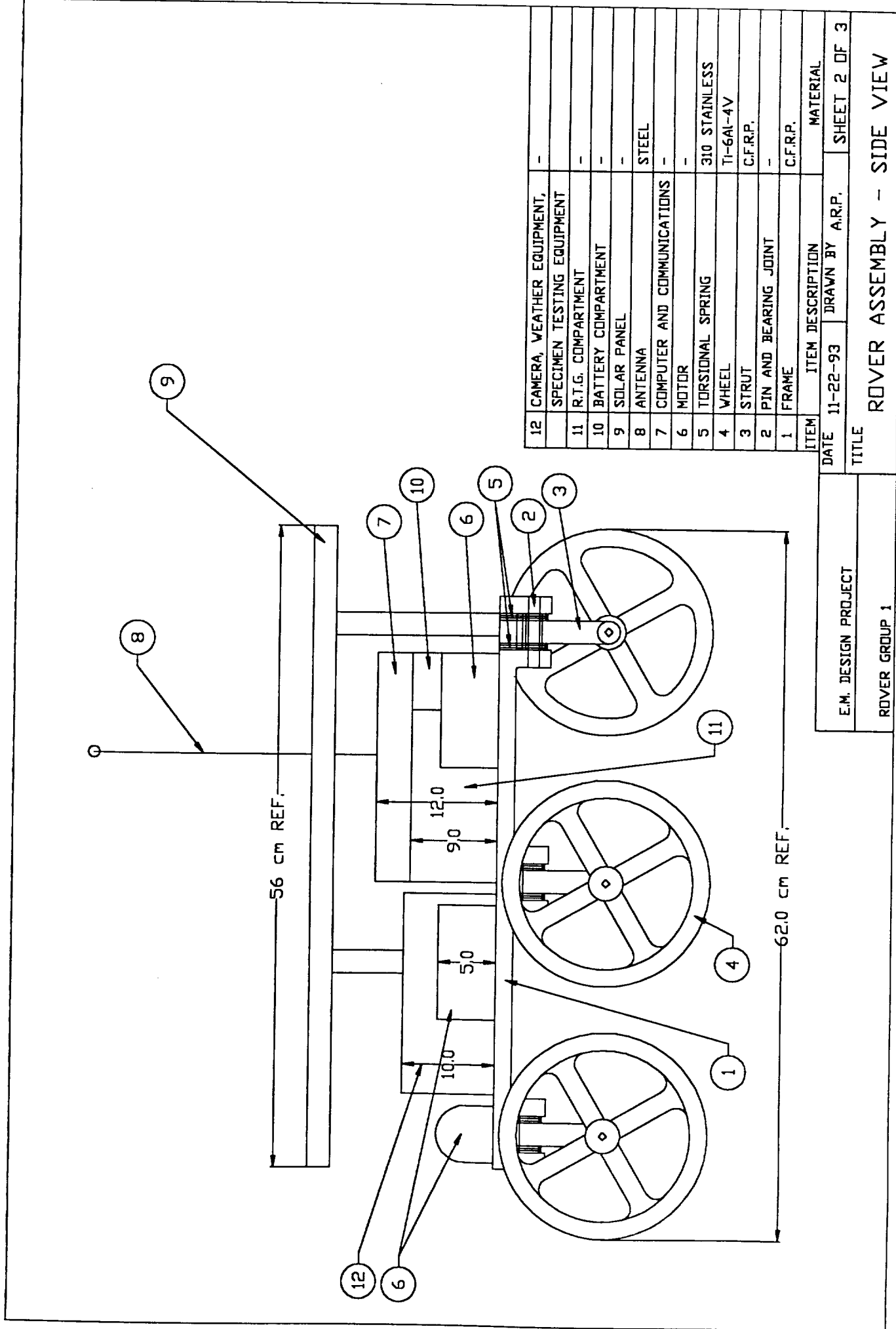


Figure 2.1 C1 Rover Assembly - Rear View

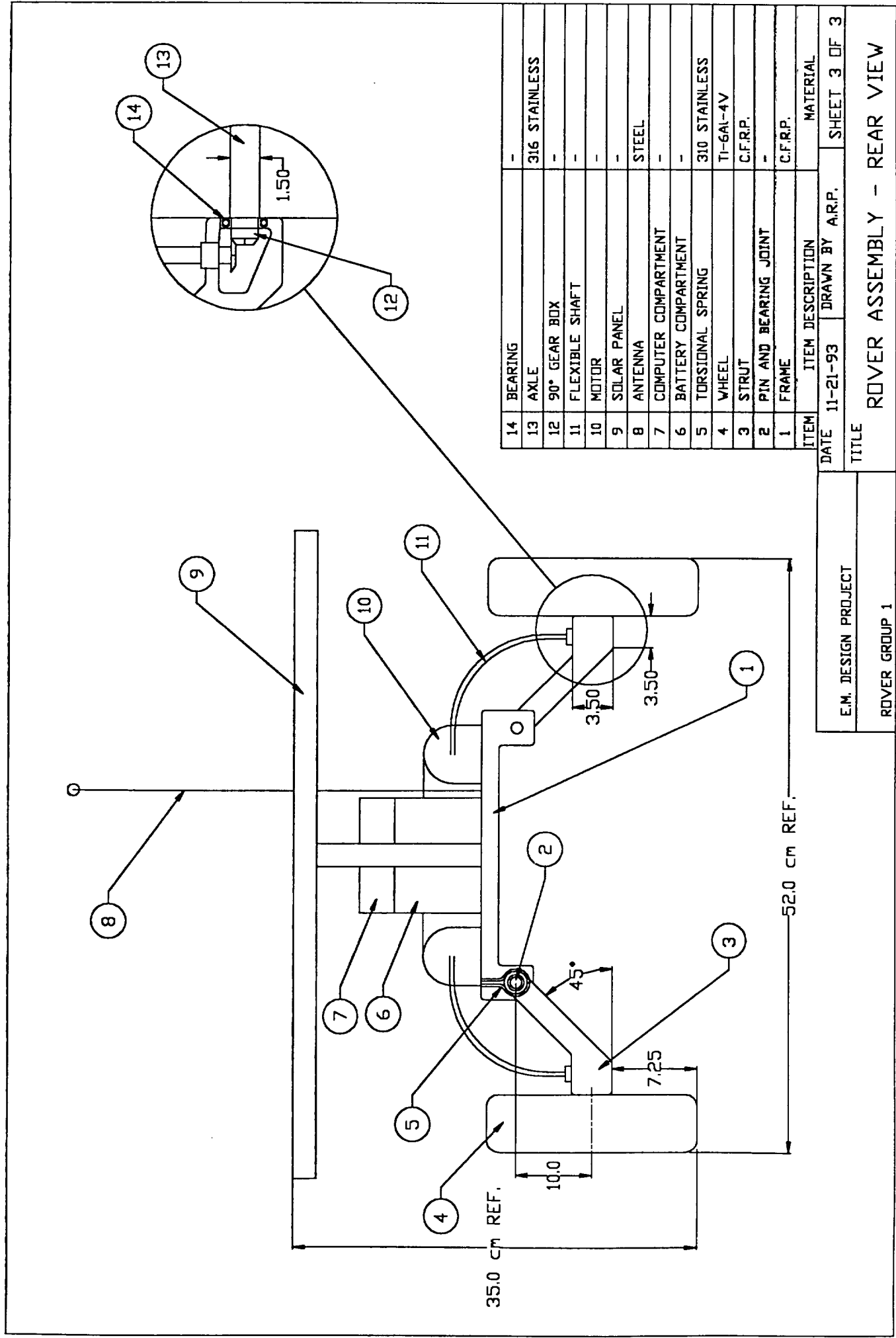


Figure 2.1 d: Rover Assembly - Isometric View

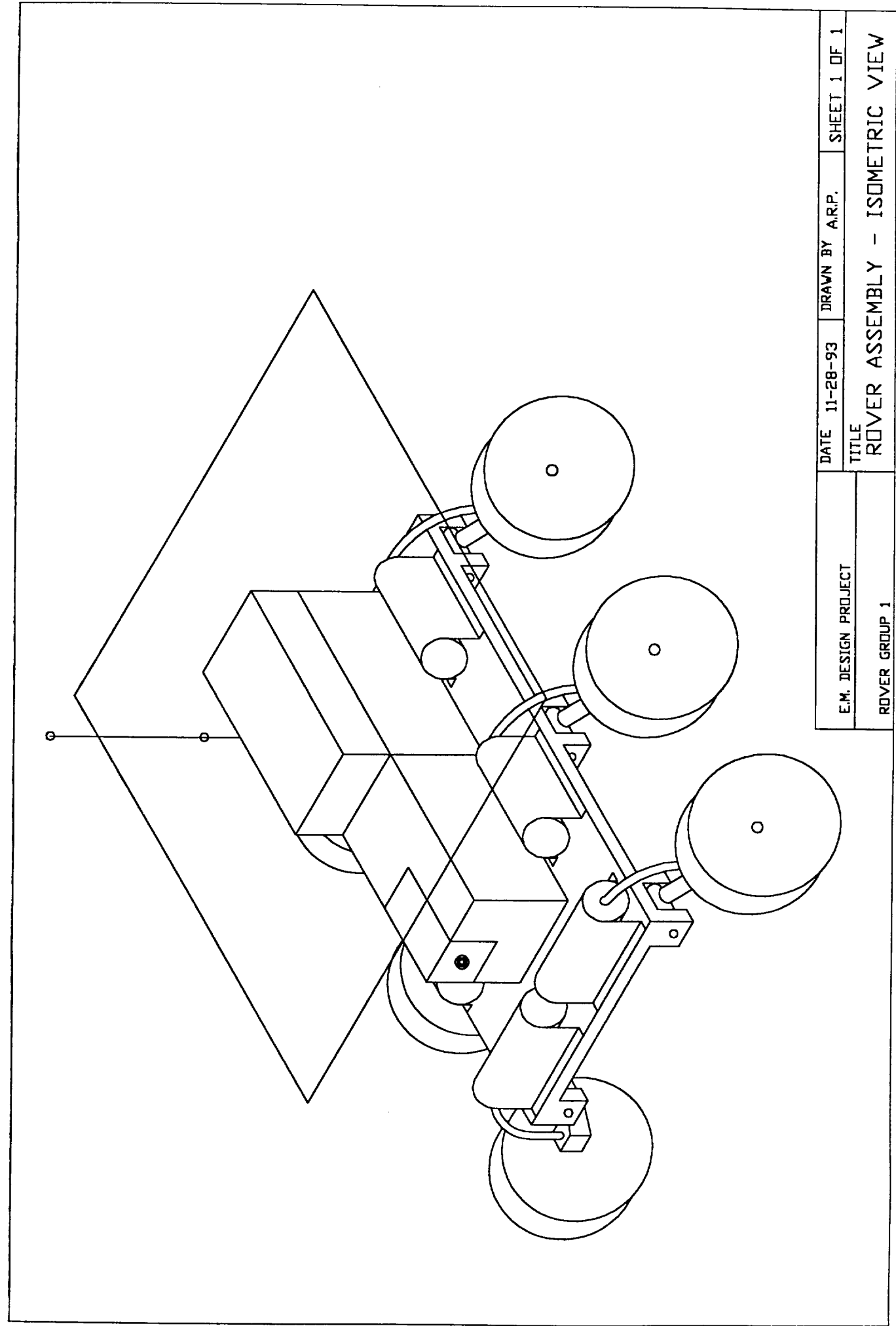
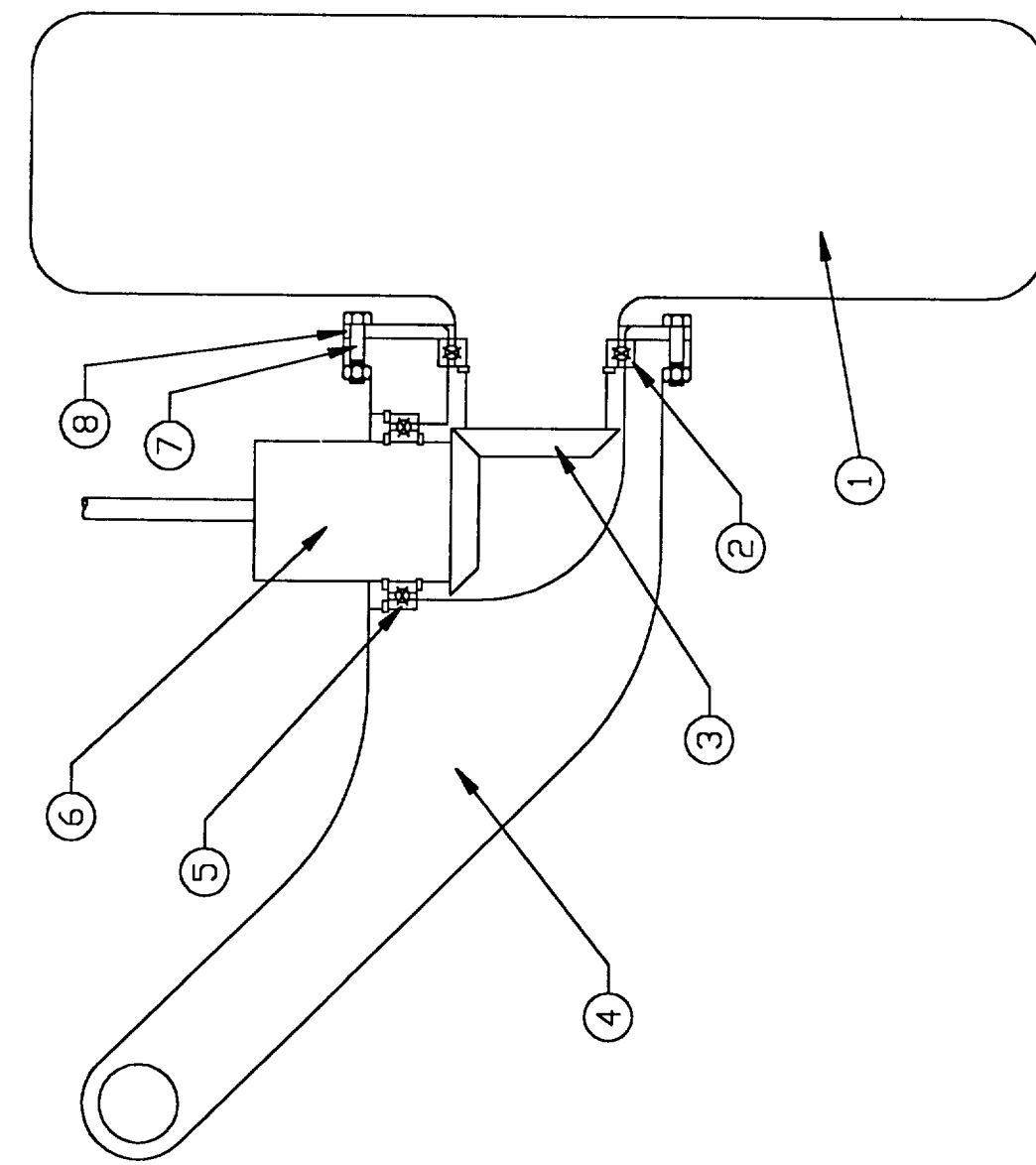


Figure 2.2: Wheel Joint Assembly



ITEM	ITEM DESCRIPTION	MATERIAL
8	COVER PLATE	CFRP
7	BOLT AND NUT	STEEL
6	FLEXIBLE SHAFT COUPLING W/ GEAR	STEEL
5	X-CONTACT BEARING, 3 SNAP RINGS	310 STAINLESS
4	STRUT	CFRP
3	BEVEL GEAR	310 STAINLESS
2	X-CONTACT BEARING, 1 SNAP RING	310 STAINLESS
1	WHEEL	Ti-6Al-4V

E.M. DESIGN PROJECT	DRAWN BY A.R.P.	SHEET 1 OF 1
ROVER GROUP 1		

Figure 2.20: Wheel Assembly

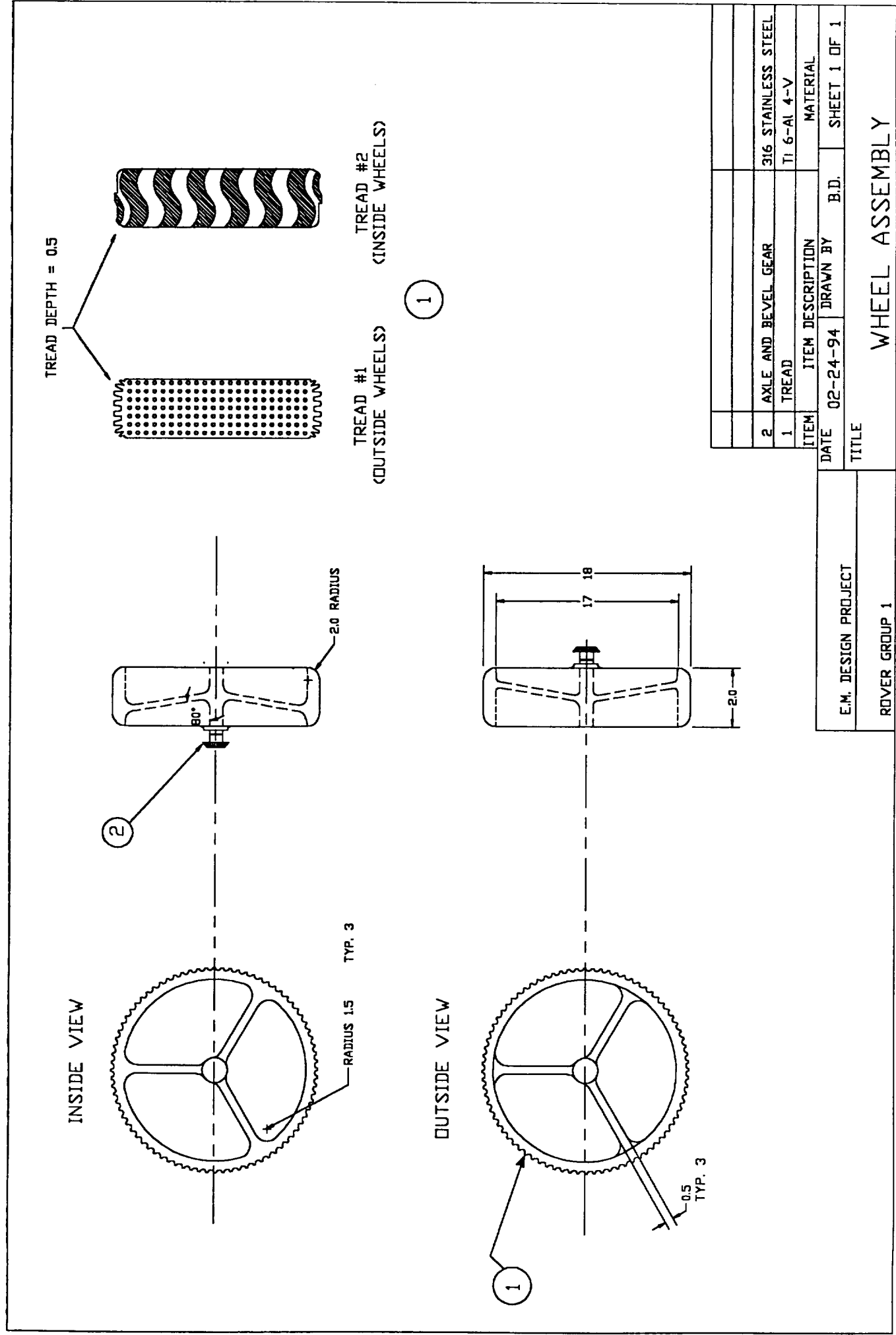


Figure 2.2 b: X-Contact Bearing

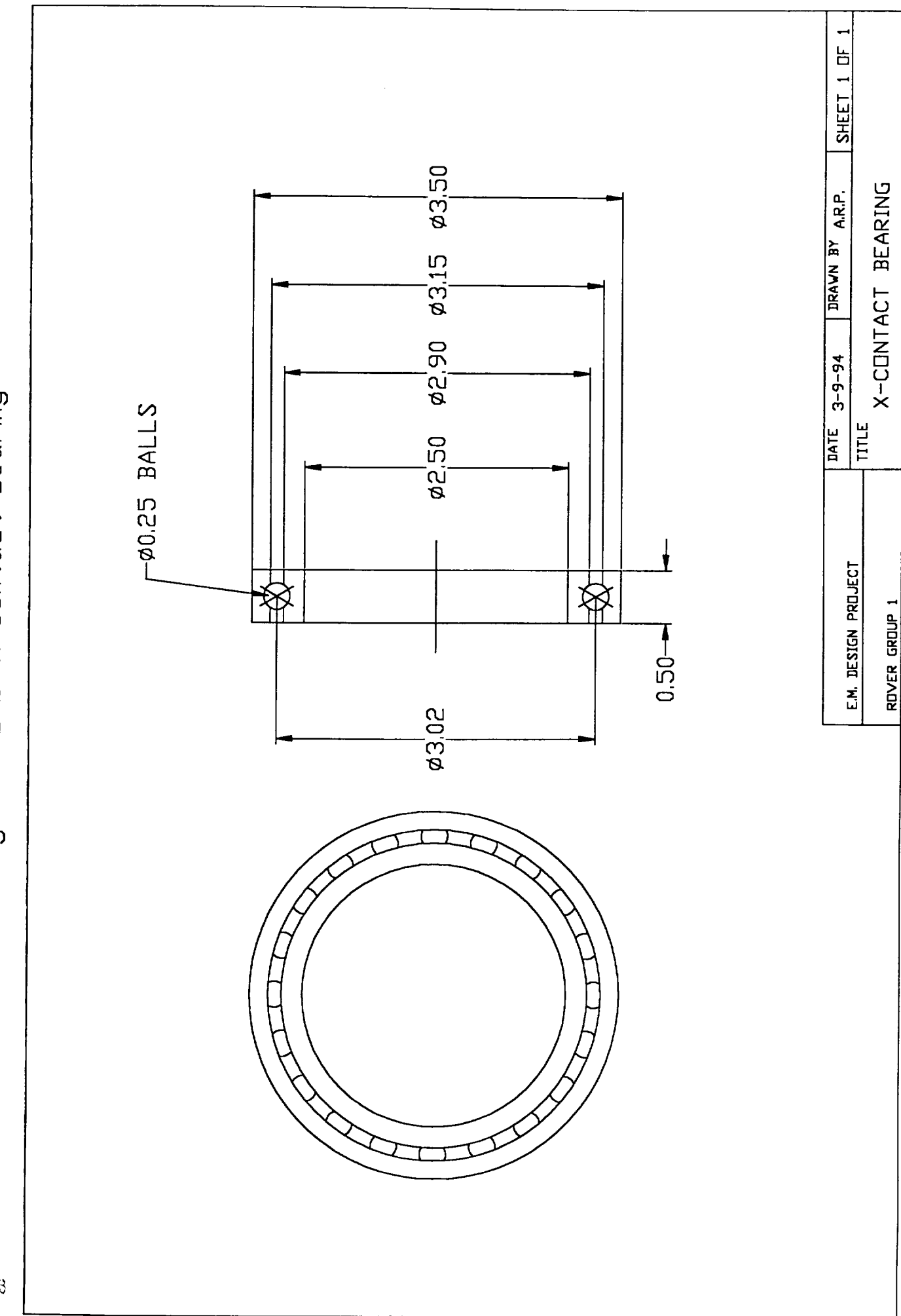
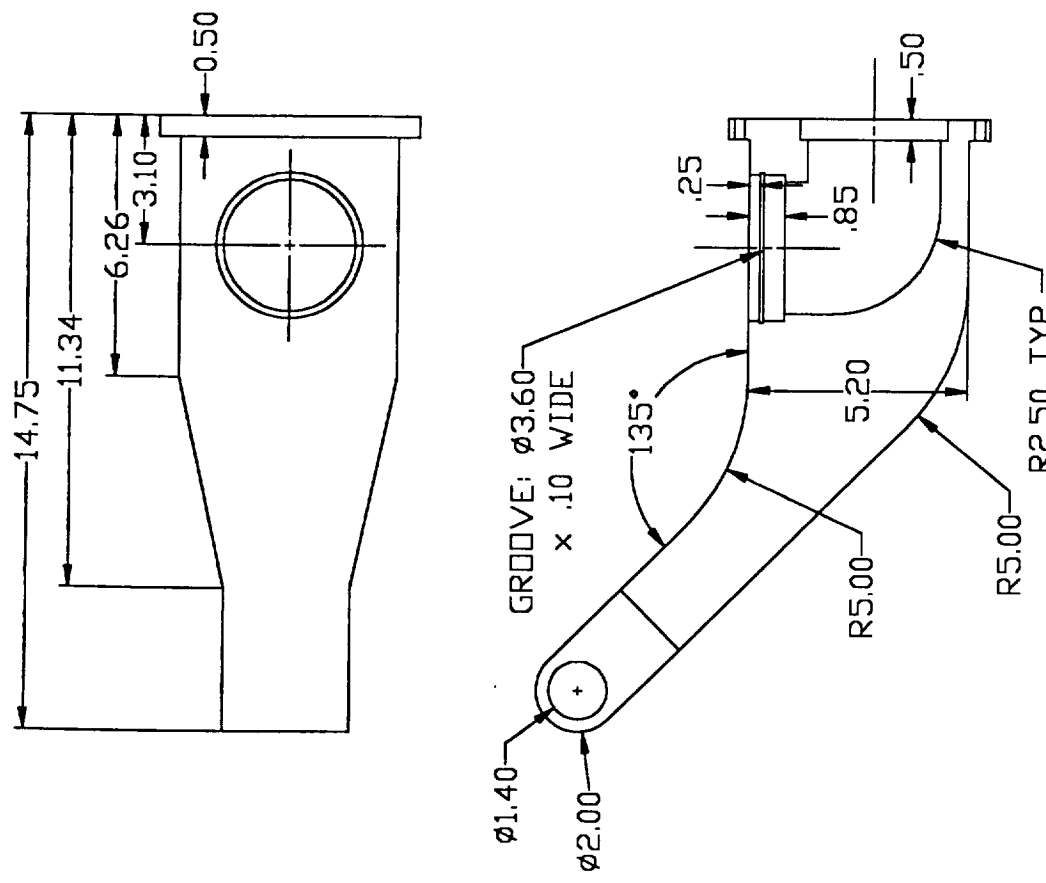


Figure 2.2 CI Strut



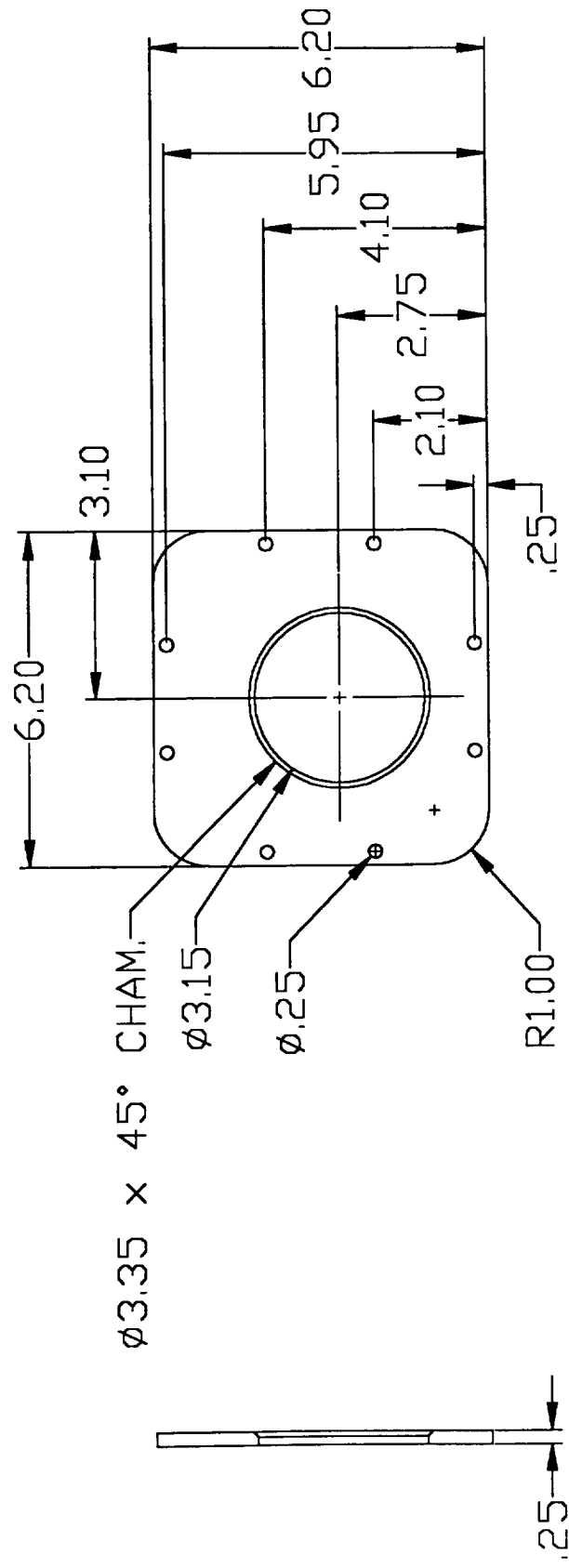
NOTE: 8 BOLT HOLES ARE EQUIDISTANT FROM THE EDGE, SYMMETRIC WITH 6.2 SQUARE.

E.M. DESIGN PROJECT DATE 3-9-94 DRAWN BY A.R.P. SHEET 1 OF 1

TITLE STRUT

ROVER GROUP 1

Figure 2.2 d: Bearing Cover Plate

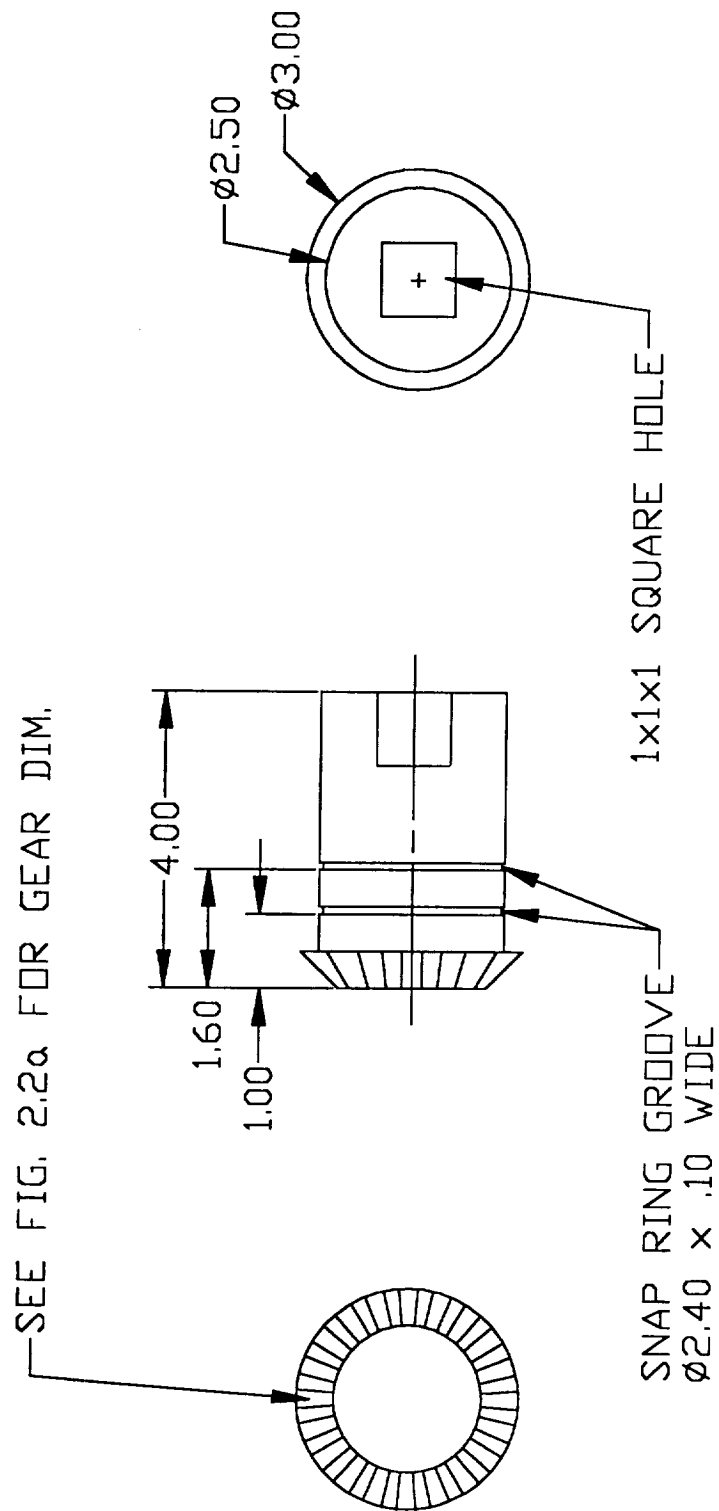


NOTE: 8 BOLT HOLES ARE EQUIDISTANT FROM THE EDGE SYMMETRIC WITH 6.2 SQUARE.

DATE 3-10-94 DRAWN BY A.R.P. SHEET 1 OF 1

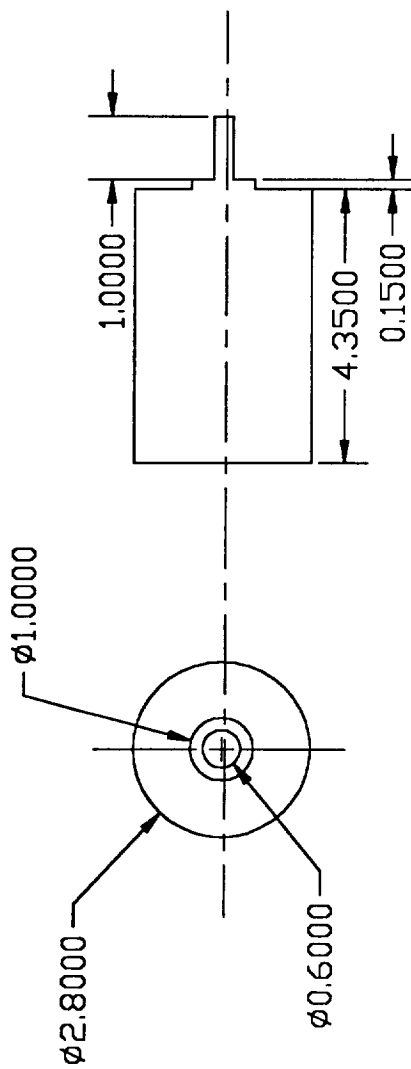
E.M. DESIGN PROJECT	
TITLE	BEARING COVER PLATE
REVER GROUP 1	

Figure 2.2 e: Flexible Shaft Coupling



E.M. DESIGN PROJECT	DATE 3-11-94	DRAWN BY A.R.P.	SHEET 1 OF 1
ROVER GROUP 1	TITLE FLEXIBLE SHAFT COUPLING		

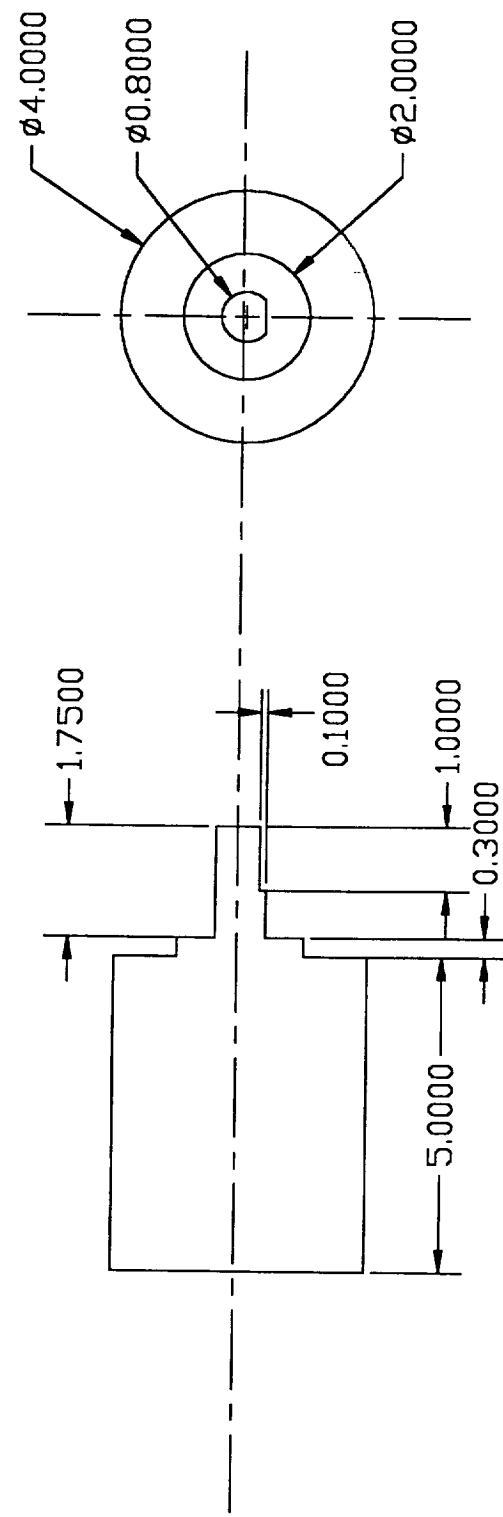
Figure 2.3 ai Motor



ALL DIMENSIONS ARE IN CM.

1	ITEM	DESCRIPTION	MATERIAL
	ITEM	DRAWN BY N. Saunders	SHEET 1 OF 3
E.M. DESIGN PROJECT	DATE 11-21-1993		
ROVER GROUP 1	TITLE MOTOR		

Figure 2.3 b: Gearbox

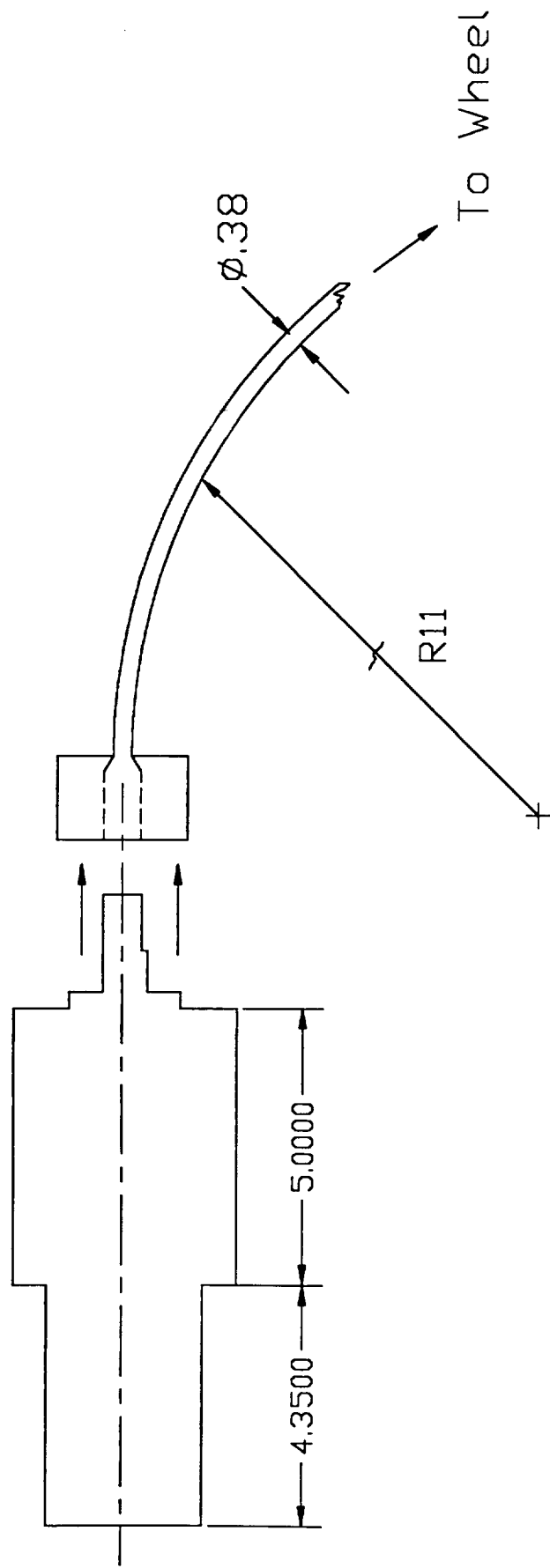


ALL DIMENSIONS ARE IN CM.

ITEM	ITEM DESCRIPTION	MATERIAL
E.M. DESIGN PROJECT	DATE 11-21-1993 DRAWN BY N. Saunders	SHEET 2 OF 3
ROVER GROUP 1		TITLE GEARBOX

E
I

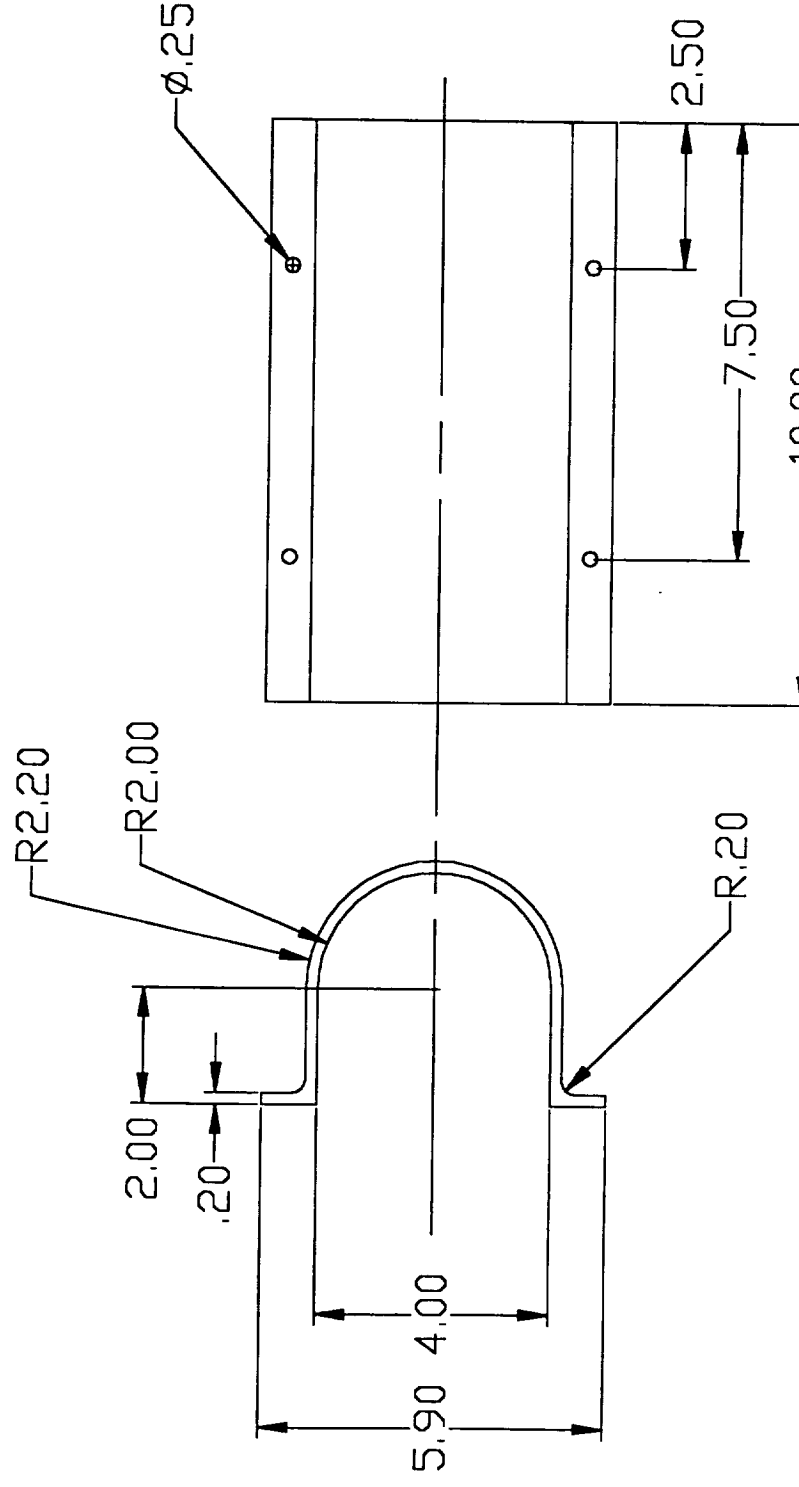
Figure 2.3 c: Gearmotor - Flexible Shaft Assembly



ITEM	ITEM DESCRIPTION	MATERIAL
	DATE 11-21-1993 DRAWN BY N. Saunders	SHEET 3 OF 3
E.M. DESIGN PROJECT		TITLE
ROVER GROUP 1		GEARMOTOR W/ FLEX, SHAFT

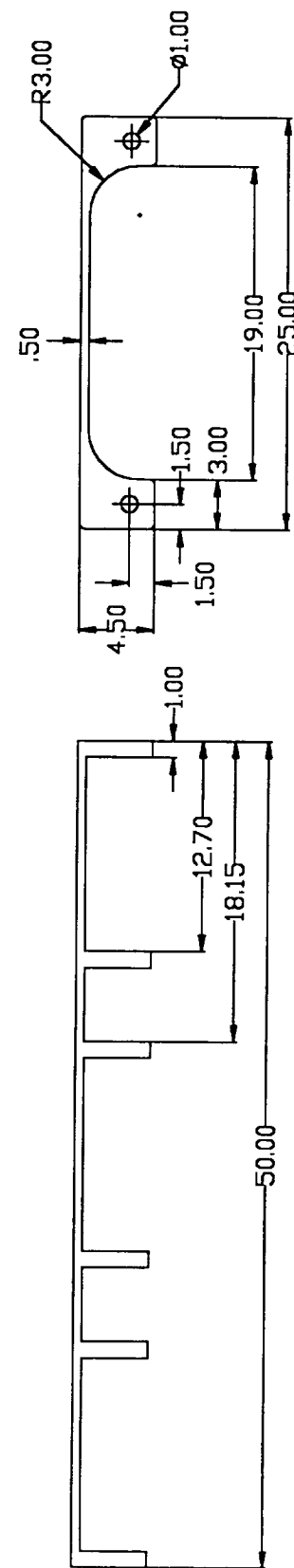
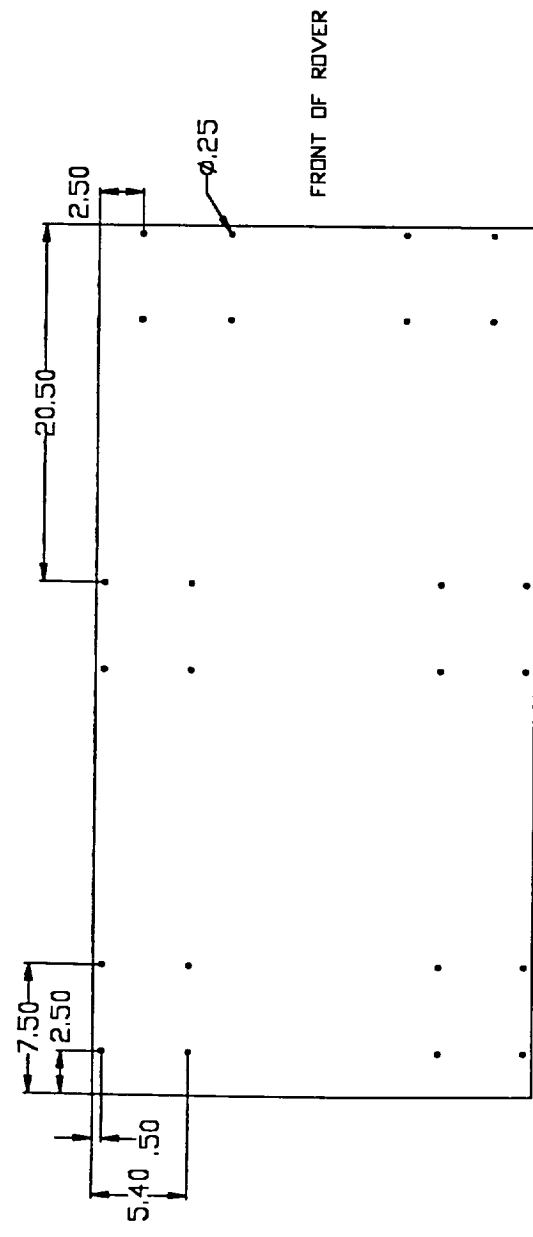
ALL DIMENSIONS ARE IN CM.

Figure 2.3 d: Motor Retaining Bracket



E.M. DESIGN PROJECT	DATE 3-10-94	DRAWN BY A.R.P.	SHEET 1 OF 1
ROVER GROUP 1	TITLE	MOTOR RETAINING BRACKET	

Figure 2.4: Frame



NOTE: STRUCTURE IS SYMMETRIC IN SIDE & FRONT VIEWS.

NOTE: SINCE DIFFERENT HARDWARE HAS VARIOUS PLACEMENTS,
BOLT HOLES FOR MOTORS SHOWN ONLY.

E.M. DESIGN PROJECT	DATE 3-12-94	DRAWN BY A.R.P.	SHEET 1 OF 1
ROVER GROUP 1	FRAME		

Figure 2.5: SALSA

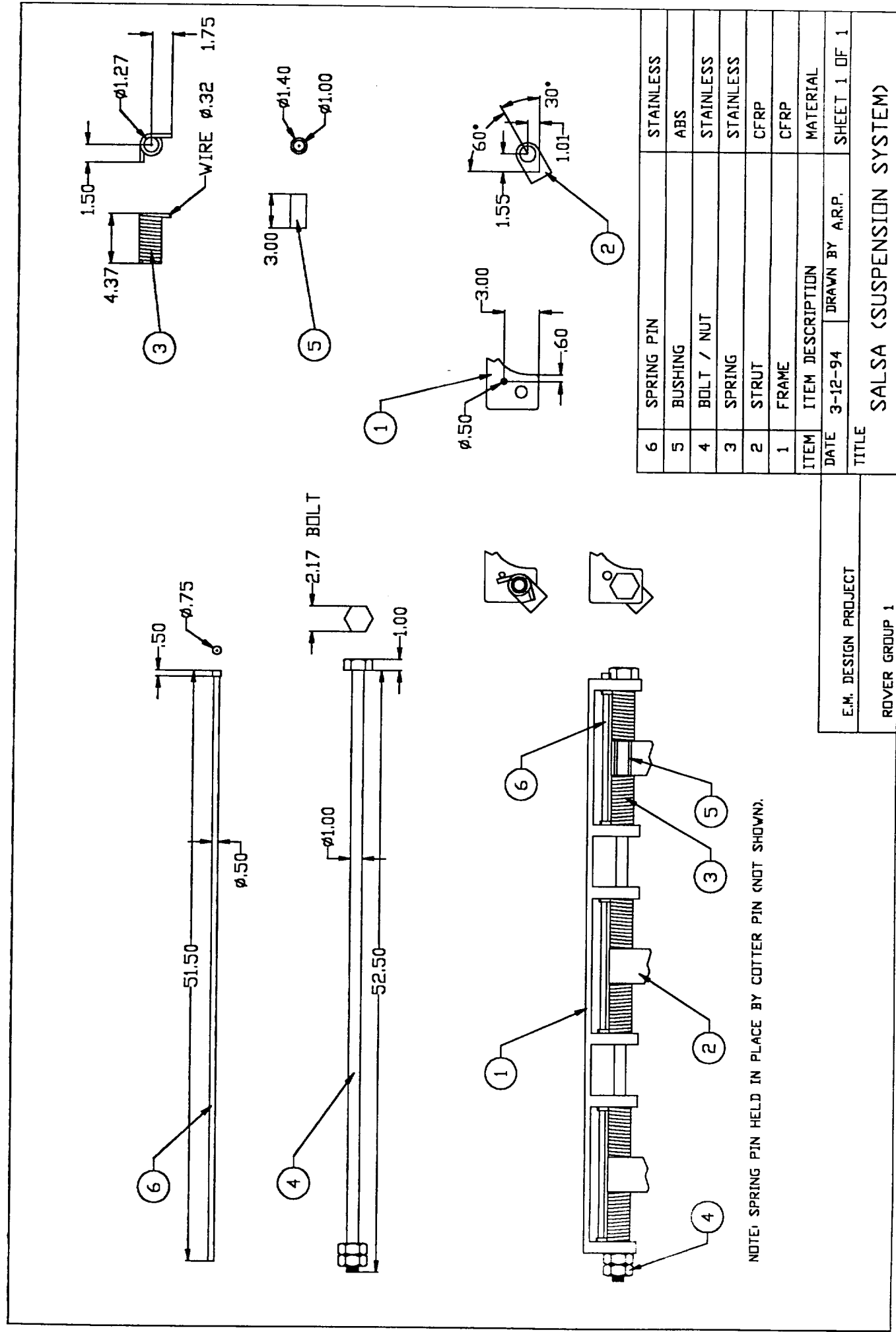


Figure 2.6: Rover Electronics Schematic

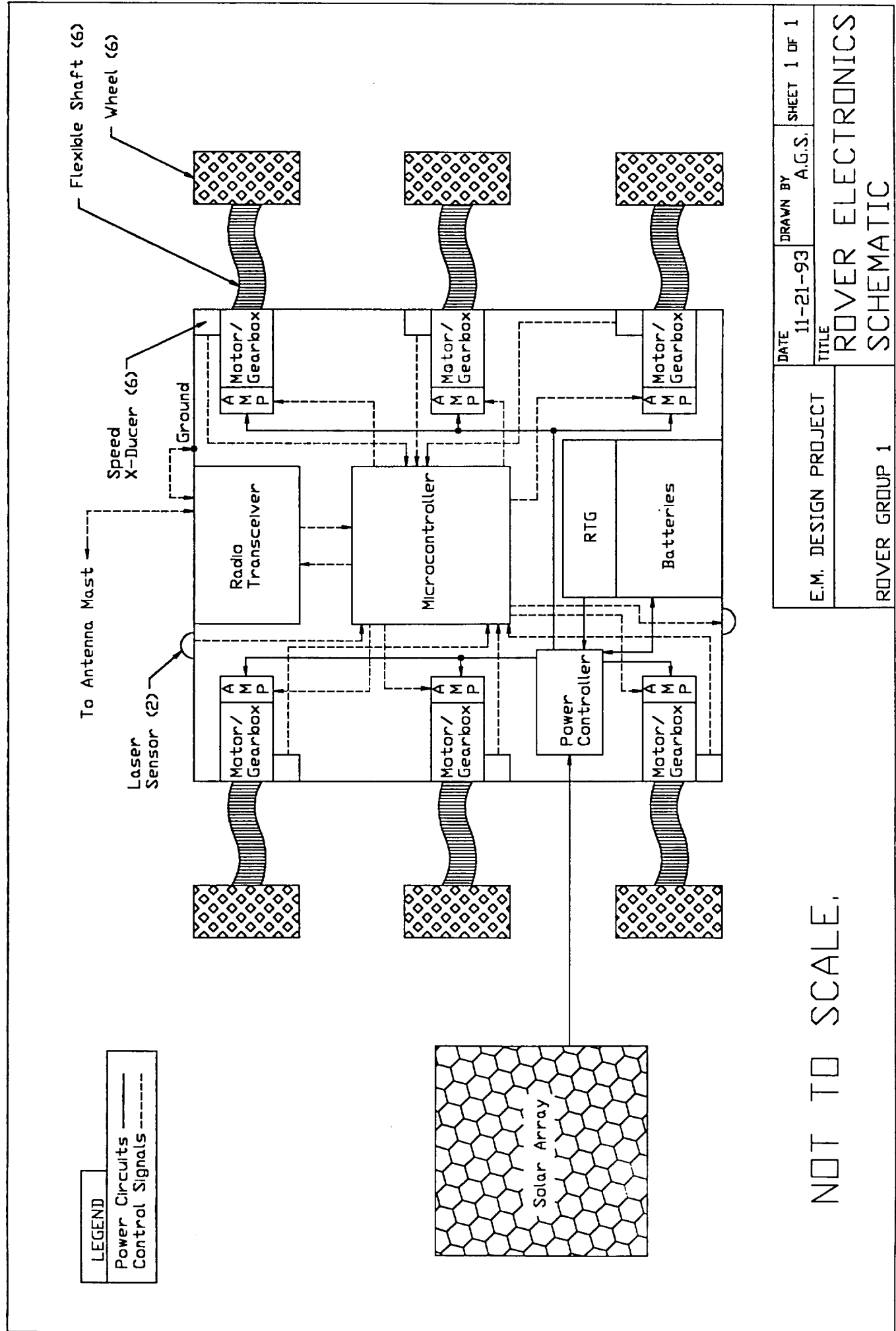


Figure 2.7: Solar Panel

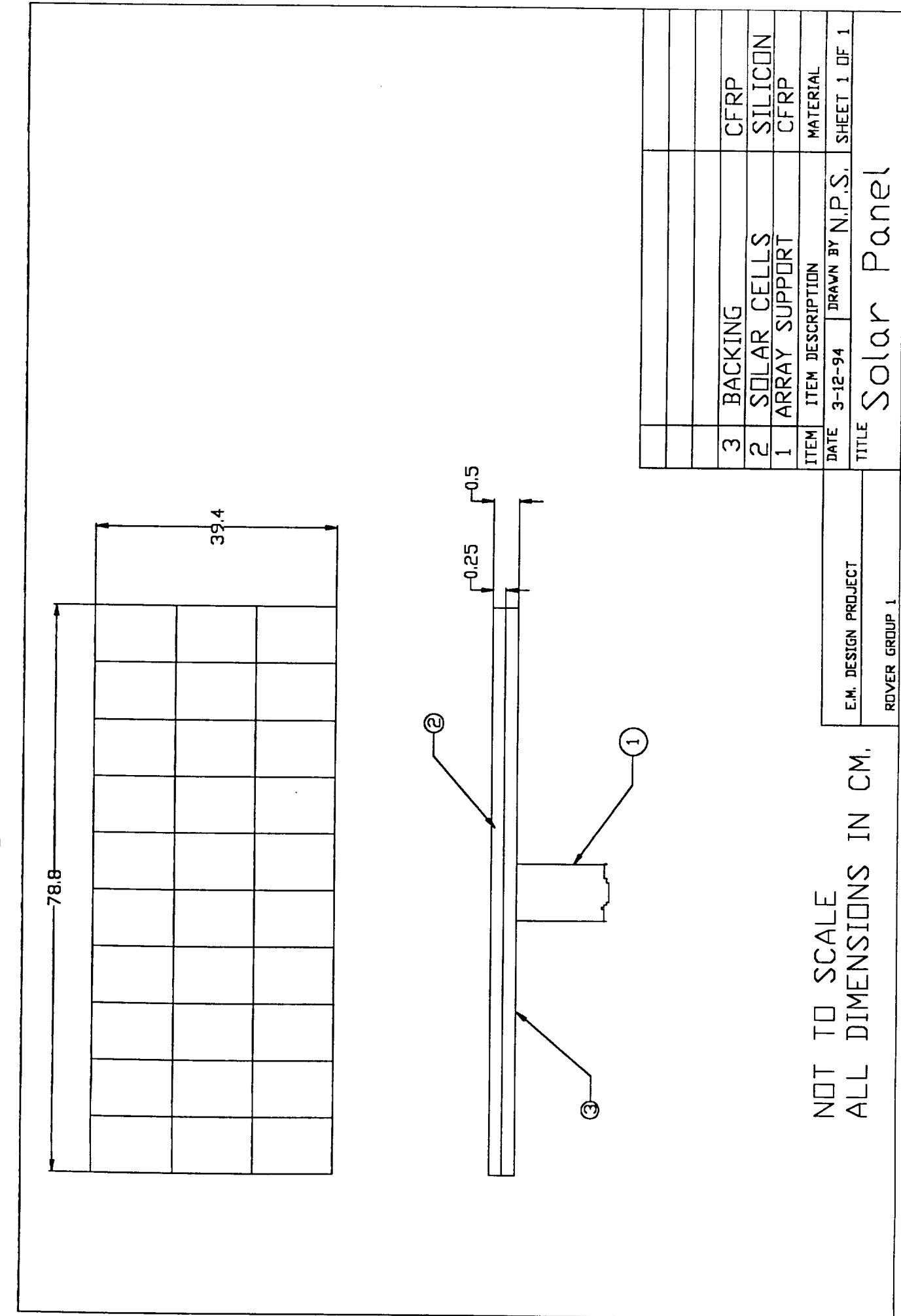
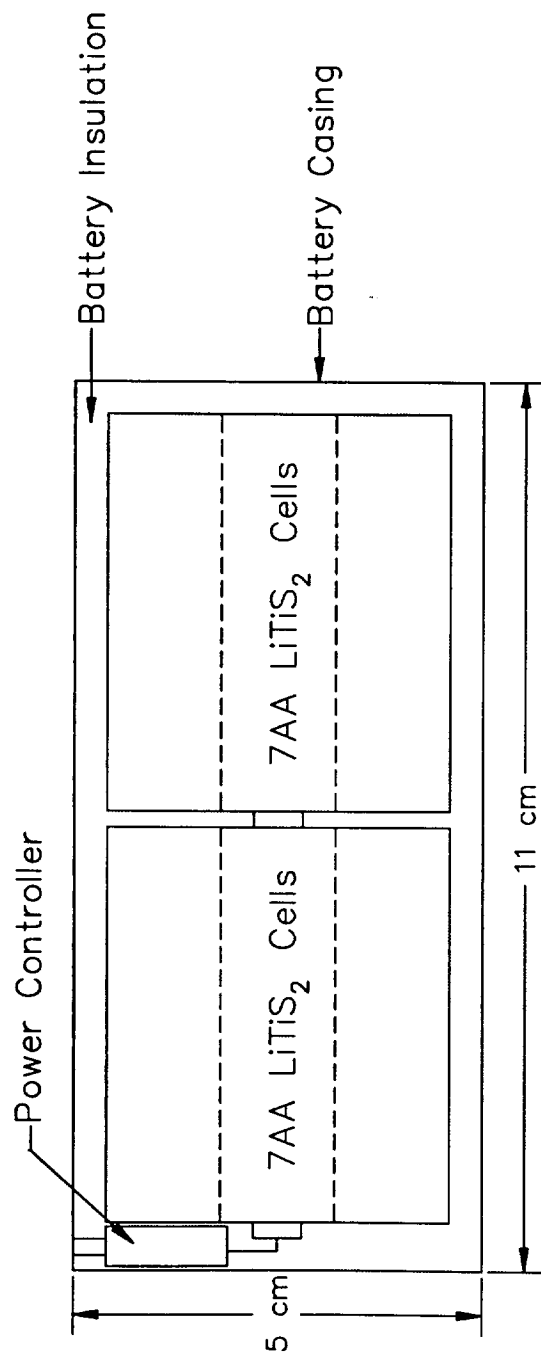


Figure 2.8a: Batteries

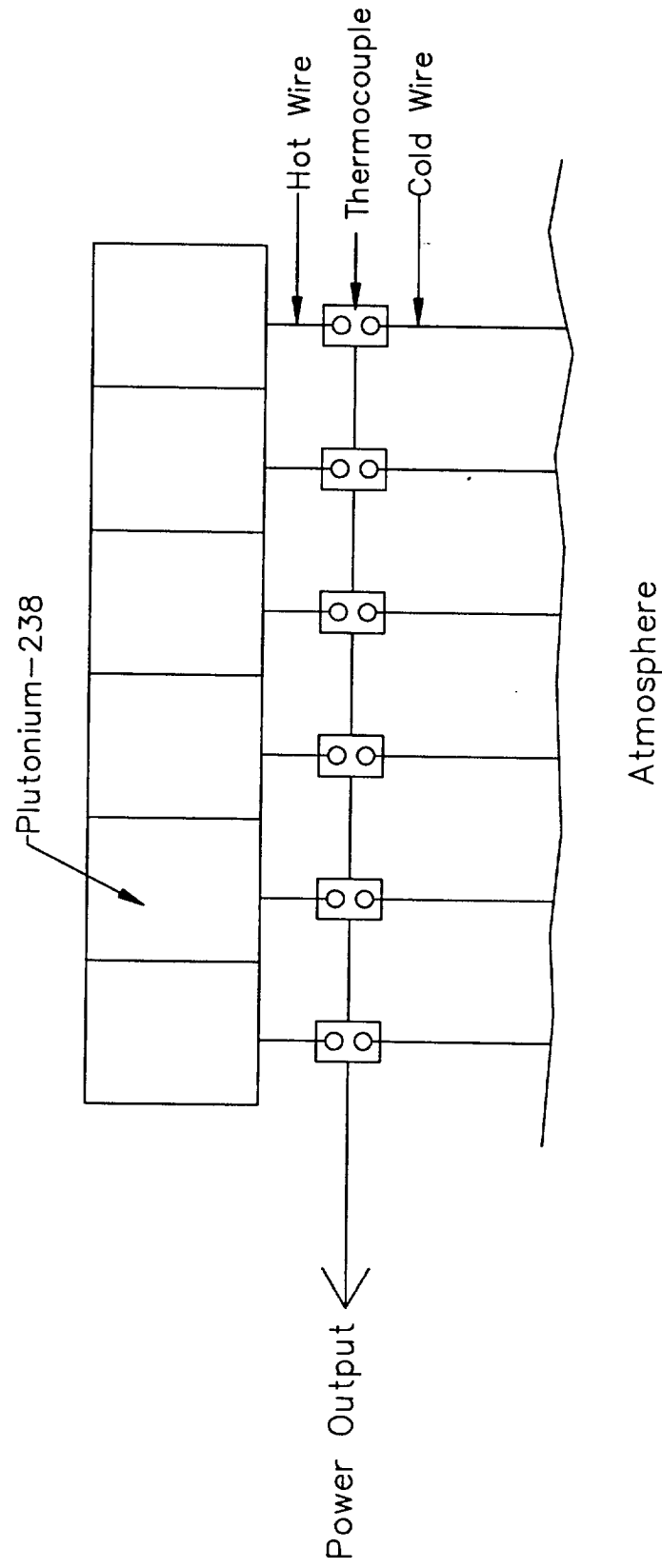
5
10



Cross-Section: Cylindrical

ITEM	ITEM DESCRIPTION	MATERIAL	
		LiTIS2	MATERIAL
1	Batteries		
E.M. DESIGN PROJECT	DATE 3-7-94	DRAWN BY T.L.R.	SHEET 1 OF 1
ROVER GROUP 1	TITLE	BATTERY DIAGRAM	

Figure 2.8b: Radioisotope Thermonuclear Generator



ITEM		ITEM DESCRIPTION	MATERIAL
1	RTG		Plutonium-238
E.M. DESIGN PROJECT	DATE 3-7-94	DRAWN BY T.L.R.	SHEET 1 OF 1
ROVER GROUP 1	TITLE		SCHEMATIC OF AN RTG

ANALYSIS

The following section summarizes the calculations made during the design phase of this project. Generally, the analysis pages list assumptions made followed by major calculations. Each analysis also gives the basic results and an explanation of the meaning behind the results

The first section outlines the SALSA system for the suspension. It also covers the calculations done for the spring which is the primary component of the articulating struts. The second covers the solar array, and the other power related inquires. The following section addresses the navigation and communication followed by the laser systems and the heated compartment. The section concludes with takeoff and landing analysis, stress analysis, failure analysis and finally, cost analysis.

4.42 - 4.47
PREVIOUS PAGE BLANK NOT FILMED

Section 3.1: SUSPENSION SYSTEM

Section 3.1.1 - Calculations for Torsion Springs.¹⁵

This torsion spring design process is outlined in reference (15) in a step-by-step manner, along with several charts and graphs of empirical data used in the design process. The calculations have been carried out in English units in order to avoid complexity.

The following guidelines have been used to establish the design process:

- There are 2 torsion springs on each of the six legs.
- The weight of the rover on Mars is approximately 10 lbs.
- The maximum torque required of the springs is approximately quadruple the steady-state torque.
- The springs are made of 310 stainless steel.
- The perpendicular distance from the pivot point to the wheel is 4 inches.
- The spring is on a shaft of 0.5 in diameter.

The steady-state moment about each pivot point is given by

$$\begin{aligned} M &= (\text{Weight of Rover}) \times (\text{Moment Arm}) / (\text{Number of Legs}) \\ M &= (10 \text{ lb})(4 \text{ in}) / (6) = 6.67 \text{ in-lb.} \end{aligned} \quad (3.1.1.1)$$

The moment which must be provided by each spring is therefore

$$M_1 = M / 2 = 3.34 \text{ in-lb,} \quad (3.1.1.2)$$

and the maximum moment is

$$M_2 = 4M_1 = 13.36 \text{ in-lb.} \quad (3.1.1.3)$$

The stress ratio is given by

$$S_r = (M_2 - M_1) / M_2 = 0.75 \quad (3.1.1.4)$$

From this, reading across a table gives (for stainless steel) a correction factor, $A=0.514$, if an infinite number of cycles are desired. This gives the corrected moment as

$$M_T = M_2 / A = (13.36 \text{ in-lb}) / (.514) = 26.0 \text{ in-lb.} \quad (3.1.1.5)$$

Reading across another table gives the wire diameter, $d=.125$ in. The table also gives basic stress, $S=141,000$ psi.

Given the shaft diameter $D_S=0.500$ inches gives a mean spring diameter of

$$D_T=(1.1)(d+D_S)=(1.1)(.125+.500)\text{in}=.688 \text{ in.} \quad (3.1.1.6)$$

Since

$$D_T/d=.688/.125=5.50 \quad (3.1.1.7)$$

is less than 10, a stress concentration factor must be incorporated by using a new corrected moment,

$$M_T=(26.0 \text{ in}\cdot\text{lb})(1.11)=28.9 \text{ in}\cdot\text{lb.} \quad (3.1.1.8)$$

This gives the same values from the table for wire diameter and basic stress.

The spring index, c , is given by

$$c=D/d=(.500)/(.125)=4.0, \quad (3.1.1.9)$$

and the moment gradient, K , is defined as

$$K=(M_2-M_1)/(\theta_2-\theta_1) \quad (3.1.1.10)$$

Choosing the spring to range from M_2 to M_1 over 45 degrees gives

$$K=(3)(3.34 \text{ in}\cdot\text{lb})/(45^\circ)=0.223 \text{ in}\cdot\text{lb}/\text{deg.} \quad (3.1.1.11)$$

This gives a required wire length, L , of

$$\begin{aligned} L &= d^4 E / (1170 \cdot K) \\ &= (0.125 \text{ in})^4 (29 \times 10^6 \text{ psi}) / (1170)(0.223 \text{ in}\cdot\text{lb}/\text{deg.}) = 27 \text{ inches.} \end{aligned} \quad (3.1.1.12)$$

With 1/2" arms at each end of the coil ($l_1=l_2=0.5"$), the active length becomes

$$L_b=L-1/3(l_1+l_2)=26.7 \text{ inches.} \quad (3.1.1.13)$$

The tentative number of coils is therefore

$$N_T=L_b/\pi D_T=(26.7 \text{ in})/(3.14)(.688 \text{ in})=12.4 \text{ coils.} \quad (3.1.1.14)$$

To make the arms end up at 90° to each other, this can be changed to $N'=12.75$. From this, the body length of the coil is

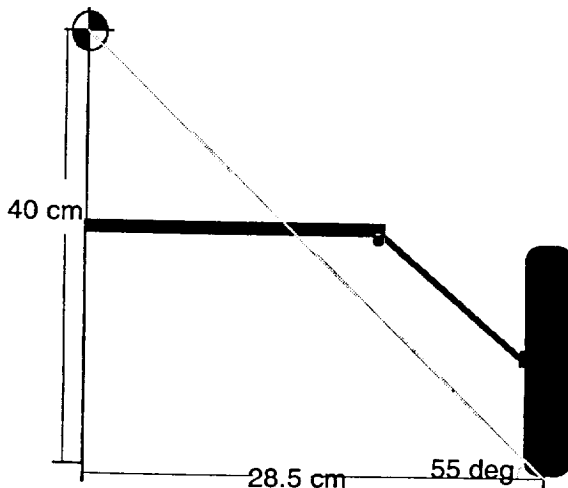
$$h'=d(N'+1)=(.125 \text{ in})(13.75)=1.72 \text{ inches.} \quad (3.1.1.15)$$

Thus, in metric units, the coil springs are made of 3.2mm wire, with 12.75 coils around a 12.7mm ID, for a total spring length of 43.7mm. Each spring provides a moment of 0.377 N·m at $\theta=0$ and 1.51 N·m at $\theta=45^\circ$.

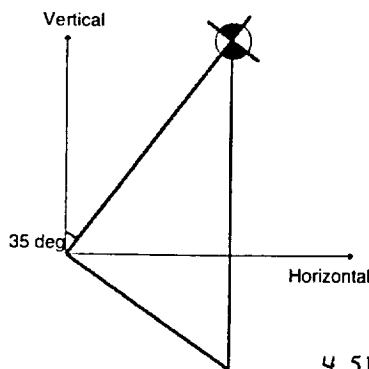
Section 3.1.2 - Suspension and Lateral Stability Assembly (SALSA)

To determine the lateral stability of the Mars Rover a few assumptions about its physical dimensions must be made. It should be noted that the dimensions used here are extreme, used because they give a reasonable safety factor and allow room for variation in environmental assumptions made earlier. It should be noted that wind effects were not considered in this calculation, and momentum effects were also neglected.

The primary concern of the study of the rovers lateral stability is to prevent a roll over which would leave the rover useless, since it is unable to right itself. The rover in



Simple Picture of Half of Rover (as viewed from front)



Roll Over Situation

this calculation will be represented by a simple point mass and a representative footprint. The point mass is located at a position which is assumed to be higher than the actual center of gravity.

The rover will occur when the center of gravity is no longer above the base of support. This will occur when the vertical normal of the rover is approximately 35 ° off of the gravitational vertical.

Since the number is a general one, it is advisable to reduce it in the interest of safety and referring to the mission profile (which assumed a maximum environmental slope of 15°). Therefore the rover should be limited to attempting to navigate a lateral slope of 20° , and not attempt to navigate lateral slopes that are any larger.

Section 3.2: POWER

Section 3.2.1 - Mechanical Power Requirement

The mechanical power needed to move the rover at the required speed (0.1 m/s) was calculated in order to choose appropriate motors. A worst case condition was used in this calculation; the rover is assumed to be at rest on a 15° incline. The maximum power required from the motors would occur when the rover must proceed up the incline at a speed of 0.1 m/s.

Several assumptions were made in the following calculation. The local acceleration of gravity at the polar cap was assumed to be a constant, 3.73 m/s². No mechanical power loss was assumed between the flexible drive shafts, the wheel bearings and right angle gear. Power loss in the bearing and gearbox were assumed negligible, while the power loss in the flexible shafts are quoted in the manufacturer's specifications*, and are taken into account in motor selection.

The mass of the on board science equipment (OSE) is an approximate figure. The figure is conservative in order to assure that the OSE mass will not exceed that of the figure used in calculations. The entire rover mass was calculated by adding up the masses of the individual components. Several abbreviations are used: f=frame; st=struts; mgs=motors, gears, and shafts; b=batteries; w=wheels, e=electronic equipment.

$$M_{rover} = M_f + M_{st} + M_{mgs} + M_b + M_w + M_{ose} + M_e \quad (3.2.1.1)$$

The mass of each component is equal to its material density multiplied by its volume.

$$M_f = d_f * v_f = (2.2 \text{ g/cm}^3)(625 \text{ cm}^3) = 1375 \text{ g}$$

$$M_{st} = d_{st} * v_{st} = (2.2 \text{ g/cm}^3)(66.6 \text{ cm}^3) = 146.5 \text{ g}$$

$$M_w = d_w * v_w = (5.1 \text{ g/cm}^3)(304 \text{ cm}^3) = 1551 \text{ g}$$

The mass of the motors, shafts, and gears are taken from the manufacturer's specifications*. Six of each will be used, requiring a factor of six for the mass.

$$M_{mgs} = (6)(125 \text{ g} + 155 \text{ g} + 20 \text{ g}) = 1800 \text{ g}$$

The mass of the battery equipment and electronics is also supplied by the manufacturers*.

$$M_b = (130 \text{ g} + 300 \text{ g} + 1200 \text{ g}) = 1630 \text{ g}$$

$$M_e = 900 \text{ g}$$

$$M_{ose} = 2410 \text{ g}$$

$$M_{rover} = (1375 + 146.5 + 1551 + 1800 + 1630 + 900 + 2410) \text{ g} * (1 \text{ kg} / 1000 \text{ g}) \\ = \underline{9.81 \text{ kg}}$$

$$\text{Weight on Mars} = M_{rover} * g = (9.81 \text{ kg})(3.73 \text{ m/s}^2) = \underline{36.6 \text{ kg m/s}^2}$$

Figure 3.2.1.1 shows a free body diagram of the rover on a 15° incline. W is the weight of the rover, F_s is the force due to surface friction on the wheels, and F_b represents the friction of the wheel bearings. The force P is that which is required to move the rover up the incline at a pre-determined speed.

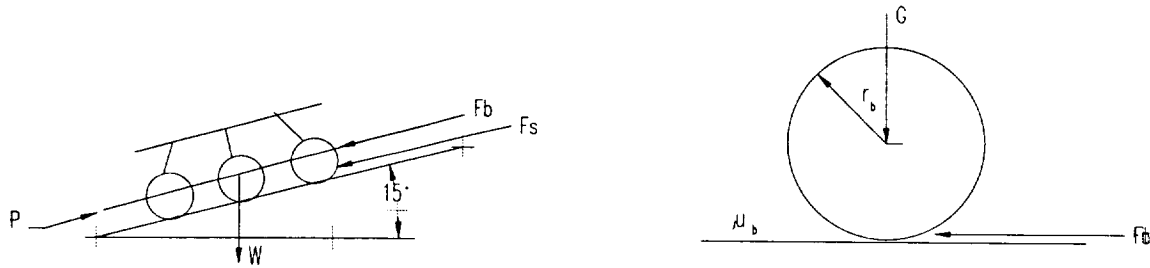


Figure 3.2.1.1: Free body diagram of the rover and a bearing.

In calculating the surface friction F_s , the value of static friction between the surface and the wheels, μ_s , was assumed to be a worst case value, $\mu_s = 0.3^*$. The friction force is equal to the normal force at the wheel times the coefficient of static friction.

$$F_s = n * \mu_s \quad (3.2.1.2)$$

The normal force is found from simple trigonometry.

$$n = w_{rover} * \cos (15^\circ) \quad (3.2.1.3)$$

$$= (36.6 \text{ kg m/s}^2) * (.9659) = (35.35 \text{ kg m/s}^2)$$

Therefore,

$$F_s = (35.35 \text{ kg m/s}^2)(0.3) = 10.61 \text{ kg m/s}^2 \quad (3.2.1.4)$$

The next step is to calculate the friction force of the bearing. The coefficient of friction of the bearing, μ_b , is approximately 0.05. This value was determined from the properties of CFRP and steel*. The rolling condition is that $\mu_b * G$ must be greater than the friction force F_b^* . The equation for finding F_b is

$$F_b = (l/r_b)G \quad (3.2.1.5)$$

where l is the lever arm of rolling resistance, equal to $0.25r_b^*$. The value of G is taken to be the weight of the rover minus the weight of its wheels.

$$G = (w_{rover} - w_{wheels}) \quad (3.2.1.6)$$

$$= (36.6 - 5.78) \text{ kg m/s}^2 = 30.82 \text{ kg m/s}^2$$

Therefore,

$$F_b = (.00125 \text{ m} / .005 \text{ m}) * 30.82 \text{ kg m/s}^2 = 7.71 \text{ kg m/s}^2$$

From Figure 3.2.1.1a, equilibrium requires that the sum of the forces in the $+15^\circ$ \angle must be zero. Therefore,

$$P = [w_{rover} * \sin(15^\circ)] + F_s + F_b \quad (3.2.1.7)$$

$$= [36.6 \text{ kg m/s}^2 * 0.259] + 10.61 \text{ kg m/s}^2 + 7.71 \text{ kg m/s}^2$$

$$= 27.79 \text{ kg m/s}^2$$

The required power to drive the rover up the incline at 0.1 m/s is equal to the applied force P from the motors times the speed of the rover.

$$\text{Power} = P * s \quad (3.2.1.8)$$

$$= (27.79 \text{ kg m/s}^2)(0.1 \text{ m/s})$$

$$= 2.78 \text{ kg m}^2/\text{s}^3 = \underline{\underline{2.78 \text{ W}}}$$

Appendix C contains a computer code which computes the required power and torque to move the rover up various inclines, ranging from 0 to 60 degrees. The results are shown below, in Figure 3.2.1.2.

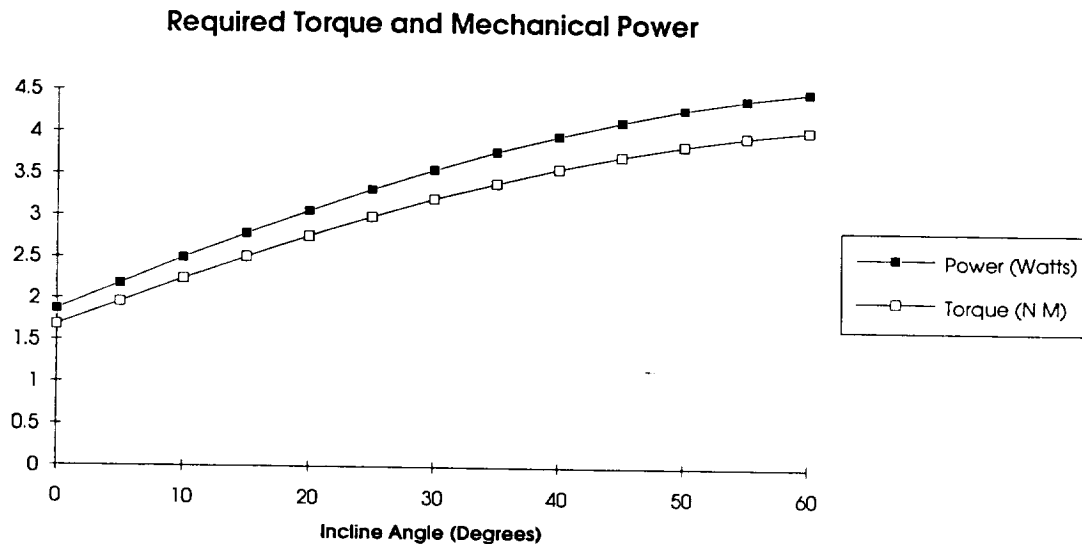


Figure 3.2.1.2 : Chart of power and torque vs. incline angle.

Sufficient power to drive the rover will be produced by the solar panel during the summer months. During the winter, the rover will likely be stationary, due to the relatively large amount of power required to mobilize the vehicle.

Section 3.2.2 - Motor Power Requirement

Six motors and six gearboxes need to be selected to provide enough torque to the wheels to allow the rover to travel up a 15 degree incline at a velocity of 0.1 m/s. The mechanical power required was determined from section 3.2.1 and from this the torque for each wheel can be found. It is then a matter of sizing the motor and gearbox with the power output from the solar array. The following equations are from the 93/94 edition of the Escap motor catalog.³

Incline and Wheel Figures for Torque Determination

$$v=0.1 \text{ m/s}$$

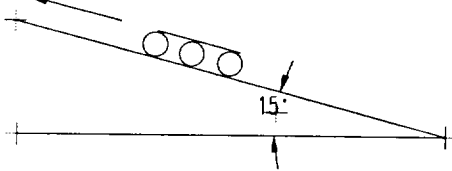


Figure 3.2.2.1 (a)

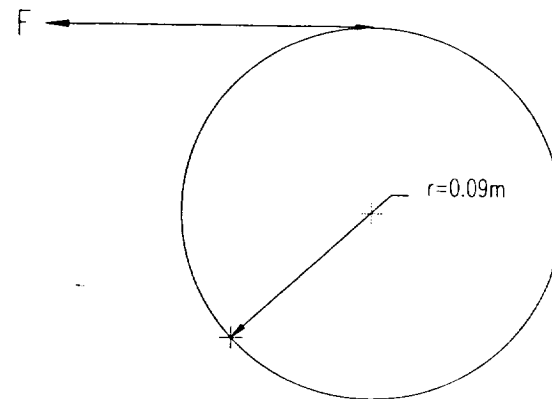


Figure 3.2.2.1 (b)

The mechanical power, calculated earlier in section 3.2.1, required to move the rover up a 15 degree incline at 0.1 m/s is 2.78 Watts. From this value the force required for each wheel can be determined by the equation:

$$F = P_M / v \quad (3.2.2.1)$$

Then the torque required is found by the equation:

$$T = F * r \quad (3.2.2.2)$$

The power output from the solar array was calculated to be 10.5 Watts, from section 3.2.3. The flexible shafts are 85% to 95% efficient.³² The gearbox efficiency is 55%.³³ To account for frictional losses, the torque lost by the right angle gear box and the flexible shafts is computed and then this result is added to the original torque required by each wheel. The following equations show this process.

Determine force for each wheel:

$$(2.78 \text{ W} / 0.1 \text{ m/s}) = 27.8 \text{ N} * (1/6 \text{ wheels}) = 4.63 \text{ N/wheel} \quad (3.2.2.3)$$

Calculate torque:

$$T = (4.63 \text{ N/wheel}) * (0.09 \text{ m}) = 0.42 \text{ Nm/wheel} \quad (3.2.2.4)$$

Torque lost due to friction:

$$2*[0.42 \text{ Nm} - (0.42 \text{ Nm})*(0.85)] = 0.126 \text{ Nm/wheel} \quad (3.2.2.5)$$

Torque produced by gearbox:

$$(0.42 \text{ Nm/wheel} + 0.126 \text{ Nm/wheel}) = 0.546 \text{ Nm/wheel} \quad (3.2.2.6)$$

The angular velocity was computed using the following equation:

Revolutions per minute of the wheel:

$$(0.1 \text{ m/s})*(1/(2*\pi*0.09\text{m}))*(60 \text{ s/min}) = 10.6 \text{ rev/min} \quad (3.2.2.7)$$

Using this number and the maximum input speed of the gearbox, which is 5000 rpm, the required gear reduction was found to be approximately 471.7:1.³ This number was found from the following equation:

Gear ratio:

$$i \leq n_{max}/n_L \quad i \leq 5000\text{rpm}/10.6\text{rpm} = 471.7 \quad (3.2.2.8)$$

For this rover a gear reduction of 405:1 was chosen. The efficiency of this gearbox is 55%.³

Now the motor speed and the required torque must be calculated. The speed of the motor has to be less than 5000 rpm which is the maximum input speed of the gearbox. To calculate the speed of the motor multiply the speed of the wheel by the gear reduction. For this rover the speed required by the motor is 4,293 rpm. To calculate the torque required by the motor use the following equation:

Torque required by the motor:

$$M_M = M_L/(i*\eta) \quad M_M = 0.546\text{Nm}/(405*0.55) = 2.45 \text{ mNm/wheel} \quad (3.2.2.9)$$

Next the current the current required by the motors is determined:

Current required by the motor: (3.2.2.10)

$$I = M/k \quad I = 2.45 \text{ mNm}/11 \text{ mNm} = 0.22 \text{ Amps}$$

The temperature and resistance of the rotor have to be determined by using the following equations:

Determine temperature and resistance of rotor:

$$T_r = \frac{(R_{22} * I^2 * R_{th} * (1 - 22 * \alpha) + T_{amb})}{(1 - R_{22} * I^2 * R_{th} * \alpha)} \quad (3.2.2.11)$$
$$\alpha = 0.0039 \text{ 1/deg C} \quad R_{22} = 1.45\Omega \quad T_{amb} = -40 \text{ deg C}$$
$$R_{th} = 17 \text{ deg C/W} \quad I^2 = 0.048A^2$$

T_r is determined to be -39.1 Deg. C. From this the resistance of the rotor at that temperature is found by:

Resistance of the rotor at -38.63 deg C: (3.2.2.12)

$$R = R_{22} * [1 + \alpha * (T_r - 22 \text{ deg C})]$$

The resistance of the rotor is determined to be 1.1 Ohms. Now the voltage of the motor can be determined by the following equation:

Voltage required by the motor: (3.2.2.13)

$$V = R * I + k * \omega \quad V = (1.1 \Omega * 0.22 A) + (2\pi * (4293 \text{ rpm} / 60)) * (11 \text{ mNm}) = 5.187 \text{ Volts}$$

The power required by all six motors is found by multiplying the voltage by the current times six wheels equals 6.85 Watts.

Section 3.2.3 Solar Array Size, Power Output, and Tracking System

A solar array is needed to produce electricity to supply power to the motors and to also charge the batteries and provide power to the electronics. The array area is initially set to 0.31 m². The solar cells are made up of silicon and are covered by a clear coating to protect them from dirt and radiation. The area of the array can be increased to increase the power output or decreased to reduce the size of the array, but this has the effect of reducing the power output.

Some assumptions made for this particular array are that the solar intensity on a

clear day on the surface of Mars is 30 mW/cm^2 , the light hitting the array surface is perpendicular to it and is maintained by rotating the array with a sun tracking device, the degradation factor is set at 0.75, and the efficiency of the solar cells can be assumed to be 15%.

To determine the power output of the solar array use the following equation:²⁹

$$A_A * s * \cos \Gamma * \eta * F = P_A \quad (3.2.3.1)$$

Substituting in the values:

$$0.31\text{m}^2 * 300\text{W/m}^2 * (\cos 0) * 0.15 * 0.75 = 10.5 \text{ Watts.}$$

The solar array tracking system is designed to rotate the solar panel so the light hitting the surface is perpendicular to the panel. This assures the maximum output of the solar panel. There will be four linear servos controlling the direction of the solar panel. The computer will determine which solar cells are producing the most electricity and then activate the linear servos to balance out the power output from all the solar cells. The linear servos will not continuously run. They will only be activated when needed so as to reduce the power drain.

The following figure show the possible motion of the array.

Rotation of Array

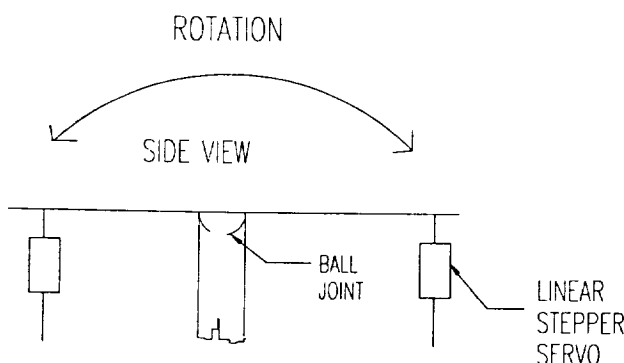


Figure 3.2.3 (a)

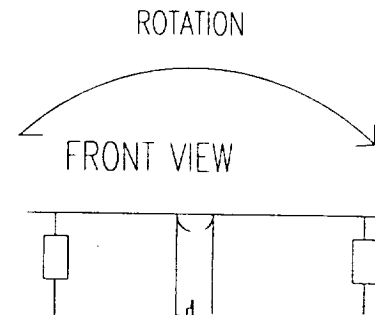


Figure 3.2.3 (b)

Section 3.2.4 RTG Power Output

The Radioisotope Thermoelectric Generator, or RTG, is the most reliable and consistent power source being employed on the rover. It will be used to power almost every rover system at one time or another throughout the Martian year. An RTG works by converting heat directly into electricity. An electric voltage is produced when two dissimilar, electronically conductive materials are joined in a closed circuit and the two junctions are kept at different temperatures. In an RTG, these pairs of junctions are called thermocouples. The thermocouples use heat from the radioactive decay of a radioisotope, which is Plutonium-238 in this case, to heat the hot junction and cold ambient air to produce a low temperature at the cold junction. The power output is a function of the temperature of each junction and of thermoelectric materials properties. A schematic diagram of an RTG is shown in Figure 2.8b. The particular RTG that will be used here is the Modular (MOD) RTG, because of its excellent specific power in comparison to other RTG models.

$$\text{Specific Power} = 7.5 \text{ W}_e/\text{kg}$$

$$\text{Converter Efficiency} = 7.6\%$$

The data available on the MOD-RTG is:

$$\text{Mass} = 41.1 \text{ kg}$$

$$\text{Size} = 1.08 \text{ m long} \times .33 \text{ m dia. (cylindrical shape)}$$

This is obviously too large and heavy for the micro rover, so a conversion must be made to modify the size. The MOD-RTG scales down in a nearly linear fashion which simplifies the conversion. A size for the RTG was selected through an optimization comparison between available space and power required. The down-scaling was performed using the volume of the above unit.

$$\text{Volume of original MOD-RTG} = \pi(.33/2)^2(1.08) = .09 \text{ m}^3$$

The size of the RTG required by our rover is:

$$\text{Size} = .22 \text{ m long} \times .07 \text{ m dia.}$$

This is used to find the volume of the unit for the micro-rover.

$$\text{Volume of RTG for Rover} = \pi(.07/2)^2(.22) = .00085 \text{ m}^3$$

The ratio between the two volumes allows the power output to be scaled down from the larger unit.

$$\text{Scale Ratio} = .09/.00085 = 106$$

$$\text{Mass of RTG} = 41.1 \text{ kg}/106 = .388 \text{ kg}$$

$$\text{Power output of rover RTG} = (.388 \text{ kg})(7.5 \text{ W/kg}) = \mathbf{2.91 \text{ W}}$$

Section 3.2.5 Battery Power Output

Secondary, or rechargeable batteries are useful in a micro rover to assist in fulfilling peak power requirements. The batteries used in this rover are LiTiS₂ AA cells that are taken from the design of the Power Stick, a radioisotope heater unit. Two sets of fourteen AA cells were selected to deliver adequate auxiliary and peak power to the rover and its subsystems. A diagram of the batteries is provided in Figure 2.8a. The data for the batteries follows:

$$\text{Energy density} = 120 \text{ W-hr/kg}$$

$$\text{Mass} = (.220 \text{ kg})(2 \text{ sets}) = .440 \text{ kg}$$

$$\text{Size} = .11 \text{ long} \times .047 \text{ m wide} \times .095 \text{ m high}$$

$$\text{Output} = (.440 \text{ kg})(120 \text{ W-hr/kg}) = \mathbf{52.8 \text{ W-hr}}$$

Section 3.2.6 Radiation Effects

The rover will obviously be exposed to some level of hard radiation during the space voyage from Earth to Mars, as will all the instrumentation, but this is considered to be beyond the scope of this report. The radiation source of chief concern is the RTG, containing a pile of Pu²³⁸, which has a radioactive activity of 1.3×10^5 Ci (Curies.) However, very little radiation will escape as the product of Pu²³⁸ decay is alpha particles, which can be effectively shielded by thick paper. The rover components which will be most sensitive to any escaping radiation are the microelectronics devices such as the CCD video camera and the microchips in the computer system. The metal components will be mostly immune to radiation effects, but almost all plastics have their performance degraded by exposure to radiation, so this must also be considered.

It is assumed that to avoid damaging the microelectronics components of the rover, the radiation levels seen must be reduced to the same order as those seen by similar components used in terrestrial applications. The plastic materials must likewise receive the same level of protection. The best way to accomplish this is to place a shield around the entire RTG with a thin layer of dense material, such as lead, although some more bulky material may offer a weight advantage.

The analysis of radioactive shielding is extremely dependent upon the geometry of the system, the shielding material (and its micro structure), and the type of radiation(s) involved. Much of what is done with shielding is still semi-empirical. The design will have to be achieved by experimentally reproducing the conditions on Mars, including the temperatures, and measuring radiation levels as well as degradation rates of the materials around the RTG. It is also desirable to physically remove the microelectronics from the RTG as an extra measure of safety.

Section 3.3: NAVIGATION AND COMMUNICATIONS

Section 3.3.1 - Rover Navigation Logic

There are two primary concerns involved in the rover's navigation logic pattern: self-preservation and completion of the mission. The rover will be expected to travel in a straight line for as long as possible, until stopped by an obstacle or a command. The movement of the rover is not totally independent; the lander and Earth based operators need to have input. The rover is programmed to move in a straight line, referring occasionally to the onboard navigation memory to maintain its path. While traveling in a straight line, the rover's computer will monitor both the laser ranging system, and the artificial horizon for possible obstacles. If the rover comes to an obstacle it will attempt to avoid it by the methods detailed here.

The rover, as is designed , is capable of navigating a slope of 15° , and overcoming an obstacle of 10cm. The rover has to be able to do is detect situations which exceed these parameters, and then decide what course of action it needs to take.

There are four distinct situations which the rover will have to deal with: an up-slope in excess of 15° , a down-slope in excess of 15° , an obstacle exceeding 10cm in height, and an excessive lateral slope. Of these situations, the first three are to be detected by the laser ranging system, the fourth will have to be addressed by an artificial horizon.

When dealing with an up-slope in excess of 15° , the rover must first stop to decide its course of action. If the slope in not significantly greater than 15° , and the slope is gentle and even, the rover can transverse the slope laterally, moving across the slope such that the real angle it is climbing is less than 15° . This tactic is based upon the fact that the 15° limit was used in determining the maximum power required by the motors, but it is limited by the uncertainty of the static coefficient of friction on the surface, as well as the tire's tread pattern and the resistance it presents to lateral sliding. If, on the other hand, the slope is greatly in excess of 15° , the rover will have to reverse its direction

move for a short distance (either by backing up, or by rotating and moving away), and attempt to move forward on a slightly different path. In this situation it would be helpful if the Earth based operators altered the desired direction of travel, because the conditions vary widely from the predicted situation.

A down-slope of greater than 15° , can be dealt with in a similar method as the excessive up-slope. One option is to traverse the descent for minor and stable situations, or retreat for reconsideration for excessive ones. An important question is raised by these excessive slope situations: should a rover be sent, if a situation arises from which it might not escape, to investigate unexpected phenomenon?

The 10cm obstacle is the situation which the rover has the greatest latitude. If the obstacle is reasonably small, i.e. between 10cm and 15cm above the general surface, the rover may choose to travel over it. Using the rovers exceptional ground clearance, the rover can attempt to just "drive over" the obstacle. However care must be taken that the obstacle is limited in dimensions, because the rover may not be able to rotate if the obstacle (like a ridge or a "wall") is underneath it. If the obstacle is significantly large, the rover should reverse course for a short interval (to distance itself from the obstacle), rotate to a new heading, and move forward and around the obstacle.

There are two dangers involved with an excessive lateral slope. First the rover may slide down the slope, and into a situation from which it would be difficult, or impossible, to extricate itself. The second, and far more dangerous, risk is of a roll over. If a roll over were to occur, the rover would become totally inactive because its solar panel array may be out of the light and there is no procedure or designed gear that might be used in righting an overturned rover. While the critical lateral slope has yet to be determined, it is unlikely that it will be below 25° . Lateral slopes would have to be detected by an artificial horizon since the laser ranging system only is able to detect forward slope relative to the orientation of the rover.

While the rover may be instructed as to what general direction the Earth-bound controls wish, the rover must decide which exact route to take. In referring to exact route, the meaning is meant to apply to a very short range: less than a few meters in front of the rover. When the situation arises that the rover cannot deal with an obstacle by the reverse and re-attempt or other methods, it will have to get help. The rover will have to "look" at a map. It would be cumbersome to have the rover's computer do this itself, thus it would seek instructions from a remote navigation advice and instruction system. This could be done by a dedicated mapping subsystem administrated by the lander (where power and size restrictions are less critical).

There is one more variable to consider in the rover's navigation logic, and that is direct orders from Earth. If pictures, or returned data, were very interesting, it may be desired that the rover move to a specific location for further sampling, or if a surface anomaly is noticed, the Earth based operators may wish the rover to investigate. Thus it must be made possible that Earth based operators be able to order the rover to proceed in a new direction, and to override the obstacle limits set by the rover's programming. New mission priorities, sent from Earth, would be stored by the lander, and transmitted to the rover. These new prerogatives would reset the directives given by the rover's onboard navigation memory; thus redirecting it with the added advantage that the rover will still attempt to avoid obstacles.

The rover's purpose is exploration, and unlike human astronauts, it is expendable. If a situation was deemed worthy of the risk of losing a rover, Earth based operators would be able to order the rover into situations it normally would avoid. These "direct order movement" commands, relayed by the lander from Earth to the rover, must be able to override the movement logic commands of the rover. The rover will still note the situation into which it is traveling but will continue regardless of the predicament. The rover will still attempt to avoid obstacles, but only to a lesser extent. Movement will be much slower in this situation, partially because the rover may have to wait for orders on

how to avoid an obstacle, but also because more consideration will have to be given as to what is the best course upon which to proceed.

Section 3.3.2 - Rover Communications

The communications system consists of the transmitters, receivers and antennae, as well as the communications protocol used and the set of commands and responses which can be understood by the rover. The former can be designed fairly completely within the parameters of the mission, while the latter can only be outlined in a more general sense until the experimenters' desires are more clearly defined and more in-depth design work on the rover's microcontroller begins.

A frequency range to which the Martian polar caps are largely transparent is 100MHz to 300 MHz¹. These frequencies are easily high enough to carry the anticipated data rate, and result in an antenna of manageable size. However, the radar mapping system makes use of a frequency in this range (150 MHz¹), so care would have to be taken to avoid interference with this system.

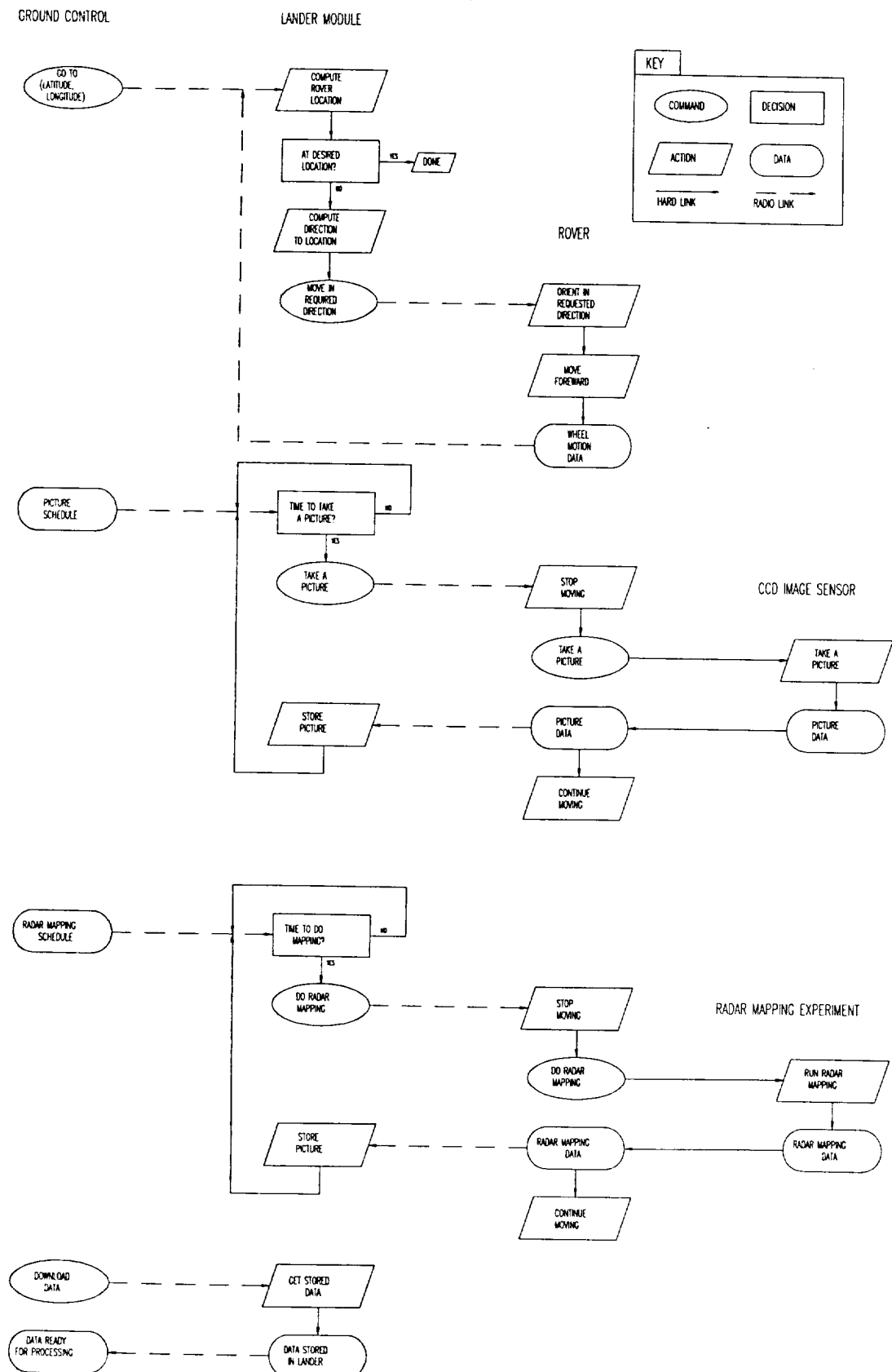
Once the frequency has been chosen, the transceivers can be designed and their power requirements estimated. It is possible that a commercial transceiver system will be suitable to the task, although it may be difficult to find one suitable for the rigors of the Martian polar environment.

The required data transfer rate needs now to be estimated. It is assumed that the commands and replies will represent a very small load on the system, and that the main problem will lie in transmitting photographic data from the CCD video camera.

The camera which will be used is a Kodak KAI-0370C, which has 767 x 484 pixel resolution, so that a total of about 40,000 bytes need to be transmitted for each picture². To transmit in a reasonable amount of time (say, 30 seconds,) this requires about 1300 bytes/second, or a minimum of 10 k-Baud transfer rate. This is quite reasonable, as 19.2k-Baud modems are fairly commonplace.

The most efficient error correction routine is probably convolutional encoding, which was used by the Voyager program in the 1980's to transmit photographic data with great success³.

The following diagram illustrates the logic of some selected rover command / communication sequences in flowchart format. The commands not shown will follow essentially the same format when implemented. The hierarchical structure (Ground Control → Lander Module → Rover → Experiments) is intended to allow the design of the electronic systems to be as modular as possible. It would therefore be relatively simple to replace the radar mapping system with, for example, an infrared mapping system for some other mission.



Section 3.3.3 Range of the Rover

Because the main source of power for the motors is the solar array, locomotion will occur only during periods of bright sunshine. For one Martian year, the summer season of bright sunshine at the northern pole will occur from September 1999 to March 2000, a period of about 180 days.

Much of the rover's time will be spent taking radar mapping images of the surface, determining navigable routes, and communicating with Earth via the lander. It will have to stop after every 3 to 4 meters of progress in order to map the surface of the surrounding area, a process which takes approximately 5 minutes. If the rover needs instructions or help from the mission operators on Earth, communication time is 80 minutes, round trip. The rover will also require time to process its own information from the laser sensors, which seek out large obstacles which it must avoid.

Taking these factors into account, the estimated time of locomotion per 24 hour period is only about 1.5 hours. Multiplied by 180 days, the time of travel during the entire summer season is estimated as 270 hours. At the standard speed of 0.1 m/s, the rover could possibly cover a range of 97 kilometers during the summer. There is also the possibility of limited movement during the season changing months of July-September 2000, and April-July 2001. Using a conservative estimate of 1/5 maximum movement time during these periods, there could be an additional terrain coverage of 16 or more kilometers. This brings the total annual range of the rover to about 110-115 kilometers.

Section 3.4: LASER SYSTEMS

The method by which the rover perceives its local environment is through a set of simple sensors and systems.

The first of these systems is the laser ranging system which allows the rover to perceive slopes and obstacles in its path. A laser source, in this case a laser diode, is maintained in the heated compartment of the rover. Laser light is carried by fiber optics from the heated compartment to emitters on the front edge of the rover. These emitters are fitted with special line generator lenses that filter the light in such a way as to result in a laser strip being projected on the surface. A charge-coupled device (CCD) imaging chip system receives the returning reflected light waves, and then sends its image to the computer which deciphers the data. The image would be a picture of the landscape, with the laser light stripe bold against the background. By determining the position of the light stripe within the picture, a computation of the relative elevation can be made; thus, slope and characteristics of the forward terrain can be determined, and a safe course plotted.

This laser ranging system has several advantages. The first is that this system has no moving parts, limiting the probability of a mechanical failure. This laser ranging system is inexpensive, with commercially available hardware. Tests conducted at Jet Propulsion Laboratory have shown that the system's effectiveness increases with lower temperatures; the tests varied temperatures between +30°C and -80°C. Tests of thermal cycling have shown no ill effects. Finally the system is highly accurate, having a success rate on the order of 98% (with the laser stripe 1.7x ambient light levels), and up to 99.4% (with the laser stripe 2.1x ambient light levels).¹⁰

A second system is required to determine the angle of the rover relative to the local gravitational field. This is necessary because the laser ranging system can only determine slopes relative to the forward direction of the rover. Excessive lateral slopes have to be avoided otherwise the rover could either tip over, or slide into an inescapable position. The solution to this situation is to create an artificial horizon for the rover that

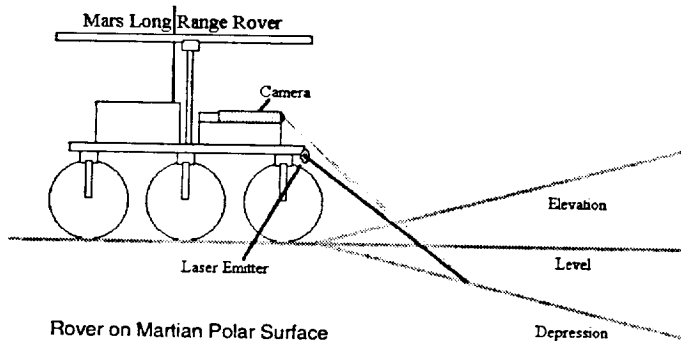
will monitor the orientation of the rover with respect to vertical. One way to do this is with a gyrocompass. However the gyrocompass was discarded as an option for two reasons: 1) the gyrocompass requires constant power, 2) the gyrocompass has significant dimensions and weight.

Since accuracy of the gyrocompass is not a necessity, only some sort of warning system is, ideally, a set of mercury switches to be used as an artificial horizon are the choice. Mercury switches are switches that are usually motion or angle sensitive, which use liquid mercury to close a circuit when moved or rotated. By arranging a set of mercury switches at different angles, a reasonably effective, while not totally accurate, artificial horizon can be made; as the angular orientation of the rover changes, circuits will be opened or closed depending on the change. The rover's computer can monitor the status of the switches, determine the orientation of the rover, and use this data to determine its path. The mercury switch artificial horizon has several advantages: it requires basically no power, there are no moving parts (other than the liquid mercury), it is inexpensive, it can be made in small or odd shapes to fit in available spaces, and the output is simple for the rover's computer to understand.

Thus by using these two onboard systems the rover can accurately move across the Martian polar surface.

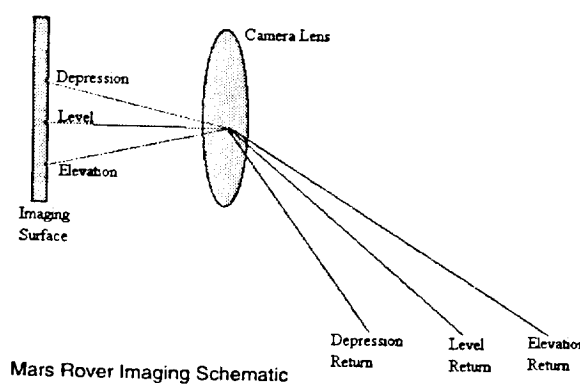
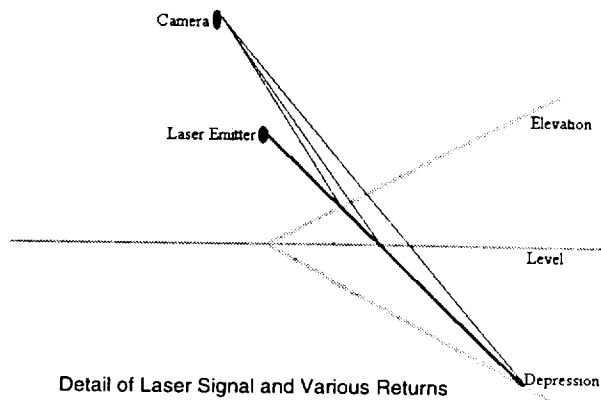
Section 3.4.1 Laser Ranging System

Before the logic the rover uses in navigating its environment can be discussed,



for obstacle avoidance: primarily the avoidance of large depressions and severe slopes. A laser diode is maintained in the rover's heated compartment, and its light is carried by fiber optics to a series of emitters arranged along the front edge of the

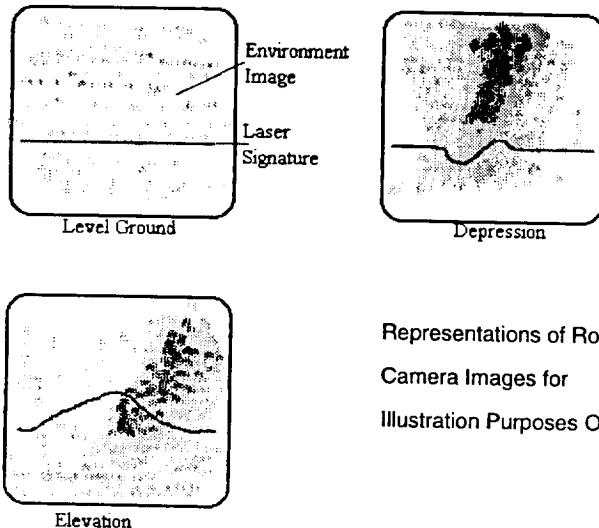
how the rover perceives its surroundings must be overviewed. The primary device used for this purpose will be a high precision, lightweight camera. The camera will not only be used for taking panoramic pictures of the Mars polar surface, it will also be used



rover. The laser light is reflected from the surface and received by the camera. The rover's computer can then determine the elevation of the ground ahead by noting the vertical position of the laser return in the camera's image and

computing the triangulation calculations required for the determination of the elevation.

The largest drawback of this system is that it can only detect elevation relative to the position and orientation of the rover. An additional sensor is required to determine the orientation of the rover. A simple set of mercury switches could act as an artificial



see it during the brightest part of the day.

horizon for the rover. The camera must also be very accurate to be effective, and the laser line on the ground must be bright enough that the camera can easily

Section 3.4.2 Rover Logic

The primary concern involved in the rover's logic patterns is self-preservation. The rover, as it is designed, is capable of navigating a slope of 15°, and overcoming an obstacle of 10cm. What the rover has to be able to do is detect situations which exceed these parameters, and then determine what course of action it needs to take to avoid difficulties. While the rover may be instructed as to what general direction the Earth-bound controllers wish, the rover must decide which exact route to take. In referring to exact route, short range means less than a meter in front of the rover. With the necessity of being able to avoid unfavorable situations the rover must have a limited amount of memory dedicated to the terrain in the immediate area which it has just traveled through. This on board "mapping" function is required because the ranging system is limited to

forward only ranging, since there will be only one camera permanently fixed camera. This fact is partially negated by the rover's mobility: the designed ability to turn in place.

There are four distinct situations which the rover will have to deal with: an up-slope in excess of 15° , a down-slope in excess of 15° , an obstacle exceeding 10cm in height, and an excessive lateral slope. Of these situations, the first three are anticipated to be navigated using the laser ranging system, the fourth will have to be addressed by an "artificial horizon" type of instrument.

When dealing with an up-slope in excess of 15° , the rover must first stop to decide its course of action. If the slope is not significantly greater than 15° , and the slope is gentle and even, the rover can transverse the slope laterally, moving across the slope such that the real angle it is climbing is less than 15° . This tactic is based upon the fact that the 15° limit was used in determining the maximum power required by the motors, but it is limited by the uncertainty of the static coefficient of friction on the surface, as well as the tire's tread pattern and the resistance it presents to lateral sliding. If, on the other hand, the slope is greatly in excess of 15° , the rover will have to reverse its direction (either by backing up, or by rotating and moving forward) move for a short distance, and attempt to find another path. In this situation it would be helpful if the Earth based operators were to alter the desired direction of travel, because the situation varies widely from the predicted situation.

A down-slope of greater than 15° can be dealt with in a similar method as the excessive up-slope: transverse descent for minor and stable situations, retreat and re-evaluation for excessive situations. This is detailed in the Navigation and Communication Section. (Section 3.3)

Lateral slopes would have to be detected by an "artificial horizon" since the laser ranging system only is able to detect forward slope relative to the orientation of the rover. The "artificial horizon" is a device used to determine orientation of an item relative to the local gravitational field. A series of mercury switches arranged in a pattern, or an

equivalent solid-state device, could be used to detect the orientation of the rover. When the rover reached a critical angle, a circuit would be closed, sending a message to the rover's command and control system. At this point, the rover could take two courses: reverse and retry or rotate and traverse the slope.

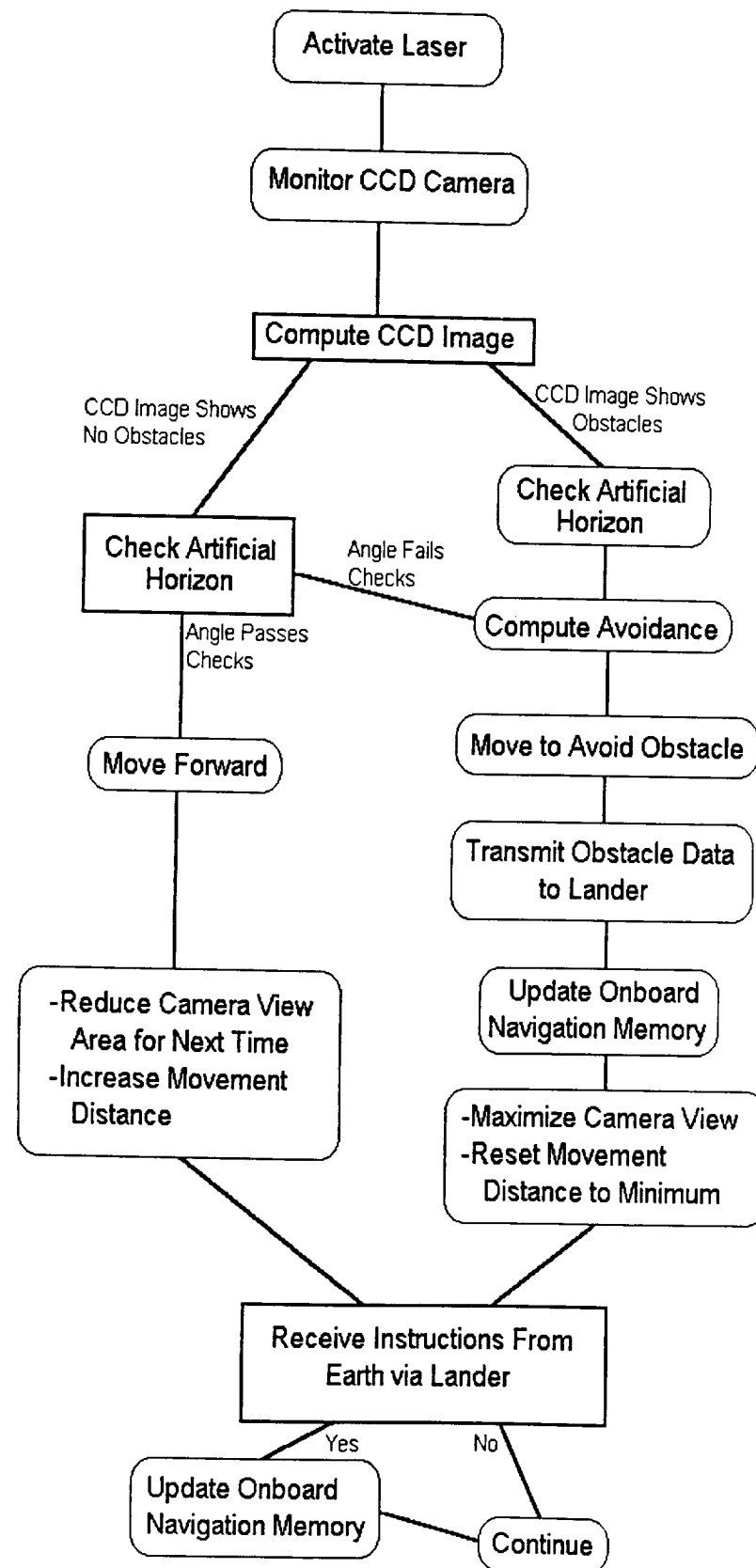


Figure 3.4.2.1: Rover Navigation Logic

P-4.78

Section 3.5: HEATED COMPARTMENT

The heated compartment on the rover, which will house the micro controller and batteries, must be kept at a temperature above -20° C in order to ensure proper operation of the equipment. The following analysis computes the heat required to maintain the temperature of the compartment at -20° for the worst case ambient Mars temperature of -150° C.

Three types of heat loss will occur in the Martian polar environment: conduction, convection, and radiation. Assuming an initial steady state temperature in the compartment, the heat loss occurs in three modes as follows.

- ① Heat will be delivered from inside the compartment to the insulation layer by convection, conducted through the insulation and wall material from the inner edge to the outer edge.
- ② Convection will occur at the outside walls of the box, where heat energy will be released to the thin Martian atmosphere.
- ③ Heat energy will radiate from the walls of the compartment to the Martian surface.

Conduction and Convection

The first two modes of transfer are governed by the equation for a composite wall with fluid boundaries. The equation governing heat transfer between fluids through a composite wall is:

$$q = (T_1 - T_4) / [(x_2 - x_1)/k_{12} + (x_3 - x_2)/k_{23}] = h(T_{f1} - T_1) = h(T_3 - T_{f3}) \quad (3.5.1)$$

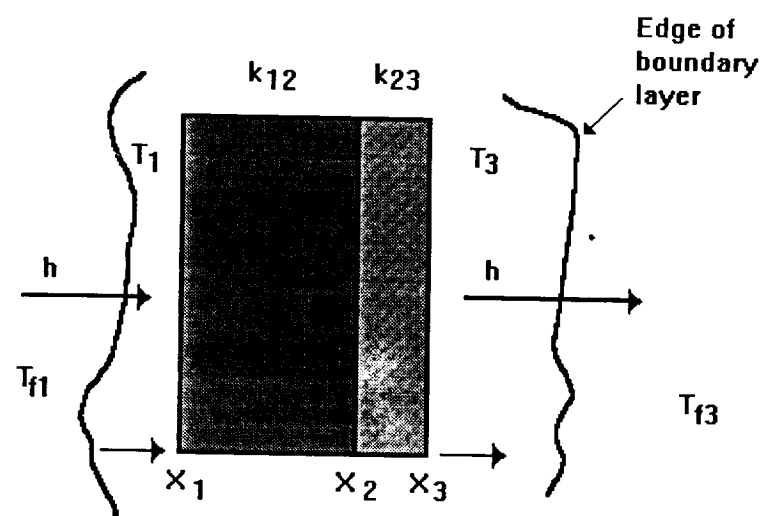


Figure 3.5.1 Composite wall with fluid boundaries.

There are two different materials which make up the conduction media of the compartment: the wall material and the insulation material. The insulation selected is known as silica aerogel, or 'santocel'. It will line the inner surface of the walls on top, bottom, and all sides. It has a thermal conductivity of 0.010 W/m K at -150° C. The thickness of the santocel insulation is 2 cm.

The wall material selected is an aluminum - magnesium alloy (95 Al - 5 Mg), due to its light weight, relatively low thermal conductivity ($k=87$ W/m K at 150°C) , and good radiation shielding properties, to protect the electronic components from any potentially harmful radiation from the RTG. The wall thickness of the aluminum is 0.3 cm. The dimensions of the aluminum walls are shown in figure 3.5.2.

The value T_{f1} is the air temperature in the compartment, 253 K. T_{f3} is the free stream temperature of the Mars atmosphere, 123 K. The value T_1-T_3 is approximated as 130 K.

$$q = 130 \text{ K}/[(.02-0)/.010 + (.023-.02)/87] \\ = 65 \text{ W/m}^2$$

From equation 3.5.1:

$$h(T_{fl} - T_1) = 65 \text{ W/m}^2$$

Therefore:

$$T_3 = T_{f3} + q/h \\ = 123 + (65)/11 \\ = 128.9 \text{ K} \quad (3.5.2)$$

where $h = 11$ for free convection¹³.

To find the heat loss rate Q , the value q is multiplied by the total inside surface area of the compartment.

$$\text{Inside surface area} = 2(8\text{cm} * 8\text{cm}) + 4(18 \text{ cm} * 8 \text{ cm}) = 704 \text{ cm}^2$$

$$\text{Outside surface area} = 2(10\text{cm} * 10\text{cm}) + 4(20\text{cm} * 10\text{cm}) = 1000 \text{ cm}^2$$

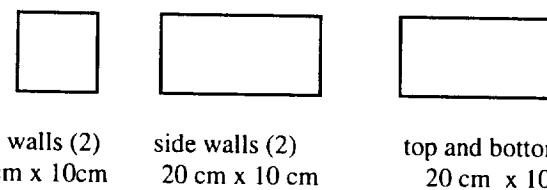


Figure 3.5.2: Dimensions of the heated compartment.

$$Q = 65 \text{ W/m}^2 \times (.074 \text{ m}^2) = 4.81 \text{ W}$$

Radiation

It will be assumed that the walls of the compartment are "gray" bodies, that is, $\epsilon = \alpha$ at a given temperature. This is a fundamentally significant assumption which is commonly used in engineering practice¹³.

Let the compartment be assumed a small gray body, so that the governing equation for total emissive power is:

$$\begin{aligned} q_r &= \epsilon \sigma T_3^4 \\ &= (0.049)(56.7 \text{E-12 kW K}^4/\text{m}^2)(128.9 \text{ K})^4 \\ &= 0.767 \text{W/m}^2 \end{aligned} \tag{3.5.3}$$

Then the power loss from radiation is:

$$Q = (0.1 \text{ m}^2)(0.767 \text{ W/m}^2) = \mathbf{0.077 \text{ W}}$$

Total thermal power loss is 4.89 Watts. This should be easily generated by the RTG, which is the source of the heat. The thermal output of the RTG is expected to be about 39 Watts. The heat will be delivered from the RTG to the warm compartment by a small duct.

Section 3.6: TAKEOFF AND LANDING IMPACT ANALYSIS

It is assumed that the impact of the lander on Mars will produce the highest loads seen by the rover during the mission. The maximum expected acceleration is 50 g's, or about 500 m/s^2 . The rover and its packaging must therefore be designed with this acceleration in mind.

To analyze the behavior of most of the rover's systems during this phase is beyond the scope of this report, and probably not necessary. The electronics, for instance, will all be solid state, and any chance of the circuit boards jarring loose can be prevented by potting everything in place. The robustness of the various experiments will be the responsibility of the designers of those experiments. The RTG and batteries are essentially solid-state devices, and should not be affected by this load.

The only systems which obviously need analysis in this area are the solar cells and the leg-wheel assemblies. The solar cell array is basically a thin plate supported at several points. The leg assemblies are more difficult to analyze, as they will start out with some play in the leg-body joint, then accelerate into the fully extended position until they impact onto the hard stop. It is this hard stop, then, which would have to be designed to take the impact force this will produce.

Alternatively, a packaging system for the rover could be designed to protect the solar panel and leg assemblies during the impact. A plausible packaging system must have the following qualities:

- Low mass
- Good cushioning qualities
- Easy rover self-extrication
- Minimum bulk beyond rover

This appears to be the most practical solution, as the analysis of a "free-floating" rover is made extremely difficult due to the unknown orientation at impact.

A very desirable material for rover packaging would be a plastic foam which could be made to break down on demand. Another possibility is to contain the rover in a bag of tightly packed foam balls. In this case it would only be necessary to break the bag to allow the rover to simply drive out. This appears to be quite a practical solution and would require only that the rover be designed with no openings large enough to admit the packing material, which could cause damage by clogging up motors or gearboxes.

The proposed design to handle the landing of the rover, then, shall be a roughly cubic plastic bag containing the rover and tightly-packed foam beads. Thin metal wires embedded in the plastic bag will have an electric current passed through them on landing, locally melting the plastic and causing the bag to break apart. The wires would be arranged in several redundant systems to reduce the chances of non-deployment. This system will ensure that the rover will arrive intact on Mars and be successfully deployed.

Section 3.7: STRESS ANALYSIS

The stress analysis of the rover is divided into five separate analyses. The individual analyses are of the following parts: the frame, the strut, the wheel, the strut pin, and the torsional spring. The stress analysis of the frame, the strut, and the wheel are performed utilizing the finite element programs I-DEAS™ and ANSYS™, while the stress analysis of the strut pin is performed using theory from any Basic Strength of Materials course. The torsional spring is analyzed using theory from reference 15 and is discussed in Section 3.1. All simulations were run for the worst case ambient temperature of -150°C.

Section 3.7.1 Frame Stress Analysis

The stress analysis of the frame consists of two parts. The first part of the analysis determines the necessary thickness of the frame. The second part of the analysis determines the cross-sectional dimensions of the strut connection tabs. Both parts are modeled using two-dimensional thin shell elements and symmetry of the part is observed. The shells are given a thickness which is representative of the material at that element.

Frame Platform

A 12.5 cm x 50 cm rectangle represents half of the frame. Boundary conditions are used to simulate the plane of symmetry and the three strut pin locations. The symmetry edge is restrained in every displacement except rotation about the x-axis, which simulates a 'pinned' type restraint. The nodes which join the platform to the strut connection tabs are fixed in all y-axis displacements, x-axis translation, and z-axis rotation. Pressures represent the "running load" weights of the experimental and power components atop the frame. The loading and boundary conditions are shown on Figure 3.7a.

From this analysis the stresses, the displacements, and the resultant forces at the boundary condition nodes are found. The thickness of the slab has been reduced from 1.5 cm. to 0.5 cm. through the use of I-DEASTTM. The stresses and safety factors for the frame and for all parts analyzed are listed in Table 3.7.1. According to the output, the highest reaction force is 14 Newtons. Using a safety factor of 1.5 this force becomes 20 Newtons and is used in the next analysis. Color plots of the maximum principal and shear stresses are shown in Figures 3.7b and c.

	Frame	ConnectionTabs	Struts	Wheel Rim	Wheel Spokes
Maximum Shear (MPa)	0.094	0.313	0.085	0.214	97.1
Maximum Principal (MPa)	0.188	0.521	1.1	0.358	194
Yield Stress (MPa)	650	650	650	870	870
Safety Factor	3457	1248	591	2430	4

Table 3.7.1: Stress Analysis Results

Strut Connection Tabs

The geometry of the strut connection tabs of the frame are the emphasis of the second part of this analysis. The fillet radius and necessary thickness of the tab were checked in this part. This two-dimensional thin plate model represents half of the frame cross-section with symmetry being observed. The boundary conditions and loading are shown in Figure 3.7d. The load consists of a single force of 20 Newtons at the strut pin location. The boundary conditions bound the symmetry plane and the vertical movement of the frame at points where components are located. Resulting color plots of the stresses are also shown in Figures 3.7e and f.

Section 3.7.2 Strut Analysis

The struts were analyzed to check for buckling and yielding of the material. The original geometry concept for the struts was to make them as curved, hollow cylindrical members, but as a result of other analyses that reduced the weight and power requirements for the rover, they evolved into a different, solid configuration. Nonetheless, the cylindrical member approach was used to make the finite element analysis less tedious. Also, favorable stresses for this hollow geometry would prove the viability of the solid members.

Solid three-dimensional elements were used to model a strut in ANSYSTM as a .003 m thick curved, hollow cylinder (Figure 3.7g). This analysis resembles a fixed-pinned column problem with the exception that the column has a 45° curve in it. The model was fixed in all directions at the end that connects to the wheel and was fixed at the other end with the exception of being allowed vertical displacements and rotations along the axis of rotation of the strut (Figure 3.7h). A force of 20N, representing the affect of the total weight of the rover on the strut plus a safety factor, was uniformly applied to the end of the strut connecting to the frame. Also, a temperature of -150°C was placed on the whole model.

The maximum principle stresses and shear stresses obtained from this analysis are shown in Figures 3.7i and j, respectively. As can be seen in Table 3.7.1, the stresses were low enough to provide a safety factor of 594. Therefore, the actual design of the strut should easily be able to handle any situation which it will encounter. The resultant forces at the boundary conditions were used in the wheel stress analysis and also in determining loads for the x-contact bearing for the wheel axle.

Section 3.7.3 Wheel Analysis

Because the wheel is one of the heaviest parts and made of titanium, stress analysis is primarily used for reducing this part's weight, which affects the overall performance of the rover. The number of wheel spokes and the dimensional thicknesses were determined from this analysis. The wheel was divided into two separate members, the rim and the spoke, in order to analyze the stresses more objectively.

Wheel Rim

A two dimensional mesh of thin shell quadrilateral elements with a thickness was used to model the rim. The load on the wheel axis is the reaction load from the strut stress analysis plus the weight of the strut. Three spokes were assumed initially. The load was represented in the worst case position, in which the spokes are arranged at angles of 90° , 210° , and 330° , where 0° is horizontal. Loading in this position results in the largest shear and principal stresses. The boundary conditions were determined to be:

- ① Zero y-axis displacement, x-axis rotation, and z-axis translation where the rim meets the ground surface.
- ② Zero x and y axis rotation, and z-axis displacement where the spokes meet the rim.

Figures 3.7 k, l, and m show the loadings, boundary conditions, and stresses. The thickness of the rim was reduced to 0.5 cm. Although the stresses are still relatively low for this thickness, no further reduction was made because an impact loading on the wheels (resulting from a fall or collision) could produce catastrophic failure in a very thin part.

Spokes

The spoke was also modeled as a two dimensional thin shell mesh, with a defined thickness. Each end of the spoke was assumed to be clamped, except for small possible

displacements (1E -05 m) in the x direction. These displacements allow for the development of shear stresses, as would occur in a physical model. The y translation was free. Color plots of the model are shown in Figures 3.7 n, o, and p.

The spokes were reduced to a diameter of 0.5 cm, and they still have a significant safety factor. This large reduction of size is possible because of the redundancy in a spoke-rim type wheel. A large impact may cause failure in one member, but the other spokes may then take up the load and remain within a reasonable safety factor of the yield stress.

Section 3.7.4 Strut Pin Analysis

Because of its important function, stress analysis of the strut pin is necessary. The loading and boundary conditions on the pin are very simple. A 1.0 cm diameter pin is fixed at both ends and subjected to a running load, $Q = 6.25 \text{ N/cm}$ (due to the weight) on the entire length, $L = 3.2 \text{ cm}$, between the two ends.

A reasonable approach is to use the familiar bending stress equation, $\sigma = M c / I$, where σ is the bending stress, M is the maximum bending moment, c is the distance between the neutral axis and the outer fiber, and I is the moment of inertia. Because this problem is a "handbook" case, M is easily found.

$$M = Q L^2 / 12 = 6.25 (3.25)^2 / 12 = 5.33 \text{ N-cm} \quad (3.7.4.1)$$

The moment of inertia of a circular cross-section with the appropriate substitutions for this case is:

$$I = \pi R^4 / 4 = \pi(.5)^4 / 4 = 0.049 \text{ cm}^4 \quad (3.7.4.2)$$

The distance between the neutral axis and the outer fiber, c , is equivalent to the radius. Thus, $c = 0.5 \text{ cm}$. Substituting the above results into the bending stress equation yields:

$$\sigma = 5.33 (.5) / 0.049 = 54.3 \text{ N/cm}^2 = \underline{\underline{5.43E +05 \text{ N/m}^2}}. \quad (3.7.4.3)$$

This result is well below the yield stress of steel.

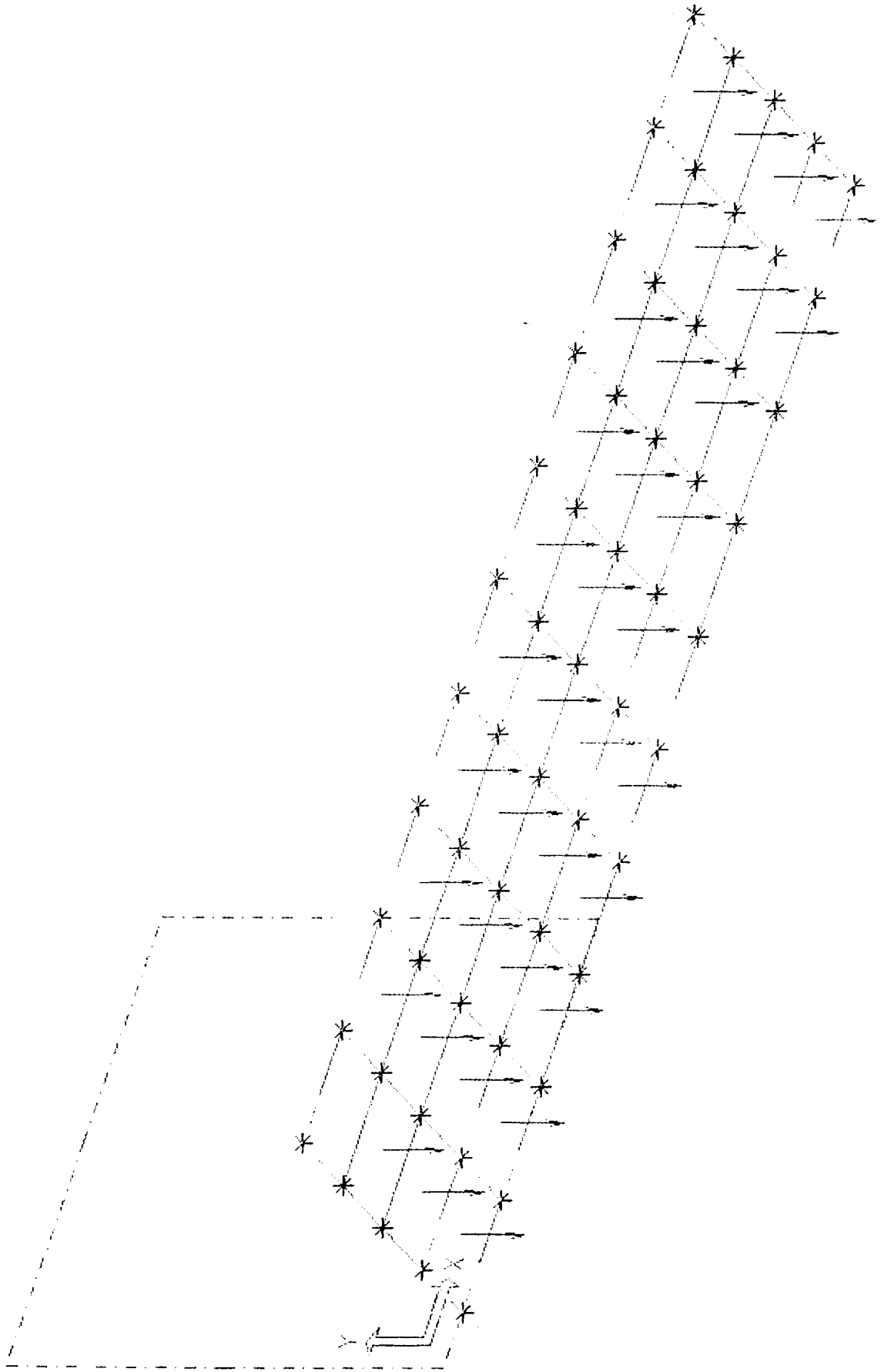
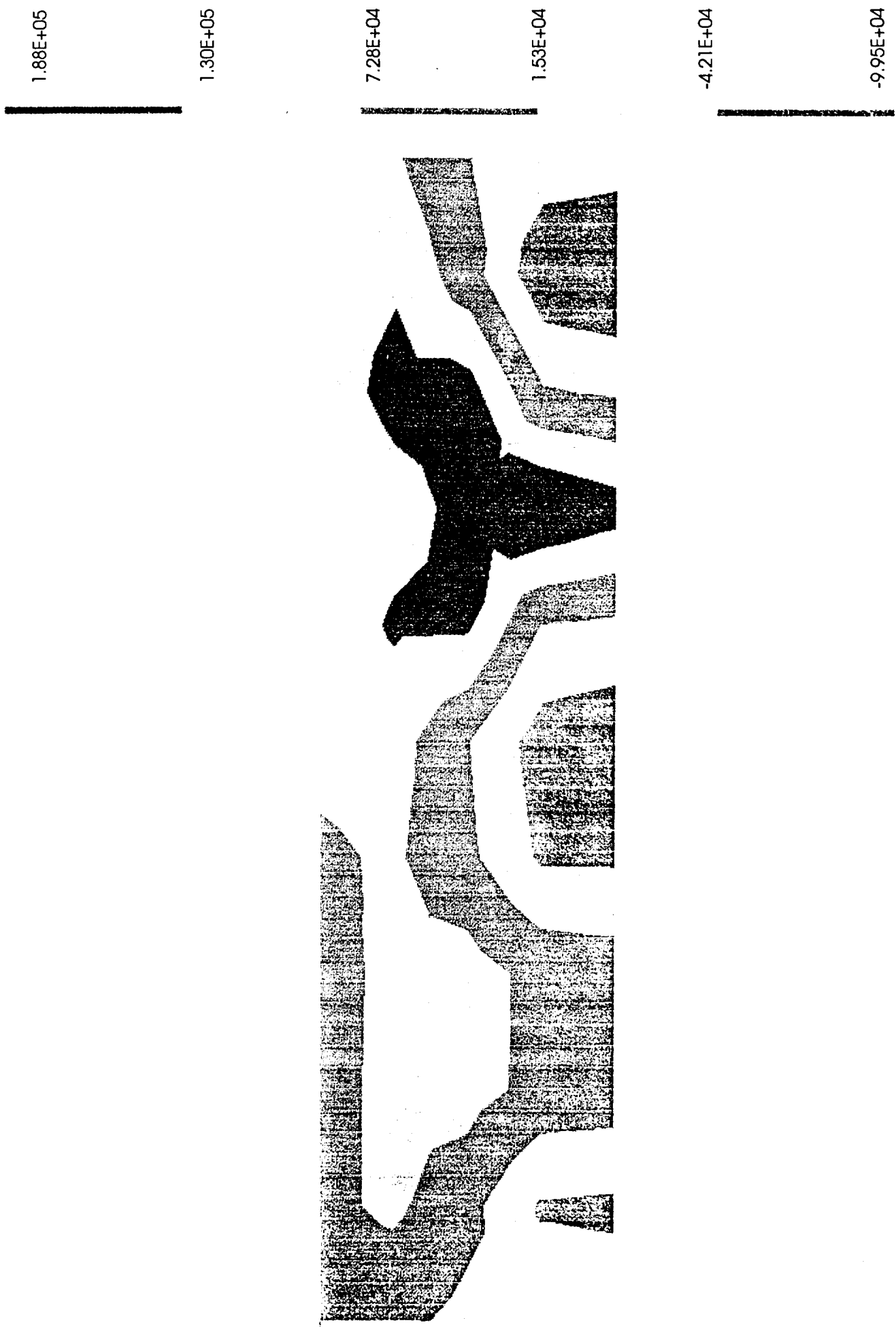


Figure 3.7 a : FRAME - Boundary Conditions and Loading

Figure 3.7 b : FRAME - Max. Principal Stress



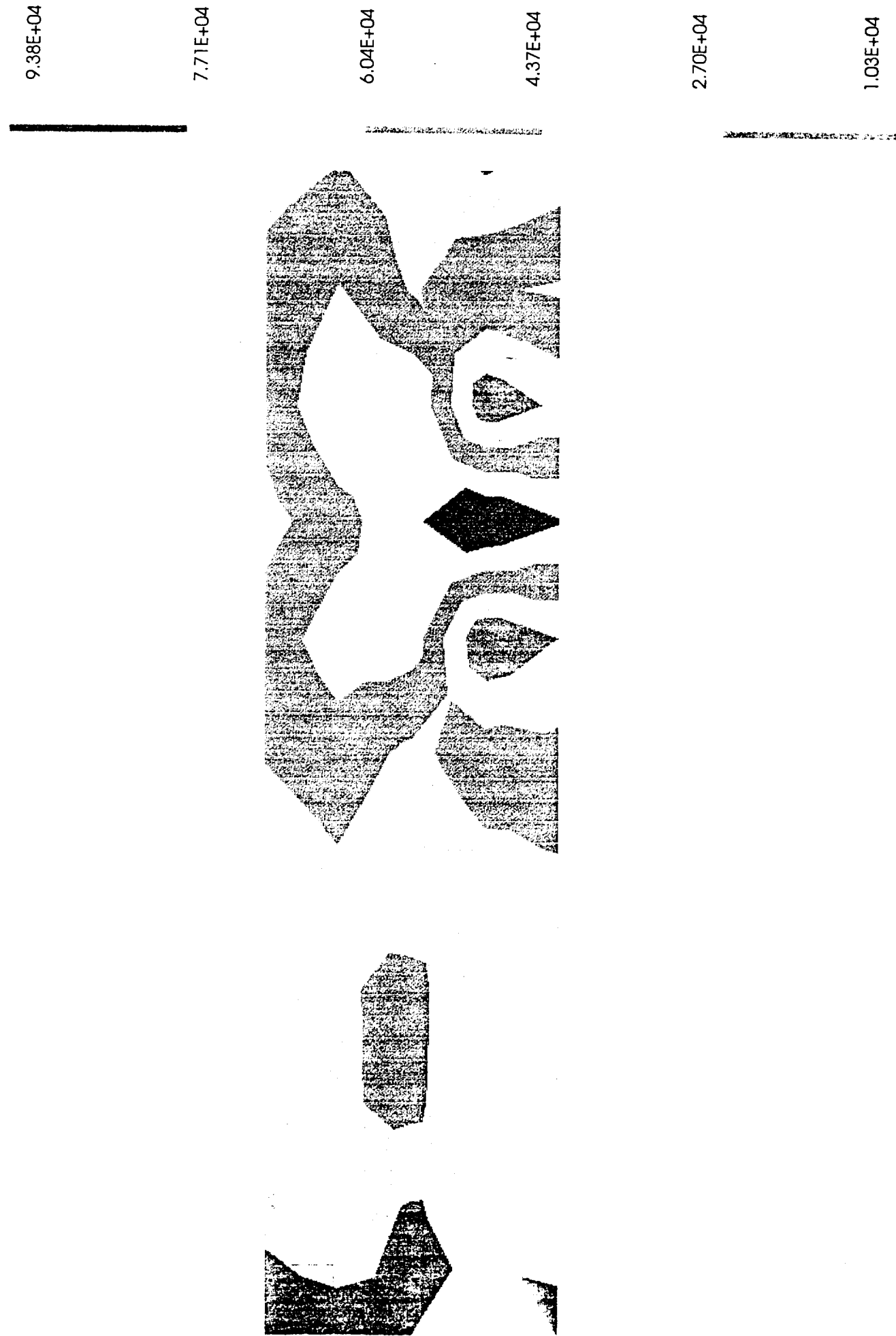


Figure 3.7 c : FRAME - Max. Shear Stress

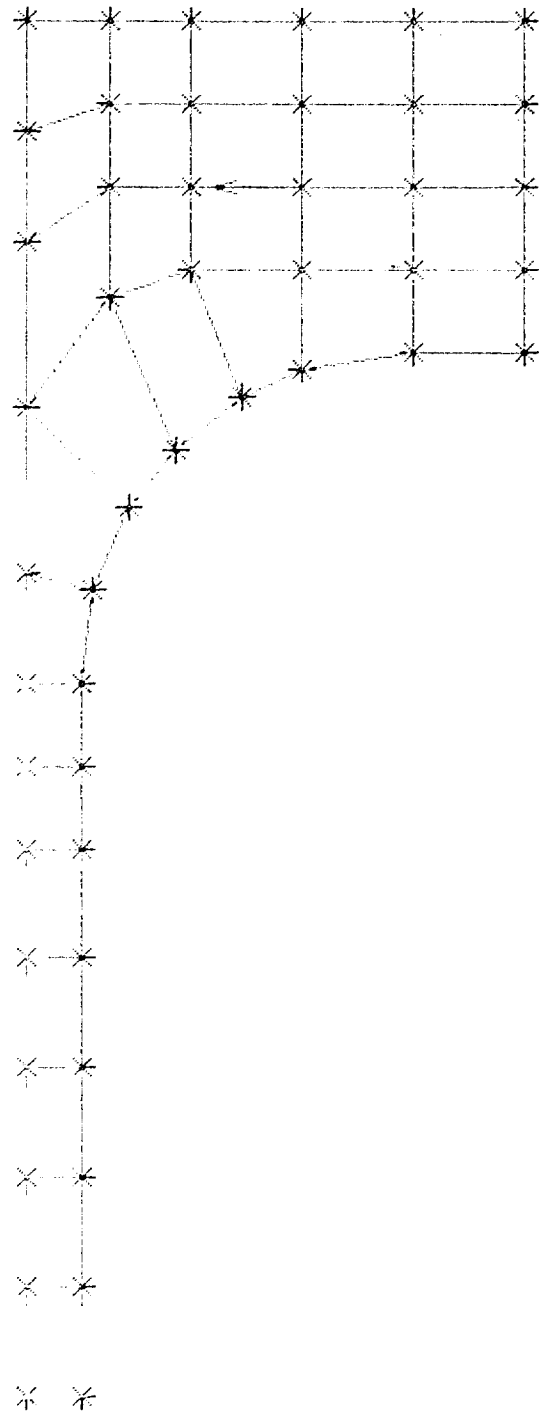


Figure 3.7 d : STRUT CONNECTING TAB - Boundary Conditions and Loading

-8.62E+04

3.52E+04

1.57E+05

2.78E+05

3.99E+05

5.21E+05

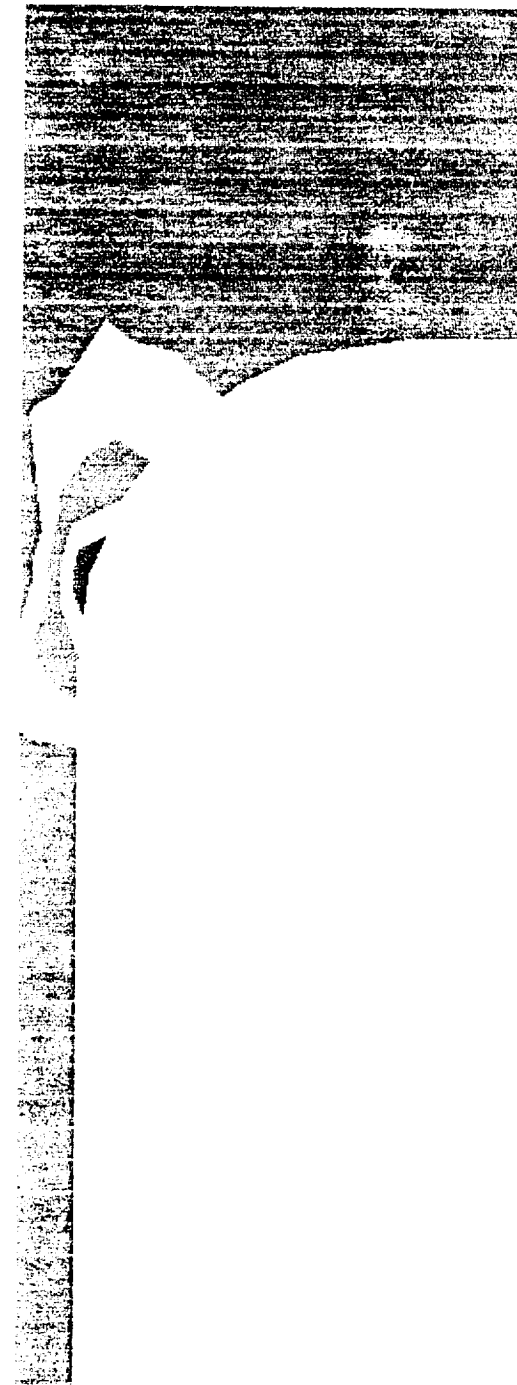


Figure 3.7 e : STRUT CONNECTING TAB - Max. Principal Stress

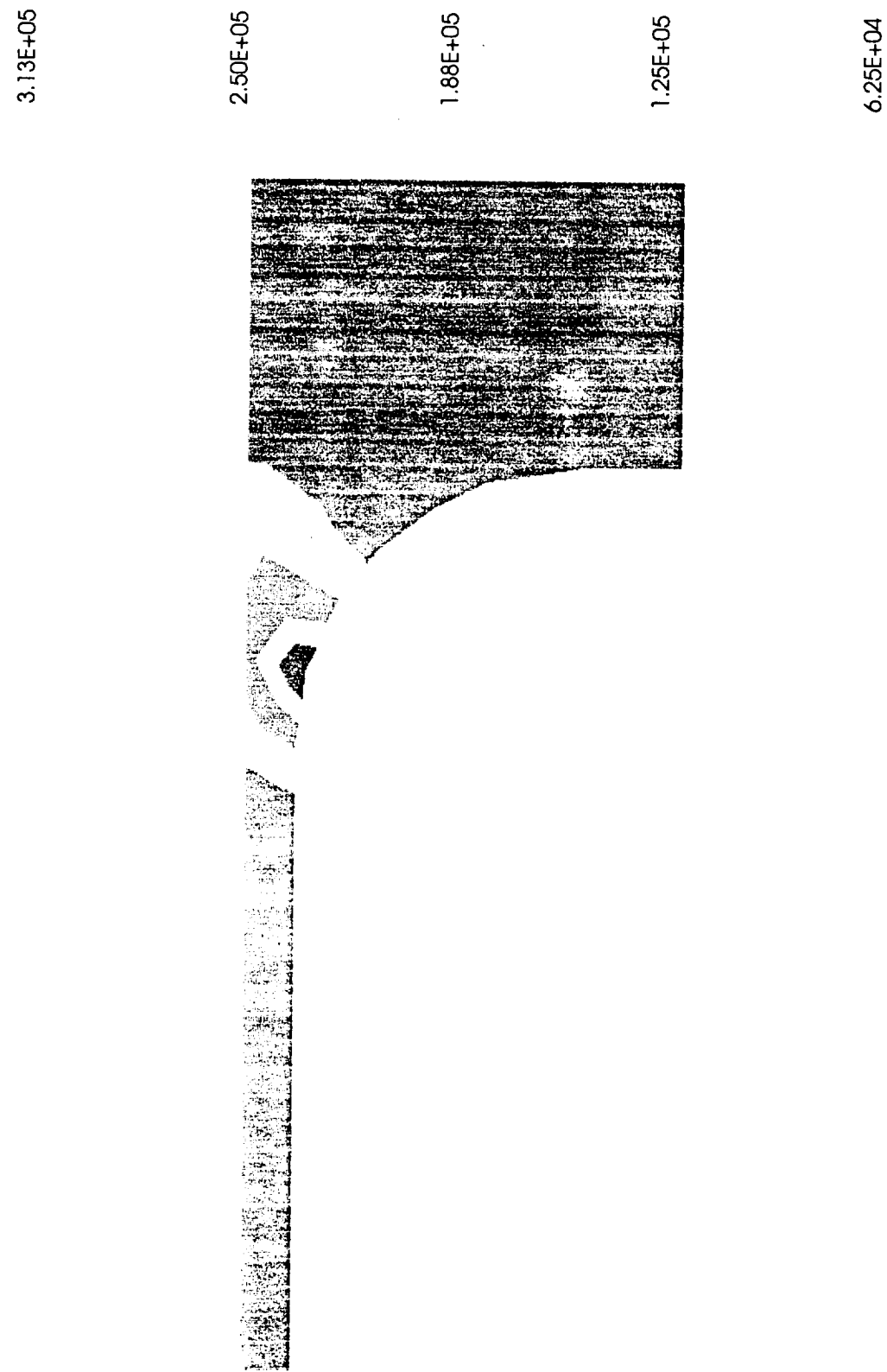


Figure 3.7 f : STRUT CONNECTING TAB - Max. Shear Stress

Figure 3.7 g: STRUT - Solid Model

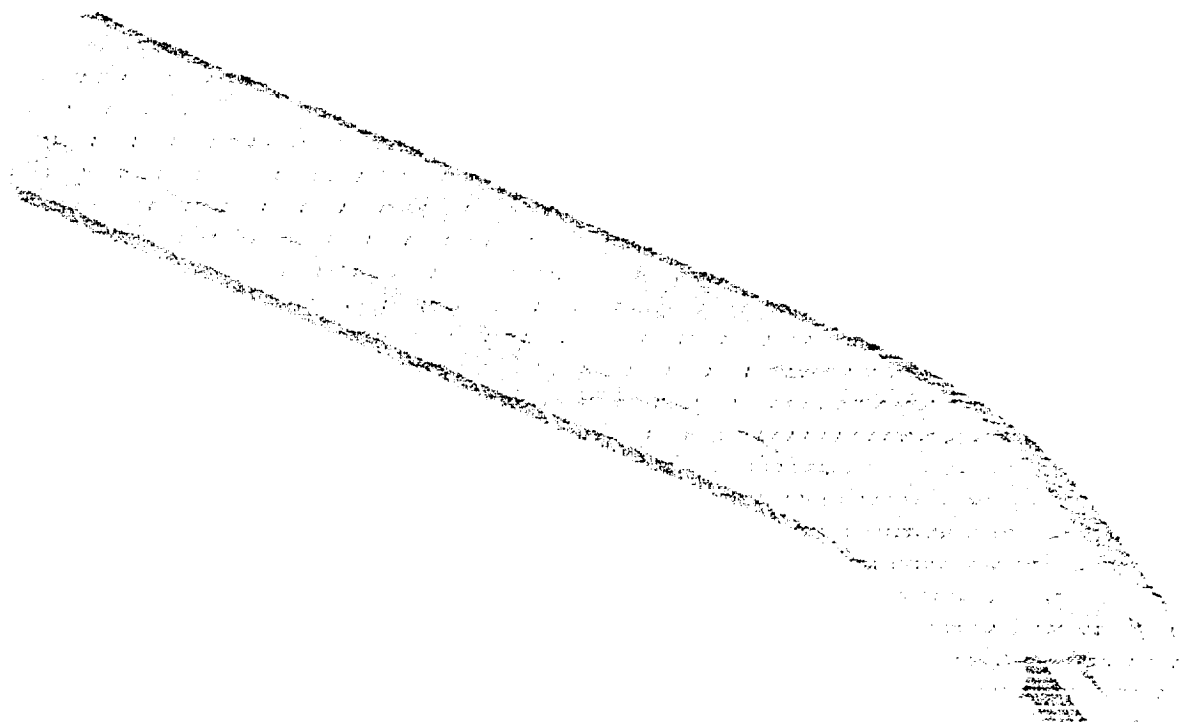


Figure 3.7 h: STRUT - Boundary Conditions and Loading



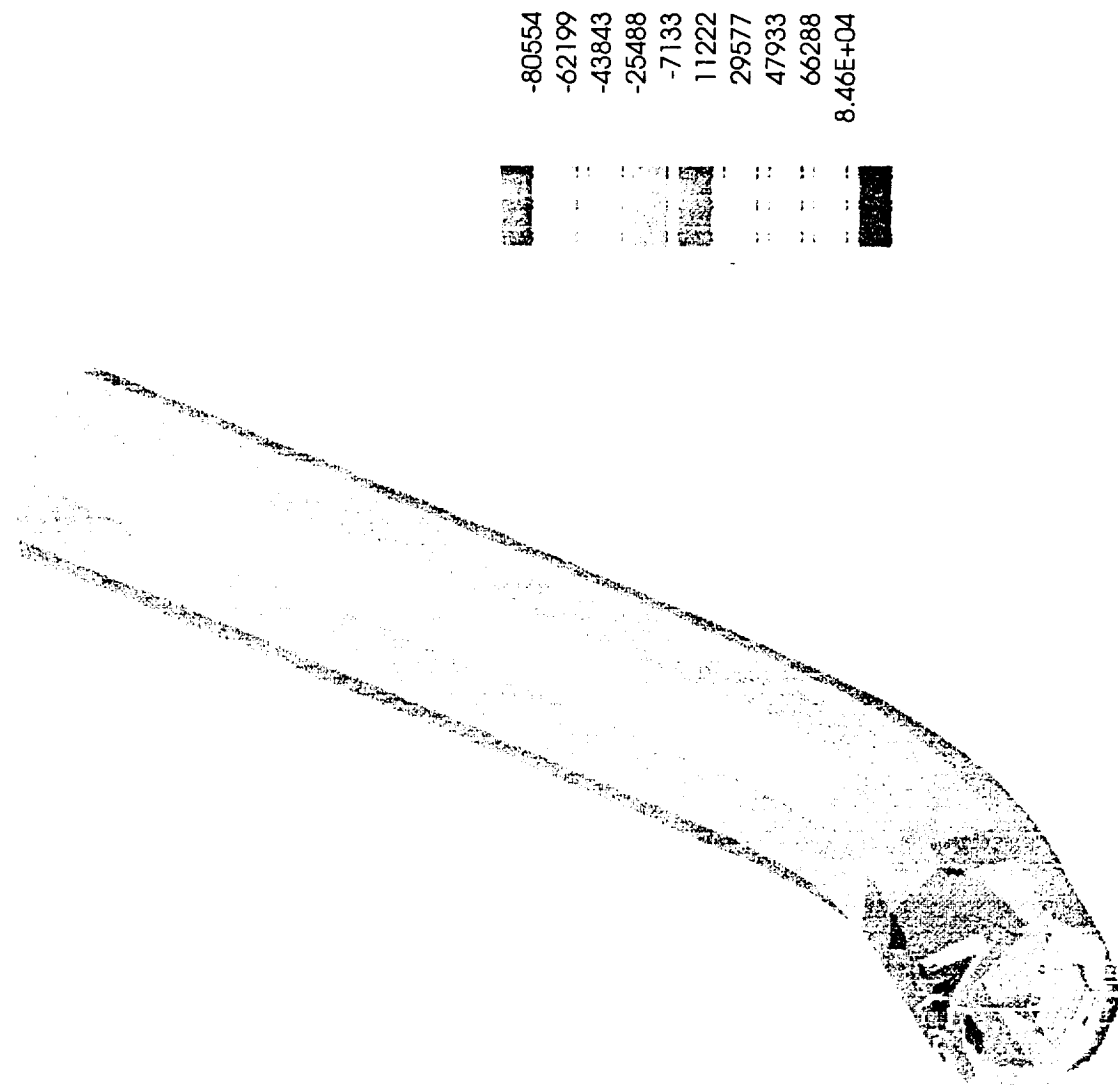
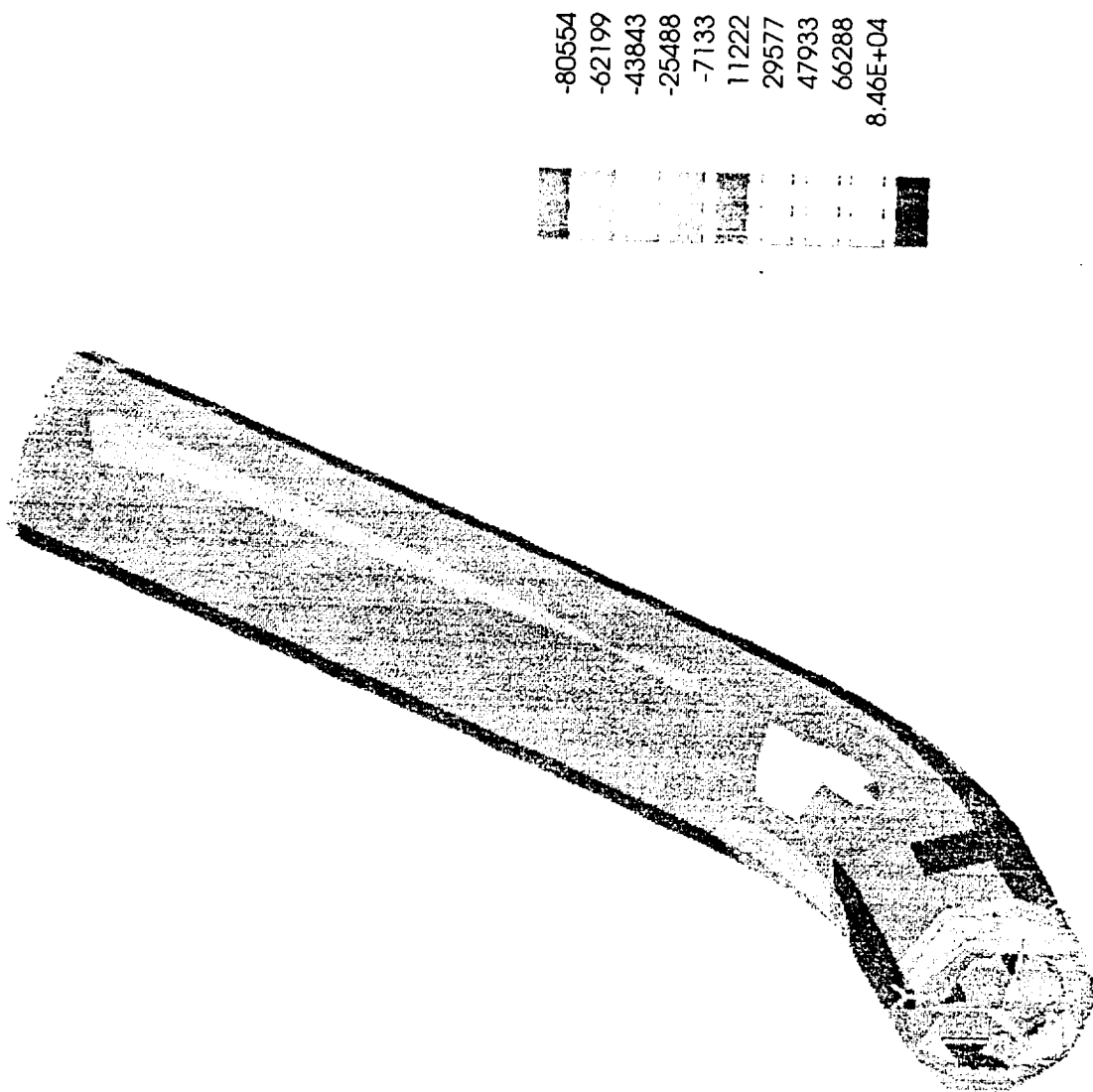


Figure 3.7 i: STRUT - Max. Principal Stress

Figure 3.7 j: STRUT - Max. Shear Stress



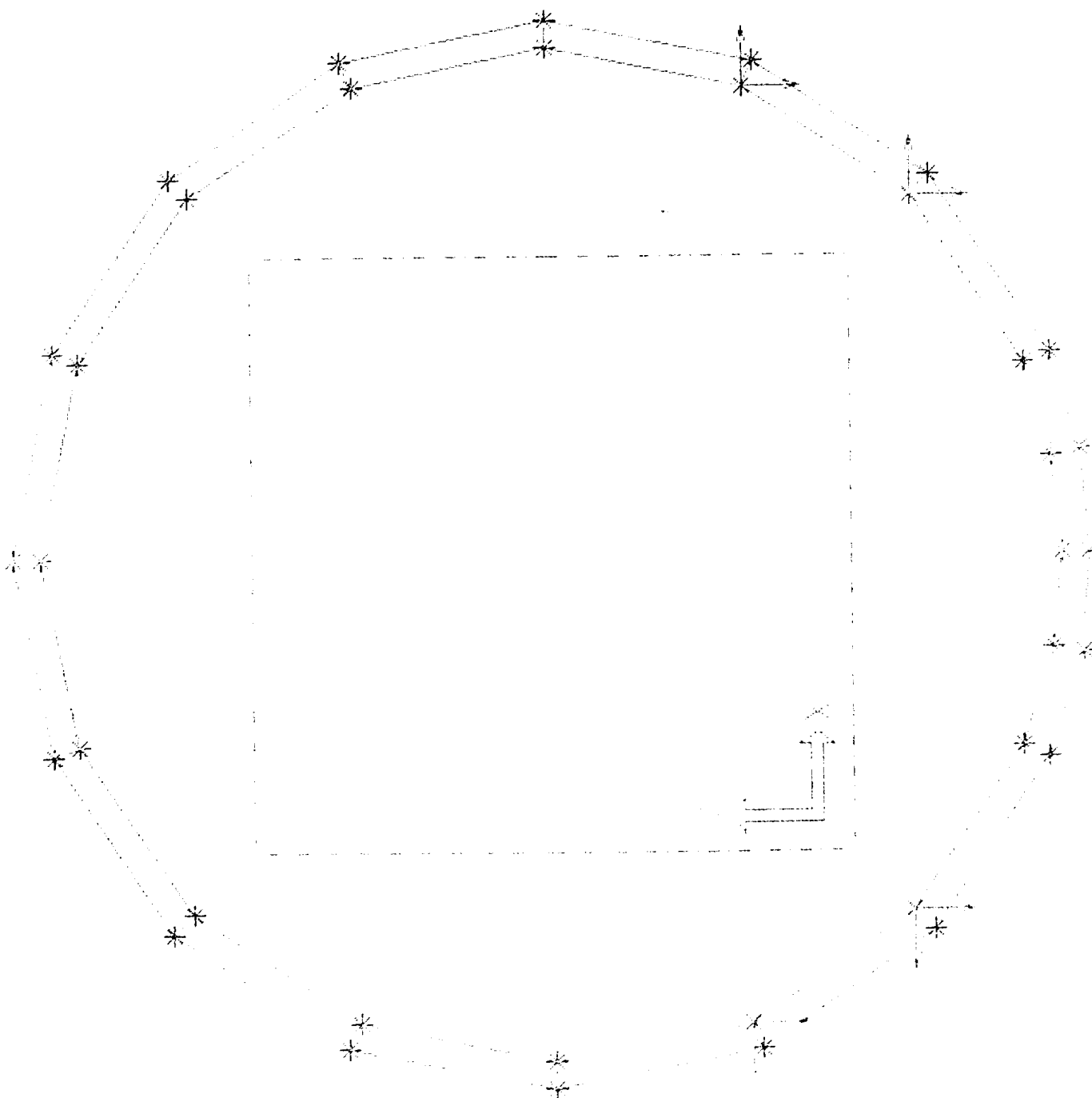


Figure 3.7 k : WHEEL RIM - Boundary Conditions and Loading

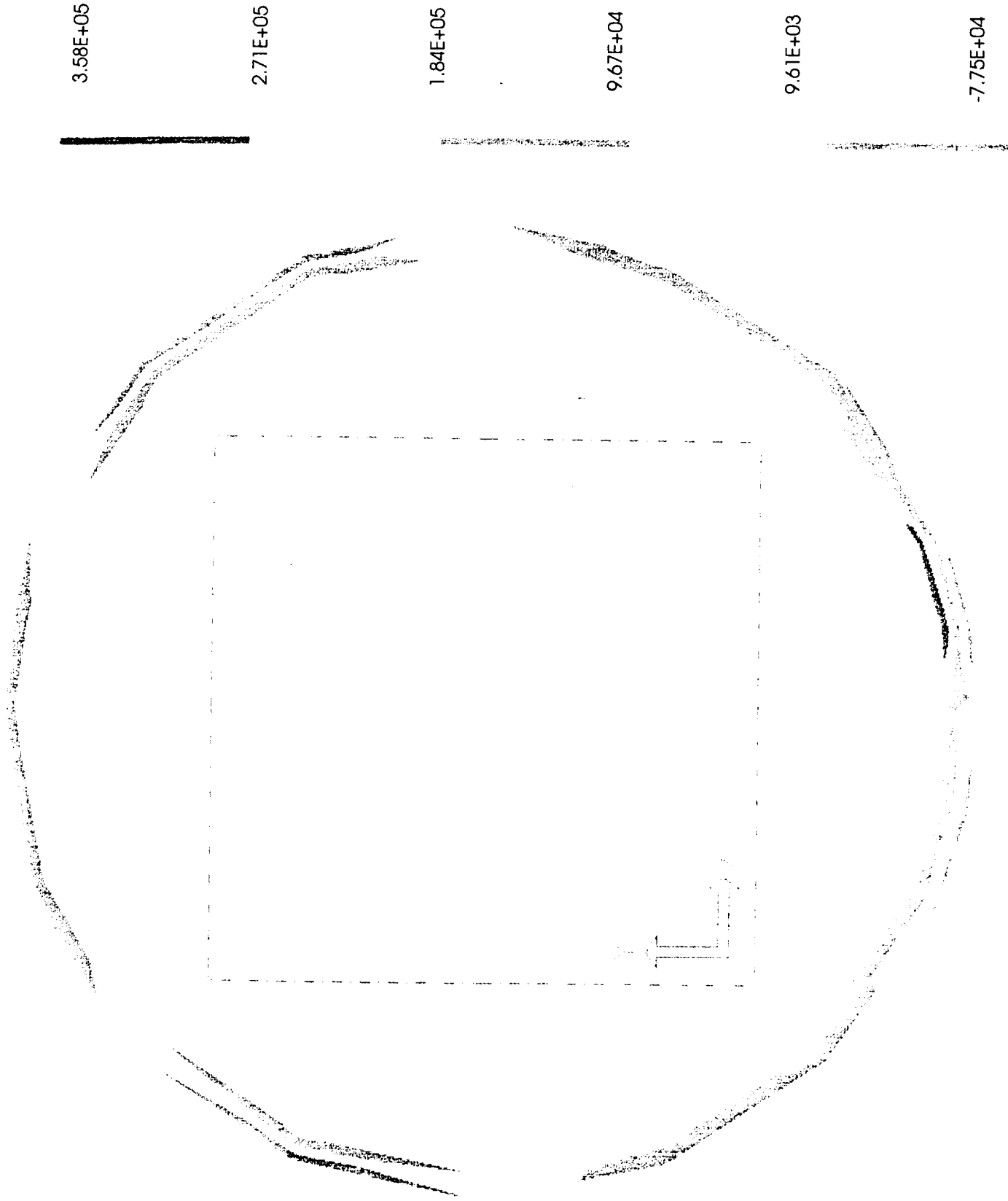


Figure 3.7.1 : WHEEL RIM - Max. Principal Stress

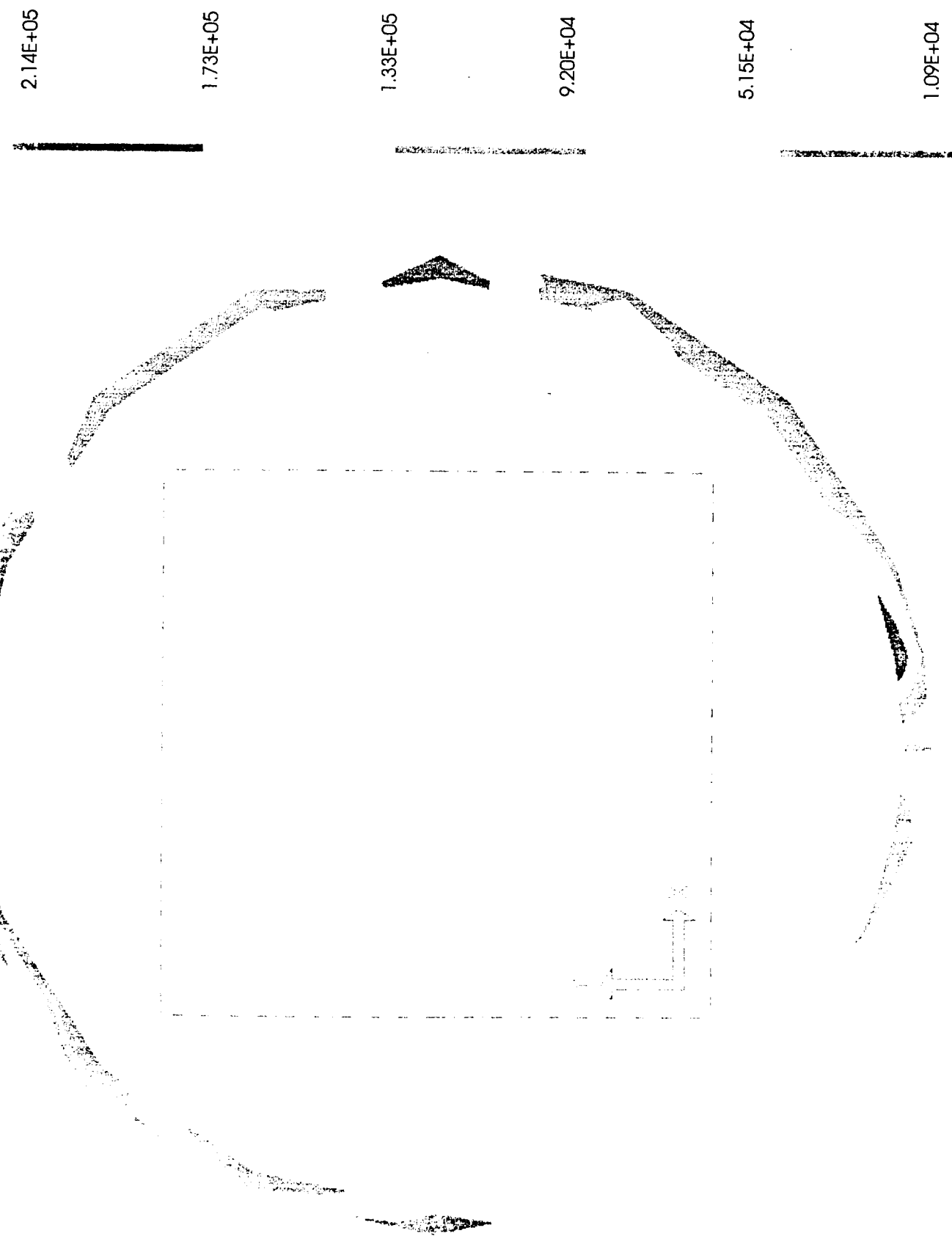


Figure 3.7 m : WHEEL RIM - Max. Shear Stress



Figure 3.7 n : SPOKE - Boundary Conditions and Loading

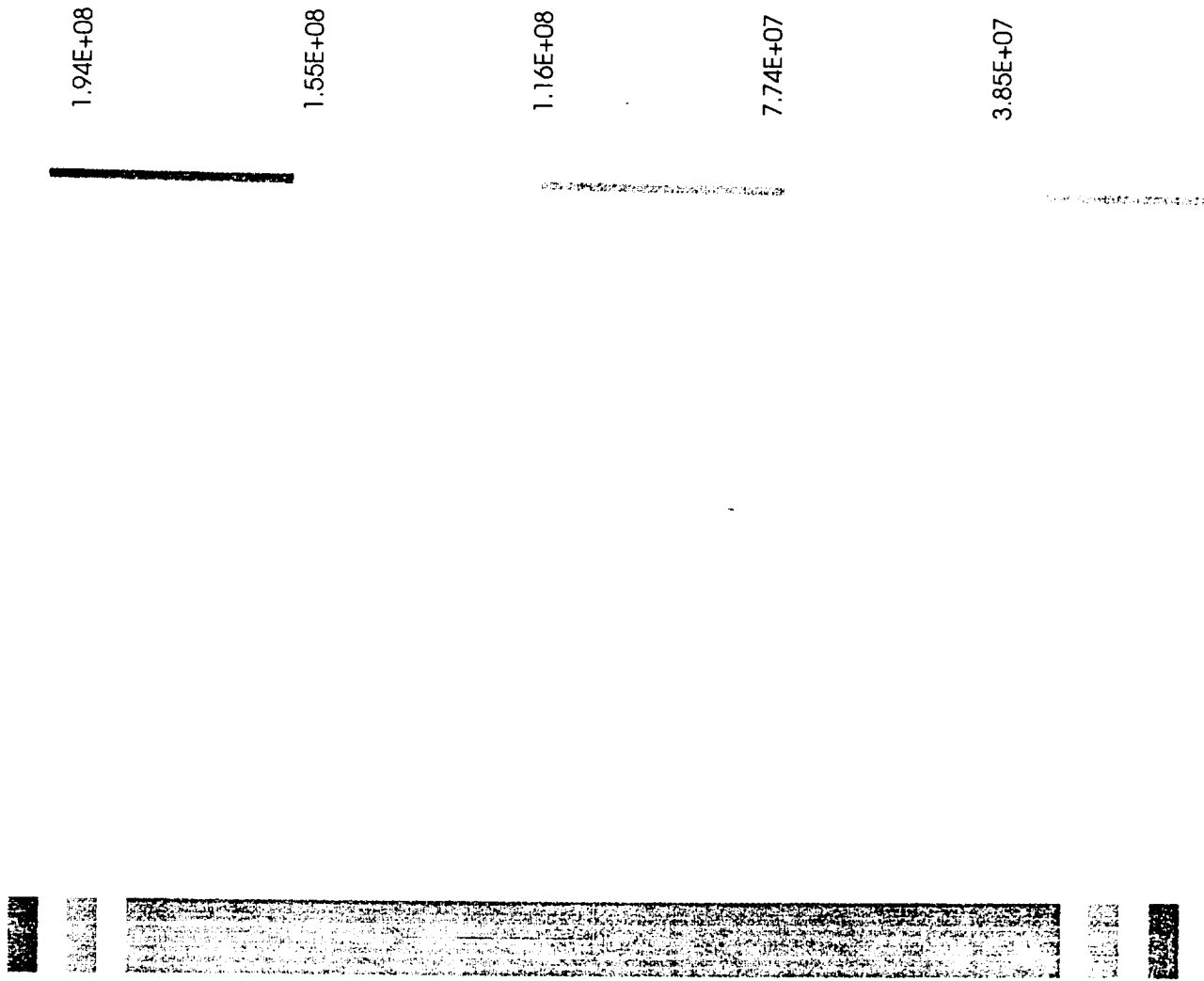


Figure 3.7 o : SPOKE - Max. Principal Stress

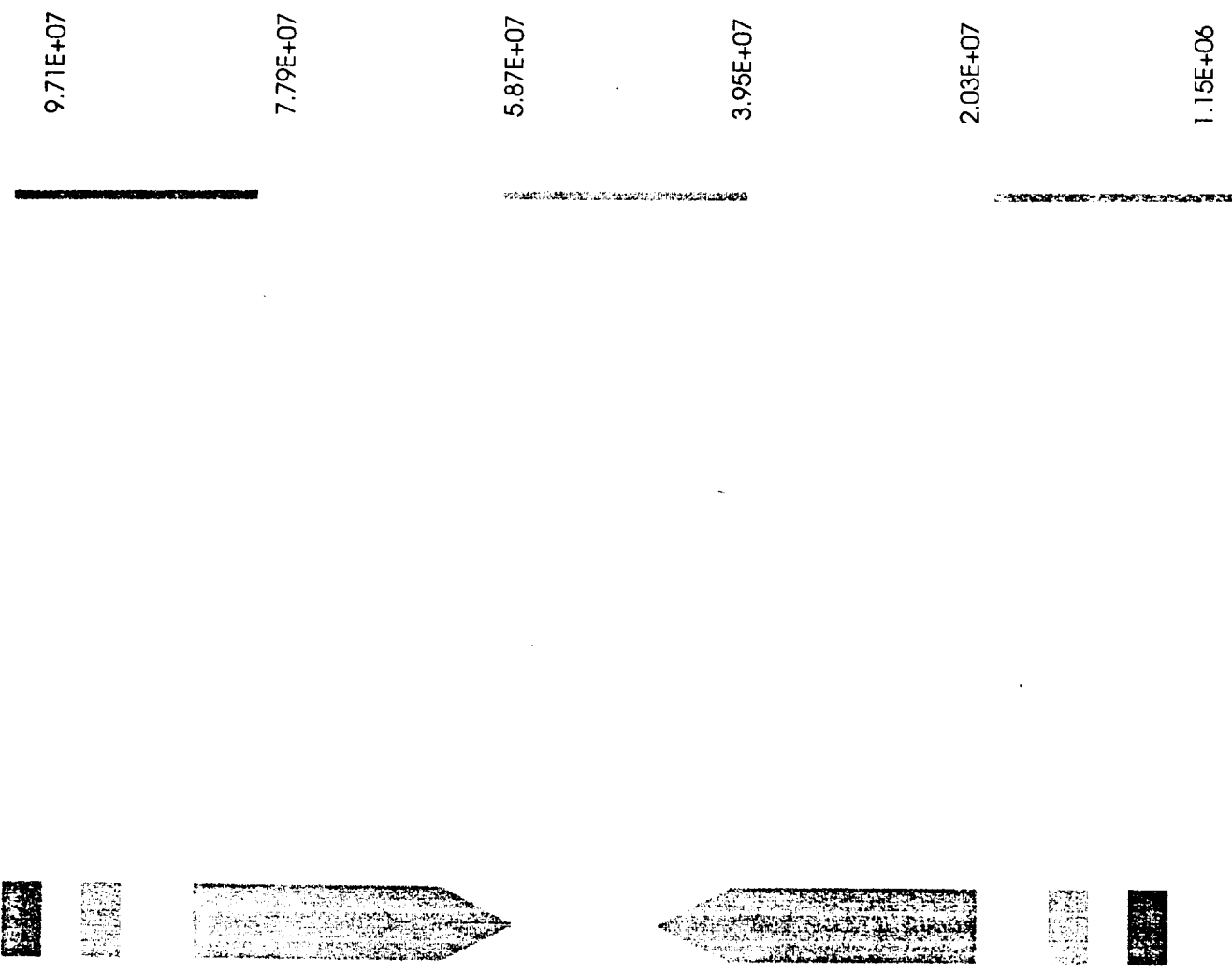


Figure 3.7 p : SPOKE - Max. Shear Stress

Section 3.8: FAILURE ANALYSIS

Section 3.8 Failure Mode and Effects Analysis

Part Name & Function	Potential Failure Mode	Effect of Failure	Cause of Failure	Design Verification	Recommended Actions
Frame -- Base that supports all the mechanical, electrical, and scientific equipment.	Frame cracks upon impact.	1) No effect. 2) Possible collapse of frame resulting in unstable or inoperable condition.	1) Incorrect material specified. 2) Incorrect thickness of frame.	Stress and material analysis.	Do stress analysis with material properties at cold temperatures and do drop tests.
Solar Array -- Converts light to electrical power.	Array cracks upon impact.	1) Reduced power output from solar array. 2) No power output from solar array.	Plane stresses too high.	Stress analysis and testing.	Do stress analysis and drop tests.
Solar Array	Dirt and carbon dioxide frost build up on solar array surface.	Reduced power output.	Contaminants settling on array surface.	Subject solar array to conditions on Mars.	Test solar array and determine if a wiper is needed to keep array clean.
Solar Array	Radiation degrades the solar cells.	Reduced power output.	Improper material coating on surface of array.	Subject solar array to high radiation levels.	Test solar array and determine if a new coating is needed.
Linear Stepper Servo (Solar Array) -- Rotate array to maximize light striking the surface.	Servo fails.	Array can only rotate in one direction.	Cold temperature.	Test servos under similar Mars surface conditions.	Test servos and determine if a warm box is needed.
Sensors & Lasers -- Detect obstacles in path of the rover.	Sensors or lasers become dirty.	Rover will not avoid obstacles which could lead to the loss of the rover.	Dust or carbon dioxide frost contaminating the sensors or lasers.	Test sensors and lasers in Martian environment simulator.	Test and determine if there is a coating that will prevent contaminants from adhering to the lasers and sensors.
Fiber Optics (Lasers) -- Channels laser light to the laser emitters.	Fiber optic breaks on impact.	Obstacle avoidance system becomes inoperative and rover does not avoid obstacles.	Fiber optic to thin and brittle.	Test fiber optics in drop test.	Test fiber optics in drop test and determine if a new material is needed.
Electronic Component(s) -- Control science experiments, communications, and all motor movement.	One or more electronic components fail.	Experiments, communication, or movement may be affected.	Overheating of components, power surge, or radiation exposure.	Test electronics assembly under actual conditions.	Test electronics assembly and correct for overheating, power surges, and radiation exposure.
Gear Motor -- Provides torque to rotate the shafts which rotates the wheels.	Gearbox or motor locks up.	Wheel(s) will not rotate.	1) Cold temperature. 2) Improper lubrication. 3) Internal contamination.	Test gear box and motors under harsh environmental conditions.	Test gear box and motors and determine if a sealed enclosure is needed.
Flexible Shafts -- Transmit power from the gear motor to the wheels.	Shaft(s) lock up.	Wheel(s) will not rotate. If several shafts lock up this will result in the rover becoming immobile.	1) Improper lubrication. 2) Dust contamination in shaft.	Test shaft with lubrication in cold atmosphere.	Test shaft. Try new lubrication and environmentally sealed shaft casing if needed.
Flexible Shaft	Shaft(s) break.	Shaft will not rotate and therefore the wheel(s) will not rotate.	Too much torque being transmitted through the shaft.	Test shaft performance under high torque conditions.	Test shafts.
Bearings -- Allow wheel to rotate while strut remains fixed.	Bearing(s) lock up.	Wheel(s) will not rotate.	1) Contamination of dust. 2) Improper lubrication.	Test the bearing under harsh environmental conditions.	Test bearings. Re-evaluate bearing seals and lubrication if necessary.
Torsion Spring -- Fixes strut at a specific position, but allows it to rotate if going over an object.	Spring(s) break.	Strut does not resist rotating.	1) Improper material. 2) Improper dimensions. 3) Too much stress.	Stress and material analysis and testing.	Stress analysis and testing. Re-evaluate material if necessary.

Section 3.9: COST ANALYSIS

Any cost analysis made at this point will result in a "ballpark" figure, at best. The costs of some components, such as the motors, flexible shafts, and solar array are known. Most of the framework and chassis is dependent upon both materials and machining costs, and the electronics system will have a high R&D cost.

The following costs are known to some degree of accuracy, since the components have been selected from stock or semi-custom commercially available items:

Item	Unit Cost	Quantity	Total
Motor	\$139/ea.	6	\$834
Gearbox	\$210/ea.	6	\$1,260
Flex. Shaft	\$45/ea.	6	\$270
Solar Array	\$0.50/cm ²	3100cm ²	\$1,550
			\$3,914

The costs of the frame components can be estimated, due to the fact that in most work of this kind, the machining cost far exceeds the materials cost unless some exotic material is used. The following are estimates of fabricated component costs:

Item	Est. Total
Struts	\$3,000
Frame	\$3,000
Wheels	\$2,000
Misc. Hrdwr.	\$1,000
	\$9,000

These costs can only be considered rough figures, based on current machining costs and composite fabrication costs in the aerospace industry.

The electronics system inherently requires a lot of expensive design and layout work. Due to the consequences of system failure, the system must be made extremely fail-safe, but without the complexity of redundant systems, which add excessive bulk. Therefore, much time will have to be invested in testing the system under simulated

mission conditions to verify that it does not fail. It is recommended that at least \$25,000 be set aside for the development, testing, and manufacturing of the electronics system.

The RTG will be by far the most expensive rover component. The nuclear pile consists of Pu²³⁸, of which there is only about 40 kg of fairly pure material in US military stockpiles, with no new material being produced. An RTG small enough for the purposes of the rover has also not been fully developed, so there will be a large R&D cost to absorb. It has been estimated that the RTG power unit will cost on the order of \$100,000.

The laser sensor for rover guidance has an estimated "space-worthy system" cost of \$25,000 from the manufacturer. The "artificial horizon" sensor for the rover has been estimated at \$5,000. The motors and controllers to align the solar array are expected to total an additional \$5,000. The science experiment costs are considered to be outside the control and scope of this design, and have not been included in any cost estimate.

These estimates entail all the major rover components. A preliminary cost estimate, therefore, for the rover less experiments, is just under \$200,000. The final cost of the rover will more likely be over than under this budgetary figure based on past experience in designs of such complexity.

Appendix A

Code to Perform Calculations from Gear Analysis Section

```

//Code to calculate torque, gear reduction, and motor characteristics
//given the mechanical power and velocity.
//User enters some specifications about the gearbox and motor.

#include <iostream.h>
#include <conio.h>

main()
{
start: clrscr();
        //set up variables
        int tamb, rth, rth1, rth2, nmax, eff, ia, ans;
        float pm, f, v, t, r, tf, tt, angv, i, mm, rtr;
        float nm, I, k, volt, angvmo, tr, r22, alp, power;

        //define mechanical power, velocity, wheel radius, & alpha
        pm=3.4;
        v=.1;
        r=.09;
        alp=.0039;

        //evaluate force required for each wheel
        f=((pm*1.356*550)/(746*v))/6;
        cout << "\nThe required force for each wheel is " << f << " Newtons";
        //evaluate torque required for each wheel
        t=f*r;
        cout << "\nThe torque required for each wheel is " << t << " Nm";

        //evaluate torque lost due to friction in shaft and right angle
        //gearbox
        tf=2*(t-(t*.85));
        cout << "\nThe torque lost due to friction is " << tf << " Nm";

        //evaluate total required torque by gearbox
        tt=tf+t;
        cout << "\nThe total torque required by each gearbox is " << tt << " Nm"

        //evaluate angular velocity of wheel
        angv=(v/r)*(1/(2*3.1415))*60;
        cout << "\nThe angular velocity of each wheel is " << angv << " rad/sec

        //***user finds gearbox with adequate torque output and enters
        //its maximum input speed***
        cout << "\nEnter the maximum input speed of the gearbox (rpm) ";
        cin >> nmax;

        //evaluate the gear reduction
        i=nmax/angv;
        cout << "\nThe required gear ratio is less than or equal to " << i << ":";

        //***user enters the gear ratio that is less than or equal to i
        //***user also enters the efficiency of the gearbox
        cout << "\nEnter the gear ratio (##:#1) ";
        cin >> ia;
        cout << "Enter the efficiency of the gearbox (%) ";
        cin >> eff;

        //evaluate torque required by the motor
        mm=((tt*1000)/((ia*eff)/100));
        cout << "The torque required by each motor is " << mm << " mNm";

```

```

//evaluate speed of the motor
nm=angv*ia;
cout << "\nThe speed of the motor to achieve this torque is " << nm << "

//***user enters the torque constant, R22, rth1, rth2, tamb for
//***the motor
cout << "\nEnter the torque constant of the motor (mNm/A) ";
cin >> k;
cout << "Enter the terminal resistance of the motor (Ohms) ";
cin >> r22;
cout << "Enter the thermal resistance of the rotor-body (deg C/W) ";
cin >> rth1;
cout << "Enter the thermal resistance of the body-ambient (deg C/W) ";
cin >> rth2;
cout << "Enter the ambient temperature (deg C) ";
cin >> tamb;
rth=rth1+rth2;
k=k/1000;
mm=mm/1000;

//evaluate current required by the motor
I=(mm/k);
cout << "\nThe current required by each motor is " << I << " Amps";

//evaluate temperature of the rotor
tr=((r22*I*I*rth*(1-22*alp)+tamb)/(1-r22*I*I*rth*alp));
cout << "\nThe temperature of the rotor is " << tr << " Celsius";

//evaluate resistance at tr
rtr=r22*(1+alp*(tr-22));
cout << "\nThe resistance at that temperature is " << rtr << " Ohms";

//evaluate voltage required by the motor
volt=(rtr*I)+(k*2*3.1415*(nm/60));
cout << "\nThe voltage required by each motor is " << volt << " Volts";

//evaluate total power required by all 6 motors
power=(volt*I*6);
cout << "\nThe total power required by all six motors is " << power << "

//***tell user to check that the current required is not greater than
//***the maximum continuous current for the motor
cout << "\nCheck that the required current is less than the max cont cur

//Do another analysis?
cout << "\nDo you want to do another analysis? (y=1 or n=2) ";
cin >> ans;
if (ans==1)
{
    goto start;
}
return(0);
}

```

The required force for each wheel is 5.665147 Newtons
The torque required for each wheel is 0.509863 Nm
The torque lost due to friction is 0.152959 Nm
The total torque required by each gearbox is 0.662822 Nm
The angular velocity of each wheel is 10.610642 rad/sec
Enter the maximum input speed of the gearbox (rpm) 5000

The required gear ratio is less than or equal to 471.225006:1
Enter the gear ratio (###:1) 405
Enter the efficiency of the gearbox (%) 55
The torque required by each motor is 2.985686 mNm
The speed of the motor to achieve this torque is 4297.310059 rpm
Enter the torque constant of the motor (mNm/A) 11
Enter the terminal resistance of the motor (Ohms) 1.45
Enter the thermal resistance of the rotor-body (deg C/W) 5
Enter the thermal resistance of the body-ambient (deg C/W) 12
Enter the ambient temperature (deg C) -40

The current required by each motor is 0.271426 Amps
The temperature of the rotor is -38.613274 Celsius
The resistance at that temperature is 1.107232 Ohms
The voltage required by each motor is 5.250531 Volts
The total power required by all six motors is 8.550784 Watts
Check that the required current is less than the max cont current of the motor.
Do you want to do another analysis? (y=1 or n=2)

Appendix B

Material Properties

MATERIAL PROPERTIES TABLE
at T = -150 to -20 degrees C

MATERIAL	USED IN	YIELD STRENGTH (MPa)	DENSITY(g/cm**3)	E (GPa)	THERMAL EXPANSION (10-6/K)
CFRP	Frame, Struts, Bearings	650	2.2	150	negligible
316 Stainless	Axles, Bearings, Pins, Shafts	400 - 470	8.5	200	16
Ti-6Al-4V	Wheel rims and spokes	870 - 1150	4.5	115	6.7 - 9.8
310 Stainless	Torsion Springs	800 - 900	8.4	200	15

Appendix C

Code to Determine Mechanical Power Requirements

```
C PROGRAM FOR COMPUTING THE MECHANICAL POWER REQUIREMENT
C AND TORQUE OF MARS LONG RANGE ROVER MOTORS
C SLOPE RANGES FORM 0 TO 60 DEGREES
C
C
IMPLICIT REAL (A-H,L-Z)
PI=3.1415927
DANGLE=-5
WRITE(*,*) 'INPUT ROVER WEIGHT (N)'
READ(*,*) WEIGHT
WRITE(*,*) 'INPUT THE TOTAL WHEEL WEIGHT(N)'
READ(*,*) WHEELS
WRITE(*,*) 'ANGLE (DEG) PEAK POWER (WATTS) REQUIRED TORQUE
(N*M)'
C CALCULATE Fs
DO 10 C=0,12
DANGLE=DANGLE+5
RANGLE=DANGLE*PI/180
FS=WEIGHT*DCOS(RANGLE)*0.3
C CALCULATE Fb
G= WEIGHT-WHEELS
FB=(.00125/.005)*G
P=(WEIGHT*DSIN(RANGLE))+FS+FB
POWER=P*.1
C CALCULATE TORQUE
FORCE=POWER/0.1
TORQUE=FORCE*.09
WRITE(*,*) DANGLE,POWER,TORQUE
10 CONTINUE
END
```

Appendix D

Rover Specifications Table

OBJECT	Dimensions(cm)	Material	Mass	Power
Frame	50x25x.5	Composite	1.375 kg	n/a
Leg (1 of 6)	<i>See Illustration</i>	Composite	.16 kg	n/a
Wheel (1 of 6)	18(od)x17(id)x2	Ti-6Al-4V	.963 kg	n/a
Flexible Shaft (1 of 6)	Ø0.33x30	Stainless Steel	.022 kg	n/a
Motor and Gearbox (1 of 6)	10x6x4	n/a	2.76 kg	8.5 W peak
Batteries	.11mx.047x.095	LiTiS ₂	.440kg	52.8 W-hr peak
Camera	15x4x4	n/a	.25 kg	200 mW peak
Solar Panel	0.31 m ² 78.8x39.4x.5 cm	Silicon	negligible	10.5 W peak
Heated Compartment	20x10x10	n/a	24.8 kg	4.81 W peak to heat
Laser Diode	1x1x3	n/a		700 mW
Merc. Horizon	negligible	n/a	negligible	n/a
Computer		n/a		3 W peak
Comm. Gear		n/a		3 W peak
Seismometer	5x3x3	n/a	.2 kg	100 mW peak
Radar Mapping Gear	20x15x10	n/a		5-10 W peak for 5 minutes
CCD Sensor Camera	6.5x6.5x9	n/a	.28 kg .1 kg est.)	200 mW std 350 mW peak
RTG	.22x..07 dia (m)	n/a	.388kg	2.91 W peak
Laser Emmiters w/ fiber optics	negligible	n/a	negligible	n/a

REFERENCES

Periodicals

1. Eberhart, Jonathon. "Mars: Let it Snow, Let it Snow...(Mars' Polar Caps)". V138, *Science News*, Nov. 3, 1990, p.286.
2. David, Leonard. "Move Over Red Rover". *Ad Astra*, Nov.-Dec. 1992, p.5.
3. Escap Motion Systems. Manufacturer's Catalog. 1993/94 edition.
4. Flynn, Faye. "Swarms of Mini-Robots Set to Take on Mars Terrain". *Science*. Sept. 18, 1992, p.1621.
5. Fishman, David. "Freewheeling on Mars". *Discover*. Aug. 1990. p.22.
6. Intel Corp. "Intel Micro-controller Handbook". 1986. Santa Clara, CA.
7. Motorola Inc. "Motorola Semiconductor Master Selection Guide and Catalog". 1984. Phoenix, AZ.
8. Nichols, Robert G. "An All-Terrain Mars Car". *Astronomy*. May 1990. p.14.
9. Wolansky, Ernest B. "Torsion Spring Material Weights". *Machine Design*. May 23, 1991. p.119.

Books

10. American Geophysical Union. Scientific Results of the Viking Project (reprinted from Journal of Geophysical Research, Sept. 30, 1977). ©1977. American Geophysical Union.
11. ASM International. Engineering Materials Handbook Vol. 1. ©1987. ASM International. Metals Park, OH.
12. Bayley, F. and J. Owen. Heat Transfer. ©1972. Thomas Nelson and Sons, LTD. London.
13. Corzine, Robert G. Four Arm Spiral Antennas. ©1990. Artech House Inc. Norwood, MA.
14. Chironis, Nicholas P (editor). Spring Design and Application. ©1961. McGraw Hill. New York.

15. Crane, F.A.A., J.A. Charles. Section and Use of Engineering Materials. ©1984. Butterworth and Co., London.
16. Clark, A. and R. Reed. Non-Metallic Materials and Composites at Low Temperatures. ©1979. Plenum Press. New York.
17. CRC Material Section Handbook. ©1993. CRC Press.
18. Delmonte, John. Technology of Carbon and Graphite Fiber Composites. ©1987. R. Krieger Publishing.
19. Flinn, Richard, Paul Trojan. Engineering Materials and Their Applications, Fourth Ed. ©1990. Houghton Mifflin Co.
20. Forsell, Börge. Radionavigation Systems. ©1991. Prentice Hall International.
21. Friedrich, Klaus. Friction and Wear of Polymer Composites. ©1986. Elsevier.
22. Gieck, K. and R. Gieck. Engineering Formulas. ©1990. McGraw Hill, New York.
23. Hands, B.A. Cryogenic Engineering. ©1986. Academic Press. New York.
24. Lipsky, Stephen E. Microwave Passive Direction Finding. ©1987. John Wiley, and Sons. New York.
25. Mark's Standard Handbook for Mechanical Engineers 8th ed. ©1978. McGraw Hill.
26. Miller, Frank, Nicholas Booth. Race to Mars. ©1988, Harper and Sons.
27. Murray, Bruce. The Planets. ©1983. W.H. Freeman and Sons.
28. Pattan, Bruno. Satellite Systems: Principles and Technologies. ©1993. Van Nostrand and Reinhold, New York.
29. Rosenbach, H.S. Solar Cell Array Design Handbook. ©1980. Litton Educational Publishing.
30. Sarafini, Tito T. and Jack Koenig (editors). Cryogenic Properties of Polymers. ©1968. Marcel Dekker, Inc. New York.
31. Wilford, John Noble. Mars Beckons. ©1990. Knopf, Inc.

5.0 REMOTE POWER SUPPLY

Robert Stubbers
Ralph Winiarski

Executive Summary

In order to provide remote power generation for the Mars microrover, several alternative methods have been examined. These options include solar cells, batteries, fuel cells, thermionic direct energy converters (DEC), charged particle DEC, and radioisotope thermoelectric generators. In selecting among these alternative methods several design criteria were used. These criteria included: 1. length of mission, 2. mass restrictions on payload, and finally 3. economics considerations. Radioisotope thermoelectric generators were selected because they best matched the design criteria.. In order to provide the most efficient and economical power source, it was decided to design a RTG for the proposed mission, rather than using an existing one. This allowed a RTG to be designed which was "taylor made" for the Mars mission. Since most of the equations used in RTG design are interdependent upon one another, a computer code was written to perform all the necessary calculations. Also, in order to provide the best design, an analysis on total weight was built into the program so that it could be determined whether a single 10 W_e was better than a 10 W_e source comprised of 4 2.5 W_e modular sources. The overall dimensions and weight to generate the 10 W_e required is given below:

	Single 10 W _e	Modular 2.5 W _e
Outer Radius	6.448 cm	6.015 cm
Mass	600 grams	240 grams
Total Mass	600 grams	960 grams

Therefor it appears that from a weight analysis, the single 10 W_e source is better than the modular, 2.5 W_e source. However, with the modular power source, a total fialure of the power system is much less likely. With a single source, a failure could potentially end the mission. Thus the choice between sources becomes a PRA decision.

It should be noted that this value is lower then what will be expected as there will be additional insulation on the end caps of the RTG and other electrical regulators which will add to the overall weight of the RTG. It has been estimated that the total weight of the single RTG will be approximately 1 kilogram and each modular RTG will weigh approximately 600 grams, or 0.6 kg due to the fact that each RTG has to be insulated heavily in order to channel the flow of heat. Therefore the estimated total weight of the modular source will be 2.4 kg.

Table of Contents

- Authors' Note
- Frontispiece
- Executive Summary
- 1.0 Introduction
 - 1.1 The Mission and Plan for the 1993/94 NASA Advanced Design Program
 - 1.2 The Contents of this Report
- 2.0 Astrophysical and Geophysical Background Information on Mars
 - 2.1 Astrophysical Characteristics of Mars (Comparison with Earth)
 - 2.2 The Martian Environment
 - 2.2.1 Martian Atmosphere and Pressure
 - 2.2.2 Composition and Topography of the Martian Surface
 - 2.2.3 Climatology of Mars
 - 2.2.3.1 Dust Storms and Wind
 - 2.2.3.2 Temperatures
 - 2.2.3.3 Clouds
 - 2.3 Estimates of Solar Radiation Incident Upon the Surface of Mars
- 3.0 Survey of Potential Power Systems for the Mars Mission
 - 3.1 Introduction
 - 3.2 Fuel Cells
 - 3.2.1 Basic Theory
 - 3.2.2 Thermally Nonregenerative Fuel Cells
 - 3.2.3 Thermally Regenerative Fuel Cells
 - 3.3 Batteries
 - 3.3.1 General Features and applicability of Batteries
 - 3.3.2 Specific Battery Types for Space Use
 - 3.3.3 Conclusions
 - 3.4 Solar-Powered Systems

- 3.5 Nuclear Powered Systems
 - 3.5.1 Radioisotope Thermoelectric Generators (RTG's)
 - 3.5.2 Thermionic Devices
 - 3.5.3 Charged-Particle Converters
 - 3.6 Summary and Conclusions
-
- 4.0 Radioisotope Thermoelectric Generators and Design Considerations
 - 4.1 Introduction
 - 4.2 Fundamental Principles of Thermoelectric Power Generators
 - 4.3 Selection of Radioisotope Fuel
 - 4.3.1 Criteria and Selection Process
 - 4.3.2 Power Density and Fuel Cost Estimates
 - 4.3.3 Radiological Safety
 - 4.3.4 Conclusions and Fuel Choice
 - 4.4 Existing RTG Designs
 - 4.4.1 Very Low Power, Long Lifetime RTG's (The Powerstick)
 - 4.4.2 Relatively High Power
 - 4.5 Need for a "Mission Specific" Design
 - 4.6 Literature Search for Mission-Specific Design Aids
 - 4.6.1 Annotated Bibliography of General Information Sources
 - 4.6.2 Primary Literature Sources Useful to the Design
 - 4.6.3 Secondary Literature Sources for this Project
-
- 5.0 Design of a RTG for Mars Mission
 - 5.1 General Considerations
 - 5.2 Selection of Optimum Thermoelectric Element
 - 5.3 Thermal Analysis
 - 5.4 Computer Code Development
 - 5.5 Weight/Size Comparison
 - 6.0 Summary and Conclusions

Appendices

- A Conceptual Designs of Alternative Small Nuclear Power Systems for Mars Mission
 - A.1 Radioisotope Fueled Thermionic Vacuum Diode System
 - A.2 Charged Particle Direct Energy Conversion (DEC) System
- B Principles of Thermoelectricity
 - B.1 Onsager Relationships
 - B.2 Magnitude of Thermoelectric Power, S_A
 - B.3 Real Thermocouples
 - B.4 Power from Thermoelectricity
 - B.5 Estimate of Optimum Efficiency of a Thermoelectric Generator
- C Selection of "Fuel" for RTG's in Space Power Systems
 - C.1 Determination of Specific Thermal Power (W/kg)
 - C.1.1 Radioactive Decay Law
 - C.1.2 Activity
 - C.1.3 Energy Released per Disintegration
 - C.1.4 Specific Power (W/kg)
 - C.1.5 Specific Thermal Power (W/kg)
 - C.2 Criteria for Radioisotope Fuel
 - C.3 Selection of Radioisotope
 - C.4 Comparison of Characteristics of ^{90}Sr and ^{238}Pu Power Source
- D Radiological Safety Comparisons of Strontium-90 with Plutonium-238 as Fuel for RTG Space Power System
- E RTG Analysis Code

1.0 Introduction

1.1 The Mission and Plan for the 1993/94 NASA Advanced Design Program

The University of Cincinnati, through its Space Engineering Research Center, has been awarded a grant to participate in the NASA University Space Research Association's Advanced Design Program. Specifically, the 1993/94 Advanced Design Project is the design of a robotic survey of the planet Mars. The overall mission to which this project is directed may be stated as: "To gather information about Mars through insitu (robotic) scientific investigations of the nature and resources of the Martian environment, the purpose being to provide a more detailed foundation for future explorations, building upon the knowledge gained from previous Mars missions." The specific information sought in this current mission concerns the potential fuel and life-support resources (primarily the water content of the North Polar cap), the geochemical nature of the Martian crust, and the general atmospheric conditions.

The plan for collecting the information is as follows. Five or six landers will be sent to the North Polar region, spaced at five-degree increments along a specified longitude (yet to be determined). Each of these landers will contain one or two micro-Rovers* equipped primarily to perform a longitudinal radar mapping of the surface substrate over its (their) five-degree domain. An additional six landers will be sent to the 15-20-degree latitude, spaced circumferentially at 60-degree intervals. Each of these landers will also contain one or two micro-Rovers, equipped for geochemical studies along the latitude within its (their) 60-degree sector. The landers themselves will function as base stations for collection of atmospheric data. To execute this plan, a mission exploration time of one Martian year (687 earth days) is deemed necessary. Since the transit time from Earth to Mars is of the order of one year, all systems thus must have a minimum capability of three earth years.

*The term "micro-Rover" has been coined by the Jet Propulsion Laboratory (JPL) for a miniaturized version of the land Rover. A popular description of the Rocky IV micro-Rover is presented by Kim Reynolds in the April, 1993 issue of Road & Track. More Technical descriptions are found in various JPL technical memoranda.

The role of the Nuclear Engineering design group, in support of the above mission and plan, is to provide the instrumentation power sources, both for the electronics themselves and for the maintenance of the required temperature for their functioning. The above-stated plans call for a maximum of 36 primary power sources (for the 12 landers and the two micro-Rovers in each), although many of these power sources may be identical. Since the detailed power requirements are pending the outcome from the other design groups in the College of Engineering, the power design group must provide a selection (options) of power sources over the expected power range from milliwatts to several hundred watts. These power sources must have enduring delivery capability under the adverse conditions of space travel, landing impact, and the harsh Martian environment.

1.2 The Contents of This Report

The approach to designing a power source for the prescribed Mars mission starts with an understanding of the environment in which the system must, or may, operate. The second section of this report is devoted entirely to a descriptions of the features of the Martian environment believed to be pertinent to both the selection and the design of the power source. Information from previous Martian exploration is drawn upon to present data on temperatures, pressures, clouds, winds, storms, and composition and topography of the Martian surface. Armed with these data, a survey of potential power systems is then presented in Section 3 of this report. The survey includes fuel cells, batteries, solar-powered systems, and nuclear-powered systems. As a result of this study, the Radioisotope Thermoelectric Generator (RTG) appears to present the best match with the environmental and mission constraints.

Section 4 presents both background information on RTGs (principles of thermoelectric power generation, components of RTGs, and existing designs) and design considerations (selection of radioisotope fuel, general design criteria, and the need for a mission-specific design). It concludes with a presentation of the literature searched for mission-specific design aids.

The groundwork laid, as summarized in the preceding four sections, culminates in the

actual RTG design for this mission, as presented in Section 5. This design is the "heart" of the project and centers on a 10 We system, either singly, or comprised of 2.5 We modules, should lesser (or greater) electrical power demands appear as a final requirement for this mission. This design has been integrated with the requirements from the other design groups on this project within the College of Engineering, University of Cincinnati, as made known to the authors.

The design section is then followed by a summary and conclusions resulting from this study (Section 6). The report concludes with five Appendices presenting details from ancillary lectures, designs of alternative systems, and radiological studies supporting the effort presented in the main body of the text.

2.0 Astrophysical and Geophysical Background Information on Mars

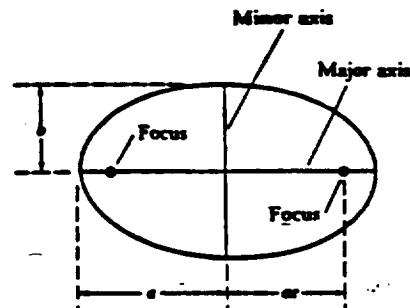
2.1 Astrophysical Characteristics of Mars (Comparisons with Earth)

Although the Universe is currently believed to be about 15 billion years old¹, our solar system has a relatively young age of 5 billion years.* The four inner planets: Mercury, Venus, Earth and Mars, are composed primarily of rock and are called terrestrial planets. They are the smallest and most dense planets in our solar system. "Mountains, craters, canyons, and volcanoes are common on their hard, rocky surfaces."² The terrestrial planets are composed mostly of heavy elements (iron, silicon, magnesium, sulfur, and nickel) and have atmospheres composed mostly of gases heavier than hydrogen and helium; carbon dioxide, oxygen, and nitrogen being the prevalent ones. The remaining planets, with the exception of Pluto, are huge, gaseous planets -- called Jovian planets -- with relatively low density, and are composed primarily of such light elements as hydrogen and helium.²

*Calculation of the geological age of the Earth from the alpha-particle decay chain of uranium-238 indicates an age of 5.3 billion years.

Most of the nine planets in our solar system orbit about the sun in approximately the same plane*. Mercury and Pluto are exceptions, with more elliptical orbits and with planes of motion significantly inclined to that of the others (7° and 17.1° inclinations to the ecliptic**, respectively). The orbital characteristics of Earth and Mars, and their major physical properties, are presented in Table 2-1.

*The orbits of the planets are more accurately described as elliptical rather than circular. Referring to the drawing below, the largest diameter across an ellipse is called the **major axis** and has length designated as $2a$. The shortest diameter through the center of the ellipse is called the **minor axis**, and is the perpendicular bisector of the major axis. The distance from the center of the ellipse to one focus is (ae) , where e is the "eccentricity." Note that $e = 0$ is the condition for a circular orbit. As seen from the data in Table 2-1, both the Mars and Earth orbits (especially of the Earth) have small eccentricities, hence nearly circular orbits.



"For the purpose of the report, the ecliptic may be taken as the plane of motion of the Earth's orbit. More specifically, the ecliptic is defined as the apparent path of the sun on the "celestial sphere."¹

Table 2-1. Astrophysical Characteristics of Mars and Earth*

Item	Mars Data	Earth Data
Mean distance from the Sun**	$1.524 \text{ AU} = 2.279 \times 10^8 \text{ km}$	$1.000 \text{ AU} = 1.496 \times 10^8 \text{ km}$
Maximum Distance from Sun	$1.666 \text{ AU} = 2.492 \times 10^8 \text{ km}$	$1.017 \text{ AU} = 1.521 \times 10^8 \text{ km}$
Minimum distance from Sun	$1.381 \text{ AU} = 2.067 \times 10^8 \text{ km}$	$0.983 \text{ AU} = 1.471 \times 10^8 \text{ km}$
Mean orbital velocity	24.1 km/s	29.8 km/s
Sidereal period	686.98 days = 1.88 years	365.256 days = 1.00 years
Rotation period	$24^h 37^m 22^s$	$23^h 56^m 7^s$
Inclination of equator to orbit	$25^\circ 11'$	$23^\circ 26'$
Inclination of orbit to ecliptic	$1^\circ 50' 59''$	—
Eccentricity of orbit	0.093	0.017
Diameter (equatorial)***	6786 km	12,756 km
Diameter (Earth = 1)	0.532	—
Mass	$6.42 \times 10^{23} \text{ kg}$	$5.976 \times 10^{24} \text{ kg}$
Mass (Earth = 1)	0.107	—
Mean density	3950 kg/m^3	5520 kg/m^3
Surface gravity (Earth = 1)	0.380	—
Escape speed	5.0 km/s	11.2 km/s
Surface Temperatures	Max: $20^\circ\text{C} = 70^\circ\text{F} = 293\text{K}$ Min: $-140^\circ\text{C} = -220^\circ\text{F} = 133\text{K}$	Max: $60^\circ\text{C} = 140^\circ\text{F} = 333\text{K}$ Mean: $20^\circ\text{C} = 70^\circ\text{F} = 293\text{K}$ Min: $-90^\circ\text{C} = -130^\circ\text{F} = 183\text{K}$

* Data from William J. Kaufmann III, Universe, Fourth Edition, (W. H. Freeman and Company, New York, 1994).

** 1 AU = 1 astronomical unit = average distance between the Earth and the Sun = $1.496 \times 10^8 \text{ km} = 93 \text{ million miles.}$

***Both Mars and Earth shapes deviate by a relatively small amount from being perfectly spherical, and are more accurately described as oblate spheroids. Since there are no oceans on Mars to aid in describing a mean geopotential reference surface, and oblate spheroid describing the 6.1 mbar level in the atmosphere from the Mariner 9 measurements is used for this purpose (Cain et al., 1973). This oblate spheroid has an equatorial radius (r_e) of 3393.4 km and a polar radius (r_p) of 3375.5 km.³

Although all of the Mars data presented in Table 2-1 bears at least indirectly on this project, the most pertinent data concern the size, sidereal period, rotational period, and surface temperatures. To a lesser significance are the data on mean distance from the sun, inclination of the polar axis, and the surface gravity.

As Mars and Earth circulate in their respective orbits, the Earth catches up with Mars every 780 days (about 2-1/7 years). These close encounters are called oppositions. Because of the actual elliptical nature of the orbits, the closest oppositions (termed "favorable" oppositions) occur when Mars is simultaneously at opposition and near perihelion. (The sun is one focus of the elliptical orbit. When the planet approaches the major axis near this focus, it is said to be near perihelion.) During a favorable opposition, the Earth-to Mars distance can be as small as 56×10^6 km (35 million miles). During the oppositions of this present decade, it is typically at a distance of $85 - 100 \times 10^6$ km (53 - 63 million miles). By comparison, as seen from the data in Table 2-1, the distance between the average (circular) orbits of Mars and Earth is 78×10^6 km (49 million miles).¹

Two tiny moons, Phobos and Deimos, move around Mars in orbits close to the Martian surface. These moons are jagged, heavily cratered, football-shaped rocks, perhaps captured by Mars from the nearby asteroid belt. Phobos is roughly 28 by 23 by 20 km (about 17 by 14 by 12 miles), and the smaller moon Deimos is roughly 16 by 12 by 10 km (about 10 by 7 by 6 miles). Their average orbits are only 6,000 km (3,700 miles) and 20,000 km (12,400 miles) from the planet surface. By comparison, the Earth's moon has a diameter of about 3,500 km (about 2,200 miles) and orbits at an average of 376,000 km (235,000 miles) above the Earth's surface.²

The intensity of solar energy (radiation) incident upon Mars is significantly less than that incident upon Earth because of the $1/r^2$ - law behavior (r is the distance of the planet from the center of the sun).

¹William J. Kaufmann III, *Universe*, Fourth Edition, (W. H. Freeman and Company, New York, 1994).

²William J. Kaufmann III, op. cit., Chapter 7.

Measurements above the Earth's atmosphere indicate 1370 W/m^2 solar radiation normally incident upon Earth.³ From the data of Table 2-1, on mean distance of the planets from the sun, the $1/r^2$ - law predicts $1/(1.524)^2 = 0.431$ of this amount, or hence 590 W/m^2 solar radiation normally incident upon Mars. However, the planets reflect some of the incident radiation. A planet's albedo is defined as the ratio of the total amount of radiant energy reflected by the planet in all directions to the amount it receives from the sun. The albedos for Earth and Mars are 0.39 and 0.15, respectively.⁴ Hence the net normally-incident radiations for the two planets are $[(1370)(0.61) = 836 \text{ w/m}^2]$ and $[(590)(0.85) = 502 \text{ w/m}^2]$, respectively.

Additionally, since this net solar radiation strikes the normal area (πR^2) along the line-of-centers between the sun and the planet of interest, where R is the (spherical) planet radius, and in the course of a complete rotation period (a "day" for the planet of interest) the spherical surface area $4\pi R^2$ shares this incident radiation, the daily average solar energy received by the planet surface is $(\pi R^2)/(4\pi R^2) = 1/4$ of the net normally-incident values. Thus, on the average, the Earth surface receives $(836)/4 = 209 \text{ w/m}^2$ and the Mars surface receives $(502)/4 = 126 \text{ w/m}^2$ (both located at their mean distance from the sun). Since the mean orbital distances have been used, these values are, in fact, "annual" averages, neglecting atmospheric interferences, e.g., clouds in the case of Earth and dust storms in the case of Mars, as will be discussed later in this section. Because of the lesser solar radiation received by the Martian surface, the surface temperatures would be expected to be considerably colder than those of Earth. Indeed, the data in Table 2-1 indicates such a difference.

³Excerpted from the document "Model Profiles of the Mars Atmosphere for the Mars Rover and Sample Return Mission," by D. E. Pitts, J. E. Tillman, J. Pollack, and R. Zurek, Jet Propulsion Laboratory, 1988, to be published by NASA as a technical memorandum.

⁴V. M. Blanco and S. W. McCuskey, Basic Physics of the Solar System, (Addison-Wesley Publishing Company, Inc., Reading, Massachusetts, 1961).

2.2 Martian Environment

2.2.1 Martian Atmosphere and Its Pressure

The Martian atmosphere is similar to that of Earth's in that they both have regional and seasonal weather patterns, clouds, and global winds. However, they differ significantly in composition and pressure. In analyzing the atmosphere of Mars, there are several things to take into consideration, such as the chemical composition, pressure and its variations, thermal analysis, and the dynamics of the system. This section of the report presents information on the chemical composition, pressure analysis and , to a lesser degree, the dynamics aspects.

The methods used to determine the composition of the Martian atmosphere were quantitative interpretations of spectroscopic observations, and through the use of mass spectrometers on the Viking 1 and 2 landers. The results of these observations and measurements are listed in Table 2-2.⁵

Table 2-2. Typical Lower Atmospheric Composition at Low Latitudes

Gas	Mixing Ratio	Gas	Mixing Ratio
CO ₂	93.32 %	H ₂ O	0.03 %
N ₂	2.7 %	Ne	2.5 ppm
Ar	1.6 %	Kr	0.3 ppm
O ₂	0.13 %	Xe	0.08 ppm
CO	0.07 %	O ₃	0.03 ppm

⁵V. A. Krasnopol'sky, Photochemistry of the Atmospheres of Mars and Venus, (Germany: Springer-Verlag Berlin Heidelberg, 1986).

Table 2-2 shows that the major part of the atmosphere is carbon dioxide, unlike Earth where nitrogen is the major component. The values listed in Table 2-2 apply to low latitudes. Mars is a fairly dry place, having low amounts of water vapor in the atmosphere, typically less than 100 prm (precipitable microns)⁶. Additionally, there is a large seasonal variation in the water vapor and ozone concentration in the atmosphere^{4,6}, and variations in the mixing ratios of nitrogen and the noble gases can be up to a factor of 1.3 times listed values at low and middle latitudes due to the seasonal effect on the CO₂ content. In higher latitudes, specifically the polar regions, the variations are even greater due to the greater effects of condensation and evaporation of CO₂ from the polar "ice caps".⁵

In order to determine atmospheric pressure, radio occultation measurements were performed. These measurements found that the mean atmospheric pressure was 6 mbars,⁵ less than one percent that of Earth's. This value is significantly lower than the original estimates made by the scattering of sunlight. It was determined that those values were influenced by the amount of dust suspended in the air and haze. Surface pressure varies seasonally by about ± 15 percent due to the condensation and sublimation of CO₂ at the poles. This fact was verified by the Viking landers. Viking 1 landed at 22.2° N 47.97° W, called the Utopia Planitia. The measured pressure variations show the exchange of at least 8.0×10^{12} tons of CO² between the polar caps and the atmosphere.⁵

Figure 2-1 shows the surface pressure versus time during a year, as measured by the Viking 1 and 2 landers.⁷ (A sol = 1 Martian day, slightly longer than 1 Earth day, as indicated in Table 2-1). The difference in pressure between the two landers is due to the altitude difference between the two sites.

⁶M. H. Carr, The Surface of Mars, (Yale College: Yale University, 1981).

⁷From a lecture to the University of Cincinnati, USRA Advanced Design Class, by John F. Connolly, NASA Johnson Space Center, "Mars Exploration", Martian Surface and Atmospheric Characteristics, (November 10, 1993).

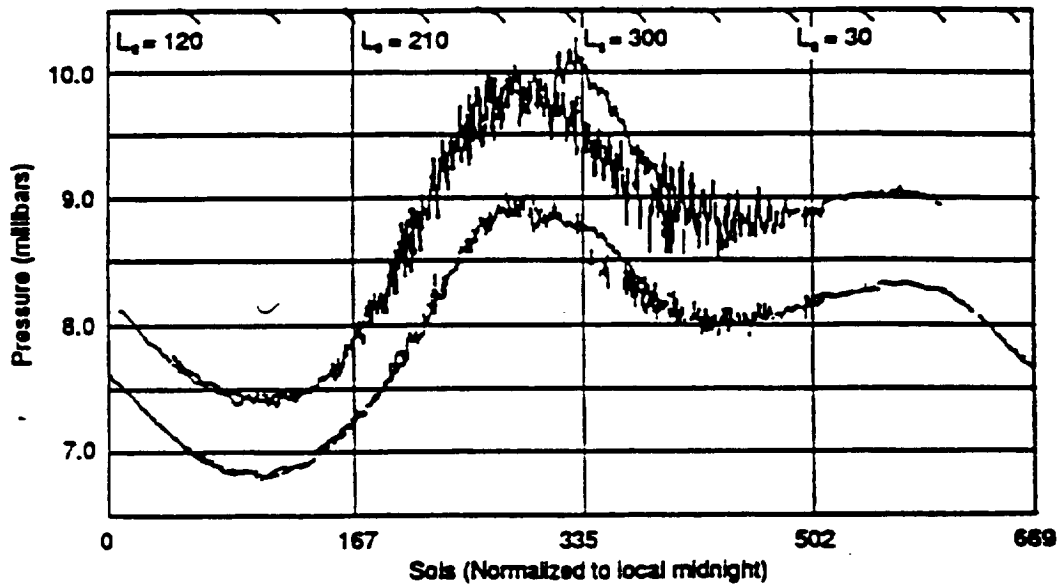


Figure 2-1 Surface pressure versus time for Viking Landers 1 and 2

As suggested by the two pressure curves in Figure 2-1, the pressure of the Martian atmosphere is a strong function of elevation, a fact of particular significance due to the considerable surface relief found on Mars. The rate at which pressure decreases with height is defined in terms of "scale height" - the vertical distance over which the pressure decreases by a factor of $1/e = (0.368)$.⁶ The scale height of the Martian atmosphere is close to 8 km, which gives a range of Martian surface pressure of almost a factor of ten. (See next section of this report for a discussion of surface topography.) This is why the Viking landers were directed to land in relatively low areas.⁶

2.2.2 Composition and Topography of the Martian Surface

Most of the measurements to date concerning the chemical makeup of the Martian soil have come from the Viking landers. The data gained from these measurements are listed below, in Table 2-3.⁶

Duricrust refers to calichelike deposits, up to a few cm thick. Fines refer to small, dust particles. As can be seen from this table, most of the surface is composed of silicon dioxide and iron oxides. It should be noted that the measurements were performed on the loose soils found around the lander sites. Thus they are not necessarily representative of the entire planet. Also note that the measurements do not total 100 percent. It has been suggested that the missing mass is due to H₂O and CO₂, and as carbon, hydrogen, and oxygen. The method of measurement could detect only elements of mass number greater than 11. The presence in the absorption spectrum of a 2.85 m line has been suggested as being caused by bound water, and possibly indicates that the regolith* could contain between 0.3-3.0 percent water by weight (Houck and colleagues).⁶ The most common suggestion for the precursor to the dust particles are forms of clay. In fact the Martian regolith can best be described as an iron-rich clay. The reddish appearance of Mars (the Red Planet) may be caused by rust (iron oxides) in the regolith.¹

Panoramic views of Chryse Planitia obtained by the Viking lander revealed generally a dust-like surface with dune drifts from which protrude rocks of a variety of sizes, shapes, and morphologies.

*The regolith is the layer of blanket of material that overlies the bedrock and forms the surface of the land.

Table 2-3 Chemical Composition of the Martian Soil

Compound wt %	Chryse Fines	Chryse Duricrust (1)	Chryse Duricrust (2)	Utopia Fines	Estimate Absolute Error
SiO ₂	44.7	44.5	43.9	42.8	5.3
Al ₂ O ₃	5.7	n.y.a.	5.5	n.y.a.	1.7
Fe ₂ O ₃	18.2	18.0	18.7	20.3	2.9
MgO	8.3	n.y.a.	8.6	n.y.a.	4.1
CaO	5.6	5.3	5.6	5.0	1.1
K ₂ O	<0.3	<0.3	<0.3	<0.3	—
TiO ₂	0.9	0.9	0.9	1.0	0.3
SO ₃	7.7	9.5	9.5	6.5	1.2
Cl	0.7	0.8	0.9	0.6	0.3
Sum	91.8	n.y.a.	93.6	n.y.a.	—
Rb, ppm	≤30			≤30	
Sr, ppm	60±30			100±40	
Y, ppm	70±30			50±30	
Zr, ppm	≤30			30±20	

In the field of Utopia Planitia, the drifts were both scarce and small, and the area between the rocks was primarily a crusty surface littered with clods of soil.⁸ Data were also obtained on the physical properties of the soil materials in the sample fields of the Viking landing sites. These data are summarized in Table 2-4.⁷

⁸H. J. Moore and B. M. Jakosky, "Viking Landing Sites, Remote Sensing Observations, and Physical Properties of Martian Surface Materials". Preliminary draft, 1988.

Table 2-4. Estimates of Mechanical Properties and Remote Sensing Signatures of the Surface Materials in the Sample Fields at the Viking Landing Sites.

	Grain Size (μm)	Bulk density (kg/m^3)	Cohesion (kPa)	Angle of internal friction (degrees)	Fraction of area covered	Thermal inertia (10^{-3} cgs units)	Dielectric constant
Lander 1							
Drift Material	0.1 - 10.0	1150±150	1.6±1.2 0 - 3.7	18.0±2.4	0.14	3	2.35 2.11 - 2.62
Blocky material	0.1 - 1500	1600±400	5.5±2.7 2.2 - 10.6	30.8±2.4	0.78	9.3±0.5 ¹	3.27 2.43 - 4.50
Rocks	35×10^3 240×10^3	2600	1000 - 10,000	40 - 60	0.08	40	8
Sample field		1624 1298 - 1850	-	-	1	-	3.33 2.61 - 4.32
Remote sensing		1612 1292 - 1857 1486 1857 - 2026	-	-		9.0±0.5	3.3±0.7 3.0 4.0 - 4.6
Lander 2							
Crusty to cloddy material	0.1 - 10.0	1400±200	1.1±1.2 0 - 3.2	34.5±4.7	0.86	6.3±1.5 ²	2.81 2.43 - 3.27
Rocks	35×10^3 450×10^3	2600	1000 - 10,000	40 - 60	0.14	40	8
Sample field		1568 1396 - 1740	-	-	1		3.19 2.81 - 3.64
Remote Sensing			-	-	0.20±0.10	8.0±1.5 8.3 - 8.8	2.8 - 12.5

¹Thermal inertia is 8.2±1.4 if fraction of area covered by rock is taken as 0.15.

²Thermal inertia is 5.6±1.4 if fraction of area covered by rock is taken as 0.20.

The Martian surface has a greater extreme of topography than that found on earth.

Surface features include volcanoes, rifts filled with dust, and craters. The largest volcano seen is Olympus Mons, which measures about 26 km (16 miles) in height and is almost 595 km (270 miles) wide at its base. It is located in the northern hemisphere at approximately 20° N 134° W.

The largest crater is called Hellas, and has been measured at 2000 km (1250 miles) wide and at least 4 km (2.5 miles) deep. It is located in the southern hemisphere at approximately 46° S 306° W. Most canyons are located in the equatorial regions. The largest of these, Valles Marineris (actually a series of canyons) ranges for over 4800 km (3000 miles), up to 480 km (300 miles) wide and can have depths of more than 6.4 km (4 miles). The topography of the North Polar Cap, where a part of the proposed mission is located, appears to be fairly uncratered, having a relatively flat area for landing. Its seasonal variation is smaller than that of the South Pole, the winters being longer and colder in the South. At its maximum, the North Polar Cap extends down to the 65th parallel. The residual cap is not centered exactly over the pole, instead varying between 80° to 85° N. It has been speculated that below the CO₂ ("dry ice") layer of the North (only) Polar Cap is ordinary ice (frozen H₂O).⁷ If indeed this is the case, then a large source of hydrogen and oxygen fuels will be available to future Martian expeditions.

2.2.3 Climatology of Mars

This portion of Section 2 presents information on the Martian surface temperature, winds, storms, and clouds, pertinent to the design project. Because of the strong interaction of the dust storms and winds with the surface and near-surface temperatures, information on these phenomena is first presented separately, and then entwined in the discussion of temperatures.

The general features of the Martian seasons in the northern hemisphere (the region of interest for this project) is as follows. The Martian year is 687 earth days long and is broken up as follows, in the northern hemisphere: Spring is 199 days, Summer 182 days, Fall 146 days, and Winter 160 days.⁹ Also, the cold season tends to be longer and colder, and the warm season is shorter but hotter in the southern hemisphere.

⁹McGraw-Hill Encyclopedia. Science & Technology, United States of America, (McGraw-Hill, 1992), pp. 491-495.

2.2.3.1 Dust Storms and Winds

Winds on Mars come from a variety of sources such as variations in temperature, condensation and evaporation of CO₂ at the poles, and Coriolis forces. They are also affected by the topography of the region through which they flow. The general patterns of Martian winds have been modeled theoretically, using the same techniques that are used on Earth's atmosphere.⁶ Average wind speeds were measured by the Viking landers and found to be about 5 m/sec.

Dust storms have been detected on Mars since early observations. It has been noted that most of the dust storms occur in the hemisphere having Winter, thus alternating between hemispheres depending upon the season. An exception is the presence of dust storms in the southern hemisphere during the summer season. These southern storms may become so large that they affect the entire planet. Dust storms moved with velocities of 14-32 m/sec. Wind speeds of approximately 14-17 m/sec, with gusts up to 26 m/sec were measured at the Viking lander sites during dust storms.⁶ Cyclonic dust storm frequency was measured at the Viking 2 site, and they were found to occur at an average of one every 3.3 days, for a period of 100 days.

2.2.3.2 Temperatures

Temperatures at the Martian surface depend on latitude, season, time of day, atmospheric winds and dust, and the properties of the surface itself (mainly its albedo and thermal inertia).¹⁰ The lowest temperatures on Mars occur at the South Pole during the winter of the Martian year (687 earth days), where they extend as low as 148K. Over the course of a Martian day (24 hours, 37 minutes), the temperature may vary as much as 50°C or as little as 10°C.¹⁰

Thermal Inertia (a measure of the responsiveness of a medium to changes in heat flow) is defined as $(k\rho C)^{1/2}$, where k is the thermal conductivity, ρ is the density, and C is the specific heat.¹⁰ If a material has a low thermal inertia, its temperature will respond rapidly to any change in heat input or output; if the thermal inertia is high, it will respond slowly. Predawn temperatures of the surface are sensitive measures of thermal inertia. For areas of the same

¹⁰M. H. Carr, *op. cit.*, pp. 18-19, pp. 25-34, pp. 169-180.

latitude, season, and albedo, the predawn temperatures are highest where the thermal inertia is highest (where there are coarse-grained surface materials). Bright areas (as determined by spectroscopic data) have low thermal inertias, and probably have fine-grained surface materials; dark areas have higher thermal inertias, and probably have more coarse-grained surface materials.¹¹ Surface temperatures were measured continuously by the Viking landers during a Martian year, with results as shown in Figure 2-2.⁷

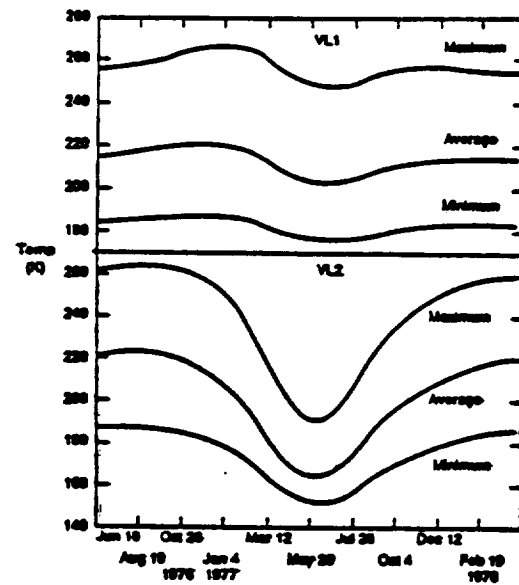


Figure 2-2. Daily maximum, minimum, and average surface temperatures at the two Viking landing sites through a Martian year. The maximum temperature occurs about 1 hr. after noon; the minimum occurs at dawn (Kieffer, 1976).

¹¹Bonnie Cooper and Associates, "Variations in Water Content of Martian Soils," Space Resource News, 2, no. 7, pp. 1-2, (July, 1993).

As mentioned previously, atmospheric circulation on Mars is driven by seasonal temperature gradients and movement of the atmosphere from pole to pole. The Martian atmosphere moves from pole to pole because 25-30 percent of it (of the CO₂) condenses on the Winter pole.¹⁰ Because the atmosphere of Mars is so thin, it has a small heat capacity; therefore, it cools and heats faster than Earth's atmosphere.

In the absence of dust, Mars' atmosphere absorbs little sunlight directly. The temperature of the gases at the surface is governed largely by the temperature of the ground and the amount of dust in the atmosphere. At the start of the Viking mission, the Martian atmosphere was relatively free of dust, and the diurnal temperature cycles at both landing sites (Chryse Planitia and the Utopia Planitia) were consistent from day to day,¹⁰ as seen from Figure 2-2. At the first site, the temperature had a minimum, at dawn, of just under 190K, and a maximum, close to noon, of 240K. Temperatures at the second site (Utopia Planitia) were 5-10°C cooler. The minimum air temperatures were close to the minimum surface temperatures, but the maximum air temperature fell approximately 20°C short of the peak surface temperatures. As northern winter approached, there was a slow seasonal cooling which was most noticeable at the second site (see Figure 2-2). This steady cooling pattern was sharply interrupted by the two major dust storms of 1977. These dust storms increased the opacity of the atmosphere, and resulted in a considerable narrowing of the diurnal temperature range. At the second site, the diurnal range was reduced from 50K (when the atmosphere was clear) to 10K.

Dust storms have a great effect on surface temperatures and atmospheric opacity. At the first Viking landing site, before the dust storms, the optical depth of the atmosphere (a measure of its opacity) had a value close to 1 (clear).^{*} The difference between the daily maximum and minimum temperatures was about 50°C. After the arrival of the first dust storm, the optical depth had increased to about 3; with the arrival of a second storm, the optical depth increased to a value of almost 6. With this increased opacity, the daily minimum and maximum temperature difference was reduced to about 15°C.¹⁰ A number of theories have been proposed to explain global dust storms. The most plausible appears to be a feedback mechanism that develops

*For vertical illumination, $I = I_0 e^{-d}$, where I is the intensity of light at the surface, I₀ is the intensity of light entering the upper atmosphere, and d is the optical depth.

between dust storms and diurnal wind tides.¹⁰ The preferential location of local dust storms in areas of known slopes and around the retreating seasonal polar cap suggests that dust is initially raised into the atmosphere as a result of slope winds, i.e. winds that develop as a result of the large temperature gradients adjacent to the polar cap. The presence of dust increases the absorption of insolation (the radiation from the sun received by a surface) in the atmosphere, which increases tidal winds. Under certain circumstances, this reinforcement of local winds may result in more dust being raised, further amplifying the tidal winds. This causes a runaway situation, in which tidal winds amplify themselves by raising more and more dust into the atmosphere over a wider and wider area. The dust storms may turn themselves off by raising so much dust into the atmosphere that the near-surface temperature gradient during the day decreases drastically. As a consequence, convective coupling with the strong tidal winds aloft is diminished, and the velocity of the near-surface winds drops so much that they can no longer pick up dust.

2.2.3.3 Clouds

Another feature which both Earth and Mars have in common is the presence of clouds. Clouds form on Mars because, even though at its usual temperatures and pressures there are only trace amounts of water vapor, the atmosphere is close to saturation. From spacecraft imaging, various types of individual clouds have been seen.⁶ (1) Polar hood - seen in the fall, consists of a general haze of water-ice, or maybe carbon dioxide-ice, more prominent in the North. These tend to dissipate when the water-ice precipitates out in the Winter. (2) Wave clouds - tend to form in the lee of large obstacles. (3) Convective clouds - form at high areas at midday, due to surface heating. (4) Orographic clouds - tend to form from air uplifting over large scale topography. (5) Ground hazes - usually seen in low areas during the cool part of the day; thought to consist of water-ice. (6) High altitude clouds - thought to consist of both water-ice and carbon dioxide-ice.

2.3 Estimates of Solar Radiation Incident Upon Martian Surface

As indicated in Section 2.1, the net average annual solar radiation incident upon Earth and Mars is 209 W/m^2 and 126 W/m^2 . Further validity, at least to the Earth's average value, is found from direct surface measurements. The annual average solar radiation received by horizontal surfaces at 79 locations throughout the continental (48 states) United States is 185 W/m^2 .¹² The fact that this value is 11 percent less than the average 209 W/m^2 can be readily explained by the occasional presence of clouds, and the second order effects of location and tilt of the Earth's polar axis. Because of the thinness of the Martian atmosphere, the attenuation of solar radiation by both atmosphere and cloud layers may be assumed to be small. An exception occurs during the global dust storms, during which times the opacity of the atmosphere is greatly increased (see discussion of Section 2.2.3).

From the above discussion, one might expect a solar radiation intensity of approximately 125 W/m^2 at the Martian Northern 20° latitude of interest to this project, and a significantly reduced value at the North Polar cap. (Theoretically, in the absence of a tilt to the rotational axis, the normally-incident radiation at the North Pole would be zero.)

3.0 Survey of Potential Power Systems for the Mars Mission

3.1 Introduction

Early estimates of the power requirements for the instrumented micro-rovers to be used in this Mars mission, as determined by the several design groups within the College of Engineering, University of Cincinnati, indicated a general order of magnitude of 10 watts (electrical). The principal guiding criteria for the power source are weight (associated transportation costs) and "ruggedness". The latter criterion is interpreted as a requirement for no,

¹²B. Y. H. Lin and R. C. Jordan, "Analysis of Solar Energy Data Applicable to Building Design," ASHRAE Journal, (December, 1962).

or few, moving parts; and capability for withstanding the Martian environment for the 2-year exploration duration. The general magnitude of the required power output, and the criteria of mission weight and ruggedness preclude the use of more conventional power generation from thermal machines (Rankine cycle, Brayton cycle, etc.) with flowing systems involving such items as pumps and turbines. The significance of the weight of the power source is clearly seen through the costs of transporting material from Earth to Mars: of magnitude \$1 million/10 kg.¹³ Such high costs and the current budget for NASA space exploration indeed place a premium on light-weight systems, and have motivated the design efforts for miniature spacecraft. Given the above-stated considerations, one is led to the so-called direct energy conversion (DEC) devices (in which there are no moving parts or flowing systems) to seek an appropriate power source design.

This section of the report surveys the "most common" DEC systems, namely: fuel cells, batteries, solar energy devices, and several types of nuclear (radioisotopic) generators. Within each type there are several possibilities, in various steps of technological development. The goal of this survey is to seek the most promising, most practical solution for the mission at hand. It should be pointed out that almost all of the DEC systems summarized herein are indeed options. However, most of these "options" demand a penalty for acceptance, primarily in the matter of weight and, secondarily, in the practicality of the current stage of development of the power system.

¹³"Design of a Lunar Propellant Processing Facility", Senior Design Project of Engineering Students at the University of Cincinnati, NASA 9th Annual Summer Conference, University Space Research Association (USRA) Advanced Design Program, Houston, Texas (June, 1993).

3.2 Fuel Cells

Fuel cells, like batteries, convert chemical energy into electrical energy; however, they are only limited in their capacity by the size of their fuel tanks¹⁴. In a fuel cell, the fuel and oxidizer are stored in tanks (external from the cell). The cells themselves consist of an electrolyte and two electrodes. There are four types of commonly used electrolytes: acid, alkali, neutral, and molten salt¹⁴. Fuel cells generally have theoretical efficiencies on the order of 80% to 99%¹⁵, but thermally regenerative fuel cells require separators, heat exchangers, and pumps¹⁶.

3.2.1 Basic Theory

The power in a fuel cell comes from the change in free energy of a reversible reaction¹⁵. The maximum power produced by a fuel cell is equal to the difference in the standard free energies of formation of the reactants and the products. The ideal potential difference (voltage), E_r , of the fuel cell is given by

$$E_r = \frac{-\Delta G}{n_e F} \quad 3-1$$

where ΔG is the Gibbs Free energy change, n_e is the number of moles of electrons released per mole of product, and F is Faraday's constant (96,500 coulomb/equivalent)¹⁵. The maximum efficiency of a fuel cell depends only upon the reactants, and is given by

$$\eta_{max} = \frac{\Delta G}{\Delta H_{fo}} \quad 3-2$$

¹⁴Gregory, D.P. Fuel Cells, (London: Mills and Boon Limited, 1972).

¹⁵Sutton, George W., ed. Inter-University Electronics Series, Vol. 3: Direct Energy Conversion, (San Francisco: McGraw-Hill Book Company, 1966).

¹⁶Brockis, J. and Srinivansan, S. Fuel Cells: Their Electrochemistry, (New York: McGraw-Hill Book Company, 1969).

where ΔH_{f0} is the change in the heat of formation¹⁶.

From equations (3-1) and (3-2), the actual efficiency of a fuel cell is given by

$$\eta = \frac{n_e F E_a}{\Delta H_{f0}} \quad 3-3$$

where E_a , the actual electrode potential, is used in place of the ideal potential E_r .

3.2.2 Thermally Nonregenerative Fuel Cells

From the previous equations, and assuming a power of 10 watts electric, the necessary quantities of fuel can be determined. Because of its high power density, the hydrogen-oxygen reaction will be considered here; an overall efficiency of 83% (the theoretical maximum for hydrogen) will also be assumed. The reactions of interest depend on the electrolyte used (acidic or alkaline). For an acidic electrolyte, the reactions of interest are the following¹⁷:



For an alkaline electrolyte, the reactions of interest are:



Thermally nonregenerative fuel cells (i.e. hydrogen-oxygen cells) are not tied to thermodynamic cycles, so their efficiency is not limited to the Carnot efficiency. For a 10W_e fuel cell operating

¹⁷Berger, Carl. Handbook of Fuel Cell Technology. New Jersey: Prentice-Hall, inc., 1968, pp. 30-31.

continuously during the Martian year mission duration, the total energy required is given by

$$\text{Total Energy} = (.01 \text{ kW}) (687 \text{ days}) (86,400 \frac{\text{seconds}}{\text{day}}) = 594,000 \text{ kJ}$$

For an ideal hydrogen-oxygen fuel cell, the amount of energy per gram of fuel is equal to ΔG_{water} (Gibbs free energy of water); $\Delta G = -13.16 \text{ kJ/g}$ for water¹⁸. Therefore, the mass of hydrogen and oxygen required is given by

$$m_{H_2+O_2} = \frac{594,000 \text{ kJ}}{13.16 \frac{\text{kg}}{\text{g}}} \times 0.001 \frac{\text{kg}}{\text{g}} = 45.1 \text{ kg of } H_2 \text{ and } O_2 .$$

The weight of the fuel cell itself (not including fuel) would be approximately 0.1 lb/watt or higher (depending on the required voltage)¹⁵; thus the cell contribution adds a weight of only 1 lb (0.45 kg) for a 10 watt_e system. These considerations yield a total system weight of approximately 45.6 kg. Clearly, on the basis of mass alone, this system has marginal practicality for the proposed Mars rover.

¹⁸Brown, Theodore L. and LeMay, H. Eugene. Chemistry: The Central Science. New Jersey: Prentice-Hall, inc., 1988, p. 977.

3.2.3 Thermally Regenerative Fuel Cells

Thermally regenerative fuel cells, unlike nonregenerative fuel cells, are limited to the Carnot efficiency

$$\eta = 1 - \frac{T_c}{T_h} \quad 3-6$$

where T_h is the "hot reservoir" absolute temperature and T_c is the temperature of the "reservoir" to which heat is rejected. The electrolytes used for thermally regenerative fuel cells are molten salts which require operating temperatures on the order of 630°C (963K) or higher¹⁶. In addition to high temperatures, these devices require separators, pumps, and heat exchangers; all of which add to its size and weight, and decrease overall efficiency. The required operating temperature and added equipment make this option impractical.

Thermally nonregenerative fuel cells are not a practical power source for the Mars rover mission because of their size and weight. Also, thermally regenerative fuel cells are not a practical source of power because of their low efficiencies, size, complexity, and high temperatures.

3.3 Batteries

3.3.1 General Features and Applicability of Batteries

Batteries are simply a set of cells which contain two electrodes which are separated by a solution called an *electrolyte*. The battery gains energy by an endothermic chemical reaction which converts the input electrical energy into stored chemical energy. When the process is run in reverse the stored energy is then discharged back into electrical energy.

Batteries are generally considered a good option for low power needs because they are compact, versatile, and maintenance free. This type of power is relatively safe and is a good alternative for earth-bound mobile power needs or storage of electrical power from another source. New battery technologies are being developed mainly by the automotive industry in their attempt to create an electric car that can compete with gas powered vehicles. The major drawback of using electric batteries is their weight, but new types of batteries are bringing the energy capacity (watt-hours/kg) up by 4 to 5 times higher than the current and most common lead-acid batteries. Researchers are currently testing batteries that use lithium polymers as the negative electrode and high energy density materials such as vandium oxide as the cathode. The lithium polymer battery is desirable because it uses thin sheets of lithium polymers which can be rolled up into small volumes and shaped to fit whatever space remains after the vehicle is designed. Lithium-aluminum/iron disulfide batteries can also be useful.¹⁹

As mentioned earlier, the major drawback in the use of batteries for a space mission is their weight. Previous estimates* indicate a specific weight of the order of 2 kg/watt_e, i.e. approximately 20 kg for a 10 W_e source. Although the weight is competitive with fuel cell technology (both of which are considered too massive for the current mission), for continuous operation for the required 2-year mission, means for recharging the batteries must be provided.

¹⁹1992-93 NASA USRA Advanced Design Program, Nuclear Engineering Fall Quarter Design Project Report (LEAD, Inc.), University of Cincinnati, Cincinnati, Ohio.

*This specific weight more accurately applies to battery power of the order of 1 kW_e. The lower-power requirement of this mission will probably have a higher associated specific weight, i.e. the 2 kg/watt is considered to be an optimistic estimate.

Another problem that batteries have is that low temperatures affect the rates at which the chemical reactions take place, thus lowering the available discharge voltage of the battery. In a combination battery-nuclear RTG power supply, this problem could be avoided through the use of the waste heat from the nuclear RTG diverted to warming up the batteries. A potential problem also arises in the length of time required for the actual recharging of the battery. Typical recharge rates run about 10 hours or more for earthbound traction batteries. This would mean that the rover would essentially shut down all operations during the night in order to store the energy required for the next day. According to Levy²⁰, batteries face an unavoidable deterioration with time. Short-term accelerated experiments have been developed to reveal potential battery lifetimes, under certain conditions. To date, however, these tests have not been universally applied to the potential contenders for space applications.²⁰

3.3.2 Specific Battery Types for Space Use

A preliminary battery design has already been developed by JPL regarding a rover for use on Mars. The battery it uses is a lithium-iodide D cell.²¹ It was designed to supply up to 150 W-hrs. (Note: A watt-hour is defined as the product of the average discharge voltage and the ampere-hour capacity of the battery).²² Since the power requirement was listed as 14 W-hr for day use and 8.0 W-hr for nighttime operations, it was expected to run for "lots of days" but only one night. This range is far too limited for the desired length of operation for this design project, (one Martian year).

²⁰P. Bro, and S. Levy, Quality and Reliability Methods for Primary Batteries, (John Wiley & Sons Inc., Pennington, New Jersey. 1990).

²¹Kim Reynolds, "JPL ROCKY IV" Road & Track, April, 1993.

²²G. Smith, Storage Batteries, (Pittman, London, England, 1980).

The Goddard Space Flight Center has held battery workshops which have looked at a variety of batteries and discussed the advantages and disadvantages of their use. Typical proceedings are those presented from the 1985 workshop.²³ (Unfortunately most of the applications which have been discussed are for satellite applications, which typically have a very small power requirement). Listed below is a brief synopsis of several battery types and their individual advantages and disadvantages drawn from the workshop proceedings.

Li-SO₂ (as used in the Galileo probe)

The cells used in the Galileo probe were 13 D-cells connected in series. They appear to be able to provide only 19.0 A-hrs. (At an average voltage of 1 volt, they would only be rated at 19.0 W-hrs).

Li-TiS₂ (as being developed by Jet Propulsion Lab.)

Present day experimental batteries have been developed which possess 10.4 Volts, 0.4 A-hr power levels. It has been projected that future developments will allow a specific energy of 100 W-hrs/kg for 35 Ah Li-TiS₂ cells. These cells would be ambient temperature rechargeable. Should projections become reality, this battery type may warrant further review in the future.

Ni-Cd (as developed by General Electric)

General Electric delivered Ni-Cd batteries of 50 Ah design for testing by NASA. During testing these batteries displayed voltages of up to 1.5 volts per cell. However, the resultant energy of only 75 W-hr falls considerably short of the presently estimated 10 W load expected to be needed for a full Martian year. While they are rechargeable, a separate source of power would be required to charge them.

²³G. Morrow, The 1985 Goddard Space Flight Center Battery Workshop. (NASA, Scientific and Technical Information Branch).

Lithium-Iodide D-Cell (as developed by JPL)

Power output is listed as 150 W-hr for 12 cells. These cells are not rechargeable, but the design includes solar cells, which provide up to 100 W-hr/day, on a sunny day. These solar cells face the problems of reduced incident solar flux as well as the dust storms which periodically arise on Mars, as discussed in the next portion of this section.

3.3.3 Conclusions

From a brief survey of battery characteristics and applicability to the mission at hand, the following tentative conclusions have been drawn. Although there are a variety of battery types in use and currently under development, the general features appear to be:

1. Batteries are compact, versatile and maintenance free low power supplies
2. Their weight is prohibitively large for this mission, very comparable in this regard to that of fuel cells
3. A significant fraction of the Martian-year mission duration will be required for recharge time
4. Auxiliary heating of the battery "compartment" is required to maintain the discharge voltage of the batteries (to maintain the chemical reaction rate)
5. Chemical batteries face unavoidable deterioration; the extent and impact on the various contenders for space use is uncertain at present.

From the considerations presented above, batteries do not appear to be a practical power source for the Martian mission under study.

3.4 Solar-Powered Systems

As discussed in Section 2.3 of this report, the annual average solar radiation intensity at the Martian Northern 20° latitude of interest to this project is expected to be approximately 125 W/m², with a significantly reduced value at the North Polar cap. For design discussion purposes, consider the "best" case of the 20° latitude solar intensity estimate (125 W/m²).

One generally associates the following pertinent advantages to power from solar energy: (1) the energy source is "free" and inexhaustible, (2) systems using solar energy directly have few moving parts, if any, and this requires very little to no maintenance, and (3) the energy source is "clean", presenting no environmental problems. On the other hand, because of the "day-night" dependency, solar systems require energy storage device(s) for continuous power output. This dependence tends to result in relatively large deployment mass for solar-powered systems. Additionally, the power generation is significantly influenced by the nature of the atmosphere between the solar collector panels and the sun's radiation.

There are three principal systems that can be used to harness the sun's energy: thermal solar power which uses concentrated solar energy in a heat engine to produce direct electricity (Carnot Cycle), photovoltaic (PV) cells to produce direct electricity, and a photochemical system in which electromagnetic radiation is used directly in a chemical process (much like photosynthesis). Each of these systems is discussed briefly as follows.

Thermal solar power uses the sunlight as a heat source. Collectors focus the electromagnetic radiation on a carrier fluid (water, air, Na salts, etc.) which is heated by the sunlight. The fluid is expanded in a turbine, in a Rankine or Brayton cycle, or in another thermodynamic cycle to produce AC electric power. Currently operating thermal solar power plants on earth have efficiencies of approximately 15%, with expectations of 20-25% in the future.²⁴ However, such a system is impractical for the low-power requirements (on the order of 10W-electric) for this project.

²⁴ Autumn quarter, 1992, USRA/NASA Senior Nuclear Engineering Design Project Report, Scott A. Snider, Lead, inc. (Nuclear Engineering Project Team), University of Cincinnati, Cincinnati, Ohio.

The use of photovoltaic cells involves a process which converts the energy of the sunlight directly into electricity without a thermodynamic cycle. The electricity produced is in the form of DC. If AC is desired, conditioners and converters are needed. Currently, there are no appropriate options to store the electric energy produced from photovoltaic cells for the Mars mission. Energy storage may be done with the use of chemical batteries or mechanically flywheels; however, at the 10 watt (electrical) power level, these are not good options because of added cost and weight*. Superconducting electromagnetic storage rings may be usable in the future, but are not yet available. Photovoltaic power plants on earth currently produce AC power at an efficiency of 6-8%²⁵. Advances in commercially available PV cell efficiencies (10-15% now)²⁶ are expected to result in commercial cell efficiencies of up to 40%, which have already been achieved under laboratory conditions.²⁷ Typical advanced photovoltaic cell outputs are of the order of 40mA per cm² of solar cell surface, at a voltage of 500 mV.²⁶ However, without an energy storage system, use of photovoltaic cells in the mission at hand restricts exploration and operational performance to sunlight hours.

In a photochemical process, the sun's electromagnetic radiation is applied to drive chemical processes in the same way process heat is now used. The advantage of sunlight over process heat is in the wavelengths of the energy. The sun has a temperature of 5800 K, much higher than the temperatures reached in process heat furnaces. This sunlight has shorter wavelengths than those from infrared heat sources. This allows for more efficient use of the energy in certain chemical processes. This field of research is still new and relatively unexplored. Therefore the use of photochemical processes is assumed to be at a non-commercial stage of development and unavailable to this project.

Of the three principal solar systems described, the photovoltaic system appears to be most applicable for consideration for the Mars mission. With an optimistic assumption of 15%

*See discussion of batteries for space use in preceding section.

²⁵Winter, Sigmann and Vant-Hall (Editors), Solar Power Plants, Part 3, 1990.

²⁶Photovoltaic Solar Energy Conference: Proceedings of the International Conference, London, U.K., April 15-19, 1985.

²⁷Proceedings of Executive Conference on Photovoltaic Systems for Electric Utility Applications, December 2-9, 1990, p. 81.

efficiency, and an incident intensity of 125 watt/m², the photovoltaic system would have an electric power output of approximately 18 watts/m². Thus, for example, a 10 watt electric system would require a solar panel with an effective area of only 5/9 m² (6ft²). Although a bit bulky, such an area appears to be within the realm of possibility for a microrover.

However, even with the acceptance of "sunlight-only" operation, and with a 6ft² collector area, two major problems in this solar application yet exist. The first one is the matter of providing heat for the protection of the instrumentation on the microrover from the harsh martian temperatures and temperature changes (see Figure 2-2). Previous space missions have solved the thermal problem by including a radioisotope thermal unit (RHU) or multiple RHU's aboard the system.²⁸ This unit is a 1-watt (thermal) encapsulated PuO₂ source, available from the U.S. Department of Energy, and qualifies for space missions.²⁹ Either this type of unit, or an alternative auxiliary heating system, is a definite requirement.

The second major problem concerns the "global" dust storms, referred to in Section 2.2.3 of this report. These cyclonic dust storms have been observed to occur at an average frequency of every 3.3 days and span a 100-day period. Such dust storms not only greatly increase the opacity of the Martian atmosphere to the solar radiation, but can potentially deposit dust layers on the photovoltaic sensors, rendering them ineffective. If one accepts these dust-storm interruptions of the exploration program, at least some means will be required to periodically "clean" the surface of the PV sensors.

From this brief survey of solar energy systems, it appears that photovoltaic cells can possibly be used in the Mars mission, but with the limitations of: (1) "sunlight-only" operating periods, (2) approximately 6 ft² of effective collector area per microrover, (3) requiring an auxiliary heating unit to protect the instrumentation, and (4) requiring a means for periodic cleaning of the surface of the sensors. Limitations (1) and (3) could be removed by including an

²⁸Private communication dated October 25, 1993, to J. N. Anno, University of Cincinnati, from Richard B. Bennett, Advanced Power Systems Analysis, Jet Propulsion Laboratory, Pasadena, Ca.

²⁹Ernest W. Johnson, "Light-Weight Radioisotope Heater Unit Final Safety Analysis Report (LWRHU-FSAR)", Report MLM-3540, UC-744, Mound Laboratories, Miamisburg, Ohio, (October, 1988).

energy storage system, with the attendant penalties of increased direct cost and a large weight
mission.

3.5 Nuclear-Powered Systems

3.5.1 Radioisotope Thermoelectric Generators (RTG's)

As the name implies, RTG's (Radioisotope Thermoelectric Generators) operate by the principle of thermoelectricity. Basically, the generator is comprised of an encapsulated heat source (the radioactive isotope) to which are attached numerous thermocouples. The thermocouple simply consists of two wires of dissimilar metals, or dissimilar semiconductors, which are joined at a hot reservoir (the heat source) with respect to a colder junction (the "cold reservoir" of the Martian environment, in this case). An emf appears at the junction which has a magnitude determined by the particular pair of thermocouple material selected. The efficiency of producing electricity from the heat source in this manner is a strong function of the temperature difference between the hot and cold reservoirs. For reasonably large temperature differences, the output voltage from a single thermocouple is several tens of millivolts. Higher voltages are obtained by clustering the thermocouples, such a cluster being called a "thermopile".

The efficiency of this direct (heat to electricity) energy conversion (DEC) option is optimized by appropriate selection of the output load resistance with respect to the internal resistances of the thermocouple wires. (See Appendix B for the detailed design criteria.) Although efficiencies greater than 10 percent are theoretically achievable, typical efficiencies of practical space power RTG's used in the past have been in the range of 5-7 percent.

The lifetime of the power source is determined primarily by the half-life of the radioisotope fuel. Commonly used radioisotope sources are strontium fluoride ($^{90}\text{SrF}_2$) which has a half-life of approximately 28 years, and plutonium dioxide ($^{238}\text{PuO}_2$) which has a half-life of about 88 years. Thus usable lifetimes can readily exceed 10 years.

The simplicity of the direct energy conversion, the continuous power output, and the ruggedness and lifetime, make it an attractive power system for remote applications. The initial uses of these advantages included powering remote navigation and weather monitoring stations, e.g. weather stations fixed to buoys located in the oceans. Only a short time later (since 1961),

RTGs were brought into the U.S. space programs, followed by a generation SNAP[°]-designated designs for specific NASA and DoD missions. Practical systems with power outputs of up to approximately 1 kW have been developed for space use during the past three decades. Figure 3-1 shows the principal power level history in the development of RTGs for space power use.³⁰

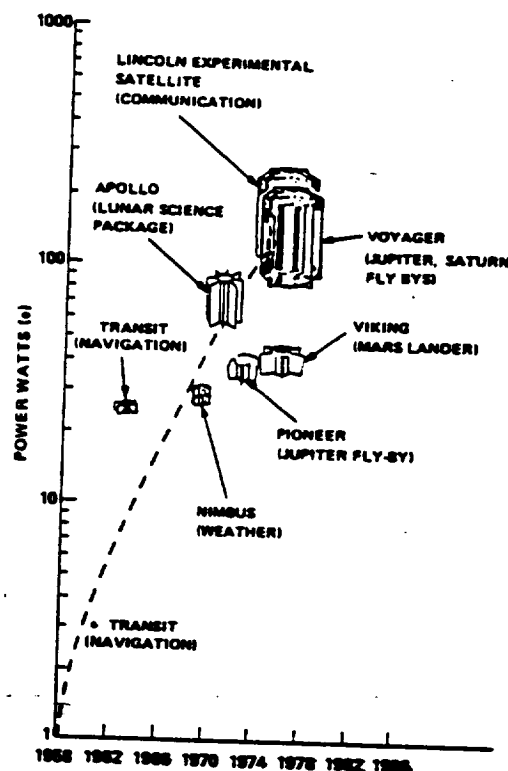


Figure 3-1 RTG power level history

Even with its relatively low efficiency, the simplicity of the RTG components results in a relatively high specific power for the "low power" range (up to about 500 watts electrical) of the order of 2-5 watts/kg.³⁰ When compared with the alternative power sources, the continuous power output over a relatively long lifetime stands out as one of the principal advantages.

[°]SNAP is an acronym for Systems for Nuclear Auxiliary Power.

³⁰Joseph A. Angelo, Jr. and David Buden, Space Nuclear Power (Orbit Book Company, inc., Malabar, Fla., 1985).

Because of its attractiveness for the Mars mission conditions, for the reasons stated above and others to be stated later, the RTG has been selected as the power source on this project. Section 4 of this report and its associated appendices present more detailed information on the RTG power system, and a general overview is presented for example, in the text Space Nuclear Power.³⁰

3.5.2 Thermionic Devices

The question was raised as to whether or not the RTG was the "best" choice for nuclear power sources in the 10-watt power range for the Mars mission. Two alternative nuclear power concepts were briefly studied; both of which appear to be impractical in this application.

The first system considered was a thermionic emission device. Thermionic emission is basically thermally enhanced quantum-mechanical "tunneling" of electrons interior to a surface through the surface potential barrier. Such tunneling is extremely temperature-dependant, requiring an emitter temperature of the order of 2000K. With a vacuum gap between the emitter surface and that of the collector, large electron current flow causes a space charge density which limits further flow. This space charge limitation can be relieved by developing a (cesium) plasma sheath between the electrodes. However, to do so requires a rather delicately balanced system providing a precise quantity of cesium vapor at the proper concentration. This complexity was deemed to be impractical to maintain during the entire mission, from launch to landing subject to two years of continuous functioning. Therefore, the thermionic device concept explored was that of the vacuum diode, accepting the space charge limitation to current emission.

The details of the conceptual design of a radioisotope fueled thermionics vacuum diode system are presented in Section A.1 of Appendix A. The results of the conceptual design produced a multi-cell power source, the unit cell of which is of coaxial cylindrical geometry. The central Tungsten electrode, inside of which is strontium-90 in the form of SrTiO₃ radioisotope fuel (melting point of 2180 K)*, is completely thermally isolated from the surroundings, and emits

*Strontium titanate is an earlier used strontium compound. Strontium fluoride is in current production, but has a melting point of only 1460K.

thermionically across a 1-mm vacuum gap to a cesiated-tungsten collector. Assume a 2-inch diameter emitter, 18 inches in length (total emitter surface area of $113 \text{ in}^2 = 0.0729 \text{ m}^2$). The space charge limited power output from the arrangement is 18.0 watt/m^2 , or hence 1.38 watts for the unit cell. An approximately 10 watt device therefore contains 7 cells. The required emitter temperature under these conditions is 2000 K.

Aside from the problems of maintaining a 1-mm gap at the required high temperatures and of maintaining a vacuum during the 3 year mission duration, however, probably the overwhelming problem is the heat losses from the emitter by thermal radiation. A simple black-body radiation calculation from a 2000 K surface yields heat fluxes far in excess of the thermionic power density, resulting in a thermal efficiency of less than 0.1 percent for the system. It is thus concluded that the thermionic vacuum diode concept is impractical in this application.

3.5.3 Charged-Particle Energy Convertors

A second nuclear-powered alternative to the RTG, that of a charged-particle direct energy conversion (DEC) system, was also studied. The details of the conceptual design of this system are presented in Section A.2 of Appendix A.

An alpha or beta-decay of a radioisotope leads to the emission of an initially energetic charged particle. A charged particle in motion is, indeed, direct electricity. If the isotope is distributed in a sufficiently thin layer, and appreciable fraction of all of the alpha (or beta) particles produced in the layer can escape from the surface with much of their initial energy and charge intact. These particles can be collected on an insulated electrode. The first few particles reaching the electrode will deposit their charge and dissipate their kinetic energy as heat. However, after a number of them have been collected, the insulated electrode, by virtue of its surplus of positive charge, will attain a high voltage with respect to the emitter layer. Subsequent charged particles "do work" against the electric field. They arrive at the electrode with their initial kinetic energy exhausted and deposit only their charge. The space between the electrodes is evacuated to approximately 10^{-5} torr to prevent energy loss by ionization of intervening gas and to permit high voltage buildup by serving as an electrical insulator. The voltage characteristic of the process is

E_0/Z_0 , the ratio of the initial kinetic energy of the particle (in electron volts) divided by its initial charge magnitude. Since E_0 is typically of the order of a million electron volts and the charge is 1 or 2 (beta or alpha particle), the characteristic voltage of the process is near a megavolt. (For the lower-energy beta particles, the characteristic voltage is about 0.1 megavolt.)

In effect, the above described system is analogous to a capacitor, with the charged-particles from radioactive decay creating the charge. The charge separation caused by the energetic charged particles driving their way to the insulated collector electrode is materialized by a flow of electrons through an external circuit (load). This electron flow through the external circuit is a source of direct electricity, produced without the use of a heat cycle. The high-voltage DC electricity thus produced can be stepped down to a more usable lower DC voltage.

Because of secondary electron production as alpha particles emerge from an emitter surface, a third electrode (a grid) is required to suppress these oppositely charged particles.³¹ This added complexity directed the conceptual design studies to a beta particle converter; with beta particles, a third electrode is unnecessary. Using parallel plane geometry, and a $^{90}\text{SrF}_2$ beta emitter (0.546 MeV and point beta energy)*, the requirements for a 10 watt system were examined. The results are summarized in Table 3-1.

³¹A. M. Plummer, W. J. Gallagher, R. G. Mathews and J. N. Anno, "The Alpha-Cell Direct-Conversion Generator", report NASA CR-54256, prepared for NASA under Contract NAS3 -2797 (November 30, 1964).

*The contributions from the decay of the ^{90}Y daughter were inadvertently omitted from this analysis. However, the conclusions remain as stated

Table 3-1 Summary of Design Characteristics of a 10 Watt(e) ^{90}Sr beta particle DEC system
 (Parallel Plate Geometry)

Item	Quantity or Value
Source Material	$^{90}\text{SrF}_2$
Electrical Power Output	10 watts (electrical)
Energy Conversion Efficiency	4.2%
Output Voltage	91 kV
Output Current	0.110 mA
Mass of SrF_2	732 g
Activity of Source Material	74.3 kCi
Thickness of SrF_2 Coating	8.54 μ
Required Vacuum Between Electrodes	10-5 torr

As seen from the summary in this table, aside from the problem of converting the 91 kV output to a more usable form, and from the problem of maintaining the required 10-5 torr vacuum during the 3 year mission, the required 20.3 m^2 surface area for the 10 watt (e) system makes it impractical as a potential power source for the Mars mission.

3.6 Summary and Conclusions

Based upon the rather brief survey of alternative energy sources for this space mission which has been presented in this section, a general comparison of the most applicable candidate in each category can be made. Table 3-2 presents both a summary and the comparison in the categories surveyed: fuel cells, batteries, solar devices, and nuclear power sources. The authors have ranked the "feasibility" of what appears to be the most promising candidate for this mission. It is seen from this summary and comparison that RTGs appear to best meet the mission requirements. Fuel cells, except for the extremely important drawback of weight, meet most of

the other requirements. However, their "excessive" mass (in the form of fuel) would seem to rank them below solar cells which, themselves, are plagued with disadvantages for this proposed mission.

On the basis stated above, RTGs have been selected as the power source for the design project. The next section of this report elaborates on the general characteristics of these Radioisotope Thermoelectric Generators.

Table 3-2 Comparison of Various Power Sources for the Robotic Survey of Mars Mission

Power Sources	Type	Advantages	Disadvantages	Acceptability for Mission	Desirability Ranking by Authors
Fuel Cells	Thermally nonregenerative	Simple, rugged, reliable, high efficiency, continuous power	Mass of fuel required for mission	not acceptable (too massive)	3
Battery	Rechargeable	Simple, rugged, reliable, high efficiency	Mass of system, limited lifetime requires recharging energy source (not continuous power)	not acceptable (too massive, limited lifetime)	4
Solar	Photovoltaic	External (free and "unlimited") energy source, simple, "clean"	Power output limited to "daylight" hours, subject to interference by dust storms, no power to heat instrumentation during darkness	Marginal acceptability	2
Nuclear (Radioisotope)	RTG	Simple, rugged, reliable, continuous power output, previous space use experience, relatively low mass, long lifetime	Relatively low efficiency, radiation safety required	Acceptable	1

4.0 Radioisotope Thermoelectric Generators and Design Considerations

4.1 Introduction

Based upon the results of the survey and comparisons of potential power sources for the stated Mars mission, as summarized in Section 3.0 of this report, the Radioisotope Thermoelectric Generator (RTG) was selected as the power source most appropriate for the mission.

Radioisotope thermoelectric generators have been used successfully in space applications since 1961. These applications range from navigational satellites to deep space interplanetary probes.³⁰ The current trend in RTG design is towards increasing power levels. The first RTGs had a power level of a few watts electric (SNAP-3B) while the latest ones have a few hundred watts electric (Galileo probe).³⁰ While most of the heat sources to date have been plutonium, strontium-90 has been used before (SNAP-17 and various AEC satellites). One of the most important concerns driving the actual design of RTG's has been the containment of the radioisotope in the event of an accident. At first, the goal was to have the fuel burn-up and disperse in the atmosphere, but this was changed to fuel containment during reentry. Now, the overriding concern is fuel containment both during reentry and upon impact. This leads to the addition of various protective layers which complicates the RTG design.³⁰ Overall, however RTGs have provided safe and reliable power for numerous space applications.

This section of the report and the associated Appendices present details of the RTG principles of operation and the radioisotope "fuel" selection, along with a brief review of existing RTG designs. The discussion of this section concludes with the need for a "mission specific" design, and a summary of the results of a literature search for design information on an RTG pertinent to this Mars mission.

4.2 Fundamental Principles of Thermoelectric Power Generation

RTG's use the radioisotope fuel as a heat source, with thermocouples attached to the (high temperature) surface of the heat source to convert the thermal energy directly to electrical energy. Since the flows of thermal and electrical energy (actually entropy) are coupled, as expressed through the Onsager relationship, the "imbalance" of such flows through two dissimilar materials leads to the development of an emf at the junction of the two materials. The two dissimilar materials are said to constitute a "thermocouple". The basic theory of such thermocouple operation, and thermoelectric power generators are summarized in Appendix B.

Using Lorentz's law that, for "good conductors", the electrical and thermal conductivity are approximately proportional as

$$\left(\frac{k}{\sigma T} \right) \approx 2.23 \times 10^{-8} \frac{(\text{volts})^2}{(\text{K})^2}$$

4-1

where k = thermal conductivity, σ = electrical conductivity, and T = absolute temperature; it is shown in Appendix B that an approximate upper limit to the output of a thermocouple composed of dissimilar metals is $83 \mu\text{V}/^\circ\text{F}$. For example, as metallic thermocouples operating between a heat source temperature of 200°F above ambient ("cold junction") temperatures could be expected to produce about 17 milliwatts. In practice, real metallic thermocouples yield about 0.10 to 0.5 of the approximate upper limit. A simplified circuit for thermoelectric power generation is shown in Figure 4-1. In this diagram, the heat source is the radioisotope fuel, and the "cold junction" is in the shell of the power source housing exposed to the Martian atmosphere, or the atmosphere, itself. A and B are the dissimilar materials comprising the thermocouple and R_L is the external load through which the electrical power is supplied.

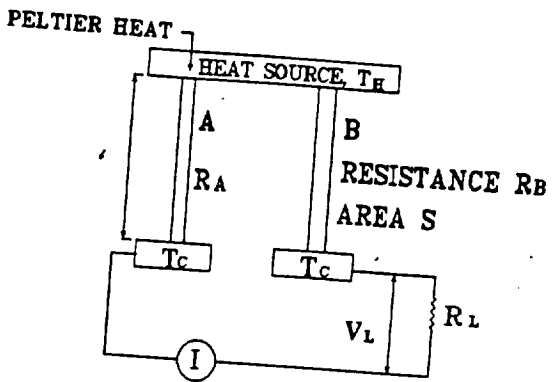


Figure 4-1 Simplified Thermoelectric Power Circuit (From Appendix B)

With the definitions:

$$m = \frac{R_L}{R_A + R_B} = \frac{\text{Load Resistance}}{\text{Internal Resistance}} \quad 4-2$$

$$Z = \frac{\alpha_{A,B}^2}{(\lambda_A + \lambda_B)(R_A + R_B)} = \text{Figure Of Merit} \quad 4-3$$

where $\alpha_{A,B}$ = Seebeck coefficient of the thermocouple pair and is defined as $(dE_{A,B}/dT)$, where $E_{A,B}$ = emf generated by the dissimilar materials and

$$\lambda = \frac{ks}{l}$$

$$\eta_c = 1 - \frac{T_c}{T_H} \quad 4-4$$

where S = cross sectional area of thermocouple material ("wire") and l = length of the thermocouple material ("wire").

The efficiency of the thermoelectric power generator can be shown to be (see Appendix B)

$$\eta = \frac{\eta_c m}{\frac{(m+1)^2}{Z T_H} - \frac{(T_H - T_C)}{Z T_H} + (m+1)} \quad 4-5$$

The efficiency has an optimum with respect to the resistance ratio, m;

$$m_{opt} = \sqrt{1 + Z \bar{T}}$$

$$\text{where } \bar{T} = \frac{T_H + T_C}{2} = \text{Average Temperature of the Thermocouple} \quad 4-6$$

Maximum achievable efficiencies are of the order of 10 - 15 percent.

Although not obvious from equations 4-5 and 4-6, the performance of the RTG is increased with increasing figure of merit, Z. For metallic thermocouples, Z is limited to approximately (see Appendix B)

$$(Z)_{Upper\ Limit} \approx \frac{1}{4\bar{T}} \quad 4-7$$

which significantly limits the RTG performance. However, by use of semi-conductor material, larger figures-of-merit are achievable. A part of the RTG design, therefore, is to select the appropriate thermocouple material for the power source for the conditions (design) of the microrovers to be employed under the Martian environment to achieve the mission. This consideration is factored into the design formulation presented in Section 5 of this report.

4.3 Selection of Radioisotope Fuel

For a space mission, a material with a small mass and a large thermal power density is desirable. Therefore, it follows that an ideal fuel source should have the following properties:

- large Q
- $f = 1.00$ (α or β emitter) (f = fraction of emitter particle captured within the fuel)
- long half-life relative to mission time
- small A_w (molecular mass)
- high radioisotope purity

Compromises, of course, must be made for the real world selection of the proper fuel based upon other criteria for the mission as discussed below.

4.3.1 Criteria and Selection Process

There are several fundamental criteria to be met:

1. Half life in the proper range - Considering the proposed mission, at least 3 Earth years, along with the desire for high specific power (see later discussion), the half-life range of interest is roughly between 10 and 100 years in order to provide a reasonably constant power output.
2. Health Physics (shielding and biological effects)
 - a. Shielding adds weight to the system - no gamma emitters
 - b. Biological effects suggest that no half-lives near the human generation time should be used (in conflict with criteria a.); therefore a compromise is required, but criterion a. still holds
3. High Power Density - minimum possible weight is desired
4. Availability - Isotope must be attainable through presently-available outlets.

In addition to the above fundamental criteria, several secondary criteria exist:

5. Large energy release per decay (large Q of decay reaction)
6. Stability of fuel
7. Strength of fuel
8. Cost: Although smaller mass systems reduce transport costs, the fuel cost cannot be "extremely high".

These eight criteria (stated above) narrow the over 1300 known radioisotopes to a small number of possibilities.

1. First, consider naturally occurring alpha-emitters. None of these radioactive species meet the half-life requirements of the mission.
2. Next, examine "common" radioisotopes (107 of them listed, for example, in reference 32).³² Half-life restrictions eliminate all but four of these common radioisotopes, and these four are eliminated by the two other criteria of "no gamma" and "large Q" [criteria (2)(a) and (3), respectively].
3. Then, consider "special" radioisotopes.

Considerations such as illustrated previously in criteria (1) and (2) reduce the >1300 radioisotopes to a select few of interest as power sources. These are listed in Table 4-1.³³ From this list of "special" radioisotopes, only four (⁹⁰Sr, ¹³⁷Cs, ²³⁸Pu, and ²⁴⁴Cm) meet the half-life criteria for the mars space mission. Of these four, ¹³⁷Cs is ruled out by its gamma-ray emission;

³²Richard Stephenson, Introduction to Nuclear Engineering, (McGraw-Hill Book company, inc., New York, 1954), Table II. "Common Radioisotopes".

³³Thomas J. Connolly, Foundations of Nuclear Engineering, (John Wiley & Sons, New York, 1978), Table 6.3.

^{244}Cm , while still a possibility, is unlikely because of its low availability and high cost. This leaves ^{90}Sr and ^{238}Pu as the most likely RTG sources. ^{90}Sr would be in the form of strontium fluoride (SrF_2), and ^{238}Pu would be in the form of plutonium dioxide (plutonia). The following two sections compare the characteristics of ^{90}Sr and ^{238}Pu power sources.

Table 4-1 Radioisotopes of Interest as Power Sources³³

Isotope	Half-Life	Specific Activity (Ci/g)	Specific Power (W/1g)	% Energy From			Source
				Alpha	Beta	Gamma	
Cobalt-60	5.26 yr	1133	17.4	-	3.6	96.4	Cobalt (α, γ)
Strontium-90	28.1 yr	141	0.95	-	100	neg	Fission Product
Cesium-137	30 yr	87	0.42	-	25.4	74.6	Fission Product
Cerium-144	284 day	3191	0.33	-	95.1	4.9	Fission Product
Promethium-147	2.62 yr	928	0.33	-	100	0	Fission Product
Thallium-170	130 day	9900	12.1	-	99.0	1.0	Thallium (α, γ)
Poisonous-210	138 day	4500	141	100	-	neg	Bismuth (α, γ)
Plutonium-236	86 yr	17.5	0.56	100	-	neg	^{237}Np (α, γ)
Cerium-342	163 day	3310	120	100	-	neg	Reactor spent fuel
Cerium-344	17.6 yr	83.3	2.8	100	-	neg	Reactor spent fuel

4.3.2 Power Density and Fuel Cost Estimates

Having narrowed the radioisotope fuel for this mission to either plutonia or strontium fluoride, it is next of interest to compare specific power outputs and costs.

Plutonia Fuel

^{238}Pu decays by alpha emission (5.49 MeV alpha particle) to ^{234}U , with a half-life of 87.7 years. (The ^{234}U daughter has a half-life of 2.45×10^5 years, and can be treated as stable for the purposes of the present mission). A very small fraction of the ^{238}Pu disintegrates by spontaneous fission, giving rise to neutrons having energies ranging from 1 to 10 MeV. Additionally relatively low energy photons are also emitted.^{34,35} A detailed description of the ^{238}Pu decay scheme accompanies Appendix D of this report.

Since the mission life of $t \sim 3$ Earth years is much less than the ^{238}Pu half-life of 87.7 years, the specific thermal power from a plutonia source is

$$P_s^{th} = \frac{\lambda N_A Q f e^{-\lambda t} p}{A_w} \approx \frac{\lambda N_A Q f}{A_w} \frac{kW}{kg} \quad 4-8$$

where: λ = decay constant of radioisotope, sec⁻¹

N_A = Avogadro's number

Q = energy release per decay, joule

f = fraction of energy captured within source

A_w = atomic weight of compound

p = purity of isotope in compound

³⁴E. Browne and R. B. Firestone, Table of Radioactive Isotopes, Lawrence Berkeley Laboratory, University of California (Wiley Interscience Publication).

³⁵E. Normand, L. A. Proud, J. L. Wert, D. L. Obery and T. L. Criswell, "Effect of Radiation from an RTG on the Installation, Personnel, and Electronics of a Launch System", Space Nuclear Power Systems, 1989. (Orbit Book Company, Malabar, Florida, 1992).

For $f = 1.00$ (alpha emitter) and $p = 0.8362$,²⁹

$$P_{\text{th}} = \frac{(0.8362)(0.6931)(6.023 \times 10^23)(8.947 \times 10^{-13})}{(2.769 \times 10^9)(270)} = 0.418 \frac{\text{Watt}}{\text{g PuO}_2} \cdot 4-9$$

This calculation is in excellent agreement with the 1.11 watts generated by 2.664 grams of the PuO_2 fuel used in the LWRHU system.²⁹ Plutonium 238 is currently available in two isotopic purities: 97% and 87%³⁶. The cost of the 97% enriched plutonia is \$7.50/mg, and the cost of the 87% enriched plutonia is \$3.60/mg (not including handling fees)³⁶. Table 4-2 shows the cost per curie, gram, and thermal watt for each enrichment.

Table 4-2 Costs of Plutonia

	97% Enriched PuO_2	87% enriched PuO_2
dollars/gram	\$7,500/gram	\$3,600/gram
dollars/curie	\$512.39/curie	\$274.22/curie
dollars/watt thermal	\$15,478.24/ W_{th}	\$8,284.59/ W_{th}

The fuel cost for each rover can be estimated by

$$\text{Cost} = \frac{P_c C}{n P_c} \quad 4-9$$

³⁶Telephone conversation of Robert Stubbers, Nuclear Engineering Program, University of Cincinnati, with Isotope Sales Department personnel, Oak Ridge National Laboratories, Oak Ridge, Tennessee (February, 1994).

where P_e = electrical power, C = cost per curie, η = generator efficiency, and P_c = thermal power per curie. Using this formula, the fuel cost of a 97% PuO₂ source for a 10 watt (electrical) RTG with 10% efficiency is estimated to be

$$\frac{(10 \text{ electrical watts}) (\$512.39/\text{curie})}{(0.10) (0.331 \text{ watts/curie})} = \$1,547,824.$$

The fuel cost of an 87% PuO₂ source is estimated to be

$$\frac{(10 \text{ watts electric}) (\$274.22/\text{curie})}{(0.10) (0.0331 \text{ watts/curie})} = \$828,459.$$

Neglecting size and weight considerations, the 87% enriched source is the least expensive form of plutonium. Another cost associated with using plutonia is shielding. Since the plutonium used in the plutonia is not 100% pure, there are usually other isotopes in the mixture, some of which are gamma emitters. These isotopes have to be shielded and the cost and additional weight for this shielding will increase the overall cost of using plutonia.

Strontium Fluoride Fuel

⁹⁰Sr decays by beta emission (0.546 MeV endpoint beta energy) with a half-life of 28.5 years, to ⁹⁰Y. In turn, the ⁹⁰Y decays by beta emission (2.282 MeV endpoint beta energy) with a half-life of only 2.67 days, to stable ⁹⁰Zr.³⁴ Secular equilibrium is established in the ⁹⁰Sr-⁹⁰Y complete in 2 to 3 weeks, so that for use as an RTG fuel, the energy level from both beta decays is available as sensible heat; and the "effective" half-life is that of the ⁹⁰Sr. Since the average energy of the emitted beta particles is approximately 1/3 of the endpoint energy, for the purposes of RTG design, $(0.546 + 2.82)/3 = 0.943$ MeV would be taken as the available energy per decay of ⁹⁰Sr (i.e. $Q = 1.51 \times 10^{-13}$ joule). A detailed description of the ⁹⁰Sr - ⁹⁰Y decay scheme accompanies Appendix D of this report.

Again, since the half-life of ^{90}Sr is much longer than the mission life, the entire right hand side of equation 4-8 can be used to calculate the specific thermal power from a $^{90}\text{SrF}_2$ source. With $f = 1.00$ and an isotopic purity of 55 percent ($p = 0.55$)³⁷, the specific thermal power is

$$P_{th} = \frac{(0.55) (0.6931) (6.023 \times 10^{23}) (1.51 \times 10^{-13})}{(0.8869 \times 10^9) (126)} = 0.310 \frac{\text{Watts}}{\text{gm of SrF}_2}$$

Early experiments used strontium-90 in the form of strontium titanate (SrTiO_3) as a thermoelectric heat source. However, strontium fluoride, a cheaper compound, has been used in recent years as a replacement for strontium titanate.³⁷ Table 4-3 shows the price of strontium fluoride per gram, curie, and thermal watt.

Table 4-3 Cost of Strontium Fluoride

	Strontium Fluoride
dollars/gram	\$164.86/gram
dollars/curie	\$1.60/curie
dollars/thermal watt	\$495.36/W _{th}

The fuel cost for a 10 watt (electric), 10 % efficient strontium fluoride source is estimated from equation 4-9 to be \$53,810, or about 1/15th the cost of the 87% enriched plutonium fuel.

³⁷Telephone Conversation of Robert Stubbers, Nuclear Engineering Program, University of Cincinnati, with Grant Culley, Hanford Nuclear Site (February, 1994).

4.3.3 Radiological Safety

At the request of this design team, a discussion of the radiological safety aspects of ^{90}Sr and ^{238}Pu radioisotope fuels for RTG's was prepared by Mr. Shoaib Usman, a doctoral student in the Nuclear Engineering Program at the University of Cincinnati. His complete discussion is presented in Appendix D of this report, and summarized in this section. Summary comparisons of the potential dose received in an accident from ^{90}Sr and ^{238}Pu sources are extracted from Appendix D, as follows.

For both inhalation and ingestion pathways, the Annual Limit of Intake (ALI) for all the important isotopes have been computed⁽¹⁰⁾ by the International Commission on Radiological Protection (ICRP). This limit suggests that the maximum intake of a radionuclide (in Bq.) in a specific chemical and physical form (i.e. solubility class) without exceeding the allowable effective dose, i.e., 5 rem for the whole body and 50 rem for any specific organ.*

The dosimetric comparison of the two RTG fuels is based on the ALI's. It is appropriate for this study to compare the respective ALI's (for both pathways i.e. inhalation and ingestion) of the two isotopes in question to estimate their relative radiological impact. Using these ALI's, the limiting weight of the radionuclide in question (^{238}Pu for PuO_2 fuel and ^{90}Sr for SrF_2 fuel) and hence the maximum allowable mass intake of the fuel can be determined (i.e. mass of PuO_2 and SrF_2) for each pathway. These numbers along with the respective specific power will provide the dose per unit power produced for the case when as a result of an accident all the fuel was inhaled or ingested by individuals.

These estimates are highly conservative because not every gram of fuel will realistically be taken up by individuals. For the case of inhalation, dose is calculated assuming a particle size of 1 μm diameter. This again is very conservative and the average actual size of the particles would be much larger. The fuel particle sizes of PuO_2 RTG are reported to be 50-250 μm diameter⁽¹²⁾.

*See Footnotes associated with Appendix D for the references presented in this material for the remainder of section 4.3.3, which has been extracted from Appendix D.

These larger particles will be filtered out during inhalation and the actual dose would be significantly lower. With these conservative approximations, the following comparison is possible (indicated in the tables which follow);

Comparison of Inhalation Pathway.

	P_u	$\frac{D}{r}$
01 compound.	P_{u_2}	$\frac{D_f}{r_2}$
02 specific power watt/gm fuel.	0.418	0.304
03 solubility class.	y	d
04 f1+ fraction of activity absorbed through skin.	10^{-4}	0.3
05 all 9b. 0 w b 9b / 0.05 v.	$6.0 \cdot 2$	$7.0 \cdot 5$
06 critical organ.	b one surface.	b one surface.
07 all 9b. 0 c. 9b / 0.5 v.	$6.0 \cdot 2$	$8.0 \cdot 5$
08 limiting mass of the isotope gm / 0.5 v.	$9.50 \cdot -10$	$1.53 \cdot -7$
09 maximum allowable useful mass intake gm / 0.5 v.	$7.00 \cdot -10$	$5.90 \cdot -6$
10 dose per Ugm of fuel intake $\frac{9a}{v} / \text{Ugm}$.	716.23	8.45
11 dose per unit power $\frac{9a}{v} / \text{watt}$.	1713.5	27.79

Comparison of Ingestion Pathway.

	P_u	s_r
01 compound.	P_{u_1}	s_{r_1}
02 specific power w/ gm fuel.	0.418	0.304
03 solubility loss.	y	d
04 fraction of activity absorbed through gut	10^{-4}	0.3
05 all 9b 0 w b 9b / 0.05 v.	$3.0 \cdot 6$	$1.0 \cdot 6$
06 critical organ.	b one surface.	b one surface.
07 all 9b 0 c o - 9b / 0.5 v.	$3.0 \cdot 6$	$1.0 \cdot 6$
08 limiting mass of the isotope gm / 0.5 v.	$4.74 \cdot 6$	$1.90 \cdot 7$
09 maximum allowable fuel mass intake gm / 0.5 v.	$3.50 \cdot 6$	$7.40 \cdot 6$
10 dose per Ugm of fuel intake $\frac{98}{v} / \text{Ugm}$	0.143	6.67
11 dose per unit power $\frac{98}{v} / \text{w att}$	0.342	21.94

The summary and conclusions of the radiological safety analysis (Appendix D) are as follows.

Three operational periods with the potential for human exposure were identified for the RTG. External exposure is most significant for transportation and launch pad periods. Launch pad period also has a potential for exposure to the instrumentation and electronics. Neutrons and photons from a ^{238}Pu RTG can cause a significant dose rate while the ^{90}Sr RTG will pose external dose problem only due to the bremsstrahlung. This external dose from a ^{90}Sr RTG is likely to be significantly lower than that from a ^{238}Pu RTG.

Fabrication period is the most plausible period for internal exposure to the workers, both under normal operation and under accidents. Launch and re-entry periods were identified as the most significant potential for both public and workers internal exposure under accident scenarios.

The internal dosimetry analysis requires extensive data on the various parameters involved in pathway analysis. However, this initial comparison based on very conservative assumptions indicated that the inhalation per unit mass of fuel from ^{238}Pu is 2 orders of magnitude higher than the dose per unit mass intake of ^{90}Sr . This makes ^{238}Pu much more serious concern for internal dosimetry via inhalation. Results were found to be quite reverse for dose due to ingestion where the dose from a unit mass intake of ^{90}Sr was an order of magnitude higher than that from ^{238}Pu .

However, it should be kept in mind that extensive monitoring and a greater degree of control is possible for ingestion as opposed to inhalation. Therefore, the actual potential hazard from ^{238}Pu RTG is considered to be much more than that from a ^{90}Sr RTG.

It was also pointed out that both the chemical and physical form are likely to change during various fabrication stages and in a post accident pathway. This aspect of pathway analysis was identified as important but could not be accounted for in this preliminary study. A parallel set of detailed safety analysis is recommended for each one of the RTG fuel candidates for a precise comparison.

4.3.4 Conclusions and Fuel Choice

While the plutonia has a higher power density than the strontium fluoride, the economic considerations demonstrate that using the plutonia will cost approximately a factor of ten more in fuel costs. The desire for inexpensive rovers led to the choice of strontium in the form of strontium fluoride as the isotope for this particular mission. This choice is reinforced by the radiological safety analysis, which indicated that in the event of an accident, the potential inhalation dose from the SrF_2 source is much less than that from PuO_2 .

Although a more detailed analysis of the fuel choice will ultimately be required, based upon the evidence in this report, the power source design, as presented in Section 5 of this report, is based upon the use of strontium fluoride as the RTG fuel.

4.4 Existing RTG Designs

As indicated in the introduction to this section of the report, RTG's have been in use for over three decades, with the first isotopic power generator being produced in 1959. Further, with the requirements imposed by the space program, both power level (see Figure 3-1) and the sophistication of the designs have increased. However, the fundamentals of the RTG have retained their simplicity. The basic elements of the RTG design are shown in Figure 4-2.³⁸

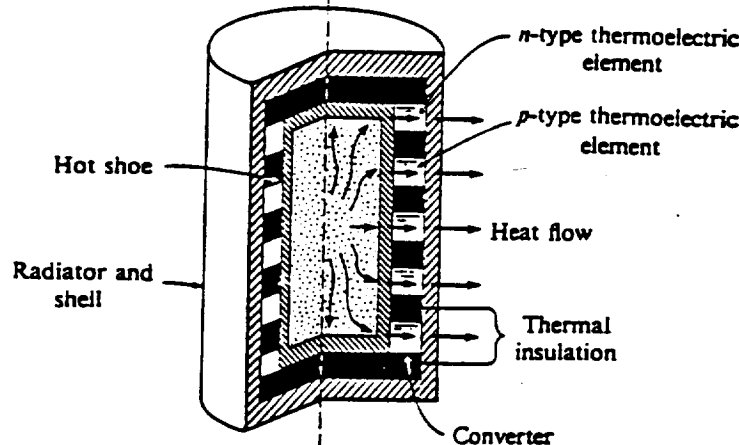


Figure 4-2 Thermoelectric isotopic power generator

In its simplicity, the design of an RTG consists of six basic elements:

1. Selection of Fuel
2. Selection of Thermoelectric Element
3. Encapsulation of System
4. Safety of Design
5. Waste Heat Removal
6. Economics

How these elements are combined is determined by the purpose (mission) of the RTG under consideration. Examples of previous design are presented in this portion of Section 4.0.

³⁸ Arthur R. Foster and Robert L. Wright, Jr., Basic Nuclear Engineering, Third Edition (Allyn and Bacon, inc., Boston, Mass., 1977), p. 175.

4.4.1 Very Low Power, Long Lifetime RTG's (The Powerstick)

To satisfy the need for a small, relatively lightweight, and reliable power source for micro-spacecraft and microrovers, the Jet Propulsion Laboratory has developed a Powerstick RTG unit.²⁸ The Powerstick is a miniature power source consisting of a Radioisotope Heater Unit (RHU), a thermoelectric thermopile, and a bank of small LiTiS₂ batteries, as shown in the drawing of Figure 4-3.²⁸ The RHU is a 1-watt plutonia (PuO₂) thermal source available from the Department of Energy, and qualified for earth launch and space applications.²⁹ The thermoelectric system using this heat source produces 14 volts at 3 milliamperes current flow, with only a 1 volt degradation after 10 years of operation. The 40+ milliwatts of continuous electric power is used to trickle-charge the lithium batteries, providing peak power as needed. All Powerstick components are currently available, off-the-shelf items, with proven reliability. The total mass of the Powerstick is 380 grams. The "waste heat" from the RHU is used to maintain the internal temperature of the power unit within the operating limits of the components, under the harsh environments of space applications.

POWERSTICK

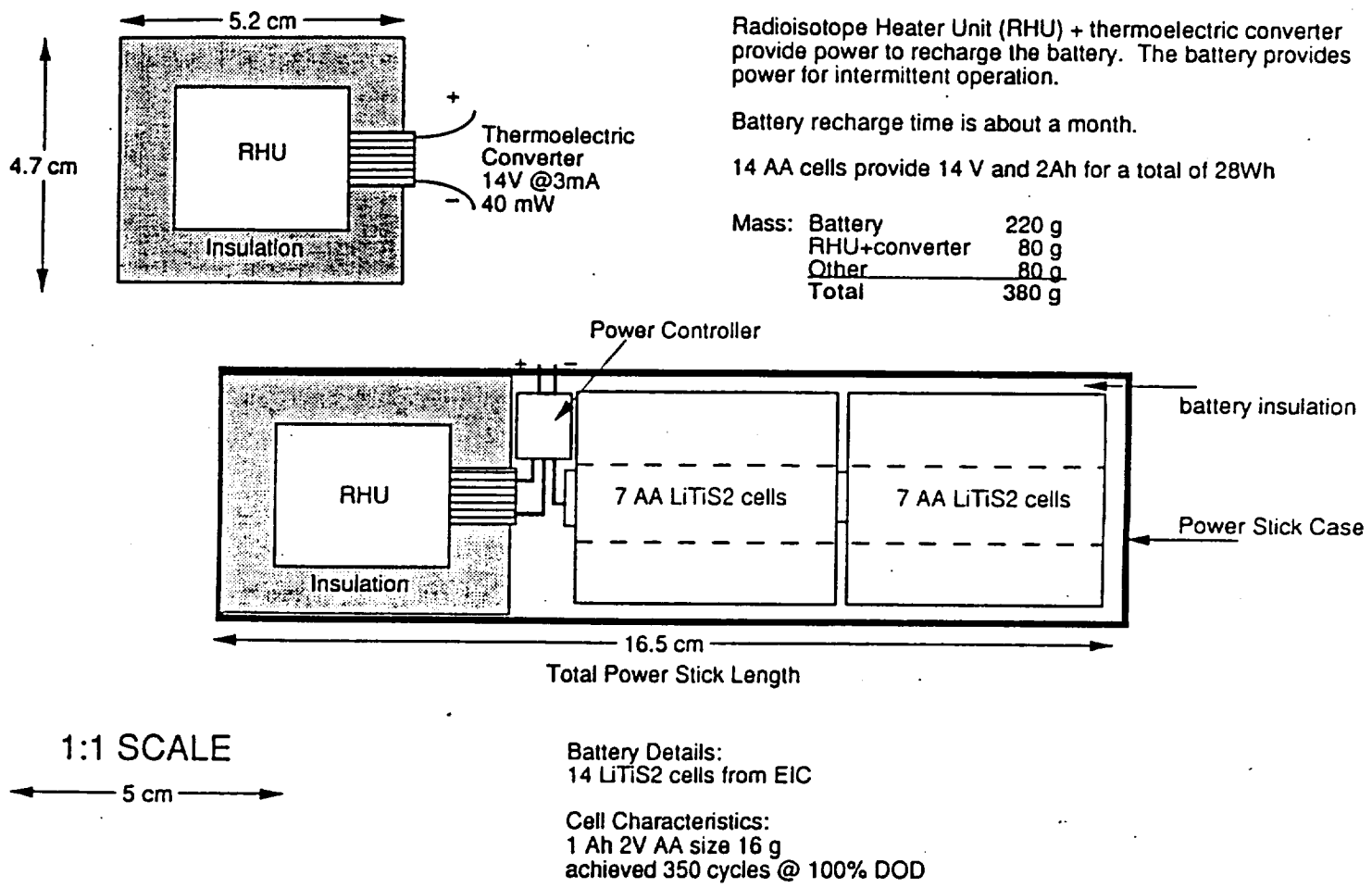


Figure 4-3 Drawing of the JPL Powerstick

4.4.2 Relatively High Power

A sampling of the relatively high power systems (in comparison with multiwatt type systems such as described above) used for space missions is given in Table 4-4.³⁰ The missions have varied from the Transit missions (navigational satellites) to the more recent multi-hundred watt (MHW) systems for communication satellites and the GPHS-RTG, developed for the Galileo project (Jupiter exploration) and other NASA and DoD missions. It can be seen from this tabulation that power outputs have ranged over two orders of magnitude (2.7 W_e to 290 W_e), power source mass has ranged over a factor of about 20 (2.1 kg to 54.4 kg), and thermoelectric material selection has varied, while fuel choices and efficiency have remained essentially unchanged.

Table 4-4 High Power Systems Used for Space Missions

Mission	SNAP-3B	SNAP-9A	SNAP-19	SNAP-27	Transit-RTG	MHW	GPHS-RTG
Mission	Transit	Transit	Nimbus Pioneer Viking	Apollo	Transit	LES 8/9 Voyager	Galileo
Fuel form	Pu metal	Pu metal	PuO ₂ -Mo cermet	PuO ₂ microspheres	PuO ₂ -Mo cermet	Pressed PuO ₂	Pressed PuO ₂
Thermoelectric material	PbTe	PbTe	PbTe-TAGS	PbSnTe	PbTe	SiGe	SiGe
BOL ¹ output power (W _e)	2.7	26.8	28-43	63.5	36.8	150	290
Mass (kg)	2.1	12.2	13.6	30.8 ²	13.5	38.5	54.4
Specific power (W _e /kg)	1.3	2.2	2.1-3.0	3.2 ³	2.6	4.2	5.2
Conversion efficiency (%)	5.1	5.1	4.5-6.2	5.0	4.2	6.6	6.6
BOL fuel inventory (W _{th})	52	565	645	1480	850	2400	~4400
Fuel quantity (curies)	1800	17,000	34,400 - 80,000	44,500	25,500	7.7 × 10 ⁴	1.3 × 10 ⁵

¹BOL = beginning of life

²without cask

³includes 11.1-kg cask

4.5 The Need for a Mission Specific Design

As seen from the preceding Table 4-4, and from Figure 3-1, the trend in the past has been for "bigger and better" RTGs. However, within the recent decade, the "ground rules" have changed. The current trend, imposed primarily by budget considerations, is now toward "smaller and cheaper" space application vehicles, and hence the associated power source (RTG in the present case). Examples of budgetary limitations and the drive for a number of relatively small units, compared with the history of a few large units, is shown by the following literature excerpts.

Concerning the Mars Environmental Survey (MESUR) Pathfinder and its Microrover Flight Experiment (MFEX): "MESUR Pathfinder development is cost-capped at \$150 million (in FY92 dollars). The MFEX, which is not included in that amount, is cost-capped at \$25 million (in real-year dollars)...NASA has sought to make MFEX a "better, faster, cheaper program"³⁹

"Developing a swarm of landers is a huge technical challenge, however, and money is tight. NASA will test a new, low-cost exploratory scheme with a single lander called "pathfinder"...NASA expects to build the initial lander for \$150 million, and its microrovers for an additional \$25 million - bargain basement prices for space exploration."⁴⁰

Concerning the Discovery Program: "as summarized here, this next phase would involve using the information obtained by survey-style missions to identify regions of the planet of unusually high scientific interest, and then developing a series of focused, low-cost missions aimed at answering specific questions relating to these regions."⁴¹

³⁹Donna Shirley Pivirotto, "Finding the Path to a Better Mars Rover", Aerospace America (September, 1993), pp. 12.

⁴⁰William J. Cook, Science and Society, "The Invasion of Mars", U. S. News and World Report (August 23, 1993), p. 59.

⁴¹David A. Paige, University of California, Los Angeles, "The Mars Polar Pathfinder", Concept #83, Discovery Program Workshop, (September, 1992).

Concerning the design philosophy for the microrover: "Develop a Micro-Rover consistent with MESUR mission cost, schedule, and risk constraints, (per the MESUR project implementation plan)."⁴²

Thus the trend is for the development of small, cheap systems, with weight of course going hand-in-hand with the development. In the past, small mass, in itself, has been a dominant design criteria. With the new ground rules, cost looms even more significant. (In this report, the use of SrF₂ as the radioisotope fuel appears, at least on the surface, to be one of the steps toward a low expense RTG, based upon the information presented in this report.) With this new design philosophy, the earlier designs of the "bigger and better" RTG are no longer completely applicable. Therefore, the undertaking of a new mission-specific design is required.

4.6 Literature Search for Mission-Specific Design Aids

As a step in approaching the mission-specific design under the new ground rules, a search of the literature was performed, and is summarized here as three distinct sub-sections. First, an annotated bibliography is presented on general orientation and background of thermoelectric generators. This study was performed only in the present project. Second, a listing of the primary sources found useful to the mission-specific design is presented and, finally a brief listing of secondary sources is given. Specific use of most of these various information sources is referred throughout this report, in order of appearance. Other general references, not listed below, on "non-design" items (e.g. astrophysical characteristics of Mars) are also identified separately in the text of this report.

⁴²W. E. Layman and J. A. Matijevic, "Micro-rover Technical Baseline: Highlights and Design Philosophy", JPL Interoffice Memorandum (June 24, 1993).

4.6.1 Annotated Bibliography of General Information Sources

1. Angelo, J., Jr., and D. Buden. 1985. Space Nuclear Power. Malabar, Florida: Orbit Book Company. pp. 88, 92, 93, 133, 137. This book contains most everything which could be needed in considering a nuclear powered thermoelectric generator. From the basics of radioactivity to actual derivation of thermoelectrical efficiency. Although most of the book is devoted to nuclear reactors, enough material is presented about direct energy conversion to gain a fairly thorough notion of it's principles.
2. Arnas, O., and D. Miller. 1978. Of an Irreversible Thermodynamic Analysis of Thermoelectric Devices. Proceedings of the Second International Conference on Thermoelectric Energy Conversion. (pp. 36-40). Arlington, Texas: The Institute of Electrical and Electronics Engineers. In order to develop a useful relationship for calculating the efficiency of the thermoelectric generator, several principles and relationships can be coupled together. This results in an equation which links the efficiency of the generator to the figure of merit of it's thermocouple materials and the temperature at which it operates.
3. Cobble, M. 1980. Optimal Thermoelectric Efficiency. Proceedings of the Third International Conference on Thermoelectric Conversion. (pp. 78-81). Arlington, Texas: The Institute of Electrical and Electronics Engineers. The power generated by a thermoelectric generator is dependant on the input heat. Accordingly, the efficiency of the device should be as high as possible, in order to minimize the heat which will be left over at the end of the cycle. A detailed understanding of the efficiency is therefore essential to the design of a specific thermoelectric generator.

4. Hager, B., and W. Chang, and A. Feild. 1993. Effects of Payload Heat Flux on Space Radiator Area. Journal of Spacecraft and Rockets 30:255-6. Enormous savings in the area necessary for a waste heat radiator can be realized through temperature management. By minimizing the temperature drops within the system, the area of the radiator can be reduced. This is achieved by operating the radiator at a higher temperature. Thus the weight previously used for this can be diverted to other needs.
5. Harpster, J. 1980. Improved Spacecraft Heat Rejection With Practical Thermoelectric Materials. Proceedings of the Third International Conference on Thermoelectric Energy Conversion. (pp. 126-129). Arlington, Texas: The Institute of Electrical and Electronics Engineers. Another use of thermoelectric generators is in heat rejection from other systems. Since thermoelectric generators are very dependable, they are desired for different systems. By placing a thermoelectric device between two components of a system, a more uniform temperature differential or change was observed. This has potential in improving the control of heat transfer throughout the system.
6. Incropera, F., and D. DeWitt. 1990. Introduction to Heat Transfer (2nd ed.). West Lafayette, Indiana: John Wiley & Sons. This extremely useful book contains most of the equations and relationships which are necessary to derive the rate of heat transfer between the source and whatever heat "sink" is chosen. For radiative heat transfer the primary mechanism is found through the Stephen-Boltzman law. For convective heat transfer Newtons law of cooling is used.

7. Jaklovszky, J., and G. Aldica. 1978. Measurement of Seebeck Coefficient in the Temperature Range of 300-530 K. Proceedings of the Second International Conference on Thermoelectric Energy Conversion. (pp. 104-106). Arlington, Texas: The Institute of Electrical and Electronics Engineers. Determining the Seebeck coefficient in the operating temperature range of a thermoelectric generator is important. Using a simulator to examine the dependence of the Seebeck coefficient to the operating temperature a curve for various temperatures can be found for a given material. This can be used in selecting the proper material to use for the thermocouples.
8. King, M., and R. Simms. 1967. Systems Analysis Of Radioisotope Thermoelectric Generators. Advances in Energy Conversion Engineering. 1967 Intersociety Energy Conversion Engineering Conference. (pp. 189-196). Miami Beach, Florida: The American Society of Mechanical Engineers. Through the use of computer simulation, a new thermoelectric generator can be optimized for a given set of operating parameters. This allows for a cheaper and more effective way to design new thermoelectric generators for custom use.
9. Landecker, K. 1978. The Application of the "Vortex" Cooling Tube to the Cooling of Thermojunctions. Proceedings of the Second International Conference on Thermoelectric Energy Conversion. (pp. 134-136). Arlington, Texas: The Institute of Electrical and Electronics Engineers. Through the use of a pressurized fluid (like air) in a cooling "vortex" excellent heat transfer from the hot junction of the thermoelectric generator can be achieved. The physical design of the vortex is shown schematically. This could be used in transferring the heat to the electronics package.

10. Mason, T. 1991. Comment "On the Use of Oxides for Thermoelectric Refrigeration". Materials Science and Engineering B10:257-260. Through a review of a previous article on thermoelectric refrigeration, it is shown that a relationship exists between the Seebeck coefficient and the electrical conductivity of a given material. This is helpful in the selection of a material for use in the thermocouple, given the electrical conductivity since the Seebeck coefficient cannot be directly measured.
11. Raag, V. 1980. Power Output Dependence on the Heat Input. Proceedings of the Third International Conference on Thermoelectric Energy Conversion. (pp. 75-77). Arlington, Texas: The Institute of Electrical and Electronics Engineers. The disposal of waste heat is an important consideration in the design of a thermoelectric generator. Since this is so, the amount of heat input must be minimized in order to reduce the amount of heat which must be disposed. It turns out that the power output is dependant on heat input so a reasonable balance must be found between them.
12. Rocklin, S. 1967. Design and Development of a High Efficiency Cascaded and Segmented Thermoelectric Module. 1967 Intersociety Energy Conversion Engineering Conference. (pp. 207-219). Miami Beach, Florida: The American Society of Mechanical Engineers. One way to improve the efficiency is to choose thermocouple's which when arranged properly will be reasonably efficient. Through a new technique of joining the thermocouple material, this higher efficiency can be realized.
13. Stapfer, G. 1980. The Thermoelectric Technology Program at the Jet Propulsion Laboratory. Proceedings of the Third International Conference on Thermoelectric Energy Conversion. (pp. 70-74). Arlington, Texas: The Institute of Electrical and Electronics Engineers. Since a thermocouple's material plays such an important role in the efficiency of a thermoelectric generator, it is important to obtain quantitative answers. This was done by the Jet Propulsion Laboratory and provides some information on both selenide and silicon germanium materials.

14. Wartanowicz, T., and D. Szczesniewska. 1980. Optimization of Microgenerator Design. Proceedings of the Third International Conference on Thermoelectric Energy Conversion. (pp. 210-216). Arlington, Texas: The Institute of Electrical and Electronics Engineers. Future developments in thermoelectric generators lie in either miniaturization of the devices or making them larger and more powerful. Through the use of a mathematical model, optimized construction with a varying heat source can be found.

4.6.2 Primary Literature Sources Useful to the Design

15. Gregory, D.P. Fuel Cells. London: Mills and Boon Limited, 1972, p. 1,23
16. Sutton, George W., ed. Inter-University Electronics Series, Vol.3: Direct Energy Conversion. San Francisco: McGraw-Hill Book Company, 1966, p. 41.
17. Brown, Theodore L. and LeMay, H. Eugene. Chemistry: The Central Science. New Jersey: Prentice-Hall, inc., 1988, p. 977.
18. Sutton, George W., ed. Inter-University Electronics Series, Vol.3: Direct Energy Conversion. San Francisco: McGraw-Hill Book Company, 1966, p. 65.
19. Brockis, J. and Srinivansan, S. Fuel Cells: Their Electrochemistry. New York: McGraw-Hill Book Company, 1969, pp. 599-600.
20. Anno, J.N. A Brief Summary and Review of Nuclear Thermionic Power for Lunar Applications, Based upon an original lecture series. Cincinnati, Ohio: Nuclear Engineering Program, University of Cincinnati, 1993.

21. Anno, J.N. Charged Particle Direct Energy Converters in a Lunar Application, Based upon an original lecture series. Cincinnati, Ohio: Nuclear Engineering Program, University of Cincinnati, 1993.
22. Mosely, H.G.J., and Harling, J. The Attainment of High Potentials by the Use of Radium. Proc. Roy. Soc., 88, 1913. pp. 471-476.
23. Anno, J.N., Stubbers, R., and Winiarski, R. Power Sources for a Robotic Survey of Mars. Cincinnati, Ohio: Nuclear Engineering Program, University of Cincinnati, 1993.
24. Reynolds, Kim, "JPL ROCKY IV" Road & Track, April, 1993.
25. Morrow, G., The 1985 Goddard Space Flight Center Battery Workshop. NASA, Scientific and Technical Information Branch. 1985.
26. Connolly, Thomas J. Foundations of Nuclear Engineering. John Wiley and Sons, New York, 1978. Table 6.3.
27. Schock, A., Or, C.T., and Skrabek, E.A. Thermal and Electrical Analysis of Mars Rover RTG, and Performance Comparison of Alternative Design Options. in Space Nuclear Power Systems, Malabar, Fl: Orbit Book Company Inc., 1989. p. 189.
28. EG&G Mound Applied Technologies. Light-Weight Radioisotope Heater Unit Final Safety Analysis Report (LWRHU FSAR). U.S. Department of Energy: MLM-3540; Nov. 30, 1988. P. 86
29. Incropera, Frank P., and DeWitt, David P. Introduction to Heat Transfer. John Wiley and Sons, New York, 1990. p. 9, 98, 115, 493, 497, 500, 509.

4.6.3 Secondary Literature Sources for this Project

30. Egli, Paul H. Thermoelectricity. John Wiley & Sons, New York, 1960.
31. Luikov, A.V. Analytical Heat Diffusion Theory. Academic Press, New York, 1968.
32. Cadoff, Irving B., and Miller, Edward. Thermoelectric Materials and Devices. Reinhold Publishing Co., New York, 1960.
33. Heikes, Robert R., and Ure, Roland W. Thermoelectricity: Science and Technology. Interscience Publishers, 1961.
34. El-Genk, Mohamed S., and Hoover, Mak D. Symposium on Space Nuclear Power Systems 1986, Vol. 5. Orbit Book Company Inc. Malabar, Fl, 1987.
35. El-Genk, Mohamed S., and Hoover, Mak D. Symposium on Space Nuclear Power Systems 1989, Vol. 10. Orbit Book Company Inc. Malabar, Fl, 1992.

5.0 Radioisotope Thermoelectric Generator Design

5.1 General Considerations

In actual design of a RTG there are several design criteria among which compromises must be made. These criteria include: ruggedness, reliability, cost, practicality, weight/size, lifetime of use, radiological safety, efficiency, availability, ability to withstand extreme environments.

5.2 Selection of Optimum Thermoelectric Material

In order to optimize the thermoelectric generator, the efficiency of the thermocouples must be optimized. The most efficient thermocouples to date have used semiconductors, so this report will be limited to semiconductor thermocouples. The semiconductor materials that will be considered are the following.³⁰

Bismuth-Tellurides

Bi_2Te_3 -75Sb₂Te₃ (p-type)

Bi_2Te_3 -25Sb₂Te₃ (n-type)

Lead-Tellurides

4N-PbTe (n-type)

3N-PbTe (n-type)

3P-PbTe (p-type)

2P-PbTe (p-type)

Silicon-Germanium

SiGe (n-type)

SiGe (p-type).

To analyze the thermocouples requires a knowledge of the following: hot and cold reservoir temperatures, the Seebeck coefficient (or figure-of-merit) as a function of temperature, the electrical resistivity, and the thermal conductivity of each semiconductor material. The thermocouple analysis must be performed for every combination of semiconductor material and temperature range. A computer code is necessary to perform this task in a timely manner.

Because the temperature of the hot and cold leg junctions (and therefore the thermal efficiency) are dependant on the geometry of the thermocouple, the optimum leg geometry must be found. This can be expressed in terms of α_{opt} (the area of the n leg as a fraction of total area of the n and p legs), which is given by:⁴³

$$\alpha_{opt} = [1 + \sqrt{\left(\frac{k_n}{k_p}\right)\left(\frac{\rho_p}{\rho_n}\right)}]^{-1} \quad 5-1$$

where k_n is the thermal conductivity of the n-type semiconductor, k_p is the thermal conductivity of the p-type semiconductor, ρ_n is the electrical conductivity of the n-type semiconductor, and ρ_p is the electrical conductivity of the p-type semiconductor.

From the figure-of-merit, the optimum output voltage, V_{opt} , can be found using the following equations:⁴³

$$V_{opt} = SAT[1 + \frac{1}{\sqrt{1 + ZT}}]^{-1} \quad 5-3$$

$$\begin{aligned} S &= \text{Seebeck Coefficient} \\ AT &= T_{hot} - T_{cold} \end{aligned} \quad 5-4$$

$$Z = \text{Figure- of- merit} = \frac{S^2}{(\sqrt{k_n\rho_n} + \sqrt{k_p\rho_p})^2} \quad 5-5$$

$$\bar{T} = \frac{S_h T_h + S_c T_c}{2S}. \quad 5-6$$

⁴³Schock, A., Or, C.T., and Skrabek, E. A. Thermal and Electrical Analysis of Mars Rover RTG, and Performance Comparison of Alternative Design Options in Space Nuclear Power Systems, Malabar, Fl: Orbit Book Company inc., 1989. p. 189.

The maximum efficiency of a thermocouple is given by:⁴³

$$\eta' = \frac{(S_{\Delta T}/V - 1)^{-1}}{[\frac{\sqrt{k_n \rho_n} + \sqrt{k_p \rho_p}}{S_{\Delta T} - V_{opt}}]^2 \Delta T + \frac{S_h T_h + S_c T_c + S_{\Delta T}}{2(S_{\Delta T} - V_{opt})} - \frac{1}{2}}. \quad 5-7$$

The optimum efficiency is obtained by putting these equations into a computer (with libraries of Z, k, and ρ) and solving for the efficiency of each thermocouple combination using a large number of temperature ranges.

Although the bismuth-telurides and lead-telurides had higher figures-of-merit, their limited temperature ranges made them undesirable choices. Silicon-Germanium semiconductors possess greater flexibility over a wide range of temperatures and it was that fact which lead to the selection of silicon-germanium as the thermoelectric material of choice. The values of the figure of merit were taken from a chart and fitted to a polynomial curve using a fortran program.

5.3 Thermal Analysis

The optimum leg to area ratio determined in section 5.2 determines the proportions of the thermocouples, but a thermal analysis is required to obtain the actual dimensions of the thermocouples. This requires a conduction analysis of the entire RTG. The RTG consists of 7 concentric cylinders with 11 different materials. The inner-most material is the strontium fluoride. The second layer (the hot-shoe material) is silicon-molybdenum. The third layer consists of 5 materials:

- 1) p-type semiconductor
- 2) n-type semiconductor
- 3) insulation
- 4) parallel/series leads (copper)
- 5) strip seal (aluminum).

The fourth layer is an electrical insulator (alumina). The fifth layer is pyrolytic graphite which prevents the dispersion of the SrF₂ if the fine weave pierced fabric should fail.⁴⁴ The sixth layer is the aeroshell (fine weave pierced fabric)⁴⁴ which prevents the spread of strontium-90 in the event of a reentry accident. The seventh layer is the aluminum casing. Neglecting end losses, this becomes a one-dimensional heat conduction problem with natural convection and radiation at the surface.

Because the desired hot and cold temperatures are known (from determination of maximum efficiency), the length of the thermocouples can be determined by an energy balance and temperature distribution across the generator. The heat analysis of the thermocouple region will not be solved analytically, because there are two regions with heat generating medium (which is very difficult to solve analytically). Instead, a computer code will be written to solve the necessary equations.

For the Strontium fluoride (region 1), the total heat generation is q''' , and the temperature distribution is given by:⁴⁵

$$T(r) = \frac{q'''r_1^2}{4k} \left(1 - \frac{r^2}{r_1^2}\right) + T_{s1} \quad 5-8$$

where r_1 is the radius of the SrF₂ cylinder, k is the thermal conductivity of the SrF₂, and T_{s1} is the surface temperature of the SrF₂ cylinder. The total heat conducted across the SiMo clad is the same as the total heat transfer across the surface of the cylinder, and is given by:

$$q = q''' \pi r_1^2 H \quad 5-9$$

where H is the axial height of the strontium fluoride cylinder. The temperature distribution across

⁴⁴EG&G Mound Applied Technologies. Light-Weight Radioisotope Heater Unit Final Safety Analysis Report (LWRHU FSAR). U.S. Department of Energy: MLM-3540; Nov. 30, 1988. P. 86

⁴⁵Incropera, Frank P., and DeWitt, David P. Introduction to Heat Transfer. John Wiley and Sons, New York, 1990. P. 9, 98, 115, 493, 497, 500, 509.

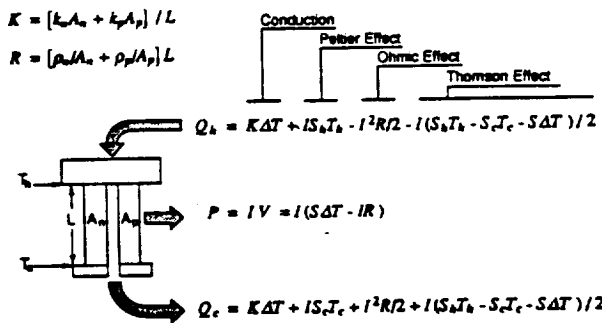
the SiMo is:⁴⁵

$$T(x) = \frac{T_{s1} - T_{s2}}{\ln(r_1/r_2)} \ln(x/r_2) + T_{s2} \quad 5-10$$

where r_2 is

the outer radius of the SiMo cladding, and T_{s2} is the temperature of the outer cladding surface.

The third layer contains thermocouple materials (both n and p type), insulation around the thermocouples, copper parallel/series leads, and aluminum strip seals. The energy balance equations for the unicouple are the following:⁴³



The rest of the layers of the RTG can be treated as one-dimensional conduction heat transfer without heat generation. The general solution to a one dimensional conduction problem through a hollow cylinder is of the same form as the solution for the temperature distribution in the SiMo cladding.

The last layer of the heat analysis must account for natural convection and radiation. The outer surface temperature of the aluminum casing (region 7) is determined by applying a heat balance across the surface. From Newton's Law of Cooling, the surface temperature of the aluminum casing is given by:²⁶

$$T_s = \frac{q_{conv}}{2\pi r_s h} + T_\infty \quad 5-11$$

where q_{conv} is heat removed by natural convection, H is the axial height of the RTG, r_o is the outer radius of the aluminum casing, T_b is the temperature of the surrounding atmosphere, and h is the average convective cooling coefficient. The average convective cooling coefficient, h , is given by the following correlation:⁴⁵

$$\bar{h} = \frac{k \overline{Nu}_D}{D} \quad 5-12$$

where k is the thermal conductivity of the atmosphere (approximated as CO_2), D is the diameter of the RTG, and \overline{Nu}_D is the average Nusselt number of CO_2 . The average Nusselt number is given by:⁴⁵

$$\overline{Nu}_D = \left\{ 0.60 + \frac{0.387 Ra_D^{1/6}}{\left[1 + (0.559/Pr)^{9/16} \right]^{6/27}} \right\}^2 \quad (10^{-5} < Ra_D < 10^2) \quad 5-13$$

where Ra_D is the Rayleigh number, and Pr is the Prandtl number.

The Rayleigh number is given by:⁴⁵

$$Ra_D = Gr_D Pr = \frac{g \beta (T_s - T_\infty) D^3}{v^2} Pr. \quad 5-14$$

In the above equation, v is the viscosity of the atmosphere, β is the volumetric thermal expansion coefficient⁴⁵ ($\approx 1/T_b$), and g is the acceleration of gravity.

The total heat removed must be equal to the heat removed by natural convection and the heat removed by radiation. The heat removed by radiative heat transfer is given by the Stephan-Boltzman Law of Radiative heat transfer:

$$q_{\text{rad}} = e \sigma (T_s^4 - T_\infty^4) \quad 5-15$$

where ϵ is the emissivity of the aluminum, and σ is the Stephan-Boltzman constant.

To complete the convective/radiative portion of the heat transfer problem requires that a surface temperature be guessed, until the sum of the radiative and convective heat transfer are equal to the total heat removal. The computer code will perform all of these tasks.

5.4 Computer Code Development

Using the equations mentioned in sections 5.2 and 5.3, a computer code was developed to analyze the heat transfer and electrical properties of the RTG. To perform this task, the RTG was divided into three parts; the strontium source and its cladding, the thermocouple region, and the surrounding materials. One dimensional heat transfer (conduction) was assumed for regions one and three. In region one and three analytical solutions were found for the one-dimensional heat conduction equations. However, in the second region, internal heat generation existed within the thermocouple legs (Joule heating) which made a one dimensional analysis inadequate. To overcome this, the thermocouple region (which consisted of the thermoelements, and insulation) was analyzed using a three dimensional mesh. The three dimensional mesh portion of the code accounted for both heat generation within the thermocouple legs, and heat transfer between the thermocouple legs and the surrounding insulation. A listing of the computer source code can be found in Appendix E. The code iterated between three distinct (but interdependent) calculational procedures. These were the following: a thermocouple optimization section, a heat transfer section (heat removal), and the 3-D mesh section (thermocouple region). A flowchart of the calculational procedure performed by the code is shown in Figure 5-1.

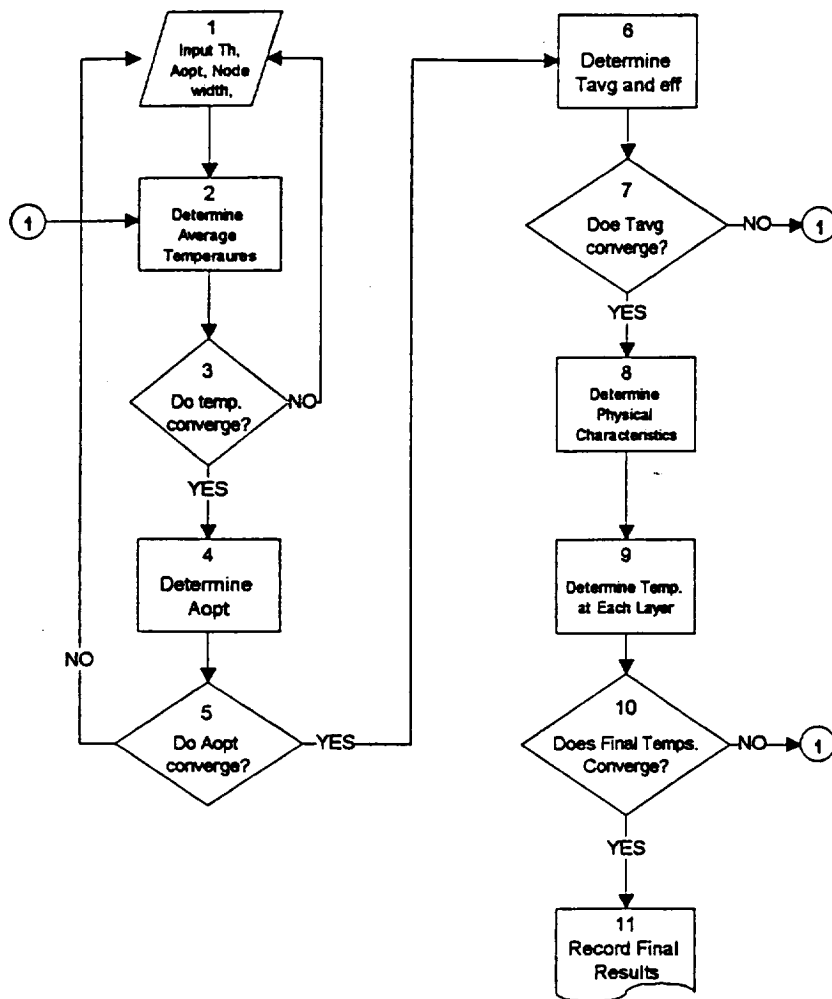


Figure 5-1 Flowchart of Calculational Procedures for the RTG Analysis Code

5.5 Weight/Size Comparison

Using the analysis code, two different RTGs were analyzed - a 10 watt (electric) and a 2.5 watt (electric) RTG. The modular, 2.5 watt, RTG was considered because it offered a more flexible power supply which would not fail in the event of a single RTG failure, and was, possibly, a lighter system than the full 10 watt system. The primary deciding factors, however, were weight and size. The 10 watt power supply had a lower weight (about 1kg with full insulation), and occupied less volume than the four 2.5 watt RTGs. The 10 watt RTG was chosen and had the following geometric characteristics:

10 We RTG

Sr centerline temp:	1321.1 K
RTG surface temperature:	273.2 K
T_{hot} :	1239.6 K
T_{cold} :	334.5 K
Efficiency:	9.3%
Length of Sr:	5.0 cm
Radius of Sr:	2.10 cm
Radius of SiMo:	2.19 cm
Length of TEs:	2.0 cm
Radius of Cu leads:	4.29 cm
Radius of Al seals:	4.79 cm
Radius of PG:	5.15 cm
Radius of fwpf:	5.45 cm
Radius of Casing:	6.45 cm
Estimated Total Mass:	1 kg

and the modular 2.5 watt RTG had the following characteristics:

2.5 We RTG

Sr centerline temp:	1291.1 K
RTG surface temperature:	273.1 K
T _{hot} :	1239.5 K
T _{cold} :	334.0 K
Efficiency:	9.2%
Length of Sr:	5.0 cm
Radius of Sr:	1.67 cm
SiMo Thickness:	1.76 cm
Length of TEs:	2.0 cm
Radius of Cu leads:	3.86 cm
Radius of Al seals:	4.36 cm
Radius of PG:	4.72 cm
Radius of fwpf:	5.01 cm
Radius of Casing:	6.01 cm
Estimated Unit Mass:	0.6 kg
4 × Unit Mass:	2.4 kg

6.0 Summary and Conclusions

In order to provide remote power generation for the Mars microrover, several alternative methods have been examined. These options include solar cells, batteries, fuel cells, thermionic direct energy converters (DEC), charged particle DEC, and radioisotope thermoelectric generators. In selecting among these alternative methods, several design criteria were used. These criteria included: 1. length of mission, 2. mass restrictions on payload, and finally 3. economic considerations. Radioisotope thermoelectric generators were selected because they best matched the design criteria. In order to provide the most efficient and economical power source, it was decided to design a RTG for the proposed mission, rather than using an existing one. This allowed a RTG to be designed which was "tailor made for the Mars mission. Since most of the equations used in RTG design are interdependent upon one another, a computer code was written to perform all the necessary calculations. Also, in order to provide the best design, an analysis on total weight was performed so that it could be determined whether a single 10 W_e was better than a 10 W_e source comprised of 4 2.5 W_e modular sources. The overall dimensions and weight to generate the 10 W_e required is given below:

	Single 10 W _e	Modular 2.5 W _e
Outer Radius	6.448 cm	6.015 cm
Estimated Mass	1 kg	0.6 kg
Estimated Total Mass	1 kg	2.4 kg

Therefore it appears that from a weight analysis, the single 10 W_e source is better than the modular, 2.5 W_e source. However, with the modular power source, a total failure of the power system is much less likely. With a single source, a failure could potentially end the mission. Thus the choice between sources becomes a probability risk assessment (PRA) decision.

It should be noted that this value of the mass of the RTG is lower than what will be expected as there will be additional insulation on the end caps of the RTG and other electrical regulators (i.e. voltage regulators) which will add to the overall weight of the RTG. The total material cost of a 10 We RTG is estimated to be \$100,000 (approximately twice the fuel costs).

Appendix A. Conceptual Designs of Alternative Small Nuclear Systems for Mars Mission

A.0 Conceptual Designs

The question was raised as to whether or no the RTG was the "best" choice for nuclear power sources in the 10-watt range, for use in the Mars rover mission. This section of the appendices presents the results of brief studies of two alternative nuclear power systems, both of which appear to be inferior to the RTG, particularly in regards to feasibility.

A.1 Radioisotope Fueled Thermionic Vacuum Diode System

Thermionic emission is basically thermally-enhanced quantum mechanical "tunneling" of electrons interior to a surface through the surface potential barrier. The situation is sketched in Figure A-1. The interior electrons have wave properties (DeBroglie wavelengths) which result in a finite probability for tunneling through the surface barrier (termed the "work function").

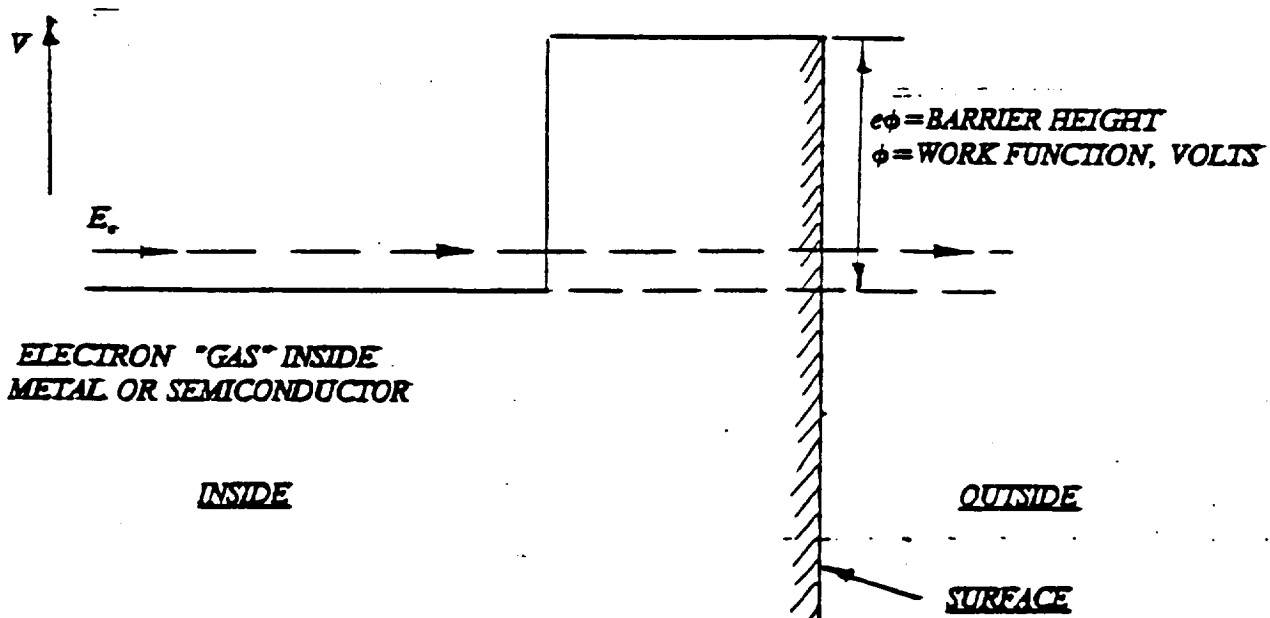


Figure A-1 Tunneling of Electrons Through a Surface Potential Barrier

The higher the absolute temperature of the "emitter" material, the larger the energy of the electron, and hence the larger the probability for barrier penetration. "Straightforward" tunneling theory gives the Richardson Equation for thermionic emission,*

$$j \left(\frac{\text{amp}}{\text{m}^2} \right) = A T^2 e^{-\frac{\Phi_e}{kT}} \quad \text{A-1}$$

where $A = 1.20 \times 10^6 \text{ amp/m}^2\text{-K}^2$ $k = \text{Boltzman constant}$
 $T = \text{absolute temperature, Kelvin}$

As the Richardson Equation indicates, the current emission is very strongly dependant on the temperature of the emitter surface. In fact, for thermionic current emission to be in a range of practical interest, absolute temperatures of the order of 2000 K are required (almost refractory scale temperatures). A typical high-temperature emitter material is tungsten, which has a work function of $\Phi_e = 4.55 \text{ eV}$.

To obtain electrical power from the thermionic emission principles, a diode is used, with a current collector material with a work function Φ_c less than that of the emitter material (see sketch of Figure A-2). The voltage output from such a diode is

$$V = \Phi_e - \Phi_c \quad \text{A-2}$$

The emitter current is independent of the collector work function Φ_c so long as

$$\Phi_e \geq \Phi_c + V_L \quad (\text{saturation mode}) \quad \text{A-3}$$

*Conyers, Herring and M. H. Nichols, "Thermionic Emission", Rev. of Modern Physics, 21, No. 2, pp. 191, FF (April, 1949).

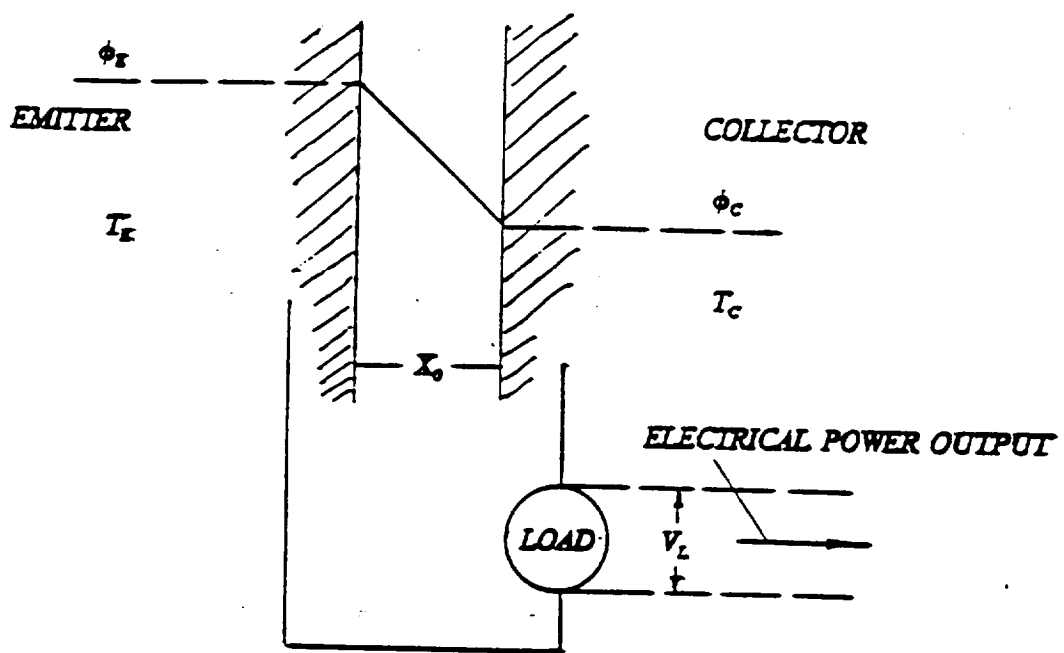


Figure A-2 Thermionic Diode Power System

In practice one obtains ~1/2 the Richardson Equation current, and actual power is reduced by 10% due to voltage drops in the converter's electrical leads,³⁰ thus

$$POWER\ OUTPUT = P_s \left(\frac{WATT}{m^2} \right) \approx \frac{0.9 j_R (\Phi_e - \Phi_c)}{2}$$

For highest power (large as possible voltage, $\Phi_e - \Phi_c$), one wants a collector with relatively low work function. Cesium has one of the lowest work functions of the metals:

CESIUM: $\Phi_c = 2.14 \text{ eV}$ $\rho = 1.9 \text{ gm/cm}^3$ $A_w = 132.95$

MELTING POINT = 28°C $Z = 55$ BOILING POINT = 690°C

Since its boiling point is less than the thermionic temperature region of interest, a "cesiated" tungsten electrode is used, then $V = \Phi_e - \Phi_c = 4.55 - 2.14 = 2.41 \text{ eV}$. The power output from such a W-Cs is then

$$P_s \left(\frac{WATT}{m^2} \right) \approx \frac{(0.9)(2.41)}{2} j_R = 1.08 j_R \quad A-5$$

A graph of this power output from the tungsten/cesiated-tungsten thermionic diode is shown in Figure A-3. Note the large surface area required and attendant ultra-high temperature to achieve power outputs in the 10+ watt range. However, these are not the limiting problems for such thermionic diodes. A vacuum gap can maintain only so much current flow before shear space charge density becomes so large that further flow is stopped. This space charge limitation is, for a vacuum diode

$$j_{LIMIT} = \left(\frac{4\sqrt{2}}{9} \right) \frac{\epsilon_0 V^{3/2} \sqrt{e/m}}{x_0^2} \left(\frac{AMP}{m^2} \right) \quad A-6$$

A-5

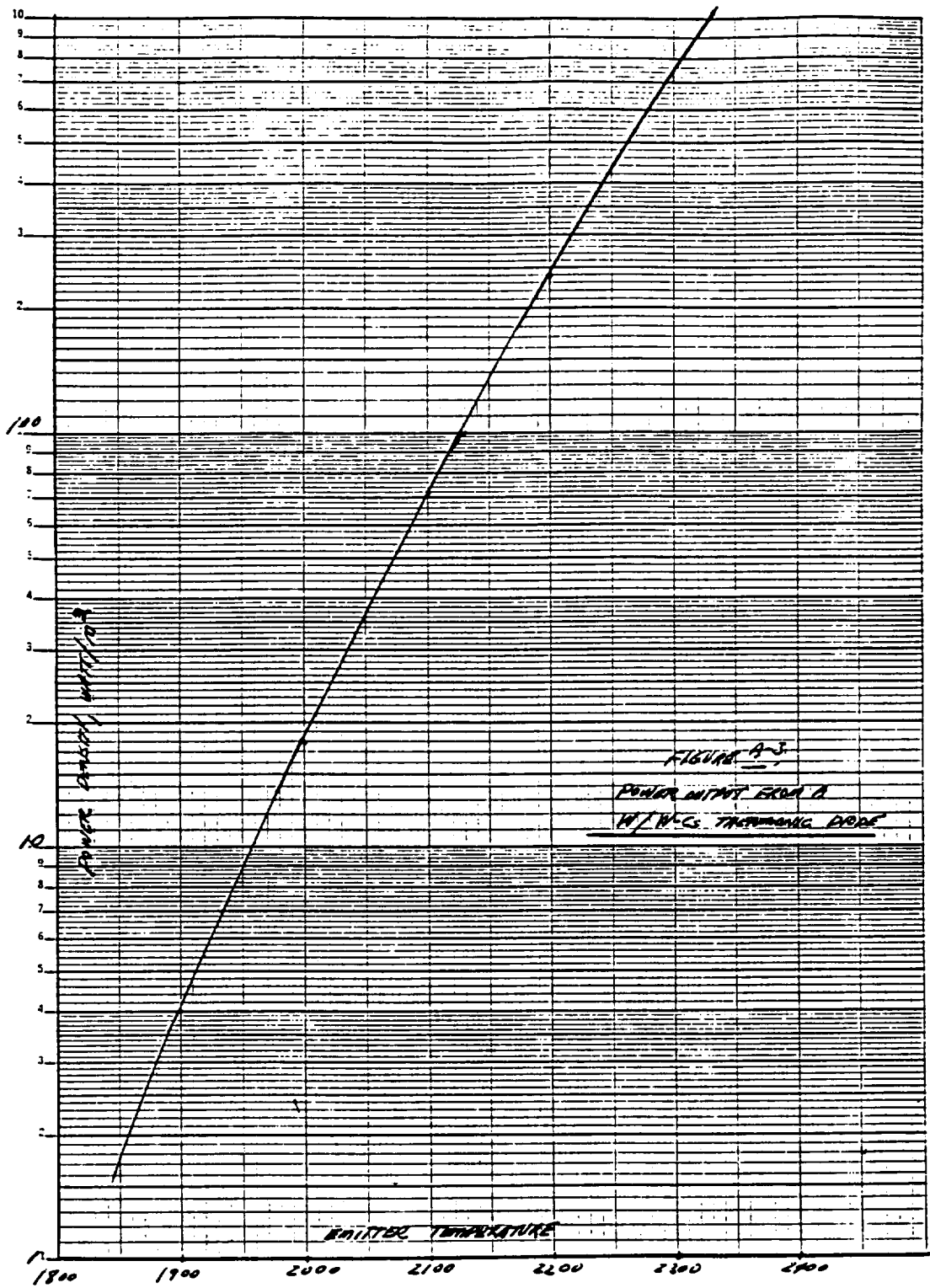


Figure A-3 Power Output from a W/W-Cs Thermionic Diode

As mentioned previously, for a W-Cs electrode system, $V = \Phi_e - \Phi_c = 2.41$ eV and thus

$$j_{LIMIT} = \frac{8.7 \times 10^{-6}}{X_0^2} \quad \frac{\text{AMP}}{\text{M}^2}$$

A-7

where X_0 is the gap width, in meters. For appreciable current densities, hence power densities, one might therefore use an extremely small gap.

An alternative, which permits a larger gap, is to fill the inter-electrode space with a cesium gas. The emitter electrons and the associated high temperatures produce a plasma sheath of thickness d within the gap, which "spreads" the space-charge limitation from X_0 to $d > X_0$; thereby enabling a larger (more manageable) gap width. However, the precise control required on the cesium vapor, and the means to introduce it and maintain it within the gap, introduces complexities and reduce ruggedness of the power source to the degree that such a scheme is thought to be inappropriate for the Mars mission under consideration.

If one accepts the simple vacuum diode, with its inherent space charge limitation, then the associated limitation on the power source is

$$P_s (\text{limit}) = j_{LIMIT} V = \frac{(8.7 \times 10^{-6})}{X_0^2} (2.41) (0.90)$$

$$= \frac{18.9 \times 10^{-6}}{X_0^2} \quad \frac{\text{watt}}{\text{M}^2}$$

A-8

where a 10 percent reduction in power output due to voltage drops in the power source electrical leads have been included. The following design can then be conceived.

Figure A-4 shows a conceptual design of the thermionic vacuum diode system, the unit cell of which is of coaxial cylindrical geometry. The central tungsten electrode, inside of which is

A-7

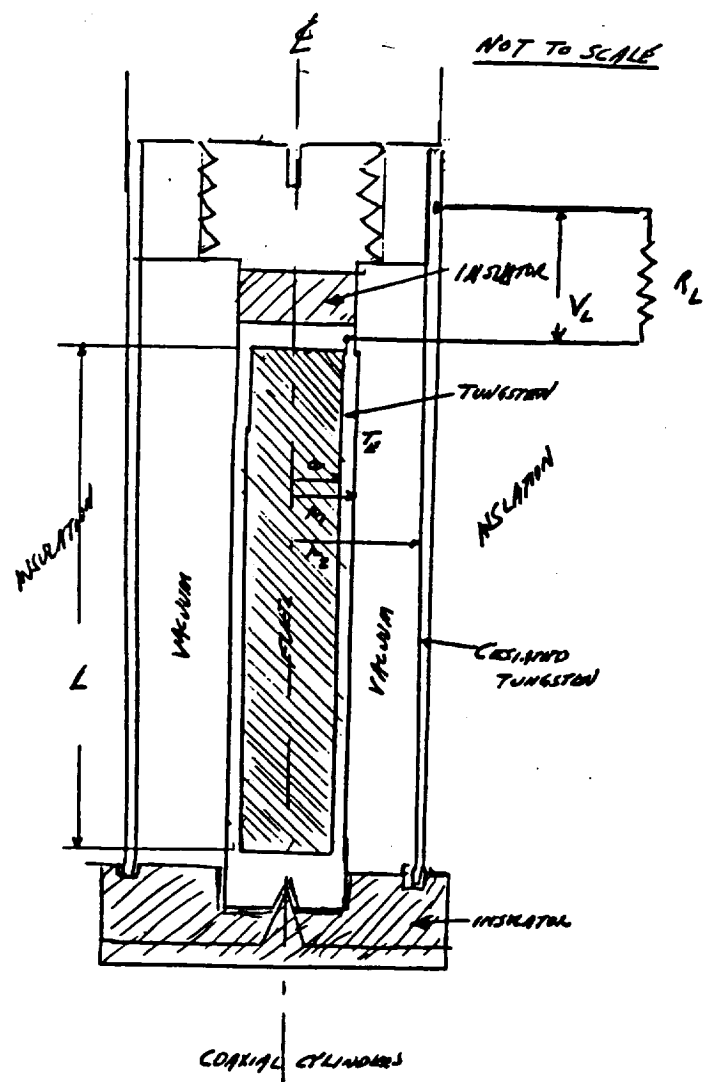


FIGURE A-4
RADIOISOTOPE FUELED
THERMIONIC VACUUM DIODE

SPACE POWERED DESIGN
NOT TO SCALE

VACUUM GAP: $X_0 = \mu_2 - \mu_1 = 0.1 \text{ cm}$
 VOLTAGE, $V_L = \phi_0 - \phi_c = 2.71 \text{ V.}$
 TEMPERATURE
 OF ANODE, $T_A = 2000 \text{ K}$
 SPECIFIC RESISTANCE
 OF ANODE: $R_s = 18.7 \text{ ohms/cm}^2$
 WITH $\mu_1 = 1 \text{ mV}$,
 $L = 18 \text{ m},$
 POWER OUTPUT/cell = $1.4 \text{ watts (2000 K)}$

Figure A-4 Conceptual Design of the Thermionic Vacuum Diode

SrTiO_3 radioisotope fuel (melting point of 2180 K)* is completely thermally isolated from the surroundings, and emits thermionically across a 1 mm gap to a cesiated-tungsten collector. Assume a 2 inch diameter emitter, 18 inches in length (total emitter surface area of $113 \text{ in}^2 = 0.0729 \text{ m}^2$). From equation (A-8), the space-charge-limited power output is 18.9 watts/ m^2 , or 1.38 watts (electrical) for the unit cell. An approximately 10 Watt device would therefore contain 7 cells. From the graph of Figure A-3, the required emitter temperature is 2000 K.

Aside from the problems of maintaining a 1 mm gap at the required temperature, and of maintaining a vacuum during a 3 year mission duration, probably the overwhelming problem is heat loss from the emitter by thermal radiation. In order to restrict the radiation heat losses to the same order of the diode electrical power output, the collector temperature must be held to less than 1 K of the emitter temperature! A simple calculation of black-body radiation from a 2000 K surface yields radiant heat transfer in the range 0.1 to 1.0 megawatt/ m^2 . Therefore, unless the heat flux is returned to the surface, the radiation heat loss overwhelms the 18.9 watts/ m^2 electrical output, i.e. the efficiency of the system is almost nil (less than 0.003 percent). It is thus concluded that the thermionic vacuum diode concept is impractical in this application.**

* Strontium titanate is an earlier used strontium compound. Strontium fluoride is in current use, but has a melting point of only 1460 K.

** In the plasma diode, the thermal radiation losses are partially overpowered by operating at much higher emission current densities (higher emitter temperatures).

A.2 Charged Particle Direct Energy Conversion (DEC) Systems

The alpha- or beta-decay of a radioisotope leads to the emission of an initially energetic, charged particle. A charged particle in motion is direct electricity. The discovery that charged-particle emission can build up a voltage on a properly insulated electrode may be traced back to Mosely in 1913.⁴⁷ The direct application of this idea for high-voltage generators has been considered by others during later decades, for example, the work of Linder and Christian at RCA⁴⁸. Consider the following situation (shown in Figure A-5) for positively-charged emission (e.g. alpha particles) from a surface which is electrically connected through a (load) resistance to a collecting surface.

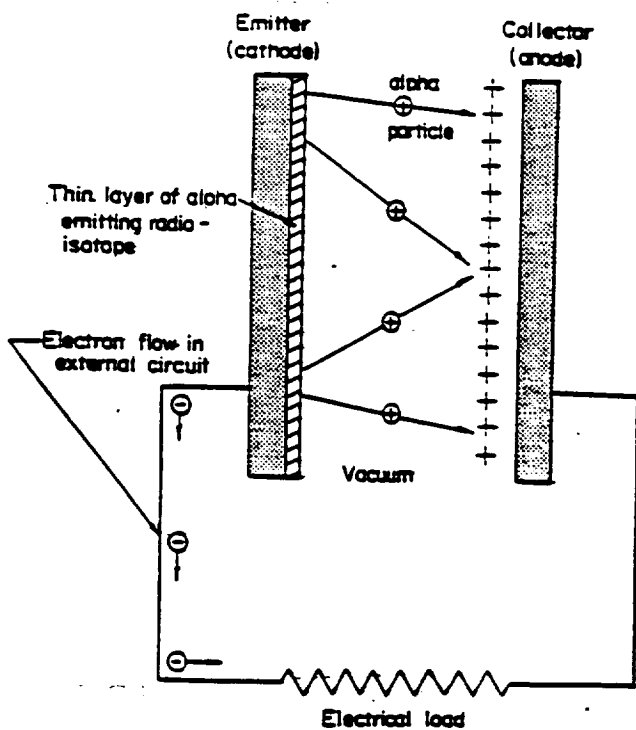


Figure A-5 Basic Principles of Charged-Particle Direct Energy Conversion

⁴⁷H. G. J. Mosely and John Harling, "The Attainment of High Potentials by the Use of Radium," Proc. Roy. Soc., 88, 471-476 (1913).

⁴⁸E. G. Linder and S. M. Christian, "The Use of Radioactive Material for the Generation of High Voltage," J. Appl. Phys., 23 (11), 1213-1216, (November 1952).

If the isotope is distributed in a sufficiently thin layer rather than in a thick fuel region, an appreciable fraction of all alpha particles produced in the layer can escape from the surface with much of their initial energy and charge intact. These particles can be collected on an insulated electrode. The first few alphas reaching the electrode will deposit their charge and dissipate their kinetic energy as heat. However, after a number of alphas have been collected, the insulated electrode, by virtue of its surplus of positive charge, will attain a high voltage with respect to the emitter layer. Subsequent alpha particles will "do work" against this electric field. The alphas arrive at the electrode with their initial kinetic energy exhausted and deposit only their charge.

The space between the electrodes is evacuated to $\sim 10^{-15}$ torr (approximately determined)

Table A-1

**MAXIMUM CONVERSION EFFICIENCIES FOR
THREE COMMON GEOMETRIES**

Geometry	Maximum Theoretical Efficiency	
	One-Sided Emission	Two-Sided Emission
Parallel Planes	7.4	14.8
Coaxial Cylinders	19.2	38.4
Concentric Spheres	50.0	100.0

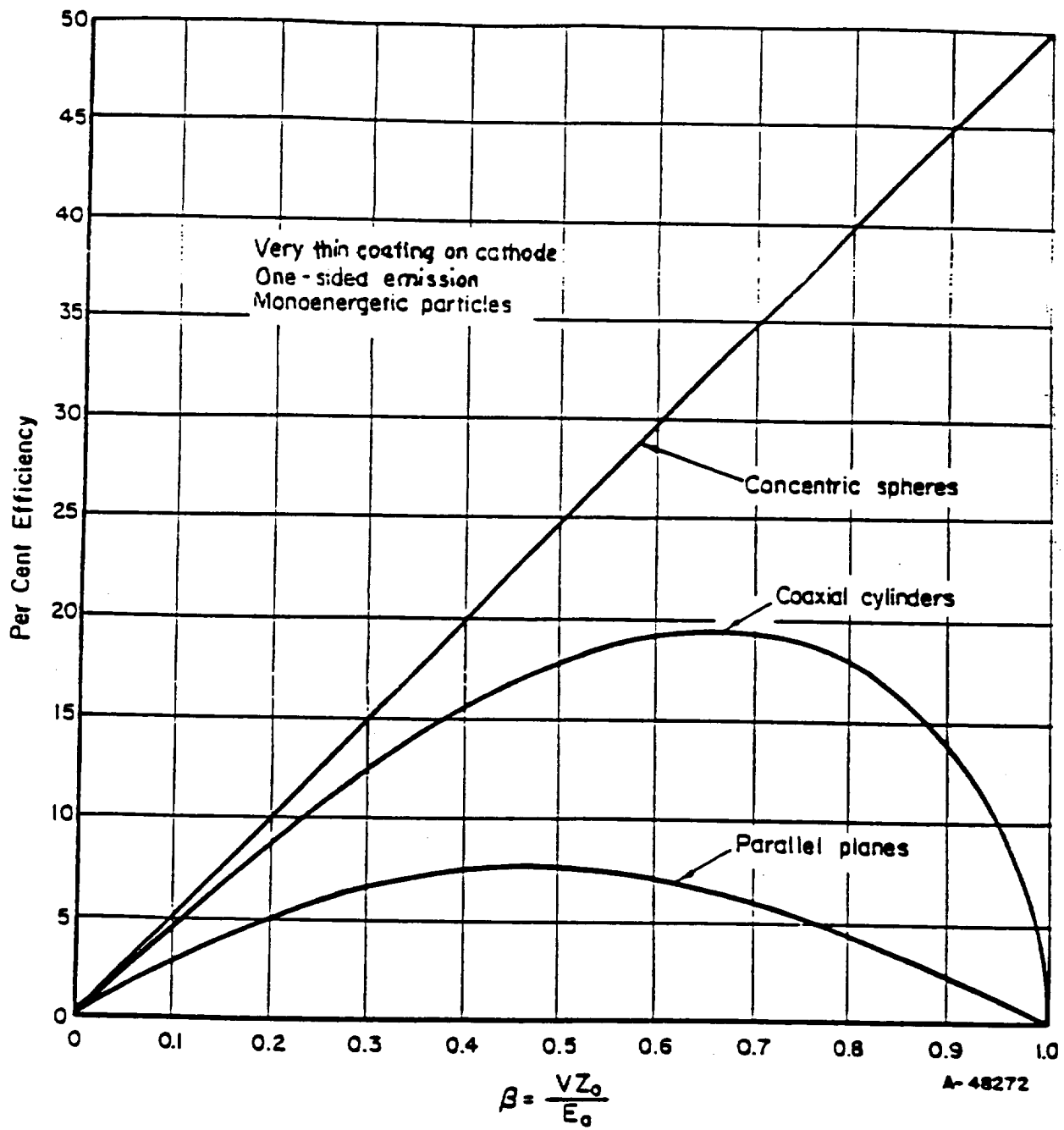


Figure A-6 Efficiency Versus Voltage for Three Common Geometries

Experiments and design considerations for using alpha particles with this direct conversion system are presented in detail in research reported in the 1960's.^{49, 50} One of the problems in using alpha particles is that low-energy secondary electrons accompany the alpha-particle emerging from the fuel surface layer, and must be suppressed by an intervening negatively-biased grid electrode. This complication, and the extremely high voltage resulting from alpha-particle energies, suggest a simpler beta-particle system for possible use in the Mars mission.

Use of beta emitters, rather than alpha-particles, can indeed be realized in practice. However, as a power source the beta-particle DEC's have at least two disadvantages:

1. Beta particles are not monoenergetic, as shown in the energy spectrum sketch of Figure A-7. Hence many particles are lost (much energy is lost) in "fall-back" particles with insufficient energy to work against the collector field (voltage).
2. No grid is required (although inherently simpler) which means there is no way to control collector voltage (except by varying load resistance).

Despite these drawbacks, the resulting simpler (more rugged) design and lower voltages (as will be seen) suggest that a beta-emitter option be explored for the Mars mission. Using parallel plane geometry (similar to that of Figure A-5) and a $^{90}\text{SrF}_2$ beta emitter (0.546 MeV end point beta energy), the requirements for a 10 watt (electrical) system were examined. The results are summarized in Table A-2.

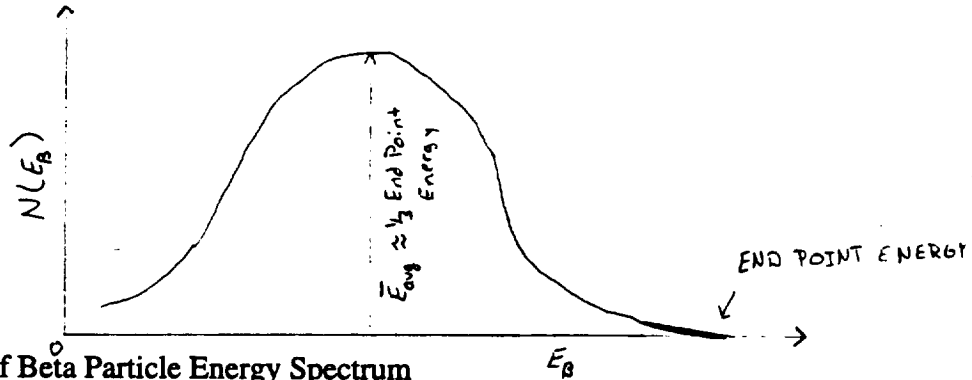


Figure A-7 Sketch of Beta Particle Energy Spectrum

⁴⁹A. M. Plummer, "Conversion of Alpha Particle Kinetic Energy into Electricity," ANL-6802, 170-180 (Paper Presented at AMU-ANL Conference on Direct Energy Conversion, November 4-5, 1963).

⁵⁰A. M. Plummer, W. J. Gallagher, and R. G. Matthews. "The Alpha-Cell Direct-Conversion Generator," Report NASA CR-54256, prepared for NASA under Contract NAS 3-2797 (Nov. 30, 1964).

Table A-2
 Summary of Design Characteristics of a 10 Watt, ^{90}Sr Beta Particle DEC System*
 (Parallel Plane Geometry)

<u>Item</u>	<u>Quantity or Value</u>
Source Materials	$^{90}\text{SrF}_2$
Electrical Power Output	10 watts (electrical)
Energy Conversion Efficiency	4.2%
Output Voltage	91 kilovolts
Output Current	0.11 milliamperes
Mass of $^{90}\text{SrF}_2$	732 grams
Activity of $^{90}\text{SrF}_2$ Coating	74.3 kilocuries
Thickness of Emitter Surface Coating	8.54 microns
Required Emitter Surface Area	20.3 m^2
Required Vacuum Between Electrodes	10^{-5} torr (10^{-5} mmHg)

*The contributions of the ^{90}Y daughter were inadvertently omitted from the analysis. However, the overall conclusions remain unchanged.

As seen from the summary in Table A-2, aside from the problem of converting the 91-kilovolt output to a more usable form, and from the problem of maintaining the required 10^{-5} torr vacuum during the 3 year mission, the required 20.3 m^2 surface area for the 10 watt system makes it impractical as a potential power source for the Mars mission.

Appendix B. Principles of Thermoelectricity*

*Based upon an original lecture series by J. N. Anno, Nuclear Engineering Program,
University of Cincinnati, Cincinnati, Ohio, (November, 1993).

B.1 Onsager Relationships

Figure B-1 is a simplified diagram of a thermocouple. A and B are wires of different materials. Because the flow of heat and

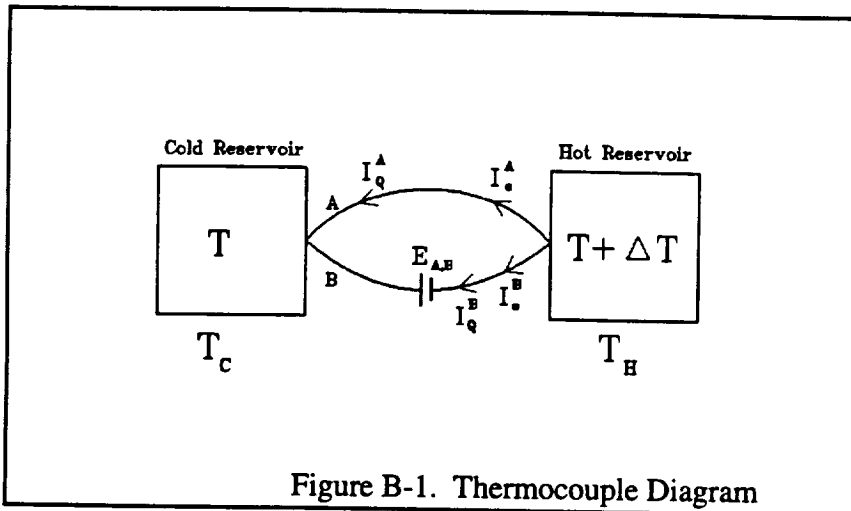


Figure B-1. Thermocouple Diagram

the flow of electrons are coupled, entropies are coupled; the electron flow through the potential difference (voltage) ΔE means that there is, also, an energy flow. Onsager proposed the following relationships:

$$\left. \begin{array}{l} \text{Heat Entropy} \quad I_s = \frac{I_q}{T} = L_{11} \frac{\Delta T}{T} + L_{12} \frac{\Delta E}{T} \\ \text{Electron Current} \quad I_s = L_{21} \frac{\Delta T}{T} + L_{22} \frac{\Delta E}{T} \\ \text{Entropy} \end{array} \right\} \text{B-1}$$

where, $L_{12} = L_{21}$.

From these two equations, the ratio

$$\frac{\text{Heat Entropy Carried Through A}}{\text{Electricity Carried Through A}} \Big|_{(\text{TEMP})} \text{CONST} = \frac{I_s}{I_s} \Big|_{(\text{TEMP})} \text{CONST} = \frac{L_{12}}{L_{22}} = S_A^* \quad \text{B-2}$$

where S_A^* = "Thermoelectric Power" of A.

B-2

Now, at $I_e=0$,

$$\Delta E = -\frac{L_{21}}{L_{22}} \Delta T = -\frac{L_{12}}{L_{22}} \Delta T = -S_A^* \Delta T$$

,hence,

$$S_A^* = \left. \frac{\Delta E}{\Delta T} \right|_{I_e=0} = \text{Thermoelectric Power of } A \quad \text{B-3}$$

B.2 Magnitude of Thermoelectric Power, S_A^*

For "good conductors," Lorentz's law states that

$$\epsilon = \frac{k}{\sigma T} = 2.23 \times 10^{-8} \frac{v^2}{\kappa^2} \quad \text{B-4}$$

where k = the thermal conductivity, σ = the electrical conductivity, and T = absolute temperature. Fourier's law of heat conduction through a "wire" of length ℓ and area, S , gives

$$I_e = \frac{I_Q}{T} = \frac{q'}{T} = -\frac{kS}{\ell T} \Delta T \quad (q' = -kS \frac{dT}{dX}). \quad \text{B-5}$$

Ohm's law for current flow is

$$I_e = \frac{\Delta E}{R} = \frac{\sigma S}{\ell} \Delta E. \quad \text{B-6}$$

By dividing equation B-5 by equation B-6, we obtain

$$\frac{I_e}{I_e} = -\left(\frac{\Delta T}{\Delta E}\right) \left(\frac{k}{\sigma T}\right) = -\epsilon \frac{\Delta T}{\Delta E} = \frac{\epsilon}{S_A^*} \quad \text{B-7}$$

where

$$S_A^{*'} = -\frac{\Delta E}{\Delta T}$$

, but

$$\frac{I_e}{I_e} \Big|_{\text{CONST}} = S_A^* = -\frac{\Delta E}{\Delta T} \Big|_{I_e=0}. \quad \text{B-8}$$

For a "small ΔT ," we argue that $S_A^* \approx S_A^{*'} \approx S_A^*$, so that, from equations B-7 and B-8,

$$S_A^* \approx \frac{\epsilon}{S_A^{*'}} , \text{ hence } (S_A^{*'} S_A^*) \approx (S_A^*)^2 = \epsilon.$$

$$\therefore S_A^* \approx \sqrt{\epsilon} = \sqrt{2.23 \times 10^{-8}} = 149 \frac{\mu V}{K} = 83 \frac{\mu V}{^{\circ}F}. \quad \text{B-9}$$

Therefore, all good conductors have approximately the same thermoelectric power, and, from B-3, for two different wires,

$$E_{A,B} = \int_{T_0}^T (S_A^* - S_B^*) dT \quad \text{B-10}$$

would be zero.

B.3 Real Thermocouples

The Seebeck Coefficient defined for a thermocouple with wires A and B different materials is the following:

$$\alpha = \alpha_{A,B} = \frac{dE_{A,B}}{dT} = S_A^+ - S_B^+ \quad \text{B-11}$$

Since the entire thermocouple performance depends on deviations from Lorentz's law (ideal behavior), $\alpha_{A,B}$ would be expected to be a fraction of $83 \mu\text{V}/^\circ\text{F}$, i.e.,

$$\alpha_{A,B} < \sqrt{\epsilon} \quad (\text{Expected}) \quad \text{B-12}$$

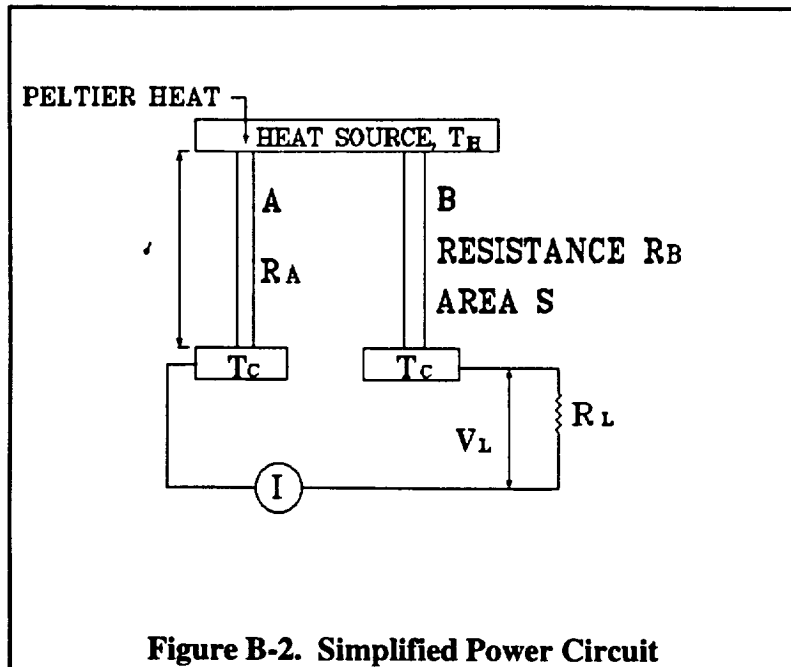
Table B-1. Range and Sensitivity of Thermocouples

Thermocouple	Type	Range, $^\circ\text{F}$	α , Seebeck Coefficient, $\mu\text{V}/^\circ\text{F}$
Copper-Constantan	T	-300 to 700	28
Iron-Constantan	J	200 to 1400	32
Chromel Alumel	K	-200 to 2300	23
Platinum-10% Rhodium-Platinum	S	1000 to 2650	6.5
Chromel-Constantan	E	32 to 1400	40

Indeed, as shown in Table B-1, $\alpha < 83 \mu\text{V}/^\circ\text{F}$ is found to be the case.

B.4 Power from Thermoelectricity

The thermocouple principles can be used for the direct conversion of heat to electricity, a simplified "power circuit" is shown in Figure B-2.



The efficiency of this device (the Thermoelectric generator) is of interest.

$$\eta = \frac{W_L'}{Q_{IN}'} = \frac{\text{Electrical Power output}}{\text{Thermal power input}} \quad \text{B-13}$$

The electrical power output is

$$W_L' = R_L I^2 \quad \text{B-14}$$

where the current, I, in the system is

$$I = \frac{\text{Total EMF in System}}{\text{Total (series) Resistance}} = \frac{\alpha_{A,B} (T_H - T_C)}{R_A + R_B + R_L} . \quad \text{B-15}$$

Thus,

$$W'_L = \frac{R_L \alpha_{A,B}^2 (T_H - T_C)^2}{(R_A + R_B + R_L)^2} . \quad \text{B-16}$$

The thermal power input is

$$\begin{aligned} Q'_{IN} &= (\text{Heat Conducted through A,B}) + (\text{Heat Input Peltier Cooling of hot reservoir}) \\ &\quad - (\text{Part of Joule Heating Dissipated in Thermocouple circuit}) \\ &= \left[\left(\frac{k_A S}{\ell} + \frac{k_B S}{\ell} \right) (T_H - T_C) \right] + (\text{Peltier Cooling at } T_H) - \frac{1}{2} (R_A + R_B) I^2 \end{aligned} \quad \text{B-17}$$

It is conventional to assign $\frac{1}{2}$ of the I^2R heating to each junction. The Peltier effect is the entropy flow induced by the current flow from equation B-2, at the hot junction, T_H ,

$$\left(\frac{I'}{I_e} \right)_A = \left(\frac{I_Q}{T_H I_e} \right)_A = S_A^* .$$

And similarly, with wire B, the net effect is heat input (cooling of the T_H reservoir) of

$$(I_Q)_{NET} = (S_A^* - S_B^*) T_H I = \alpha_{A,B} T_H I = \text{Peltier Cooling} \quad \text{B-18}$$

For convenience, define $\lambda_i = k_i S / \ell$, then, from B-17 and B-18,

$$Q'_{IN} = (\lambda_A + \lambda_B) (T_H - T_C) + \alpha_{A,B} T_H I - \frac{1}{2} (R_A + R_B) I^2 \quad \text{B-19}$$

From equations B-13, B-15, B-16, and B-19, and with

$$m = \frac{R_L}{R_A + R_B} = \frac{\text{Load Resistance}}{\text{Internal Resistance}} \quad \text{B-20}$$

$$Z = \frac{\alpha_{A,B}^2}{(\lambda_A + \lambda_B)(R_A + R_B)} = \text{Figure of Merit} \quad \text{B-21}$$

$$\eta_C = \left(1 - \frac{T_C}{T_H}\right) = \text{Carnot Efficiency} \quad \text{B-22}$$

the efficiency (equation B-13) becomes

$$\eta = \frac{\eta_c m}{\frac{(m+1)^2}{Z T_H} - \frac{(T_H - T_C)}{2 T_H} + (m+1)} \quad \text{B-23}$$

This efficiency expression has an optimum with respect to the resistance ratio, m ;

$$m_{opt} = \sqrt{1 + Z \bar{T}} \quad \text{B-24}$$

where $\bar{T} = (T_h + T_c)/2$ = average temperature of thermocouple wire.

B.5 Estimate of Optimum Efficiency of a Thermoelectric Generator

Assume that the deviations from Lorentz's law are scattered about the average value, and take

$$\bar{\lambda} = \frac{\lambda_A + \lambda_B}{2} = \frac{\bar{k} S}{\ell}; \quad \bar{R} = \frac{R_A + R_B}{2} = \frac{\ell}{\bar{\sigma} S}$$

so that an optimistic estimate for the Seebeck coefficient (equations B-9 and B-11) is

$$\alpha_{A,B} \approx S^* = \sqrt{\epsilon} = \sqrt{\frac{\bar{k}}{\bar{\sigma} \bar{T}}}.$$

Hence, the figure of merit is

$$Z = \frac{\alpha_{A,B}^2}{(\lambda_A + \lambda_B)(R_A + R_B)} \approx \frac{\frac{\bar{k}}{\bar{\sigma} \bar{T}}}{(2 \bar{\lambda})(2 \bar{R})} = \frac{1}{4 \bar{T}} \quad \text{B-25}$$

which gives the optimum (resistance ratio) to be (from B-24)

$$m_{opt} = \sqrt{1 + Z \bar{T}} = \sqrt{1 + \frac{1}{4}} = 1.12$$

from equation B-23, with $m = 1.12$ and $Z = 1/4\bar{T}$,

$$\eta \approx \frac{1 - \frac{T_c}{T_H}}{8.46 (1.12 + \frac{T_c}{T_H})} \quad \text{B-26}$$

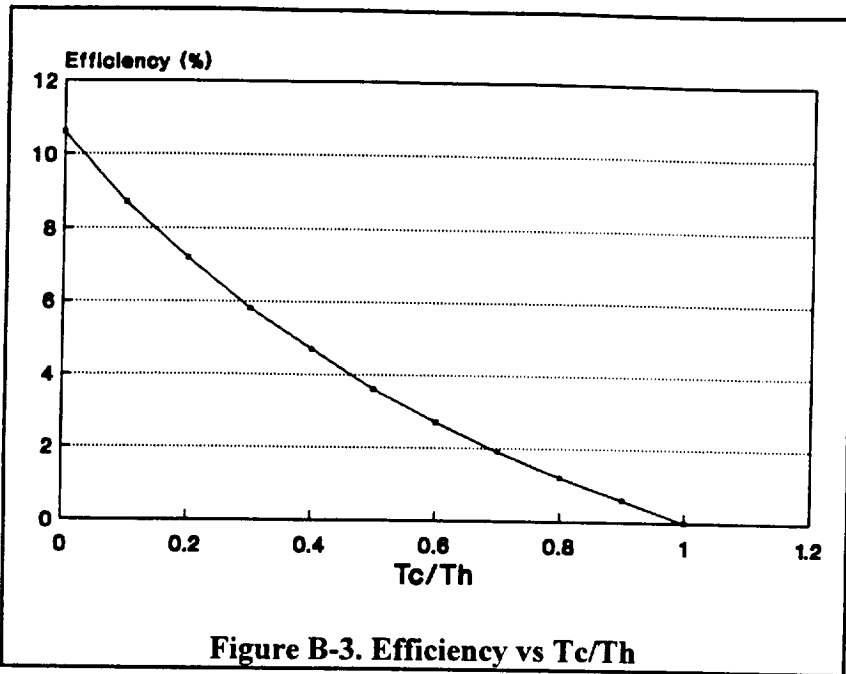


Figure B-3. Efficiency vs T_c/T_h

Note that with these approximations, the maximum achievable efficiency ($T_c/T_h \ll 1$) is 10.6%. For realistic temperatures (say, for example, $T_c = 273$ K, $T_h = 600$ K, so that $T_c/T_h = 0.46$, i.e., of the order of $\frac{1}{2}$) with $T_c/T_h \sim \frac{1}{2}$, $\eta \approx 3.7\%$.

Practical thermoelectric generators are found to have efficiencies in the 5-7% range. Some gains can be made through the use of high-temperature semiconductor materials, which have higher figures of merit ($Z > 1/4T$). Thus equation B-26 is a "lower limit" estimate for the theoretical efficiency of semiconductor systems, and strictly applies to metal systems only.

Appendix C. Selection of Fuel for RTGs in Space Power Systems

C.1 Determination of Specific Thermal Power (kW/kg)

C.1.1 Radioactive Decay Law

The number density of radioactive atoms, N (atoms/cm³), is a function of time and is given by

$$N = N_0 e^{-\lambda t} \quad C-1$$

where N_0 is the initial concentration of radioactive atoms (N at $t=0$), and λ is the decay constant. The decay constant, λ , can also be expressed in terms of the isotope's half-life as follows:

$$\lambda = \text{decay constant} = \frac{\ln 2}{T_{1/2}} = \frac{0.6931}{T_{1/2}} \quad C-2$$

for a pure emitter. The initial number density is determined using the following equation:

$$N_0 = \frac{\rho N_A}{A_w} = \frac{\text{atoms or molecules}}{\text{cm}^3} \quad C-3$$

where ρ = physical density, g/cm³

N_A = Avagadro's number = 6.023×10^{23} particles/mole

A_w = atomic or molecular mass, g/mole.

C.1.2 Activity

The activity of a radioactive isotope is given by the following:

$$A = \left| \frac{dN}{dt} \right| = \left| -\lambda N \right| = \lambda N \frac{\text{disintegrations}}{\text{sec cm}^3} \quad C-4.$$

The most commonly used units for activity are the Becquerel and the Curie:

1 dis/sec ≈ 1 Becquerel = 1 bq

$$3.7 \times 10^{10} \text{ dis/sec} \equiv 1 \text{ Curie} = 1 \text{ Ci.}$$

From equations C-1, C-3, and C-4, the activity can be written as

$$A = \frac{\lambda \rho N_A e^{-\lambda t}}{A_w} \quad \text{C-5.}$$

The specific activity (the activity on a per gram basis) is given by

$$A_g = \frac{\lambda N_A e^{-\lambda t}}{A_w} \frac{\text{disintegrations}}{\text{sec gm}} \quad \text{C-6}$$

for 100% radioactive atoms.

C.1.3 Energy Released per Disintegration

Because both the emitted particle and the recoil particle energy are available for heat generation in an RTG, the energy released for each reaction of interest is the Q value of that reaction (in general, $Q >$ energy of emitted particle). For non-relativistic particles (i.e. α particles),

$$Q = \left(1 + \frac{m}{M}\right) (\text{K.E.}) \quad \text{C-7}$$

where m is the mass of the α -particle, M is the mass of the recoil nucleus, and (K.E.) $_{\alpha}$ is the kinetic energy of the emitted α particle.

C.1.4 Specific Power (kW/kg)

From equation C-6, with energy Q released per disintegration, the total energy released per second per unit mass is the specific power,

$$P_s = \frac{\lambda N_A Q e^{-\lambda t}}{A_w} \frac{kW}{kg} \quad C-8,$$

where Q has units of Joules (1 MeV = 1.6×10^{-19} Joule).

C.1.5 Specific Thermal Power (kW/kg)

Let f = the fraction of the decay energy (Q total) captured in the "fuel." For practical purposes, f = 1.00 for a pure α emitter and a shielded beta emitter, but f < 1.00 for a gamma emitter. From equation C-8, the specific thermal power of the radioisotopic fuel is

$$P_s^{th} = \frac{\lambda N_A Q f e^{-\lambda t}}{A_w} \frac{kW}{kg} \quad C-9.$$

For the case in which t (design lifetime) $\ll T_{1/2}$, equation C-9 reduces to

$$P_s^{th} = \frac{\lambda N_A Q f}{A_w} \frac{kW}{kg} \quad C-10.$$

for 100% radioactive atoms. This specific thermal power is reduced for materials in which not all atoms are the radioactive isotope of interest.

For a space mission, a material with a small mass and a large P_s^{th} is desirable; therefore, it follows from the above relationships that an ideal fuel source should have the following properties:

- large Q
- f = 1.00 (α or β emitter)
- small λ (long half-life) relative to mission time

- small A_w (molecular mass)
- good radioisotope purity.

Compromises, of course, must be made for the "real world" selection of the proper fuel based upon other criteria for the mission as discussed in the following section.

C.2 Criteria for Radioisotope Fuel

There are several fundamental criteria to be met:

1. Half-life in proper range - Considering mission(s), say at least 3 earth years, along with the desire for high specific power (see later discussion), the half-life range of interest is roughly between 10 and 100 years.
2. Health Physics (Shielding and Biological effects)
 - a. Shielding adds weight to system → no gamma emitters
 - b. Biological effects suggest that no half-lives near the human generation time should be used (in conflict with criteria a); therefore, a compromise is required, but criterion (B)(i) still holds.
3. High Power Density - minimum possible weight is desired
4. Availability - Isotope must be attainable

In addition to the above fundamental criteria, several secondary criteria exist:

5. Large energy release per decay (large Q of decay reaction)
6. Stability of fuel
7. Strength of fuel
8. Cost.

Although smaller mass systems reduce transport costs, the fuel cost cannot be "extremely high".

C.3 Selection of Radioisotope

The eight criteria previously stated narrow the over 1300 known radioisotopes to a small number of possibilities.

1. First consider naturally occurring alpha-emitters. The 24 naturally occurring alpha emitters are listed in Table C-1.⁵¹ None of these radioactive species meet the half-life requirements of the mission.
2. Next, examine "common" radioisotopes (107 of them). From Table C-2,⁵² it can be seen that half-life restrictions eliminate all but four of these listed radioisotopes, and these four are eliminated by the two other criteria of "no gamma" and "large Q" (criteria (B)(i) and (C), respectively).
3. "Special" Radioisotopes

Considerations such as illustrated previously in (A) and (B) reduce the >1300 radioisotopes to a select few of interest as power sources. These are listed in Table C-3,⁵³ and their properties listed in Table C-4.⁵⁴ From this list of "special" radioisotopes, only four (⁹⁰Sr, ¹³⁷Cs, ²³⁸Pu, and ²⁴⁴Cm) meet the half-life criteria for the mars space mission. Of these four, ¹³⁷Cs is ruled out by its gamma-ray emission; ²⁴⁴Cm, while still a possibility, is unlikely because of its low availability and high cost. This leaves ⁹⁰Sr and ²³⁸Pu as the most likely RTG sources. ⁹⁰Sr would be in the form of strontium flouride, and ²³⁸Pu would be in the form of plutonium dioxide (plutonia).

⁵¹J. N. Anno, Wave Mechanics for Engineers, (Lexington books, D.C. Heath and Company, Lexington, Massachusetts, 1976) Table 8.1).

⁵²Richard Stephenson. Introduction to Nuclear Engineering, (McGraw-Hill Book Company, inc., New York, 1954), Table II.

⁵³Thomas J. Connolly, Foundations of Nuclear Engineering, (John Wiley & Sons, New Youk, 1978) Table 6.3.

⁵⁴Authur R. Foster and Robert L. Wright, Jr. Basic Nuclear Engineering, 4th ed., (Allyn and Bacon, inc., 1983) Table 7.1.

C.4 Comparison of Characteristics of ^{90}Sr and ^{238}Pu Power Sources

1. ^{238}Pu Source

a. Properties of PuO_2 source

Molecular mass:	270 g/mol
Energy released per decay, Q^{55} :	5.592 MeV
Half-life, $T_{1/2}^{56}$:	87.74 years
Physical density ⁵⁶ :	10.0 g/cm ³
Purity of source (see Table C-5) ⁵⁶ :	87.4% $^{238}\text{PuO}_2$
Neutron emission ⁵⁶ :	5190 ± 130 n/g sec
Radiation from 100 Watt ⁵⁷ :	neutron - 0.53 mRem/hr
Bare source at 1 yard:	gamma - 0.01 mRem/hr

b. Calculation of Specific Thermal Power of $^{238}\text{PuO}_2$ Fuel

For a mission life of ~3 years and a half-life of 87.7 years for ^{238}Pu , $t \ll T_{1/2}$; therefore, equation C-10 may be used to calculate P_s^{th} . Assuming $f = 1.00$, and an isotopic purity of 83.62% (see Table C-5),

$$P_s^{\text{th}} = \frac{(0.8362) (0.6931) (6.023 \times 10^{23}) (8.947 \times 10^{-13})}{(2.769 \times 10^3) (270)} = 0.418 \frac{\text{Watt}}{\text{g } \text{PuO}_2}.$$

This calculation is in excellent agreement with the 1.11 watts generated by 2.664 grams of the PuO_2 fuel used in the LWRHU system⁵⁶.

⁵⁵Thomas J. Connolly, op. cit., Table A.3.

⁵⁶Ernest W. Johnson, op. cit., pp. 28-33.

⁵⁷Harold L. Davis, "Radionuclide Power for Space - Part I," Nucleonics, **21**, 61 (March, 1963).

2. ^{90}Sr Power Source (SrF_2)

a. Properties of SrF_2

Molecular Mass:	128 g/mole
Energy Released per decay, Q^{55} :	0.546 MeV
Half-life, $T_{1/2}^{55}$:	28.1 years
Mass range of end-point β ($\rho \bar{r}$) ⁵⁸ :	0.185 g/cm ²
Neutron and Gamma emission:	none
Purity of SrF_2 Source (as fabricated) ⁵⁴ :	55% ^{90}Sr 43.9% ^{88}Sr 1.1% ^{86}Sr

Other properties include: Cheap and plentiful (millions of curies available at DOE waste facilities), SrF_2 is insoluble in water, resistant to shock, and has a high melting point (1460K). 1975 reported cost estimates are listed in Table C-6. ^{238}Pu is 30 to 50 times more expensive than ^{90}Sr .

Table C-6. Cost estimates for ^{238}Pu and ^{90}Sr Fuels⁵⁴

Isotope Source	\$/gram	\$/Watt (thermal)
^{90}Sr	42	45
^{238}Pu	1250	2200

b. Calculation of Specific Thermal Power of SrF_2 Fuel

Again using equation C-10, and with a shielded source such that $f = 1.00$, and an isotopic purity of 55%,

⁵⁸R. D. Evans, The Atomic Nucleus, (McGraw-Hill Book Company, inc., New Youk, 1955) p. 625.

$$P_s^{th} = \frac{(0.55) (0.6931) (6.023 \times 10^{23}) (0.8736 \times 10^{-13})}{(0.8869 \times 10^9) (128)} = 0.129 \frac{\text{Watts}}{\text{g of } SrF_2}$$

The results of this brief comparison of ^{238}Pu and ^{90}Sr is summarized in Table C-7.

Table C.7 Comparison of PuO_2 and SrF_2 Sources for Space Power RTG's

Advantages	Cheap	no gamma in pure form
	Plentiful	high power density
	Acceptable Power Density	$T_{1/2}$ in good range
	$T_{1/2}$ in acceptable range	
	no gamma or neutron	PuO_2 high temperature
	SrF_2 insoluble in water, shock resistant, and high melting point	ceramic, strength good, and good stability
Disadvantages	Affinity for Bone Marrow (damaging to blood production)	Many times more expensive than ^{90}Sr
		neutron emitter as currently fabricated

Table C-1. Natural Alpha Emitters⁵¹

Symbol	Z	Atomic weight	Half-life	Decay Constant sec ⁻¹	Particle Energy (MeV)
Bi	83	210.987	2.16 min	0.00535	6.617
Bi	83	211.989	60.5 min	1.91 \wedge 10 ⁻⁴	6.043
Bi	83	213.995	19.7 min	5.86 \wedge 10 ⁻⁴	5.443
Po	84	209.983	138.40 day	5.80 \wedge 10 ⁻⁶	5.299
Po	84	210.987	0.52 sec	1.33	7.448
Po	84	211.989	0.304 usec	2.28 \wedge 10 ⁻⁸	8.780
Po	84	213.995	0.1637 msec	4,230	7.680
Po	84	214.999	1.83 msec	379	7.380
Po	84	216.002	0.158 sec	4.39	6.775
Po	84	218.009	3.05 min	0.00379	5.998
Rn	86	219.010	3.92 sec	0.177	6.813
Rn	86	220.011	51.0 sec	0.0136	6.282
Rn	86	222.018	3.823 day	2.10 \wedge 10 ⁻⁸	5.486
Ra	88	223.019	11.68 day	6.87 \wedge 10 ⁻¹¹	5.867
Ra	88	224.020	3.64 day	2.20 \wedge 10 ⁻⁸	5.681
Ra	88	226.025	11622 year	1.89 \wedge 10 ⁻¹²	4.777
Th	90	227.028	18.17 day	4.41 \wedge 10 ⁻¹¹	6.036
Th	90	228.029	1.91 year	1.15 \wedge 10 ⁻¹⁰	5.4214
Th	90	230.033	8.0 \wedge 10 ⁴ year	2.74 \wedge 10 ⁻¹³	4.682
Th	90	232.038	1.39 \wedge 10 ⁶ year	1.58 \wedge 10 ⁻¹⁴	4.007
Pa	91	231.036	3.43 \wedge 10 ⁴ year	6.40 \wedge 10 ⁻¹³	5.010
U	92	234.041	2.48 \wedge 10 ⁵ year	8.84 \wedge 10 ⁻¹⁴	4.768
U	92	235.044	7.10 \wedge 10 ⁶ year	3.09 \wedge 10 ⁻¹⁷	4.391
U	92	238.051	4.51 \wedge 10 ⁹ year	4.88 \wedge 10 ⁻¹⁸	4.195

Table C-2. Common Radioisotopes⁵²

Radionuclide	Half life	Beta particle, Mev	Gamma ray, Mev	Radionuclide	Half life	Beta particle, Mev	Gamma ray, Mev
H ³	12 yr	0.018	None	Sr ⁸⁵	112 days	K capture	0.09
Li ⁷	0.9 sec	12	Weak	Sr ⁸⁵	60 days	2.37 max (see charts)	2.3 max (see charts)
Be ⁷	54.5 days	K capture	0.48 (12%)	Tm ¹⁴⁷	8 days	0.80 (86%), 0.32 (15%)	0.638 (15%), 0.364 (85%)
Be ¹⁰	2.5 × 10 ⁴ yr	0.56	None	Tm ¹⁴⁷	6.7 hr	0.47 (35%), 1.0 (40%)	1.3, 1.7
B ¹⁰	0.03 sec	13	Weak			1.4 (25%)	
C ¹⁴	5800 yr	0.155	None	I ¹³¹	22 sec	Delayed neutrons	0.247
N ¹³	10 min	1.24 (e ⁻)	None	Xe ¹³⁶	9.2 hr	0.93	
N ¹³	7.35 sec	10 (18%), 3.8–4.6 (82%)	6.2	Ca ⁴⁵	2.3 yr	0.658 (74%), 0.09 (26%)	0.794, 0.602, 0.568 (26%)
O ¹⁸	2 min	1.68 (e ⁻)	None	Ca ⁴⁵	37 yr	1.2 (5%), 0.31 (95%)	0.669 (from 2.6-min Ba ¹³⁷)
O ¹⁸	29.4 sec	2.9 (70%), 4.5 (30%)	1.6 (70%)	Be ¹¹¹	12 days	K capture	0.26, 0.5 (strong)
F ¹⁹	12 sec	5.1	2.2	Be ¹¹¹	12.3 days	1.022 (60%), 0.48 (40%)	0.54 (40%)
Na ²²	2.8 yr	0.575 (e ⁻)	1.28	La ¹⁴⁰	40 hr	2.26 (10%), 1.67 (20%)	2.5 (6%), 1.6 (77%), other low-energy gammas
Na ²²	15 hr	1.39	2.76 and 1.38			1.32 (70%)	
Mg ²²	9.6 min	1.8 (80%), 0.9 (20%)	1.01 (20%), 0.84 (100%)	Ce ¹⁴⁴	28 days	0.56 (30%), 0.41 (70%)	0.141 (70%)
Al ²⁶	2.3 min	3.01	1.8	Ce ¹⁴⁴	273 days	0.32	0.13 (strong)
Si ³¹	2.7 hr	1.6	None	Pr ¹⁴¹	19 hr	2.15 (96%), 0.64 (4%)	1.57 (4%)
P ³³	14.3 days	1.71	None	Pr ¹⁴¹	13.8 days	0.92	None
S ³⁵	87 days	0.167	None	Nd ¹⁴⁴	11 days	0.78 (67%), 0.17 (33%)	0.035 (strong), 0.58 (weak)
Cl ³⁶	4 × 10 ⁴ yr	0.7	Weak	Pr ¹⁴⁴	2.7 yr	0.23	None
Cl ³⁶	38 min	4.81 (53%), 2.77 (16%), 1.6 (31%), 2.13 (47%)		Sr ⁸⁵	47 hr	0.8 (33%), 0.88 (67%)	0.10, 0.07
A ³⁷	34 days	K capture, L capture	None	Hf ¹⁸⁴	46 days	0.42	0.34 (22%), 0.48 (78%)
A ³⁷	1.8 hr	1.2	1.3	Ta ¹⁸⁰	122 days	0.50	1.2 max, many others
K ⁴⁰	12.4 hr	3.58 (73%), 2.04 (25%)	1.51 (25%)	W ¹⁸²	77 days	0.43	0.134
Ca ⁴⁰	152 days	0.25	None	W ¹⁸²	25 hr	1.32 (30%), 0.63 (70%)	0.68 max, others
Sc ⁴³	85 days	1.49 (2%), 0.38 (98%)	1.12 (98%), 0.89 (100%)	Ra ¹⁸⁰	90 hr	1.00 (67%), 0.95 (30%)	0.132 (37%), 0.275 (23%)
V ⁵¹	3.9 min	2.3	1.45	Os ¹⁸⁴	15 days	0.14	0.13, 0.04
Cr ⁵¹	26.5 days	K capture	0.32 (3%), 0.267 (weak)	Ir ¹⁹²	70 days	0.67	0.65 max, many others
Mn ⁵⁴	310 days	K capture	0.84	Ag ¹⁸⁰	2.7 days	0.97	0.411
Mn ⁵⁴	2.6 hr	2.86 (60%), 1.05 (25%)	0.845, 1.81 (25%), 2.13 (15%)				
Fe ⁵⁴	2.9 yr	K capture	None	Hg ¹⁹⁷	2.7 days	K capture	0.077
Fe ⁵⁴	47 days	0.46 (50%), 0.28 (50%)	1.3 (50%), 1.1 (50%)	Hg ¹⁹⁷	44 days	0.205	0.286
Co ⁵⁷	270 days	0.26 (e ⁻)	0.131	Tl ²⁰⁴	2.7 yr	0.78	None
Co ⁵⁷	5.3 yr	0.31	1.17 and 1.33	Pb ²¹⁰	22 yr	0.028	Soft
Ni ⁵⁸	85 yr	0.06	None	Bi ²¹⁰	5 days	1.17	None
Cu ⁶¹	12.9 hr	0.57 (35%), 0.65 (e ⁻ 20%), K capture (45%)	1.34 (1%)	Po ²¹⁰	138 days	4.95 (alpha)	None
Cu ⁶¹	4.3 min	2.7	1.32	Ra ²²⁶	3.82 days	5.49 (alpha)	None
Zn ⁶⁵	250 days	0.32 (8% e ⁻), K capture (97%)	1.11 (46%)	Ra ²²⁶	1620 yr	6.7 (alpha)	0.188
Zn ⁶⁵	14 hr	IT	0.439	Th ²²⁸	1.39 × 10 ⁴ yr	4.1 (alpha)	None
Ge ⁷³	14 hr	3.17 max (see charts)	2.5 max (see charts)	Th ²²⁸	23.5 min	1.2	None
As ⁷⁵	27 hr	3.12 max (see charts)	2.1 max (see charts)	Th ²²⁸	24.1 days	0.206 (80%), 0.11 (20%)	0.093 (20%)
As ⁷⁵	40 hr	0.7	None	Pa ²³⁴	27.4 days	0.58 max (see charts)	0.471 max (see charts)
Se ⁷⁵	113 days	K capture	0.405 max (see charts)	Pa ²³⁴	1.2 min	2.32 (96%), also IT	See charts
Br ⁷⁶	38 hr	0.465	0.547, 0.787, 1.35	U ²³⁴	1.6 × 10 ⁴ yr	4.82 (alpha)	0.04
Br ⁷⁶	53.6 sec	2 (53%), 8 (45%), delayed neutrons	3	U ²³⁴	2.5 × 10 ⁴ yr	4.76 (alpha)	Weak
Rb ⁸³	19.5 days	1.32 (80%), 0.72 (20%)	1.1 (20%)	U ²³⁴	8.8 × 10 ⁴ yr	4.5 (alpha)	0.17
Se ⁸⁴	33 days	1.5	None	U ²³⁴	2.5 × 10 ⁷ yr	4.5 (alpha)	None
Y ⁸⁵	61 hr	2.2	None	U ²³⁴	4.5 × 10 ⁸ yr	4.18 (alpha)	None
Ze ⁸⁸	63 days	0.887 (2%), 0.4 (98%)	0.708 (98%)	U ²³⁴	23.5 min	1.2	0.074
Nb ⁹³	33 days	0.148	0.758				
Mo ⁹⁶	67 hr	1.2 (73%), 0.5 (23%)	0.141, 0.726				
Tc ⁹⁸	3 × 10 ⁴ yr	0.30	None				
Ru ¹⁰⁰	2.8 days	K capture	0.23				
Ru ¹⁰⁰	42 days	0.33 (50%), 0.665 (50%)	0.5 (50%)				
Pd ¹⁰⁰	13 hr	0.93	None				
Ag ¹⁰²	270 days	2.36 max (see charts)	1.5 max (see charts)				
Ag ¹⁰²	7.5 days	1.06	None				
Cd ¹⁰⁴	43 days	1.67	0.5				
In ¹¹³	50 days	IT, 2.03 (97%), K capture (3%)	0.192, 0.715 (3%), 0.548 (3%)				

Table C-3. Radioisotopes of Interest as Power Sources⁵³

Isotope	Half-Life	Specific Activity (Ci/g)	Specific Power (W(t)/g)	% Energy From			Source
				Alpha	Beta	Gamma	
Cobalt-60	5.26 yr	1133	17.4	--	3.6	96.4	Cobalt (n, γ)
Strontium-90	28.1 yr	141	0.95	--	100	neg	Fission Product
Cesium-137	30 yr	87	0.42	--	25.4	74.6	Fission Product
Cerium-144	284 day	3191	0.33	--	95.1	4.9	Fission Product
Promethium-147	2.62 yr	928	0.33	--	100	0	Fission Product
Thulium-170	130 day	5900	12.1	--	99.0	1.0	Thulium (n, γ)
Polonium-210	138 day	4500	141	100	--	neg	Bismuth (n, γ)
Plutonium-238	86 yr	17.5	0.56	100	--	neg	^{231}Np (n, γ)
Curium-242	163 day	3310	120	100	--	neg	Reactor spent fuel
Curium-244	17.6 yr	83.3	2.8	100	--	neg	Reactor spent fuel

Table C-4. Properties of Available Radioisotopic Power Sources

Properties of Available Radioisotopic Power Sources									
	¹⁴⁴ Ce	⁹⁰ Sr	¹³⁷ Cs	¹⁴⁷ Pm	⁶⁰ Co	²⁴² Cm	²⁴⁴ Cm	²¹⁰ Po	²³⁸ Pu
Compound	<chem>Ce2O3</chem>	<chem>SrTiO3</chem>		<chem>Pm2O3</chem>		<chem>Cm2O3</chem>	<chem>Cm2O3</chem>		
Half-life	284.5 days	27.7 yr	30 yr	2.67 yr	5.26 yr	162.5 days	18.1 yr	138 days	<chem>PuO2</chem> 86 yr
Activity (Ci/g)	440*	33	16	742	360 max.	3044	72.6		
Specific power (W/g)	2.84	0.223	0.0774	0.41	5.32	44.1	2.53	140	0.4
Thermal energy (Ci/W)	126	148	207	2440	65.1	1950	29.2	31.2	
Melting point (°C)	2680	1910		2350	1480	1950	1950	590	
Strength		Fair	Brittle	Good	Excellent	Fair	Fair		Good
Stability	Good in air	Good	Decreases above 1000°C	Good	Excellent	In inert gas			Good
Shielding†	3.5	1.0	3.6	Little	5.7	Neutron	Neutron		
Capsule compatibility	Reacts above 1400°C	Excellent	Excellent	Excellent	Excellent				Neutron

* After a 1-year decay.

† Number of centimeters of uranium necessary to attenuate radiation to 0.1 Gy/h at 100-cm distance with 100 W of power.

Table C-5. Savannah River Plant Feed for Plutonia Fuel Pellets

	<u>ISOTOPE</u>	<u>CONTENT</u>	
PLUTONIUM ISOTOPES	²³⁶ Pu:	0.00007	ISOTOMIC PERCENTAGE
	²³⁸ Pu:	83.62	"
	²³⁹ Pu:	13.98	"
	²⁴⁰ Pu:	1.96	"
	²⁴¹ Pu:	0.41	"
	²⁴² Pu:	0.14	"
ACTINIDES	²⁴¹ Am:	254	WT. PPM
	²³⁷ Np:	203	"
	²³² Th:	232	"
	²³⁴ U:	6,191	"

**Appendix D. Radiological Safety Comparisons of Strontium-90 with Plutonium-238 as
Fuel for RTG Space Power System**

by

Shoaib Usman*

*Doctoral student in Nuclear Engineering Program, University of Cincinnati, Cincinnati, Ohio
(April, 1994)

INTRODUCTION:

The use of the Radioisotope Thermoelectric Generators (RTG) for space applications has long been investigated and several have been used for deep-space missions. The basic principle of operation of the RTG is absorption of energy from the decay and recoil of the radioactive "fuel" and the conversion of this energy into electricity. Thus far, plutonium has been the main candidate for the RTG fuel. In a recent study at the University of Cincinnati⁽¹⁾, fuel selection criteria were evaluated with the objective to explore new fuel materials for this application.

The following four technical criteria were considered to be most significant in the selection of a fuel for space applications⁽²⁾:

(1) Half Life:

In view of the duration of the space missions of concern (about three earth years) and the demand for high specific power, a fuel with a half life of 10 to 100 years is considered to be necessary.

(2) Power Density:

A high power density is required because of the constraints on payload mass and size.

(3) Availability:

The fuel must be abundant and chemically stable and have adequate strength and proper mechanical properties to be feasible for use in an RTG.

(4) Health Physics:

Since use of massive shielding is not possible in space, the selected fuel must not produce adverse radiation exposure to personnel and instrumentation.

In view of the economics and technical considerations, the selection of fuel for an RTG is limited to only a few special radioisotopes including ^{90}Sr , ^{137}Cs , ^{238}Pu and ^{244}Cm . Use of ^{90}Sr as a fuel appears to be a likely alternative⁽¹⁾ to ^{238}Pu . Continued studies at the University of Cincinnati will determine the feasibility of the use of ^{90}Sr for RTG fuel. A dosimetric comparison will be made to investigate the potential risks to individuals from the use of ^{238}Pu and ^{90}Sr in a space vehicle.

Three periods in the manufacture and use of an RTG have been identified in which the potential exists for radiation exposure to workers and the general population. Accordingly, a safety analysis of these periods is presented;

- (1) Fabrication
- (2) Transportation, Storage and pre-Launch
- (3) Launch and Re-entry.

(1) Fabrication Period:

Details associated with the manufacture and assembly of the RTG must be considered. Dose estimates to individuals working with the RTG must be made for various stages of fuel fabrication under normal operation. These estimates must consider the chemical and physical form of the fuel isotopes at the various stages of fabrication. Moreover, realistic accident scenarios should be developed and analyzed on a probabilistic basis and include dose estimates for workers and the general public.

In the absence of details regarding the fuel fabrication procedures for the two RTG's this comprehensive analysis is not yet possible.

(2) Transportation, Storage and Launch Pad Period:

A detailed study of the form and method of storage and transportation is also required. Dose received during normal operations and possible accident scenarios should be developed for storage and transportation activities.

The spacecraft is brought to the launch pad several weeks before the launch date. This presents a long period of time during which workers have the potential to receive exposure. Dose estimates for personnel working near the RTG must be determined. Instrumentation in close proximity to the RTG will also receive exposure which may impact their operation.

(3) Launch and Re-entry Period:

The launch and re-entry period represent two times when the general population may be at risk of exposure. Therefore, a detailed probabilistic risk assessment is required for all the major malfunctions and/or accidents including determination of dispersion mechanisms and any change in chemical or physical form that may occur in the RTG fuel as a result of the accident.

A detailed comparative dosimetric study of the two RTG fuels for all the above operations is presently not available because some relevant information is lacking. Therefore, a general comparison of the two isotopes is given assuming that the fuel remains unchanged. Likewise, the solubility class of the fuel does remain unchanged.

EXTERNAL RADIATION HAZARDS:

External radiation exposure from the RTG can be significant under normal operation of transportation, storage and launch pad periods. The following factors are considered important for external dosimetry;

- (1) Type of Radiation and Abundance.
- (2) Distance and Shielding.
- (3) Duration of Exposure.

(1) Type of Radiation and Abundance:

^{238}Pu decays by alpha emission into ^{234}U , which has a half life of 2.45E5 yrs and hence can be treated as stable for an RTG during a three year mission. A very small fraction of ^{238}Pu disintegrates by spontaneous fission giving rise to neutrons having energies ranging from 1 to 10 MeV⁽³⁾. Due to a higher RBE (Relative Biological Effectiveness), these neutrons represent a serious external dose hazard and contribute about 80% of the total dose rate at any point⁽³⁾. Capture of neutrons is often followed by gamma ray emission. These photons must also be included when estimating the external gamma dose rate.

There are also some photons emitted by ^{238}Pu . A detailed description of the ^{238}Pu decay scheme is summarized⁽⁴⁾ in appendix A-1. These photons add to the external dose rate and, with the neutrons and captured gamma rays, can produce a significant external radiation exposure problem.

Both ^{90}Sr and ^{90}Y (the radioactive progeny of ^{90}Sr) emit beta particles. The half life of ^{90}Sr is approximately 30 years. The half life of ^{90}Y is only 64 hrs and decays to stable ^{90}Zr . Secular equilibrium will be established in only 2 to 3 weeks. A detail decay scheme of these isotopes is reproduced⁽⁴⁾ in appendix A-2.

For a properly designed RTG using ^{90}Sr , all the energy from ^{90}Sr and ^{90}Y will be fully absorbed reducing the external beta ray exposure to zero. However, the dose due to the *Bremsstrahlung* that are produced when the beta particles are absorbed in matter may be significant and must also be considered when calculating the external dose rate. This calculation requires specific information about the RTG design, which is not yet available.

However, for a well designed RTG using ^{90}Sr , which uses low Z material to minimize bremsstrahlung, the external dose rate from these bremsstrahlung is likely to be much smaller than that produced by the neutrons and gamma dose rate from a ^{238}Pu RTG.

(2) Distance and Shielding:

In the design of an RTG, the fuel is shielded by the cell body. For a bare sources, increasing the distance from the source is the only practical method for reducing the dose rate. Dose rates from alpha or beta particles is easily reduced to zero if the distance from the source is increased greater than the range of the particles. For alpha particle this range is very small i.e. a few centimeters in air⁽⁵⁾, hence these alpha particles do not pose any external radiation hazards. In fact even the most energetic alpha particles cannot penetrate the dead layer of the skin. Beta particles from ^{90}Sr have a range of about 143 cm in air. However, beta particles from ^{90}Y have a range of 845 cm! This aspect of shield design cannot be ignored during design of a ^{90}Sr RTG cell.

Neutrons and gamma dose rate produced by the ^{238}Pu fuel can be reduced by using shielding. For fast neutrons, shielding is based on moderation and subsequent absorption. Although borated Polyethylene⁽³⁾ can be used for this purpose, the added weight does not permit its use in space applications. For similar reasons, gamma shielding is also not feasible. The external dose rate from a ^{238}Pu RTG can be significant. According to one estimate⁽³⁾ the worst case total dose for 25 ground operation personnel can be on the order of 20 person-rem. The maximum exposure to any one individual is estimated to be 3 rem. These doses suggest that for a ^{238}Pu RTG, the external dose hazard is a serious concern.

In comparison, the external dose rate from a ^{90}Sr RTG is likely to be much lower because of the absence of neutron emission. Bremsstrahlung poses a problem for external exposure, but proper design and material selection can reduce this potential source of exposure.

(3) Duration of Exposure:

Radiation hazard for both of these RTG's can significantly be reduced by limiting the time of exposure to the radiation. This requires careful operation planning and management. Unfortunately some of these operations, such as transportation, handling etc., cannot be totally avoided. However, the exposure can be reduced by good planning.

INTERNAL RADIATION HAZARDS:

Potential for internal radiation exposure exists during the fabrication period, where various processes are performed to produce RTG's. The RTG units contain fuel isotopes in a sealed form. Therefore, there is no likelihood for internal radiation exposure under normal operation. However, in case of an accident during transportation and launch period there is some potential for exposure. This risk for public exposure is even more critical for accidents during launch and re-entry period.

A detailed safety analysis of these periods would involve probabilistic risk assessment of all of the potential accident scenarios. The dose estimates for these cases should carefully analyze the specific pathway. This type of investigation requires extensive specific data and is therefore beyond the scope of the present work.

There are two significant pathways (for radionuclides) for internal exposure: inhalation and ingestion. Comparison of both of these pathways is required for the two fuel isotopes. The

It is important to keep in mind that the chemical form of an isotope is important in determining its biological pathway and the dose to an exposed individual. For example ^{90}Sr , when inhaled as a soluble salt (such as SrCl_2), clears very rapidly⁽⁶⁾. This will result in a much smaller dose than if the ^{90}Sr was inhaled as SrTiO_3 , which clears much more slowly. Following ingestion, however, the dose from a unit intake of a soluble salt of ^{90}Sr is greater than the insoluble compound.

The isotopes of alkaline earth materials with radioactive half lives greater than 15 days are assumed to be uniformly distributed throughout the volume of mineral bone⁽⁷⁾, whereas isotopes with the radioactive half lives less than 15 days are assumed to be distributed in a thin layer over bone surface. ^{90}Sr is therefore assumed to be uniformly distributed throughout the volume of mineral bone. ^{90}Y produced due to the decay of ^{90}Sr is also assumed to decay and deposit its energy at the location of its birth ($T_{1/2} = 64$ hrs). This makes bone the critical organ for ^{90}Sr .

Based on the extensive data available it is suggested that no compound of plutonium should be considered to be very soluble⁽⁸⁾. PuO_2 is assumed to be insoluble⁽⁸⁾. All the other compounds of plutonium are intermediate in solubility⁽⁸⁾. The retention of Plutonium in the lungs is very complex. It is generally agreed that ^{238}Pu inhaled eventually concentrates in the skeleton and the liver⁽⁹⁾. Slower clearance from bone makes it the critical organ for ^{238}Pu . Retention of ^{238}Pu by gonads is also reported in literature, but the retention factor is much too small to cause any significant dosimetry effects.

For both inhalation and ingestion pathways, the Annual Limit of Intake (ALI) for all the important isotopes have been computed⁽¹⁰⁾ by the International Commission on Radiological Protection (ICRP). This limit suggests that the maximum intake of a radionuclide (in Bq.) in a specific chemical and physical form (i.e. solubility class) without exceeding the allowable effective dose, i.e., 5 rem for the whole body and 50 rem for any specific organ⁽¹¹⁾.

The dosimetric comparison of the two RTG fuels is based on the ALI's. It is appropriate for this study to compare the respective ALI's (for both pathways i.e. inhalation and ingestion) of the two isotopes in question to estimate their relative radiological impact. Using these ALI's, the limiting weight of the radionuclide in question (^{238}Pu for PuO_2 fuel and ^{90}Sr for SrF_2 fuel) and

hence the maximum allowable mass intake of the fuel can be determined (i.e. mass of PuO_2 and SrF_2) for each pathway. These numbers along with the respective specific power will provide the dose per unit power produced for the case when as a result of an accident all the fuel was inhaled or ingested by individuals.

These estimates are highly conservative because not every gram of fuel will realistically be taken up by individuals. For the case of inhalation, dose is calculated assuming a particle size of 1 μm diameter. This again is very conservative and the average actual size of the particles would be much larger. Fuel particles size of PuO_2 RTG is reported to be 50-250 μm diameter⁽¹²⁾. These larger particles will be filtered out during inhalation and the actual dose would be significantly lower. With these conservative approximations, the following comparison is possible (indicated in the tables which follow);

Comparison of Inhalation Pathway.

	Pu	Sr
01) Compound.	PuO_2	SrF_2
02) Specific Power Watt/ gm fuel.	0.418	0.304
03) Solubility Class.	Y	D
04) f_1 = Fraction of activity absorbed through G.I. Track.	10^{-5}	0.3
05) ALI (Bq.) Whole Body (Bq/0.05 Sv.).	6.0 E2	7.0 E5
06) Critical Organ.	Bone Surface.	Bone Surface.
07) ALI (Bq.) Critical Organ (Bq/0.5 Sv.).	6.0 E2	8.0 E5
08) Limiting Mass of the Isotope(gm /0.5 Sv.).	9.50 E-10	1.53 E-7
09) Maximum Allowable Fuel Mass Intake(gm/0.5 Sv.).8	7.00 E-10	5.90 E-8
10) Dose per μgm of fuel Intake (Sv./ μgm).	716.23	8.45
11) Dose per unit Power (Sv./ μWtt).	1713.5	27.79

Comparison of Ingestion Pathway.

	Pu	Sr
01) Compound.	PuO ₂	SrF ₂
02) Specific Power Watt/ gm fuel.	0.418	0.304
03) Solubility Class.	Y	D
04) f1= Fraction of activity absorbed through G.I. Track.	10 ⁻⁵	0.3
05) ALI (Bq.) Whole Body (Bq/0.05 Sv.).	3.0 E6	1.0 E6
06) Critical Organ.	Bone Surface.	Bone Surface.
07) ALI (Bq.) Critical Organ (Bq/0.5 Sv.).	3.0 E6	1.0 E6
08) Limiting Mass of the Isotope(gm /0.5 Sv.).	4.74 E-6	1.90 E-7
09) Maximum Allowable Fuel Mass Intake(gm/0.5 Sv.).	3.50 E-6	7.40 E-8
10) Dose per μ gm of fuel Intake (Sv./ μ gm).	0.143	6.67
11) Dose per unit Power (Sv./Watt).	0.342	21.94

SUMMARY AND CONCLUSION:

Three operational periods with the potential for human exposure were identified for the RTG. External exposure is most significant for transportation and launch pad periods. Launch pad period also has a potential for exposure to the instrumentation and electronics. Neutrons and photons from a ^{238}Pu RTG can cause a significant dose rate while the ^{90}Sr RTG will pose external dose problem only due to the bremsstrahlung. This external dose from a ^{90}Sr RTG is likely to be significantly lower than that from a ^{238}Pu RTG.

Fabrication period is the most plausible period for internal exposure to the workers, both under normal operation and under accidents. Launch and re-entry periods were identified as the most significant potential for both public and workers internal exposure under accident scenarios.

The internal dosimetry analysis requires extensive data on the various parameters involved in pathway analysis. However, this preliminary comparison based on very conservative assumptions indicated that the inhalation per unit mass of fuel from ^{238}Pu is 2 order of magnitude higher than the dose per unit mass intake of ^{90}Sr . This makes ^{238}Pu much more serious concern for internal dosimetry via inhalation. Results were found to be quite reverse for dose due to ingestion where the dose from a unit mass intake of ^{90}Sr was an order of magnitude higher than that from ^{238}Pu .

However, it should be kept in mind that extensive monitoring and a greater degree of control is possible for ingestion as opposed to inhalation. Therefore, the actual potential hazard from ^{238}Pu RTG is considered to be much more than that from a ^{90}Sr RTG.

It was also pointed out that both the chemical and physical form are likely to change during various fabrication stages and in a post accident pathway. This aspect of pathway analysis was identified as important but could not be accounted for in this preliminary study. A parallel set of detailed safety analysis is recommended for each one of the RTG fuel candidates for a precise comparison.

REFERENCES:

- (1) Anno, J. N., Stubbers, R., and Winiarski, R.; "Selection of fuel for RTG's in space power systems", Work in progress at the University of Cincinnati.
- (2) Anno, J. N., Private Communication, University of Cincinnati, December 12, 1993.
- (3) Normand, E., Proud, L. A., Wert, J. L., Oberg, D. L. and Criswell T. L.; "Effect of Radiation from an RTG on the Installation, Personnel and Electronics of a Launch System", Space Nuclear Power Systems, 1989, Orbit Book Company, Malabar, FL, 1992.
- (4) Browne, E. and Firestone, R. B.; "Table of Radioactive Isotopes", Lawrence Berkeley Laboratory, University of California, Wiley Interscience Publication.
- (5) Camber, H. "Interaction of Radiation with matter":, Introduction to Health Physics, 2nd Edition, Pergamon Press, New York.
- (6) Morrow, P. E., Gibb, F. R., Davies, H. and Fisher, M.; "Dust removal from the Lung parenchyma"; an investigation of clearance simulation Toxicol. Appl. Pharmacol. 12, 372-396, 1968.
- (7) ICRP Publication 30, Part 1, "Limits for intakes of radionuclides by workers", Chapter 7 (Dosimetric Model for Bone).
- (8) ICRP Publication 19, "The Metabolism os Compounds of Plutonium and Other Actinides", Pergamon Press, New York, 1972.
- (9) Park, J. F., Catt, D. C., Craig, K. D., Olson, R. J. and Smith, V. H.; "Solubility Changes of Pu^{238} Oxides in water suspension and effect on biological behavior after inhalation by Beagle dogs", In: Proc. Third Int. Cong. Int. Rad. Prot. Assn., Washington, D.C., September 1973, Ed. Snyder, W. S., Vol. 1. 719-724.
- (10) ICRP Publication 30, "Limits for intakes of radionuclides by workers", Pergamon Press, New York.
- (11) ICRP Publication 26, "Recommendation of the International Commission on Radiological Protection", Pergamon Press, New York.
- (12) Prosser, D. L., "SNAP-27 Radioisotopic Heat Source Summary Report", Mound Laboratory, November 11, 1969.

Appendix E. RTG Analysis Code

```

integer dumx,dumy,dumz,m,n,p
dimension T(27,27,27), q(27,27,27), k(27,27,27)
real dx,dy,dz,th,tc,thavg,dt,tcavg,rp,rn,nm,pm,l
real rins,mup,mun,nu,nud,kins,kfwpf,kal,kcu,kpg
real rsr,hsr,ksr
l=2.0
print*, 'enter Th'
read*, th
thavg=th
print*, 'guess average Tc'
read*, tcavg
print*, 'enter number of nodes in each direction'
read*, m
print*, 'enter initial radius of p leg'
read*, rp
qgen=1.5372
thmo=0.0889
ksr=.02093
kpg=1.0
kal=4.01
kfwpf=.60
kcu=3.80
thcu=0.1
thal=0.5
thalumina=1.0
print*, 'Enter thickness of Pyrolytic Graphite'
read*, thpg
print*, 'Enter thickness of Fine-Weave-Pierced-Fabric'
read*, thfwpf
thcasing=1.0
print*, 'Enter temperature of surroundings'
read*, tbulk
print*, 'Enter initial guess of surface temperature'
read*, tsurf
print*, 'Enter desired power level (in watts)'
read*, pwr
c This sets the desired output voltage, change as needed
vdes=24
print*, 'Enter the number of parallel leads'
read*, npara
print*, 'Enter the desired length of SrF2 source'
read*, hsr
qins=25.0

```

```

thot = 0
tcold = 0
count = 0
countp=0
lcount=0
countn=0
countins=0
thins=0
tcins=0
prevc=10
prevh=20
c Definition of thermo material properties
do 310 w=1,20
dt=thavg-tcavg
qe=1.6E-19
nm=1E18
mun=1900
alphan=2.6
kn=5.0
pm=1E18
mup=500
alphap=2.3
kp=5.0
kins=.0175
dt=thavg-tcavg
ron=(1+alphan*((thavg**2-tcavg**2)/(2*dt)-292))*1(1/(mun*nm*dt*qe))
rop=(1+alphap*((thavg**2-tcavg**2)/(2*dt)-292))*1(1/(mup*pm*dt*qe))
aopt=1/(1+((kn/kp)*(rop/ron))**.5)
rn=rp*(aopt/(1-aopt))**.5
if (thavg.gt.1300) then
  thavg=1300
endif
zhn=(-.595+.00531*thavg-8.54E-6*thavg**2+4.6E-9*thavg**3+
1 1.21E-12*thavg**4-1.25E-15*thavg**5)*.001
zhp=(-.227+.00205*thavg-2.29E-6*thavg**2+1.61E-9*thavg**3-
1 3.77E-13*thavg**4-1.19E-16*thavg**5)*.001
zcn=(-.595+.00531*tcavg-8.54E-6*tcavg**2+4.6E-9*tcavg**3+
1 1.21E-12*tcavg**4-1.25E-15*tcavg**5)*.001
zcp=(-.227+.00205*tcavg-2.29E-6*tcavg**2+1.61E-9*tcavg**3-
1 3.77E-13*tcavg**4-1.19E-16*tcavg**5)*.001
shn=(zhn*ron*kn)**.5

```

```

shp=(zhp*rop*kp)**.5
scn=(zcn*ron*kn)**.5
scp=(zcp*rop*kp)**.5
sh=(shn+shp)/2
sc=(scp+scn)/2
s=sh+sc
z=(s**2)/(((kn*ron)**.5 + (kp*rop)**.5)**2)
tavg=(sh*thavg + sc*tcavg)/(2*s)
dummy=(1+z*tavg)**.5
vopt=s*dt*(1/(1+1/dummy))
effte=(dummy)/(((dummy+1)**2)/(z*dt)+(.5+(tavg/dt))*(dummy+1)-.5)
print*, effte
c This starts the third segment
c Calculate dimensions of SrF2 source
qtot=pwr/effte + qins
vol=qtot/qgen
c Determine the axial positions
nser=(vdes/vopt)+1
rsr=(vol/(3.14159*hsr))**0.5
n=m
p=m
dx=hsr/(npara*m)
dy=(3.14159*rsr)/(nser*n)
dz=l/p
deltax=hsr/npara
deltay=(2*3.14159*(rsr+thmo))/nser
c Calculate centerline temp of SrF2
qnode=qtot/(nser*npara)
tmoi=(qnode*log((rsr+thmo)/rsr))/(2*3.14159*hsr*ksr)+thavg
tcenter=((qgen*rsr**2)/(4*ksr))+tmoi
c Calculate surface temperature of RTG
rrtg=(rsr+thmo+l+thcu+thal+thalumina+thpg+thfwpf+thcasing)
drtg=2*rrtg
asurf=2*3.14159*rrtg*hsr
beta=(1/tbulk)
nu=(2.248388E-10)*(tbulk**1.845)
230 rad=(3.75*0.76*beta*(tsurf-tbulk)*drtg**3)/(nu**2)
nud=(0.6+0.32296*(rad**0.16667))**2
h=(nud*15.2E-3)/drtg
qprime=h*asurf*(tsurf-tbulk)+4.608E-8*asurf*(tsurf**4-tbulk**4)
eps=(Qprime-qtot)/qtot
if (eps.gt.1) then
    Tsurf=Tsurf-.01

```

```

    goto 230
  endif
  if (eps.lt.-1) then
    Tsurf=Tsurf+.01
    goto 230
  endif
  Rthree=rsr+thmo+l
  Rfour=rthree+thcu+thal
  Rfive=rfour+thpg
  Rsix=rfive+thfwpf
  Rseven=rsix+thcasing
  Tone=qtot/(2*3.14159*hsr)
  Ttwo=(log(rfive/rfour))/kpg
  Tthree=(log(rsix/rfive))/kfwpf
  Tfour=(log(rseven/rsix))/kal
  tfive=(2*3.14159*hsr*kins)/(log(rfour/rthree))
  tsix=((log(rfour/rthree))/(2*3.14159*hsr*kcu)+(log(rfour/rthree))/
  1(2*3.14159*hsr*kal))**-1
  tcshoe=tone*(ttwo+tthree+tfour)+tsurf+qtot*(tfive+tsix)**-1
  current=pwr/vdes
  if (lcount.gt.1) then
    goto 300
  endif
  do 10 z=2,p+2
  do 20 x=2,m+2
  do 30 y=2,m+2
    t(x,y,z)=300
    lcount=2
    distn=((x-1)*dx-.25*m*dx)**2+((y-1)*dy-.5*n*dy)**2
    distp=((x-1)*dx-.75*m*dx)**2+((y-1)*dy-.5*n*dy)**2
    if ((distn.gt.rn**2).and.(distp.gt.rp**2)) then
      q(x,y,z)=0
      k(x,y,z)=1.75
    endif
  300  if (distn.le.rn**2) then
    k(x,y,z)=5
    q(x,y,z)=(current/(npara*nser))**2 * ((3.14159*ron*rn**2)/l)
    countn=1
  endif
  if (distp.le.rp**2) then
    k(x,y,z)=5
    q(x,y,z)=(current/(npara*nser))**2 * ((3.14159*rop*rp**2)/l)
    countp=1

```

```

    endif
30 continue
20 continue
10 continue
if (countn.lt.1) then
    i=distn
    j=.5*n
    do 40 kz=2,p+2
        k(i,j,kz)=5
        q(i,j,kz)=((current/(npara*nser))**2) * ((3.14159*ron*rn**2)/l)
40 continue
endif
if (countp.lt.1) then
    i=distp
    j=.5*n
    do 50 kz=2,p+2
        k(i,j,kz)=5
        q(i,j,kz)=((current/(npara*nser))**2) * ((3.14159*rop*rp**2)/l)
50 continue
endif
do 60 x=1,m+3
do 70 y=1,n+3
    t(x,y,1)=th
70 continue
60 continue
do 90 x=1,m+3
do 100 y=1,n+3
    t(x,y,p+3)=tcshoe
100 continue
90 continue
do 200 it=1,100
do 110 z=2,p+2
do 120 x=2,m+2
do 130 y=2,n+2
    termone=((dy*dz)/dx)*(t(x+1,y,z)+t(x-1,y,z))
    termtwo=((dx*dz)/dy)*(t(x,y+1,z)+t(x,y-1,z))
    termthr=((dx*dy)/dz)*(t(x,y,z+1)+t(x,y,z-1))
    termfour=(q(x,y,z)*dx*dy*dz)/k(x,y,z)
    termfive=(dy*dz)/dx+(dx*dz)/dy+(dx*dy)/dz
    t(x,y,z)=.5*(termone+termtwo+termthr+termfour)/termfive
130 continue
120 continue
110 continue

```

```

do 140 z=2,p+2
do 150 x=2,m+2
  t(x,1,z)=t(x,3,z)
  t(x,n+3,z)=t(x,n+1,z)
150  continue
  do 160 y=2,n+2
    t(1,y,z)=t(3,y,z)
    t(m+3,y,z)=t(m+1,y,z)
160  continue
140  continue
200  continue
  tcold=0
  tcins=0
  do 170 y=2,n+2
  do 180 x=2,m+2
    Tcold=t(x,y,p+2)+tcold
    if (q(x,y,P+2).eq.0) then
      tcins=tcins+t(x,y,p+2)
    endif
180  continue
170  continue
  countins=0
  qpres=0
  countq=0
  thot=0
  thins=0
  do 220 y=2,n+2
  do 210 x=2,m+2
    thot=thot + t(x,y,2)
    if (q(x,y,2).eq.0) then
      countins=countins+1
      thins=thins+t(x,y,2)
    endif
210  continue
220  continue
  do 280 x=2,m+2
  do 270 y=2,n+2
  do 260 z=2,p+2
    if (q(x,y,z).eq.0) then
      qpres=kins*dz*(t(x,y,z-1)-t(x,y,z+1))+qpres
      countq=countq+1
    endif
260  continue

```

```

270 continue
280 continue
tcavg=tcold/((m+1)*(n+1))
thavg=thot/((m+1)*(n+1))
tcinsavg=tcins/(countins)
thinsavg=thins/(countins)
rfour=rsr+thmo+l+thcu+thal
rtwo = rsr+thmo
Rins=(log(rfour/rtwo))/(2*3.14159*hsr*kins)
qins=qpres/countq
hconverge=(thavg-prevh)/prevh
cconverge=(tcavg-prevc)/prevc
prevh=thavg
prevc=tcavg
310 continue
efficiency=pwr/qtot
open (unit=15,file='theend',status='unknown')
write (15,*) 'Sr centerline temp: ',tcenter
write (15,*) 'surface temperature: ',tsurf
write (15,*) 'thot: ',thavg
write (15,*) 'tcold: ',tcavg
write (15,*) 'efficiency: ',efficiency
write (15,*) 'Radius of Sr: ',rsr
write (15,*) 'SiMo Thickness: ',thmo,rtwo
write (15,*) 'Length of TEs: ',l,rthree
write (15,*) 'thickness of Cu leads: ',thal,(rfour-thal)
write (15,*) 'thickness of Al seals: ',thcu,rfour
write (15,*) 'thickness of PG: ',thpg,rfive
write (15,*) 'thickness of fwpf: ',thfwpf,rsix
write (15,*) 'thickness of Casing: ',thcasing,rseven
stop
end

```

6.0 SOIL ANALYSIS

Richard Hampton
Marlon Santos

TABLE OF CONTENTS

6.1 INTRODUCTION.....	6.1
6.2 DESIGN GOAL	6.1
6.2.1 THERMAL/DRILL PROBE	6.1
6.2.2 X-RAY DIFFRACTOMETER.....	6.2
6.3 PROPOSED DESIGN.....	6.3
6.3.1 THERMAL/DRILL PROBE	6.3
6.3.2 THERMAL/DRILL PROBE SUPPORT EQUIPMENT.....	6.8
6.3.3 SOIL SAMPLING/PREPARATION INTRODUCTION	6.8
6.3.4 X-RAY DIFFRACTOMETER.....	6.13
6.4 DESIGN BASIS	6.22
6.4.1 THERMAL/DRILL PROBE AND SUPPORT EQUIPMENT	6.22
6.5 REFERENCES	6.25
6.6 APPENDIX	6.26

6.1 INTRODUCTION

This is the design of a soil analysis system including an x-ray diffractometer and a thermal/drill probe. The thermal/drill probe is a device that could simultaneously melt and drill its way through the frozen polar caps of the martian surface, take pictures, and collect data from several sensors at varying depth below the surface. The x-ray spectrometer would be used to analyze mineral contents of the martian soil. We already know from previous martian expeditions that heavy elements such as silicon and aluminum are found in the crust; but not what form they are in, such as alumina or silica. An x-ray diffractometer would provide this information. This report will describe a possible design for an x-ray diffractometer and thermal/drill probe that could be used in space.

Some of the issues to be discussed for the x-ray generation are soil sample preparation and scattering detection. X-ray generation is complicated by a limited power supply and target cooling method (no constant running water supply). Soil sample preparation is complicated by large amounts of ice present in the polar region. These and many other problems and limitations were addressed during the design of this diffractometer.

6.2 DESIGN GOAL

6.2.1 Thermal/Drill Probe

The design goal for the thermal/drill probe is to develop a platform and vehicle for several sensors to preform and collect data below the martian polar cap. The first objective is to develop the probe itself. The second objective is to develop support equipment and housing for the probe.

The main concern of the first objective is the actual composition and consistency of the polar cap. It is known from previous martian expeditions that the surface soil has a consistency ranging from boulders, to gravel, to dust. Dust storms are prevalent, therefore, the consistency of the ice and dust is questionable. The probe design will have the ability to descend through the ice at a fairly constant rate, to acquire data at varying depths. The martian gravitational pull is roughly one-third that of Earth. Since the probe should be light and compact, the reliance of the martian gravity as a method of movement and guidance is not very good.

It is apparent that the thermal/drill probe is not part of the vital function of the martian lander. But, it is an additional piece of scientific equipment. Therefore, the design of the support equipment and housing contains some flexibility. This design is dependent on the capabilities of the rover. If the rover is capable of carrying or dragging the thermal/drill system, then it would allow for data collection at multiple sites. If the rover is not capable of performing these tasks, then the thermal/drill system will reside in the lander. The support equipment will consist of a computer & power system. The computer will be for data collection and storage. It would also be used for the thermal/drill guidance control and sensory operations.

6.2.2 X-ray Diffractometer

The goal for the Materials Science group was to design an x-ray diffractometer that could be transported to Mars aboard a proposed unmanned martian polar probe. NASA has recently been trying to cut costs recently by using more commercial products. In the past nearly all parts used for NASA equipment were specially designed for a single application. This is very expensive. Many commercial products can be used with slight or no modification. Part of the goal for this project is to try and find as many commercial products as possible to be used in the

design of the diffractometer. This design is limited by the amount of power that can be supplied, the amount of mass that can be taken, and a lack of a constant water supply used in nearly all commercial diffractometers as a cooling agent. Power up to 250 Watts will be available from batteries, solar cells, etc.. Most commercial diffractometers require at least 2 kilowatts. While there was no specific size goal it should generally be designed on a small scale. Cathode ray tubes used for the diffractometer will melt if not properly cooled, typically done by running a constant stream of water behind the target anode. The design goal for this problem will be to propose a cathode ray tube with an alternate method of heat removal, one that doesn't produce so much heat or a combination of both. Another design consideration is to develop a method of soil sample preparation. Soil cannot be analyzed as is, it must be powdered. Thus processes and equipment to deal with these problems and limitations will be discussed in this paper.

6.3 PROPOSED DESIGN

6.3.1 Thermal/Drill Probe

The thermal/drill probe consist of two parts. The first is the thermal/drill probe itself. The second is the support equipment and housing.

The thermal/drill probe is shown in Figure 1; the dimensions and shape of the probe are similar to an enlarged "test tube." The probe housing contains the motor, several sensors, lamps, mirror, camera, and coil coaxial cable. The housing has the appropriate windows for the camera and sensors that require it. The external features are the lower thermal/drill head and the four upper thermal guiding fins.

The thermal/drill head is directly connected to the motor shaft. The drill is designed for slow speed drilling with grooved track on the flat side of the head (the drill-housing interface

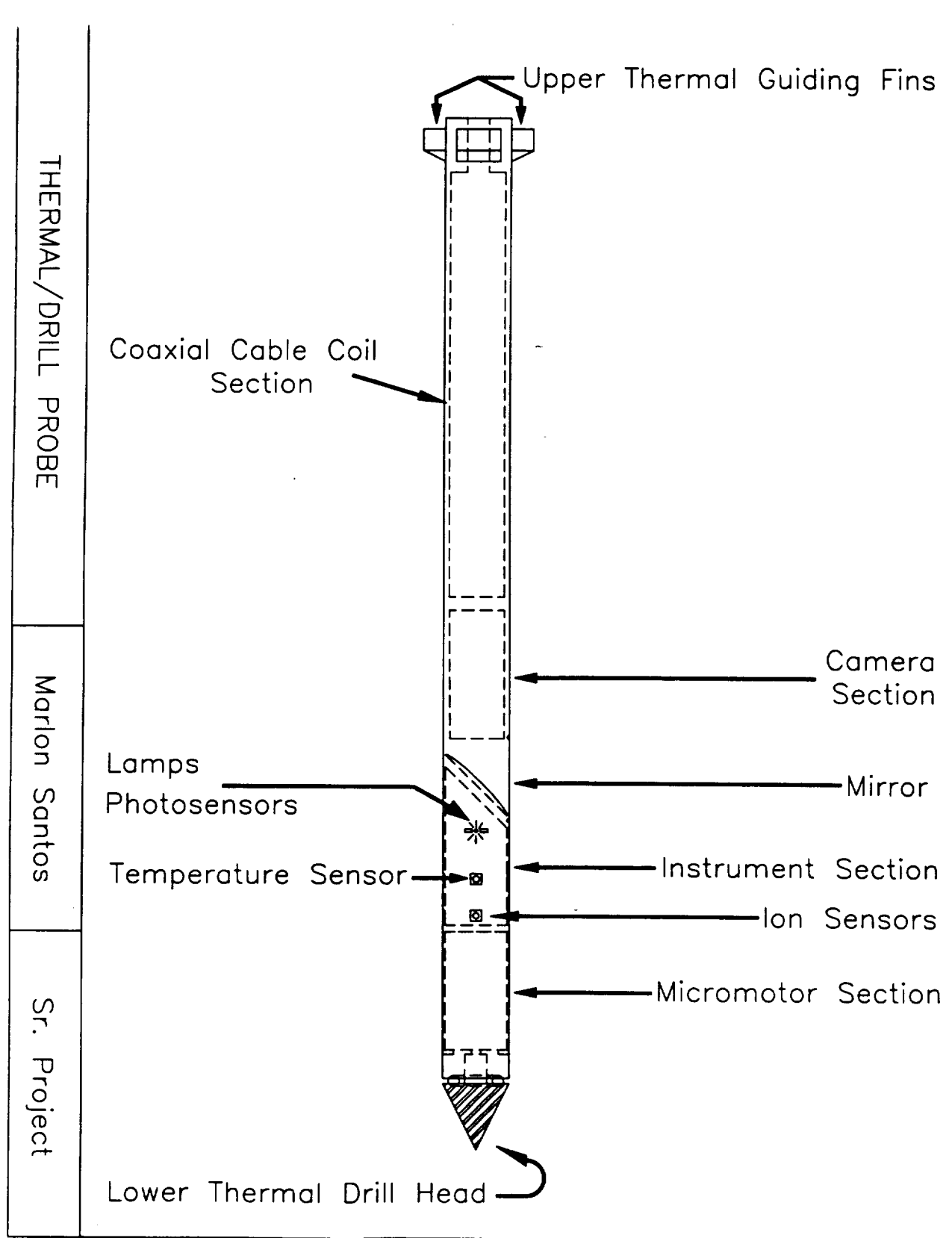


FIGURE 1. Thermal/Drill Probe Design

area) [See Figure 2]. This groove is for ball bearings to sit in. There are heating elements within the drill head which disburse the heat throughout.

6.3.1.1 Motor

The motor to drive the thermal/drill head is mounted to the lower part of the probe housing. The motor's speed is controlled by the computer. The concept is very simple; it is similar to the throttle of a remote control car. The only difference is that the computer and the program is the operator, rather than a person.

6.3.1.2 Ball Bearings

The ball bearings sit in the doughnut shape groove between the lower part of the probe housing and the thermal/drill head. It has three functions. The obvious one is to allow for free movement of the drill head. The second function is to give support to the probe housing to the thermal/drill head, because the weight of the probe is transferred to that area. The third function is to be an electrical connection from the probe housing to the heating elements within the drill head.

6.3.1.3 Thermal Fins

The four thermal fins on the upper part of the probe housing is use to help guide the probes decent through the ice. It contains heating elements within, which would be controlled by the computer.

6.3.1.4 Instrumentation

The instrument section will contain a camera-mirror system, high precision temperature sensor, pressure transducers, electrical resistivity sensors, solid state ion sensors, and four multispectral photometers. The sensors will be flush mounted along the outside of the probe housing.

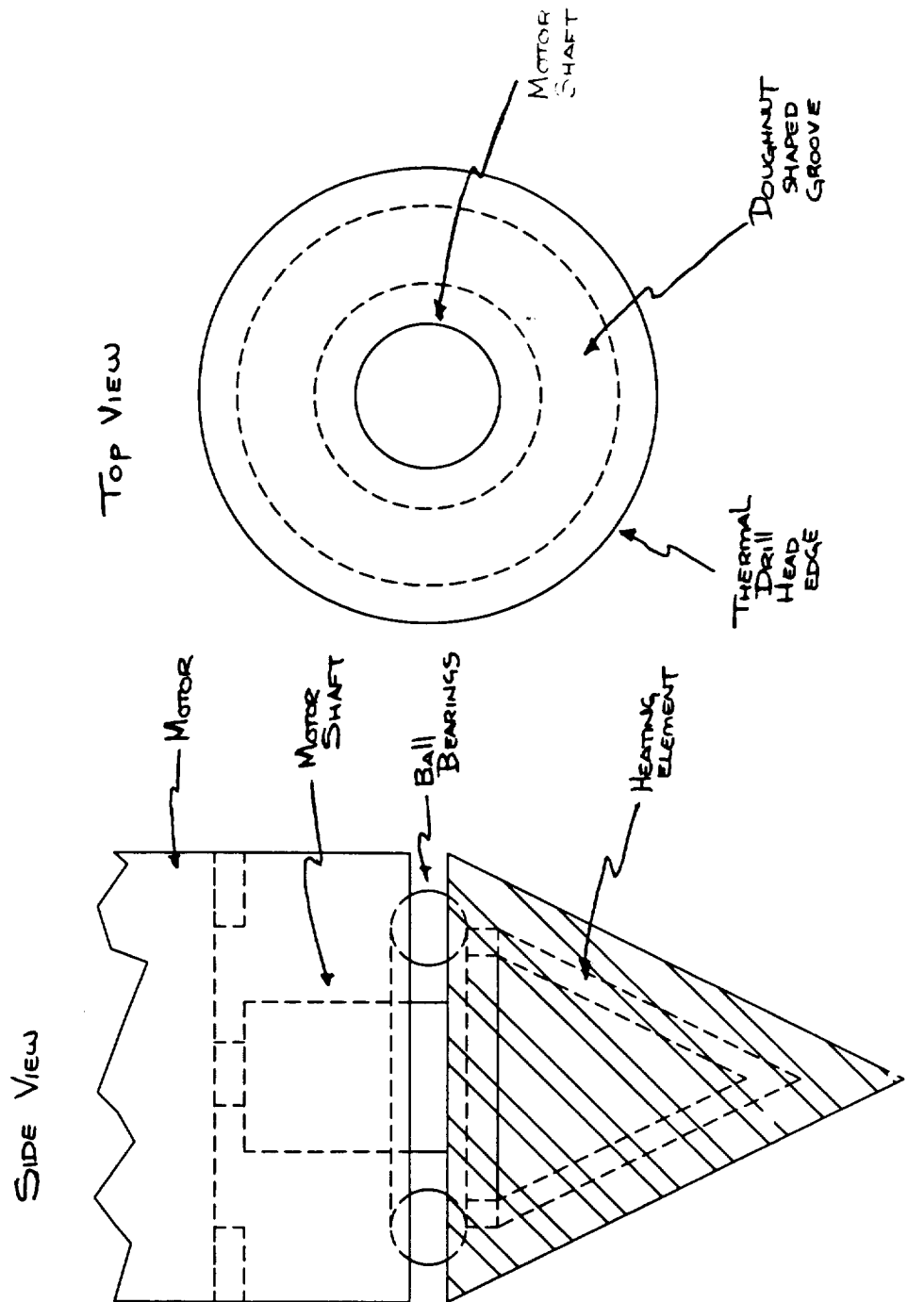


FIGURE 2. Thermal/Drill Head Design

Thermal/Drill Head Design

Marlon Santos Sr. Project

6.3.1.4.1 Camera and Mirror

The camera system will allow for a visual depiction as the probe descends through the ice. The camera is a Sony XC-999 cigar type CCD camera which is focused at an angled mirror and out the window of the probe housing.

6.3.1.4.2 Sensors

The high precision temperature sensors will be used to determine the ambient temperature of the ice. The pressure transducer will collect pressure data as it descends through the ice. AC and DC electrical resistivity sensors will provide information concerning the ambient electrical conductivity of the ice, and the total ionic content of the melt water. The solid state ion sensors are electrodes made from uniform solid materials that produce differential voltages in proportion to the log of the concentration of specific aqueous ionic species (Orion, 1927). Using present-day commercially available technology, the concentration of H^+ , Na^+ , Cl^- , S_2^- , in the meltwater that surrounds the thermal probe can easily be measured with these electrodes as function of depth. The multispectral photometers will consist of 8 channel linear reticon arrays on either side of small tungsten lamps mounted on all four sides of the probe. Every 5 seconds, the lamps will briefly illuminate the walls of the water filled cavity created by the probe as it descends. The windows for the arrays will focus and disperse the light reflected from the walls of the cavity to give crude reflectance spectra at eight wavelengths (Paige 1992).

6.3.1.5 Coiled Cable

The coiled cable compartment will contain 150 meters of coaxial cable, which is contained in a orthocyclically-wound coil for maximum dense packing. This is its link for power and data handling the cable is capable of handling up to 440W at 300V DC. The high voltage power supply is required to minimize ohmic dissipation in the cable (Paige, 1992).

6.3.2 Thermal/Drill Probe's Support Equipment

The support equipment and home for the thermal/drill probe has 3 options.

6.3.2.1 Option 1: The "Mine Design"

"Drop and forget," this option (shown in Figure 3) is a total self-reliant thermal/drill probe. The basis of this design is the dependency on the rover capabilities. This design would include the thermal/drill probe, computer system, battery system, and transmitting system. The dome shell would protect the support equipment and would be covered with flexible solar cells to serve as a source of power and to recharge the battery system.

6.3.2.2 Option 2: The "Tethered Design"

"Drag and drop," the basis of this design (shown in Figure 4) is contingent on whether the rover could carry the lightened equipment and drag the umbilical cord to the lander. The transmitting system would be eliminated and the battery system, solar cells array, and computer system, would be apart of the main system aboard the lander. The over all carried equipment would be the thermal/drill probe, relay equipment, and the protective shell. The tethered cord would be the umbilical cord to the lander where support equipment resides.

6.3.2.3 Option 3: The "Lander Design"

This option is the fall back design because everything is housed on the lander. No rover system is required. The support equipment is essentially a part of the main lander system, which consist of the battery system, computer system and the solar cell arrays.

6.3.3 Soil Sampling/Preparation Introduction

Diffraction of soil samples is a common practice in the field of geology. Geologists have profiled mineral contents of soil from all around the world. This is an important practice for finding rich areas of resources. It is accomplished by a fairly simple process. Obtain soil

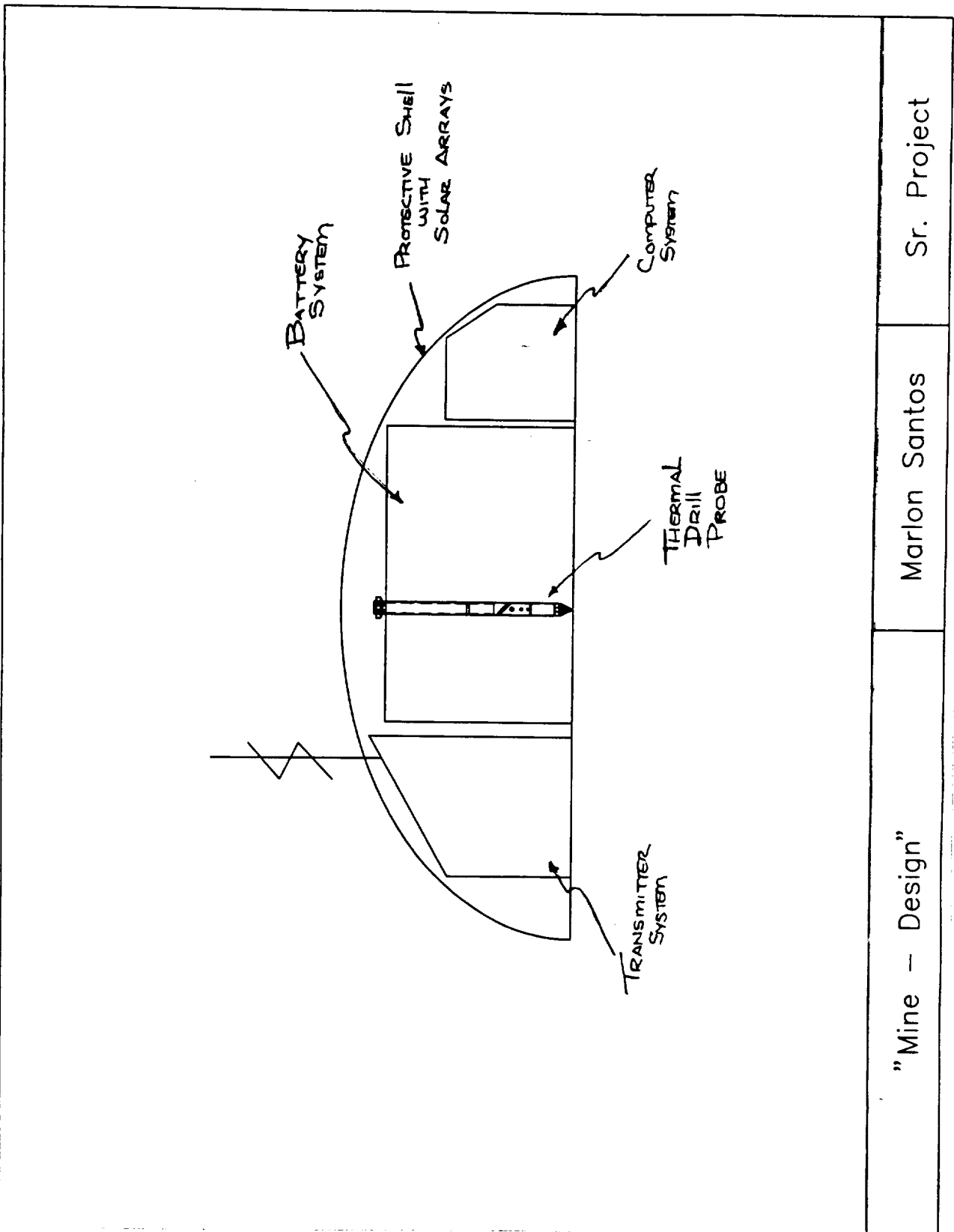


FIGURE 3. The Mine Thermal/Drill Probe

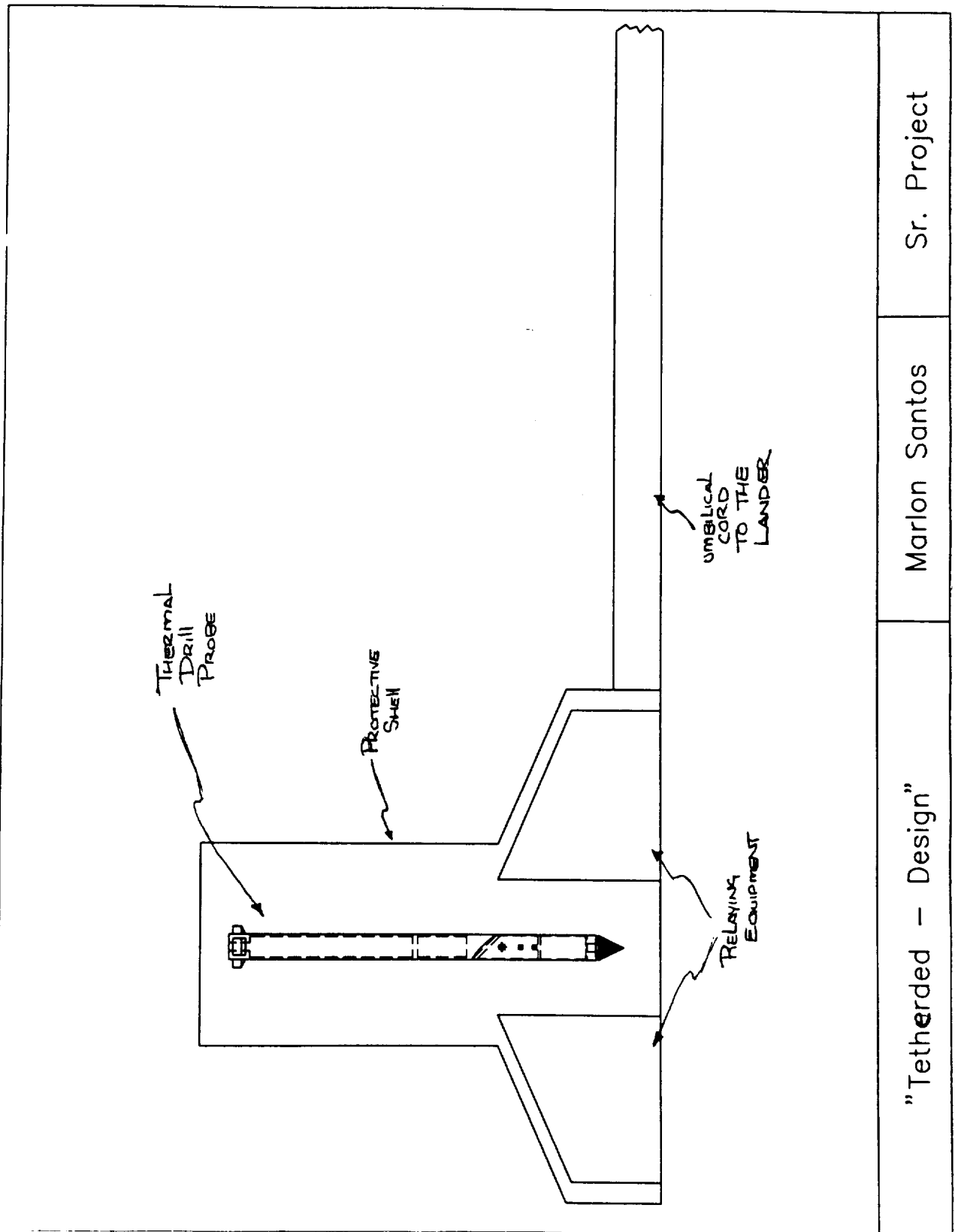


FIGURE 4. The Tethered Thermal/Drill Probe

samples. Dry off water content with heat. Crush the dried soil, and use a standard commercial diffractometer (built by Philips, Siemens, Rigaku etc.) to obtain diffraction patterns which can be compared to known data for nearly all materials. This process can be followed in designing a method for diffraction on Mars except that commercial diffractometers are too bulky and fragile for transport through space.

6.3.3.1 Soil Sampling

The first necessity for diffraction is a soil sample. This can be obtained easily by use of the rovers. The short range rovers are equipped with an auger and a sampler. The auger is used for digging into and profiling the ice and soil. This will produce broken up soil around the auger which could be picked up by the sampler. While there are other uses for the soil samples, the rover could return to the lander with enough soil for diffraction. It would require approximately one cubic inch of material. The rover would deposit such a sample into an orifice leading to preparation for diffraction. The rover has already been designed with these capabilities and requires no special designing on our part.

6.3.3.2 Soil Sample Preparation

As previously stated, the soil must be dried and powdered. This can be done as follows. When the rover drops the soil sample in the orifice it will fall into a small mortar dish (See Figure 5). Inside this stainless steel mortar is where the sample will be wrapped with common heating coils such as 'calrod' used as stove top heating units. Due to the extremely low pressure of the Martian atmosphere, water will vaporize well below 100 °C and proper drying can occur at a temperature between 100-150 °C. This temperature range can be achieved in the small chamber by running 200 watts of power at 100 volts through the calrod coils (most ovens using calrod run at 1000 watts and 200 volts and achieve temperatures over 500 °C and must heat a

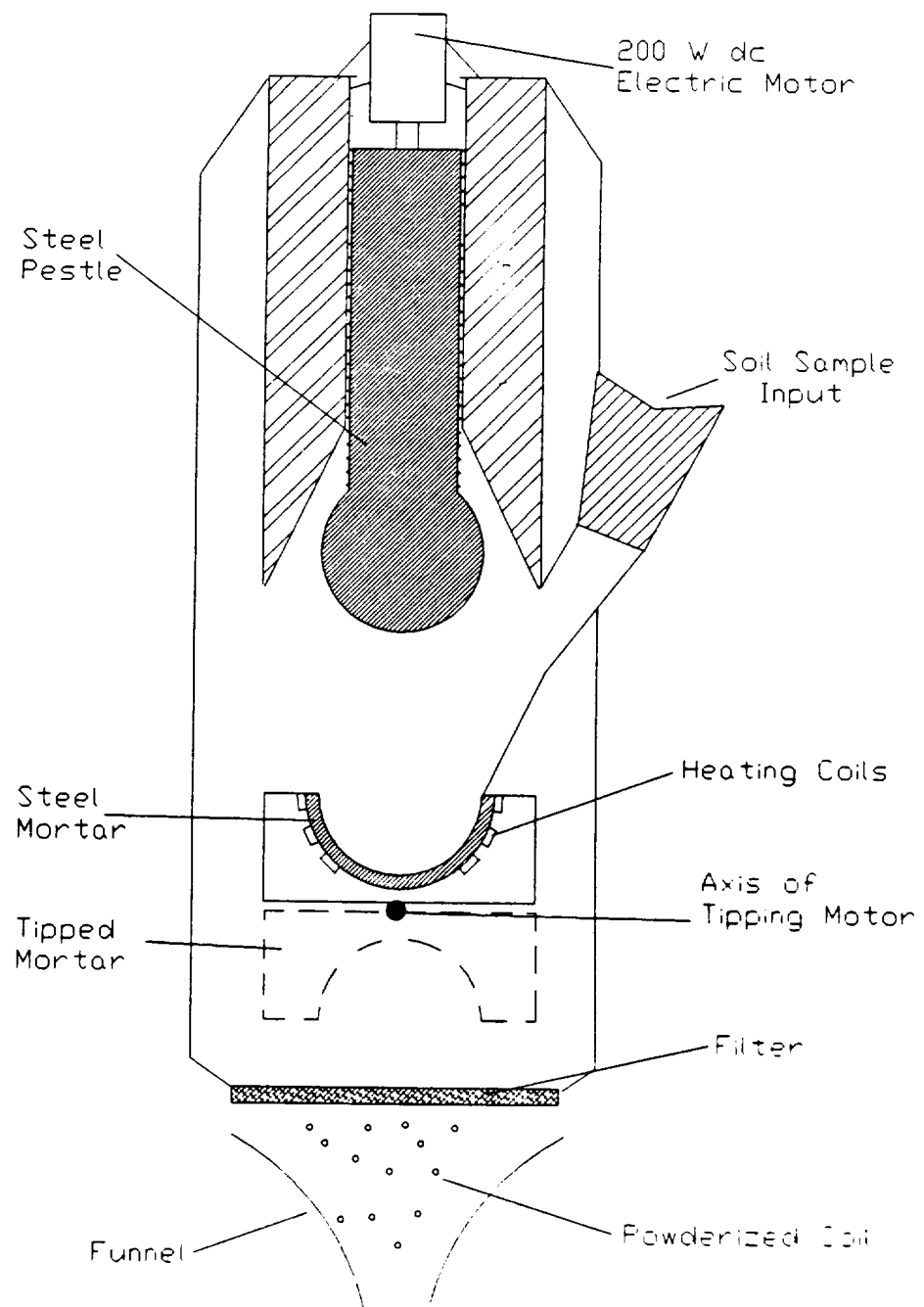


FIGURE 5. Soil Crushing Apparatus

much larger volume). Drying time should be no less than two hours as the water content in the soil will be in solid form and will have to absorb large amounts of heat to vaporize fully. Next, the power will be transferred to an electric motor controlling a pestle. The head of the pestle should be just slightly smaller than the mortar, and will be lowered onto the soil by rotation through a threaded region. The pestle will move up and down crushing the soil with approximately 20 pounds of force (including the weight of the pestle). This crushing should occur about 20 times. Manual tests have shown that about 20 repetitions of pressing and rotating a pestle into a mortar containing hard soil does a good job of powderizing. Another way of powderizing materials is by milling, but it was not chosen due to its inability to break up hard minerals such as quartz. It is unknown what form the large amounts of silicon is in discovered by the Viking expeditions, and preparations must be taken for the possibility of hard phases of materials such as quartz. Next, the mortar containing the powdered soil will be tipped over and agitated to allow the powder to fall through a 50 micron screen. As the smaller soil particles fall through the screen, they will enter a small plastic funnel. This is a form ready for diffraction. Tables 1 and 2 display the equipment, power, etc required for the described process. It should be noted that most of the equipment will not be used simultaneously, but the same power source can be accessed for each step.

6.3.4 X-ray Diffractometer

6.3.4.1 X-ray Diffractometer Introduction

A device that NASA should be interested in sending to Mars is an x-ray diffractometer. This would reveal a mineral analysis of our neighboring planet. We already know what elements make up the red planet but it would be important to know what mineral resources would be

available to man upon future colonization. Arguments against sending a diffractometer are weight and power limitations. These constraints can be met through design engineering.

TABLE 1 Power Distribution

Equipment	Description	Volts (V)	Power (W)
Calrod Heating Coils	Dissipate moisture in soil	24	200
Rev. Electric Motor	Drive pestle to powderize soil	24	220
Electric Motor	Tip mortar and agitate	24	25
Power Converters (7)	Boost electric potential	24	210
Cathode Ray Tube	Generate X-Rays	30K	210
Electric Motors	Rotate sample and counter	24	15
Power Converter	Boost potential to counter	24	30
Scintillation Counter	Detect X-Rays	1000	30

Max Power Used at Same Time: 250W

TABLE 2 Equipment Size and Weight Dimensions

Weight Equipment	X	Y/Diam.	Z	(lb)
Cathode Ray Tube	12"	Max diam 4"		10
Power Converters (7 stacked)	14"	5.7"	5.7"	42
D 5000 Rotating Disk for Sample & Counter	2"	diam.18"		35
Scintillation Counter	3"	3"	12"	10
Soil Prep Chamber (Includes mortar, pestle etc.)	14"	3"	7"	40
High V Wiring etc.	--	--	--	12

Total Weight: 149 lb (70 kg)

6.3.4.1 X-ray Generator

The generation of x-rays is generally done with a cathode ray tube (See Figure 6). An extremely high potential electric power source causes electrons to jump from a tungsten filament cathode to a target metal anode. When the electrons bombard the anode they cause the inner shell electrons of the atoms of the target to change energy levels. When this change occurs an x-ray is emitted. Since the energy levels of the electrons are fixed, and the wavelength of emitted x-ray is proportional to the difference in energy levels, many x-rays of the same wavelength are emitted called characteristic x-rays of the target metal. These monochromatic (same wavelength) x-rays can then be filtered and aimed at a soil sample (or any material). The x-rays will diffract off at angles characteristic of the soil following the Bragg Law

$$\lambda = 2d \sin\theta$$

where λ is the wavelength of the x-rays, d is the spacing between atomic planes in the material and θ is the diffraction angle. The diffracted x-rays can then be detected and compared to known data for nearly all materials.

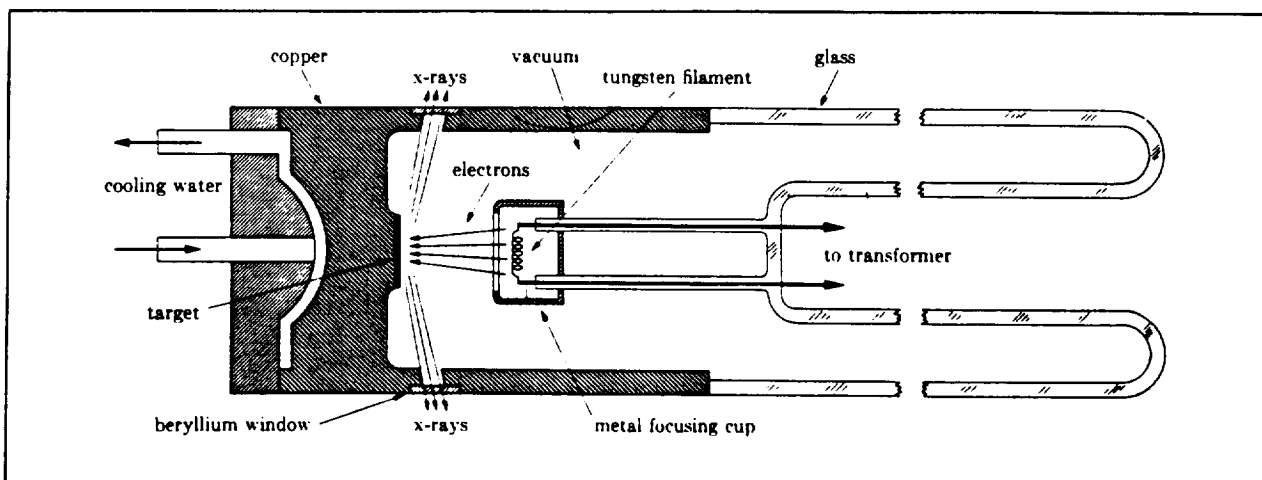


FIGURE 6. Cathode Ray Tube Schematic

Many commercial diffractometers are made to run on ac. This requires a large bulky transformer to boost the electric potential. Normal cathode ray (CRT) tubes will work whether the power source is ac or dc, thus most any commercial cathode ray tube could be adapted to work in a dc circuit. Figure 7 shows an ordinary CRT actual size about one foot long. Good CRTs like this one can be purchased from Rigaku. The leads can be connected to the dc source. An advantage with dc in this case is that it is easier to obtain the high potential necessary for electron emission. As stated earlier, to boost voltage in an ac circuit requires a large bulky transformer. Power converters can be used in the dc case which are smaller and not as heavy. EMCO and Spellman are manufacturers of electronics. They produce several power converters that could be used in this case (some of these are displayed in the appendix). For example, if one wanted to run a 210 watt CRT at 30 kV it could be done by running 7 of the Spellman EPM 30*30 model power converters in parallel. Power is additive by voltage when in series and by current when in parallel. These modules are only 5.7" X 5.7" X 2" each and convert an input of 30 W at 24 V dc to a 30 kV output. This potential is on the same order as commercial diffractometers but the power is only one tenth. The next section deals with the actual design.

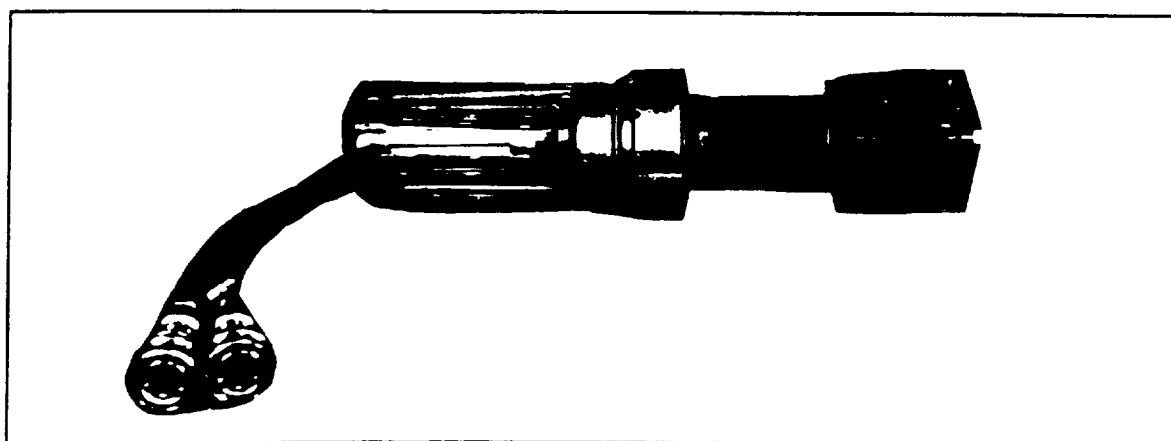


FIGURE 7. A commercially available cathode ray tube

6.3.4.2 X-ray Source Design

Now that it has been explained how x-ray generation is done and how some of the equipment works, this section is a proposal for an x-ray source aboard the Mars lander.

The maximum input power is 250 Watts dc. 210 Watts of this at 24 Volts will be used for x-ray generation (saving the rest for x-ray diffraction and detection). This energy will first be converted to a 30 kV potential at 7 mA by running it through a circuit of seven Spellman EPM 30*30 HV power converters in parallel. This will then be connected to an altered cathode ray tube used by Rigaku. The alterations include change in target anode metal and a change in the heat dissipation process. The target metal selected is chromium. It is desirable to have a material capable of exhibiting its characteristic x-rays at lower potentials or power and also for the wavelengths of these characteristic x-rays to be within a reasonable range. If they are too long or short the Bragg angle will be difficult to detect and also x-rays over 2.5 Å are more easily absorbed by air. Chromium begins exhibiting characteristic x-rays at only 5.989 kV whereas targets such as molybdenum require 20 kV. Since the potential produced by the power converters is 30 kV, this will ensure extremely high intensity peaks of characteristic radiation. The wavelength of the most pronounced intensity for Cr emissions is 2.28962 Å, just slightly longer than the most commonly used targets of copper (1.54051) and iron (1.93597). Rigaku CRTs (the ones they use and can be purchased from them) come with a selection of target metals including chromium, and could be altered to remove the other targets and fix the Cr one in place.

The other alteration to be made is in the cooling system. Running water cooling is out of the question for this application, these parts should be removed or amputated from behind the CRTs anode and replaced with heat dissipation fingers. Under ordinary conditions fingers would not be able to remove heat fast enough and the anode would melt, but under the circumstances

involved it will. First, the power level involved is one tenth, ordinarily 2000 W to only 210 W. This lower power means that fewer electrons will bombard the target per unit time (they will still strike it with the same momentum as the potential is still of the same order) resulting in much less heat production. Second, the atmospheric temperature of the martian poles is on the order of -100 to -150 degrees C. These conditions should require no cooling method, but since the atmospheric pressure on Mars is only 1/100th that of earth's convection of heat will be very slow and more surface area will be required to dissipate the heat. Fingers made of a good conductor of heat (Cu) should be made to extend from behind the chromium anode of the CRT. These adaptations can be seen in Figure 8.

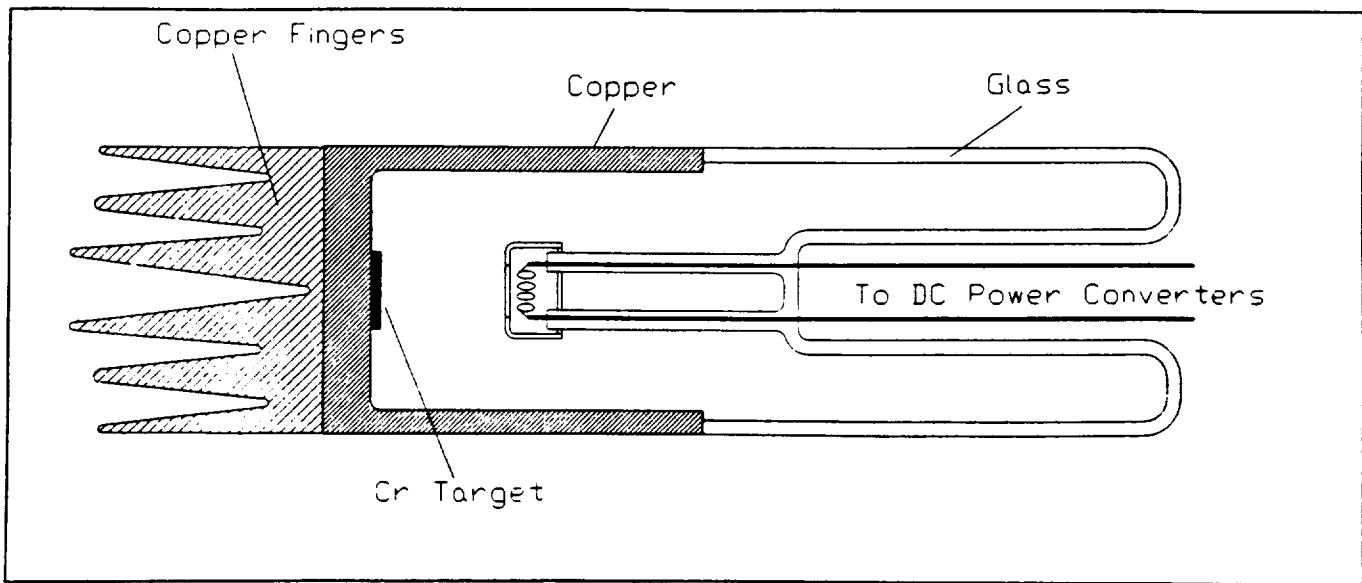


FIGURE 8. Modified CRT

The proposed system will produce a continuous spectra of x-rays with several intensity peaks the most prominent at $\lambda=2.28962$. This emitted radiation will exit the CRT through the window, but are not yet ready for diffraction. The continuous spectra creates a large amount of background radiation that can cloud up diffraction patterns. The radiation must be filtered. This

can be done by allowing the radiation to pass through a thin vanadium foil. This is possible due to the absorption characteristics which allow materials to absorb some wavelength radiation more or less (Vanadium's absorption edge allows it to absorb a large amount of background radiation and relatively small amounts of Cr characteristic radiation 2.28962). Commercial vanadium filters used for Cr radiation are about .016 mm thick. This absorbs 80% of background radiation and only 50% of characteristic radiation. The number of x-rays generated by this system is already almost an order of magnitude less than common equipment so it would be recommended to use a thinner filter allowing more x-rays to pass. A vanadium filter .012 mm thick will allow up to 60% characteristic radiation to pass will only allowing slightly more background radiation to pass (25%). This filter should be used.

The final step to this x-ray generation process is to columnize it. The radiation that gets diffracted must all come from the same direction. Columnators are standard tools in diffraction. It is a metal tube in which the radiation enters and exits through a small slit aimed directly at the sample (soil). No special modifications would be necessary, columnators of all sizes are readily available.

6.3.4.3 X-ray Diffraction and Detection

The best method for mineral analysis is powder diffraction. This is the method for which the soil will be prepared as previously described. As the columnated monochromatic radiation hits the soil sample it is diffracted at angles characteristic of the minerals it contains. In order to ensure that all orientations of the crystals are exposed to radiation the sample is rotated. The most common detection devices for x-rays are proportional counters and scintillation counters. For this application, scintillation counters would be more desirable. This is due to the relatively low intensity radiation needed to be detected. Scintillation counters amplify the incident x-rays

by converting it to light and then an electron which is multiplied by a series of dynodes as shown in Figure 9. Proportional counters do not amplify. Scintillation counters also require a high potential power source to excite the electrons to jump from dynode to dynode. Siemens manufactures a diffractometer with parts that could be used for this application. The D 5000 series diffractometer is displayed in Figure 10 with arrows pointing to the usable parts. It is equipped with two rotating tracks, one for the sample and one for the counter. The counter is a scintillation counter able to read intensities at incrementing angles of 0.1 degree. While it was made for an ac circuit, the rotation could be done by small power electric motors. The remaining power used by the counter.

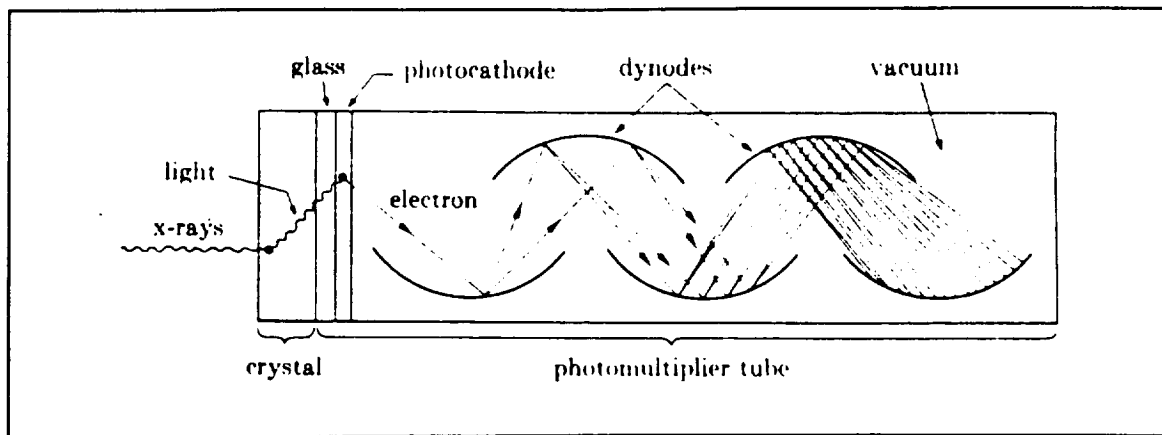


FIGURE 9. Scintillation Counter Schematic

The output being electric impulses would be sent to a computer and transmitted back to earth where it would be analyzed.

The analysis is relatively simple. It is known what elements are in the soil so we know what minerals are possible to find. Diffraction data for all these minerals is available from the Joint Committee on Powder Diffraction Standards (JCPDS). Data on quartz silica and magnetite iron oxide are shown as an example in the appendix. This shows the d spacings and relative

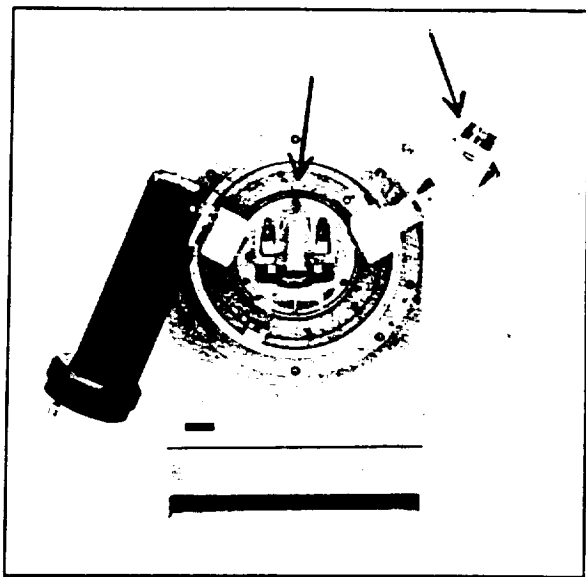


FIGURE 10. Siemens D5000 Diffractometer

intensities for atomic planes. By knowing the d spacings of the most intense diffraction planes and the wavelength of the incident radiation we can calculate the expected angles at which peaks should occur. Many angles characteristic of different materials are identical but some common sense will solve this problem. We know what minerals are possible and many are impossible.

6.3.4.4 Conclusions

The described process should be able to distinguish minerals in amounts over 10% content in soil. The power requirements, weight specifications and cost of this project are outlined in the following tables. The described process should work in theory, but as always it would have to be built and tested to work the 'kinks' out of it.

One of the arguments against having a diffractometer is that it 'hogs' power and space and there are many other data collecting instruments being considered. A possible solution to this is to send different equipment on each lander. The proposed mission includes 12 of these

martian landers. One might send a diffractometer on 3 or 4 landers, and thermal probe on several others. This would allow for more information to be collected on the mission.

6.4.0 DESIGN BASIS

6.4.1 Thermal/Drill Probe and Support Equipment

This proposed design is a modification of the Mars Polar Pathfinder probe which was based on a improved design by Haldor W.C. Aamot. Haldor a member of the U.S. Army CRREL designed the pendulum probe, "such self-contained thermal probes have a long history of use in the exploration of polar ice sheets on earth." (Paige, 1992) [See Figure 11]

The principal driving force of the Mars Polar Pathfinder probe is the thermal tip. Beyond that, it is relying on gravity and the weight of the probe. The probe is small and light without taking in consideration that Mar's gravitational pull is one third of Earth's. Also, the weight of the probe is greatly decreased as it descends in the ice, because the coaxial cable is unravelling out of the probe which happens to be a good majority of the probes weight. My concern with the Mars Polar Thermal probe is that the probe's design is based on the principle to follow. The minimum power required to operate the thermal probe is equal to the sum of the power required for melting the ice, and the power required to balance lateral heat losses until the complete length of the probe has passed given point. Ideally then, at the rear (upper) end of the probe, melt water is just beginning to freeze, and the hole size is the same as the probe diameter. If the probe is too long, or rate at which lateral heat is supplied is insufficient, the probe will become frozen in. An optimum probe speed exists, above which the lateral heat produced is excessive, the hole becomes oversized, and energy is wasted (Aamot, 1967a). It is obvious that the dimensions and the power requirements are related and are critical. It is to risky, considering, the consistency

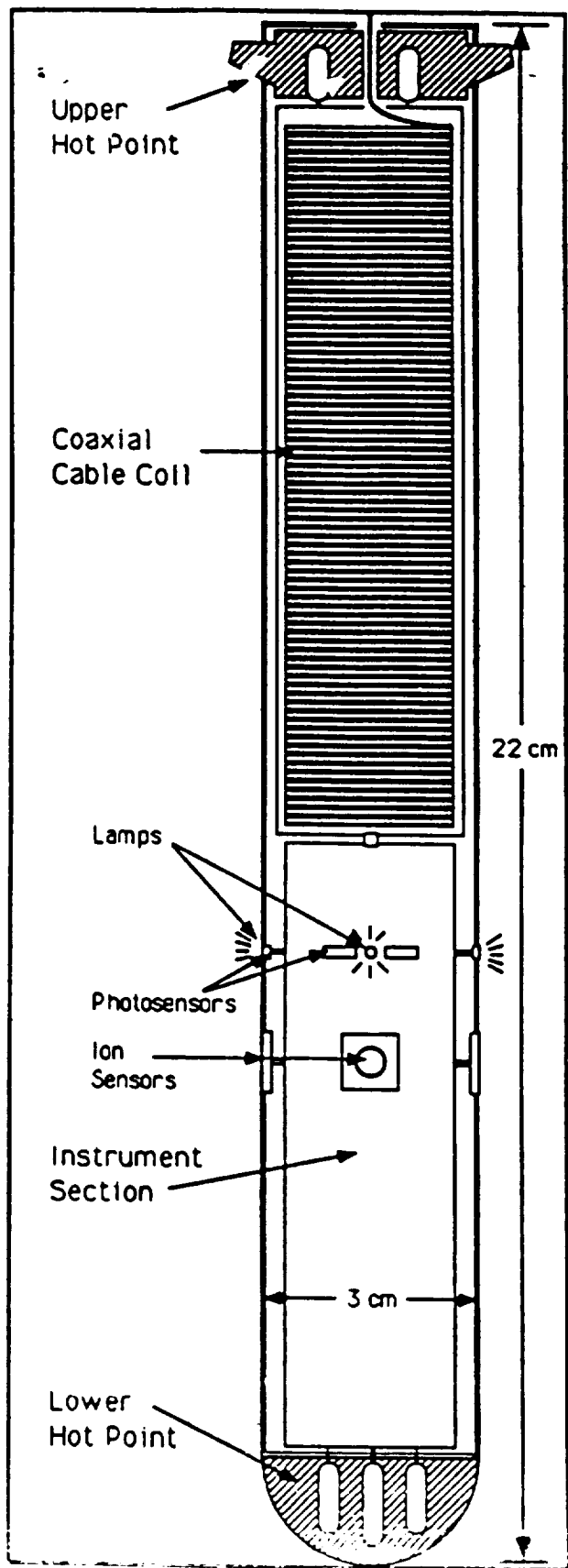


FIGURE 11. Probe used for Mars Polar Pathfinder Mission

of the ice/dust is unknown. The second concern is that the probe is operating on an "on/off" cycle. This gives it a greater probability to get "frozen in" the ice. This is where modification and development of the thermal/drill had came about. This would give the probe capabilities of drilling through the ice. Essentially, it has the best of both driving forces. It utilizes the drilling capabilities, the thermal aspect to melt the ice, and the gravitation pull. This design will reduce the power. The possibility of getting "frozen in" is reduced. The rate of decent of the probe would be more consistent, especially with the computer control.

The options for support equipment and home is greatly dependent on the rover system. If the rover could carry one or multiple thermal/drill probes then this would give the scientific community more data and information to work with.

TABLE 3 Probe Design

Design	Thermal/Drill Probe
Dimension	28cm (l) x 3cm (w)
Mass	1 to 2 kg

TABLE 4 Cable

Type	Coaxial, Beryllium-Copper conductors, Teflon insulation
Length	150 m (uncoiled)
Outer Diameter	1 mm
Center Conductor	29 Gauge (AWG)
Voltage Rating	300 V

TABLE 5 Probe Power Supply and Data System

Capacity	Less than 440W, 300 V DC
Mass	Option 3 about 10 kg Increasing Mass with Option 2 & 1 (Respectively)
Data Rate	1000 bps (operating), 1 bps (idle)
Total Data Volume	10 Mbytes

6.5 REFERENCES

- 1) Baird, Casto, Clark. "The Viking X-Ray Fluorescence Experiment: Sampling Strategies and Laboratory Simulations." *Journal of Geophysical Research* Vol 82 No 28 Sept 30, 1977 pg 4595.
- 2) Clark, Baird, Rose. "The Viking X-Ray Fluorescence Experiment: Analytical Methods and Early Results." *Journal of Geophysical Research* Vol 82 No 28 Sept 30, 1977 pg 4577.
- 3) Cullity B.D. Elements of X-Ray Diffraction 2nd Ed. Addison-Wesley publishing Co. Inc. 1978.
- 4) Kakudo, Kasai. X-Ray Diffraction by Polymers Elsevier Publishing Co. 1972 Kodonsha Ltd.
- 5) Ladd, Palmer. Structure Determination by X-Ray Diffraction Plenum Press 1977.
- 6) Paige, David. "The Mars Polar Pathfinder" Discovery Program Workshop Concept #83 Sept 1992.
- 7) Paige, David. "Drill/Borescope System" Mars Polar Pathfinder Video #1 March 5, 1993.
- 8) Schwartz, Cohen. Diffraction of Materials Academic Press 1977.
- 9) Beard, D. "D 5000 Diffractometer Introduced." X-Ray Update Issue 1 July 1990 Siemens Manufacturing.
- 10) Selected Powder Diffraction Data for Minerals. Joint Committee on Powder Diffraction Standards 1974 entries 5-0490, 19-629.
- 11) "Rigaku X-Ray Diffractometer System." Rigaku Sales Pamphlet.
- 12) Spellman High Voltage Company products listings in EEM 1991.
- 13) EMCO High Voltage Company products listings in EEM 1991.

APPENDIX

5-0490 MINOR CORRECTION

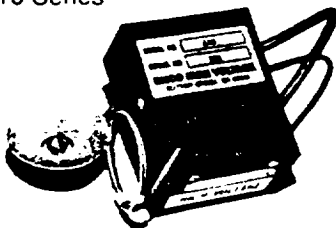
d	3.34	4.26	1.82	4.26	SiO_2
I/I ₁	100	35	17	35	
SILICON OXIDE					QUARTZ, LOW
d Å	I/I ₁	hkl	d Å	I/I ₁	hkl
Rad. CuK α_1 A 1.5405 Filter Ni			4.26	35	100
Dia. Cut off			3.343	100	101
I/I ₁ G.C. DIFFRACTOMETER			2.458	12	110
Ref. SWANSON AND FUYAT, NBS CIRCULAR 539, VOL. III 1953			2.282	12	102
Sys. HEXAGONAL S.G. D ₃ ⁴ - P ₃ ₁ ₂₁			2.237	6	111
a ₀ 4.913 b ₀ c ₀ 5.405 A C 1.10			2.128	9	200
a ₀ b ₀ c ₀ Y Z 3			1.980	6	201
Ref. Ibid.			1.817	17	112
Ref. Ibid.			1.801	<1	003
Ref. Ibid.			1.672	7	202
Ref. Ibid. 1.544 1.553 Sign +			1.659	3	103
3V D 2.647 mp Color			1.608	<1	210
Ref. Ibid.			1.541	15	211
SAMPLE FROM LAKE TOXAWAY, N.C. SPECT. ANAL.: <0.01% Al; <0.001% Ca,Cu,Fe,Mg.			1.453	3	113
X-RAY PATTERN AT 25°C.			1.418	<1	300
3-0427, 3-0444			1.382	7	212
Replaces 1-0649, 2-0458, 2-0459, 2-0471, 3-0419,			1.375	11	203
			1.372	9	301
			1.288	3	104
			1.256	4	302

19-629

d	2.53	1.49	2.97	4.85	Fe_3O_4
I/I ₁	100	40	30	8	
Iron Oxide (Magnetite)					
Rad. CuK α_1 A 1.5405 Filter Ni Dia.					
Cut off I/I ₁ Diffractionmeter					
Ref. National Bureau of Standards, Monograph 25, Sec. 5 31 (1967)					
Sys. Cubic S.G. Fd _{3m} (227)					
a ₀ 8.396 b ₀ c ₀ A C					
a ₀ b ₀ c ₀ Y Z 8 Dx S. 197					
Ref. Ibid.					
Ref. Ibid.					
Ref. Ibid.					
Sample obtained from the Columbian Carbon Co., New York 17, New York.					
Spectrographic analysis showed the following major impurities: 0.01 to 0.1% Co, 0.001 to 0.01% Ag, Al, Mg, Mn, Mo, Ni, Si, Ti and Zn.					
Pattern taken at 25°C.					

MINIATURE RUGGED CRT SUPPLY

10,000 VDC @ 10 Watts
A10 Series



FEATURES

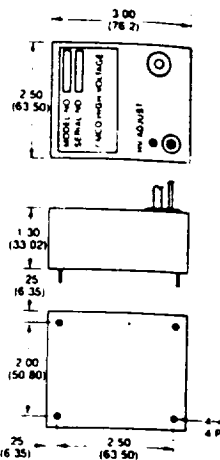
- PRECISION REGULATED & RIPPLE
- SHORT CIRCUIT PROOF
- REVERSE POLARITY PROTECTION
- RFI FILTERING/SHIELDING
- AIRBORNE APPLICATION TO 70,000 FEET

ELECTRICAL SPECIFICATIONS

INPUT VOLTAGE: +24 to +32 VDC
INPUT REGULATION: .01%
HIGH VOLTAGE OUTPUT: +10,000 VDC @ 1 MA
OUTPUT REGULATION: 0.025%
OUTPUT RIPPLE: 0.025%
ADJUSTMENT RANGE: +/- 5%
AUXILIARY OUTPUT: +500 VDC @ 1mA
OPERATING TEMPERATURE: -55 to +80 Degrees C

OPTIONS

- Other Input Voltages
- Alternate High Voltage Outputs
- Auxiliary Output Voltages
- Single Output Only
- Alternate Input/Output Connectors



PRECISION CRT MULTIPLE OUTPUT

14,000 VDC @ 14 Watts
S143 Series

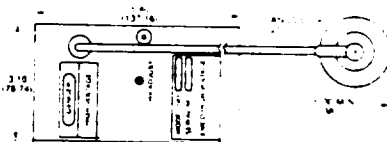


FEATURES

- PRECISION REGULATION & RIPPLE
- REMOTE ON/OFF CONTROL
- REMOTE SCREEN & FOCUS PROGRAMMABILITY
- SHORT CIRCUIT PROOF
- REVERSE POLARITY PROTECTION
- RFI FILTERING/SHIELDING
- AIRBORNE APPLICATION TO 70,000 FEET

ELECTRICAL SPECIFICATIONS

INPUT VOLTAGE: +13 to +32 VDC
INPUT REGULATION: .05%
OPERATING TEMPERATURE: -55 to +80 degrees C
STORAGE TEMPERATURE: -55 to +90 degrees C
OUTPUT NO. 1:
HIGH VOLTAGE OUTPUT: +14,000 VDC @ 1 MA
OUTPUT REGULATION: 0.05%
OUTPUT NO. 2:
VIDEO VOLTAGE OUTPUT: +75 Volts (Fixed) @ 50 Ma
OUTPUT REGULATION: 0.5%
OUTPUT RIPPLE: 0.5%



OUTPUT NO. 3:

FOCUS VOLTAGE OUTPUT: +1,500 to 3,000 VDC @ 20 U

OUTPUT REGULATION: 0.1%

OUTPUT RIPPLE: 0.1%

PROGRAMMING VOLTAGE: 0 to -5 VDC

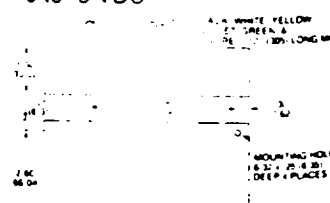
OUTPUT NO. 4:

SCREEN VOLTAGE OUTPUT: +500 to +1,000 VDC @ 50 uA

OUTPUT REGULATION: 0.1%

OUTPUT RIPPLE: 0.1%

PROGRAMMING VOLTAGE: 0 to -5 VDC



EMCO
Emco High Voltage Company

11126 Ridge Rd., Sutter Creek, CA 95685

209-223-EMCO • TELEX: 510-100-8006 • FAX: 209-223-2779

ORIGINAL PAGE IS
OF POOR QUALITY



High Voltage Electronics Corp

7 Fairchild Avenue Plainview NY 11303 • (516) 349-8686 • FAX (516) 349-8699 • TWX 510-221-2155

EPM, LCM & UM SERIES

EPM Series 30W Modular HV Power Supplies

Features:

- Output voltages from 1kV to 30kV @ 30 watts
- Voltage programming from zero to rated output
- Current programming from zero to rated output
- Inhibit control of output via TTL signals
- Test points for output current and voltage
- Overvoltage protection
- Designed to meet UL[®] requirements
- Compact package
- Low stored energy

The EPM series utilizes proprietary circuitry enabling these high voltage power supplies to yield full output current from near zero to maximum output voltage. Current regulation is standard on all models and is particularly valuable in applications that require a current source into the load such as

- Electrophoresis
- Electron Beam
- Ion Sources
- Photomultipliers
- Laboratory Applications

Specifications:

- Input: +24V DC ±10%
- Output: 8 models from 1kV to 30kV. Each model is available in positive or negative polarity outputs
- Load Regulation
Static: 0.01% of output voltage for NL to FL change
Dynamic: 10V 100µA NL to FL
- Line Regulation
±0.01% for a ±10% input voltage change
- Ripple: 0.1% p-p of output voltage.
- Physical: 5.7" x 5.7" x 2"
- Input Connector: 9 pin AMP Metri-Mate
- Output Cable: 18" ±1" of UL[®] approved high voltage wire
- Voltage Stability 0.01% per 8 hours
- Voltage Temperature Coefficient: 0.01% per °C
- Voltage Test Point: 10V ± 2% = Max. rated output
- Current Test Point: 10V ± 2% = Max. rated output

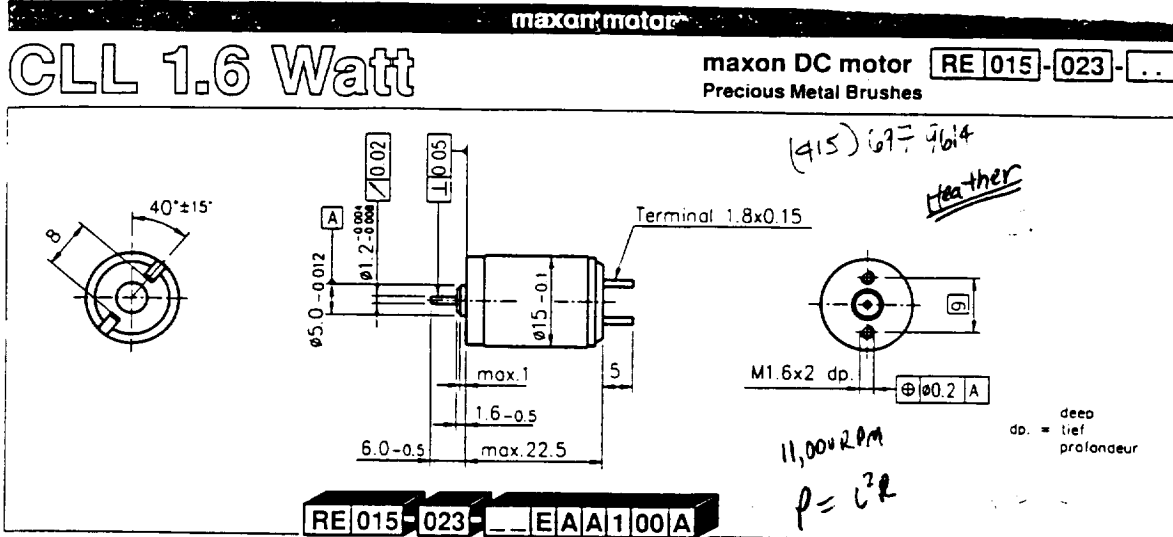
Spellman engineers designed the EPM to be very flexible so that it can be easily customized to fit your OEM and special require-



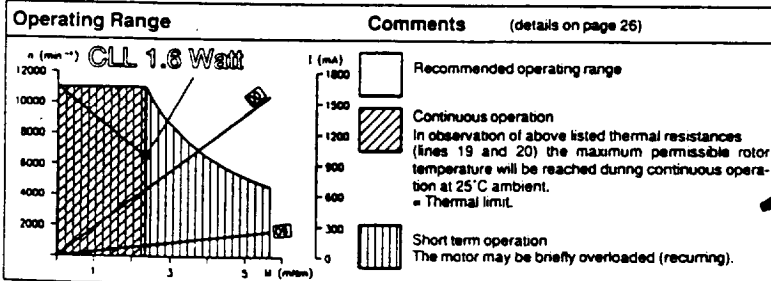
Maximum Rating	Model Number
kV	mA
1	30
3	10
5	6
10	3
15	2
20	1.5
25	1.2
30	1

* Specify "P" for positive polarity or "N" for negative polarity
models. Please contact Spellman's Sales Department to discuss your application's requirements

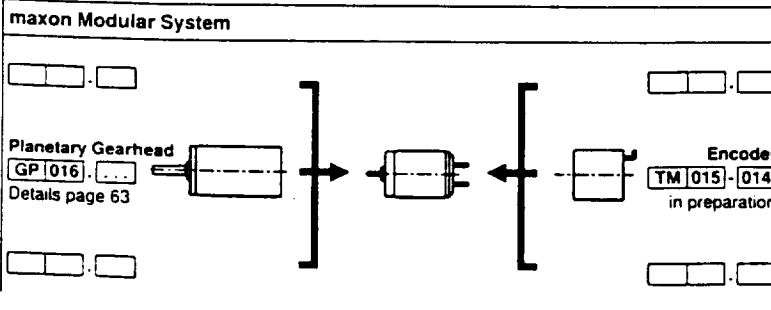
ORIGINAL PAGE IS
OF POOR QUALITY



Motor Data	Winding Number (Order Number)										
		01	02	03	04	05	06	07	08	09	10
1 Assigned power rating	W	1.6	1.6	1.6	1.6	1.6	1.6	1.6	1.6	1.6	1.6
2 Nominal voltage	Volt	3.00	3.50	3.70	4.50	6.00	7.20	9.00	12.00	15.00	24.00
3 No load speed	rpm	7740	7660	7450	7420	7950	7710	7680	8330	8080	9850
4 Stall torque	mNm	4.07	4.12	4.03	3.96	4.22	4.11	4.06	4.27	4.20	5.03
5 Speed/torque gradient	rpm/mNm	1950	1900	1890	1920	1930	1920	1940	2000	1970	2000
6 No load current	mA	27.0	22.9	20.9	17.1	14.0	11.2	8.91	7.40	5.69	4.56
7 Starting current	mA	1130	967	871	700	599	472	371	318	243	221
8 Terminal resistance	Ohm	2.681	3.62	4.25	6.43	10.0	15.3	24.2	37.8	61.8	109
9 Max. permissible speed	rpm	11000	11000	11000	11000	11000	11000	11000	11000	11000	11000
10 Max. continuous current	mA	500	500	500	419	335	272	216	173	135	102
11 Max. continuous torque	mNm	1.81	2.13	2.32	2.37	2.36	2.37	2.35	2.32	2.34	2.33
12 Max. power output at nominal voltage	mW	811	811	772	754	862	814	801	915	872	1280
13 Max. efficiency	%	71.9	72.0	71.8	71.6	72.2	72.0	71.8	72.2	72.1	73.8
14 Torque constant	mNm/A	3.81	4.26	4.63	5.65	7.04	8.71	10.9	13.4	17.3	22.8
15 Speed constant	rpm/V	2640	2240	2060	1690	1360	1100	874	711	551	419
16 Mechanical time constant	ms	10.3	10.2	10.2	10.1	10.1	10.1	10.1	10.1	10.1	10.1
17 Rotor inertia	kgm²	0.503	0.511	0.513	0.503	0.500	0.501	0.497	0.482	0.489	0.482
18 Terminal inductance	mH	0.05	0.07	0.08	0.12	0.19	0.29	0.46	0.69	1.15	1.99
19 Thermal resistance housing-ambient	K/W	35.00	35.00	35.00	35.00	35.00	35.00	35.00	35.00	35.00	35.00
20 Thermal resistance rotor-housing	K/W	8.20	8.20	8.20	8.20	8.20	8.20	8.20	8.20	8.20	8.20



- Stock program
- Standard program
- Special program
- Axial play 0.05 - 0.15 mm
- Max. sleeve bearing loads
 - axial (dynamic) 0.2 N
 - radial (5 mm from flange) 0.5 N
 - press-fit force (static) 20 N
- Radial play/sleeve bearings 0.014 mm
- Ambient temperature range -20/+65°C
- Max. rotor temperature +85°C
- Number of commutator segments 5
- Weight of motor 20 g
- Values listed in the table are nominal. For applicable tolerances (see page 25) and additional details please request our computer printout.



$$1g = 0.35 \text{ ounce}$$

$$20g = 0.35 =$$

Planetary Gearhead GP 016 - ...

GP 016

Technical Data									
Planetary gearhead straight teeth Bearing at output sleeve bearing Radial play 0.02 mm Axial play max. 0.15 mm Max. permissible axial load 6 N Max. permissible force for press fits 100 N Average backlash no load per stage Recommended input speed <1°/min Recommended temperature range <6000 rpm -15/+65°C									
Number of stages: 1 2 3 4 5 Max. radial load., 6 mm from flange 27 N 33 N 36 N 36 N 36 N Efficiency 90% 81% 73% 65% 59%									

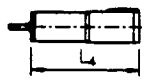
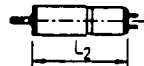
Gearhead Order Number	Reduction	No. of stages	max. Torque		Sense of direction	g	Weight	L ₁ max. mm	L ₂ max. mm	L ₃ max. mm	L ₄ max. mm
			continuous Nm	inter. Nm							
GP016-015-044 AA-00A	44 : 1	1	0.1	0.15	-	20	15.1	37.3			
GP016-019-0019 BA-00A	192 : 1	2	0.15	0.2	-	23	18.7	40.9			
GP016-023-0084 CA-00A	843 : 1	3	0.2	0.3	-	27	22.3	44.5			
GP016-026-0370 DA-00A	369.6 : 1	4	0.25	0.35	-	31	25.9	48.1			
GP016-030-1621 EA-00A	1620.5 : 1	5	0.3	0.4	-	35	29.5	51.7			

* Absolute reduction ratio per stage: $\frac{44}{13} + 1 = 4.3846$

In preparation	44.3									
	47.9									
	51.5									
	55.1									
	58.7									

+ Motor Order Number

- **RE 015 - 023 - [] E A A 1 00 A A**
Basic motor RE015-023..EAA100A
see page 48
- **RE 015 - 023 - [] E A B 1 00 A A**
in preparation
- **20 17 [] 63 16 2 0 0 0**
Basic motor 2017....-22.162-000
see page 37



+ Tacho/Encoder

Encoder
in preparation

TM 015 - 014

57

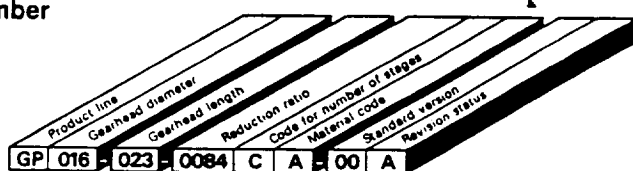
60

51

29.5 + 3 + 22.5

Structure of Gearhead Order Number

Example:



Product Line
GP Planetary gearhead
GS Spur gearhead

Gearhead diameter in mm

Gearhead length in mm

Reduction ratio
Example: 84 : 1

Revision status A - Z	
Standard version Shaft, bearing, lubrication, mounting and temperature range as shown in the catalogue	
Material code Material pairing, internal gears	
Code for number of stages A 1 stage B 2 stages C 3 stages etc.	

7.0 SOLAR TRACKING SYSTEM

Michael Sonby

TABLE OF CONTENTS

7.1 INTRODUCTION.....	7.1
7.2 SYSTEM JUSTIFICATION.....	7.2
7.3 SYSTEM DESIGN	7.4
7.4 APPENDIX.....	7.7

7.1 INTRODUCTION

The NASA Space Research Center has designed the foundation for a rover-based mission to Mars. A series of rovers and landers will be launched to gather data about the polar regions of Mars. A sun tracking system was designed for this mission. Its purposes is to power some of the rovers with solar energy; this sun tracker should help maximize the power for the rover.

The tracking system design proceeded as follows:

- the power output was calculated from both a stationary solar panel and a panel following the sun by use of a tracking system. From this, a potential gain could be determined
- a general feedback loop was designed for the entire system. From this loop, I was able to decide what part of the system can be handled with software and what should be handled with hardware
- appropriate hardware was chosen for the system, and the connection between the hardware and the software was designed
- software was created (using both the C language and MATLAB programming) that would operate the system
- a simulated solar panel was built, with four solar cells used as locators
- the system was tested

A working model of the solar tracking system was demostrated. This system will maneuver the solar array towards the greatest amount of sunlight using two rotational axes from a robotic arm.

7.2 SYSTEM JUSTIFICATION

This first step was to make a study to determine the potential gain by using the tracking system. Based on a chapter about solar geometry, I was able to convert the variables to their Martian equivalents. Then a chart was created based on the day of the Martian year, the energy received by an ideal solar tracker (able to move in all axis), and the energy received by a flat-plat collector. Due to the fact that the rover will be at the poles, the solar panel will not receive any sunlight for several months. However, when the sun is at the pole, the chart indicates that a collector with an ideal tracker received ten times more energy than a flat-plate collector.

From the calculations made from the study, the amount of solar energy hitting the solar panel with the tracking system would range from 0 Joules/m² to 52,404,534 Joules/m², depending on the day of the Martian year. Given an area of 0.31 m² and a time of 88596 second per Martian day, that created a maximum power of 183.4 Watts on a summer day. This does not take into account the efficiency of the solar panels (around 15 percent), nor the effect of dust or clouds. However, even assuming only 8% of possible solar radiation was turned into energy for the rover, that would give the rover 14.6 Watts, more than the amount needed (10.5 Watts, from the rover section of the NASA project) to run the rover. Figure 1 is a chart showing the power output for both the case of a stationary solar panel and one following the sun.

**Power Output from two solar panels (Area=0.31 m²,
Beta=0.75, Eff.=0.15)**

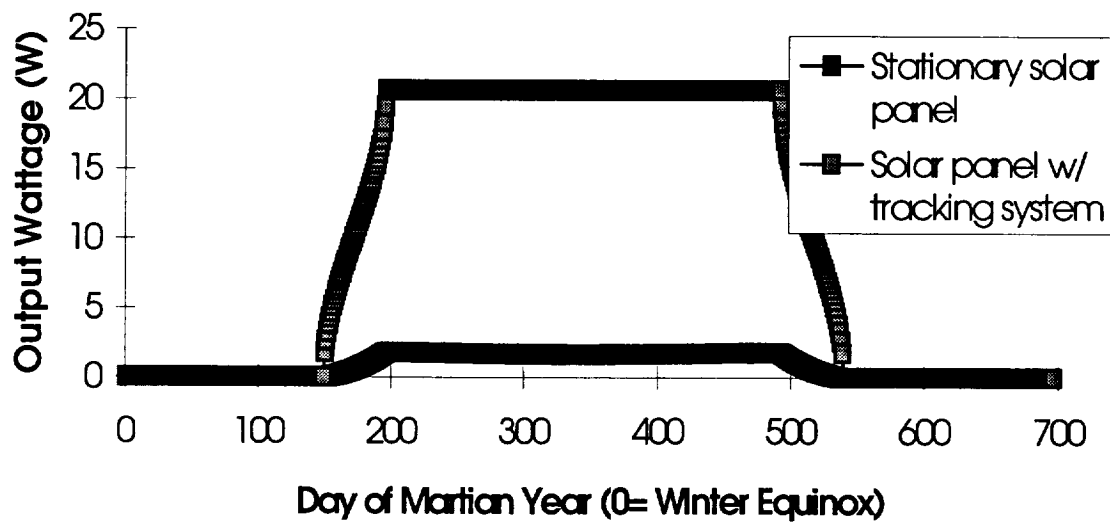


FIGURE 1. Comparison of energy available from a stationary solar panel to that equipped with a solar tracking system

7.3 SYSTEM DESIGN

The system operates as follows. Light will hit four solar cells, one at each corner of a rectangular array. The sensors are connected to an A/D converter, which will send the four voltages to a computer. A C program is used to read the voltages from the A/D converter. From there, the voltages will enter a MATLAB program, and be converted into the coordinates for the best location of the panel. A robot control program will then be activated, telling the robot to maneuver the array into the ideal location. The system will be a feedback loop, allowing for the best measurement possible. Figure 2 shows the feedback loop diagram.

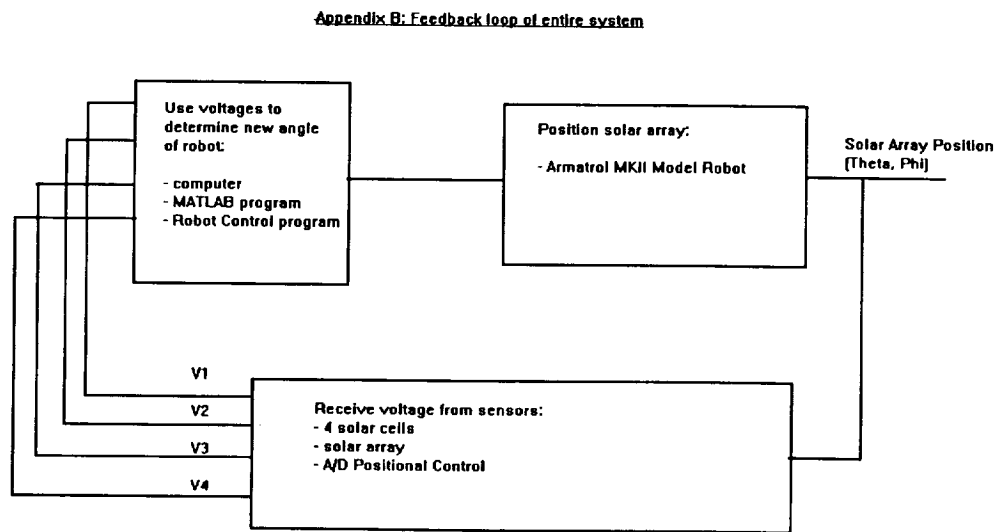


FIGURE 2. Feedback control loop

The MATLAB control will take the 4 voltages (ranging from 0-0.55 V), and convert them into two angles. These angles will then be converted into a new position for the solar array. With four sensors, the system is redundant, and able to be modified if any of the sensors break down. The MATLAB program is the base program; it will activate the two C programs when needed. A listing of the MATLAB and C programs is included in the Appendix.

Rather than building legs to hook up the sun tracker, an Armatrol robot was used to hold the array. This was chosen for several reason. Expense was one. It is cheaper to use a functioning robot than to build a new mechanical system to hold the array. Also, by using a working mechanical system, more time can be spent emphasizing the electrical control system. Finally, the robot already has a computer program that enables the robot to be positioned.

John Phillips created a program that would allow the robotic arm to learn commands and repeat them. By using several subroutines from his program, I was able to create a C program that would read the four variables that would move the robot's base, shoulder, elbow and wrist. However, only two of the variables (the base and elbow angles) would change from one position to the new position.

The program has two modes. The continuous mode will run the feedback loop without stopping. The best fit mode will adjust the solar array until the V1 and V4 voltages are within 0.25 volts of each other. The beginning of the program will ask for which mode the user wants.

The system will be tested by either shining a bright flashlight from an angle towards the solar panel. Then, once the program begins, the robotic arm should position the panel so that it faces the flashlight (or is at least in the best position possible). This should be the case no matter where the light is positioned. Another test is to block one of the voltages, and see how the array positions itself.

The solar tracking system was a successful senior design project. During the year, I learned a great deal about control systems and robotics for the project. The system tested successfully, and the project worked according to its' goal.

7.4 APPENDIX

```

/*
   Program for solar tracking system
*/
/* Des.m- MATLAB program that moves robotic arm for solar tracking system */
/* by Michael Sonby */

v1=1;
v2=2;
v4=4;
forever= ('Enter a 1 for continuous mode, other key for best fit mode ');
if forever ~=1           /* if 1 is pressed, set forever=1;      */
    forever=0;            /* otherwise, forever=0;          */
end;
while abs(v1-v4)+forever>0.25      /* if forever=1, program will not stop*/
/* if forever=0, program will end when v1 & v4 are within 0.25 volts */

!del c:\robot\pat.m
!del c:\matlab\pat.m
!c:\robot\volts           /* Reads voltages from A/D converter      */
/* Writes to pat.m          */
!copy c:\robot\pat.m c:\matlab\pat.m
pat                      /* Reads and sets up 4 voltages (v1-v4)      */

v1= volts * [1; 0; 0; 0];
v2= volts * [0; 1; 0; 0];
v3= volts * [0; 0; 1; 0];
v4= volts * [0; 0; 0; 1];
v1
v2
v3
v4
vmax=0.55;             /* Maximum voltage possible from solar cells */

conv= 180/3.14159;      /* Converts radians to degrees
theta1= asin ((v2-v4)/vmax)*conv; /* Base angle #1
theta2= asin ((v1-v3)/vmax)*conv; /* Base angle #2
phi1= asin ((v1-v2)/vmax)*conv; /* Elbow angle #1
phi2= asin ((v3-v4)/vmax)*conv; /* Elbow angle #2
!del angles.txt
angles1= [theta1;theta2;phi1;phi2];
angles= [theta1;0;phi1;0];        /* Chooses what angles to use
/* For Base and Elbow
angles1
angles

```

```

coeff=[89.0;101.0;90.0;100.0];      /* Coefficients from robot.c program */
/* Sets angles number to 0-255 range */

new=angles+coeff;
factor=[255/181;255/108;255/177;255/192];
value=new.*factor;
snum=round(255-abs(value));
snum           /* Snum is 0-255 range for 4 angles */
/* Base, shoulder, elbow, and wrist (Shoulder and wrist do not change) */
base =[1 0 0 0]*snum;
shoulder=[0 1 0 0]*snum;
elbow =[0 0 1 0]*snum;
wrist =[0 0 0 1]*snum;
fprintf ('angles.txt','%g\n',base);    /* Writes the 4 snum variables */
fprintf ('angles.txt','%g\n',shoulder);/* To Angles.txt, where program */
fprintf ('angles.txt','%g\n',elbow);    /* Mike.c will move robotic arm */
fprintf ('angles.txt','%g\n',wrist);    /* To those coordinates */

!copy angles.txt c:\robot\angles.txt
!c:\robot\mike          /* Move arm */
end        /*While loop*/

```

```

/***********************/
#include <stdio.h>
#include <graph.h>
#include <conio.h>
#include <malloc.h>
#include <string.h>
main(argc,argv)
int argc;      /* MAIN DATA COLLECTION PROGRAM */
char *argv[];
{
char string[20];
FILE *infp;
float atof(),fnum;
int atoi(),waistp,sholder,elbowp,wristp,i,a,count,delay;
int huge *store;
count=0;
store= (int huge *)malloc(4000,sizeof(int));
if (store == NULL) {printf("\n NO MEMORY!!");abort();}
else   {printf("\n MEMORY BLOCK ALLOCATED\n");}

```



```

infp=fopen("angles.txt","r"); /* Opens angles.txt to read */
delay=2;
wait (delay);
while (fgets(string,4000,infp))
{++count;store[count]=atoi(string);printf("\n %d %d",count,store[count]);}
fclose(infp);

waistp=store[1];           /* Reads the first 4 numbers */
sholder=store[2];          /* of angles.txt and assigns */
elbowp=store[3];           /* them to four positions */
wristp=store[4];
printf("\n%d %d %d %d\n",waistp,sholder,elbowp,wristp);

```



```

waistp=check(waistp);  waist(waistp);
/* Move base to position waistp */ 
sholder=check(sholder); shoulder(sholder);
/* Move shoulder to position sholder */
elbowp=check(elbowp);  elbow(elbowp);
/* Move elbow to position elbowp */
wristp=check(wristp);  wrist(wristp);
/* Move wrist to position wristp */
}

```

```

check(position)          /* Checks to make certain all positions      */
int position;           /* Are in 0-255 Range                      */

{ if (position>255) {position=255;}
  if (position<0) {position=0;}
return(position);
}

wait(delay)    /* Pause function. Only used while reading angles.txt      */
int delay;
{
int i,a; a=0; for (i=0;i<delay;i++) { a=a+1; }

waist(position)          /* Function that moves Base Position*/
int position;
{
printf("\nMoving waist !");
outp(768,0);
outp(769,position);
outp(770,0);
wait(1000);
outp(770,1);
}

shoulder(position)        /* Function that moves Shoulder Position */
int position;
{
printf("\nMoving shoulder !");
outp(768,1);
outp(769,position);
outp(770,0);
wait(1000);
outp(770,1);
}

elbow(position)/* Function that moves Elbow Position      */
int position;
{
printf("\nMoving elbow !");
outp(768,2);
}

```

```
    outp(769,position);
    outp(770,0);
    wait(1000);
    outp(770,1);
}

wrist(position)/* Function that moves Wrist Position */  
int position;
{
    printf("\nMoving wrist !");
    outp(768,3);
    outp(769,position);
    outp(770,0);
    wait(1000);
    outp(770,1);

}
```

```

#include <stdio.h>
#include <conio.h>
#include <stdlib.h>
#include <time.h>
#include <signal.h>

float v1,v2,v3,v4;
int ch;
FILE *fp;

float ad(int ch)

{
int lval,hval,aval;
float va;
char value[6];

    outp(0x310,ch*2);      /* Clears output voltages */
    outp(0x310,ch*2);      /* Clears again */
    outp(0x312,ch*2);

do {lval = inp(0x316);
} while ((lval&8)==0);

    aval=inp(0x313);
    hval=(aval*16)+lval/16;
    if (hval>2047) hval=hval-4095;
    va= (float) hval/204.7;
return (va);
}

main()
{

/*get four voltage at four channels*/
ch=4;
v1=ad(ch);           /* Checks woltage at A4, sets to v1 */
printf ("ch= %i\n",ch);
ch=5;
printf ("v1= %f\n",v1);
v2=ad(ch);           /* Checks voltage at A5, sets to v2 */
ch=6;
v3=ad(ch);           /* Checks voltage at A6, sets to v3 */
ch=7;
}

```

```
v4=ad(ch);           /* Checks voltage at A7, sets to v4  */
printf ("ch= %i\n",ch);

/* Create M file with four voltages in an array */
fp=fopen("pat.m","w");
fprintf (fp,"volts=[%f %f %f %f]\n",v1,v2,v3,v4);
fclose (fp);
}
```